

Stony Brook University



OFFICIAL COPY

The official electronic file of this thesis or dissertation is maintained by the University Libraries on behalf of The Graduate School at Stony Brook University.

© All Rights Reserved by Author.

**Design, Synthesis and Biological Evaluation of Novel Trisubstituted-
Benzimidazoles as a New Class of Antitubercular Agents, Targeting FtsZ**

A Dissertation Presented

by

Kunal Kumar

to

The Graduate School

In partial fulfillment of the

requirements

for the Degree of

Doctor of Philosophy

in

Chemistry

Stony Brook University

May 2011

Stony Brook University

The Graduate School

Kunal Kumar

We, the dissertation committee for the above candidate for the

Doctor of Philosophy degree, hereby recommend

acceptance of this thesis

Professor Iwao Ojima
Dissertation Advisor
Department of Chemistry

Professor Kathlyn A. Parker
Chairman
Department of Chemistry

Professor Frank W. Fowler
Third Member
Department of Chemistry

Professor James Bliska
Outside Member
Department of Molecular Genetics and Microbiology,
Center for Infectious Diseases, Stony Brook University

This dissertation is accepted by the Graduate School

Lawrence Martin
Dean of the Graduate School

Abstract of the Dissertation

**Design, Synthesis and Biological Evaluation of Novel Trisubstituted-Benzimidazoles as a
New Class of Antitubercular Agents, Targeting FtsZ**

Kunal Kumar

Doctor of Philosophy in

Chemistry

Stony Brook University

2011

Despite extensive research in last 40 years, the treatment of TB is still limited to a cocktail of classical drugs that mostly target cell wall biosynthesis, DNA coiling, transcription, translation. Knowing the bacterial ability to develop resistance, there is a dire need for the discovery of new cellular targets to develop novel antitubercular agents which can surpass the resistance. In this context, FtsZ, a highly conserved and ubiquitous cytokinesis protein, offers an extremely promising therapeutic target. It has been observed that inhibition of FtsZ assembly leads to absence of septum formation, eventually causing cell lethality. Hence, compounds targeting FtsZ can be developed as novel anti-tubercular agents.

Libraries of novel trisubstituted benzimidazoles were created through rational drug design. A good number of these benzimidazoles exhibited promising MIC values in the range of 0.5-6 $\mu\text{g/mL}$ (2-15 μM) against *Mtb* H37Rv strain with no appreciable cytotoxicity ($\text{IC}_{50} > 200 \mu\text{M}$) against Vero cells. Moreover, five of the lead compounds also exhibited excellent activity against clinical *Mtb* strains with different drug-resistance profiles. In the light scattering experiments, the lead compounds clearly showed inhibition of FtsZ assembly in a dose dependent manner while enhancing the GTPase activity of *Mtb* FtsZ by 3-4 folds. Transmission electron microscopy (TEM) images of *Mtb* FtsZ treated with lead compound revealed an impressive dose-dependent inhibition of FtsZ assembly and a remarkable reduction in FtsZ protofilament formation. A unique *Mtb* cell morphology was observed under Scanning electron microscopy (SEM) upon treatment with lead benzimidazoles. *Mtb* cells were shorter in length with increased circumferences and altered polar caps. The TEM and SEM analyses strongly suggest that lead benzimidazoles have a novel mechanism of action on the inhibition of *Mtb* FtsZ assembly and Z-ring formation. Furthermore, as FtsZ is highly conserved in different pathogens, we also identified several hit compounds against *F. tularensis*, *B. thailandensis* and *Y. pestis*. Design, synthesis, optimization and biological evaluation of novel trisubstituted-benzimidazoles are presented.

**Dedicated to my parents,
My brother Kushal
and
my friends**

TABLE OF CONTENTS

LIST OF FIGURES	viii
LIST OF SCHEMES.....	x
LIST OF TABLES	xi
LIST OF ABBREVIATIONS.....	xii
ACKNOWLEDGEMENTS.....	xv

CHAPTER I

FtsZ: A Novel Target for the Discovery of New Class of Antitubercular Agents

§ 1.1 Introduction.....	2
§ 1.1.1 Tuberculosis.....	2
§ 1.1.2 Current TB treatments	4
§ 1.2 FtsZ – Filamentous Temperature Sensitive Protein Z	5
§ 1.2.1 Biological Role of Filamentous Temperature Sensitive Protein Z (FtsZ)	6
§ 1.2.2 FtsZ and Tubulin: Structural and functional homology	10
§ 1.3 FtsZ-A novel target for anti-TB drug discovery	11
§ 1.4 <i>Mtb</i> FtsZ inhibitors	12
§ 1.5 References.....	17

CHAPTER II

Discovery of Novel Benzimidazoles as a New Class of Antitubercular Agents: Targeting Essential Cell Division Protein FtsZ

§ 2.1 Introduction.....	25
§ 2.2 Results and Discussion	29
§ 2.2.1 Synthesis of 2,5,6-trisubstitutedbenzimidazole library	29
§ 2.2.2 Preliminary screening, re-synthesis and accurate MIC determination.....	30
§ 2.2.3 Preliminary SAR study and optimization of the 6-position of 2,5,6-trisubstituted benzimidazoles	34
§ 2.2.4 Optimization of the 2-position of 2,5,6-trisubstituted benzimidazoles	36
§ 2.2.5 Optimization of the 5-position of 2,5,6-trisubstituted library against <i>Mtb</i>	39
§ 2.2.6 Optimization of 2,5,7-trisubstituted benzimidazoles.....	41
§ 2.2.7 Early ADMET results and synthesis of metabolically stable.....	44
§ 2.3 Conclusion	45
§ 2.4 Experimental Section.....	46
§ 2.4.1 Synthesis of 2,5,6-Trisubstituted Benzimidazole Library II-A	46
§ 2.4.2 Synthesis of 2,5,6-Trisubstituted Benzimidazole Library II-B	54

§ 2.4.3 Synthesis of analytically pure trisubstituted benzimidazoles	64
§ 2.4.4 Synthesis of 2,5,6-Trisubstituted Benzimidazole Library II-C	71
§ 2.4.5 Synthesis of 2,5,6-Trisubstituted Benzimidazole Library II-D	76
§ 2.4.6 Synthesis of 2,5,6-Trisubstituted Benzimidazole Library II-E	77
§ 2.4.7 Synthesis of 2,5,7-Trisubstituted Benzimidazole Library II-F	79
§ 2.4.8 Antibacterial and cytotoxicity activity determination	85
§ 2.5 References	87

CHAPTER III

Target Confirmation and Biological Evaluation of Novel Benzimidazole-Based Anti-tubercular Agents

§ 3.1 Introduction	90
§ 3.2 Results and discussion	92
§ 3.2.1 Polymerization Assay	92
§ 3.2.2 GTPase Assay	94
§ 3.2.3 Transmission Electron Microscopy of FtsZ assembly	95
§ 3.2.4 Scanning Electron Microscopy of Mtb cells	96
§ 3.2.5 Photoaffinity labeling (PAL) of FtsZ for binding site determination	97
§ 3.2.6 Preliminary in vivo assays and formulation studies	101
§ 3.3 Conclusion	104
§ 3.4 Experimental Section	105
§ 3.4.1 Mtb FtsZ Protein Preparation	105
§ 3.4.2 FtsZ Polymerization Inhibitory Assay	106
§ 3.4.3 GTPase Assay	106
§ 3.4.4 Transmission Electron Microscopy (TEM) Analysis	107
§ 3.4.5 Ultrastructural analysis via scanning electron microscopy (SEM)	107
§ 3.4.6 Photoaffinity Labeling of FtsZ using 4-azido-SB-PIG8	108
§ 3.4.7 Synthesis of photoaffinity analogue 4-Azido-SB-PIG8	108
§ 3.5 References	110

CHAPTER IV

Discovery of Novel Trisubstituted Benzimidazole-Based Antibacterial Agents Against Other Pathogens

§ 4.1 Introduction	113
§ 4.2 Compounds targeting FtsZ from other pathogens	115
§ 4.3 Results and discussion:	123
§ 4.3.1 Preliminary screening against different bacterial strains	123
§ 4.3.2 Ex-vivo efficacy of hit benzimidazoles against <i>B. thailandensis</i> and <i>F. tularensis</i>	125
§ 4.3.3 Resynthesis of 2,5,6-trisubstituted hit benzimidazoles for accurate MIC ₉₉ determination	127
§ 4.4 Conclusion	131
§ 4.5 Experimental Section	132

§ 4.6 References.....	139
-----------------------	-----

CHAPTER V

Synthesis of CMPF for Dual-Targeting Taxoid Conjugate

§ 5.1. Introduction.....	145
§ 5.2 Results and discussion.....	150
§ 5.2.1 <i>Synthesis of CMPF derivatives</i>	150
§ 5.2.2 <i>Evaluation of binding affinity of CMPF derivatives to human serum albumin (HSA)</i>	151
§ 5.4 Conclusion.....	152
§ 5.5 Experimental Section.....	153
§5.6 References.....	159

CHAPTER VI

Synthesis of Taxoid-Based Antitubercular Agents for Co-Crystallization With FtsZ and X-ray Study

§ 6.1 Introduction.....	163
§ 6.2 Results and discussions.....	166
§ 6.3 Conclusion.....	167
§ 6.4 Experimental Section.....	168
§ 6.5 References.....	172

BIBLIOGRAPHY

Chapter I.....	173
Chapter II.....	178
Chapter III.....	180
Chapter IV.....	181
Chapter V.....	185
Chapter VI.....	186

APPENDICES

A1. Appendix Chapter II.....	189
A2. Appendix Chapter III.....	286
A3. Appendix Chapter IV.....	288
A4. Appendix Chapter V.....	310
A5. Appendix Chapter VI.....	314

LIST OF FIGURES

CHAPTER I

Figure I-1. Estimated new TB cases worldwide	2
Figure I-2. Estimated HIV prevalence in new TB cases worldwide.....	3
Figure I-3. Current drugs and their targets; Adapted and reorganized from the National Institute of Allergy and Infectious Diseases' website.....	4
Figure I-4. Structures of FDA-approved current anti-TB drugs	5
Figure I-5. Graphic presentation of the Z-ring formation and cell division.	6
Figure I-6. The spatial regulation of the Z ring assembly by MinCDE system and Nucleoid occlusion (NO).....	8
Figure I-7. Polymerization-depolymerization dynamics of FtsZ.....	9
Figure I-8. <i>Mtb</i> FtsZ inhibitors	13
Figure I-9. <i>Mtb</i> FtsZ inhibitors: Taxanes.....	16
Figure I-10. Electron micrograph of <i>Mtb</i> cells: (A) Control, (B) SB-RA-20018 and (C) SB-RA-5001.....	16

CHAPTER II

Figure II-1. FtsZ dynamics: GTP hydrolysis and Polymerization	25
Figure II-2. <i>Mtb</i> FtsZ inhibitors:Taxanes.....	26
Figure II-3. Proposed trisubstituted benzimidazoles library	27
Figure II-4. Preliminary SAR studies and optimization of the 6-position	34
Figure II-5. Optimization of the 2-position of 2,5,6-trisubstituted benzimidazole library	36
Figure II-6. Hits from the 2-position optimization	38
Figure II-7. Optimization of the 6-position.....	39
Figure II-8. Synthesis of the 5-position optimized 2,5,6-trisubstituted benzimidazole library II-D	40
Figure II-9. Synthesis of the 5-position optimized 2,5,6-trisubstituted benzimidazole library II-E	41
Figure II-10. Optimization of the 2,5,7-trisubstituted benzimidazoles.....	42
Figure II-11. Amide congeners of SB-P3G2 and SB-P8B2	44

CHAPTER III

Figure III-1. The Z-ring formation: Bacterial Cell division	90
Figure III-2. Library of Benzimidazoles and list of hit compounds	91
Figure III-3. Inhibition of FtsZ polymerization by lead benzimidazoles.....	93
Figure III-4. Inhibition of FtsZ polymerization by lead benzimidazoles.....	94
Figure III-5. Enhancement of GTPase activity of FtsZ by lead benzimidazoles.....	95
Figure III-6. Transmission electron microscope (TEM) images of FtsZ.....	96
Figure III-7. SEM of <i>Mtb</i> cells treated with SB-P3G2 (20,000X).....	97
Figure III-8. Photoaffinity analogues (PAA) taxoid and benzimidazole based anti-TB agents ..	98
Figure III-9. MALDI of digested samples of non-polymerized FtsZ with and without PAA	100
Figure III-10. MALDI of digested samples of polymerized FtsZ with and without PAA	101
Figure III-11. Mean CFU in lung and spleen after 22 days of administration of compound	102

CHAPTER IV

Figure IV-1. Graphic representation of Z-ring formation and cell division.....	114
Figure IV-2. FtsZ inhibitors against pathogens other than <i>Mtb</i>	116
Figure IV-3. FtsZ inhibitors of bacteria other than <i>Mtb</i>	117
Figure IV-4. Structures of 2,5,6-trisubstituted benzimidazoles against <i>F. tularensis</i> at 1 µg/mL with > 90 % growth inhibition.....	123
Figure IV-5. Structures of 2,5,7-trisubstituted benzimidazoles against <i>F. tularensis</i> at 1 µg/mL with > 90 % growth inhibition.....	124
Figure IV-6. Structures of hit benzimidazoles against <i>F. tularensis</i> with 40-50 % growth inhibition 0.2 µg/mL.....	124
Figure IV-7. Structures of hit benzimidazoles against <i>Y. pestis</i>	125
Figure IV-8. Structures of hit benzimidazoles against <i>B. thailandensis</i>	125
Figure IV-9. Effect of benzimidazoles on <i>B. thailandensis</i> Bt38 efflux mutant infection of raw macrophages.....	126
Figure IV-10. Effect of benzimidazoles on <i>F. tularensis</i> LVS infection of raw macrophages..	127
Figure IV-11. Percent growth inhibition of <i>F. tularensis</i> LVS 110408 by lead benzimidazoles	130
Figure IV-12. MIC ₉₀ of lead benzimidazoles against <i>F. tularensis</i> LVS 110408.....	130

CHAPTER V

Figure V-1. Basic structure of drug conjugate.....	145
Figure V-2. Dual targeting taxoid conjugate.....	146
Figure V-3. Derivatives of CMPF with their binding affinities to albumin.....	147
Figure V-4. Binding affinity if methyl ester and N-methyl amide derivatives of CMPF to HSA.	148
Figure V-5. Dual targeting taxoid conjugate containing folic acid and CMPF.....	149
Figure V-6. ITC Measurements of CMPF derivatives.....	152

CHAPTER VI

Figure VI-1. Taxanes as <i>Mtb</i> FtsZ inhibitors.....	163
---	-----

LIST OF SCHEMES

CHAPTER II

Scheme II-1. Proposed synthesis of 2,5,6- and 2,5,7-trisubstituted benzimidazole library.....	28
Scheme II-2. Synthesis of 2,5,6-trisubstituted benzimidazole library II-A	29
Scheme II-3. Re-synthesis of hit compounds	30
Scheme II-4. Re-synthesis of Hit compounds.....	31
Scheme II-5. Re-synthesis of hit compounds	33
Scheme II-6. Optimization of the 6-position of 2,5,6-trisubstituted benzimidazole library.....	35
Scheme II-7. Optimization of the 2-position of 2,5,6-trisubstituted benzimidazole library.....	37
Scheme II-8. Synthesis of 2,5,6-trisubstituted benzimidazoles with pyrrolidine substituent at the 6-position	38
Scheme II-9. Synthesis of 2,5,7-trisubstituted benzimidazole library II-F.....	43

CHAPTER III

Scheme III-1. Synthesis of 4-azido SB-P1G8.....	99
---	----

CHAPTER IV

Scheme IV-1. Synthesis of 2,5,6-trisubstituted benzimidazole intermediates.....	128
Scheme IV-2. Synthesis of hit compounds	128

CHAPTER V

Scheme V-1. Proposed synthesis of CMPF analogues	149
Scheme V-2. Synthesis of CMPF precursor	150
Scheme V-3. Synthesis of alkyltriphenylphosphonium salts.....	150
Scheme V-4. Synthesis of CMPF analogues	151

CHAPTER VI

Scheme VI-1. Synthesis of SB-RA-2001.....	164
Scheme VI-2. Synthesis of SB-RA-200101.....	165
Scheme VI-3. Synthesis of SB-RA-2001 (VI-4)	166
Scheme VI-4. Synthesis of SB-RA-200101 (VI-7)	167

LIST OF TABLES

CHAPTER I

Table I-1. <i>Mtb</i> FtsZ inhibitors.....	14
Table I-2. Antimicrobial activities of taxanes against drug-sensitive and multidrug-resistant <i>Mtb</i> strains.....	15

CHAPTER II

Table II-1. Optimization of the reaction condition	30
Table II-2. Antimicrobial Activities of Selected Trisubstituted Benzimidazoles against Drug-Sensitive and Drug-Resistant Strains of <i>Mtb</i>	32

CHAPTER III

Table III-1. Formulation of lead benzimidazoles	103
---	-----

CHAPTER IV

Table IV-1. Compounds targeting FtsZ of bacteria other than <i>Mtb</i>	118
Table IV-2. Compounds targeting FtsZ for bacteria other than <i>Mtb</i>	122
Table IV-3. Re-synthesis of the hit compounds.....	129

CHAPTER VI

Table VI-1. Antimicrobial activities of taxanes against drug-sensitive and multidrug-resistant <i>Mtb</i> strains	164
---	-----

LIST OF ABBREVIATIONS

10-DAB	10-Deacetylbaccatin III
3-MBA	3-methoxybenzamide
ABC	ATP-binding cassette
ACN	Acetonitrile
ADMET	Absorption, distribution, metabolism, excretion and
AIDS	Acquired immune deficiency syndrome
ANS	1-anilinonaphthalene-8-sulfonic acid
ATP	Adenosine triphosphate
<i>B. subtilis</i>	<i>Bacillus subtilis</i>
BSA	Bovine serum albumin
CA-MRSA	Community acquired MRSA
CDC	Center for disease control and prevention
CFU	Colony forming unit
CMPF	3-carboxy-4-methyl-5-propyl-2-furanpropanoic acid
CNMR	Carbon nuclear magnetic resonance
CYP3A4	CytochromeP3A4
DAPI	4',6-diamidino-2-phenylindole
DMF	Dimethylformamide
DMSO	Dimethylsulfoxide
DNA	Deoxyribonucleic acid
<i>E. coli</i>	<i>Escherichia coli</i>
EPR	Enhanced permeability and retention
EtOAc	Ethyl acetate
<i>F. tularensis</i>	<i>Francisella tularensis</i>
FAB	Fast atom bombardment
FDA	Food & drug administration
FRAP	Fluorescence recovery after photobleaching
FtsZ	Filamentous temperature-sensitive protein Z
GDP	Guanosine diphosphate
GFP	Green fluorescent protein
GTP	Guanosine triphosphatase
GTPase	Guanosine triphosphate
HCl	Hydrochloric acid
HIV	Human immune virus
HNMR	Proton nuclear magnetic resonance
HPLC	High performance liquid chromatography

HRMS	High resolution mass spectrometry
HSA	Human serum albumin
HTP	High throughput
IC ₅₀	Half maximal inhibitory concentration
ID ₅₀	Median infectious dose
IP	Intraperitoneally
IPTG	Isopropyl β-D-1-thiogalactopyranoside
ITC	Isothermal titration calorimetry
LB	Lysogeny broth
LD ₅₀	Median lethal dose
LTBI	Latent TB infection
mp	Melting point
MABA	Microplate alamar blue assay
MALDI	Matrix-assisted laser desorption/ionization
MDR	Multidrug resistant
MDRSA	Multidrug resistant staphylococcus aureus
MDR-TB	Multi-drug resistant tuberculosis
MES	2-(<i>N</i> -morpholino)ethanesulfonic acid
MIC	Minimum inhibitory concentration
MRSA	Methicillin-resistant staphylococcus aureus
<i>Mtb</i>	<i>Mycobacterium tuberculosis</i>
NHS	<i>N</i> -hydroxysuccinimide
NIAID	National institute of allergy and infectious diseases
OADC	Oleic acid/Albumin fraction V, Bovine/Dextrose/Catalase
OD	Optical density
OTBA	3-{5-[4-Oxo-2-thioxo-3-(3-trifluoromethylphenyl)-thiazolidin-5-ylidene methyl]-furan-2-yl}-benzoic acid
PAA	Photoaffinity analogue
PAL	Photoaffinity-labeling
PBS	Phosphate buffer saline
PCR	Polymerase chain reaction
P-gp	P-glycoprotein
Pi	Inorganic phosphate
PMFS	Phenylmethylsulfonyl fluoride
RNA	Ribonucleic acid
<i>S. aureus</i>	<i>Staphylococcus aureus</i>
SAR	Structure-activity relationship
SEM	Scanning electron microscopy
STD-NMR	Saturation transfer difference NMR

TB	Tuberculosis
TBZ	Thiabendazole
TEM	Transmission electron microscopy
TES chloride	Triethylsilyl chloride
TFA	Trifluoroacetic acid
THF	Tetrahydrofuran
TLC	Thin layer chromatography
TRAs	Taxane reversal agents
VRE	Vancomycin-resistant enterococci
WHO	World Health Organization
XDR-TB	Extremely drug-resistant tuberculosis
<i>Y. pestis</i>	<i>Yersinia pestis</i>

Acknowledgments

This thesis is the result of five and half years of research work where I have been accompanied and supported by many people. It is my great pleasure to express my deepest gratitude to all of them who made it possible for me.

I would like to express my most sincere gratitude to my dissertation advisor Professor Iwao Ojima for giving me the opportunity to work in his research laboratory. His infectious enthusiasm and holistic view on research have made a lasting impression on me. I thank him for his insightful guidance, patience, never-ending encouragement and continuous support which have kept me going over the five years' of challenging graduate study. Besides my advisor, I would like to thank the member of my committee. I sincerely thank Professor Kathlyn A. Parker and Professor Frank W. Fowler, the chair and third member of my committee, respectively. I significantly benefitted from their insightful comments, suggestions and interactions throughout the course of my graduate study. I especially wish to thank Professor James Bliska for taking time out of his busy schedule to be the outside member of my dissertation committee.

I would also like to humbly acknowledge the support of our collaborators who have shared their expertise with us and made significant contribution to my doctoral research. I wish to thank Professor Richard A. Slayden and researchers from his laboratory, especially Dr. Susan Knudson and Dr. Ryan M. Troyer at Colorado State University, for performing anti-bacterial assays, cytotoxicity assays and electron microscopy on MTB cells for our lead compounds. I would like to sincerely acknowledge Sanofi-Aventis for determining ADMET properties of our lead benzimidazoles. I am thankful to Professor Peter J. Tonge and his laboratory members for their valuable advice and generous help during my doctoral study. I also acknowledge Dr. Seung-Yub Lee, Dr. Bela Ruzsicska, Dr. Henguang Li and Dr. Edward Melief for their discussions and collaboration on various aspects of the FtsZ project.

Financial support from New York State Foundation for Science, Technology and Innovation (NYSTAR), National Institutes of Health (NIH), National Institute of Allergy and Infectious Diseases (NIAID) and the Department of Chemistry at Stony Brook is gratefully acknowledged. In addition, I would like to thank many people in the Chemistry Department at Stony Brook. I wish to sincerely thank the members of the faculty of the Chemistry Department

and especially Professor Dale Drueckhammer, Professor Peter Tonge, Professor Iwao Ojima, Professor Frank Fowler and Professor Kathlyn Parker for a great foundation during my course work. I thank Dr. James Marecek, for his kind assistance in NMR spectroscopy. I thank Ms. Carol Brekke, Ms. Charmaine Yapchin and especially to Ms. Katherine Hughes for their warm-hearted assistance in a variety of matters during my stay at Stony Brook. I also thank Dr. Alvin Silverstein, Executive Officer of the department, for his kind help. As always, it is impossible to mention everyone.

I am greatly indebted to the past and present members of Professor Ojima's group. I would like to thank Dr. Joseph Kaloko, Dr. Xianrui "Ray" Zhao, Dr. Liang Sun, Dr. Bruno Chapsal, Dr. Seung-Yub Lee, Dr. Stephen J. Chaterpaul, Dr. Ce Shi, Dr. Shuyi Chen, Dr. Jin Chen, Dr. Olivier Marrec, Dr. Sunny Huang and Dr. Stanislav Jaracz for your support, encouragement and the many discussions on my research projects. Additionally, I wish to thank Edison Zuniga, Chi-Feng Lin, Chih-Wei Chien, Gary Teng, Alexandra Athan, William Berger, Joshua Seitz, Tao Wang, Wen Chen, Winnie Situ, Bora Park, and Yang Zang for all support and encouragement. A special thanks to all the undergraduate and master students, Keita Morohashi, Ping Ping, Guan-Ting Chen, Cristina Susanto and Lucy Li for their help in my research projects. I would like to thank Gary Teng, Divya awasthi, Edison Zuniga, Joshua Seitz and Joseph Kaloko for their valuable help in proofreading and formatting of my thesis.

Especially, I want to express my true appreciation to Divya Awasthi and Ilaria Zanardi. I am lucky to have such great friends and excellent partners at work. You guys made me get through the tough days with lots of laughter and fun. Research wouldn't have been as much of a wonderful experience without you all.

My special thanks go to Mrs. Yoko Ojima for her kindness and hospitality and for making life outside lab, a great experience. I want to thank Mrs. Patricia Marinaccio for all the candies and for always being so warm to me and making me feel like at home.

Finally I want to express my deepest and sincere gratitude to my parents and my brother for believing in me and supporting me through various ups and downs. I owe you the most. Also, I would like to extend my sincere thanks to all my friends for keeping up with my sporadic mood swings. Your love and encouragement have kept me going all this while. Thank you with all my heart!!!

Chapter I

FtsZ: A Novel Target for the Discovery of New Class of Antitubercular Agents

Table of Content

§ 1.1 Introduction.....	2
§ 1.1.1 Tuberculosis	2
§ 1.1.2 Current TB treatments	4
§ 1.2 FtsZ – Filamentous Temperature Sensitive Protein Z	5
§ 1.2.1 Biological Role of Filamentous Temperature Sensitive Protein Z (FtsZ).....	6
§ 1.2.2 FtsZ and Tubulin: Structural and functional homology	10
§ 1.3 FtsZ-A novel target for anti-TB drug discovery	11
§ 1.4 <i>Mtb</i> FtsZ inhibitors	12
§ 1.5 References	17

§ 1.1 Introduction

§ 1.1.1 Tuberculosis

Tuberculosis (TB), caused by *Mycobacterium tuberculosis* (*Mtb*) is a leading cause of death worldwide.¹ The primary site of infection is the lungs, followed by dissemination via the circulatory system and lymphatic system to secondary sites including the central nervous system, bones, joints, liver and spleen. Symptoms of TB infection usually include severe coughing-up of blood or sputum, chest pain, fatigue, loss of weight/appetite, and fever. TB is contagious when airborne and inhalation of air containing the bacteria is the most common route of infection. In the 19th century, TB was one of the most dreaded diseases and the eighth leading cause of death in children 1 to 4 years of age during the 1920s. There are two kinds of TB-related conditions: latent-TB infections (LTBI) and active-TB disease.² It has been estimated that 90% of those who are exposed to or infected with TB have latent-TB infections and the body is able to fight the growth of bacteria.² People with LTBI are healthy, do not show any symptoms and can't spread infection. However, during sickness or in cases of weak immune systems, there is a 10 % chance that these bacteria can progress to an active-TB disease.² Hence, LTBI, even though it is not contagious, should be eradicated to eliminate any possibilities of it growing to an active disease.

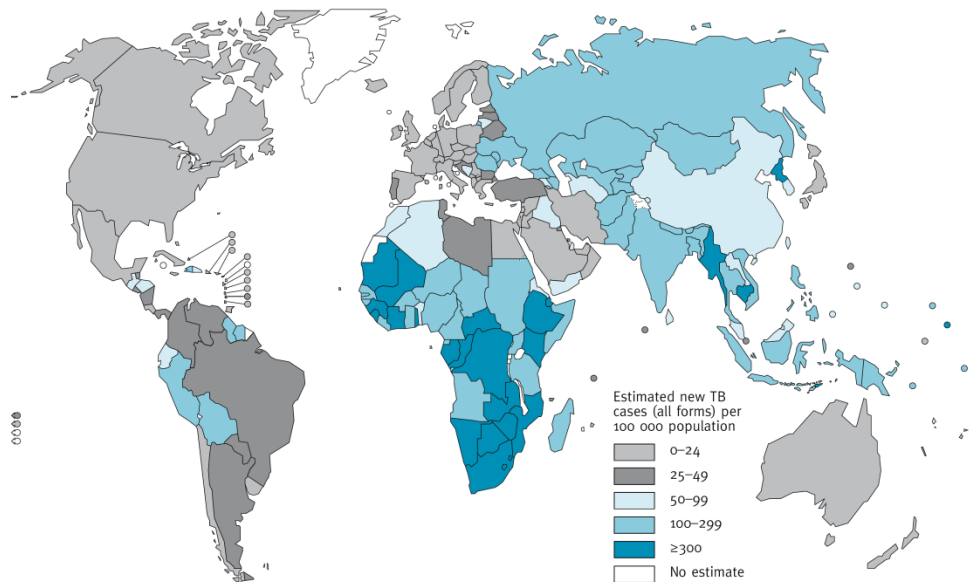


Figure I-1. Estimated new TB cases worldwide³

Recent statistics from World Health Organization (WHO) in the year 2009 estimate that there are an estimated 9.4 million new TB incident cases globally every year with a global mortality rate of 23 % (**Figure I-1**).³ Most of these cases occurred in Asia (55%) and Africa (30 %).³ The Global Burden of Disease study by the WHO indicates that women account for an estimated 3.3 million cases equal to 35 % of all cases.³

However, with the emergence of HIV/AIDS in the last couple of decades, TB has become the most common opportunistic infection for HIV/AIDS patients. Among the 9.4 million estimated TB incident cases, 1-1.2 million (11-13%) were HIV-positive, which is slightly, but not significantly, lower than the previous years (**Figure I-2**).³ An estimated 1.3 million and 0.38 million deaths occurred among the HIV-negative and HIV-positive TB cases, respectively.³ Furthermore, there were 0.38 million deaths among women infected with TB infection.³

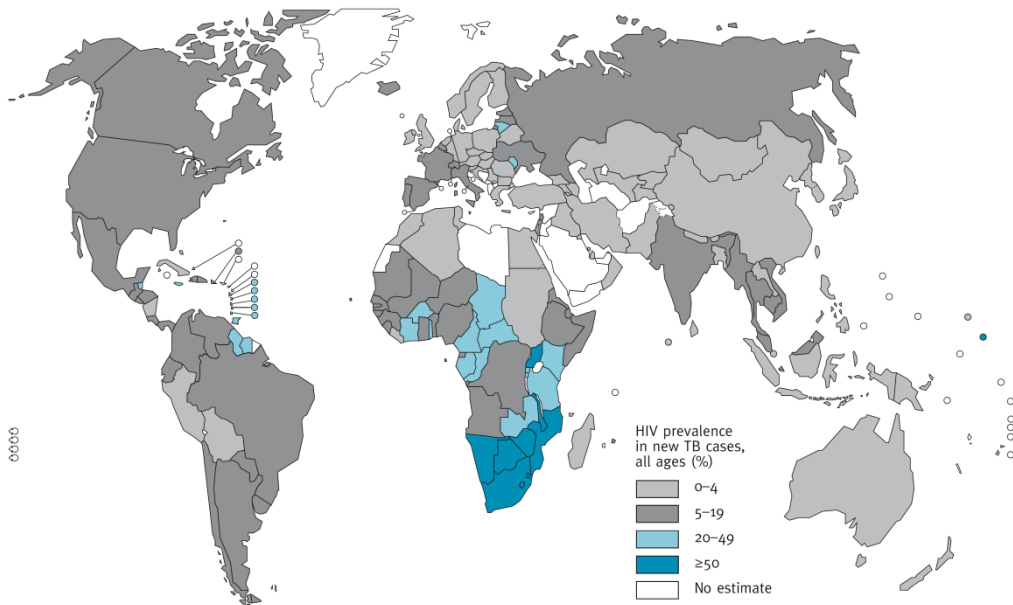


Figure I-2. Estimated HIV prevalence in new TB cases worldwide³

Poor patient compliance and inadequate control programs have led to the emergence of multi-drug resistant (MDR) strains of *Mtb*.⁴ In 2008, the WHO estimated that up to 440,000 cases of MDR-TB emerge every year leading to more than 110,000 deaths worldwide.³ Treatment of MDR-TB requires treatment time of two years with estimated cost of \$250,000 per patient in the US. Bacterial resistance to three or more ‘second-line’ antibiotics is classified as extremely drug resistant-TB (XDR-TB). Findings by WHO from 2000-2004 suggested that 4%

of MDR-TB cases meet the criteria for XDR-TB.³ By 2010, 58 countries and territories had reported at least one case of XDR-TB.³

§ 1.1.2 Current TB treatments

Primarily, TB infection can be treated by administering a combination of first-line drugs like, isoniazid, ethambutol, pyrazinamide, rifampicin, streptomycin which target cell-wall biosynthesis, RNA synthesis, protein synthesis etc (Figure I-3 and I-4).^{5,6}

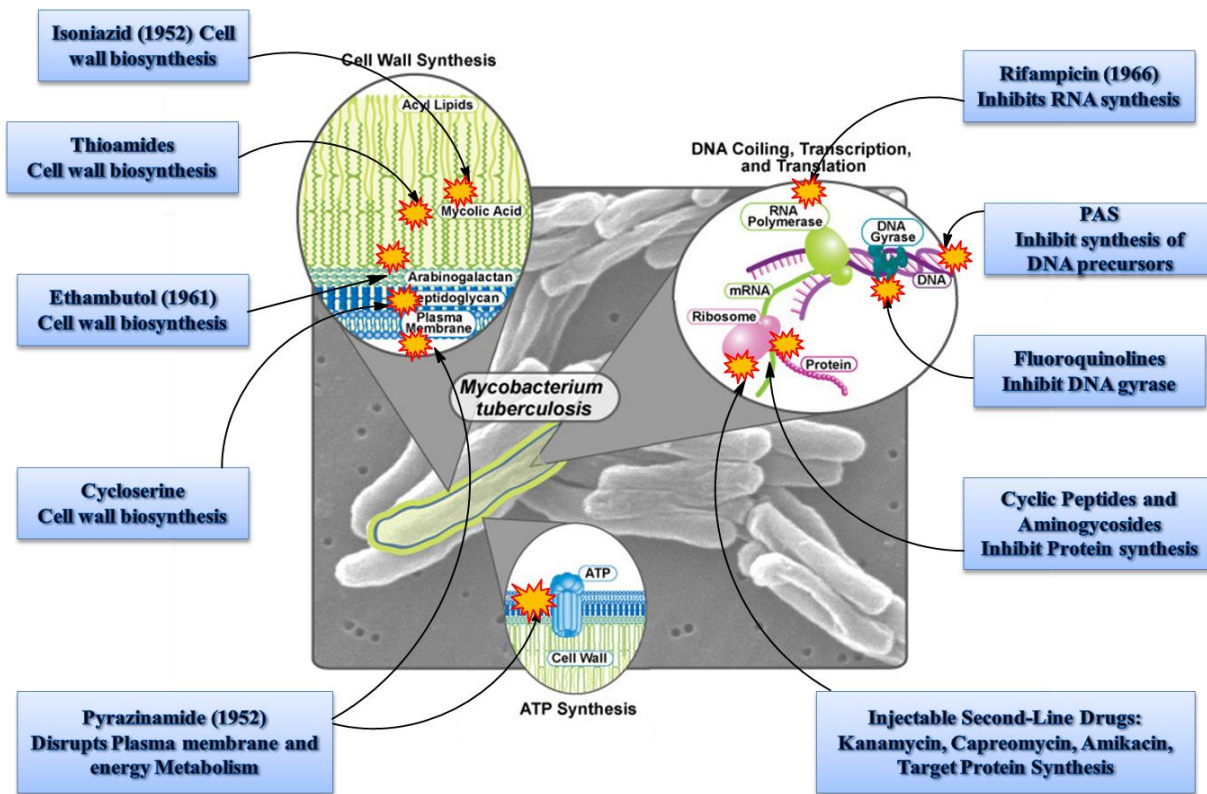


Figure I-3. Current drugs and their targets; Adapted and reorganized from the National Institute of Allergy and Infectious Diseases’ website

In the initial treatment phase, rifampicin and isoniazid are taken in combination for the first two months, followed by ethambutol and pyrazinamide for the continuation phase, which lasts 4-7 months.⁶ In cases of MDR-TB, where the bacteria become resistant to first-line drugs, such as rifampicin and isoniazid, a combination of second-line drugs comprising of thioamides, cycloserine, fluoroquinolones, cyclic peptides, and aminoglycosides are used.⁶ However, these second-line drugs come with several drawbacks. They may show additional side effects and the

treatment itself is 100 times more costly. Furthermore, there's a high possibility of MDR-TB strain developing resistance to even second-line drugs, complicating the treatment.

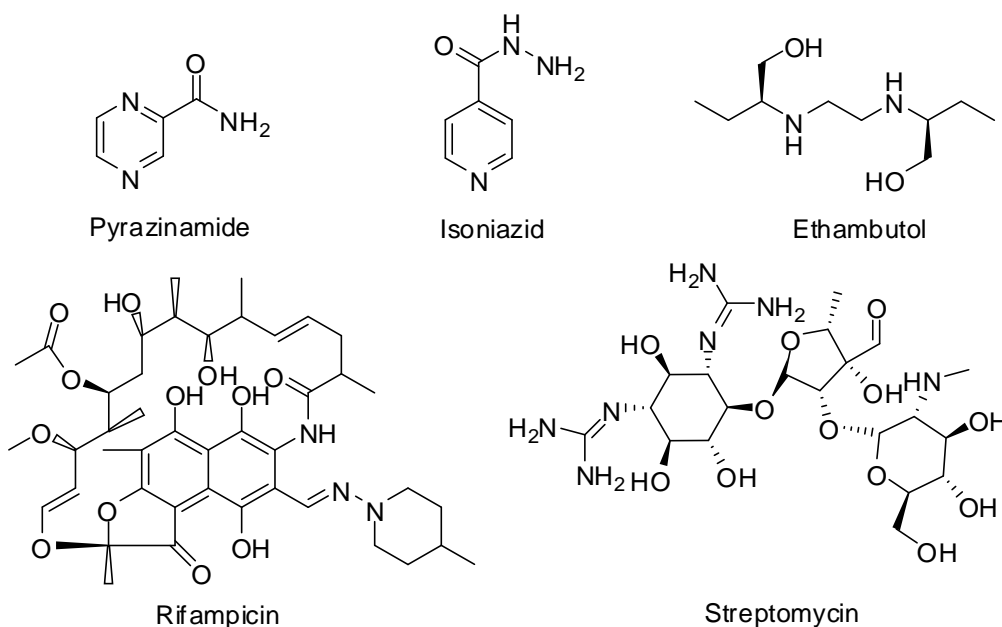


Figure I-4. Structures of FDA-approved current anti-TB drugs

Treatment for XDR-TB involves the administration of a cocktail of several first-line as well as second-line drugs for a long period of time with very limited chance of recovery. Widespread bacterial resistance to existing therapeutics due to poor drug compliance and bacterial flexibility to overcome drug effect has been a key hurdle for the complete treatment of the disease. Therefore, in order to counter attack the adaptive genetic machinery of bacteria, there is a dire need for the identification of novel therapeutic targets. In this context, FtsZ, an essential bacterial cytokinesis protein, is a highly promising therapeutic target since the disruption of cell division would lead to the inhibition/arrest of bacterial infection.^{7,8}

§ 1.2 FtsZ – Filamentous Temperature Sensitive Protein Z

Unlike drugs designed for eukaryotic cells, cytokinesis remains largely unexploited for the development of novel bacterial therapeutics. Filamentous temperature-sensitive protein Z (FtsZ), a tubulin homolog, is the most abundant bacterial cell division protein. In the presence of guanosine triphosphate (GTP), FtsZ polymerizes bi-directionally at the center of the cell on the inner membrane to form a highly dynamic helical structure known as the “Z-ring”.^{9,10,11,12,13} The recruitment of several other cell division proteins leads to Z-ring contraction, resulting in septum

formation and eventually cell division (**Figure I-5**).¹⁴ It was hypothesized that the inhibition of proper FtsZ assembly would cause an absence of septum formation, leading to bacterial cell division arrest. The bacterial cell continues to elongate, resulting in filamentation, which ultimately leads to cell death.^{15,16} Because of the central role that FtsZ plays in cell division, it is a very promising target for the development of new anti-TB drugs active against drug-resistant as well as drug sensitive *Mtb* strains.

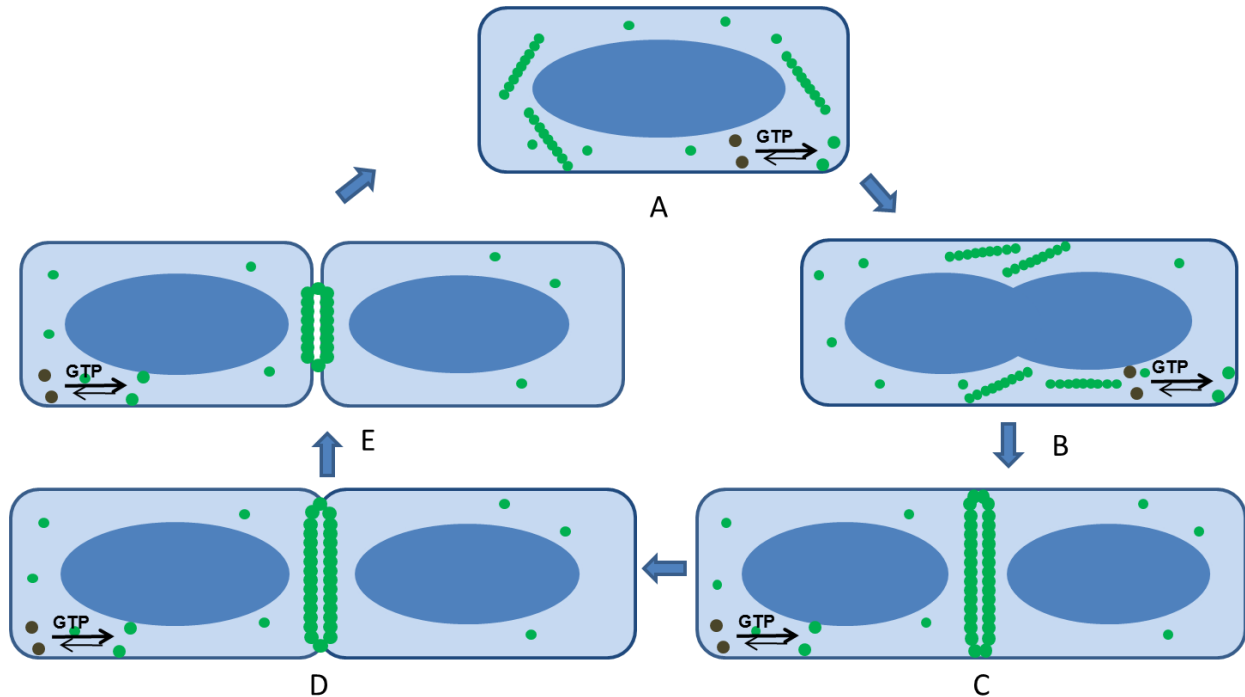


Figure I-5. Graphic presentation of the Z-ring formation and cell division.

(A) Bacterial cell before the beginning of cell division with FtsZ protofilaments scattered in the cell and undergoing continuous nucleotide exchange between GTP-bound FtsZ and GDP-bound FtsZ with rapid equilibrium, favoring GTP-bound FtsZ (B) Cell elongation and chromosome segregation, localization of FtsZ protofilaments at the mid cell. (C) Formation of the Z-ring:the ‘steady-state turnover’-- GTP hydrolysis competes continuously with protofilament growth during polymerization. (D &E) Formation of septum and subsequent constriction of the Z-ring followed by membrane fluctuation to bring about cell division.

§ 1.2.1 Biological Role of Filamentous Temperature Sensitive Protein Z (FtsZ)

FtsZ is the most essential and highly conserved cytoplasmic protein in prokaryotes.^{17,18} In the presence of GTP, at a critical concentration of 0.5-1 μM of FtsZ,^{19,20,21} FtsZ subunits are believed to display cooperative assembly to form single stranded protofilaments. They stack in a head to tail fashion, with GTP sandwiched between two FtsZ subunits.^{21,22,23} Extensive lateral

interaction between these overlapping protofilaments leads to the formation of a highly dynamic ring structure known as the “Z-ring”.²¹ However, the existence of lateral interactions among overlapping protofilaments is still debatable as accounted by several mathematical and *in vitro* models, and other alternative modes of interaction have been suggested such as annealing of protofilaments, and initial attraction of the ring.¹⁴ It has been proposed that association of the protofilaments does not necessarily involve physical contact; rather, they interact through electrostatic forces involving the ions between the protofilaments.^{24,25} Although the structure of the Z-ring formed *in vivo* is not well understood, it has been suggested that the Z-ring architecture might consist of a large number of short, overlapping protofilaments rather than a continuous ring.²⁶

While many of the proteins involved in chromosomal segregation and cell division are conserved across the taxa, others appear limited to Gram-negative or Gram-positive bacteria. Analysis of the *Mtb* genome sequence revealed that many of the genes that encode proteins involved in regulation of septum formation and cell division are not annotated.¹⁶ Much of what is known is derived from the studies in model organisms like *E. coli*, *B. subtilis*.^{27,28} It has been shown that an essential requirement for the formation of the Z-ring is the anchoring of FtsZ to the cell membrane through either FtsA or ZipA (accessory proteins), both of which are known to bind to the conserved C-terminal domain of FtsZ.^{28,27} However, it has been revealed that only one of them is required for Z-ring formation but both ZipA and FtsA are necessary for proper cytokinesis.²⁸ Since the requirement of ZipA can be bypassed by a mutation in FtsA and given that FtsA is widely conserved compared to ZipA, FtsA is believed to be the crucial factor responsible for maintaining the Z-ring integrity.^{17,29}

Fluorescence recovery after photobleaching (FRAP) along with other studies have revealed that the Z ring is very dynamic and continuously exchanging the subunits from a pool of cytoplasmic FtsZ before and during constriction. The rate of the steady-state turnover depends on the GTPase activity of the FtsZ polymer.^{30,31} Rapid turnover with no effect on the integrity of the Z-ring further suggests that it consists of short filaments of FtsZ interacting laterally with each other, presumably held together by FtsA/ZipA.^{14,32} A number of accessory proteins, especially MinCDE system and Noc (*B. subtilis*)/SIma (*E. coli*) are involved in the spatial regulation of septum formation, ensuring that the Z-ring is formed between the segregated chromosomes in the middle of the cell and not at the poles (**Figure I-6**).^{17,14}

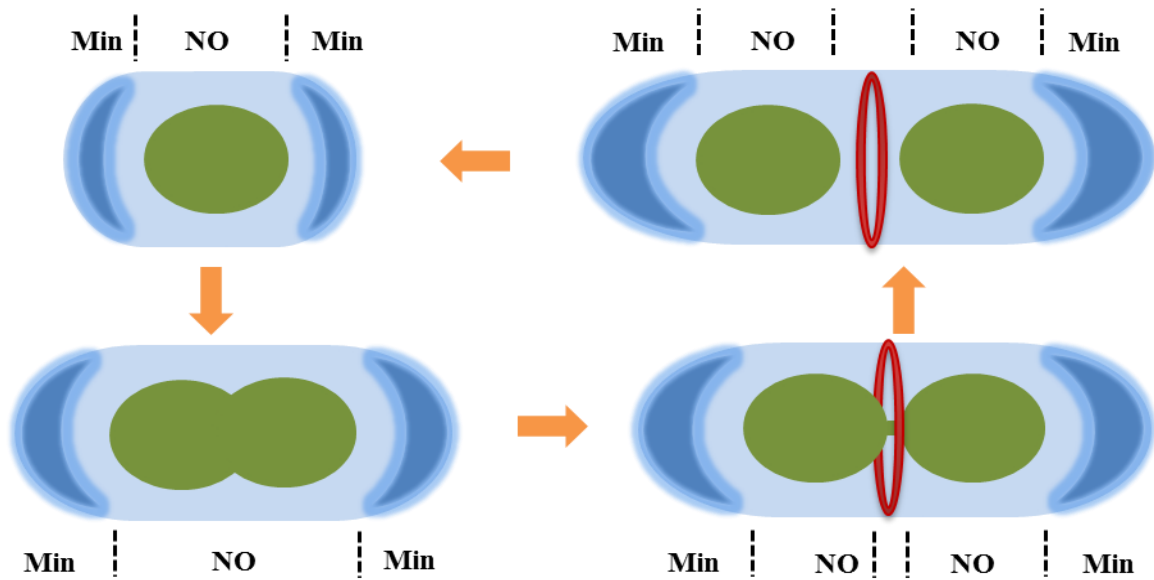


Figure I-6. The spatial regulation of the Z ring assembly by MinCDE system and Nucleoid occlusion (NO).¹⁷

In new daughter cells, Min system and NO prevents Z ring assembly at the cell poles and close to the nucleoid, respectively. During initial phase of chromosome segregation, NO continue to inhibit Z-ring formation in the cylindrical part of the cell. Finally, the progression of chromosome segregation reveals an inhibitor-free region at mid-cell, allowing the Z ring assembly.

The constant balance between assembly and disassembly of the “Z ring” is essential for bacterial cytokinesis, since small changes in FtsZ polymerization dynamics would be translated into large and rapid aberration in Z-ring structure.³³ Thus, a proper understanding of FtsZ polymerization dynamics will aid in the development of drugs that can prevent cell division by disrupting Z ring formation or function (**Figure I-7**).

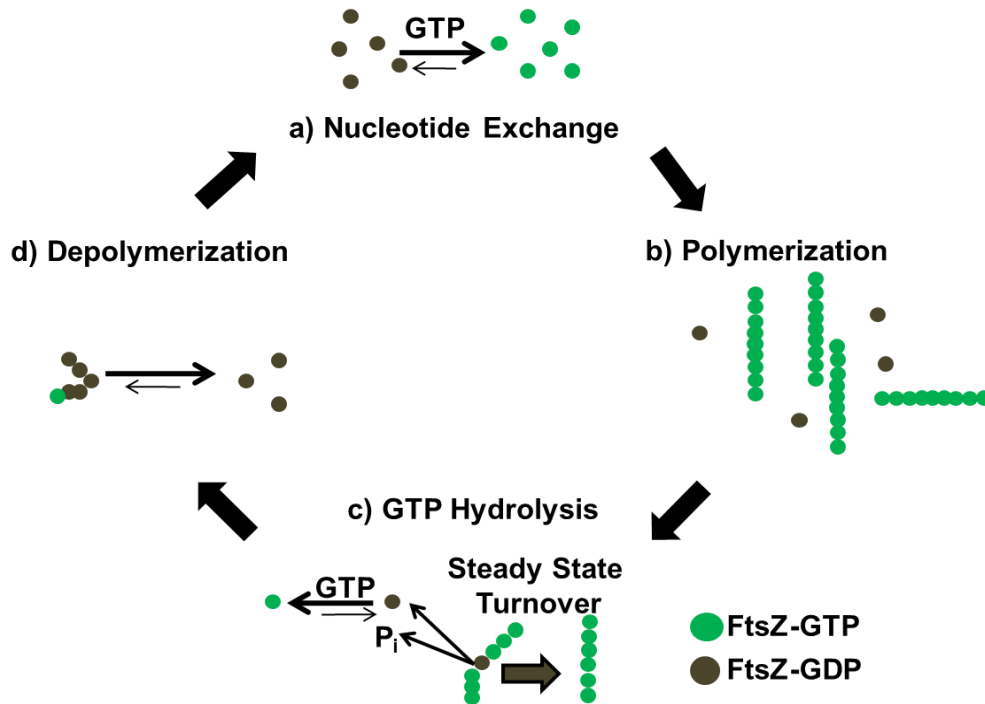


Figure I-7. Polymerization-depolymerization dynamics of FtsZ.

(A) Nucleotide exchange between GTP-bound FtsZ and GDP-bound FtsZ with rapid equilibrium, favoring GTP-bound FtsZ (B) Polymerization begins and long-strait protofilaments starts to form after a critical concentration of GTP-bound FtsZ is achieved. (C) The ‘steady-state turnover’-- GTP hydrolysis competes continuously with protofilament growth during polymerization. (D) After bacterial cell division occurs, distorted GDP-bound FtsZ protofilaments depolymerize to yields FtsZ monomers.

The relation between FtsZ polymerization and GTP hydrolysis to guanosine diphosphate (GDP) is crucial for integrity of the Z-ring. Romberg and Mitchison showed that GTP-bound FtsZ polymerizes into straight polymers, which triggers the GTPase activity of FtsZ, because the catalytic site is formed at the interface of two adjacent FtsZ monomers.^{34,35} The GTP binding domain is located in one monomer and the highly conserved tubulin-like loop 7 (T7-loop) of the other domain is located in an adjacent FtsZ monomer. During steady-state GTP turnover, the properties of the polymer are determined by the nucleotide species that predominates.³⁴ It has been shown that GTP hydrolysis is the rate-limiting step in this process, thus suggesting GTP as the major nucleotide species in the FtsZ polymer.³⁴ Upon GTP hydrolysis, polymers bound to GDP were thought to favor curved conformation as opposed to straight polymers.³⁶ It has been proposed that the GTP hydrolysis generates a force during septation where nucleotide-dependent transitions from straight to a curved polymer can transmit mechanical work to the membrane leading to the constriction of the Z-ring.^{26,36} However, the physiological role of this force

remains controversial as accounted by several experiments where FtsZ mutants with undetectable GTPase activity could still divide suggesting that FtsZ GTPase is not the source of power during constriction of the septum but is important for symmetric invagination.^{37,38}

Recent experiments with liposomes (tubular membrane) and observation of curved and straight protofilaments *in vivo* demonstrated that the protofilament bending is more likely to be a plausible mechanism for producing the constriction force.^{26,39} However it is believed that the curved conformation of the protofilaments itself can not pull the membrane to complete scission.¹⁴ It has been suggested that the final step of scission can be completed by membrane fluctuations.¹⁴ The remodeling of the cell wall, which starts from the membrane invagination, may become a positive force pushing the septum toward closure, leading to final scission.^{14,40,41}

§ 1.2.2 FtsZ and Tubulin: Structural and functional homology

The fact that FtsZ is a homologue of tubulin was first realized via the identification of a short amino acid sequence, GGGTGTG, from the crystal structure of *Methanococcus jannaschii* FtsZ, that is virtually identical to the tubulin signature motif, (G/A)GGTGSG, found in all α , β and γ -tubulins.¹⁰ Despite limited (10-18%) sequence similarity,⁴² FtsZ and tubulin share a common fold, comprised of two domains linked by an α -helix.⁴³ The residues involved in the nucleotide binding domain and a region involved in protofilament formation in tubulin are found to be conserved.⁴³ Like tubulin, FtsZ polymerizes in the presence of GTP into 5 nm wide protofilaments while depolymerizing upon GTP hydrolysis.¹¹ Amidst similarity, the proteins also differ in several ways. Unlike FtsZ, where identical subunits form protofilaments, microtubules are formed from non-identical subunits, α and β tubulin.¹¹ Furthermore, the two *Mtb* FtsZ subunits are associated laterally as compared to longitudinally in case of tubulin. Because of the structural and functional homology, compounds that are known to affect the assembly of tubulin into microtubules, can act as a lead for targeting FtsZ assembly. The limited sequence homology at protein level, affords the opportunity to discover FtsZ-specific compounds with limited cytotoxicity to eukaryotic cells.

§ 1.3 FtsZ-A novel target for anti-TB drug discovery

As described above, FtsZ, an essential bacterial cytokinesis protein, has emerged as a highly promising new target for the discovery of novel antibacterial agents. It was hypothesized that inhibition of proper FtsZ assembly would prevent septum formation, giving way to continued cell filamentation, ultimately leading to cell death.^{15,16} FtsZ offers a significant potential advantage over traditional targets. As FtsZ is highly conserved in prokaryotes, in addition to being pathogen specific, FtsZ inhibitors may be developed as broad-spectrum antibacterial agents for the treatment of a variety of bacterial infections.⁴⁴ Since FtsZ is an essential and conserved protein for bacterial cell division, it is believed that acquiring resistance to the FtsZ-targeted compounds by mutations in the protein may be demanding for bacteria.^{45,18} Recently Haydon et al have isolated staphylococcal strains resistant to anti-FtsZ compounds with relatively low frequency, reiterating the difficulty in developing resistance.⁴⁶ This suggests that resistance mechanisms against compounds developed for FtsZ inhibition may not be widespread in nature. Accordingly, FtsZ is a very promising target to develop new generation antibacterial drugs. A good number of compounds have already been identified to target FtsZ.^{44,47,48,49} As FtsZ and tubulin have close functional homology,^{50,51,52} compounds that are known to inhibit or stabilize tubulin/microtubules can serve as a good starting point for the development of novel antibacterial agents.^{8,49,53,47,54} Upon modification, these tubulin inhibitors can be made specific to target FtsZ with no appreciable cytotoxicity to eukaryotic cells.

Although drug development in this field is still in an early stage, several classes of compounds have been found effective against *Mtb* and a number of compounds have been identified as promising leads.

§ 1.4 *Mtb* FtsZ inhibitors

Inhibitors of *Mtb* FtsZ reported so far are summarized in **Table I-1** and their structures are shown in **Figure I-8**. Characteristics of these inhibitors are described below.

Totarol

Totarol is a naturally occurring diterpenoid phenol extracted from *Podocarpus totara*. Since its discovery, totarol has been shown to inhibit the proliferation of several pathogenic Gram-positive bacteria such as *S. aureus* and *Mtb*.^{55,56} Jaiswal *et al.* examined its effect on the assembly dynamics of *Mtb* FtsZ *in vitro*.⁵⁷ In the preliminary study they found that totarol increased the length of *B. subtilis* cells by several fold, indicating its inhibitory activity against cell division. Totarol inhibited the polymerized mass of *Mtb* FtsZ by 27% at 50 μ M concentration. GTPase activity was also reduced in a concentration dependent manner without affecting the binding of GTP to *Mtb* FtsZ. Transmission electron microscopy (TEM) images indicated that totarol significantly reduced the average width of FtsZ protofilaments and also induced aggregation in the absence of GTP. Totarol increased the fluorescence intensity of the FtsZ-ANS complex (ANS = 1-anilinonaphthalene-8-sulfonic acid), whereas decreased that of PM-FtsZ (PM = *N*-(1-pyrene)maliemide), indicating that totarol induced conformational changes in FtsZ.

Albendazole and Thiabendazole

Albendazole and thiabendazole are known fungicide and parasiticide, which cause degenerative alterations in the intestinal cells of worms by binding to the colchicine-sensitive site of tubulin, and inhibiting its polymerization or assembly into microtubules. Sarcina *et al.* reported that the treatment of cyanobacterial and bacterial cultures with thiabendazole resulted in cell elongation.⁵⁸ This suggested that the cell division cycle was arrested and therefore tubulin inhibitors may act, in a similar manner, on the *ftsZ* gene product. In addition, increased amount of DNA in DAPI-DNA-stained TBZ-treated *Synechococcus* 7942 cells was observed, which indicated that DNA replication still occurred in the presence of thiabendazole. Slayden *et al* examined the effect of albendazole and thiabendazole on *Mtb* cell growth.¹⁶ MIC₉₉ values of albendazole and thiabendazole were determined to be 61 μ M and 80 μ M, respectively. The cell

morphology and transcriptional response indicated cell filamentation and gene regulation causing the inhibition of septum formation in *Mtb* cells. These results suggested that thiabendazole and albendazole interfered and delayed *Mtb* cytokinesis.

2-Alkoxy carbonylaminopyridines and 2-carbamoylpteridine

Based on the premise that known tubulin inhibitors can inhibit FtsZ assembly,⁴² White, Reynolds and their coworkers screened a library of 200 2-alkoxy carbonylaminopyridines for antimicrobial activity against *Mtb*.⁵⁹ Two compounds, SRI-3072 and SRI-7614, were found to inhibit the growth of *Mtb* cells at 0.15 $\mu\text{g/mL}$ and 6.25 $\mu\text{g/mL}$, respectively. SRI-3072 and SRI-7614 inhibited *Mtb* FtsZ polymerization in a dose dependent manner with ID_{50} values of 52 μM and 60 μM , respectively. These compounds also inhibited the GTPase activity by 20-25 % at 100 μM concentration. In addition, these compounds were evaluated for their inhibitory activity against tubulin polymerization. SRI-3072 was specific to FtsZ and did not exhibit tubulin polymerization inhibition at 100 μM concentration, whereas SRI-7614 inhibited tubulin polymerization (ID_{50} 4 μM). Furthermore, SRI-3072 reduced the growth of *Mtb* in mouse-derived macrophages. However, SRI-3072 had some issues in the synthesis and purification. Thus, an optimization of this lead compounds was carried out to yield a more easily accessible and more potent (8-fold better MIC than SRI-3072) 2-carbamoylpteridine analogue of SRI-3072.⁶⁰

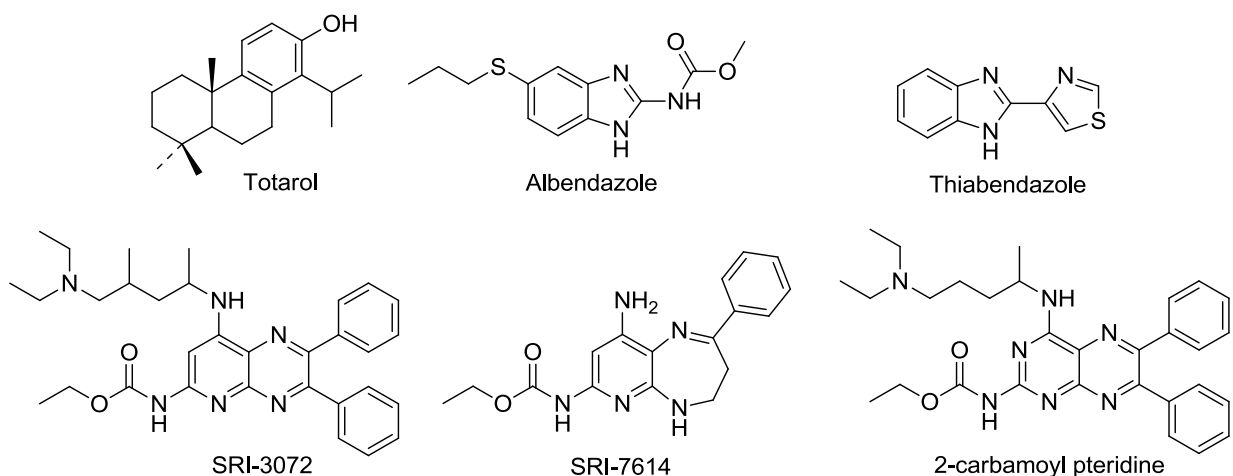


Figure I-8. *Mtb* FtsZ inhibitors

Table I-1. *Mtb* FtsZ inhibitors

	Compound	Mode of action	Assays used	MIC
1	Albendazole, Thiabendazole	filamentous phenotype response; up-regulation of gene encoding Z-ring formation	cell-based assay; cell morphology; transcriptional profiling.	Albendazole 61 μ M, Thiabendazole 80 μ M
2	Totarol	Dose dependent inhibition of GTPase and FtsZ polymerization; reduced width and aggregation of FtsZ protofilaments	GTPase and FtsZ polymerization assay; TEM	---
3.	SRI-3072, SRI-7614, 2-carbamoyl-pteridine	Inhibition of FtsZ polymerization and GTPase activity	FtsZ GTPase and polymerization assay	SRI-3072 0.15 μ g/mL SRI-7614 6.25 μ g/mL 2-carbamoylpteridine 0.25 μ g/mL
4	Taxanes	FtsZ polymer stabilization	Real time PCR-based assay, cell filamentation	1.25 -2.5 μ M

Taxanes

Paclitaxel (Taxol[®]), a microtubule-stabilizing anticancer agent, exhibits modest antibacterial activity against drug-sensitive and drug-resistant *Mtb* strains (MIC 40 μ M), although its cytotoxicity against human cancer cell lines (a benchmark for activity against human host cells) is three orders of magnitude more potent (IC₅₀ 0.019-0.028 μ M). Following the hypothesis that compounds that affect tubulin/microtubule would serve as leads for developing FtsZ inhibitors,^{42,59,58} a library of taxanes was designed and screened for antibacterial activity against *Mtb* cells. Real time PCR-based assay was employed to screen taxanes, such as cytotoxic taxanes that stabilize microtubules^{61,62,63} and non-cytotoxic taxane-multidrug resistance (MDR) reversal agents (TRAs)^{64,65,66,67,68,69,70} that inhibit the efflux pumps of ATP-binding cassette (ABC) transporters such as P-glycoprotein (P-gp).

Table I-2. Antimicrobial activities of taxanes against drug-sensitive and multidrug-resistant *Mtb* strains^a

	Taxanes	MIC <i>Mtb.</i> (μM)		Cytotoxicity (IC ₅₀ , μM)	
		H37Rv	IMCJ946.K2	MCF79	A549
1	Paclitaxel	40	40	0.019	0.028
2	SB-T-0032	5	1.25	0.65	0.65
3	SB-RA-2001	5	2.5	4.5	15.7
4	SB-RA-5001	2.5	1.25	>80	>80
5	SB-RA-5001MeO6	2.5	2.5	>80	>80
6	SB-RA-5011	2.5	1.25	>80	>80
7	SB-RA-5012	2.5	1.25	>80	>80

M. tuberculosis H37Rv is sensitive to all antibiotics tested. *M. tuberculosis* IMCJ946.K2 is resistant to drugs including INH, REF, EB, streptomycin, kanamycin, *p*-aminosalicylic acid, cycloserine and enviomycin. MCF7 and A549 cells: human breast and non-small cell lung cancer cell lines, respectively.

Of the 120 taxanes screened, several compounds exhibited significant anti-TB activity. From the MIC₉₉ values and cytotoxicity assay, **SB-T-0032** and **SB-RA-2001** (**Figure I-9**) were selected as lead compounds for further studies. SB-RA series of taxanes bearing a (*E*)-3-(naphtha-2-yl)acryloyl (2-NpCH=CHCO) group at the C-13 position exhibited MIC₉₉ between 2.5-5 μM against drug-sensitive and drug-resistant *Mtb* strains. A new library of taxanes based on this SB-RA series was prepared through modification of 10-deacetylbaaccatin III (DAB). These **SB-RA-2001** analogs were found to have higher specificity to FtsZ than microtubules and exhibited the same level of anti-TB activity as that of SB-T-0032. It has been shown that novel and effective anti-angiogenic taxoid, IDN5390,^{71,72} bearing a C-seco-baccatin moiety possesses substantially less cytotoxicity than paclitaxel. Therefore, C-seco analogs of SB-RA-2001 (**Figure I-9**) were designed, synthesized and evaluated. These novel C-seco-taxanes SB-RA-5001 and its congeners (**Figure I-9**), were found to exhibit promising anti-TB activity (MIC₉₉ 1.25-2.5 μM) against both drug-sensitive and drug-resistant *Mtb* strains without appreciable cytotoxicity (IC₅₀ > 80 μM). Thus, the specificity of these novel taxanes to microtubules as compared to FtsZ was completely reversed. The scanning electron microscopy (SEM) images of *Mtb* cells treated with SB-RA-20018 and SB-RA-5001 clearly show substantial elongation and filamentation, a

phenotypic response to FtsZ inactivation (Figure I-10). In addition, a preliminary study on the effect of SB-RA-5001 on polymerization-depolymerization, using the standard light-scattering assay exhibited a dose-dependent stabilization of FtsZ against depolymerization.

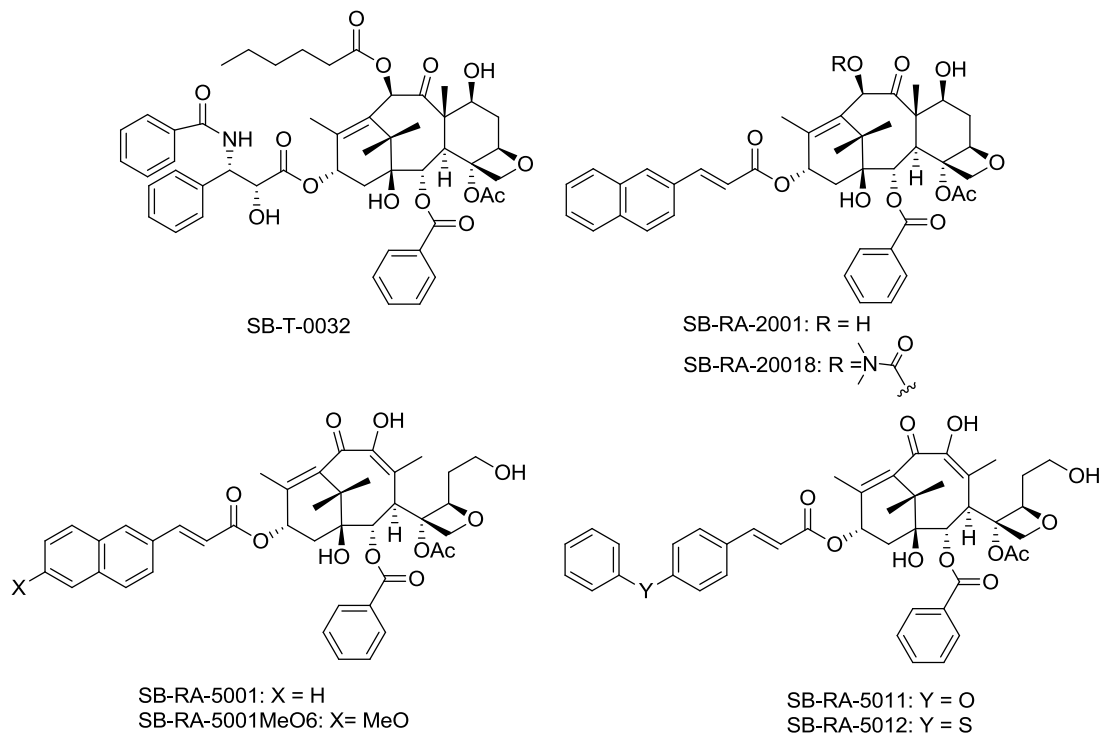


Figure I-9. *Mtb* FtsZ inhibitors: Taxanes

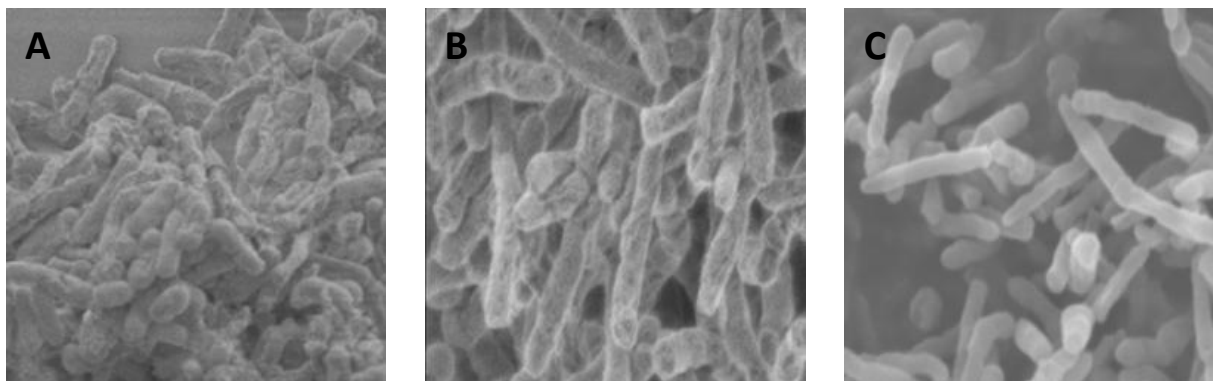


Figure I-10. Electron micrograph of *Mtb* cells: (A) Control, (B) SB-RA-20018 and (C) SB-RA-5001.

§ 1.5 References

1. Bloom, B. R.; Murray, C. J., Tuberculosis: commentary on a reemergent killer. *Science* **1992**, *257* (5073), 1055-64.
2. Tuberculosis: Basic TB facts. Center for Disease Control and Prevention (CDC). Available from: <http://www.cdc.gov/tb/topic/basics/default.htm>.
3. Tuberculosis: Data and Country Profiles. World Health Organization (WHO) Available from: http://www.who.int/tb/publications/global_report/2010/en/index.html.
4. Raviglione, M. C., Issues facing TB control (7). Multiple drug-resistant tuberculosis. *Scott. Med. J.* **2000**, *45*, 52-5.
5. Miller, J. R.; Waldrop, G. L., Discovery of novel antibacterials. *Expert Opin. Drug Discovery* *5*, 145-154.
6. Tuberculosis: What is TB? National Institute of Allergy and Infectious Diseases (NIAID). Available from: <http://www.niaid.nih.gov/topics/tuberculosis/understanding/whatistb/Pages/default.aspx>.
7. Margalit, D. N.; Romberg, L.; Mets, R. B.; Hebert, A. M.; Mitchison, T. J.; Kirschner, M. W.; RayChaudhuri, D., Targeting cell division: Small-molecule inhibitors of FtsZ GTPase perturb cytokinetic ring assembly and induce bacterial lethality. *Proc. Nat. Acad. Sci.* **2004**, *101*, 11821-11826.
8. Vollmer, W., The prokaryotic cytoskeleton: A putative target for inhibitors and antibiotics? *Appl. Microbiol. Biotechnol.* **2006**, *73*, 37-47.
9. Ben-Yehuda, S.; Losick, R., Asymmetric cell division in *B. subtilis* involves a spiral-like intermediate of the cytokinetic protein FtsZ. *Cell* **2002**, *109*, 257-266.
10. Goehring, N. W.; Beckwith, J., Diverse paths to midcell: assembly of the bacterial cell division machinery. *Curr. Biol.* **2005**, *15*, R514-R526.
11. Leung, A. K. W.; White, E. L.; Ross, L. J.; Reynolds, R. C.; DeVito, J. A.; Borhani, D. W., Structure of Mycobacterium tuberculosis FtsZ Reveals Unexpected, G Protein-like Conformational Switches. *J. Mol. Biol.* **2004**, *342*, 953-970.
12. Moller-Jensen, J.; Loewe, J., Increasing complexity of the bacterial cytoskeleton. *Curr. Opin. Cell Biol.* **2005**, *17*, 75-81.

13. Thanedar, S.; Margolin, W., FtsZ Exhibits Rapid Movement and Oscillation Waves in Helix-like Patterns in *Escherichia coli*. *Curr. Biol.* **2004**, *14*, 1167-1173.
14. Erickson Harold, P.; Anderson David, E.; Osawa, M., FtsZ in bacterial cytokinesis: cytoskeleton and force generator all in one. *Microbiol. Mol. Biol Rev.* **2010**, *74*, 504-28.
15. Respicio, L.; Nair, P. A.; Huang, Q.; Anil, B.; Tracz, S.; Truglio, J. J.; Kisker, C.; Raleigh, D. P.; Ojima, I.; Knudson, D. L.; Tonge, P. J.; Slayden, R. A., Characterizing septum inhibition in Mycobacterium tuberculosis for novel drug discovery. *Tuberculosis* **2008**, *88*, 420-429.
16. Slayden, R. A.; Knudson, D. L.; Belisle, J. T., Identification of cell cycle regulators in Mycobacterium tuberculosis by inhibition of septum formation and global transcriptional analysis. *Microbiology* **2006**, *152*, 1789-1797.
17. Adams, D. W.; Errington, J., Bacterial cell division: assembly, maintenance and disassembly of the Z ring. *Nat. Rev. Microbiol.* **2009**, *7*, 642-653.
18. Margolin, W., Themes and variations in prokaryotic cell division. *FEMS Microbiol. Rev.* **2000**, *24*, 531-548.
19. Mukherjee, A.; Lutkenhaus, J., Dynamic assembly of FtsZ regulated by GTP hydrolysis. *EMBO J.* **1998**, *17*, 462-469.
20. Dajkovic, A.; Mukherjee, A.; Lutkenhaus, J., Investigation of regulation of FtsZ assembly by SulaA and development of a model for FtsZ polymerization. *J. Bacteriol.* **2008**, *190*, 2513-2526.
21. Chen, Y.; Bjornson, K.; Redick, S. D.; Erickson, H. P., A rapid fluorescence assay for FtsZ assembly indicates cooperative assembly with a dimer nucleus. *Biophys. J.* **2005**, *88*, 505-514.
22. Caplan, M. R.; Erickson, H. P., Apparent Cooperative Assembly of the Bacterial Cell Division Protein FtsZ Demonstrated by Isothermal Titration Calorimetry. *J. Biol. Chem.* **2003**, *278*, 13784-13788.
23. Romberg, L.; Simon, M.; Erickson, H. P., Polymerization of FtsZ, a bacterial homolog of tubulin. Is assembly cooperative? *J. Biol. Chem.* **2001**, *276*, 11743-11753.
24. Popp, D.; Iwasa, M.; Erickson, H. P.; Narita, A.; Maeda, Y.; Robinson, R. C., Suprastructures and Dynamic Properties of Mycobacterium tuberculosis FtsZ. *J. Biol. Chem.* **2010**, *285*, 11281-11289.

25. Popp, D.; Narita, A.; Iwasa, M.; Maeda, Y.; Robinson, R. C., Molecular mechanism of bundle formation by the bacterial actin ParM. *Biochem. Biophys. Res. Commun.* **2010**, *391*, 1598-1603.
26. Li, Z.; Trimble, M. J.; Brun, Y. V.; Jensen, G. J., The structure of FtsZ filaments in vivo suggests a force-generating role in cell division. *EMBO J.* **2007**, *26*, 4694-4708.
27. Erickson, H. P., The ftsZ protofilament and attachment of ZipA - structural constraints on the FtsZ power stroke. *Curr. Opin. Cell Biol.* **2001**, *13*, 55-60.
28. Pichoff, S.; Lutkenhaus, J., Unique and overlapping roles for ZipA and FtsA in septal ring assembly in Escherichia coli. *EMBO J* **2002**, *21*, 685-693.
29. Geissler, B.; Elraheb, D.; Margolin, W., A gain-of-function mutation in ftsA bypasses the requirement for the essential cell division gene zipA in Escherichia coli. *Proc. Nat. Acad. Sci.* **2003**, *100*, 4197-4202.
30. Anderson, D. E.; Gueiros-Filho, F. J.; Erickson, H. P., Assembly dynamics of FtsZ rings in Bacillus subtilis and Escherichia coli and effects of FtsZ-regulating proteins. *J. Bacteriol.* **2004**, *186*, 5775-5781.
31. Stricker, J.; Maddox, P.; Salmon, E. D.; Erickson, H. P., Rapid assembly dynamics of the Escherichia coli FtsZ-ring demonstrated by fluorescence recovery after photobleaching. *Proc. Nat. Acad. Sci.* **2002**, *99*, 3171-3175.
32. Errington, J.; Daniel, R. A.; Scheffers, D.-J., Cytokinesis in bacteria. *Microbiol. Mol. Biol. Rev.* **2003**, *67*, 52-65.
33. Romberg, L.; Levin, P. A., Assembly Dynamics of The Bacterial Cell Division Protein FtsZ: Poised at the Edge of Stability. *Annu. Rev. Microbiol.* **2003**, *57*, 125 - 54.
34. Romberg, L.; Mitchison, T. J., Rate-Limiting Guanosine 5'-Triphosphate Hydrolysis during Nucleotide Turnover by FtsZ, a Prokaryotic Tubulin Homologue Involved in Bacterial Cell Division. *Biochemistry* **2004**, *43*, 282-288.
35. Huecas, S.; Andreu, J. M., Polymerization of Nucleotide-free, GDP- and GTP-bound Cell Division Protein FtsZ: GDP Makes the Difference. *FEBS Lett.* **2004**, *569*, 43 - 48.
36. Lu, C.; Reedy, M.; Erickson, H. P., Straight and curved conformations of FtsZ are regulated by GTP hydrolysis. *J. Bacteriol.* **2000**, *182*, 164-170.

37. Mukherjee, A.; Saez, C.; Lutkenhaus, J., Assembly of an FtsZ mutant deficient in GTPase activity has implications for FtsZ assembly and the role of the Z ring in cell division. *J. Bacteriol.* **2001**, *183*, 7190-7197.
38. Oliva, M. A.; Trambaiolo, D.; Loewe, J., Structural Insights into the Conformational Variability of FtsZ. *J. Mol. Biol.* **2007**, *373*, 1229-1242.
39. Osawa, M.; Anderson, D. E.; Erickson, H. P., Reconstitution of Contractile FtsZ Rings in Liposomes. *Science* **2008**, *320*, 792-794.
40. Yanagisawa, M.; Imai, M.; Taniguchi, T., Shape Deformation of Ternary Vesicles Coupled with Phase Separation. *Phys. Rev. Lett.* **2008**, *100*, 148102/1-148102/4.
41. Zhu, T. F.; Szostak, J. W., Coupled Growth and Division of Model protocell membranes. *J. Am. Chem. Soc.* **2009**, *131*, 5705-5713.
42. de Pereda, J. M.; Leynadier, D.; Evangelio, J. A.; Chacon, P.; Andreu, J. M., Tubulin secondary structure analysis, limited proteolysis sites, and homology to FtsZ. *Biochemistry* **1996**, *35*, 14203-14215.
43. Nogales, E.; Wang, H. W., Structural Mechanisms Underlying Nucleotide-Dependent Self-Assembly of Tubulin and Its Relatives. *Curr. Opin. Struct. Biol.* **2006**, *16*, 221 - 229.
44. Lock, R. L.; Harry, E. J., Cell-division inhibitors: new insights for future antibiotics. *Nat. Rev. Drug Discovery* **2008**, *7*, 324-338.
45. Rothfield, L.; Justice, S.; Garcia-Lara, J., Bacterial cell division. *Annu. Rev. Genet.* **1999**, *33*, 423-448.
46. Haydon, D. J.; Stokes, N. R.; Ure, R.; Galbraith, G.; Bennett, J. M.; Brown, D. R.; Baker, P. J.; Barynin, V. V.; Rice, D. W.; Sedelnikova, S. E.; Heal, J. R.; Sheridan, J. M.; Aiwale, S. T.; Chauhan, P. K.; Srivastava, A.; Taneja, A.; Collins, I.; Errington, J.; Czaplewski, L. G., An inhibitor of FtsZ with potent and selective anti-staphylococcal activity. *Science* **2008**, *321*, 1673-1675.
47. Kumar, K.; Awasthi, D.; Berger, W. T.; Tonge, P. J.; Slayden, R. A.; Ojima, I., Discovery of anti-TB agents that target the cell-division protein FtsZ. *Future Med. Chem.* **2010**, *2*, 1305-1323.
48. Kapoor, S.; Panda, D., Targeting FtsZ for antibacterial therapy: a promising avenue. *Expert Opin. Ther. Targets* **2009**, *13*, 1037-1051.

49. Huang, Q.; Tonge Peter, J.; Slayden Richard, A.; Kirikae, T.; Ojima, I., FtsZ: a novel target for tuberculosis drug discovery. *Curr. Top. Med. Chem.* **2007**, *7*, 527-43.
50. Erickson, H. P.; Taylor, D. W.; Taylor, K. A.; Bramhill, D., Bacterial cell division protein FtsZ assembles into protofilament sheets and minirings, structural homologs of tubulin polymers. *Proc. Nat. Acad. Sci.* **1996**, *93*, 519-23.
51. Lowe, J.; Amos, L. A., Crystal structure of the bacterial cell-division protein FtsZ. *Nature* **1998**, *391*, 203-6.
52. Lowe, J.; Amos, L. A., Tubulin-like protofilaments in Ca²⁺-induced FtsZ sheets. *EMBO J* **1999**, *18*, 2364-71.
53. Lappchen, T.; Hartog Aloysius, F.; Pinas Victorine, A.; Koomen, G.-J.; den Blaauwen, T., GTP analogue inhibits polymerization and GTPase activity of the bacterial protein FtsZ without affecting its eukaryotic homologue tubulin. *Biochemistry* **2005**, *44*, 7879-84.
54. Huang, Q.; Kirikae, F.; Kirikae, T.; Pepe, A.; Amin, A.; Respicio, L.; Slayden, R. A.; Tonge, P. J.; Ojima, I., Targeting FtsZ for Antituberculosis Drug Discovery: Noncytotoxic Taxanes as Novel Antituberculosis Agents. *J. Med. Chem.* **2006**, *49*, 463-466.
55. Constantine, G. H.; Karchesy, J. J.; Franzblau, S. G.; LaFleur, L. E., (+)-Totarol from *Chamaecyparis nootkatensis* and activity against *Mycobacterium tuberculosis*. *Fitoterapia* **2001**, *72*, 572-574.
56. Kubo, I.; Muroi, H.; Himejima, M., Antibacterial activity of totarol and its potentiation. *J. Nat. Prod.* **1992**, *55*, 1436-40.
57. Jaiswal, R.; Beuria, T. K.; Mohan, R.; Mahajan, S. K.; Panda, D., Totarol inhibits bacterial cytokinesis by perturbing the assembly dynamics of FtsZ. *Biochemistry* **2007**, *46*, 4211-4220.
58. Sarcina, M.; Mullineaux, C. W., Effects of tubulin assembly inhibitors on cell division in prokaryotes in vivo. *FEMS Microbiol. Lett.* **2000**, *191*, 25-29.
59. White, E. L.; Suling, W. J.; Ross, L. J.; Seitz, L. E.; Reynolds, R. C., 2-Alkoxy-carbonylaminopyridines: inhibitors of *Mycobacterium tuberculosis* FtsZ. *J. Antimicrob. Chemother.* **2002**, *50*, 111-114.

60. Reynolds, R. C.; Srivastava, S.; Ross, L. J.; Suling, W. J.; White, E. L., A new 2-carbamoyl pteridine that inhibits mycobacterial FtsZ. *Bioorg. Med. Chem. Lett.* **2004**, *14*, 3161-3164.
61. Georg, G. I.; Chen, T. T.; Ojima, I.; Wyas, D. M.; Editors, *Taxane Anticancer Agents: Basic Science and Current Status. ACS Symp. Ser., 1995; 583; p 353.* 1995; p 353 pp.
62. Kingston, D. G. I.; Jagtap, P. G.; Yuan, H.; Samala, L., The chemistry of taxol and related taxoids. *Prog. Chem. Org. Nat. Prod.* **2002**, *84*, 53-225.
63. Ojima, I.; Bounaud, P.-Y.; Bernacki, R. J., Designing taxanes to treat multidrug-resistant tumors. *Mod. Drug Discovery* **1999**, *2*, 45,47-48,51-52.
64. Brooks, T. A.; Kennedy, D. R.; Gruol, D. J.; Ojima, I.; Baer, M. R.; Bernacki, R. J., Structure-activity analysis of taxane-based broad-spectrum multidrug resistance modulators. *Anticancer Res.* **2004**, *24*, 409-415.
65. Brooks Tracy, A.; Minderman, H.; O'Loughlin Kieran, L.; Pera, P.; Ojima, I.; Baer Maria, R.; Bernacki Ralph, J.; Brooks, T., Taxane-based reversal agents modulate drug resistance mediated by P-glycoprotein, multidrug resistance protein, and breast cancer resistance protein. *Mol. Cancer Ther.* **2003**, *2*, 1195-205.
66. Minderman, H.; Brooks, T. A.; O'Loughlin, K. L.; Ojima, I.; Bernacki, R. J.; Baer, M. R., Broad-spectrum modulation of ATP-binding cassette transport proteins by the taxane derivatives ortataxel (IDN-5109, BAY 59-8862) and tRA96023. *Cancer Chemother. Pharmacol.* **2004**, *53*, 363-369.
67. Ojima, I.; Borella, C. P.; Wu, X.; Bounaud, P.-Y.; Oderda, C. F.; Sturm, M.; Miller, M. L.; Chakravarty, S.; Chen, J.; Huang, Q.; Pera, P.; Brooks, T. A.; Baer, M. R.; Bernacki, R. J., Design, Synthesis and Structure-Activity Relationships of Novel Taxane-Based Multidrug Resistance Reversal Agents. *J. Med. Chem.* **2005**, *48*, 2218-2228.
68. Ojima, I.; Bounaud, P.-Y.; Bernacki, R. J., New weapons in the fight against cancer. *Chemtech* **1998**, *28*, 31-36.
69. Ojima, I.; Bounaud, P.-Y.; Oderda, C. F., Recent strategies for the treatment of multi-drug resistance in cancer cells. *Expert Opin. Ther. Pat.* **1998**, *8*, 1587-1598.
70. Ojima, I.; Bounaud, P.-Y.; Takeuchi, C.; Pera, P.; Bernacki, R. J., New taxanes as highly efficient reversal agents for multi-drug resistance in cancer cells. *Bioorg. Med. Chem. Lett.* **1998**, *8*, 189-194.

71. Appendino, G.; Danieli, B.; Jakupovic, J.; Belloro, E.; Scambia, G.; Bombardelli, E., The chemistry and occurrence of taxane derivatives. XXX. Synthesis and evaluation of C-seco paclitaxel analogs. *Tet. Lett.* **1997**, *38*, 4273-4276.
72. Taraboletti, G.; Micheletti, G.; Rieppi, M.; Poli, M.; Turatto, M.; Rossi, C.; Borsotti, P.; Roccabianca, P.; Scanziani, E.; Nicoletti, M. I.; Bombardelli, E.; Morazzoni, P.; Riva, A.; Giavazzi, R., Antiangiogenic and antitumor activity of IDN 5390, a new taxane derivative. *Clin. Cancer Res.* **2002**, *8*, 1182-1188.

Chapter II

Discovery of Novel Benzimidazoles as a New Class of Antitubercular Agents: Targeting Essential Cell Division Protein FtsZ

Table of Content

§ 2.1 Introduction.....	25
§ 2.2 Results and Discussion.....	29
§ 2.2.1 Synthesis of 2,5,6-trisubstituted benzimidazole library	29
§ 2.2.2 Preliminary screening, re-synthesis and accurate MIC determination.....	30
§ 2.2.3 Preliminary SAR study and optimization of the 6-position of 2,5,6-trisubstituted benzimidazoles	34
§ 2.2.4 Optimization of the 2-position of 2,5,6-trisubstituted benzimidazoles	36
§ 2.2.5 Optimization of the 5-position of 2,5,6-trisubstituted library against <i>Mtb.</i>	39
§ 2.2.6 Optimization of 2,5,7-trisubstituted benzimidazoles	41
§ 2.2.7 Early ADMET results and synthesis of metabolically stable	44
§ 2.3 Conclusion	45
§ 2.4 Experimental Section.....	46
§ 2.4.1 Synthesis of 2,5,6-Trisubstituted Benzimidazole Library II-A	46
§ 2.4.2 Synthesis of 2,5,6-Trisubstituted Benzimidazole Library II-B	54
§ 2.4.3 Synthesis of analytically pure trisubstituted benzimidazoles	64
§ 2.4.4 Synthesis of 2,5,6-Trisubstituted Benzimidazole Library II-C	71
§ 2.4.5 Synthesis of 2,5,6-Trisubstituted Benzimidazole Library II-D	76
§ 2.4.6 Synthesis of 2,5,6-Trisubstituted Benzimidazole Library II-E	77
§ 2.4.7 Synthesis of 2,5,7-Trisubstituted Benzimidazole Library II-F	79
§ 2.4.8 Antibacterial and cytotoxicity activity determination	85
§ 2.5 References.....	87

§ 2.1 Introduction

Tuberculosis (TB), caused by *Mycobacterium tuberculosis* (*Mtb*) is a highly infectious disease affecting one-third of the world's population.¹ In the past several decades, the increase in TB co-infection in HIV/AIDS afflicted patients along with the emergence of MDR-TB and XDR-TB has made TB the leading cause of death worldwide. Indeed, statistics from World Health Organization (WHO) estimate that there are about 9.4 million new TB cases with 1 to 1.2 million cases being HIV positive.²

Despite considerable efforts in the past 40 years, the development of new TB treatments has been entirely limited to classical drugs which target cell wall biosynthesis, ATP synthesis, RNA synthesis, protein synthesis, and other important biological mechanisms. Knowing that bacteria have the ability to develop resistance, these scientific labors have been largely inadequate. Hence, the discovery of new cellular targets represents a brilliant opportunity for the development of more effective antitubercular agents which may surpass resistance and could very well be active against drug sensitive as well as drug resistant *Mtb* strains.

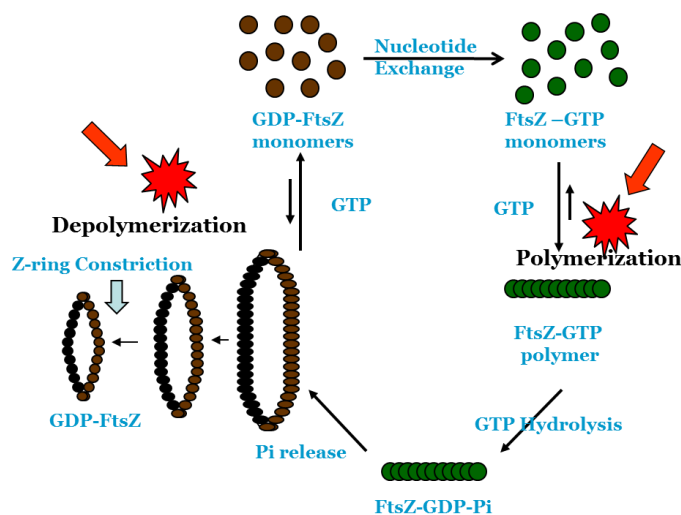


Figure II-1. FtsZ dynamics: GTP hydrolysis and Polymerization³

As discussed previously, FtsZ, a highly essential and indispensable cytokinesis protein, offers an excellent therapeutic target for the development of novel anti-TB agents (**Figure II-1**).^{3,4,5,6} The polymerization and de-polymerization of FtsZ is a dynamic and continuous process. It was hypothesized that the inhibition of either polymerization or depolymerization of FtsZ into the proper FtsZ assembly would prevent septum formation without affecting DNA replication

and nucleoid segregation. Such conditions would give way to continued cell filamentation, ultimately leading to cell death.^{6,7,8} Another interesting factor is that the concentration of FtsZ remains invariant during the cell cycle. Therefore it is less probable that it will escape the drug interaction. Because of structural and functional homology,^{9,10} compounds that are known to affect the assembly of tubulin into microtubules can act as a lead for targeting FtsZ assembly, which on modification can be made specific to target FtsZ with no appreciable cytotoxicity to eukaryotic cells. Because of the overwhelming importance of FtsZ in the bacterial cycle, it is a very promising target for the development of new anti-TB drugs active against drug-resistant and drug sensitive *Mtb* strains.

Following the hypothesis that compounds which affect tubulin/microtubule would serve as leads for developing FtsZ inhibitors,^{11,12,13} a library of taxanes was designed and screened for antibacterial activity against *Mtb* cells. Of the 120 taxanes screened, several compounds exhibited significant anti-TB activity.¹⁴ C-seco analogs of SB-RA-2001 (**Figure II-2**) were designed, synthesized and evaluated. Of these novel C-seco-taxanes, SB-RA-5001 and its congeners were found to exhibit promising anti-TB activity (MIC₉₉ 1.25-2.5 μM) against both drug-sensitive and drug-resistant *Mtb* strains without appreciable cytotoxicity (IC₅₀> 80 μM) to normal cells. Thus, the specificity of these novel taxanes to microtubules as compared to FtsZ was completely reversed through systematic and rational drug design. The scanning electron microscopy (SEM) images of *Mtb* cells treated with SB-RA-20018 and SB-RA-5001 clearly showed substantial elongation and filamentation, a phenotypic response to FtsZ inactivation.

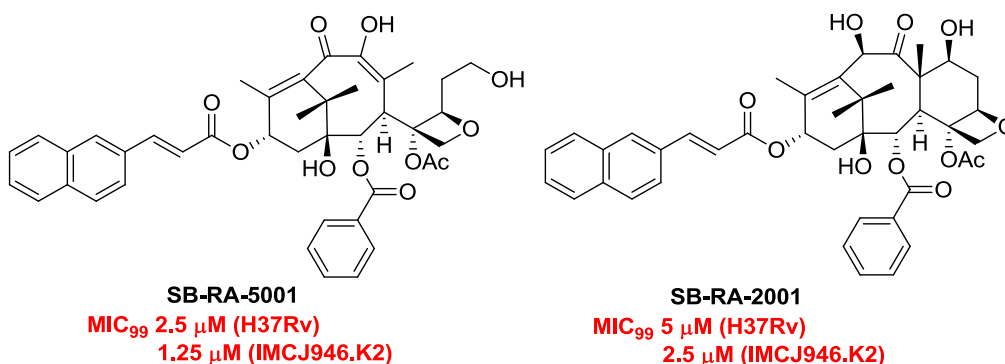


Figure II-2. *Mtb* FtsZ inhibitors: Taxanes¹⁴

Albendazole and thiabendazole are known inhibitors of tubulin polymerization. Sarcina and Mullineaux demonstrated that thiabendazole caused cell elongation in *E. coli* and cyanobacteria, which suggests that these tubulin inhibitors may act in a similar manner on the *ftsZ* gene product as they do on tubulin.¹⁵

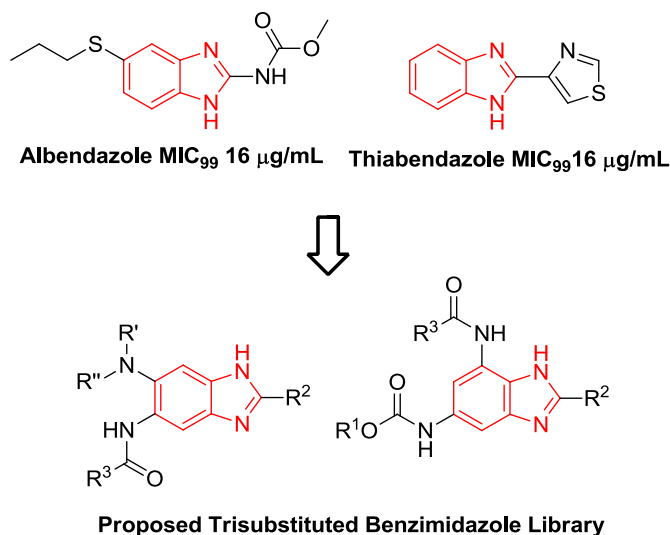
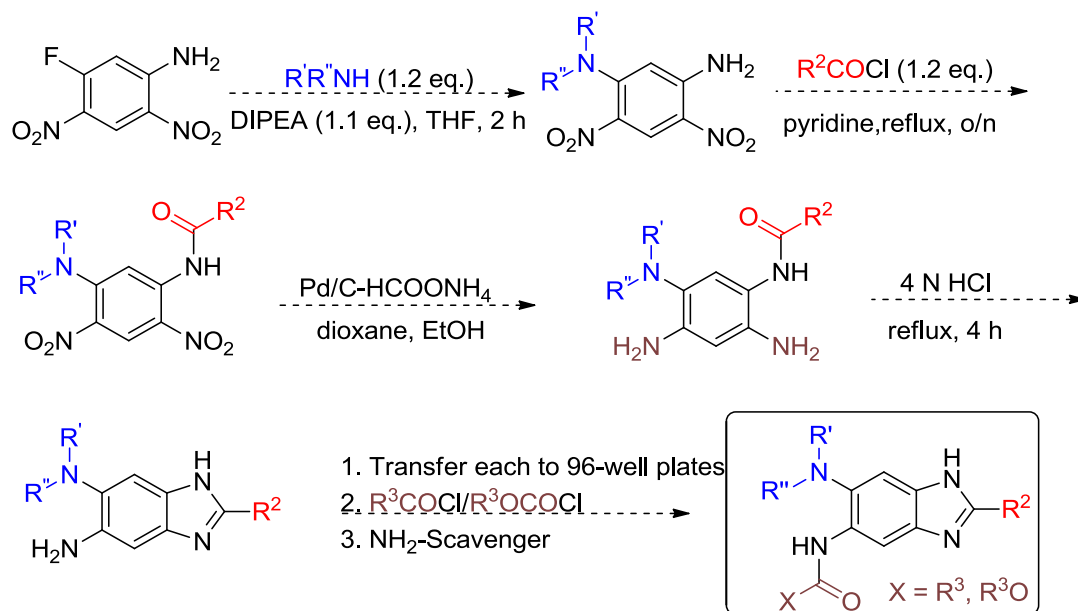


Figure II-3. Proposed trisubstituted benzimidazoles library

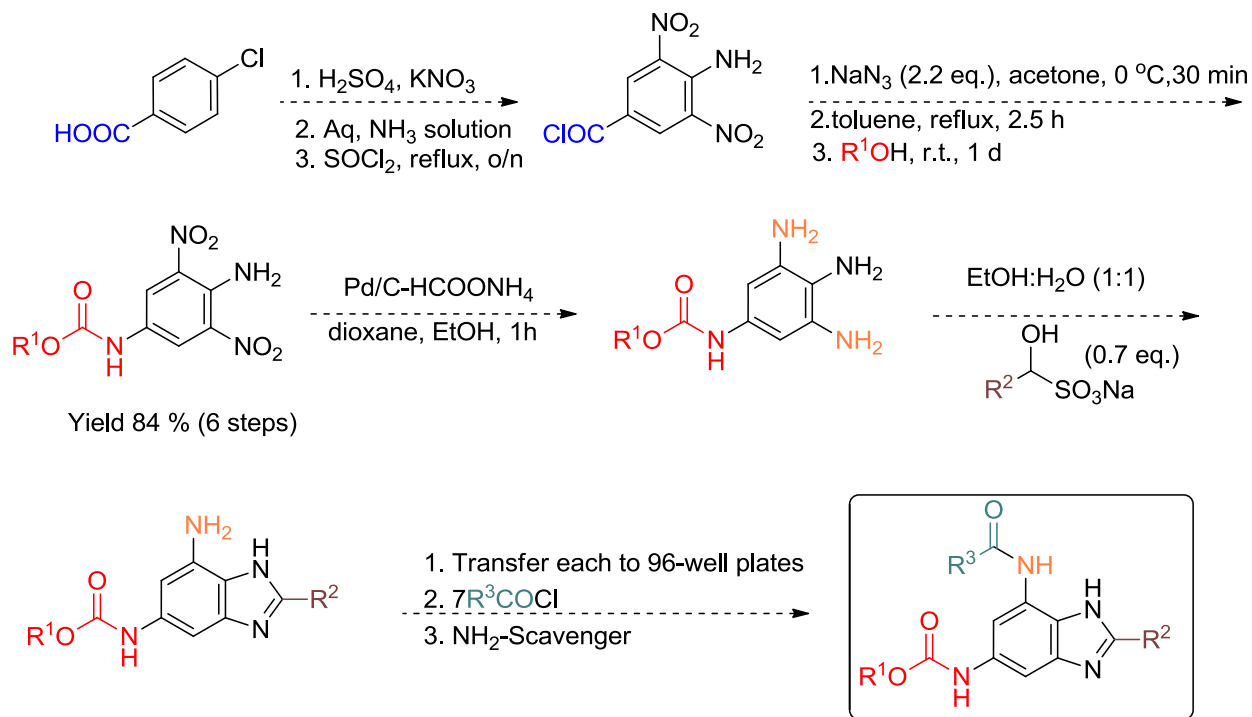
Later, Slayden, *et al.*, determined that thiabendazole and albendazole interfered and delayed *Mtb* cell division processes at 16 μg/mL (**Figure II-3**)⁸ Based on the similarity of the benzimidazole moiety to the pyridopyrazine and pteridine pharmacophores in the FtsZ inhibitors identified by White, Reynolds and others,^{10,16,17,18} it was hypothesized that the benzimidazole framework might be a promising starting point for the development of novel FtsZ inhibitors.

The benzimidazole skeleton is a privileged nitrogen-heterocycle and an important pharmacophore present in a number of widely used drugs. The pharmacological, metabolic and toxicological profiles of the benzimidazole pharmacophore have been extensively studied. Several solid- or solution-phase synthetic methods for mono or di-substituted benzimidazoles have been reported, but few deal with the synthesis of trisubstituted benzimidazoles. Furthermore, based on thorough literature search, there are very few trisubstituted benzimidazoles known in literature and they have not been investigated for their antibacterial activity. Consequently, trisubstituted benzimidazoles were selected (**Figure II-3**), especially 2,5,6- and 2,5,7- trisubstituted benzimidazoles, as the basic scaffold for the synthesis of novel benzimidazole libraries using systematic and rational design (**Scheme II-1**).

Synthesis of 2,5,6-trisubstituted benzimidazole library



Synthesis of 2,5,7-trisubstituted benzimidazole library

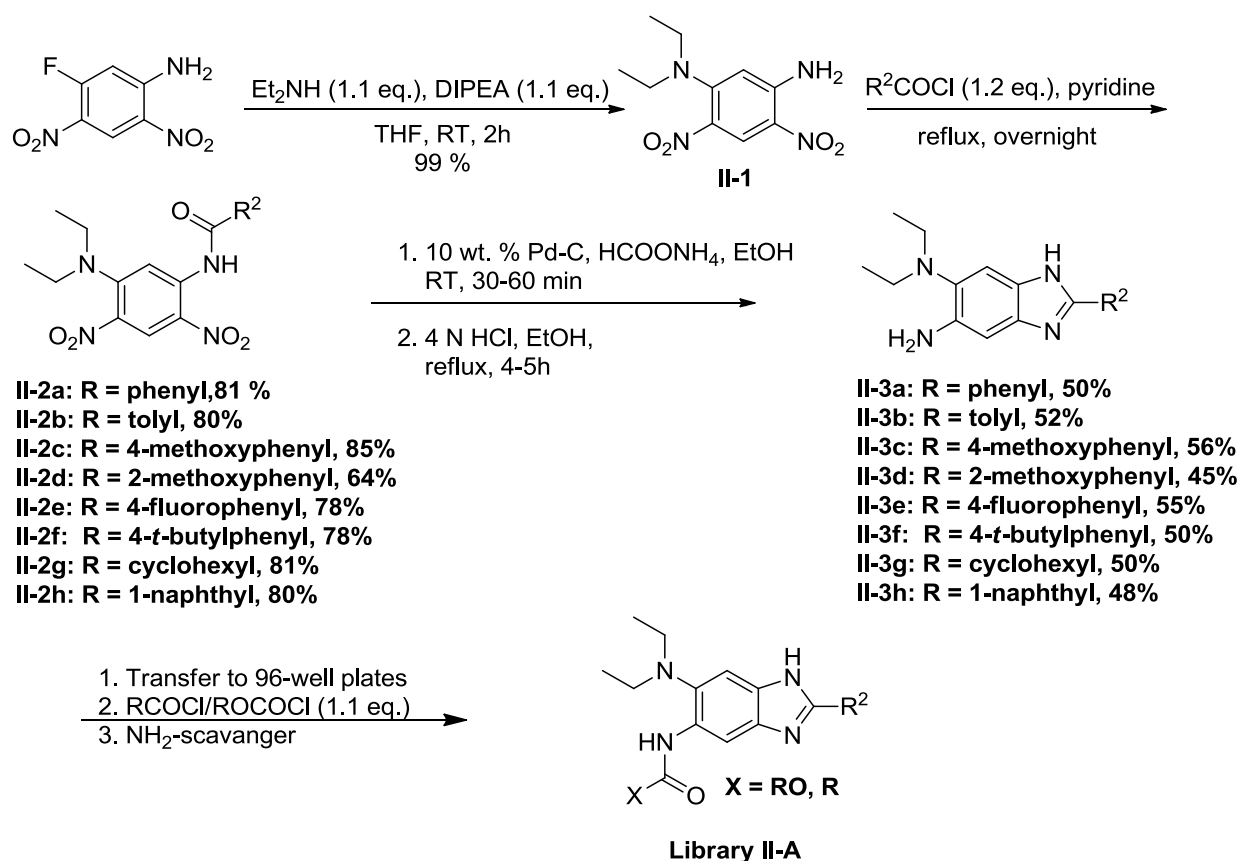


Scheme II-1. Proposed synthesis of 2,5,6- and 2,5,7-trisubstituted benzimidazole library

§ 2.2 Results and Discussion

§ 2.2.1 Synthesis of 2,5,6-trisubstituted benzimidazole library

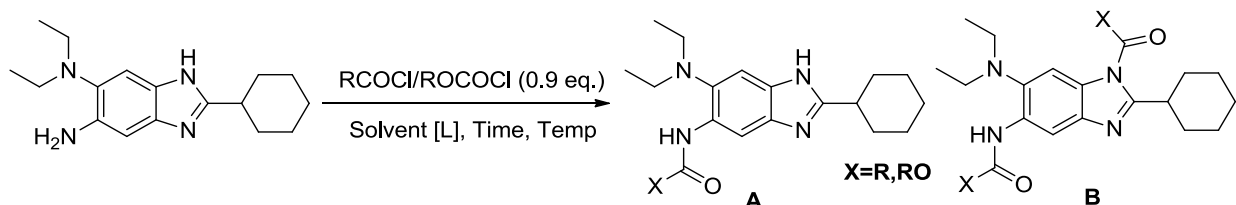
A library of 2,5,6-trisubstituted benzimidazoles was synthesized as outlined in **Scheme II-2**. The aromatic nucleophilic substitution of commercially available 2,4-dinitro-5-fluoroaniline with diethyl amine afforded **II-1** in 95-100% yield. The acylation of **II-1** with different acyl chlorides afforded **II-2a~II-2h** in 64-85% yield. The reduction and subsequent acid-catalyzed cyclization gave 5-aminobenzimidazoles **II-3a~II-3h** in 48-56% yield. The intermediates **II-3a~II-3h** were dissolved in methylene chloride and transferred to a 96-well plate. Subsequently, a series of 33 different acyl chlorides and/or alkyl chloroformates were added to afford library **II-A** of 272 compounds with good to high purity (see the experimental section for detailed structures of library).



Scheme II-2. Synthesis of 2,5,6-trisubstituted benzimidazole library II-A

§ 2.2.2 Preliminary screening, re-synthesis and accurate MIC determination

The library **II-A** (272 2,5,6-trisubstituted benzimidazoles) was screened in a 96-well format (single point assay). Of these, 26 compounds were identified to inhibit the growth of *Mtb* H37Rv with MIC₉₉ values ≤ 5 $\mu\text{g/mL}$ in triplicates. Furthermore, among the 26 hits, 8 compounds showed MIC₉₉ values of 0.5-6.1 $\mu\text{g/mL}$. In order to confirm accurate MIC values, hit compounds were re-synthesized in an analytically pure form (**Scheme II-3**, **Table II-1**). Unfortunately, the re-synthesis of the hit compounds showed product selectivity problems. For reactions where acyl chlorides were used as reagents at room temperature, relatively better product selectivity in favor of the desired mono-substituted products was observed (**Entry 1**). Following the same reaction conditions with butyrylchloroformate (**Entry 2**), showed very poor product selectivity and mostly disubstituted product was observed. The poor selectivity could be attributed to high reactivity of the chloroformates. Hence, reaction was repeated with a slow addition of 0.9 equivalents of the reagent at lower temperature and higher dilution (**Entry 3-5**). There was some improvement in the selectivity, but not significant.



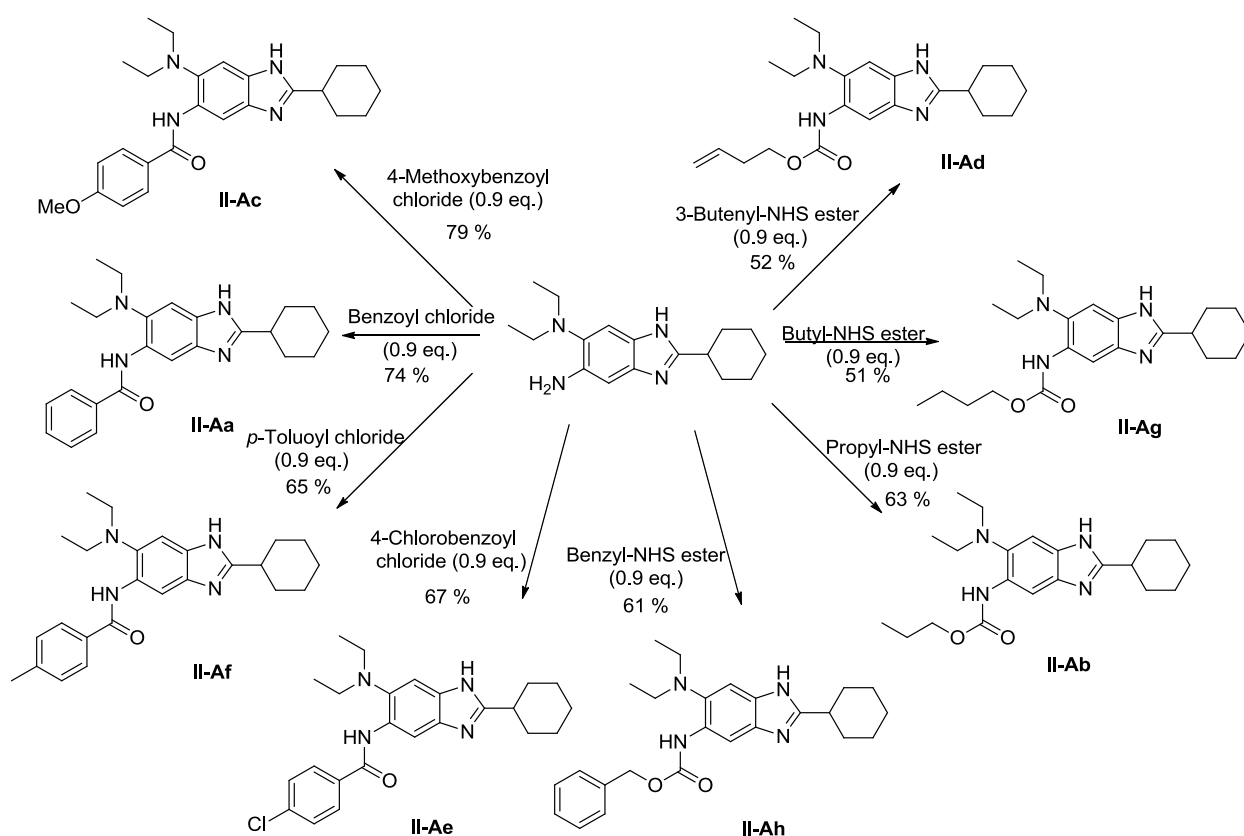
Scheme II-3. Re-synthesis of hit compounds

Table II-1. Optimization of the reaction condition

Entry	RCOCl/ROCOCl	Solvent [C]	Temp	Time	A (yield)	B (Yield)
1.	PhCOCl (1 eq.)	CH ₂ Cl ₂ [0.02]	RT	15 h	74 %	12 %
2.	BuOCOCl (1 eq.)	CH ₂ Cl ₂ [0.02]	RT	15 h	13 %	46 %
3.	BuOCOCl (0.9 eq.)	CH ₂ Cl ₂ [0.01]	0°C-RT	15 h	20 %	35 %
4.	BuOCOCl (0.9 eq.)	CH ₂ Cl ₂ [0.02]	0°C-RT	15 h	20 %	35 %
5.	BuOCOCl (0.9 eq.)	CH ₂ Cl ₂ [0.02]	-50°C -RT	15 h	20 %	40 % ^a
6.	Bu-NHS ester (0.9 eq.)	CH ₂ Cl ₂ [0.02]	0°C-RT	15 h	61 %	14 % ^a

^aReaction did not go to completion. Some starting material was recovered.

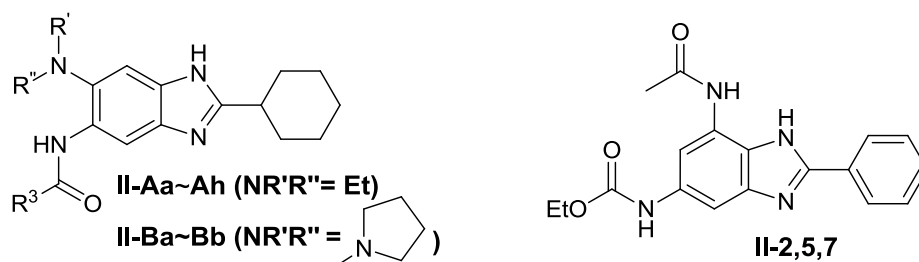
Following a suggestion given by Dr. Henry Li, *N*-hydroxysuccinimide (NHS) esters of the corresponding chloroformates were used under the presumption that the NHS-ester will have lower reactivity compared to chloroformates. As expected, it was observed that using 0.9 equivalent of NHS ester at 0 °C - RT improved the product selectivity to a greater extent with 50-60 % yield of the desired mono-substituted product (**Entry 6**). The reaction may warrant additional optimization to further improve the product selectivity. Nevertheless, this procedure was used for the re-synthesis of all the hit compounds with carbamate functionality at the 5-position (**Scheme II-4**). (Please see the Experimental Section for the structures and synthetic procedure of the hit compounds.)



Scheme II-4. Re-synthesis of Hit compounds

The eight analytically pure hit compounds showed MIC values of 2-15 μ M against drug sensitive H37Rv Mtb strain based on accurate Alamar blue assay, consistent with the preliminary screening results (**Table II-2**).

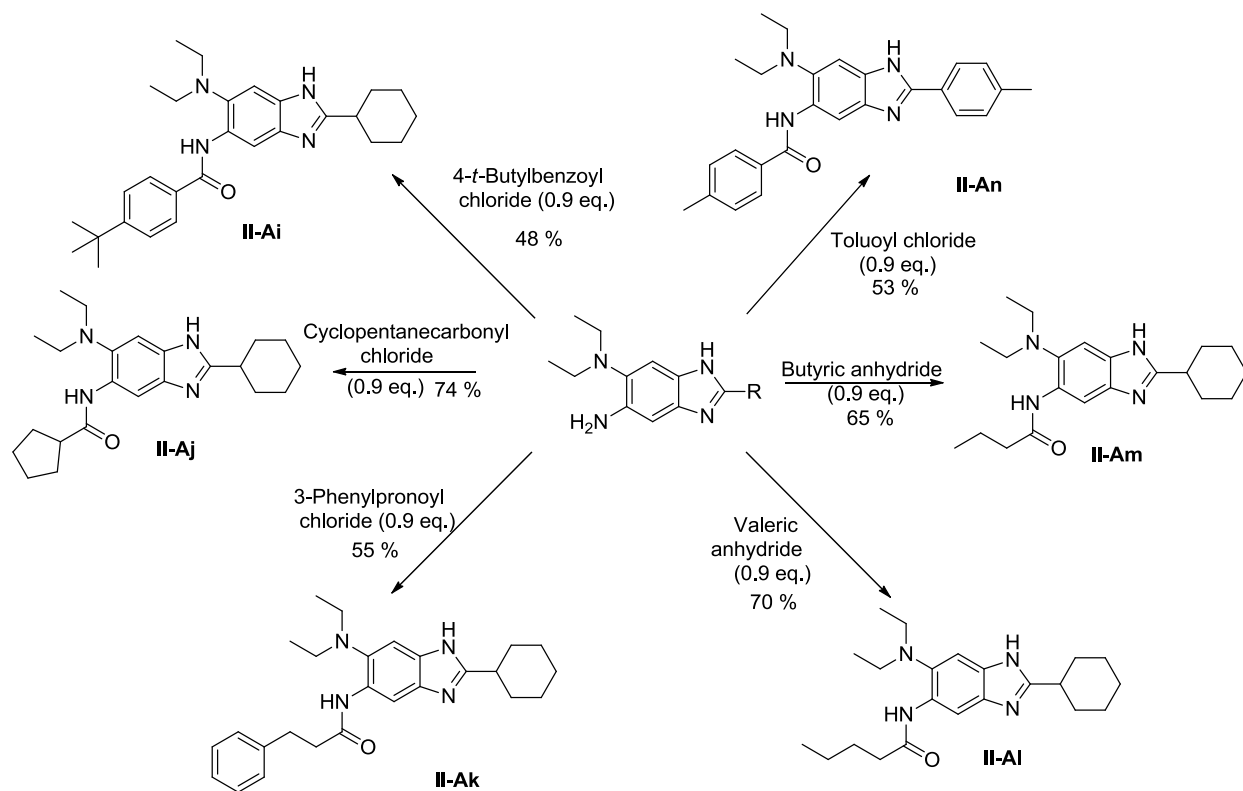
Table II-2. Antimicrobial Activities of Selected Trisubstituted Benzimidazoles against Drug-Sensitive and Drug-Resistant Strains of *Mtb*^a



Entry	Benzimidazole	R ₃	MIC ₉₉ (μM) <i>Mtb</i> strains						Cytotoxicity (IC ₅₀ μM) Vero cells
			H37Rv	W210	NHN20	NHN335	NHN382	TN587	
1	II-Aa		7.9						>400
2	II-Ab		4.3						>400
3	II-Ac		7.4						>400
4	II-Ad		4.2	4.2	4.2	4.2	4.2	4.2	>400
5	II-Ae		14.1						>400
6	II-Af		15.1						>400
7	II-Ag		2.0	4.0	4.0	4.0	2.0	4.0	>400
8	II-Ah		3.8						>400
9	II-Ba		1.0	1.0	1.0	1.0	1.0	1.0	>200
10	II-Bb		3.7	3.7	3.7	3.7	3.7	3.7	>200
11	II-257	Me	1.6	4.6	4.6	4.6	4.6	4.6	>200

Mtb H37Rv is a standard drug sensitive strain. *Mtb* W210, NHN20, NHN335, NHN382 and TN587 are clinical strains with differing drug resistant profiles.

None of the pure lead compounds showed any appreciable cytotoxicity ($IC_{50} > 200 \mu M$) against Vero cells (**Table II-2**). Two lead compounds, **II-Ad** and **II-Ag**, were also evaluated for their activities against clinical isolates of *Mtb* strains W210 (drug-sensitive),¹⁹ NHN20 (drug-sensitive),¹⁹ NHN335-2 (isoniazide-resistant; KasA G269S mutation),²⁰ NHN382 (isoniazide-resistant; Kat G S315t mutation)¹⁹ and TN587 (isoniazide-resistant; KatG 3315T mutation),¹⁹ which showed no difference between the drug-sensitive and drug-resistant strains, as anticipated, exhibiting excellent MIC_{99} values in the range of 0.39-1.56 $\mu g/mL$ (1-4.6 μM). These compounds have been advanced to the *in vivo* rapid model assay in mice. The remaining 26 hit compounds have also been re-synthesized for extensive structure activity relationship (SAR) studies and their biological evaluation is currently in progress (**Scheme II-5**) (Please see the experimental section for the synthetic procedure and the structures).



Scheme II-5. Re-synthesis of hit compounds

§ 2.2.3 Preliminary SAR study and optimization of the 6-position of 2,5,6-trisubstituted benzimidazoles

Preliminary SAR studies of 2,5,6-trisubstituted lead compounds indicated that cyclohexyl and diethyl amino groups at the 2- and 6-position, respectively, were critically important for antibacterial activity (**Figure II-4**).

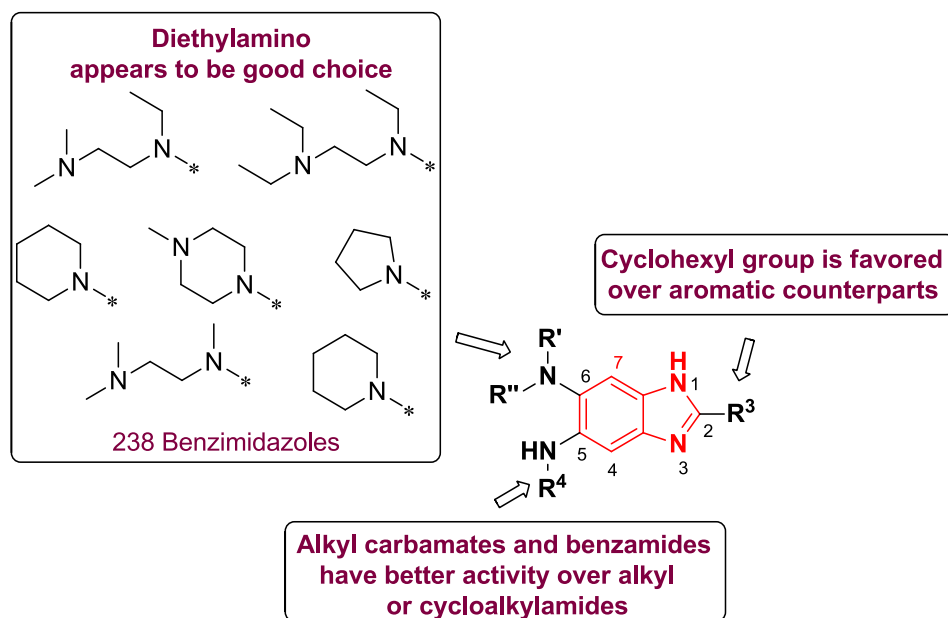
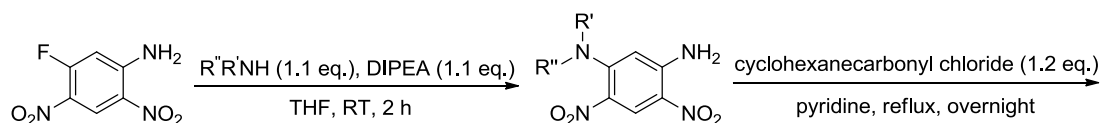


Figure II-4. Preliminary SAR studies and optimization of the 6-position

Based on these observations, another library (**II-B**) of 238 2,5,6-trisubstituted benzimidazoles was synthesized with various diethylamino-like substituents at the 6-position retaining the cyclohexyl substituent at the 2-position (**Scheme II-6**) (procedures are similar to the synthesis of library **II-A**, see experimental section for the structures of library **II-B**). As the final acid catalyzed cyclization step to form the benzimidazole intermediates with desired substitution pattern was giving low yield, it was decided to optimize the reaction conditions. During the process, it was observed that one pot reaction using tin (II) chloride dihydrate and 4 N HCl improved the yield drastically. Also the reaction was much cleaner with single spot on TLC and baseline impurities, making purification simpler.



II-4a: R''R'N = 4-methylpiperazinyl, 98 %

II-4b: R''R'N = pyrrolidinyl, 100 %

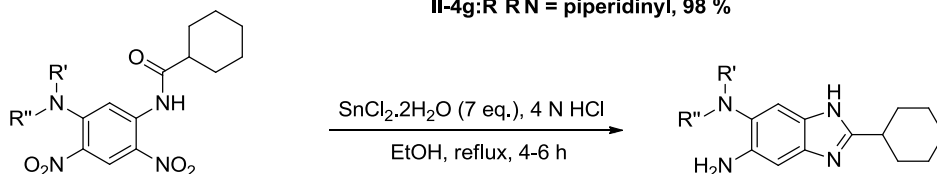
II-4c: R''R'N = morpholino, 93 %

II-4d: R''R'N = *N,N,N*-triethylethylenediamino, 99 %

II-4e: R''R'N = *N,N,N*-trimethylethylenediamino, 93 %

II-4f: R''R'N = *N,N*-dimethyl-*N*-ethylethylenediamino, 88 %

II-4g: R''R'N = piperidinyl, 98 %



II-5a: R''R'N = 4-methylpiperazinyl, 74 %

II-5b: R''R'N = pyrrolidinyl, 83 %

II-5c: R''R'N = morpholino, 93 %

II-5d: R''R'N = *N,N,N*-triethylethylenediamino, 94 %

II-5e: R''R'N = *N,N,N*-trimethylethylenediamino, 83 %

II-5f: R''R'N = *N,N*-dimethyl-*N*-ethylethylene-diamino, 50 %

II-5g: R''R'N = piperidinyl, 98 %

II-6a: R''R'N = 4-methylpiperazinyl, 82 %

II-6b: R''R'N = pyrrolidinyl, 50 %

II-6c: R''R'N = morpholino, 79 %

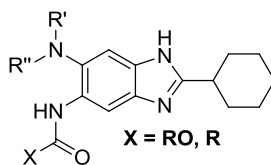
II-6d: R''R'N = *N,N,N*-triethylethylenediamino, 81 %

II-6e: R''R'N = *N,N,N*-trimethylethylenediamino, 59 %

II-6f: R''R'N = *N,N*-dimethyl-*N*-ethylethylene-diamino, 74 %

II-6g: R''R'N = piperidinyl, 82 %

1. Transfer to 96-well plates
2. RCOCl/ROCOCl (1.1 eq.)
3. NH₂-scavanger



Library II-B

Scheme II-6. Optimization of the 6-position of 2,5,6-trisubstituted benzimidazole library

Based on the Alamar Blue Assay, 54 compounds were identified from library **II-B**, which inhibited the cell growth with MIC₉₉ values ≤ 5 μg/mL. Among the 54 hits, re-synthesized pure **II-Ba** and **II-Bb** showed MIC₉₉ values of 0.39 μg/mL (1.2 μM) and 1.56 μg/mL (13 μM), respectively (**Table II-2**). Two lead compounds, **II-Ba** and **II-Bb**, were also assayed for their activities against clinical isolates of *Mtb* strains W210 (drug-sensitive)¹⁹, NHN20 (drug-sensitive)¹⁹, NHN335-2 (isoniazide-resistant; KasA G269S mutation)²⁰, NHN382 (isoniazide-resistant; Kat G S315T mutation)¹⁹ and TN587 (isoniazide-resistant; KatG 3315T mutation)¹⁹, which showed no difference in activity against drug-sensitive and drug-resistant strains. As anticipated, **II-Ba** and **II-Bb** exhibited excellent MIC₉₉ values in the range of 0.39-1.56 μg/mL (1-4.6 μM). These compounds have been advanced to the *in vivo* rapid model assay in mice.

§ 2.2.4 Optimization of the 2-position of 2,5,6-trisubstituted benzimidazoles

While we were waiting for the results from the 6-position optimization, the 2-position optimization with the piperidine group at the 6-position was carried out. The 2-position was modified with heteroaromatic substituents which are found in many drug-like molecules (**Figure II-5**).

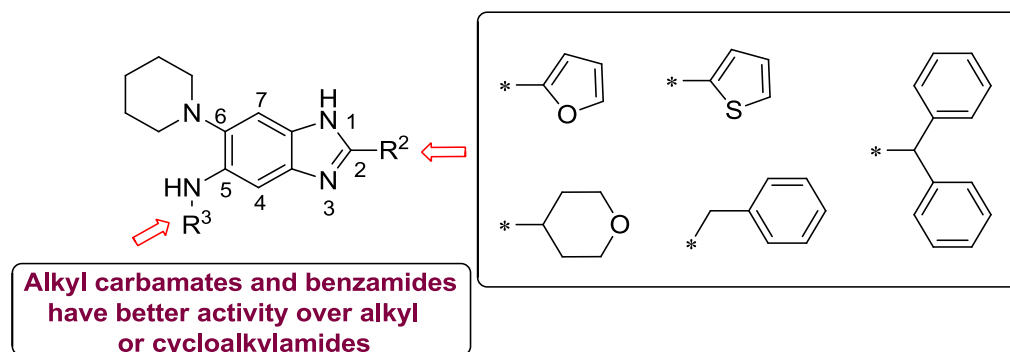
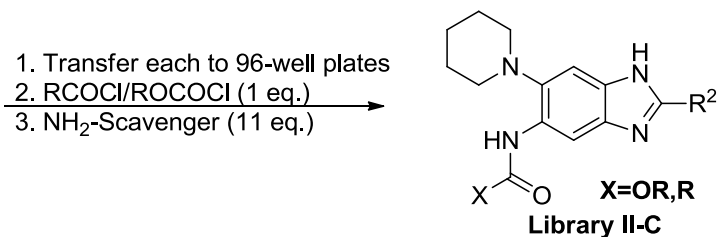
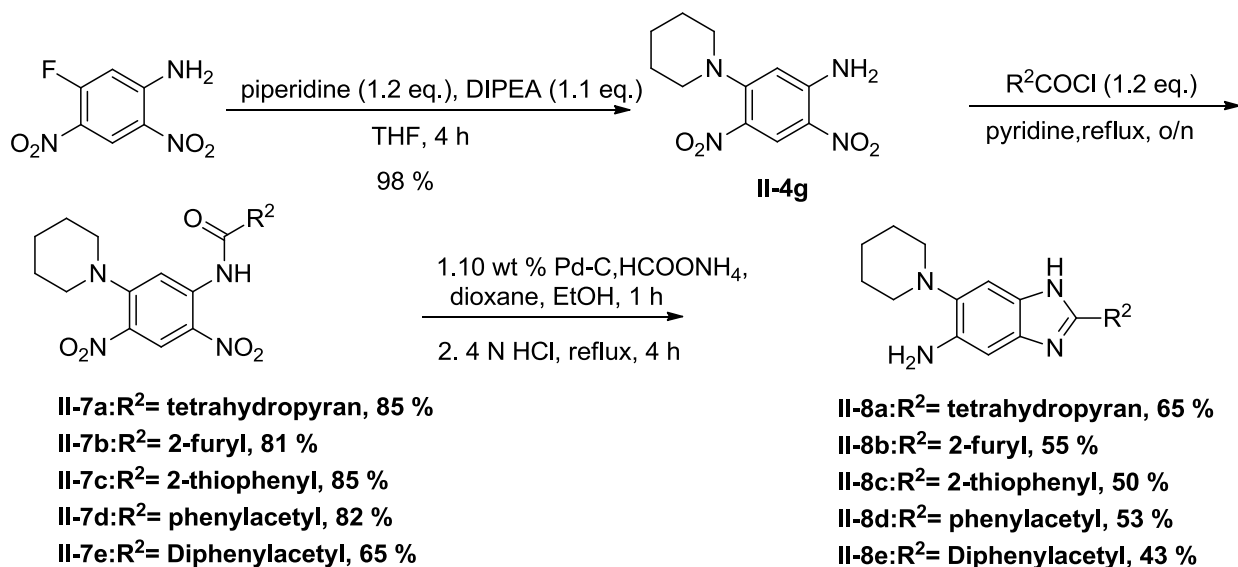


Figure II-5. Optimization of the 2-position of 2,5,6-trisubstituted benzimidazole library

In addition, diphenyl and benzyl groups were also installed at the 2-position to assess the flexibility of the 2-position (**Figure II-5**). With these modifications, another library (**II-C**) of 147 2,5,6-trisubstituted benzimidazoles was synthesized with various aromatic and heteroaromatic substituents at the 2-position (**Scheme II-7**) (procedures are similar to the synthesis of library **II-A**, see experimental section for the structures of library **II-C**).



Scheme II-7. Optimization of the 2-position of 2,5,6-trisubstituted benzimidazole library

Based on the Alamar Blue Assay, 12 compounds were identified, which inhibited cell growth with MIC₉₉ values of ≤ 10 $\mu\text{g/mL}$. Among the 12 hits, 3 compounds exhibited MIC₉₉ values of ≤ 5 $\mu\text{g/mL}$ and 5 compounds exhibited MIC₉₉ values of ≤ 10 $\mu\text{g/mL}$ (**Figure II-6**). Some of the compounds have been re-synthesized and sent for accurate MIC₉₉ determination. The rest of the compounds are currently being re-synthesized.

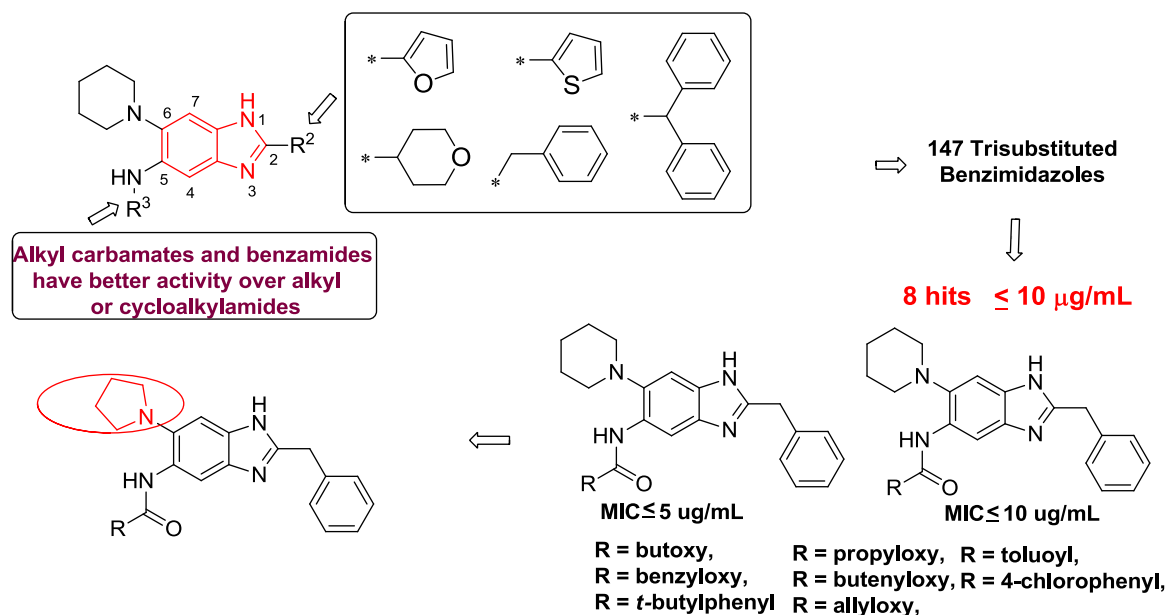
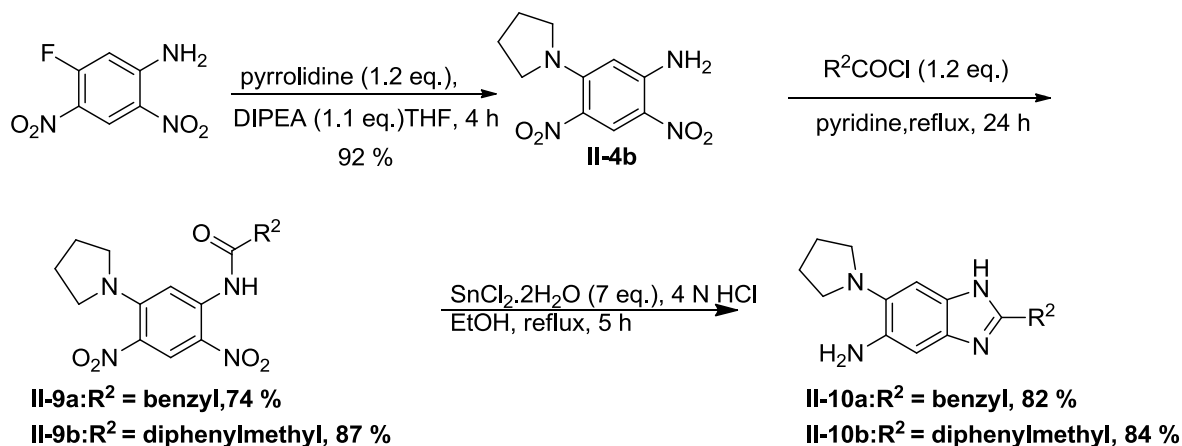


Figure II-6. Hits from the 2-position optimization

As mentioned before, a pyrrolidine substituent at the 6-position is critical for anti-TB activity. Thus, the 2-position optimization was done using a pyrrolidine substituent at the 6-position (**Scheme II-8**). These intermediates are being used to synthesize active compounds which may exhibit improved biological activity.



Scheme II-8. Synthesis of 2,5,6-trisubstituted benzimidazoles with pyrrolidine substituent at the 6-position

§ 2.2.5 Optimization of the 5-position of 2,5,6-trisubstituted library

So far only amide or carbamate functionalities have been explored at the 5-position using a limited number of acyl chlorides and chloroformates. In order to expand the scope of the library and investigate other functionalities such as urea, thiourea, and sulfonamide, substituent optimization at the 5-position was evaluated using various isocyanates, isothiocyanates, and sulfonyl chlorides as outlined (**Figure II-7**).

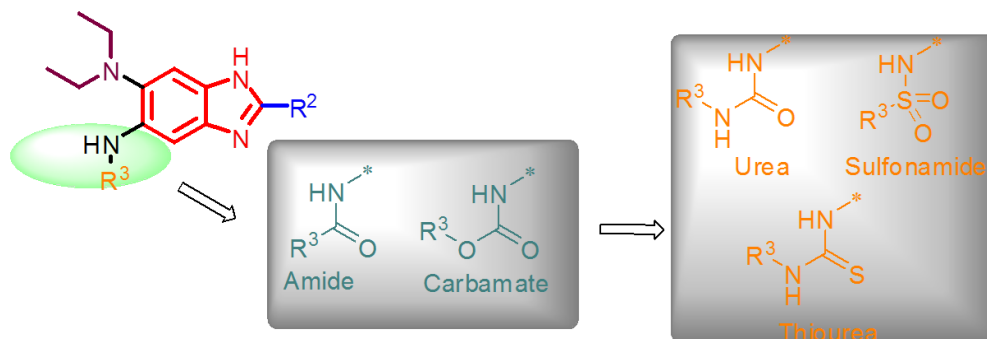


Figure II-7. Optimization of the 6-position

For the optimization of the 5-position, a new library (**II-D**) of 180 compounds was synthesized using various isocyanate, isothiocyanate and sulfonyl chlorides as reagents (**Figure II-8**). In a preliminary screening against drug sensitive H37Rv cells, compound **II-Da**, with a thiourea functionality at the 5-position, was found to exhibit good activity (MIC value of ≤ 5 $\mu\text{g/mL}$). Moreover, for two compounds, **II-Db** and **II-Dc** no visible growth with active respiration was observed. This led us to believe that these compounds may be bacteriostatic: rather than killing the bacteria the compounds either slow down or inhibit their growth. These findings need to be confirmed using analytically pure compounds.

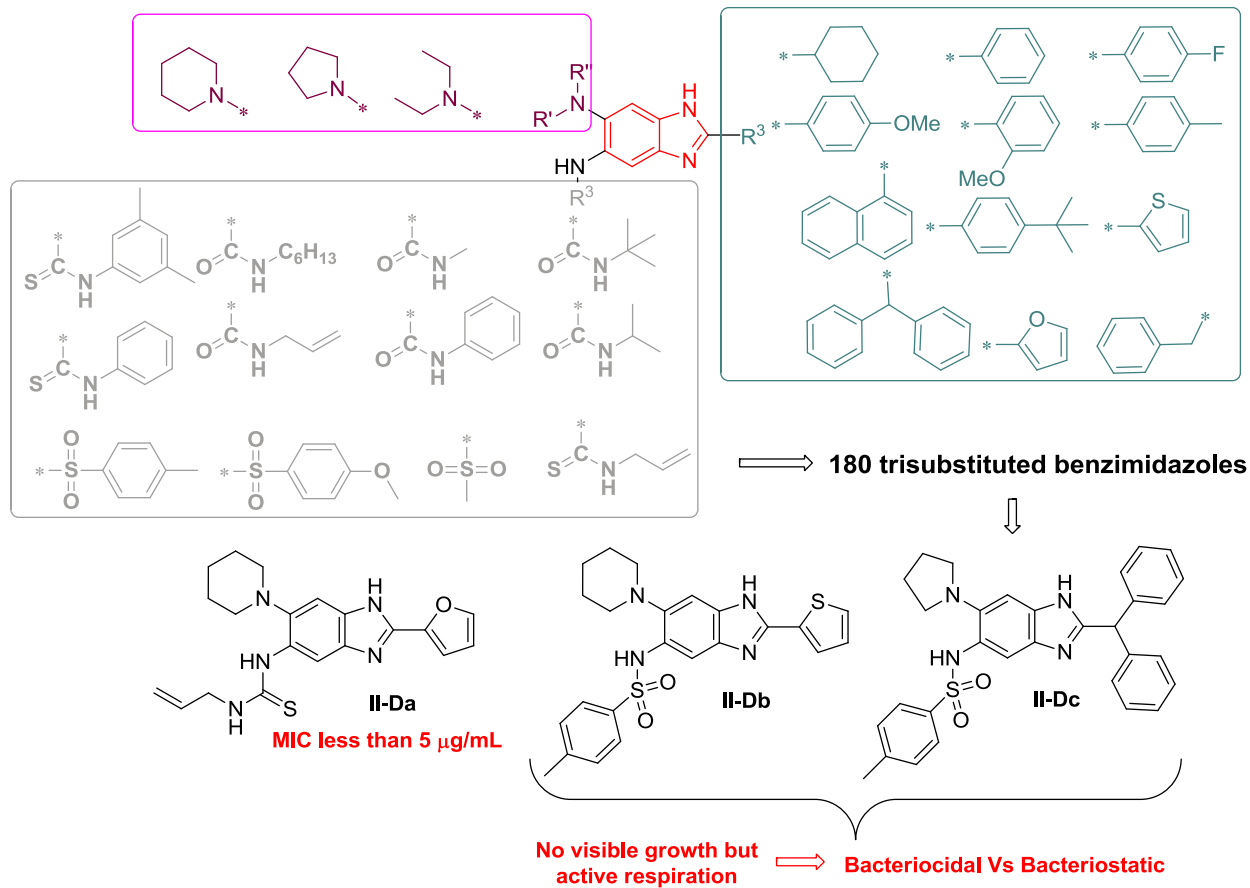


Figure II-8. Synthesis of the 5-position optimized 2,5,6-trisubstituted benzimidazole library II-D

Furthermore, acylating reagents that have been used so far are very limited in their structure versatility and functional properties. Mostly, we have focused on alkyl or aromatic acylating reagents. Hence it was important to extend the series to assorted reagents with diverse structural and functional features. In an attempt to diversify the 5-position, a series of different acylating reagents was used for the synthesis of library **II-E** (**Figure II-9**). The biological evaluation of this library of compounds is currently in progress.

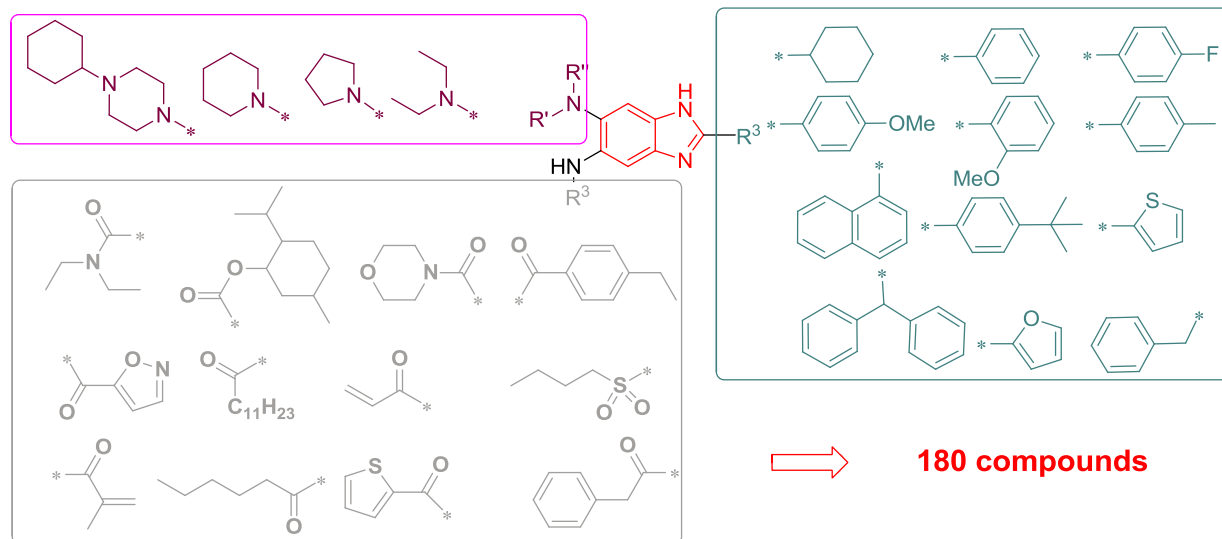


Figure II-9. Synthesis of the 5-position optimized 2,5,6-trisubstituted benzimidazole library II-E

§ 2.2.6 Optimization of 2,5,7-trisubstituted benzimidazoles

Previously in the Ojima lab, a library of 77 2,5,7-trisubstituted benzimidazoles was synthesized for the discovery of novel compounds against *Mtb*. In a preliminary screening against *Mtb* strains, one compound **II-257** was identified, which inhibited cell growth with an MIC₉₉ value of ≤ 0.5 $\mu\text{g/mL}$. Upon accurate MIC₉₉ determination, **II-257** exhibited MIC₉₉ value of 0.5 $\mu\text{g/ml}$ and 1.56 $\mu\text{g/ml}$ against drug-sensitive and drug-resistant cell lines, respectively (**Table II-2**). In order to optimize the lead compounds, a more diverse library of 2,5,7-trisubstituted benzimidazoles with different substitution patterns was synthesized (**Figure II-10**). In the case of 2,5,6-trisubstituted benzimidazole library, a cyclohexyl group at the 2-position proved to be very crucial for anti-TB activity. Thus, a cyclohexyl moiety was used at the 2-position for the 2,5,7-trisubstituted library as well. Moreover, in addition to ethoxycarbamate substituent at the 5-position, we also decided to expand the scope by using various other carbamates as well.

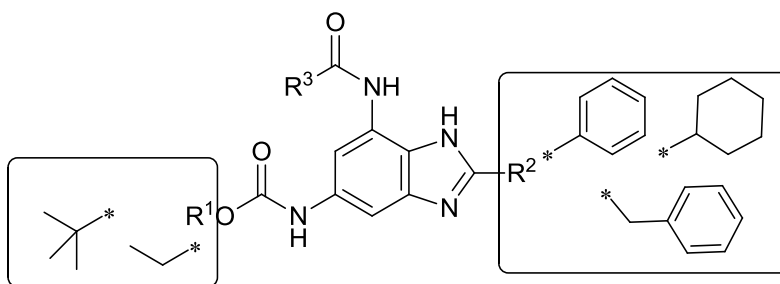
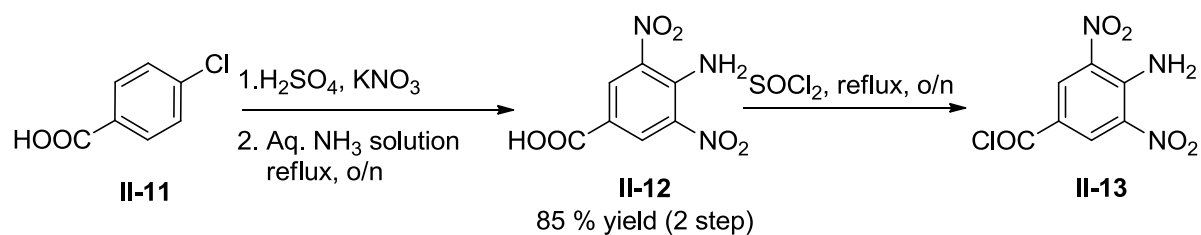
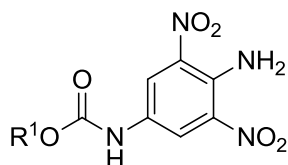


Figure II-10. Optimization of the 2,5,7-trisubstituted benzimidazoles

A library of 2,5,7-trisubstituted benzimidazole was synthesized as outlined in Scheme II-9. Earlier, the synthesis of a 2,5,7-trisubstituted library was carried out starting with 4-amino-3,5-dinitrobenzamide (**II-12**). Unfortunately, this compound is no longer commercially available or very expensive. Hence, we decided to start the synthesis from relatively cheaper, commercially available 4-chlorobenzoic acid (**II-11**). Nitration of **II-11** in the presence of potassium nitrate and sulfuric acid followed by the substitution of the chloride by an amino moiety using ammonia solution in methanol generated the intermediate 4-amino-3,5-dinitrobenzoic acid (**II-12**) as yellow solid in 85 % yield (2 steps). The intermediate **II-12** was converted to acyl chloride **II-13**. The reaction of **II-13** with sodium azide afforded the corresponding acyl azide, which was subjected to the Curtius rearrangement to give the corresponding isocyanate. The isocyanate was subsequently reacted with *t*-butanol or ethanol to give the corresponding carbamates **II-14a** ($R^1 = \text{Et}$) or **II-14b** ($R^1 = t\text{-Bu}$) in 78-84 % yield (for 4 steps) as a bright red solid. The reduction of **II-14a/II-14b** followed by cyclocondensation with the bisulfite salts of different aldehydes afforded 7-aminobenzimidazoles **II-15a~II-15f** in 40-64 % yield. The final acylation of **II-15a~II-15f** in the same manner as that for the library of **II-A** gave the library of 126 2,5,7-trisubstituted benzimidazoles **II-F** with good to high purity (see the experimental section for the detailed experimental procedures, structures of intermediates and library).



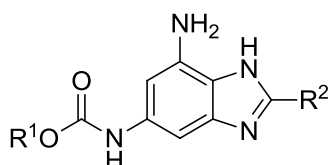
1. NaN_3 (2.2 eq.), acetone, 0°C -RT, 30 min
 2. toluene, reflux, 3-4 h
 3. R^1OH , RT, o/n



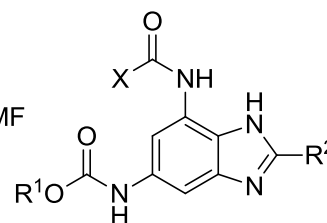
II-14a: $\text{R}^1 = \text{Et}$, 78 %
II-14b: $\text{R}^1 = t\text{-Bu}$, 84 %

1. 10 wt % Pd-C, HCOONH_4 , EtOH
 RT, 30-60 min

2. $\text{R}^2\text{CH}(\text{OH})\text{SO}_3^-\text{Na}^+$, water
 RT, o/n



1. Transfer each to 96-well plates, DMF
 2. $\text{RCOCl}/\text{ROCOCl}$ (1 eq.)
 3. NH_2 -Scavenger (11 eq.)



X=OR, R
Library I-F

II-15a: $\text{R}^1 = \text{Et}$, $\text{R}^2 = \text{phenyl}$, 48 %
II-15b: $\text{R}^1 = \text{Et}$, $\text{R}^2 = \text{cyclohexyl}$, 42 %
II-15c: $\text{R}^1 = \text{Et}$, $\text{R}^2 = \text{benzyl}$, 64 %
II-15d: $\text{R}^1 = t\text{-Bu}$, $\text{R}^2 = \text{cyclohexyl}$, 51 %
II-15e: $\text{R}^1 = t\text{-Bu}$, $\text{R}^2 = \text{benzyl}$, 63 %
II-15f: $\text{R}^1 = t\text{-Bu}$, $\text{R}^2 = \text{phenyl}$, 59 %

Scheme II-9. Synthesis of 2,5,7-trisubstituted benzimidazole library II-F

Unexpectedly, most of the compounds were found to be cytotoxic at 5 $\mu\text{g}/\text{ml}$ based on a more accurate Alamar Blue Assay. We hypothesized that the extreme cytotoxicity of these compounds could arise from the residual DMF in the 96 well plates. Hence in order to confirm this premise, we are currently resynthesizing the compounds using volatile solvents such as ethanol, tetrahydrofuran, and acetonitrile.

§ 2.2.7 Early ADMET results and synthesis of metabolically stable benzimidazoles analogues

Considering the encouraging *in vitro* results of our lead compounds, evaluation of early *in vitro* adsorption, distribution, metabolism, excretion and toxicology (ADMET) properties of **SB-P3G2** was carried out by our collaborators at Sanofi-Aventis laboratory. The compound exhibited relatively reasonable drug-like ADMET properties with good membrane permeability, promising cardiac safety (no effect on hERG calcium-ion channel), negligible inhibition of CYP 3A4 and clean kinase profile. Additionally, the plasma stability of the compound in human plasma was excellent. However, the plasma stability in mouse plasma was poor which improved significantly on addition of PMSF (phenylmethylsulfonyl fluoride), a hydrolase inhibitor. Also, it was observed that the metabolic stability in mouse and rat microsome was suggestively low.

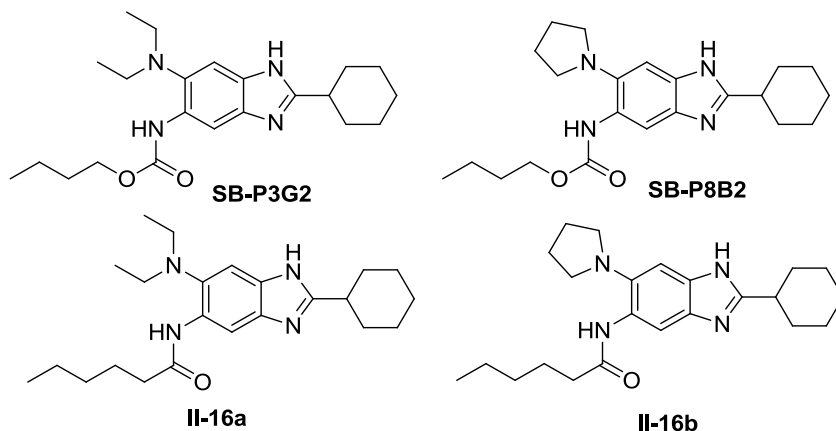


Figure II-11. Amide congeners of SB-P3G2 and SB-P8B2

As all preclinical studies will be done with mice or rats, it is necessary to develop a metabolically more stable compound that can be used for mice or rats. Knowing that the compound showed improved stability on addition of PMFS; we suspected that carbamate functionality is one possible site which is getting cleaved during the process. Therefore, it was decided to synthesize the amide congeners of two lead compounds, SB-P3G2 and SB-P8B2 (**Figure II-11**). However, these compounds need to retain their anti-tubercular activities after modification. Currently, the biological evaluation of these compounds is in progress, and depending on the results, the metabolic stability of the compounds will be evaluated. Furthermore, among the 11 hit compounds, several benzimidazoles with amide functionality at the 5 position were identified, however with lower activities compared to SB-P3G2. The

ADMET properties of these compounds will also be evaluated collaboration with Sanofi-Aventis.

§ 2.3 Conclusion

A library of 349 novel trisubstituted-benzimidazoles was synthesized using multi-step polymer-assisted solution phase synthesis through a rational and systematic design. In preliminary screening, 27 compounds exhibited MIC₉₉ values of ≤ 0.5 $\mu\text{g/mL}$ against *Mtb*. H37RV strain. Upon resynthesis and accurate MIC determination, 9 lead compounds were identified which exhibited MIC₉₉ in the range of 0.56-6.1 $\mu\text{g/mL}$. Following the initial discovery, an optimized library of 238 trisubstituted-benzimidazoles was synthesized and screened. 54 additional compounds with MIC₉₉ values ≤ 5 $\mu\text{g/mL}$ were identified as solid hits. Among the 54 hits, 2 compounds showed MIC₉₉ values of 0.39 and 1.56 $\mu\text{g/mL}$, respectively, based on the Alamar blue assay. The lead compounds showed excellent activities against drug-resistant clinical isolates of *Mtb* with MIC₉₉ values in the range of 0.39-1.56 $\mu\text{g/mL}$ without any appreciable cytotoxicity. Based on preliminary SAR studies, optimization of substituents at the 2-, 5-, and 6-position was carried out by synthesizing another series of libraries of ~1000 compounds. Unfortunately, some of the compounds were found to be cytotoxic, whereas other compounds didn't show any improvement in activities over the previous compounds. Currently, other series of libraries have been synthesized which are being screened against *Mtb*. Moreover, the lead compound SB-P3G2 has exhibited reasonable drug-like ADMET properties.

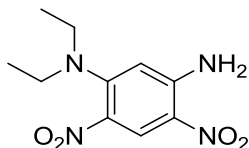
§ 2.4 Experimental Section

General Methods: ^1H and ^{13}C NMR spectra were measured on a Varian 300, 400 or 500 MHz NMR spectrometer. Melting points were measured on a Thomas Hoover Capillary melting point apparatus and are uncorrected. TLC was performed on Merck D Calufolien with Kieselgel 60F-254 and column chromatography was carried out on silica gel 60 (Merck; 230-400 mesh ASTM). High-resolution mass spectra were obtained from Mass Spectrometry Laboratory, University of Illinois at Urbana-Champaign, Urbana, IL. Purity was determined by Agilent 1100 series HPLC assembly. Two analytical conditions were used and noted as a part of the characterization data for re-synthesized compounds. **HPLC1:** Luna PFP, 3 μm , 100 \AA (pore size), 3.0 \times 150 mm column, Solvent A – $\text{H}_2\text{O}:\text{ACN}$, 95:5 (20 mM Ammonium acetate, pH 6.5), Solvent B = $\text{H}_2\text{O}:\text{ACN}$, 5:95 (20 mM Ammonium acetate, pH 6.5), Temperature 30 $^\circ\text{C}$, flow rate 0.6 mL/min, t = 0-13.5 min, gradient 15-90 % solvent B. **HPLC2:** Kinetex PFP, 2.6 μm , 100 \AA (pore size), 4.6 \times 100 mm column, Solvent A – $\text{H}_2\text{O}:\text{ACN}$, 95:5 (25 mM Ammonium acetate, pH=6.5), Solvent B = $\text{H}_2\text{O}:\text{ACN}$, 5:95 (25 mM Ammonium acetate, pH=6.5), Temperature 25 $^\circ\text{C}$, flow rate 1.0 mL/min, t = 0-15 min, gradient 20-95 % solvent B.

Materials: All chemicals were purchased from Aldrich Co., Synquest Inc., Fisher Scientific and VWR and purified before use by standard methods. Tetrahydrofuran was freshly distilled from sodium metal and benzophenone. Dichloromethane was also distilled immediately prior to use under nitrogen from calcium hydride. Aminomethylated polystyrene resin EHL (200-400 mesh) 2 % DVB was purchased from Novagen Biochem.

§ 2.4.1 Synthesis of 2,5,6-Trisubstituted Benzimidazole Library II-A

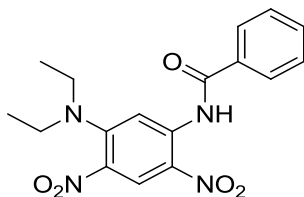
5-*N,N*-Diethylamino-2,4-dinitroaniline (II-1):



To a solution of 2,4-dinitro-5-fluoroaniline (500 mg, 2.48 mmol) and diisopropylethylamine (DIPEA) (476.3 μL , 2.73 mmol) in tetrahydrofuran (25 mL) was added a

solution of diethylamine (360 μ L, 3.48 mmol) in tetrahydrofuran (22 mL) dropwise. The reaction mixture was stirred at room temperature for 4 h. The solvent was evaporated and water was added to give a yellow precipitate. The solution was extracted with dichloromethane (30 mL x 3). The organic layer was collected, dried over anhydrous magnesium sulfate and evaporated to give **II-1** as yellow solid (626 mg, 99 % yield); mp 108-109 $^{\circ}$ C; ^1H NMR (500 MHz, CDCl_3) δ 1.18 (t, 6 H, $J = 7$ Hz), 3.23 (q, 4 H, $J = 6.5$ Hz), 6.14 (s, 1 H), 6.49 (broad s, NH), 8.71 (s, 1 H); ^{13}C NMR (125 MHz, CDCl_3) δ 12.07, 45.72, 102.7, 123.2, 128.1, 131.5, 147.7, 149.3. MS (ESI) m/z 253.1 ($\text{M}+1$) $^+$.

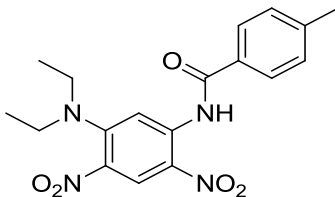
1-Benzamido-5-*N,N*-diethylamino-2,4-dinitrobenzene (**II-2a**):



A solution of **II-1a** (500 mg, 1.96 mmol) and benzoyl chloride (329 mg, 2.35 mmol) in pyridine (8 mL) was refluxed overnight. After completion of the reaction, pyridine was removed *in vacuo* to give a brown solid. This crude mixture was washed with methanol and collected by filtration to afford pure **II-2a** as a yellow solid (570 mg, 81 % yield); mp 168-170 $^{\circ}$ C; ^1H NMR (400 MHz, CDCl_3) δ 1.30 (t, 6 H, $J = 7.2$ Hz), 3.41 (q, 4 H, $J = 7.2$ Hz), 7.53 (dd, 2 H), 7.59 (dd, 1 H), 7.98 (d, 2 H, $J = 7.2$ Hz), 8.78 (s, 1 H), 8.81 (s, 1 H), 11.84 (s, 1 H); ^{13}C NMR (100 MHz, CDCl_3) δ 12.23, 46.53, 107.5, 125.1, 127.3, 129.1, 132.9, 133.5, 138.8, 149.0, 166.1. MS (ESI) m/z 359.1 ($\text{M}+1$) $^+$.

Compounds **II-2a~II-2h** were prepared in the same manner.

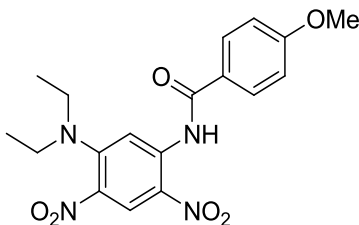
1-(4-Methylbenzamido)-5-*N,N*-diethylamino-2,4-dinitrobenzene (**II-2b**):



Yellow solid; 80 % yield; mp 200-202 $^{\circ}$ C; ^1H NMR (500 MHz, CDCl_3) δ 1.30 (t, 6 H, $J = 7$ Hz), 2.45 (s, 3 H), 3.41 (q, 4 H, $J = 7$ Hz), 7.34 (d, 2 H, $J = 8$ Hz), 7.89 (d, 2 H, $J = 8.5$ Hz), 8.80 (s, 1

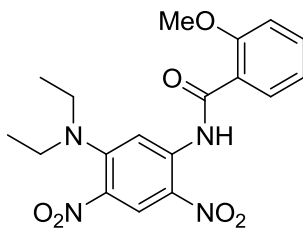
H), 8.83 (s, 1 H), 11.82 (s, NH); ^{13}C NMR (125 MHz, CDCl_3) δ 12.29, 21.57, 46.56, 107.5, 125.1, 127.3, 129.8, 130.8, 132.9, 139.0, 143.8, 149.0, 166.2. MS (ESI) m/z 373.1 ($\text{M}+1$) $^+$.

1-(4-Methoxybenzamido)-5-*N,N*-diethylamino-2,4-dinitrobenzene (II-2c):



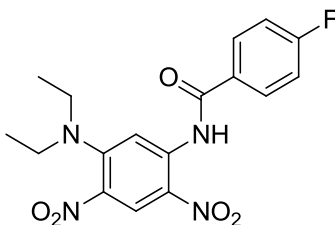
Yellow solid; 85 % yield; mp 166-167 °C; ^1H NMR (400 MHz, CDCl_3) δ 1.29 (t, 6 H, $J = 7.2$ Hz), 3.41 (q, 4 H, $J = 6.8$ Hz), 3.39 (s, 3 H), 7.01 (d, 2 H, $J = 8.4$ Hz), 7.96 (d, 2 H, $J = 8.4$ Hz), 8.82 (d, 2 H, $J = 8$ Hz), 11.77 (s, 1 H); ^{13}C NMR (100 MHz, CDCl_3) δ 12.26, 46.53, 55.53, 107.4, 114.3, 125.0, 125.7, 127.2, 129.4, 132.8, 139.1, 149.0, 163.4, 165.6. MS (ESI) m/z 389.1 ($\text{M}+1$) $^+$.

1-(2-Methoxybenzamido)-5-*N,N*-diethylamino-2,4-dinitrobenzene (II-2d):



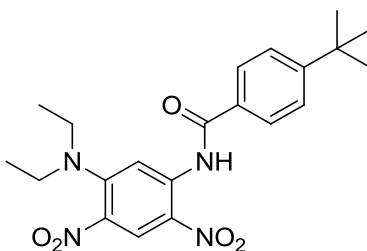
Yellow solid; 64 % yield; mp 155-157 °C; ^1H NMR (500 MHz, CDCl_3) δ 1.28 (t, 6 H, $J = 7.5$ Hz), 3.39 (q, 4 H, $J = 7$ Hz), 4.10 (s, 3 H), 7.05 (d, 1 H, $J = 8.5$ Hz), 7.11 (dd, 1 H, $J = 7$ Hz), 7.53 (m, 1 H), 8.21 (d, 1 H, $J = 9$ Hz), 8.79 (s, 1 H), 8.95 (s, 1 H), 12.5 (s, 1 H); ^{13}C NMR (125 MHz, CDCl_3) δ 12.30, 46.42, 55.67, 109.4, 111.4, 121.2, 126.1, 127.0, 132.6, 134.3, 138.8, 148.8, 157.6, 164.9. MS (ESI) m/z 389.1 ($\text{M}+1$) $^+$.

1-(4-Fluorobenzamido)-5-*N,N*-diethylamino-2,4-dinitrobenzene (II-2e):



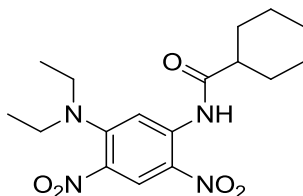
Yellow solid; 78 % yield; mp 173-174 °C; ¹H NMR (500 MHz, CDCl₃) δ 1.30 (t, 6 H, *J* = 7 Hz), 3.41 (q, 4 H, *J* = 7 Hz), 7.21 (d, 2 H, *J* = 8 Hz), 8.02 (d, 2 H, *J* = 8 Hz), 8.79 (s, 1 H), 8.81 (s, 1 H), 11.82 (s, 1 H); ¹³C NMR (125 MHz, CDCl₃) δ 12.26, 46.59, 107.5, 116.4, 125.1, 127.2, 129.8, 133.0, 138.7, 149.0, 164.5, 165.0, 166.6. MS (ESI) *m/z* 377.1 (M+1)⁺.

1-(4-*tert*-Butylbenzamido)-5-*N,N*-diethylamino-2,4-dinitrobenzene (II-2f):



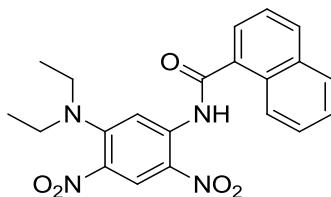
Yellow solid; 78 % yield; mp 171-173 °C; ¹H NMR (500 MHz, CDCl₃) δ 1.31 (t, 6 H, *J* = 7 Hz), 1.36 (s, 9 H), 3.41 (q, 4 H, *J* = 7 Hz), 7.57 (d, 2 H, *J* = 8.5 Hz), 7.93 (d, 2 H, *J* = 8.5 Hz), 8.81 (s, 1 H), 8.84 (s, 1 H), 11.82 (s, 1 H); ¹³C NMR (125 MHz, CDCl₃) δ 12.29, 31.07, 35.14, 46.55, 107.5, 125.2, 126.13, 127.29, 130.76, 132.9, 139.0, 149.0, 156.8, 166.2. MS (ESI) *m/z* 415.2 (M+1)⁺.

1-(Cyclohexanecarboxamido)-5-*N,N*-diethylamino-2,4-dinitrobenzene (II-2g):



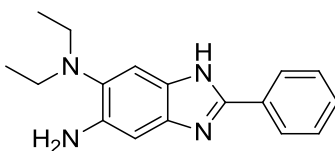
Yellow solid; 81 % yield; mp 129-131 °C; ¹H NMR (500 MHz, CDCl₃) δ 1.25 (t, 6 H, *J* = 7 Hz), 1.33-1.5 (m, 5 H), 1.69 (m, 1 H), 1.83 (m, 2 H), 2.02 (m, 2 H), 2.36 (m, 1 H), 3.33 (q, 4 H, *J* = 7 Hz), 8.62 (s, 1 H), 8.71 (s, 1 H), 10.91 (s, 1 H); ¹³C NMR (125 MHz, CDCl₃) δ 12.19, 25.24, 25.51, 28.71, 29.35, 46.40, 47.29, 107.6, 124.9, 127.0, 132.6, 138.6, 148.9, 175.9. MS (ESI) *m/z* 365.1 (M+1)⁺.

1-(Naphthalene-1-carboxamido)-5-*N,N*-diethylamino-2,4-dinitrobenzene (II-2h):



Orange solid; 80 % yield; mp 135-137 °C; ¹H NMR (400 MHz, CDCl₃) δ 1.30 (t, 6 H, *J* = 7.2 Hz), 3.41 (q, 4 H, *J* = 7 Hz), 7.57 (m, 3 H), 7.86 (t, 2 H, *J* = 8 Hz), 7.98 (d, 1 H, *J* = 8.4 Hz), 8.50 (d, 1 H, *J* = 8.4 Hz), 8.72 (s, 1 H), 8.82 (s, 1 H), 11.47 (s, NH); ¹³C NMR (100 MHz, CDCl₃) δ 12.16, 46.43, 107.4, 124.6, 124.8, 125.8, 126.6, 127.0, 127.6, 128.4, 130.0, 132.3, 132.7, 133.7, 138.5, 148.8, 167.9. MS (ESI) *m/z* 409.1 (M+1)⁺.

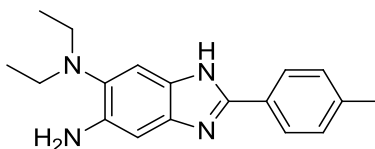
5-Amino-6-*N,N*-diethylamino-2-phenyl-1*H*-benzo[d]imidazole (II-3a):



To a solution of **II-2a** (700 mg, 1.95 mmol) in dioxane (50 mL) and ethanol (50 mL) was added ammonium formate (3.22 g) and 10 wt. % Pd-C (300 mg) with stirring. The reaction mixture turned from yellow to red and then to colorless in 45-60 min at room temperature. The catalyst and excess ammonium formate were filtered off to give the product solution. Concentrated hydrochloric acid was added to this solution and adjusted to 4 N HCl concentration. Then the mixture was refluxed for 4-6 h. The reaction mixture was basified by addition of ammonium hydroxide, extracted with ethyl acetate (40 mL x 3) and dried over anhydrous magnesium sulfate. The crude product was purified by flash chromatography on silica gel using ethyl acetate/hexanes (gradient 20-40 % ethyl acetate/hexanes) as eluent to give pure **II-3a** as a brown solid (250 mg, 50 % yield); mp 105-106 °C; ¹H NMR (300 MHz, CDCl₃) δ 0.96 (t, 6 H, *J* = 6.9 Hz), 2.92 (q, 4 H, *J* = 6.9 Hz), 6.89 (s, 1 H), 7.32 (m, 4 H), 8.05 (d, 2 H, *J* = 9.5 Hz); ¹³C NMR (100 MHz, CDCl₃) δ 15.27, 51.23, 100.2, 113.9, 128.9, 131.5, 132.0, 132.9, 137.9, 144.1, 153.0; HRMS (FAB) *m/z* calcd for C₁₇H₂₀N₄H⁺: 281.1758, Found: 281.1766 (Δ = -2.8 ppm). HPLC(2): 9.02 min, purity > 99 %.

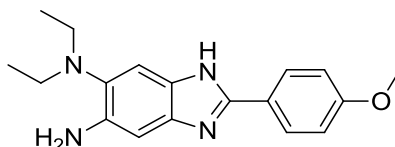
Compounds **II-3a** ~ **II-3h** were prepared in the same manner.

5-Amino-6-*N,N*-diethylamino-2-(4-methylphenyl)-1*H*-benzo[d]imidazole (II-3b):



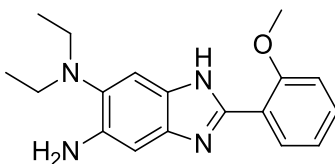
Brown solid; 52 % yield; mp 114-116 °C; ¹H NMR (400 MHz, CDCl₃) δ 0.90 (t, 6 H, *J* = 6.8 Hz), 2.30 (s, 3 H), 2.85 (q, 4 H, *J* = 6.8 Hz), 6.77 (s, 1 H), 7.12 (d, 2 H, *J* = 8 Hz), 7.21 (s, 1 H), 7.97 (d, 2 H, *J* = 8.4 Hz); ¹³C NMR (100 MHz, CDCl₃) δ 12.55, 21.27, 48.53, 97.78, 110.88, 126.2, 127.5, 129.5, 134.4, 135.0, 139.3, 141.2, 150.8; HRMS (FAB) *m/z* calcd for C₁₈H₂₂N₄H⁺: 295.1919, Found: 295.1923 (Δ = -1.4 ppm). HPLC(2): 7.20 min, purity > 99 %.

5-Amino-6-*N,N*-diethylamino-2-(4-methoxyphenyl)-1*H*-benzo[d]imidazole (II-3c):



Brown solid; 56 % yield; mp 100-103 °C; ¹H NMR (400MHz, CDCl₃) δ 0.88 (t, 6 H, *J* = 6.8 Hz), 2.83 (q, 4 H, *J* = 7.2 Hz), 3.71 (s, 3 H), 6.78 (m, 3 H), 7.18 (s, 1 H) 8.05 (d, 2 H, *J* = 8.8 Hz); ¹³C NMR (100 MHz, CDCl₃) δ 12.55, 48.49, 55.17, 97.85, 110.4, 114.2, 122.7, 128.0, 133.8, 135.0, 135.1, 141.1, 150.7, 160.5; HRMS (FAB) *m/z* calcd for C₁₈H₂₂N₄OH⁺: 311.1864, Found: 311.1872 (Δ = -2.6 ppm). HPLC(1): 9.22 min, purity > 89 %.

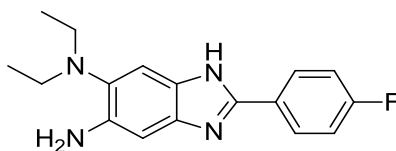
5-Amino-6-*N,N*-diethylamino-2-(2-methoxyphenyl)-1*H*-benzo[d]imidazole (II-3d):



Brown solid; 45 % yield; mp 171-175 °C; ¹H NMR (400 MHz, CDCl₃) δ 0.97 (t, 6 H, *J* = 6.8 Hz), 2.97 (q, 4 H, *J* = 7.2 Hz), 3.96 (s, 3 H), 6.88 (s, 1 H), 6.97 (d, 1 H, *J* = 8.4 Hz), 7.06 (t, 1 H, *J* = 8 Hz), 7.31 (t, 1 H, *J* = 8.5 Hz), 7.37 (s, 1 H), 8.49 (d, 1 H, *J* = 9.6 Hz); ¹³C NMR (100 MHz, CDCl₃) δ 12.49, 48.52, 55.73, 97.31, 111.3, 118.2, 121.4, 129.4, 130.2, 133.1, 134.9, 141.2,

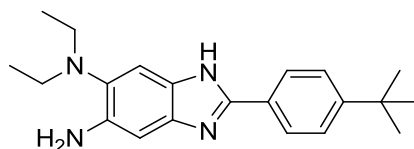
148.1, 156.2; HRMS (FAB) m/z calcd for $C_{18}H_{22}N_4OH^+$: 311.1867, Found: 311.1872 ($\Delta = -1.6$ ppm). HPLC(2): 7.99 min, purity > 99 %.

5-Amino-6-*N,N*-diethylamino-2-(4-fluorophenyl)-1*H*-benzo[d]imidazole (II-3e):



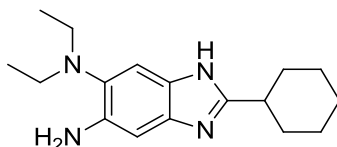
Brown solid; 55 % yield; mp 105-107 °C; 1H NMR (300MHz, $CDCl_3$) δ 0.96 (t, 6 H, $J = 7$ Hz), 2.92 (q, 4 H, $J = 7.2$ Hz), 6.85 (s, 1 H), 7.04 (t, 2 H, $J = 8.0$ Hz), 7.31 (s, 1 H), 7.98 (ddd, 2 H, $J = 1.8, 5.4, 8.7$ Hz); ^{13}C NMR (100 MHz, $CDCl_3$) δ 12.53, 48.44, 97.37, 110.8, 115.9, 116.0, 125.9, 128.2, 133.9, 134.4, 135.6, 141.7, 149.0, 162.4, 164.4; HRMS (FAB) m/z calcd for $C_{17}H_{19}FN_4H^+$: 299.1668, Found: 299.1672 ($\Delta = -1.3$ ppm). HPLC(2): 9.54 min, purity > 96 %.

5-Amino-6-*N,N*-diethylamino-2-(4-*tert*-butylphenyl)-1*H*-benzo[d]imidazole (II-3f):



Brown solid; 50 % yield; mp 95-96 °C; 1H NMR (400 MHz, $CDCl_3$) δ 0.90 (t, 6 H, $J = 6.8$ Hz), 1.25 (s, 9 H), 2.82 (q, 2 H, $J = 6.8$ Hz), 6.81 (s, 1 H), 7.26 (s, 1 H), 7.32 (d, 2 H, $J = 8.4$ Hz), 8.15 (d, 2 H, $J = 8.4$ Hz); ^{13}C NMR (125 MHz, $CDCl_3$) δ 12.57, 31.02, 34.55, 48.39, 97.15, 110.4, 125.6, 126.3, 127.4, 134.1, 135.0, 135.5, 140.9, 151.0, 152.3; HRMS (FAB) m/z calcd for $C_{21}H_{28}N_4H^+$: 337.2393, Found: 337.2392 ($\Delta = -2.7$ ppm). HPLC(2): 9.16 min, purity > 99 %.

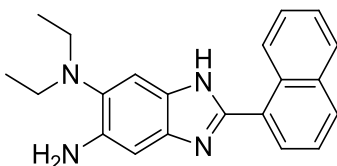
5-Amino-2-cyclohexyl-6-*N,N*-diethylamino-1*H*-benzo[d]imidazole (II-3g):



Dark brown solid; 50 % yield; mp 102-104 °C; 1H NMR (300 MHz, $CDCl_3$) δ 1.27 (t, 6 H, $J = 6.9$ Hz), 1.52 (m, 5 H), 1.75 (m, 1 H), 1.89 (m, 2 H), 2.04 (m, 2 H), 2.39 (m, 1 H), 3.37 (t, 4 H, $J = 7.2$ Hz), 8.65 (s, 1 H), 8.76 (s, 1 H); ^{13}C NMR (100 MHz, $CDCl_3$) δ 12.55, 25.62, 25.90, 31.84,

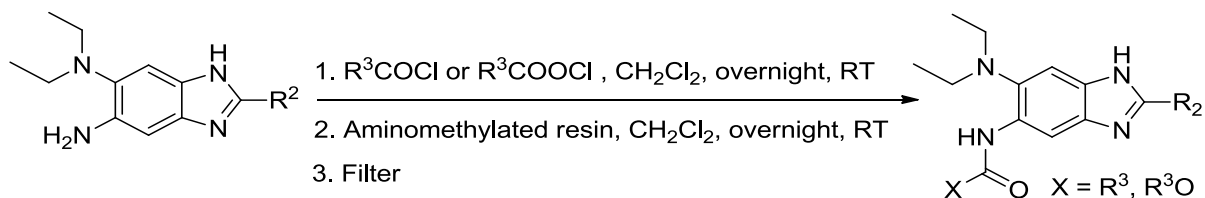
38.46, 48.66, 98.28, 109.9, 132.9, 134.1, 134.6, 140.2, 158.1. HRMS (FAB) m/z calcd for $C_{17}H_{26}N_4H^+$: 287.2231, Found: 287.2236 ($\Delta = -1.7$ ppm). HPLC(2): 8.36 min, purity > 98 %.

5-Amino-6-*N,N*-diethylamino-2-(naphth-1-yl)-1*H*-benzo[d]imidazole (II-3h):

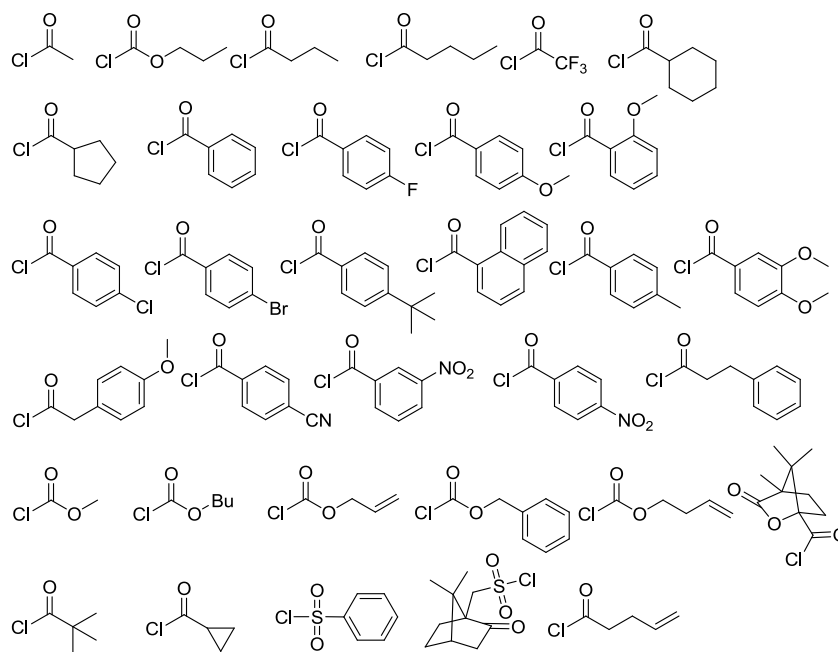


Off white solid; 48 % yield; mp 101-104 °C; 1H NMR (500MHz, $CDCl_3$) δ 0.94 (t, 6 H, $J = 7.2$ Hz), 2.95 (broad s, 4 H, $J = 7.2$ Hz), 7.54 (m, 3 H), 7.68 (s, 1 H), 7.91 (m, 3 H), 8.81 (d, 2 H, $J = 8$ Hz), 8.99 (s, 1 H), 9.4 (s, 1 H), 12.48 (s, 1 H); ^{13}C NMR (125 MHz, $CDCl_3$) δ 12.94, 24.49, 50.65, 100.9, 113.7, 124.8, 126.1, 126.3, 127.0, 127.9, 128.1, 128.5, 129.9, 131.2, 132.3, 132.5, 133.8, 134.9, 140.4, 152.2, 168.5; HRMS (FAB) m/z calcd for $C_{21}H_{22}N_4H^+$: 331.1929, Found: 331.1923 ($\Delta = -1.8$ ppm). HPLC(2): 8 min, purity > 99 %.

Synthesis of the library of 2,5,6-trisubstituted benzimidazoles II-A:



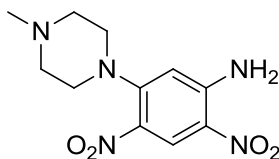
List of Acylating reagents



The intermediates **II-3a~II-3h** (0.005 mmol), thus synthesized, were dissolved in dichloromethane and transferred into 96 well plates, and to these wells were added 33 different acyl chlorides (1.1 eq.) or alkyl chloroformates (1 eq) and reacted overnight on a shaker. Acyl chlorides and alkyl chloroformates used for the library synthesis are shown in Figure S1. Aminomethylated polystyrene resin EHL (200-400 mesh), 2 % DVB (10 eq) was added to scavenge excess or unreacted acyl chlorides or alkyl chloroformates. After reacting on a shaker overnight, the resin was filtered to provide the library of 2,5,6-trisubstituted benzimidazoles **II-A**. The products were analyzed by LC-MS/UV for their purity and confirmation of the structure. The purity was in the range of 80-90 %.

§ 2.4.2 Synthesis of 2,5,6-Trisubstituted Benzimidazole Library II-B

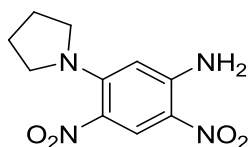
2,4-dinitro-5-(4-Methylpiperazin-1-yl)aniline (**II-4a**):



To a solution of 2,4-dinitro-5-fluoroaniline (2 g, 9.95 mmol) and DIPEA (2.01 mL, 11.94 mmol) in tetrahydrofuran (50 mL) was added a solution of *N*-methylpiperazine (1.19 g, 11.94 mmol) in tetrahydrofuran (50 mL), dropwise. The mixture was stirred at room temperature for 4 h. The reaction mixture was diluted with dichloromethane, washed with water (30 mL x 3) and dried over anhydrous magnesium sulfate. The solvent was evaporated to afford **II-4a** as a yellow solid (1.40 g, 98% yield): mp 148-150 °C: ¹H NMR (400 MHz, acetone-d₆) δ 2.26 (s, 3 H), 2.50 (t, 4 H, *J* = 4.8 Hz), 3.11 (t, 4 H, *J* = 4.8 Hz), 6.56 (s, 1 H), 7.50 (broad s, 2 H), 8.79 (s, 1 H); ¹³C NMR (100 MHz, acetone-d₆) δ 46.28, 51.55, 55.25, 105.4, 124.9, 128.6, 132.0, 150.2, 151.8; MS (ESI) *m/z* 282.1 (M+1)⁺.

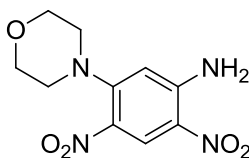
In the same manner, compounds **II-4b~ II-4g** were prepared.

2,4-Dinitro-5-(pyrrolidin-1-yl)aniline (II-4b):



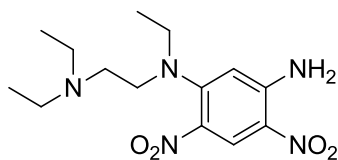
Yellow solid; quantitative yield; mp 169-171 °C; ¹H NMR (500 MHz, CDCl₃) δ 2.0 (m, 4 H), 3.27 (m, 4 H), 5.91 (s, 1 H), 6.30 (broad s, NH), 8.71 (s, 1 H); ¹³C NMR (125 MHz, CDCl₃) δ 25.63, 50.96, 98.26, 122.8, 127.9, 130.1, 146.7, 147.2; MS (ESI) *m/z* 255.1 (M+1)⁺.

2,4-dinitro-5-Morpholinoaniline (II-4c):



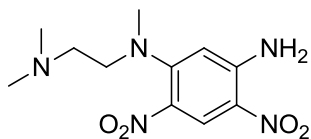
Yellow solid; 93% yield; mp 194-195 °C; ¹H NMR (400 MHz, acetone-d₆) δ 3.11 (t, 4 H, *J* = 4.8 Hz), 3.77 (t, 4 H, *J* = 4.8 Hz), 6.60 (s, 1 H), 7.54 (broad s, 2 H), 8.78 (s, 1 H); ¹³C NMR (100 MHz, acetone-d₆) δ 52.04, 66.93, 105.5, 125.2, 128.7, 131.9, 150.3, 151.9; MS (ESI) *m/z* 260 (M+1)⁺.

3-(*N',N',N*-Triethylethylenediamino)-4,6-dinitroaniline (II-4d):



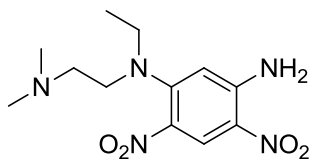
Brown oil; 99 % yield; ^1H NMR (300 MHz, CDCl_3) δ 0.99 (t, 6 H, $J = 7.2$ Hz), 1.20 (t, 3 H, $J = 7.2$ Hz), 2.50 (q, 4 H, $J = 7.2$ Hz), 2.60 (t, 2 H, $J = 7.5$ Hz), 3.25 (m, 4 H), 6.17 (s, 1 H), 6.37 (broad s, 2 H), 8.75 (s, 1 H). ^{13}C NMR (100 MHz, acetone- d_6) δ 12.54, 12.74, 47.51, 48.05, 51.20, 51.40, 104.6, 124.1, 128.2, 132.5, 149.7, 150.3; Mass (ESI) m/z 326.2 ($\text{M}+1$) $^+$.

3-(*N',N',N*-Trimethylethylenediamino)-4,6-dinitroaniline (II-4e):



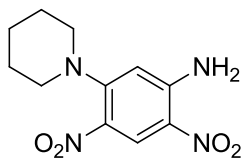
Yellow solid; 93% yield; mp 134–135 °C; ^1H NMR (400 MHz, acetone- d_6) δ 2.16 (s, 6 H), 2.55 (t, 2 H, $J = 6.4$ Hz), 2.93 (s, 3 H), 3.28 (t, 2 H, $J = 6.9$ Hz), 6.48 (s, 1 H), 7.37 (broad s, 2 H), 8.62 (s, 1 H); ^{13}C NMR (100 MHz, acetone- d_6) δ 40.17, 45.89, 53.17, 57.13, 102.7, 123.9, 128.5, 131.5, 149.7, 151.1; MS (ESI) m/z 284.1 ($\text{M}+1$) $^+$.

3-(*N',N'*-Dimethyl-*N*-ethylethylenediamino)-4,6-dinitroaniline (II-4f):



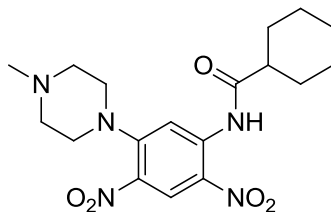
Yellow solid; 88% yield; mp 83-85 °C; ^1H NMR (400 MHz, acetone- d_6) δ 1.18 (t, 3 H, $J = 7.0$ Hz), 2.16 (s, 6 H), 2.48 (t, 2 H, $J = 7.2$ Hz), 3.29 (m, 4 H), 6.56 (s, 1 H), 7.41 (broad s, 2 H), 8.60 (s, 1 H); ^{13}C NMR (100 MHz, acetone- d_6) δ 12.67, 45.93, 47.45, 50.54, 57.33, 104.5, 124.0, 128.2, 132.4, 149.8, 150.3; MS (ESI) m/z 298.1 ($\text{M}+1$) $^+$.

2,4-Dinitro-5-(piperidin-1-yl)aniline (II-4g):



Yellow solid; 98% yield; mp 115-116 °C; ¹H NMR (400 MHz, acetone-d₆) δ 1.64 (m, 6 H), 3.08 (t, 4 H, *J* = 4.8 Hz), 6.51 (s, 1 H), 7.43 (broad s, 2 H), 8.69 (s, 1 H); ¹³C NMR (100 MHz, acetone-d₆) δ 24.64, 26.27, 52.72, 104.81, 124.6, 128.5, 131.9, 150.2, 152.2; MS (ESI) *m/z* 267.1 (M+1)⁺.

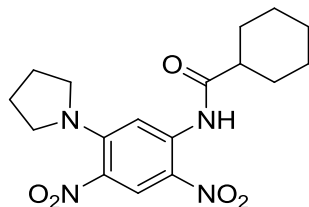
1-Cyclohexanecarboxamido-2,4-dinitro-5-(4-methylpiperazin-1-yl)benzene (II-5a):



A solution of **II-4a** (2.79 g, 9.94 mmol) and cyclohexanecarbonyl chloride (2.03 mL, 14.91 mmol) in pyridine (30 mL) was refluxed overnight. The reaction mixture was diluted with dichloromethane, washed with water (30 mL x 3) and dried over anhydrous magnesium sulfate. The crude product was purified by flash chromatography on silica gel using ethyl acetate as eluent to give **II-5a** as yellow solid (3.28 g, 74 % yield): mp 90-92 °C; ¹H NMR (400 MHz, CDCl₃) δ 1.23-1.39 (m, 3 H), 1.50 (m, 2 H, *J* = 12.4 Hz), 1.70 (d, 1 H, *J* = 12 Hz), 1.83 (m, 2 H, *J* = 12 Hz), 2.04 (m, 2 H, *J* = 12 Hz), 2.37 (m, 4 H), 2.58 (t, 4 H, *J* = 4.5 Hz), 3.33 (t, 4 H, *J* = 4.5 Hz), 8.62 (s, 1 H), 8.85 (s, 1 H), 10.91 (s, 1 H); ¹³C NMR (100 MHz, CDCl₃) δ 25.44, 29.36, 45.76, 47.28, 50.52, 54.15, 108.7, 126.2, 127.2, 132.8, 139.4, 150.2, 175.9. MS (ESI) *m/z* 392.1 (M+1)⁺.

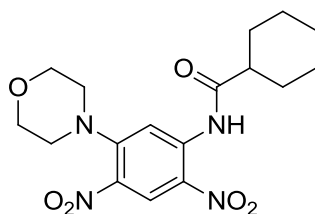
In the same manner, compounds **II-5b**~ **II-5g** were prepared.

1-Cyclohexanecarboxamido-2,4-dinitro-5-(pyrrolidin-1-yl)benzene (II-5b):



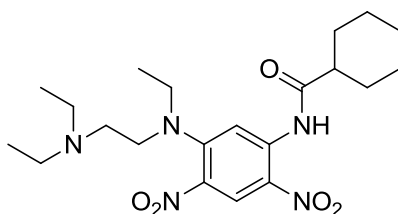
Yellow solid; 83 % yield; mp 181-182 °C; ^1H NMR (500 MHz, CDCl_3) δ 1.6-1.3 (m, 7 H), 1.73 (m, 1 H), 1.87 (m, 2 H), 2.02 (m, 6 H), 2.37 (m, 1 H), 3.37 (m, 4 H), 8.46 (s, 1 H), 8.71 (s, 1 H), 10.95 (s, 1 H); ^{13}C NMR (125 MHz, CDCl_3) δ 25.43, 25.46, 25.52, 29.33, 47.21, 51.26, 104.8, 124.2, 126.8, 130.8, 138.2, 146.5, 175.8. Ms (ESI) m/z 363.1 ($\text{M}+1$) $^+$.

1-Cyclohexanecarboxamido-2,4-dinitro-5-N-morpholinobenzene (II-5c):



Yellow solid; 93% yield; mp 160-161 °C; ^1H NMR (300 MHz, CDCl_3) δ 1.23-1.54 (m, 4 H), 1.74 (m, 2 H), 1.84-2.04 (m, 4 H), 2.37 (m, 1 H), 3.28 (t, 4 H, $J = 4.5$ Hz), 3.85 (t, 4 H, $J = 4.5$ Hz), 8.64 (s, 1 H), 8.87 (s, 1 H); ^{13}C NMR (100 MHz, CDCl_3) δ 25.43, 28.76, 29.36, 47.28, 50.97, 66.09, 108.7, 126.6, 127.1, 132.9, 139.5, 150.4, 176.0; MS (ESI) m/z 379.2 ($\text{M}+1$) $^+$.

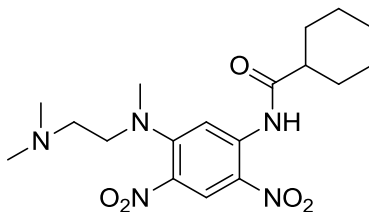
1-Cyclohexanecarboxamido-2,4-dinitro-5-*N,N,N'*-triethylethylenediaminobenzene (II-5d):



Yellow oil; 94 % yield; ^1H NMR (400 MHz, CDCl_3) δ 1.01 (t, 6 H, $J = 7.2$ Hz), 1.24 (t, 3 H, $J = 7.2$ Hz), 1.37-1.72 (m, 5 H), 1.99 (m, 2 H), 2.35 (m, 1 H), 2.61 (q, 4 H, $J = 6.8$ Hz), 2.74 (t, 2 H, $J = 7.6$ Hz), 3.38 (q, 2 H, $J = 6.8$ Hz), 3.45 (t, 2 H, $J = 6.8$ Hz), 8.62 (s, 1 H), 8.71 (s, 1 H), 10.93 (s, 1 H); ^{13}C NMR (100 MHz, CDCl_3) δ 10.72, 12.25, 25.52, 25.86, 29.3, 43.86, 46.6, 47.28,

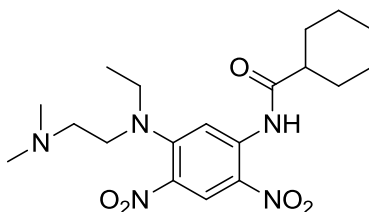
47.56, 49.35, 49.58, 107.9, 125.3, 126.9, 132.9, 138.7, 149.1, 175.7, 180.6; MS (ESI) m/z 436.2 (M+1)⁺.

1-Cyclohexanecarboxamido-2,4-dinitro-5-*N',N',N'*-trimethylethylenediaminobenzene (II-5e):



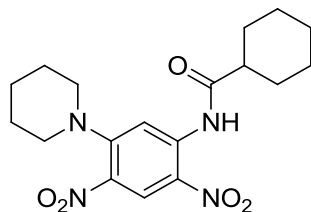
Yellow solid; 83% yield; mp 160-161 °C; ¹H NMR (300 MHz, CDCl₃) δ 1.19-1.33 (m, 3 H), 1.47 (m, 2 H, *J* = 12.4 Hz), 1.67 (m, 1 H), 1.82 (m, 2 H), 1.97 (m, 2 H), 2.22 (s, 6 H), 2.37 (m, 1 H), 2.67 (t, 2 H, *J* = 6.8 Hz), 2.96 (s, 3 H), 3.5 (t, 2 H, *J* = 6.8 Hz), 8.58 (s, 1 H), 8.71 (s, 1 H), 10.90 (s, 1 H); ¹³C NMR (100 MHz, CDCl₃) δ 25.39, 25.47, 29.29, 40.52, 45.5, 47.22, 52.48, 55.79, 106.6, 124.9, 127.1, 131.7, 138.6, 149.7, 175.6; MS (ESI) m/z 394.2 (M+1)⁺.

1-Cyclohexanecarboxamido-2,4-dinitro-5-*N',N'*-dimethyl-*N*-ethylethylenediaminobenzene (II-5f):



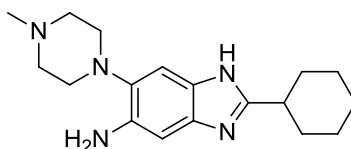
Yellow solid; 50% yield; mp 212-213 °C; ¹H NMR (400 MHz, CDCl₃) δ 1.23 (t, 3 H, *J* = 7.2 Hz), 1.35 (m, 2 H), 1.51 (m, 2 H), 1.68 (m, 1 H), 1.82 (m, 2 H), 1.98 (m, 2 H), 2.22 (s, 6 H), 2.36 (m, 1 H), 2.54 (t, 2 H, *J* = 7.2 Hz), 3.40 (m, 4 H), 8.64 (s, 1 H), 8.73 (s, 1 H), 10.93 (s, 1 H); ¹³C NMR (100 MHz, CDCl₃) δ 12.35, 25.47, 25.53, 29.38, 45.52, 47.32, 50.05, 56.09, 108.0, 125.2, 126.9, 132.9, 138.7, 149.2, 175.8; MS (ESI) m/z 408.3 (M+1)⁺.

1-Cyclohexanecarboxamido-2,4-dinitro-5-piperidinylbenzene (II-5g):



Yellow solid; 96% yield; mp 154-155 °C; ^1H NMR (400 MHz, CDCl_3) δ 1.30 (m, 3 H), 1.47 (m, 2 H), 1.69 (m, 7 H), 1.82 (m, 2 H), 2.00 (m, 2 H), 2.38 (m, 1 H), 3.22 (t, 4 H, $J = 4.2$ Hz), 8.57 (s, 1 H), 8.77 (s, 1 H), 10.96 (s, 1 H); ^{13}C NMR (100 MHz, CDCl_3) δ 25.52, 25.24, 25.36, 29.26, 47.15, 51.88, 108.3, 125.5, 127.2, 132.4, 139.1, 150.5, 175.80; MS (ESI) m/z 377.1 ($\text{M}+1$) $^+$.

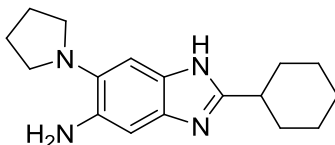
5-Amino-2-cyclohexyl-6-(4-methylpiperazinyl)-1H-benzo[d]imidazole (II-6a):



To a solution of **II-5a** (2.06 g, 5.28 mmol) in ethanol (30 mL) and dioxane (36 mL) was added solid stannous chloride dihydrate (6.99g, 37 mmol). Concentrated hydrochloric acid (33 mL) was added to the reaction mixture such that the final concentration of HCl is 4 N in the reaction flask. The reaction mixture was refluxed for 4 h. Upon completion, the reaction mixture was basified with 30% sodium hydroxide solution. Excess stannous chloride formed a soluble salt in excess base. The desired product was extracted with dichloromethane and purified by flash chromatography on silica gel using ethyl acetate/ethanol (98/2) as eluent to afford **II-6a** as a pale brown solid (1.32 g, 82 % yield): mp 143-145 °C; ^1H NMR (400 MHz, CDCl_3) δ 1.25 (m, 3 H), 1.61 (m, 3 H), 1.75 (m, 2 H), 2.02 (m, 2 H), 2.31 (s, 3 H), 2.50 (broad m, 4 H), 2.78 (m, 1 H), 2.86 (broad s, 4 H), 6.74 (s, 1 H), 7.16 (s, 1 H); ^{13}C NMR (100 MHz, CDCl_3) δ 25.70, 25.95, 30.50, 31.87, 38.47, 46.01, 51.78, 55.85, 98.89, 106.9, 132.5, 134.7, 136.4, 137.7, 158.0; HRMS (FAB) m/z calcd for $\text{C}_{18}\text{H}_{27}\text{N}_5\text{H}^+$: 314.2345, Found: 314.2348 ($\Delta = 1.0$ ppm). HPLC(1): 6.37 min, purity > 99 %.

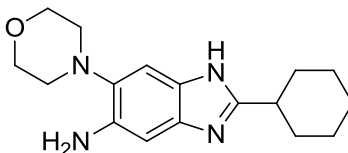
In the same manner, compounds **II-6b**~ **II-6g** were prepared.

5-Amino-2-cyclohexyl-6-(pyrrolidin-1-yl)-1H-benzo[d]imidazole (II-6b):



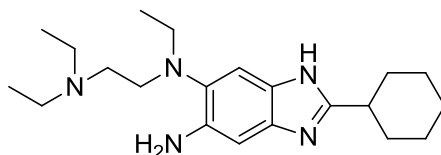
Off white solid; 50 % yield; mp 138-140 °C; ^1H NMR (300 MHz, CDCl_3) δ 1.29-1.12 (m, 3 H), 1.5-1.79 (m, 5 H), 1.85 (broad s, 4 H), 2.07 (m, 2 H), 2.81 (m, 1 H), 2.97 (q, 4 H, $J = 5.4$ Hz), 6.80 (s, 1 H), 7.23 (s, 1 H); ^{13}C NMR (100 MHz, CDCl_3) δ 23.97, 25.78, 26.01, 31.94, 38.48, 51.92, 98.81, 106.1, 132.9, 133.8, 134.78, 138.28, 157.53, HRMS (FAB) m/z calcd for $\text{C}_{17}\text{H}_{24}\text{N}_4\text{H}^+$: 285.2072, Found: 285.2079 ($\Delta = -2.5$ ppm). HPLC(2): 7.84 min, purity > 99 %.

5-Amino-2-cyclohexyl-6-(morpholino)-1H-benzo[d]imidazole (II-6c):



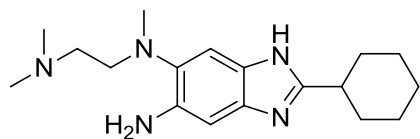
Brown solid; 79% yield; mp 124-125 °C; ^1H NMR (400 MHz, CDCl_3) δ 1.23-1.39 (m, 4 H), 1.59-1.84 (m, 5 H), 2.10 (m, 2 H), 2.82 (m, 1 H), 2.89 (t, 4 H, $J = 4.5$ Hz), 3.85 (t, 4 H, $J = 4.5$ Hz), 6.83 (s, 1 H), 7.26 (s, 1 H), 10.94 (s, 1 H); ^{13}C NMR (100 MHz, CDCl_3) δ 25.80, 29.58, 31.78, 38.30, 45.63, 52.33, 67.66, 98.19, 107.4, 136.3, 138.1, 157.3; HRMS (FAB) m/z calcd for $\text{C}_{17}\text{H}_{24}\text{N}_4\text{OH}^+$: 301.2028, Found: 301.2022 ($\Delta = -2.0$ ppm). HPLC(1): 7.09 min, purity > 99 %.

5-Amino-2-cyclohexyl-6-(*N,N,N*-triethylethylenediamino)-1H-benzo[d]imidazole (II-6d):



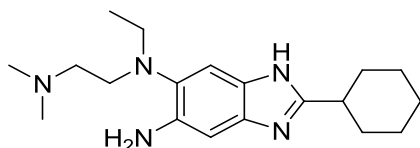
Pale brown solid; 81 % yield; mp: turned black at 120 °C; ^1H NMR (300 MHz, CDCl_3) δ 0.95 (t, 9 H, $J = 7.2$ Hz), 1.20-1.35 (m, 5 H), 1.59-1.81 (m, 6 H), 2.05 (m, 2 H), 2.42 (m, 6 H), 2.79 (m, 1 H), 2.90 (m, 2 H, $J = 6.9$ Hz), 2.98 (t, 2 H, $J = 6.9$ Hz), 6.78 (s, 1 H), 7.27 (s, 1 H); ^{13}C NMR (100 MHz, CDCl_3) δ 11.28, 12.33, 25.43, 25.51, 25.81, 31.75, 38.38, 46.94, 49.08, 51.01, 52.98, 98.05, 109.8, 133.0, 133.9, 140.1, 158.0; HRMS (FAB) m/z calcd for $\text{C}_{21}\text{H}_{35}\text{N}_5\text{H}^+$: 358.2971, Found: 358.2975 ($\Delta = 1.1$ ppm). HPLC(1): 8.74 min, purity > 96 %.

5-Amino-2-cyclohexyl-6-(*N',N',N*-trimethylethylenediamino)-1*H*-benzo[d]imidazole (II-6e):



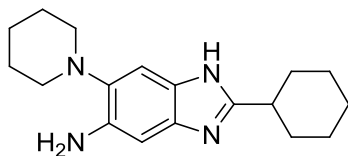
Pale brown solid; 59% yield; mp: turned black at 120 °C; ¹H NMR (400 MHz, CDCl₃) δ 1.25 (m, 3 H), 1.60-1.76 (m, 5 H), 2.04 (m, 2 H), 2.24 (s, 6 H), 2.42 (t, 2 H, *J* = 6.4 Hz), 2.59 (s, 3 H), 2.80 (m, 1 H), 2.92 (t, 2 H, *J* = 6.4 Hz), 6.75 (s, 1 H), 7.22 (s, 1 H); ¹³C NMR (100 MHz, CDCl₃) δ 25.71, 25.97, 31.89, 38.42, 42.96, 45.45, 54.74, 57.36, 98.20, 108.3, 132.6, 134.2, 136.7, 139.1, 157.8; HRMS (FAB) *m/z* calcd for C₁₈H₂₉N₅H⁺: 316.2501, Found: 316.2498 (Δ = -0.9 ppm). HPLC(1): 6.57 min, purity > 98 %.

5-Amino-2-cyclohexyl-6-(*N',N'*-dimethyl-*N*-ethylethylenediamino)-1*H*-benzo[d]imidazole (II-6f):



Pale brown solid; 74% yield; mp: turned black at 120 °C; ¹H NMR (400 MHz, CDCl₃) δ 0.89 (t, 3 H, *J* = 7.2 Hz), 1.12-1.29 (m, 3 H), 1.56-1.74 (m, 5 H), 2.01 (m, 2 H), 2.12 (s, 6 H), 2.28 (t, 2 H, *J* = 6.8 Hz), 2.73 (m, 1 H), 2.84 (q, 2 H, *J* = 6.8 Hz), 2.97 (t, 2 H, *J* = 6.8 Hz), 6.72 (s, 1 H), 7.23 (s, 1 H); ¹³C NMR (100 MHz, CDCl₃) δ 12.48, 25.68, 25.95, 31.85, 38.50, 45.54, 49.91, 52.99, 57.43, 63.38, 98.01, 110.3, 133.5, 133.9, 134.6, 140.4, 158.1; HRMS (FAB) *m/z* calcd for C₁₉H₃₁N₅H⁺: 330.2658, Found: 330.2649 (Δ = -2.7 ppm). HPLC(1): 7.61 min, purity > 99 %.

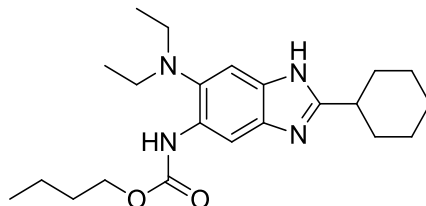
5-Amino-2-cyclohexyl-6-piperidinyl-1*H*-benzo[d]imidazole (II-6g):



Pale brown solid; 82% yield; mp > 200 °C; ¹H NMR (400 MHz, CDCl₃) δ 1.24 (m, 4 H), 1.65 (m, 8 H), 1.77 (m, 2 H), 2.07 (m, 2 H), 2.84 (broad m, 5 H), 6.89 (s, 1 H), 7.22 (s, 1 H); ¹³C NMR (100 MHz, CDCl₃) δ 24.15, 25.72, 26.01, 26.89, 32.00, 38.58, 53.58, 98.57, 107.0, 132.8, 134.3,

§ 2.4.3 Synthesis of analytically pure trisubstitutedbenzimidazoles

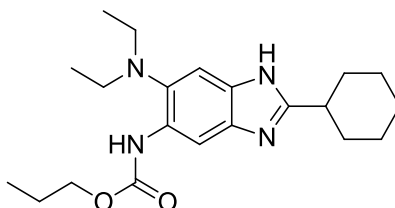
5-Butoxycarbonylamino-2-cyclohexyl-6-*N,N*-diethylamino-1*H*-benzo[d]imidazole (**II-Ag**):



To a solution of 2-cyclohexyl-5-*N,N*-diethylamino-6-amino-1*H*-benzo[d]imidazole (**II-3g**) (486 mg, 1.71 mmol) in dichloromethane (20 mL) was added a solution of *N*-butoxycarbonyloxysuccinimide (340 mg, 1.71 mmol) in dichloromethane (20 mL) dropwise at room temperature. After the addition, the reaction mixture was stirred at room temperature overnight. After the completion of the reaction, the reaction mixture was concentrated. The crude was purified via flash chromatography on silica gel (gradient 20-40% EtOAc/hexanes) to give **II-Ag** as white solid (336 mg, 51 % yield): mp 171-172 °C; ¹H NMR (500 MHz, CDCl₃) δ 0.91 (t, 6 H, *J* = 7.2 Hz), 0.96 (t, 3 H, *J* = 7.5 Hz), 1.23-1.46 (m, 5 H), 1.57-1.72 (m, 5 H), 1.81 (m, 2 H, *J* = 10 Hz), 2.07 (m, 2 H, *J* = 10 Hz), 2.85 (m, 1 H), 2.92 (q, 4 H, *J* = 7.2 Hz), 4.19 (t, 2 H, *J* = 6.5 Hz), 7.46 (s, 1 H), 8.24 (s, 1 H), 8.51 (s, 1 H); ¹³C NMR (125 MHz, CDCl₃) δ 12.72, 13.75, 19.11, 25.81, 26.02, 31.07, 31.78, 38.46, 50.43, 64.87, 98.88, 107.3, 113.3, 131.2, 132.2, 134.3, 138.5, 154.1, 158.8; HRMS (FAB) *m/z* calcd for C₂₂H₃₄N₄O₂H⁺: 387.2763, Found: 387.2760 (Δ = 0.8 ppm). HPLC(2): 10.6 min, purity >99 %.

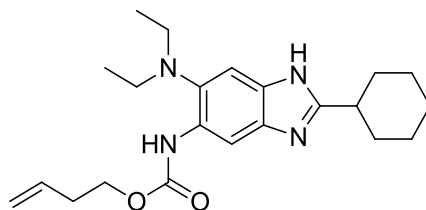
In a similar manner, **II-Ab**, **II-Ad**, **II-Ah**, **II-Ba** and **II-Bb** were synthesized and characterized.

2-Cyclohexyl-6-*N,N*-diethylamino-5-propoxycarbonylamino-1*H*-benzo[d]imidazole (**II-Ab**):



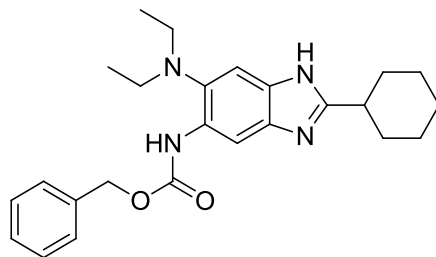
White solid; 63 % yield; mp 80-181 °C; ¹HNMR (300 MHz, CDCl₃) δ 0.92 (t, 6 H, *J* = 7.2 Hz), 0.99 (t, 3 H, *J* = 7.5 Hz), 1.25-1.41 (m, 4 H), 1.60-1.76 (m, 5 H), 1.86 (m, 2 H), 2.10 (m, 2 H), 2.87 (m, 1 H), 2.92 (m, 4 H, *J* = 6.9 Hz), 4.14 (t, 2 H, *J* = 6.6 Hz), 7.47 (s, 1 H), 8.23 (s, 1 H), 8.51 (s, 1 H); ¹³C NMR (125 MHz, CDCl₃) δ 10.28, 12.67, 22.28, 25.71, 25.96, 31.75, 38.44, 50.38, 66.56, 100.0, 112.0, 132.1, 132.4, 134.3, 136.92, 154.1, 159.0; HRMS (FAB) *m/z* calcd for C₂₁H₃₂N₄O₂H⁺: 373.2601, Found: 373.2604 (Δ = -0.8 ppm). HPLC(2): 9.98 min, purity >99 %.

5-But-3-enoxycarbonylamino-2-cyclohexyl-6-*N,N*-diethylamino-1*H*-benzo[d]imidazole (II-Ad):



White solid; 51 % yield; mp 143-145 °C; ¹HNMR (500 MHz, CDCl₃) δ 0.91 (t, *J* = 7 Hz, 6 H), 1.16-1.31 (m, 3 H), 1.56-1.66 (m, 3 H), 1.77 (d, 2 H, *J* = 13.5 Hz), 2.04 (d, 2 H, *J* = 12.5 Hz), 2.47 (t, 2 H, *J* = 6.5 Hz), 2.83 (m, 1 H), 2.88 (q, 4 H, *J* = 7.5 Hz), 4.23 (t, 2 H, *J* = 7 Hz), 5.11 (m, 2 H), 5.84 (m, 1 H), 7.41 (s, 1 H), 8.24 (s, 1 H), 8.52 (s, 1 H); ¹³C NMR (125 MHz, CDCl₃) δ 12.66, 25.72, 25.96, 31.76, 33.47, 50.39, 63.98, 99.97, 112.1, 117.1, 131.9, 132.0, 131.9, 133.9, 134.3, 137.3, 153.9, 159.2; HRMS (FAB) *m/z* calcd for C₂₂H₃₂N₄O₂H⁺: 385.2604, Found: 385.2604 (Δ = 0.0 ppm). HPLC(2): 10.1 min, purity >99 %.

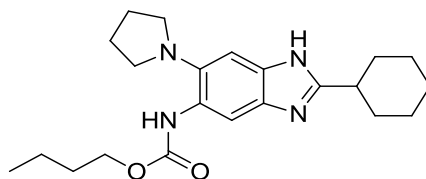
5-Benzoyloxycarbonylamino-2-cyclohexyl-6-*N,N*-diethylamino-1*H*-benzo[d]imidazole (II-Ah):



White solid; 61 % yield; mp 208-209 °C; ¹HNMR (300 MHz, CDCl₃) δ 0.90 (t, 6 H, *J* = 7.2 Hz), 1.38 (m, 4 H), 1.84-1.62 (m, 5 H), 2.11 (m, 2 H), 2.84 (m, 1 H), 2.91 (m, 4 H, *J* = 7.2 Hz), 5.22

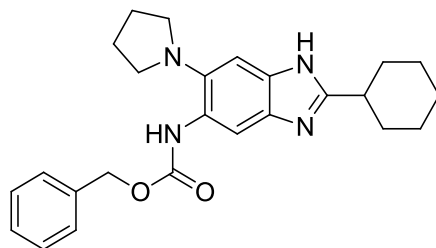
(s, 2 H), 7.45-7.35 (m, 5 H), 8.25 (s, 1 H), 8.61 (s, 1 H); ^{13}C NMR (125 MHz, CDCl_3) δ 12.62, 25.77, 25.97, 31.77, 38.46, 50.41, 66.68, 99.02, 113.2, 128.1, 128.5, 131.3, 132.0, 134.2, 136.3, 138.2, 153.7, 159.0; HRMS (FAB) m/z calcd for $\text{C}_{25}\text{H}_{32}\text{N}_4\text{O}_2\text{H}^+$: 421.2601, Found: 421.2604 ($\Delta = -0.5$ ppm). HPLC(2): 10.7 min, purity >99 %.

5-Butoxycarbonylamino-2-cyclohexyl-6-(pyrrolidin-1-yl)-1H-benzo[d]imidazole (II-Ba):



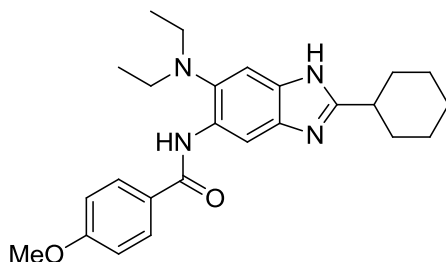
White solid; 51 % yield; mp 128-129 °C ; ^1H NMR (500 MHz, CDCl_3) δ 0.94 (t, 3 H, $J = 6.5$ Hz), 1.26-1.19 (m, 5 H), 1.73-1.55 (m, 7 H), 1.92 (bs, 4 H), 2.00 (m, 2 H), 2.76 (m, 1 H), 2.93 (bs, 4 H), 4.18 (t, $J = 6.5$ Hz, 2 H), 7.40 (s, 1 H), 7.95 (s, 1 H), 8.17 (s, 1 H); ^{13}C NMR (125 MHz, CDCl_3) δ 13.68, 19.03, 24.24, 25.71, 25.94, 30.99, 31.75, 38.45, 53.41, 64.90, 101.3, 109.80, 129.3, 131.8, 135.6, 137.5, 154.3, 159.1. HRMS (FAB) m/z calcd for $\text{C}_{22}\text{H}_{32}\text{N}_4\text{O}_2\text{H}^+$: 385.2594, Found: 385.2604 ($\Delta = -1.1$ ppm). HPLC(2): 10 min, purity >99 %.

5-Benzoyloxycarbonylamino-2-cyclohexyl-6-(pyrrolidin-1-yl)-1H-benzo[d]imidazole (II-Bb):



White solid; 68 % yield; mp 86-87 °C ^1H NMR (500 MHz, CDCl_3) δ 1.21-1.28 (m, 4 H), 1.59-1.65 (m, 4 H), 1.76 (m, 2 H), 1.91 (s, 4 H), 2.04 (d, 2H, $J = 12.5$ Hz), 2.82 (m, 1 H), 2.93 (s, 4 H), 5.22 (s, 2 H), 7.34-7.48 (m, 5 H aromatic), 8.08 (s, 1 H), 8.22 (s, 1 H); ^{13}C NMR (125 MHz, CDCl_3) δ 24.29, 25.69, 25.91, 31.72, 38.31, 53.54, 66.75, 101.5, 108.7, 128.1, 128.5, 129.6, 131.9, 136.0, 136.2, 153.8, 158.9. HRMS (FAB) m/z calcd for $\text{C}_{25}\text{H}_{30}\text{N}_4\text{O}_2\text{H}^+$: 419.2448, Found: 419.2447 ($\Delta = 0.2$ ppm). HPLC(2): 10.1 min, purity >99 %.

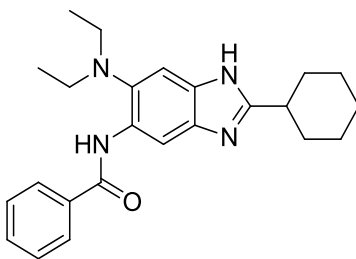
2-Cyclohexyl-6-*N,N*-diethylamino-5-(4-methoxybenzamido)-1*H*-benzo[*d*]imidazole (II-Ac):



To a solution of **II-3g** (120 mg, 0.41 mmol) in dichloromethane (10 mL) was added a solution of 4-methoxybenzoyl chloride (69 mg, 0.41 mmol) in dichloromethane (15 mL) dropwise at room temperature. After the addition, the reaction mixture was stirred at room temperature overnight. After the completion of the reaction, the reaction mixture was washed with saturated solution of sodium bicarbonate. The organic layer was dried over anhydrous magnesium sulfate and concentrated. The crude was purified by flash chromatography on silica gel (gradient: 20-40% ethyl acetate/hexanes) to give **II-Ac** as a white solid (139 mg, 79%): mp 198-199 °C; ¹H NMR (400 MHz, CDCl₃) δ 0.97 (t, 6 H, *J* = 7.2 Hz), 1.16 (m, 3 H), 1.53-1.68 (m, 5 H), 1.98 (m, 2 H), 2.71 (m, 1 H), 3.02 (q, 4 H, *J* = 7.2 Hz), 3.9 (s, 3 H), 7.05 (d, 2 H, *J* = 8.8 Hz), 7.55 (s, 1 H), 7.95 (d, 2 H, *J* = 8.8 Hz), 8.95 (s, 1 H), 10.32 (s, 1 H); ¹³C NMR (100 MHz, CDCl₃) δ 13.36, 25.85, 26.18, 31.96, 38.67, 51.02, 55.75, 101.2, 113.2, 114.2, 127.9, 128.8, 129.0, 132.1, 139.3, 135.2, 160.0, 162.6, 164.9; HRMS (FAB) *m/z* calcd for C₂₅H₃₂N₄O₂H⁺: 421.2601, Found: 421.2604 (Δ = -0.7 ppm). HPLC(2): 9.5 min, purity >99 %.

The same procedure was used for the synthesis of **II-Aa**, **II-Ae**, **II-Af**, **II-Ai~II-Ao**, **II-16a** and **II-16b**.

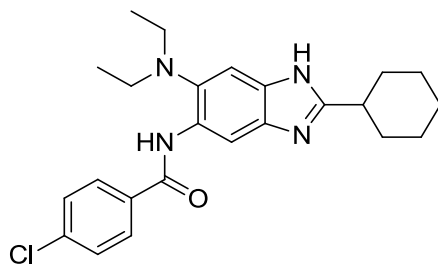
5-Benzamido-2-cyclohexyl-6-*N,N*-diethylamino-1*H*-benzo[*d*]imidazole (II-Aa):



White solid; 74 % yield; mp 180-181 °C; ¹H NMR (400 MHz, CDCl₃) δ 0.97 (t, 6 H, *J* = 7.2 Hz), 1.16 (m, 3 H), 1.65 (m, 5 H), 1.98 (m, 2 H), 2.71 (m, 1 H), 3.03 (m, 4 H, *J* = 6.8 Hz), 7.57 (m, 4

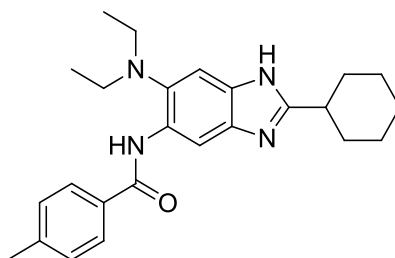
H), 7.98 (d, 2 H, $J = 6.2$ Hz), 8.97 (s, 1 H), 10.4 (s, 1 H); ^{13}C NMR (100 MHz, CDCl_3) δ 13.09, 21.48, 25.64, 25.91, 31.73, 38.40, 50.77, 100.9, 113.1, 126.9, 129.5, 131.6, 132.7, 135.15, 139.5, 159.8, 165.1; HRMS (FAB) m/z calcd for $\text{C}_{24}\text{H}_{30}\text{N}_4\text{OH}^+$: 391.2486, Found: 391.2498 ($\Delta = -3.1$ ppm). HPLC(2): 9.50 min, purity >99 %.

5-(4-Chlorobenzamido)-2-cyclohexyl-6-*N,N*-diethylamino-1*H*-benzo[d]imidazole (II-Ae):



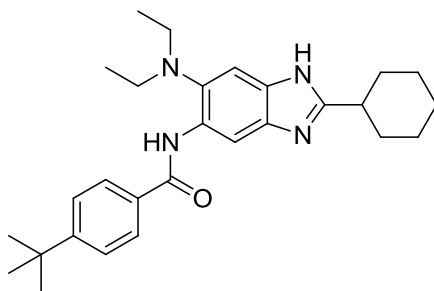
White solid; 64 % yield; mp 216-217 °C (turned brown); ^1H NMR (400 MHz, CDCl_3) δ 0.96 (t, 6 H, $J = 7.2$ Hz), 1.21-1.32 (m, 2 H), 1.59-1.81 (m, 5 H), 2.08 (m, 2 H), 2.79 (m, 1 H), 3.02 (m, 4 H, $J = 7$ Hz), 7.50 (d, 2 H, $J = 6.8$ Hz), 7.58 (s, 1 H), 7.88 (d, 2 H, $J = 8.8$ Hz), 8.82 (s, 1 H), 10.31 (s, 1 H); ^{13}C NMR (125 MHz, CDCl_3) δ 13.12, 25.75, 25.97, 29.69, 31.76, 38.47, 50.78, 100.5, 113.6, 128.3, 129.1, 131.3, 131.8, 133.9, 135.2, 137.9, 139.6, 159.5, 163.7; HRMS (FAB) m/z calcd for $\text{C}_{24}\text{H}_{29}\text{N}_4\text{OClH}^+$: 425.2108, Found: 425.2108 ($\Delta = -0.0$ ppm). HPLC(2): 10.5 min, purity >99 %.

2-Cyclohexyl-6-*N,N*-diethylamino-5-(4-methylbenzamido)-1*H*-benzo[d]imidazole (II-Af):



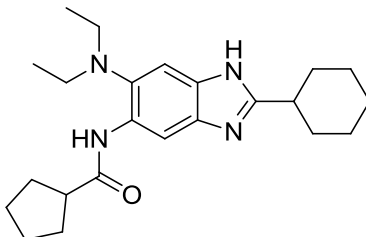
White solid; 65 % yield; mp 183-184 °C; ^1H NMR (300 MHz, CDCl_3) δ 0.97 (t, 6 H, $J = 6$ Hz), 1.2 (m, 3 H), 1.58-1.78 (m, 5 H), 2.06 (m, 2 H), 2.45 (s, 3 H), 2.76 (m, 1 H), 3.03 (q, 4 H, $J = 7.2$ Hz), 7.34 (d, 2 H, $J = 8.4$ Hz), 7.59 (s, 1 H), 7.87 (d, 2 H, $J = 8.1$ Hz), 8.91 (s, 1 H), 10.31 (s, 1 H); ^{13}C NMR (100 MHz, CDCl_3) δ 13.09, 21.48, 25.63, 25.92, 31.72, 38.40, 50.75, 100.9, 113.1, 126.8, 129.6, 131.8, 132.7, 135.0, 139.4, 142.1, 159.8, 165.1; HRMS (FAB) m/z calcd for $\text{C}_{25}\text{H}_{32}\text{N}_4\text{OH}^+$: 405.2654, Found: 405.2654 ($\Delta = -0.0$ ppm). HPLC(2): 10.1 min, purity >99 %.

2-Cyclohexyl-6-*N,N*-diethylamino-5-(4-*tert*-butylbenzamido)-1*H*-benzo[d]imidazole (II-Ai):



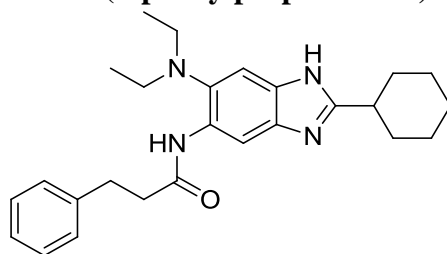
White solid; 48 % yield; mp 206-208 °C; ¹H NMR (400 MHz, CDCl₃) δ 0.99 (t, 6 H, *J* = 7.2 Hz), 1.2 (m, 3 H), 1.38 (s, 9 H), 1.58-1.67 (m, 5 H), 1.97 (m, 2 H), 2.68 (m, 1 H), 3.03 (q, 4 H, *J* = 6.8 Hz), 7.58 (s, 1 H), 7.57 (d, 2 H, *J* = 8.4 Hz), 7.95 (d, 2 H, *J* = 8.4 Hz), 9.02 (s, 1 H), 10.41 (s, 1 H); ¹³C NMR (100 MHz, CDCl₃) δ 13.09, 25.58, 25.87, 29.67, 31.16, 31.73, 31.90, 35.02, 38.40, 50.82, 100.8, 113.2, 125.9, 126.8, 131.9, 132.6, 134.9, 155.2, 159.8, 165.1; HRMS (ESI) *m/z* calcd for C₂₈H₃₈N₄OH⁺: 447.3124, Found: 447.3120 (Δ = -0.9 ppm).

2-Cyclohexyl-5-cyclopentylamido-6-*N,N*-diethylamino -1*H*-benzo[d]imidazole (II-Aj):



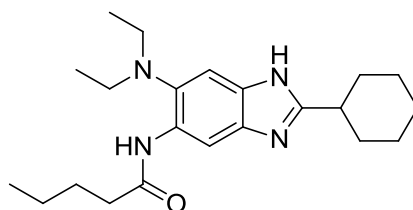
White solid; 74 % yield; mp 202-204 °C; ¹H NMR (400 MHz, CDCl₃) δ 0.92 (t, 6 H, *J* = 7.2 Hz), 1.24 (m, 3 H), 1.67-2.05 (m, 15 H), 2.91 (m, 2 H), 3.03 (q, 4 H, *J* = 7.2 Hz), 7.50 (s, 1 H), 8.65 (s, 1 H), 9.41 (s, 1 H); ¹³C NMR (100 MHz, CDCl₃) δ 12.92, 25.77, 25.79, 30.53, 31.75, 38.45, 47.70, 50.57, 101.1, 112.6, 131.9, 134.6, 138.5, 159.4, 174.1; HRMS (ESI) *m/z* calcd for C₂₃H₃₄N₄OH⁺: 383.2911, Found: 383.2913 (Δ = 0.5 ppm).

2-Cyclohexyl-6-*N,N*-diethylamino-5-(3-phenylpropanamido)-1*H*-benzo[d]imidazole(II-Ak):



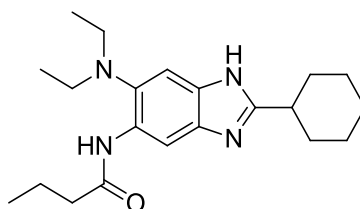
White solid; 55 % yield; ^1H NMR (400 MHz, CDCl_3) δ 0.83 (t, 6 H, $J = 6.8$ Hz), 1.23-1.29 (m, 5 H), 1.67-1.83 (m, 4 H), 2.08 (m, 2 H), 2.78 (t, 2 H, $J = 7.2$ Hz), 2.85 (q, 4 H, $J = 7.2$ Hz), 3.11 (t, 2 H, $J = 7.2$ Hz), 7.25 (m, 5 H), 7.49 (s, 1 H), 8.69 (s, 1 H), 9.33 (s, 1 H); ^{13}C NMR (100 MHz, CDCl_3) δ 12.81, 25.80, 26.04, 29.66, 31.89, 31.98, 38.53, 40.18, 50.48, 101.1, 112.5, 126.3, 128.2, 128.4, 131.7, 134.5, 138.5, 140.3, 159.4, 170.1; MS (FIA) m/z 419.2 ($\text{M}+1$) $^+$.

2-Cyclohexyl-6-*N,N*-diethylamino-5-(pentanamido)-1*H*-benzo[d]imidazole (II-AI):



White solid; 70 % yield; mp 124-126 $^\circ\text{C}$; ^1H NMR (400 MHz, CDCl_3) δ 0.92 (t, 6 H, $J = 6.8$ Hz), 0.95 (t, 3 H, $J = 7.2$ Hz), 1.27-1.48 (m, 5 H), 1.65-1.84 (m, 7 H), 2.08 (m, 2 H), 2.45 (t, 2 H, $J = 7.2$ Hz), 2.84 (m, 1 H), 2.93 (q, 4 H, $J = 7.2$ Hz), 7.51 (s, 1 H), 8.72 (s, 1 H), 9.45 (s, 1 H); ^{13}C NMR (100 MHz, CDCl_3) δ 12.93, 13.78, 22.42, 25.82, 26.11, 28.09, 31.59, 38.48, 50.63, 101.1, 112.6, 131.6, 132.0, 134.4, 138.8, 159.6, 171.2; HRMS (FAB) m/z calcd for $\text{C}_{22}\text{H}_{34}\text{N}_4\text{OH}^+$: 371.2911, Found: 371.2909 ($\Delta = -0.9$ ppm).

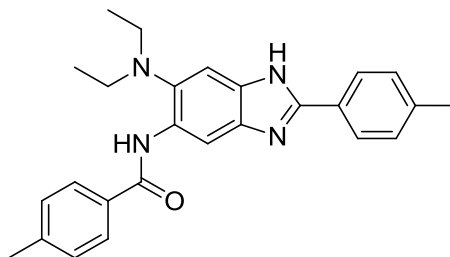
5-(Butanamido)-2-cyclohexyl-6-*N,N*-diethylamino-1*H*-benzo[d]imidazole (II-Am):



White solid; 65 % yield; mp 134-136 $^\circ\text{C}$; ^1H NMR (400 MHz, CDCl_3) δ 0.92 (t, 6 H, $J = 7.2$ Hz), 1.06 (t, 6 H, $J = 7.2$ Hz), 1.31 (m, 3 H), 1.66-1.84 (m, 7 H), 2.12 (m, 2 H), 2.45 (t, 2 H, $J = 7.2$

Hz), 2.84 (m, 1 H), 2.93 (q, 4 H, $J = 7.2$ Hz), 77.52 (s, 1 H), 8.73 (s, 1 H), 9.45 (s, 1 H); ^{13}C NMR (100 MHz, CDCl_3) δ 12.93, 13.82, 19.60, 25.84, 26.13, 31.62, 38.62, 40.68, 50.68; HRMS (ESI) m/z calcd for $\text{C}_{21}\text{H}_{32}\text{N}_4\text{OH}^+$: 357.2654, Found: 357.2653 ($\Delta = -0.3$ ppm).

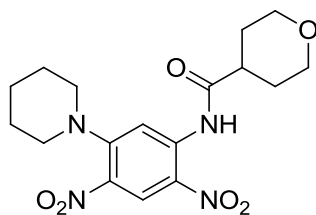
6-*N,N*-diethylamino-5-(4-methylbenzamido)-2-Toluoyl-1*H*-benzo[d]imidazole (II-An):



White solid; 53 % yield; mp > 210 °C; ^1H NMR (400 MHz, CDCl_3) δ 0.97 (t, 6 H, $J = 7.2$ Hz), 2.93 (s, 3 H), 2.45 (s, 3 H), 3.03 (q, 4 H, $J = 7.2$ Hz), 6.95 (d, 2 H, $J = 7.6$ Hz), 7.29 (d, 2 H, $J = 8$ Hz), 7.64 (s, 1 H), 7.84 (m, 4 H), 9.10 (s, 1 H); ^{13}C NMR (100 MHz, CDCl_3) δ 12.99, 21.40, 50.54, 101.5, 113.3, 126.5, 127.0, 127.1, 129.3, 129.6, 132.3, 132.7, 135.8, 139.5, 142.0, 152.6, 165.5; HRMS (ESI) m/z calcd for $\text{C}_{26}\text{H}_{28}\text{N}_4\text{OH}^+$: 413.2341, Found: 413.2341 ($\Delta = -0.0$ ppm).

§ 2.4.4 Synthesis of 2,5,6-Trisubstituted Benzimidazole Library II-C:

2,4-Dinitro-5-piperidinyl-1-tetrahydropyranocarboxamido-benzene (II-7a):

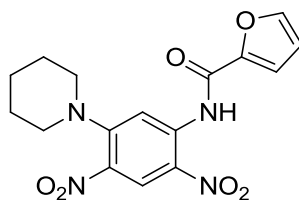


To a solution of 1-tetrahydropyranocarboxylic (300 mg, 2.32 mmol) in CH_2Cl_2 (5 mL) was added oxalyl chloride (0.3 mL, 3.48 mol) and a few drops of dimethylformamide. The reaction mixture was stirred for 90 minutes and the solvent was evaporated *in vacuo* to give the corresponding acyl chloride. The crude product was taken to the next step. A solution of **II-4g** (329 mg, 1.24 mmol) and 1-tetrahydropyrancarbonyl chloride (274 mg, 1.86 mmol) in pyridine (5 mL) was refluxed overnight. The reaction mixture was diluted with dichloromethane, washed with water (30 mL x 3) and dried over anhydrous magnesium sulfate. The crude product was purified by flash chromatography on silica gel using ethyl acetate as eluent to give **II-7a** as a

yellow solid (398mg, 85 % yield); mp 134-136 °C; ¹H NMR (400 MHz, CDCl₃) δ 1.69-1.73 (m, 6 H), 1.81-1.93 (m, 4 H), 2.65 (m, 1 H), 3.27 (m, 4 H), 3.41-3.52 (m, 2 H), 4.09 (m, 2 H), 8.61 (s, 1 H), 8.84 (s, 1 H), 11.0 (s, 1 H); ¹³C NMR (100 MHz, CDCl₃) δ 23.59, 25.35, 28.39, 28.84, 39.60, 44.00, 52.01, 66.98, 108.4, 125.6, 127.4, 132.7, 138.9, 150.7, 174.0. MS (ESI) *m/z* 379.3 (M+1)⁺.

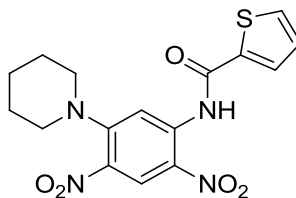
In the same manner, compounds **II-7b~ II-7e** were prepared.

2,4-dinitro-1-(2-Furyl)carboxamido-5-piperidinylbenzene (II-7b):



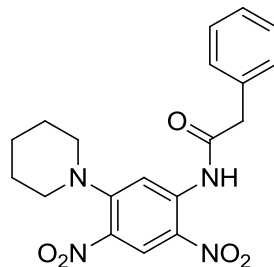
Yellow solid; 81 % yield; mp 196-198°C; ¹H NMR (400 MHz, CDCl₃) δ 1.72 (m, 6 H), 3.30 (t, 4 H, *J* = 4.8 Hz), 6.61 (dd, 2 H, *J* = 1.2 Hz, 2.4 Hz), 7.30 (d, 1 H, *J* = 3.6 Hz), 7.63 (m, 1 H), 8.68 (s, 1 H), 8.85 (s, 1 H); ¹³C NMR (100 MHz, CDCl₃) δ 23.60, 25.34, 52.01, 108.4, 112.9, 116.9, 125.8, 127.4, 132.7, 138.7, 145.7, 146.9, 150.5, 156.7; MS (ESI) *m/z* 361.3 (M+1)⁺.

2,4-dinitro-1-(2-Thiophenyl)carboxamido-5-piperidinylbenzene(II-7c):



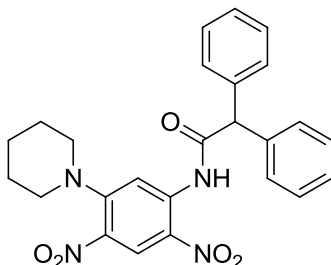
Orange solid; 85 % yield; mp 178-180 °C; ¹H NMR (400 MHz, CDCl₃) δ 1.72 (m, 6 H), 3.30 (t, 4 H, *J* = 4.8 Hz), 7.19 (dd, 1 H, *J* = 0.8 Hz, 4 Hz), 7.67 (d, 1 H, *J* = 4.8 Hz), 7.75 (d, 1 H, *J* = 4 Hz), 8.66 (s, 1 H), 8.86 (s, 1 H), 11.7 (s, NH); ¹³C NMR (100 MHz, CDCl₃) δ 23.60, 25.36, 52.03, 108.1, 125.5, 127.5, 127.6, 128.3, 129.5, 132.7, 133.0, 138.6, 139.0, 150.6, 160.6; MS (ESI) *m/z* 377.3 (M+1)⁺.

1-Benzylcarboxamido-2,4-dinitro-5-piperidinybenzene(II-7d):



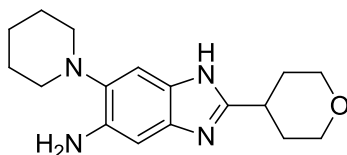
Yellow solid; 82 % yield; mp 128-130°C; ¹H NMR (400 MHz, CDCl₃) δ 1.71 (m, 6 H), 3.25 (t, 4 H, *J* = 4.8 Hz), 3.83 (s, 2 H), 7.35-7.44 (m, 5 H), 8.58 (s, 1 H), 8.78 (s, 1 H), 10.8 (s, NH); ¹³C NMR (100 MHz, CDCl₃) δ 23.59, 25.32, 45.96, 51.98, 108.3, 125.6, 127.3, 128.0, 129.3, 129.5, 132.6, 138.7, 150.5, 170.8; MS (ESI) *m/z* 385.3 (M+1)⁺.

1-Diphenylmethylcarboxamido-2,4-dinitro-5-piperidinybenzene(II-7e):



Yellow solid; 65 % yield; mp 116- 119 °C; ¹H NMR (300 MHz, CDCl₃) δ 1.69 (s, 6 H), 3.24 (d, 4 H, *J*= 5.7 Hz), 5.16 (s, 1 H), 7.28-7.41 (m, 10 H), 8.66 (s, 1 H), 8.79 (s, 1 H), 10.9 (s, 1 H); MS (ESI) *m/z* 462.1 (M+1)⁺.

5-Amino-2-tetrahydropyran-6-piperidiny-1H-benzo[d]imidazole (II-8a):

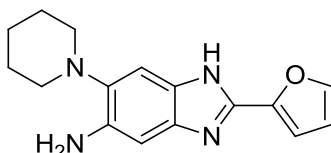


To a solution of **II-7a** (308 mg, 0.81 mmol) in dioxane (20 mL) and ethanol (20 mL) was added ammonium formate (2.0 g) and 10 wt. % Pd-C (200 mg) with stirring. The reaction mixture turned from yellow to red and then to colorless in 45-60 min at room temperature. The catalyst and excess ammonium formate were filtered off to give the product solution.

Concentrated hydrochloric acid was added to this solution and adjusted to 4 N HCl concentration. Then the mixture was refluxed for 4-6 h. The reaction mixture was basified by addition of ammonium hydroxide, extracted with ethyl acetate (40 mL x 3) and dried over anhydrous magnesium sulfate. The crude product was purified by flash chromatography on silica gel using ethyl acetate/hexanes (gradient 20 % ethyl acetate/hexanes) as eluent to give pure **II-8a** as a brown solid (160 mg, 65 % yield); ^1H NMR (400MHz, CDCl_3) δ 1.70 (m, 6 H), 1.98 (m, 4 H), 3.06 (m, 1 H), 3.45 (m, 2 H), 3.99 (m, 2 H), 6.80 (s, 1 H), 7.22 (s, 1 H); ^{13}C NMR (100 MHz, CDCl_3) δ 24.19, 26.92, 31.43, 35.67, 53.61, 67.49, 98.18, 107.4, 133.0, 134.1, 138.5, 155.3; MS (ESI) m/z 301.4 ($\text{M}+1$) $^+$.

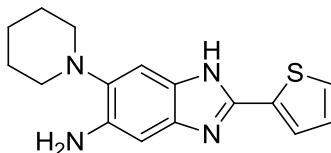
Compounds **II-8b~ II-8e** were prepared in the same manner.

5-Amino-2-furyl-6-piperidinyl-1H-benzo[d]imidazole (II-8b):



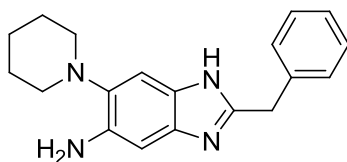
Dark brown solid; 55 % yield; mp 124-126 °C; ^1H NMR (400 MHz, CDCl_3) δ 1.68 (m, 6 H), 2.78 (broad s, 4 H), 6.45 (m, 1 H), 6.85 (s, 1 H), 7.09 (m, 1 H), 7.24 (s, 1 H), 7.40 (s, 1 H); ^{13}C NMR (100 MHz, CDCl_3) δ 24.19, 26.88, 53.48, 98.04, 107.5, 109.4, 112.1, 133.3, 133.9, 139.2, 139.3, 142.1, 143.0, 145.6; HRMS (ESI) m/z calcd for $\text{C}_{16}\text{H}_{18}\text{N}_4\text{OH}^+$: 283.1559, Found: 283.1561 ($\Delta = 0.7$ ppm).

5-Amino-6-piperidinyl -2-thiophenyl-1H-benzo[d]imidazole(II-8c):



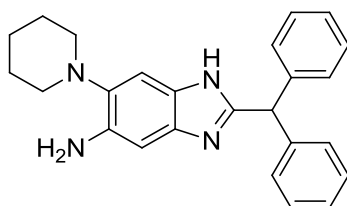
Pale yellow solid; 50 % yield; mp 145-148°C; ^1H NMR (400 MHz, CDCl_3) δ 1.64 (m, 6 H), 2.73 (broad s, 4 H), 6.80 (s, 1 H), 6.94 (t, 1 H, $J = 4.8$ Hz), 7.19 (s, 1 H), 7.24 (d, 1 H, $J = 5.2$ Hz), 7.64 (d, 1 H, $J = 3.6$ Hz); ^{13}C NMR (100 MHz, CDCl_3) δ 24.17, 26.87, 53.44, 98.05, 107.4, 125.9, 127.0, 127.9, 133.4, 134.5, 139.0, 139.2, 145.6; HRMS (ESI) m/z calcd for $\text{C}_{16}\text{H}_{18}\text{N}_4\text{SH}^+$: 299.1330, Found: 299.1330 ($\Delta = 0.0$ ppm).

5-Amino-2-benzyl-6-piperidinyl-1H-benzo[d]imidazole(II-8d):



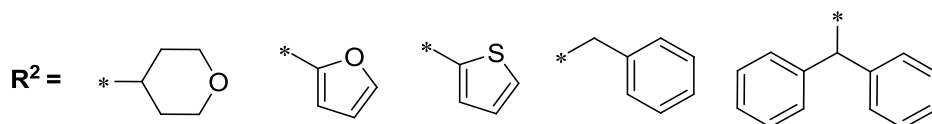
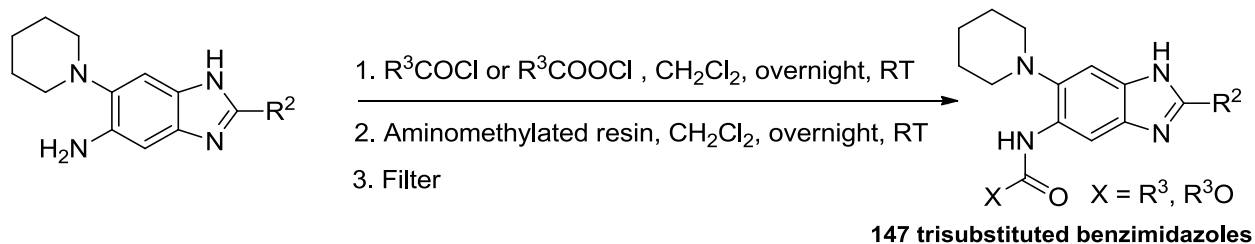
Brown solid; 53 % yield; mp 82-84 °C; ¹H NMR (400 MHz, CDCl₃) δ 1.68 (m, 6 H), 2.76 (broad s, 4 H), 4.12 (s, 2 H), 6.72 (s, 1 H), 7.15 (s, 1 H), 7.21 (m, 5 H); ¹³C NMR (100 MHz, CDCl₃) δ 24.22, 26.92, 35.50, 53.44, 98.33, 107.1, 126.9, 128.7, 128.8, 132.7, 134.2, 136.8, 138.4, 138.5, 151.4; HRMS (ESI) *m/z* calcd for C₁₉H₂₂N₄H⁺: 307.1923, Found: 307.1921 (Δ = - 0.7 ppm).

5-Amino-2-diphenylmethyl-6-piperidinyl-1H-benzo[d]imidazole(II-8e):

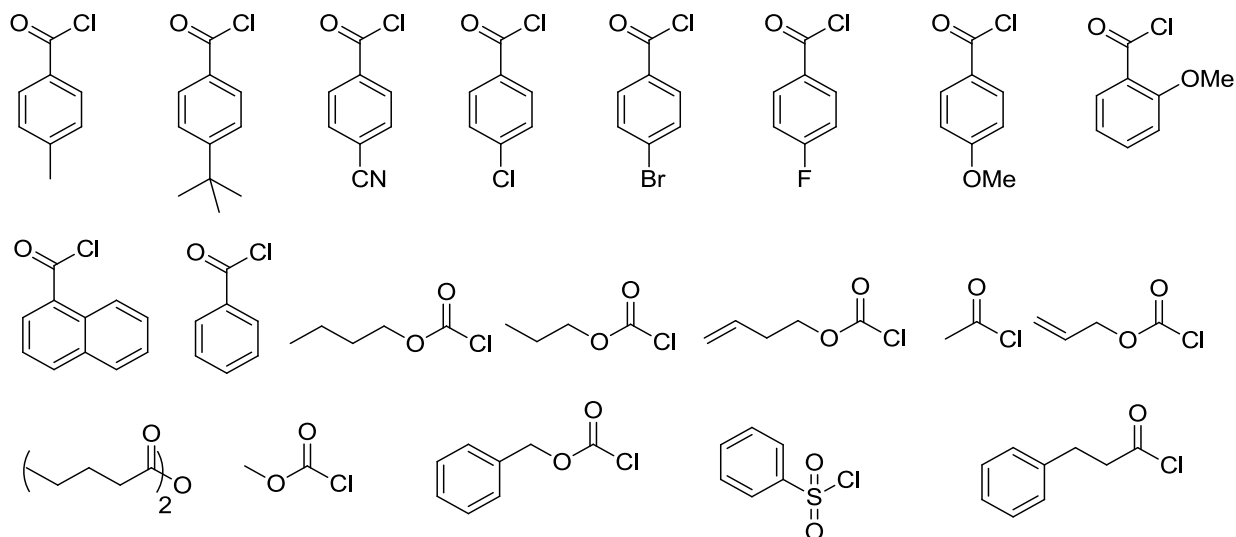


Off-white solid; 43 % yield; mp 136-138°C; ¹H NMR (400 MHz, CDCl₃) δ 1.69 (m, 6 H), 2.76 (broad s, 4 H), 5.69 (s, 1 H), 6.89 (s, 1 H), 7.20-7.30 (m, 10 H); ¹³C NMR (100 MHz, CDCl₃) δ 25.52, 28.16, 52.95, 55.04, 100.4, 108.0, 128.1, 129.7, 130.1, 139.9, 140.5, 142.4, 155.4; HRMS (ESI) *m/z* calcd for C₂₅H₂₆N₄H⁺: 383.2236, Found: 383.2234 (Δ = - 0.5 ppm).

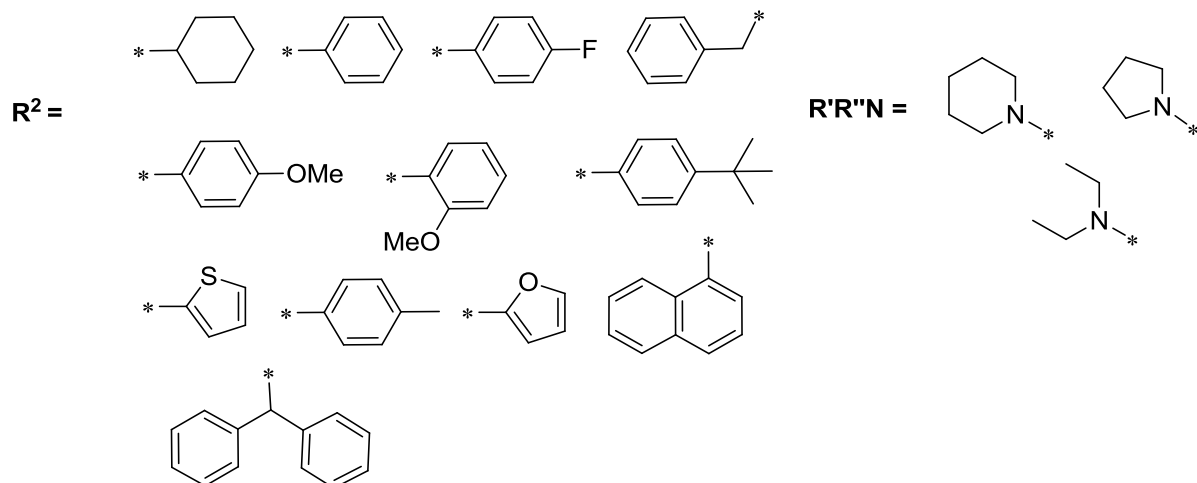
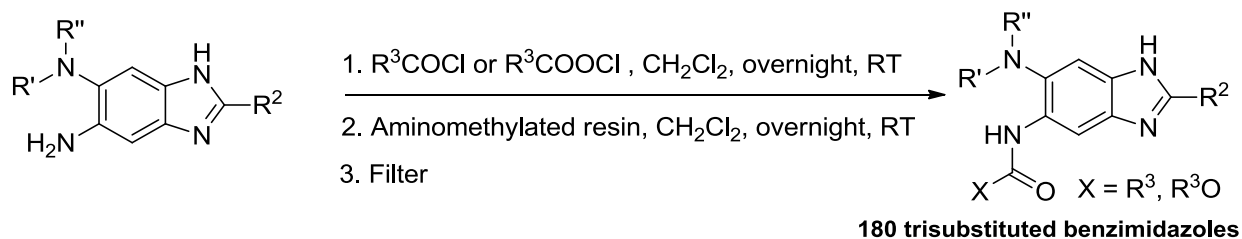
Synthesis of 2,5,6-Trisubstituted Benzimidazole Library II-C:



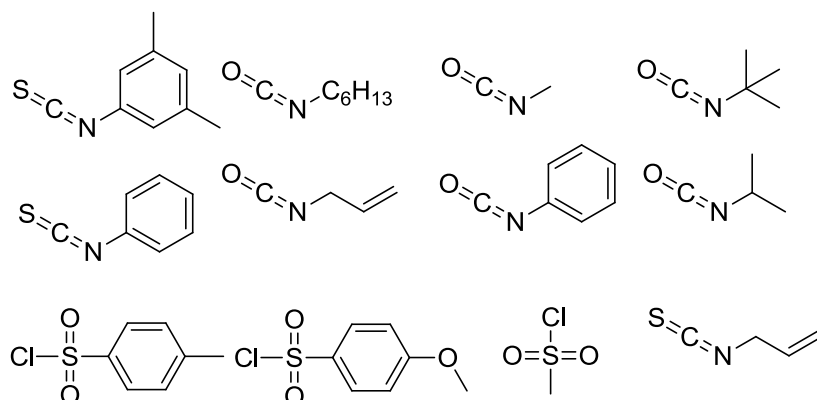
List of reagents



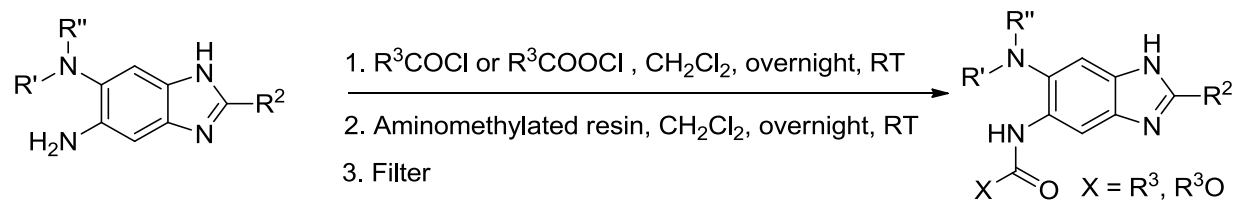
§ 2.4.5 Synthesis of 2,5,6-Trisubstituted Benzimidazole Library II-D:



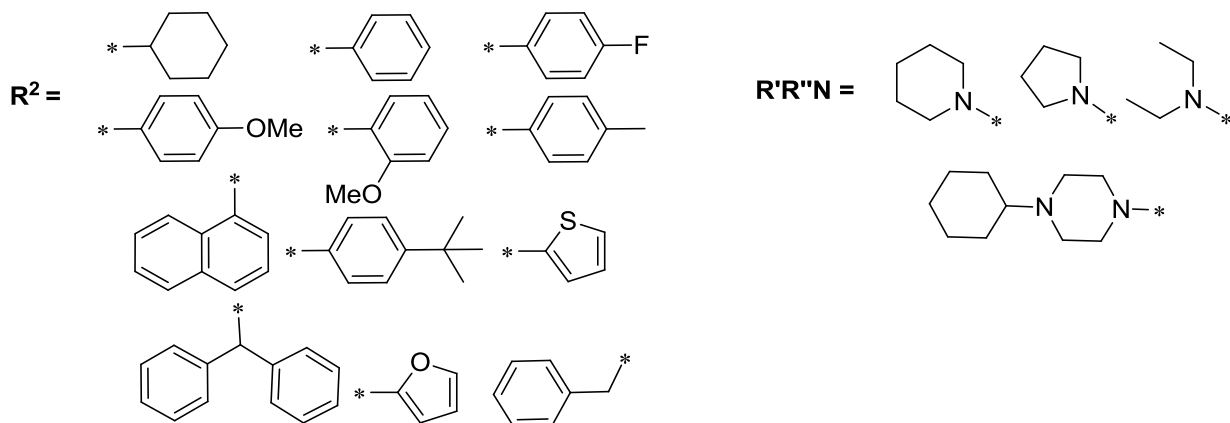
List of reagents



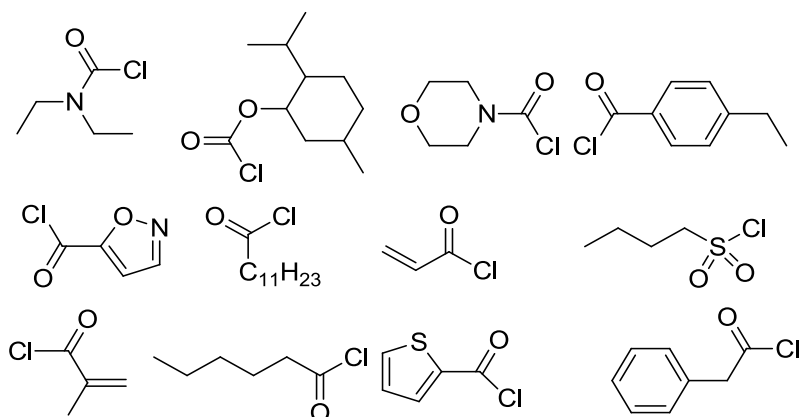
§ 2.4.6 Synthesis of 2,5,6-Trisubstituted Benzimidazole Library II-E:



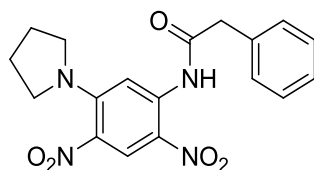
180 trisubstituted benzimidazoles



List of reagents

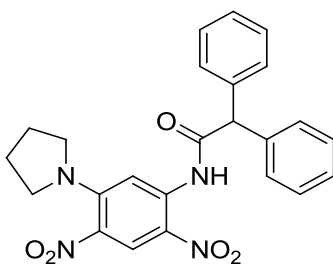


1-Benzylcarboxamido-2,4-dinitro-5-pyrrolidinylbenzene (II-9a):



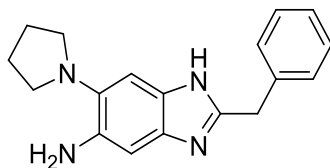
Yellow solid; 74 % yield; mp 134-138°C ¹H NMR (400 MHz, CDCl₃) δ 2.01 (m, 4 H), 3.34 (t, 4 H, *J* = 4.8 Hz), 3.82 (s, 2 H), 7.33-7.41 (m, 5 H), 8.44 (s, 1 H), 8.71 (s, 1 H); ¹³C NMR (100 MHz, CDCl₃) δ 25.50, 45.97, 51.30, 104.8, 124.2, 126.9, 128.0, 129.3, 129.5, 129.7, 131.1, 132.8, 137.8, 146.4, 170.8; MS (ESI) *m/z* 371.3 (M+1)⁺.

1-Diphenylmethylcarboxamido-2,4-dinitro-5-pyrrolidinylbenzene(II-9b):



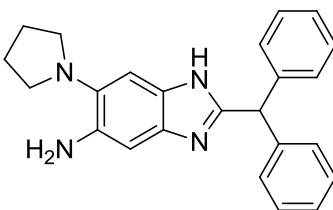
Yellow solid; 65 % yield; mp 115-117 °C; ¹H NMR (400 MHz, CDCl₃) δ 1.92 (m, 4 H), 3.28 (m, 4 H, *J* = 5.7 Hz), 5.11 (s, 1 H), 7.18-7.32 (m, 10 H), 8.48 (s, 1 H), 8.67 (s, 1 H); ¹³C NMR (100 MHz, CDCl₃) δ 25.49, 51.35, 56.95, 61.25, 104.9, 124.3, 126.9, 127.4, 127.8, 128.6, 128.9, 129.0, 131.9, 137.7, 137.8, 172.2, 178.3; MS (ESI) *m/z* 447.4 (M+1)⁺.

5-Amino-2-benzyl-6-pyrrolidinyl-1H-benzo[d]imidazole (II-10a):



Brown solid; 82 % yield; mp 82 °C; ¹H NMR (400 MHz, CDCl₃) δ 1.87 (m, 4 H), 2.95 (broad s, 4 H), 4.1 (s, 2 H), 6.71 (s, 1 H), 7.16 (s, 1 H), 7.21 (m, 5 H); ¹³C NMR (100 MHz, CDCl₃) δ 24.22, 35.92, 52.14, 98.99, 106.3, 127.2, 129.1, 133.7, 134.1, 135.3, 137.0, 138.8, 151.6; HRMS (ESI) *m/z* calcd for C₁₈H₂₀N₄H⁺: 293.1766, Found: 293.1766 (Δ = 0.0 ppm).

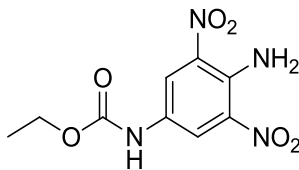
5-Amino-2-diphenylmethyl-6-pyrrolidinyl-1H-benzo[d]imidazole (II-10b):



Off-white solid; 84 % yield; mp 123-126 °C; ¹H NMR (400 MHz, CDCl₃) δ 1.87 (m, 4 H), 2.95 (broad s, 4 H), 5.68 (s, 1 H), 6.68 (s, 1 H), 7.14-7.27 (m, 11 H); ¹³C NMR (100 MHz, CDCl₃) δ 23.99, 29.16, 51.84, 100.4, 127.1, 128.7, 128.9, 135.2, 138.7, 140.9, 153.1; HRMS (ESI) *m/z* calcd for C₂₄H₂₄N₄H⁺: 369.2079, Found: 369.2080 (Δ = 0.3 ppm).

§ 2.4.7 Synthesis of 2,5,7-Trisubstituted Benzimidazole Library II-F:

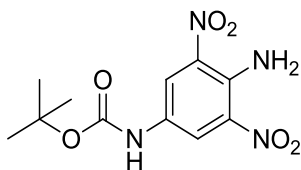
4-Amino-3,5-dinitro-1-(ethoxycarbonylamino)benzene(II-14a):



4-chlorobenzoic acid (1.52 g, 9.74 mmol) was dissolved in sulfuric acid (25 mL) at 70-100 °C and KNO₃ (5.02g) was added in portion. The reaction mixture was heated to 120-130 °C for 15 hours, cooled down to ~20 °C and poured onto ice. The precipitate was filtered to give light yellow solid, m.p. 153-154 °C (Lit m.p. 153-156 °C).²¹Product from the previous reaction was dissolved in methanol (50 mL) and aqueous NH₃ solution was added gradually. The reaction

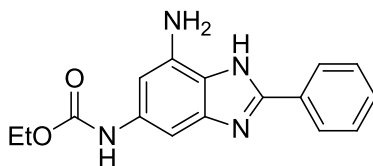
mixture was refluxed. After the completion of reaction, 1:1 solution of HCl was added to the reaction mixture. On stirring the precipitate was formed which was filtered and washed with water to obtain 4-amino-3,5-dinitrobenzoic acid (**II-12**) in 85 % yield (2 steps); $^1\text{H NMR}$ (300 MHz, DMSO-d_6) δ 8.80(s, 2H).²¹ 4-Amino-3,5-dinitrobenzoic acid **II-12** (614 mg, 2.70 mmol) was dissolved in thionyl chloride (4 mL) and refluxed overnight. The reaction mixture was cooled down to room temperature and excess thionyl chloride was distilled off to give compound **II-13**. The crude product was immediately dissolved in acetone (2.4 mL) in an ice-bath. To this solution was added dropwise NaN_3 (448 mg, 5.94 mmol) in ice-water (0.88 mL). The mixture was stirred for 20 min at 0 °C until a solid precipitated out. After dilution with ice-water (12 mL), the reaction mixture was extracted with dichloromethane (6 mL x 2), dried over anhydrous magnesium sulfate at 0 °C for 1 h, and filtered. The filtrate was concentrated on a rotary evaporator (below room temperature), and the residue dissolved in toluene (15 mL). After refluxing for 2 h, the reaction mixture was cooled down to room temperature, and ethanol (10 mL) was added. After stirring overnight at room temperature, the reaction mixture was concentrated *in vacuo* and purified by flash chromatography on silica gel (hexane/ethylacetate = 1/1) to afford 4-amino-3,5-dinitro-1-(ethoxycarbonylamino)benzene (**II-14a**) as a bright red solid (570 mg, 78 % yield); mp 163-165 °C; $^1\text{H NMR}$ (400 MHz, CDCl_3) δ 8.64 (s, 2 H), 6.59 (bs, 1 H), 4.26 (q, 2 H, $J = 6.9$ Hz), 1.33 (t, 3 H, $J = 6.9$ Hz); $^{13}\text{C NMR}$ (100 MHz, CD_3OD) δ 15.00, 62.53, 125.2, 127.9, 136.3, 139.0, 156.1; HRMS (FAB) m/z calcd for $\text{C}_9\text{H}_{10}\text{N}_4\text{O}_6\text{H}^+$: 271.0677, Found: 271.0679 ($\Delta = -0.7$ ppm).

4-Amino-3,5-dinitro-1-(tert-butoxycarbonylamino)benzene (II-14b):



Compound **II-14b** was prepared in the same manner: bright red solid; 84 % yield; mp 178-180°C; $^1\text{H NMR}$ (400 MHz, DMSO-d_6) δ 1.48 (s, 9 H), 8.19(s, 2 H), 8.65 (s, 2 H), 9.69 (s, 1 H); $^{13}\text{C NMR}$ (100 MHz, DMSO-d_6) δ 28.02, 79.97, 123.3, 126.6, 134.3, 136.9, 152.8; MS (ESI) m/z 299.2 ($\text{M}+1$)⁺.

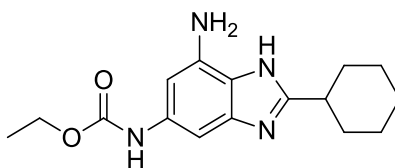
7-Amino-5-ethoxycarbonylamino-2-phenyl-1H-benzo[d]imidazole (II-15a):



To a suspension of **II-14a** (324 mg, 1.2 mmol) in ethanol (24 mL), was added ammonium formate (1.8 g) and 10 wt. % Pd-C (120 mg) under nitrogen. The mixture was stirred at room temperature overnight. The catalyst and excess ammonium formate were filtered off. The filtrate was treated with the sodium bisulfite adduct of benzaldehyde (252 mg, 1.2 mmol) at 0 °C. After the solution was stirred for 12-16 h at room temperature under nitrogen, a trace of insoluble material was removed by filtration and the filtrate was concentrated on a rotary evaporator until approximately 60-70% of the solvent was removed. To the residue an equal volume of ethyl acetate was added, and the mixture was transferred to a separatory funnel. The organic layer was separated, and the water layer was extracted with ethyl acetate (40 mL). The combined organic layers were washed with brine, dried over anhydrous sodium sulfate. The crude product was purified by flash chromatography on silica gel (hexane/ethyl acetate = 1/1) to afford **II-15a** (610 mg, 48% yield) as brown solid; mp 114-115 °C; ¹H NMR (300 MHz, CD₃OD) δ 1.30 (t, 3H, *J* = 6.9 Hz), 4.16 (q, 2H, *J* = 7.2 Hz), 6.51 (s, 1H), 7.18 (s, 1H), 7.44 (m, 3H), 8.01 (m, 2H); ¹³C NMR (100 MHz, CD₃OD) δ 15.11, 62.90, 93.72, 100.95, 127.30, 127.40, 129.11, 130.17, 130.90, 131.32, 137.19, 138.28, 139.11, 151.32, 156.47; HRMS (FAB) *m/z* calcd for C₁₆H₁₆N₄O₂H⁺: 297.1244, Found: 297.1352 (Δ = -2.7 ppm). HPLC (2): 4.50 min, purity > 99 %.

The compounds **II-15b~II-15f** were prepared in the same manner.

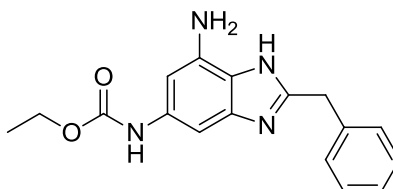
7-Amino-2-cyclohexyl-5-ethoxycarbonylamino-1H-benzo[d]imidazole (II-15b):



Brown solid; 42 % yield; mp > 200 °C; ¹H NMR (400 MHz, CD₃OD) δ 1.27 (t, 3 H, *J* = 7.2 Hz), 1.32-1.43 (m, 2 H), 1.51-1.61 (m, 2 H), 1.69-1.83 (m, 4 H), 1.98-2.04 (m, 2 H), 2.83 (m, 1 H), 4.15 (q, 2 H, *J* = 7.2 Hz), 6.57 (s, 1 H), 8.56 (s, 1 H); ¹³C NMR (100 MHz, CD₃OD) δ 15.09,

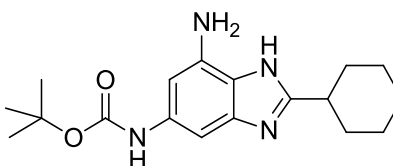
26.80, 27.00, 32.43, 38.92, 61.94, 93.18, 101.4, 123.2, 135.9, 137.6, 156.3, 157.8, 169.5; HRMS (ESI) m/z calcd for $C_{16}H_{22}N_4O_2H^+$: 303.1821, Found: 303.1821 ($\Delta = 0.0$ ppm).

7-Amino-2-benzyl-5-ethoxycarbonylamino-1H-benzo[d]imidazole (II-15c):



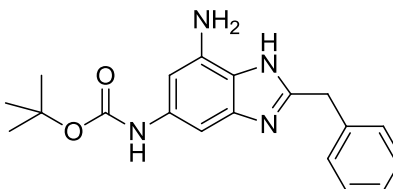
Brown solid; 64 % yield; mp > 200 °C; 1H NMR (400MHz, CD_3OD) δ 1.28 (t, 3H, $J=7.2$ Hz), 4.15 (q, 2H, $J=7.2$ Hz), 4.21 (s, 2H), 6.55 (s, 1H), 7.10 (s, 1H), 7.29 (m, 5 H), 8.35 (s, 1H); ^{13}C NMR (100 MHz, CD_3OD) δ 15.07, 35.46, 61.93, 93.51, 101.3, 125.3, 128.4, 129.9, 136.8, 137.5, 138.0, 152.7, 156.4, 167.2; HRMS (ESI) m/z calcd for $C_{17}H_{18}N_4O_2H^+$: 311.1508, Found: 311.1512 ($\Delta = 1.3$ ppm).

7-Amino-2-cyclohexyl-5-(tert-butoxycarbonylamino)-1H-benzo[d]imidazole (II-15d):



Brown solid; 51 % yield; mp > 200 °C; 1H NMR (400MHz, CD_3OD) δ 1.36 (s, 9 H), 1.54-1.63 (m, 4 H), 1.75-1.88 (m, 4 H), 2.07 (m, 2 H), 2.88 (m, 1 H), 6.51 (s, 1 H), 7.10 (s, 1 H), 8.44 (s, 1 NH); ^{13}C NMR (100 MHz, CD_3OD) δ 25.81, 27.50, 27.60, 31.33, 37.89, 79.46, 92.18, 99.70, 123.0, 135.0, 136.4, 154.2, 156.6; HRMS (ESI) m/z calcd for $C_{18}H_{26}N_4O_2H^+$: 312.2134, Found: 331.2137 ($\Delta = 0.9$ ppm).

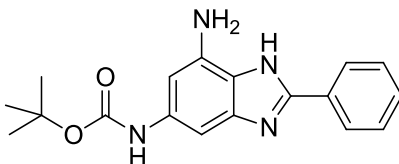
7-Amino-2-benzyl-5-(tert-butoxycarbonylamino)-1H-benzo[d]imidazole (II-15e):



Brown solid; 63 % yield; mp > 200 °C; 1H NMR (400MHz, CD_3OD) δ 1.49 (s, 9 H), 4.17 (s, 2 H), 6.5 (s, 1 H), 7.07 (s, 1 H), 7.28 (m, 5 H); ^{13}C NMR (100 MHz, CD_3OD) δ 27.59, 34.37,

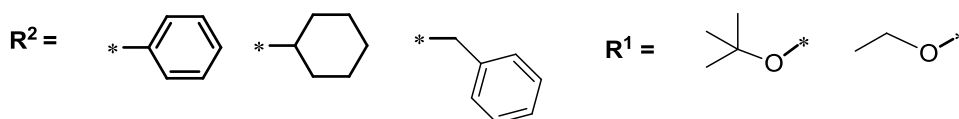
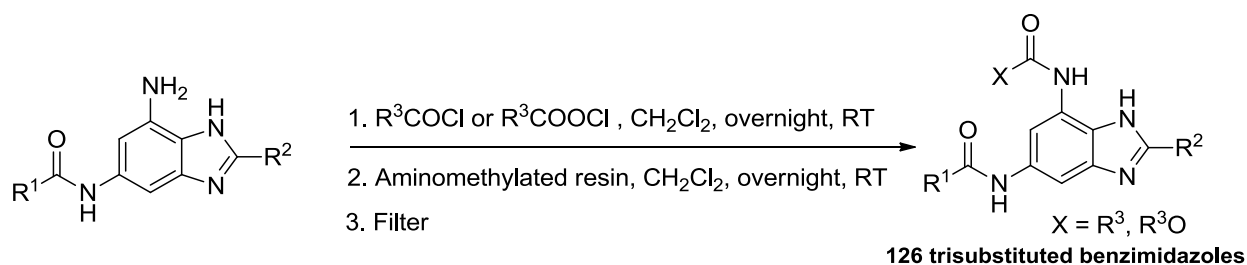
79.43, 92.35, 99.94, 124.9, 126.9, 128.5, 135.8, 136.1, 136.5, 136.7, 151.3, 154.3; HRMS (ESI) m/z calcd for $C_{19}H_{22}N_4O_2H^+$: 339.1821, Found: 339.1862 ($\Delta = 1.5$ ppm).

7-Amino-2-phenyl-5-(*tert*-butoxycarbonylamino)-1*H*-benzo[d]imidazole (II-15f):

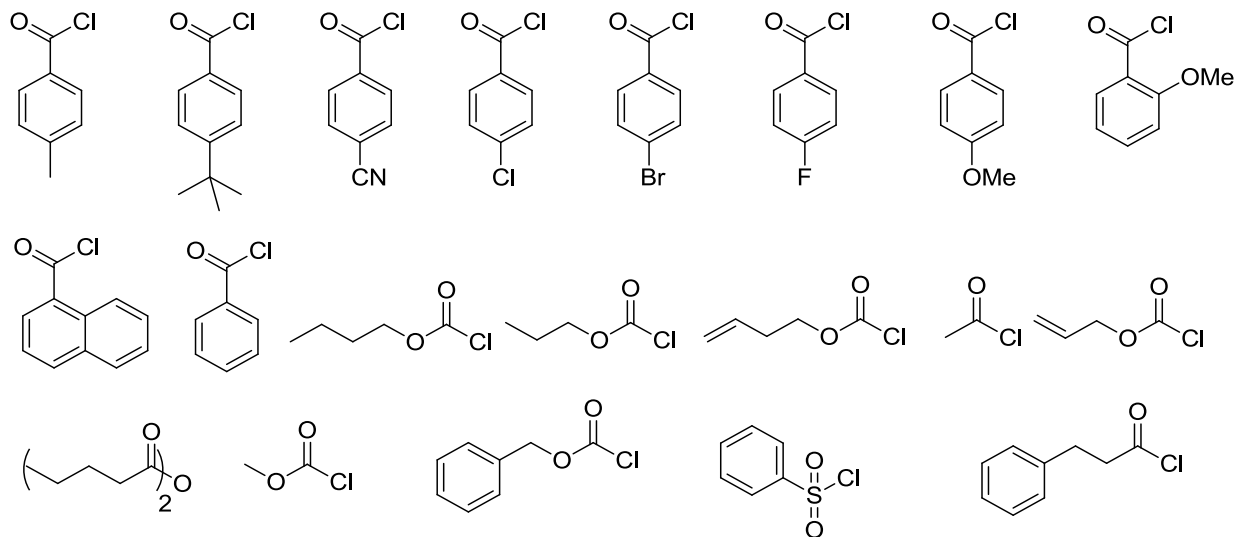


Brown solid; 59 % yield; mp > 200 °C; 1H NMR (400MHz, CD_3OD) δ 1.51 (s, 9 H), 6.49 (s, 1 H), 7.15 (s, 1 H), 7.48 (m, 3 H), 8.00 (d, 2 H, $J = 8.4$ Hz); ^{13}C NMR (100 MHz, CD_3OD) δ 28.94, 80.71, 93.64, 101.0, 127.4, 130.1, 130.8, 131.4, 137.4, 139.1, 151.2, 155.7; HRMS (ESI) m/z calcd for $C_{18}H_{20}N_4O_2H^+$: 325.1665, Found: 325.1669 ($\Delta = 1.2$ ppm).

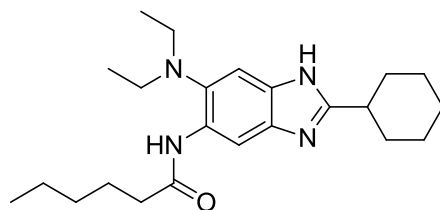
Synthesis of 2,5,7-Trisubstituted Benzimidazole Library II-F:



List of reagents

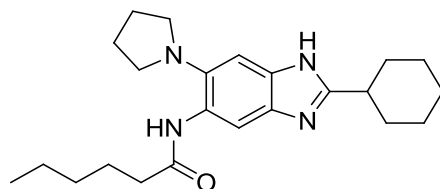


2-Cyclohexyl-6-*N,N*-diethylamino-5-(hexanamido)-1*H*-benzo[d]imidazole (II-16a):



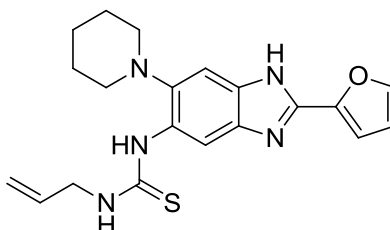
White solid; 56 % yield; mp 183-184 °C; ¹H NMR (400 MHz, CDCl₃) δ 0.91 (m (overlapping triplets), 9 H), 1.23-1.39 (m, 7 H), 1.63-1.83 (m, 7 H), 2.11 (m, 2 H), 2.47 (t, 2 H, *J* = 7.2 Hz), 2.87 (m, 1 H), 2.94 (q, 4 H, *J* = 7.2 Hz), 7.50 (s, 1 H), 8.74 (s, 1 H), 9.46 (s, 1 H); ¹³C NMR (100 MHz, CDCl₃) δ 12.89, 13.81, 22.39, 25.88, 26.11, 31.43, 31.55, 38.59, 38.72, 50.60, 101.0, 112.6, 131.6, 132.0, 134.4, 139.0, 159.7, 171.1; HRMS (ESI) *m/z* calcd for C₂₃H₃₆N₄OH⁺: 385.2963, Found: 385.2967 (Δ = -1.0 ppm).

2-Cyclohexyl-5-hexanamido-6-pyrrolidinyl-1*H*-benzo[d]imidazole (II-16b):



White solid; 61 % yield; mp 127-129 °C; ¹H NMR (400 MHz, CDCl₃) δ 0.91 (t, 3 H, *J* = 7.2 Hz), 1.2-1.43 (m, 7 H), 1.63-1.85 (m, 7 H), 1.97 (broad s, 4 H), 2.07 (m, 2 H), 2.47 (t, 2 H, *J* = 7.2 Hz), 2.84 (m, 1 H), 2.99 (broad s, 4 H), 7.52 (s, 1 H), 8.59 (s, 1 H), 8.91 (s, 1 H); ¹³C NMR (100 MHz, CDCl₃) δ 13.86, 22.43, 24.33, 25.84, 26.09, 31.43, 31.78, 38.57, 53.72, 102.3, 109.7, 129.4, 131.4, 135.5, 138.5, 159.4, 171.2; HRMS (ESI) *m/z* calcd for C₂₃H₃₄N₄OH⁺: 383.2906, Found: 383.2911 (Δ = -1.3 ppm).

5-Allylthioamido-6-piperidinyl-2-thiophene-1*H*-benzo[d]imidazole (II-Da):



White solid; 64 % yield; mp 128-130 °C; ¹H NMR (400 MHz, CDCl₃) δ 1.64 (broad s, 6 H), 2.72 (broad s, 4 H), 4.22 (broad s, 2 H), 5.12 (dd, 2 H), 5.83 (m, 1 H), 6.45 (m, 1 H), 7.11 (m, 1 H), 7.27 (s, 1 H), 7.41 (m, 1 H); ¹³C NMR (100 MHz, CDCl₃) δ 23.85, 24.46, 47.62, 53.75, 106.9, 109.1, 110.6, 112.6, 117.1, 128.5, 133.1, 136.7, 143.3, 143.7, 144.6, 145.0, 180.1; HRMS (ESI) *m/z* calcd for C₂₀H₂₃N₅OSH⁺: 382.1703, Found: 382.17022911 (Δ = 0.3 ppm).

§ 2.4.8 Antibacterial and cytotoxicity activity determination:

Bacterial Strains and Growth. H37Rv, the drug sensitive laboratory strain of *Mtb* as well as clinical *Mtb* strains W210, NHN20, HN355, NHN382 and TN587 exhibit different resistant profiles to isoniazid and rifampicin.^{10,31} For evaluation of drug sensitivity all strains were grown in 7H9 media containing 10% OADC enrichment and 0.05% Tween-80 and assessed at mid log phase growth.

Antibacterial Activity. The minimum inhibitory concentration (MIC) was determined by the Microplate Alamar Blue assay (MABA) as described previously.³² Briefly, stock solutions of the compounds were prepared in DMSO and were serially diluted 2 fold in 96 well microtiter plates and each *Mtb* strains was added to each well to an OD₆₀₀ of 0.005. Plates were incubated for 6 days at 37°C. AlamarBlue® (Invitrogen) was added to the plates and the plates were

incubated for an additional 24 h at 37 °C. Plates were monitored for color change, and MIC was determined in triplicate.

Cytotoxicity Assay. The cytotoxicity of the compounds was tested against VERO cells. Epithelial cells from the kidneys of the African Green Monkey were used to start the VERO cell line. Vero cells were grown in L15 media without CO₂. Serial two fold dilutions of the drugs were prepared in the 96 well microtiter plates. The cells were added to the plates in media containing the appropriate amount of AlamarBlue®. The cells were added to a final concentration of 2.5×10^4 / well. The plates were incubated for 3 days at 37°C. The LD₅₀ was calculated according to manufacturer directions.

§ 2.5 References

1. Bloom B. R., Murray C. J. Tuberculosis: commentary on a reemergent killer. *Science* **1992**, 257, 1055-1064.
2. Tuberculosis: Data and Country Profiles. World Health Organization (WHO)
Available from: http://www.who.int/tb/publications/global_report/2010/en/index.html.
3. Romberg, L.; Levin, P. A. Assembly dynamics of the bacterial cell division protein FtsZ: Poised at the Edge of Stability. *Annu. Rev. Microbiol.* **2003**, 57, 125-154
4. Errington, J.; Daniel, R. A.; Scheffers, D.-J., Cytokinesis in bacteria. *Microbiol. Mol. Biol. Rev.* **2003**, 67, 52-65.
5. Adams, D. W.; Errington, J., Bacterial cell division: assembly, maintenance and disassembly of the Z ring. *Nat. Rev. Microbiol.* **2009**, 7, 642-653.
6. Vollmer, W., The prokaryotic cytoskeleton: A putative target for inhibitors and antibiotics? *Appl. Microbiol. Biotechnol.* **2006**, 73, 37-47.
7. Respicio, L.; Nair, P. A.; Huang, Q.; Anil, B.; Tracz, S.; Truglio, J. J.; Kisker, C.; Raleigh, D. P.; Ojima, I.; Knudson, D. L.; Tonge, P. J.; Slayden, R. A., Characterizing septum inhibition in Mycobacterium tuberculosis for novel drug discovery. *Tuberculosis* **2008**, 88, 420-429.
8. Slayden, R. A.; Knudson, D. L.; Belisle, J. T., Identification of cell cycle regulators in Mycobacterium tuberculosis by inhibition of septum formation and global transcriptional analysis. *Microbiology*, **2006**, 152, 1789-1797.
9. de Pereda, J. M.; Leynadier, D.; Evangelio, J. A.; Chacon, P.; Andreu, J. M., Tubulin secondary structure analysis, limited proteolysis sites, and homology to FtsZ. *Biochemistry* **1996**, 35, 14203-14215.
10. Nogales, E.; Wang, H. W., Structural Mechanisms Underlying Nucleotide-Dependent Self-Assembly of Tubulin and Its Relatives. *Curr. Opin. Struct. Biol.* **2006**, 16, 221 - 229.
11. Kumar, K.; Awasthi, D.; Berger, W. T.; Tonge, P. J.; Slayden, R. A.; Ojima, I., Discovery of anti-TB agents that target the cell-division protein FtsZ. *Future Med. Chem.* **2010**, 2, 1305-1323.
12. Kapoor, S.; Panda, D., Targeting FtsZ for antibacterial therapy: a promising avenue. *Expert Opin. Ther. Targets* **2009**, 13, 1037-1051.

13. Huang, Q.; Tonge Peter, J.; Slayden Richard, A.; Kirikae, T.; Ojima, I., FtsZ: a novel target for tuberculosis drug discovery. *Curr. Top. Med. Chem.* **2007**, *7*, 527-43.
14. Huang, Q.; Kirikae, F.; Kirikae, T.; Pepe, A.; Amin, A.; Respicio, L.; Slayden, R. A.; Tonge, P. J.; Ojima, I., Targeting FtsZ for Antituberculosis Drug Discovery: Noncytotoxic Taxanes as Novel Antituberculosis Agents. *J. Med. Chem.* **2006**, *49*, 463-466.
15. Sarcina, M.; Mullineaux, C. W., Effects of tubulin assembly inhibitors on cell division in prokaryotes in vivo. *FEMS Microbiol. Lett.* **2000**, *191*, 25-9.
16. White, E. L.; Ross, L. J.; Reynolds, R. C.; Seitz, L. E.; Moore, G. D.; Borhani, D. W. Slow polymerization of Mycobacterium tuberculosis FtsZ. *J. Bacteriol.* **2000**, *182*, 4028-34.
17. White, E. L.; Suling, W. J.; Ross, L. J.; Seitz, L. E.; Reynolds, R. C. 2-Alkoxy-carbonylaminopyridines: inhibitors of *Mycobacterium tuberculosis* FtsZ. *J. Antimicrob. Chemother.* **2002**, *50*, 111-114.
18. Reynolds, R. C.; Srivastava, S.; Ross, L. J.; Suling, W. J.; White, E. L. A new 2-carbamoyl pteridine that inhibits mycobacterial FtsZ. *Bioorg. Med. Chem. Lett.* **2004**, *14*, 3161-3164.
19. Slayden, R. A.; Lee, R. E.; Barry, C. E., Isoniazid Effects Multiple Components of the Type II Fatty Acid Synthase System of Mycobacterium tuberculosis. *Mol. Microbiol.* **2000**, *38*, 514-525.
20. Collins, L.; Franzblau, S. G., Microplate Alamar blue assay versus BACTEC 460 system for high-throughput screening of compounds against Mycobacterium tuberculosis and Mycobacterium avium. *Antimicrob. Agents Chemother.* **1997**, *41*, 1004-1009.
21. Elkin, V. V.; Tolkacheva, L. N.; Chernysheva, N. B.; Karmanova, I. B.; Konyushkin, L. D.; Semenov, V. V., Hydrogenation on palladium-containing granulated catalysts 3. Synthesis of aminobenzimidazoles by catalytic hydrogenation of dinitroanilines. *Russ. Chem. Bull.* **2007**, *56*, 1216-1226.

Chapter III

Target Confirmation and Biological Evaluation of Novel Benzimidazole-Based Anti-tubercular Agents

Table of Content

§ 3.1 Introduction.....	90
§ 3.2 Results and discussion	92
§ 3.2.1 Polymerization Assay	92
§ 3.2.2 GTPase Assay	94
§ 3.2.3 Transmission Electron Microscopy of FtsZ assembly	95
§ 3.2.4 Scan Electron Microscopy of Mtb cells	96
§ 3.2.5 Photoaffinity labeling (PAL) of FtsZ for binding site determination	97
§ 3.2.6 Preliminary in vivo assays and formulation studies	101
§ 3.3 Conclusion	104
§ 3.4 Experimental Section.....	105
§ 3.4.1 Mtb FtsZ Protein Preparation	105
§ 3.4.2 FtsZ Polymerization Inhibitory Assay.....	106
§ 3.4.3 GTPase Assay	106
§ 3.4.4 Transmission Electron Microscopy (TEM) Analysis	107
§ 3.4.5 Ultrastructural analysis via scanning electron microscopy (SEM)	107
§ 3.4.6 Photoaffinity Labeling of FtsZ using 4-azido-SB-PIG8	108
§ 3.4.7 Synthesis of photoaffinity analogue 4-Azido-SB-PIG8	108
§ 3.5 References.....	110

§ 3.1 Introduction

Bacterial cell division has been proven to be very crucial for the sustenance and growth of the bacteria. However, the basic mechanism behind the cytokinesis is poorly understood and continuous efforts have been dedicated towards identifying gene products involved in cell division and their associated function. Among this pool of cytokinesis proteins, FtsZ is the most heavily studied, and has been very deservedly found to be the most essential and ubiquitous protein. The polymerization and de-polymerization of FtsZ is a dynamic and continuous process. During cell division, the recruitment of several other cell division proteins leads to Z-ring contraction, resulting in septum formation and eventually cell division (**Figure III-1**).¹

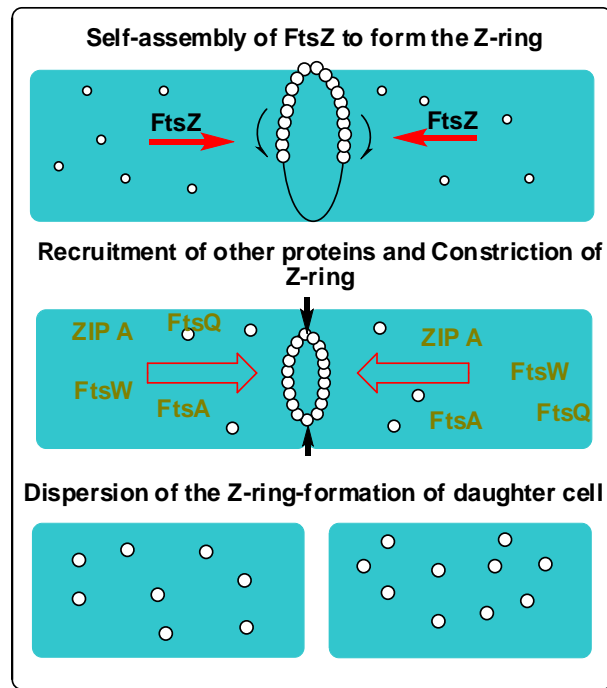


Figure III-1. The Z-ring formation: Bacterial Cell division¹

It was hypothesized that the inhibition of proper FtsZ assembly by either inhibiting polymerization or depolymerization of FtsZ would prevent septum formation without affecting DNA replication and nucleoid segregation.¹ Such conditions would give way to continued cell filamentation, ultimately leading to cell death.^{2,3} Because of the overwhelming importance of FtsZ in bacterial cycle; it is a very promising target for the development of new anti-Tuberculosis (TB) drugs active against drug-resistant *Mtb* strains.⁴ Based on this premise, several compounds have been identified to inhibit FtsZ assembly.^{5,6}

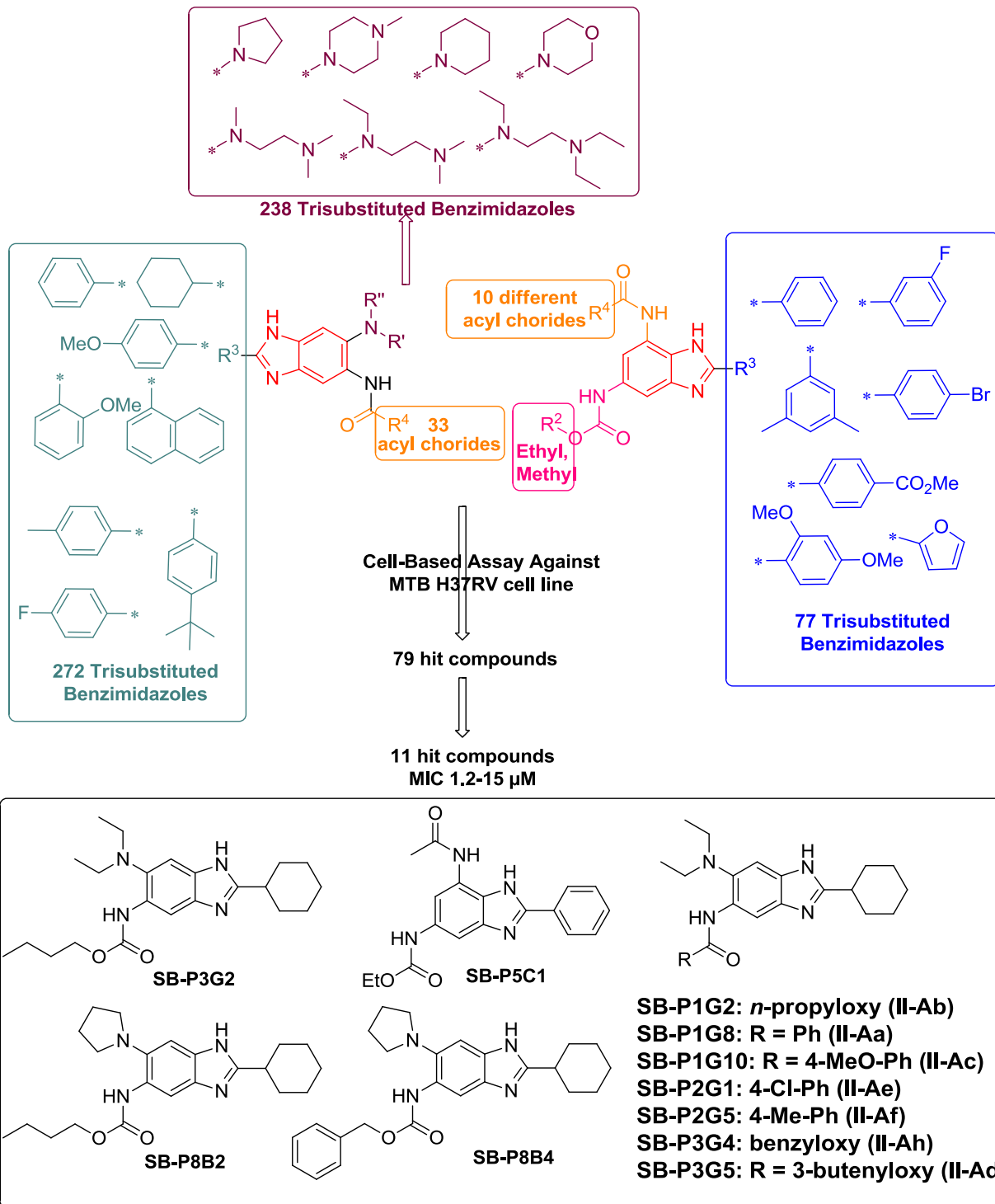


Figure III-2. Library of Benzimidazoles and list of hit compounds⁷

Following the hypothesis, a library of benzimidazole-based compounds were designed and synthesized as described in the previous chapter (Figure III-2).⁷ As expected, several compounds which exhibited Minimum Inhibitory Concentration (MIC) value of $\leq 6 \mu\text{g/mL}$

against drug sensitive as well as drug resistant *Mtb* strains were identified.⁷ However, such cell-based assays do not provide enough insightful information about the mode of action. In order to confirm that these compounds inhibit bacterial growth by interfering with the FtsZ assembly, the effect of our lead compounds on the FtsZ assembly was investigated by using several basic kinetic assays pertinent to *Mtb* FtsZ including light scattering assays, GTPase assay, TEM and SEM imaging etc.

§ 3.2 Results and discussion

§ 3.2.1 Polymerization Assay⁷

A cell-based assay was carried out wherein these re-synthesized lead compounds were screened against drug-sensitive H37Rv strain to obtain the accurate MIC. However, such cell-based assays are not informative about the mode of action. In order to confirm that these compounds inhibit *Mtb* growth by interfering with the FtsZ assembly, a light scattering experiment was carried out to investigate the effect of the lead compounds on FtsZ (de)polymerization. In this experiment, an examination of the extent of light scattering due to FtsZ (de)polymerization as a function of lead compound's concentration was studied. Initially, the critical concentration of FtsZ required for the assay was determined. FtsZ (10 and 15 μM) was incubated at room temperature in polymerization buffer (50 mM MES, 5mM MgCl_2 , 50 mM KCl, pH 6.5). Upon addition of GTP to a final concentration of 100 μM GTP, an immediate increase in light scattering was observed, reaching a plateau in about 3 min. The value for the critical concentration required for maximum polymerization was determined to be 15 μM . To study the effect of the compounds on FtsZ assembly, 15 μM FtsZ in polymerization buffer was incubated with different concentration of the compound for 3 min, after which GTP was added to a final concentration of 100 μM to initiate FtsZ polymerization. As anticipated, a reduction in the extent of light scattering was observed with increasing concentration of compounds, indicating the inhibition of FtsZ polymerization.

The assay confirmed that the compounds inhibited polymerization of FtsZ in a dose dependent manner (**Figure III-3 and III-4**). In case of **SB-P3G5**, 50 % inhibition was observed at 10-20 μM concentration and the polymerization was completely inhibited at 40 μM concentration. In the case of **SB-P1G2**, 50 % inhibition was observed at 20 μM concentration.

Strangely, there was no significant inhibition at 10 μM concentration. For **SB-P1G8** and **SB-P3G2**, similar patterns in inhibition were observed; 50 % inhibition at 10 μM and polymerization was completely shut down at 20 μM concentration. The polymerization assay confirmed that benzimidazoles inhibited the bacterial (*Mtb*) growth by inhibiting FtsZ polymerization.

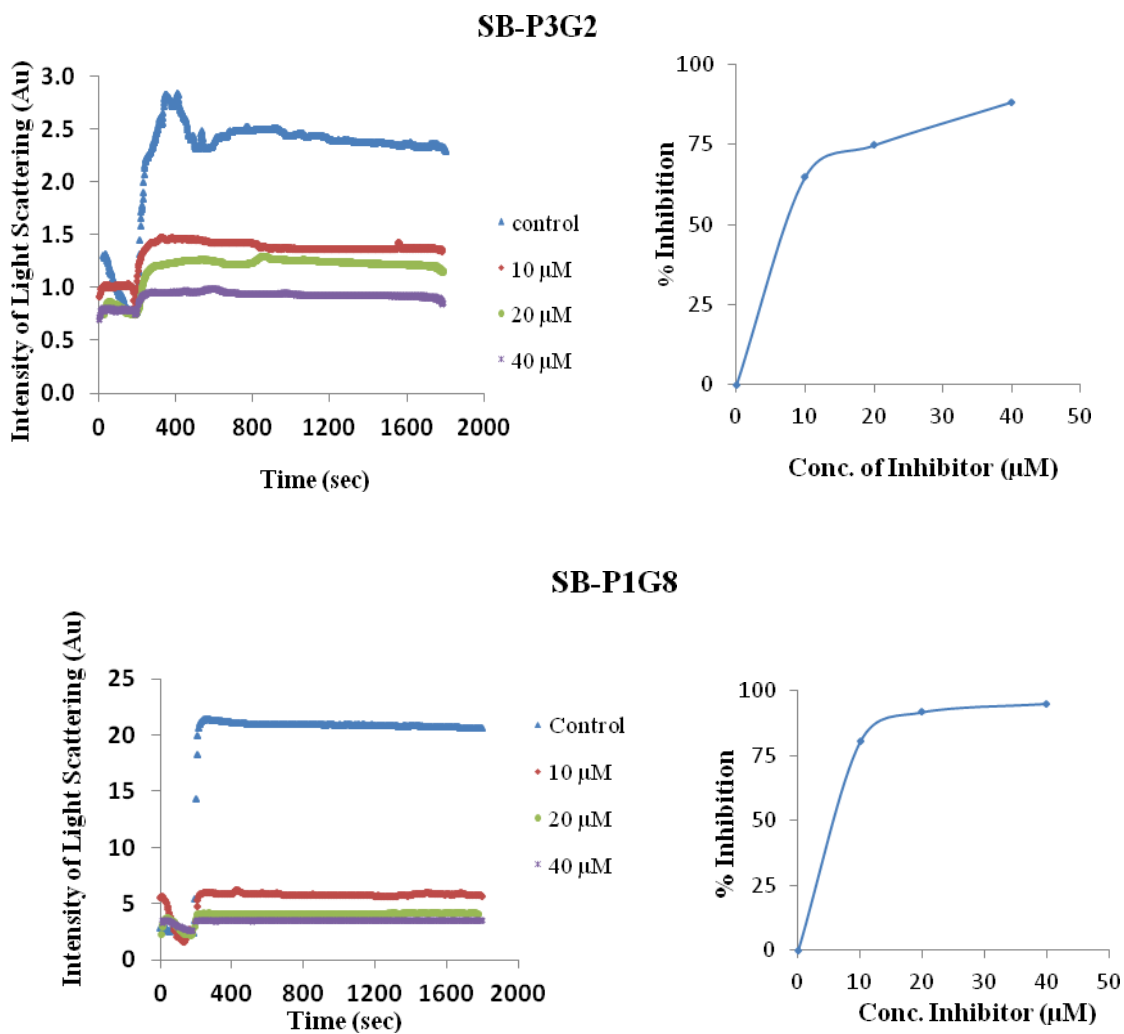


Figure III-3. Inhibition of FtsZ polymerization by lead benzimidazoles⁷

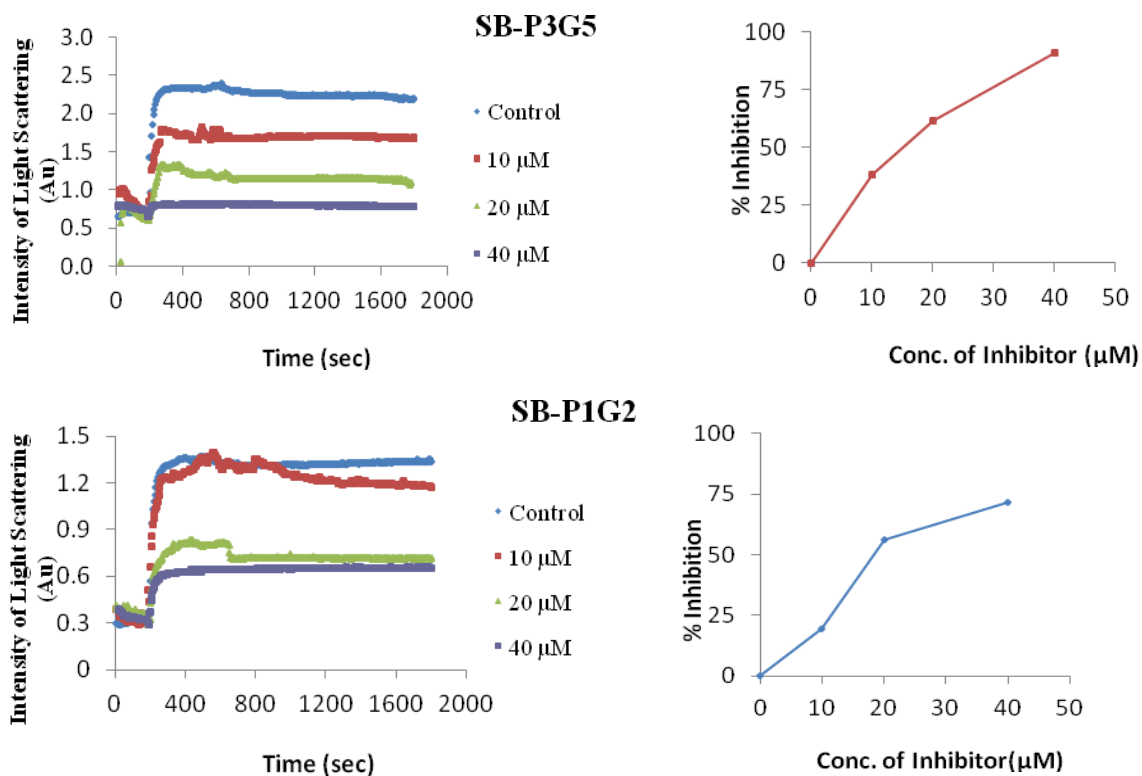


Figure III-4. Inhibition of FtsZ polymerization by lead benzimidazoles⁷

§ 3.2.2 GTPase Assay⁷

The assembly and disassembly of FtsZ protein has been shown to be GTP dependent. Since FtsZ has GTPase activity, the Malachite green assay was performed to monitor the amount of inorganic phosphate (Pi) released upon treatment of *Mtb* FtsZ with some of the lead compounds.

FtsZ protein at a concentration of 20 μM in polymerization buffer was incubated with **SB-P3G2** and polymerization was initiated by the addition of GTP. Two controls were maintained for this set of experiments. The first control was untreated protein with GTP, while the second was lead compound suspended in polymerization buffer. Upon addition of Malachite green reagent, formation of solid precipitate (believed to be the protein) in the wells containing protein was observed, therefore, accurate absorbance measurements could not be made. To prevent the precipitation of the protein, its concentration in the reaction mixture was reduced to 10 μM. Also an additional control i.e. protein suspended in polymerization buffer without any

GTP was included to eliminate any background reading. Unfortunately, this control showed absorbance upon the addition of the reagent. This indicated that the protein was already bound to inorganic phosphate, the source of which was probably the phosphate buffer used to purify the protein. The protein was washed with MES buffer (pH 6.5) to remove this inorganic phosphate. The GTPase assay was performed again with **SB-P3G2** and **SB-P3G5**. Upon treatment of *Mtb* FtsZ with the two compounds, an enhancement in GTPase activity was observed (**Figure III-5**).

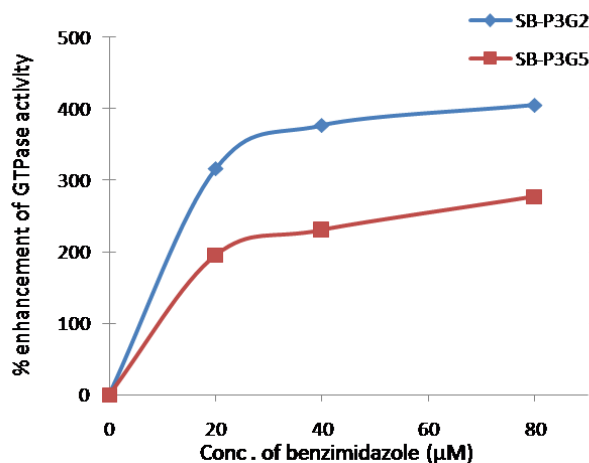


Figure III-5. Enhancement of GTPase activity of FtsZ by lead benzimidazoles⁷

This unique behavior is analogous to the effect curcumin has on recombinant *E.coli* FtsZ.¹³ Enhancement in the GTPase activity in combination with the previous data illustrating polymerization inhibition of FtsZ upon treatment with these compounds led to the conclusion that the increased GTPase activity causes the instability of FtsZ polymer. As a result of the instability, FtsZ is unable to polymerize and hence polymerization inhibition is observed.

§ 3.2.3 Transmission Electron Microscopy of FtsZ assembly⁷

To visualize the effect of the hit compounds on polymerization of FtsZ protein, TEM imaging of the treated and untreated FtsZ protein was carried out. FtsZ (12 μM) polymerized in the presence of GTP (50 μM) was transferred onto a carbon coated copper-mesh grid for TEM imaging. Unfortunately the filaments were too dense; therefore FtsZ concentration was reduced to 6 μM however, similar results were obtained. At 3 μM concentration of FtsZ, the filaments were too scattered. The method which proved successful was using 5 μM FtsZ, 25 μM GTP and diluting the sample 5 times before loading onto the grid. With the above described optimized

protocol, FtsZ protein treated with 40 μM or 80 μM **SB-P3G2** was visualized. Colchicine treated protein was used as a reference in this set of experiments (**Figure III-6**).

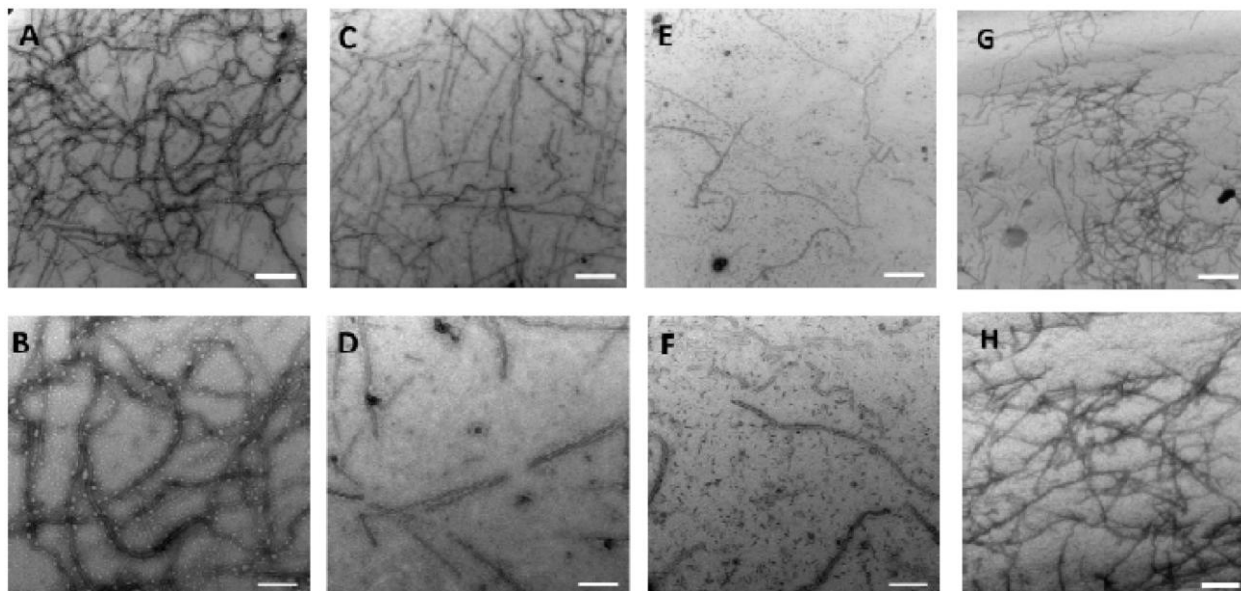


Figure III-6. Transmission electron microscope (TEM) images of FtsZ⁷

FtsZ (5 μM) was polymerized by GTP in the absence (**A, B**) and presence of **SB-P3G2** at 40 μM (**C, D**) and 80 μM (**E, F**). TEM images of the inhibition of FtsZ polymerization in the presence of colchicine at 200 μM (**G, H**) are also shown for comparison. Images (**A, C, E, G**) are at 30,000x magnification (scale bar 500 nm) and (**B, D, F, H**) are at 68,000x magnification (scale bar 200 nm).

As expected, there was considerable reduction in the extent of FtsZ protofilament formation upon treatment with **SB-P3G2** in comparison to the control experiment. At 40 μM concentration of **SB-P3G2**, the density of FtsZ protofilaments was considerably reduced. Furthermore the filaments were shorter and very thin which became more apparent at higher concentration of 80 μM . On the other hand, treatment of *Mtb* FtsZ protein with 200 μM colchicine clearly had a less profound effect on the inhibition of FtsZ polymerization. Similar formation of tiny aggregates was not observed as compared to **SB-P3G2** treated protein, reiterating the efficacy of the compound. This result definitely confirms that these novel benzimidazoles exhibit a remarkable FtsZ assembly inhibitory activity.

§ 3.2.4 Scan Electron Microscopy of *Mtb* cells⁷

Visualization of bacteria treated with 2xMIC and 4xMIC **SB-P3G2** for 2-days using scanning electron microscopy (SEM) revealed aberrant cell division indicative of FtsZ assembly

inhibition (**Figure III-7**). Specifically, cell division and elongation was inhibited in a dose dependent manner resulting in shorter bacterial cells with increased circumferences and altered polar caps. The observed altered bacterial morphology upon exposure to **SB-P3G2** is thought to result from inhibition of FtsZ leading to disruption in septum formation and recruitment of septum associated proteins involved in later steps of division and septum resolution.

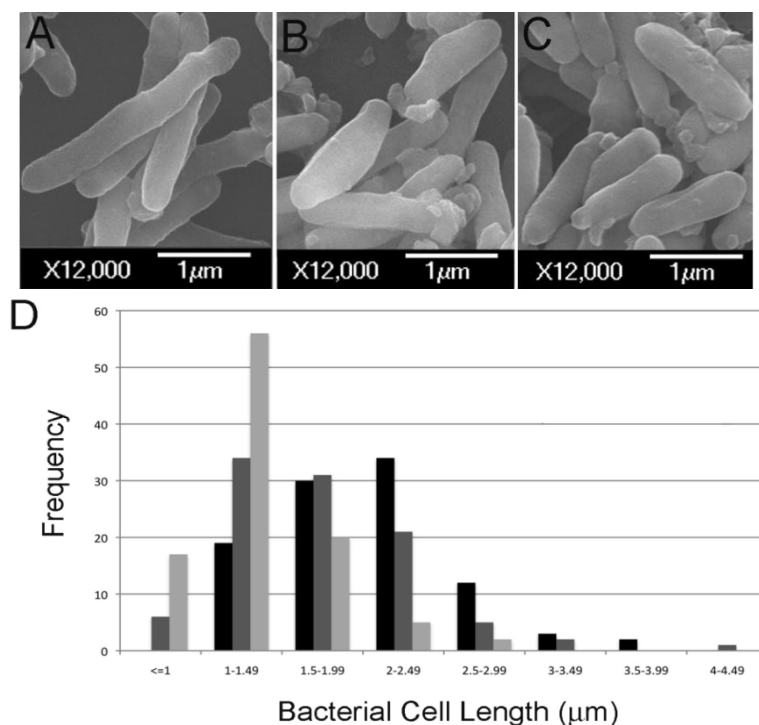


Figure III-7. SEM of *Mtb* cells treated with SB-P3G2 (20,000X).⁷

(A) Control; (B) 2x MIC; (C) 4 x MIC; (D) distribution of bacterial cell length: Control (black), 2x MIC (grey), 4x MIC (light grey)

§ 3.2.5 Photoaffinity labeling (PAL) of FtsZ for binding site determination

Though FtsZ kinetic assays confirmed that the novel trisubstituted benzimidazoles restrict the *Mtb* growth by inhibiting FtsZ polymerization, the mechanism of its action and binding site are still unknown. Furthermore, identifying the binding site could very well open a new dimension for structure-based design of more efficient inhibitors. In order to investigate the binding site of benzimidazoles, there are several experiments which can be carried out, including photoaffinity-labeling of FtsZ, co-crystallization of FtsZ and molecular docking (**Figure III-8**). Co-crystallization of *Mtb* FtsZ with our lead benzimidazole as well as taxane based-anti TB

agents could potentially be the most promising experiments to determine the binding site. For this experiment, lead taxanes as well as benzimidazoles which will be discussed in later chapters were synthesized.

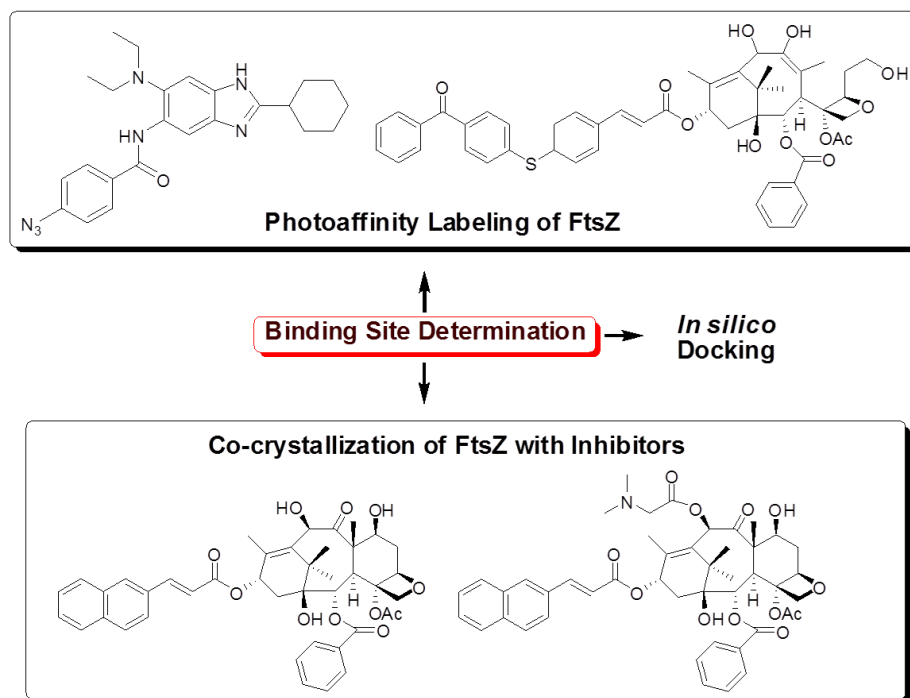
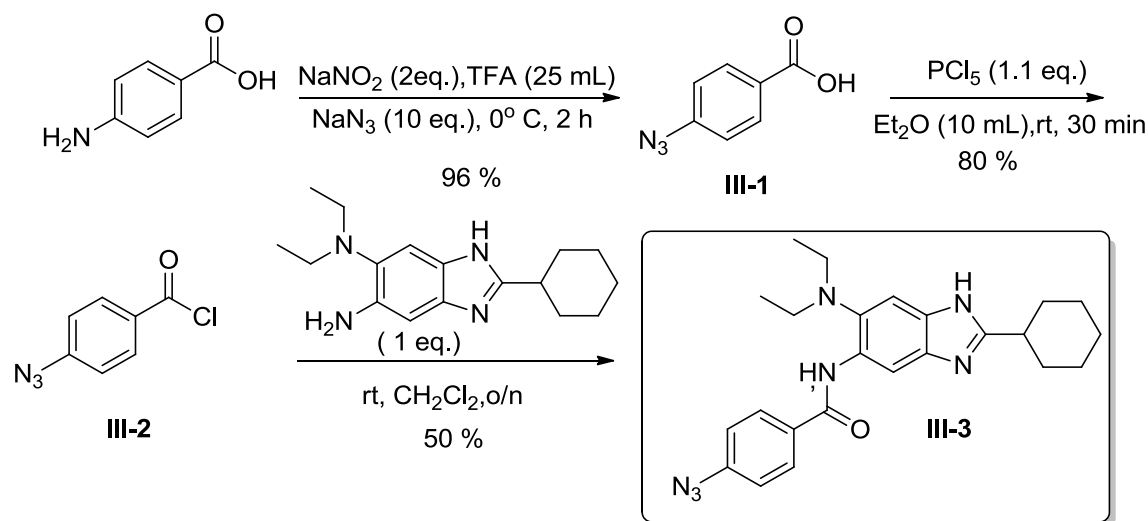


Figure III-8. Photoaffinity analogues (PAA) taxoid and benzimidazole based anti-TB agents

Photoaffinity-labeling (PAL) of FtsZ is another experiment whereby photolyzing FtsZ with the lead compounds containing photo labile group such as, azide, benzophenone will enable the identification of amino acid residues in the binding site. Thus, photoaffinity analogues of taxane-based and trisubstituted benzimidazole-based anti-TB agents were designed and synthesized to perform photoaffinity labeling experiments (**Figure III-8**). It should be noted that attachment of photoreactive groups, in this case azide and benzophenone, should not affect binding to the target proteins and hence should maintain good anti-TB activities. The taxoid based photoaffinity analogue (PAA) **SB-RA-50012** was previously investigated for its anti-TB activity and was found to show appreciable activity.⁸

The synthesis of photoaffinity analogue (PAA), 4-azido-SB-P1G8 **II-3** was carried out starting with diazotization of *p*-aminobenzoic acid and subsequent nucleophilic substitution by azido group to form *p*-azidobenzoic acid **II-1** in 96 % yield. Treatment with phosphorous

pentachloride gave *p*-azidobenzoyl chloride **III-2** in 80 percent yield. Finally coupling with the respective benzimidazole (**SB-P1G8**) gave the desired product **III-3** in 50 % yield (**Scheme III-1**).



In order to check the activity of 4-azido-SB-P1G8 (**III-3**) against *Mtb.* FtsZ, polymerization assay was carried out (**Figure III-9**). In comparing the inhibition of polymerization by **III-3** with that of **SB-P1G8**, it was concluded that no significant change was observed, confirming its activity.

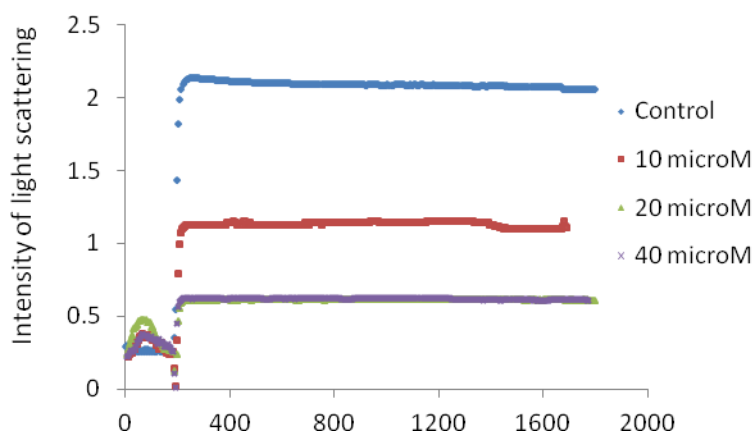


Figure III-8. Effect of 4-azido-SB-P1G8 on FtsZ polymerization

In the PAL experiment, FtsZ (polymerized and unpolymerized) was incubated with 4-azido-SB-P1G8 for 3 minutes following the polymerization conditions. The samples were then photolyzed at 360 nm for 30 minutes. After photolyzing the samples, FtsZ was precipitated using acetone method. In solution tryptic digestion of the precipitated protein was carried out, followed by MALDI analysis of the digested sample. The two control samples, polymerized and non-polymerized FtsZ with and without inhibitor were photolyzed. In the MALDI spectrum, it was expected to observe disappearance of a peptide peak and appearance of a new peptide peak with additional molecular weight (of the PAA). Unfortunately, when the MALDI spectrums were compared, no such phenomenon was observed (**Figure III-9 and Figure III-10**).

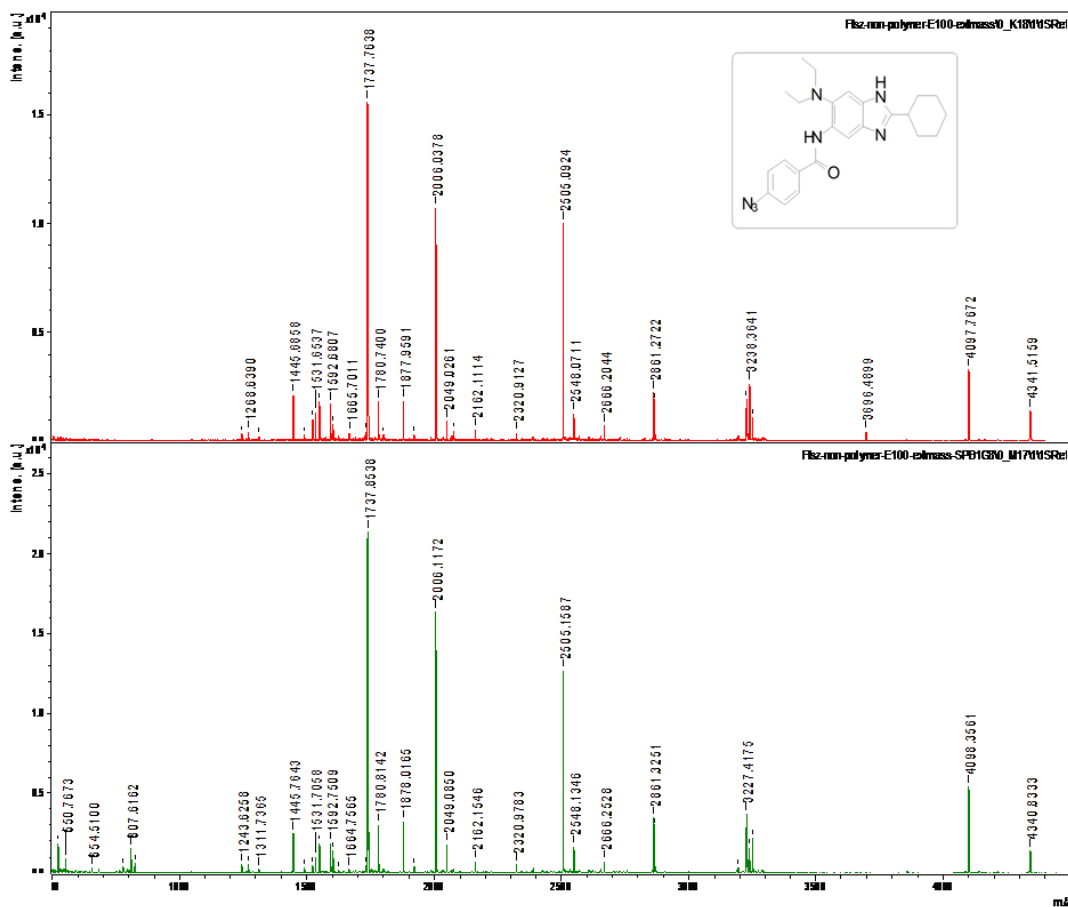


Figure III-9. MALDI of digested samples of non-polymerized FtsZ with and without PAA

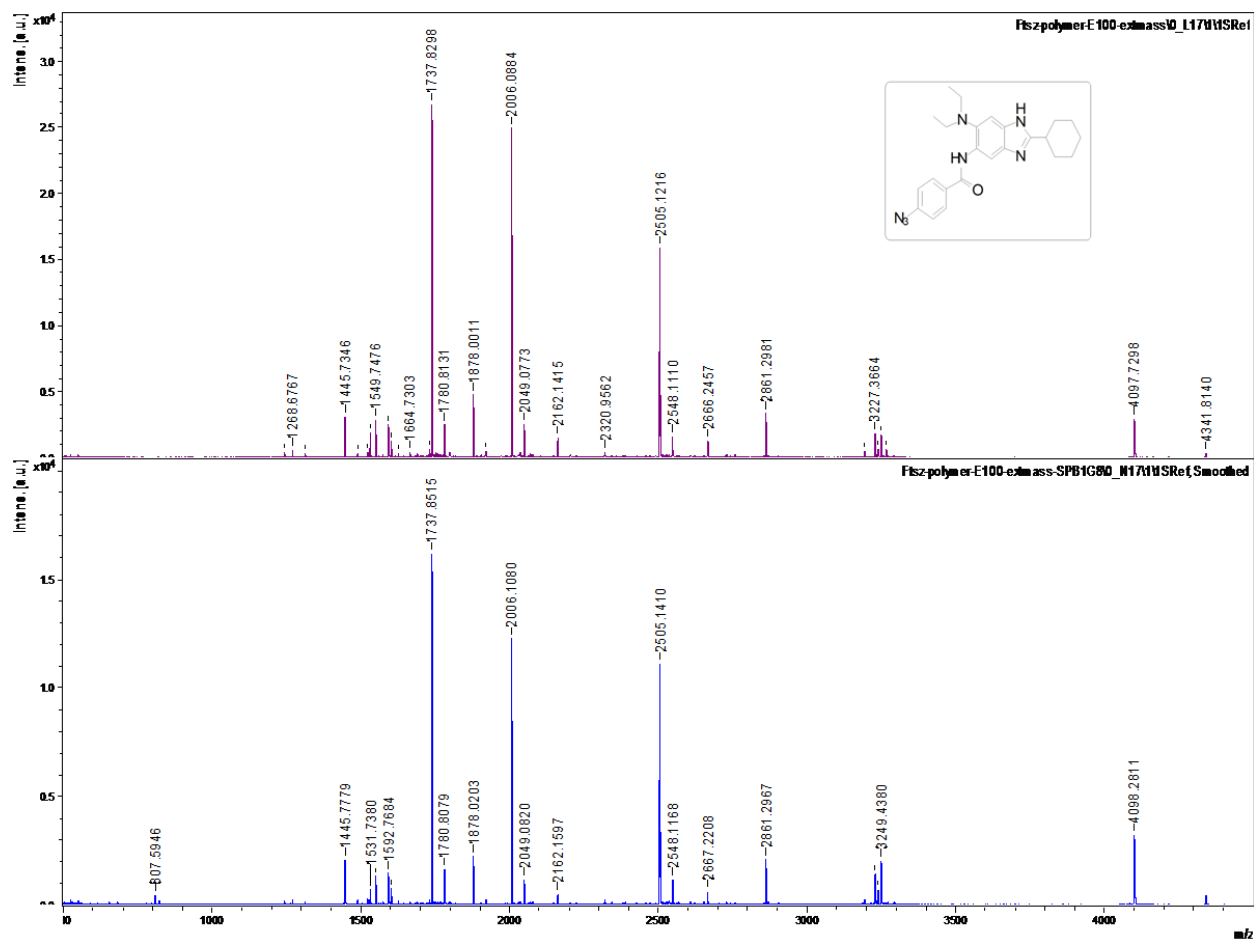


Figure III-10. MALDI of digested samples of polymerized FtsZ with and without PAA

At this end, PAL experiments have been tried with 4-azido-SB-P1G8. However, no relevant information about the binding site amino acid sequence has been gathered. Next, taxoid-based PAA will be used along with the optimization of photolysis time.

§ 3.2.6 Preliminary *in vivo* assays and formulation studies

The evidence presented by above mentioned experiments strongly suggests that the novel benzimidazoles directly inhibit FtsZ assembly by destabilizing the FtsZ polymer. The lead benzimidazole, **SB-P3G2** was advanced to *in vivo* testing. **SB-P3G2** was tested for efficacy against *M. tuberculosis* H37Rv in the *M. tuberculosis* rapid infection model. **SB-P3G2** was delivered intraperitoneally (IP) at a concentration of 150 mg/kg for 1 dose and 75 mg/kg for the last 8 doses. In the preliminary studies, it was observed the delivery of the lead compound was partial due to its poor solubility. Nevertheless, the compound demonstrated promising efficacy

based on greater than 0.3 reduction in \log_{10} CFU cutoff (**Figure III-11**). As a result, an increased effort was required to improve the solubility of our lead compounds *via* formulation (using surfactant) or by synthesizing water soluble prodrug.

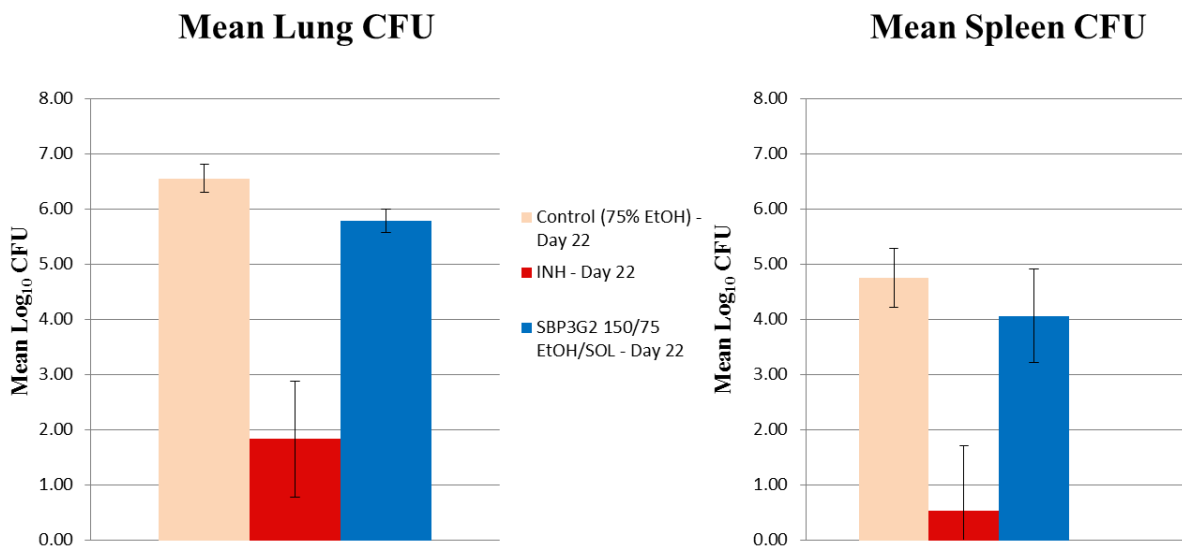


Figure III-11. Mean CFU in lung and spleen after 22 days of administration of compound

Eight groups of 5 mice each were treated for 9 days and then were assessed for bacterial burden in the lungs and spleen. SB-P3G2 was diluted in a solution of 12.5% ethanol, 10% solutol at 150mg/kg for 1 dose and 75mg/kg for the last 8 doses. There were 2 control groups (negative control group 1 received 20ul of 75% Ethanol and Positive control group 2 received isoniazid administered at 25mg/kg in water). All treatments and controls were delivered IP. Dosing was started at 12 days of infection and continued till day 21 of infection. On day 12 a pretreatment group was sacrificed and the bacterial loads for each mouse was determined prior to treatments. On day 22 the mice were sacrificed and the lungs and spleens were homogenized and plated on 7H11agar plates for CFU enumeration.

In order to develop a suitable formulation method, Solutol HS 15 was used as a solubilizing agent. The solubilizer Solutol HS 15 (polyethylenglycol 660 –12-hydroxystearate) is a non-ionic surfactant used for pharmaceutical purposes without showing any apparent toxicity. Solutol HS 15 is very efficient in solubilizing substances like fat-soluble vitamins, and active ingredients of hydrophobic nature. It has been observed that the solubilizing capacity of compounds increases linearly due to the formation of spherical micelles. To develop a suitable formulation, it is important to make sure that after injection the compound solution in solutol HS 15 should stay homogeneous without any immediate precipitation. In order to judge that, the homogeneity of the solution of our lead compounds in 1:1 (w/w) solution of solutol HS15 and EtOH when diluted by phosphate buffer saline (PBS pH 7.4) was examined. A solution of **SB-P3G2**, **SB-**

P8B2 and **SB-P8B4** in solutol HS 15/EtOH (1:1) at a concentration 20 mg/mL was diluted with PBS (Table III-1).

Table III-1. Formulation of lead benzimidazoles

A.	Solubility test of SB-P3G2 at room temperature
	1. 100 μ L of 20 mg/mL in solutol HS 15 (1:1)
	Added 300 μ L of PBS - No precipitate
	Added 100 μ L of PBS - Compound precipitated
	2. 100 μ L of 10 mg/mL in solutol HS 15 (1:1)
	Added 500 μ L of PBS - Few floating particles
	Added 200 μ L of PBS - More floating particles after 30 minutes
	Added 200 μ L of PBS - Compound precipitated
B.	Solubility test of SB-P8B2 and SB-P8B4 at room temperature
	1. 100 μ L of 20 mg/mL in solutol HS 15 (1:1)
	Added 800 μ L of PBS – No precipitate
	Left for 2 days-Homogeneous solution
	2. 100 μ L of 10 mg/mL in solutol HS 15 (1:1)
	Added 1000 μ L of PBS - No precipitate
	Left for 2 days-Homogeneous solution

SB-P8B2 and **SB-P8B4** showed better solubility results as compared to **SB-P3G2** at concentrations of 20 mg/mL and 10 mg/mL. **SB-P3G2** solution started to precipitate after 4-6 times dilution by PBS at room temperature. However, in case of **SB-P8B2** and **SB-P8B4**, the solution remained homogeneous even after 8-10 times dilution and 2 days at room temperature. Thus, it was concluded that administering 1 dose of 4 mg or 2 doses of 2 mg of the lead compound would be ideal for overcoming the solubility issues. In other words, just before injection, stock solution of the lead compounds (40 mg/mL or 20 mg/mL in solutol HS 15/EtOH) can be diluted with appropriate volume of PBS (to keep the ethanol volume to a permissible level) so that each dose has either 4 mg or 2 \times 2 mg. Presently, the *in vivo* assays are being repeated by our collaborator Prof. Slayden laboratory following our formulation.

§ 3.3 Conclusion

Several novel trisubstituted-benzimidazoles were designed and synthesized through rational and systematic design. In preliminary cell-based screening against *Mtb* H37Rv strain, several of these compounds exhibited MIC₉₉ values in the range of 1.2-15 µM along with limited cytotoxicity. In a light scattering experiment, several of these novel lead compounds exhibited inhibition of FtsZ assembly in a dose dependent manner. Additionally, GTPase activity of *Mtb* FtsZ was enhanced by 3-4 folds as observed in malachite green assay.

SEM images of *Mtb* cells treated with **SB-P3G2** showed dose dependent shortening of cell length. A visible reduction in the extent of FtsZ polymerization was observed under transmission electron microscope. The FtsZ protofilaments were shorter in length in comparison to the untreated FtsZ which became more apparent at higher concentrations of **SB-P3G2**. At this end, photoaffinity labeling of FtsZ with 4-azido-SB-P1G8 haven't been able to provide relevant information about the binding site. In the preliminary *in vivo* studies, although the delivery of our lead compounds was partially limited due to poor solubility, **SB-P3G2** demonstrated promising efficacy based on greater than 0.3 reduction in log₁₀CFU cutoff.

The evidence presented in this study strongly suggests that these novel benzimidazoles can directly inhibit proper FtsZ assembly by destabilizing the FtsZ polymer which is unequivocally confirmed by SEM and TEM images. Further optimization and *in vivo* evaluation of these newly discovered lead compounds are actively underway in our laboratories.

§ 3.4 Experimental Section

General Methods: ^1H and ^{13}C NMR spectra were measured on a Varian 300, 400 or 500 MHz NMR spectrometer. Melting points were measured on a Thomas Hoover Capillary melting point apparatus and are uncorrected. TLC was performed on Merck DCalufolien with Kieselgel 60F-254 and column chromatography was carried out on silica gel 60 (Merck; 230-400 mesh ASTM). SensoLyte® MG phosphate assay kit from Anaspec was used for Malachite Green assay. Light scattering assays were performed using a Fluorolog fluorimeter from ISA instruments. Scanning electron micrographs were obtained with a JOEL JSM-6500F scanning electron microscope. FEI Tecnai12 BioTwinG transmission electron microscope with an AMT XR-60 CCD digital camera system was used to acquire transmission electron microscopy images.

Materials: BL21(DE3)pLysS cells, Ni-NT and the buffers were purchased from Novagen. BCA kit for protein concentration determination was purchased from Sigma Aldrich. Malachite Green Carbinol Base was bought from Sigma Aldrich. Ammonium molybdate (VI) tetrahydrate was provided by Acros. Buffer salts (reagent grade or better), solvents (HPLC grade or better), and all the other chemicals were purchased from Fisher Scientific Co. (Pittsburgh, PA). The chemicals were purchased from Sigma Aldrich and Synquest Inc. and purified before use. Tetrahydrofuran was freshly distilled from sodium metal and benzophenone. Dichloromethane was distilled immediately prior to use under nitrogen from calcium hydride.

§ 3.4.1 *Mtb FtsZ Protein Preparation*^{2,9}

The appropriate (pET 15 b) plasmid (1.5 μL and 3 μL) was transformed into 100 μL of BL21(DE3) pLys cells. The transformed cells were plated onto LB plates, containing 100 $\mu\text{g}/\text{mL}$ ampicillin. The antibiotic concentration was kept the same for the following steps. The plates were incubated overnight at 37 °C. The colonies were picked and grown in 10 mL of LB media at 37 °C at 250 rpm shake rate. The inoculum was transferred to 1 L of LB media in a 4 L flask and grown to an OD of 0.4 at A600. Then, 1 mM IPTG was added to induce protein expression overnight at 32 °C at 250 rpm shake rate. Next day the cells were harvested at 5K rpm for 30 min and re-suspended in approximately 20-30 mL binding buffer (300 mM NaCl, 50 mM NaH_2PO_4 , 10 mM imidazole, pH = 8). The re-suspended cells were lysed using ultra-sonicator. The lysate

was centrifuged in an ultracentrifuge at 33K rpm for 90 min. The supernatant was filtered and loaded onto Ni²⁺-NTA column washed with 50 mL of binding buffer and eluted using a gradient of binding buffer with 50-250 mM imidazole. The eluted protein was immediately loaded onto a G-25 size exclusion chromatography column, pre-equilibrated with the polymerization buffer (50 mM MES, 5mM MgCl₂, 50 mM KCl, pH 6.5). The protein fractions were concentrated and stored at -80 °C for further use. Since the number of aromatic residues in *Mtb* FtsZ protein are low (Tyr: 1, Trp: 0), it is not reliable to follow concentration of protein by scanning at A280. The concentration of protein was therefore ascertained using the BCA kit from Sigma.

§ 3.4.2 FtsZ Polymerization Inhibitory Assay⁹

The inhibitory activity of lead benzimidazoles for *Mtb* FtsZ polymerization was determined by light scattering on a PTI Fluorescence Master Systems. The 90° light scattering was measured at 30 °C, using excitation and emission wavelength of 400 nm with slit width of 2 nm. The gain was set at 950 V. *Mtb* FtsZ (15 µM) was incubated in the polymerization buffer (50 mM MES, 5mM MgCl₂, 50 mM KCl, pH 6.5) to establish a baseline. Then, 5 mM GTP (20 µL) was added to make the final volume 1,000 µL in a 1.5 mL cuvette. The light scattering was measured for a period of 30-60 min. When DMSO was used as a solvent for the inhibitor, the control also contained the same amount of DMSO. For inhibition studies, a lead benzimidazole at various concentrations was incubated with the polymerization buffer to establish a base line. This was followed by addition of FtsZ (15 µM). Once the baseline was stabilized, 5 mM GTP (20 µL) was added to make the final volume 1,000 µL in a 1.5 mL cuvette and the light scattering was measured.

§ 3.4.3 GTPase Assay

The amount of inorganic phosphate (Pi) released during the assembly of FtsZ was measured using a standard Malachite Green/ammonium molybdate assay. Briefly, FtsZ protein (10 µM) was incubated with or without a benzimidazole at different concentrations (0, 20, 40 and 80 µM) in polymerization buffer (50 mM MES, 5 mM MgCl₂, 50 mM KCl, pH 6.5) at room temperature for 15 min. Then, 50 µM GTP was added to the reaction mixture and incubated at 37 °C to start the hydrolysis reaction. After 30 min of incubation, Malachite green reagent (20% v/v) was

added to the reaction mixtures to quench the reaction. The reaction mixtures were centrifuged at 13,000 rpm for 90 sec to remove the protein debris. The samples (100 μ L) were transferred to a 96 well plate and the absorbance of each well was measured at 620 nm. The background absorbance was subtracted from all the readings. A phosphate standard curve was prepared using phosphate standard provided with a Malachite Green assay kit (SensoLyte®). All the solutions were prepared in polymerization buffer.

§ 3.4.4 Transmission Electron Microscopy (TEM) Analysis¹⁰

Mtb FtsZ (5 μ M) was incubated with 40 μ M or 80 μ M of **SB-P3G2** in the polymerization buffer (50 mM MES, 5mM MgCl₂, 50 mM KCl, pH 6.5) for 15-20 min. To each solution was added GTP to a final concentration of 25 μ M. The resulting solution was incubated at 37 °C for 30 min. The incubated solution was diluted 5 times with the polymerization buffer and immediately transferred to carbon coated 300 mesh formvor copper grid and negatively stained with 1 % uranyl acetate. The samples were viewed with a FEI Tecnai12 BioTwinG transmission electron microscope at 80 kV. Digital images were acquired with an AMT XR-60 CCD Digital Camera System.

§ 3.4.5 Ultrastructural analysis via scanning electron microscopy (SEM)

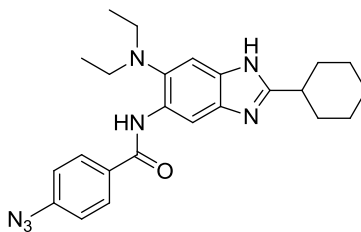
Mtb H37Rv bacteria were exposed to 2 x MIC and 4 x MIC **SB-P3G2** for 2 days. The bacteria were prepared for scanning electron microscopy as described by Slayden et. al.³ Briefly, bacteria were prepared for SEM treatment with 2.5% glutaraldehyde in 0.1 M sodium cacodylate (pH 7.2), 5mM CaCl₂ and 5 mM MgCl₂ and incubated at room temperature for 1-2 h. The fixed bacteria were harvested by centrifugation and washed in PBS, and subjected to 2.5% glutaraldehyde overnight at 4 °C. Final preparation for SEM was achieved by treatment with 1% OsO₄ in sodium cacodylate buffer and dehydration in a graded alcohol series. The bacteria were then examined using a JOEL JSM-6500F scanning electron microscope. Bacteria from all treatment groups were measured for their lengths. Size frequency graphs were prepared for each treatment group.

§ 3.4.6 Photoaffinity Labeling of FtsZ using 4-azido-SB-PIG8

500 μL of 15 μM FtsZ (polymerized and unpolymerized) was incubated with 2 μL of 10 mM photoaffinity analogues 4-azido-SB-PIG8 in polymerization buffer for 3 minutes following the polymerization conditions. Two control samples, polymerized and non-polymerized FtsZ with and without inhibitor, were photolyzed at 360 nm for 30 minutes using southern RMR3500 2 lamps. After photolyzing the samples, FtsZ was precipitated using acetone method. Four volumes of cold acetone was mixed with one volume of photolyzed protein sample and stored at $-20\text{ }^{\circ}\text{C}$ for 20-30 minutes. The solution was centrifuged at 15000g for 15 minutes. The supernatant was discharged carefully and the protein pellets were air dried. In solution tryptic digestion of the precipitated protein was carried out. The pellets were mixed with 10 M urea and 1 M Tris-HCl (pH 8.5) to bring up the solution to 8 M urea and 100 mM Tris-HCl. 100 mM TCEP (reducing agent) was added to a final concentration of 5 mM TCEP and incubated at room temperature for 20 minutes. Later, 500 mM iodoacetamide (freshly prepared) was added to a final concentration of 10 mM and incubated at room temperature in dark for 15 minutes. The above samples were diluted by a factor of four with 100 mM Tris-HCl (pH 8.5) followed by addition of 100 mM CaCl_2 to a final concentration of 1 mM. Finally trypsin (0.4 $\mu\text{g}/\mu\text{L}$) was added to the above solution, incubated overnight and quenched with 5 % formic acid solution. These samples were then subjected to MALDI analysis.

§ 3.4.7 Synthesis of photoaffinity analogue 4-Azido-SB-PIG8

4-azido-*N*-(2-cyclohexyl-6-(diethylamino)-1H-benzimidazol-5-yl)benzamide (III-3):



4-Aminobenzoic acid (1.0 g, 7.3 mmol) dissolved in TFA (25 mL) was diazotized in the dark at $0\text{ }^{\circ}\text{C}$ with NaNO_2 (1.0 g, 14.6 mmol). After stirring for 30 minutes, sodium azide (4.75 g, 73 mmol) was slowly added to the reaction mixture over a period of 5 minutes. After an additional 15 minutes, diethyl ether (20 mL) was added and the mixture was stirred for 1 hour. The reaction mixture was washed with water, extracted with diethyl ether, and dried over magnesium sulfate.

Removal of excess TFA as an azeotrope with benzene gave **III-1** as a white powder (1.12 g, 96 % yield) with m.p. 182-184 °C (lit. m.p. 185 °C)¹¹.

4-Azidobenzoic acid (259 mg, 1.58 mmol) was dissolved in diethyl ether (10 mL) followed by the addition of phosphorous pentachloride (352 mg, 1.74 mmol) The reaction mixture was stirred for 30 minutes. The diethyl ether was removed under vacuum to obtain yellow oil which crystallized under vacuum. The solid was triturated with hexane at 0 °C to give **III-2** as white solid (230 mg, 80 % yield) with m.p. 55-56 °C (Lit. m.p. 57-58 °C)¹².

To a solution of 5-Amino-6-*N,N*-diethylamino-2-cyclohexyl-1*H*-benzo[d]imidazole (38.8 mg, 0.135 mmol) in methylene chloride (mL) was added **III-2** (23 mg, 0.121 mmol) and stirred overnight. After the completion of reaction, the solvent was removed and the crude was purified by flash chromatography (gradient 20-40 % EtOAc/hexanes) to give **III-3** (15 mg, 50 % yield). ¹HNMR (300 MHz, CDCl₃) δ 0.97 (m, 6 H, *J* = 7.0 Hz), 1.25-1.28 (m, 5 H), 1.57-1.58 (m, 3H), 2.04 (m, 2 H), 2.77 (m, 1 H), 3.02 (q, 4 H, *J* = 6.9 Hz), 7.18 (d, 2 H, *J* = 4.2 Hz), 7.26 (s, 1 H), 7.58 (s, 1 H), 7.97 (d, 2 H, *J* = 4.2 Hz), 8.86 (s, 1 H), 10.3 (s, NH); ¹³CNMR (100 MHz, CDCl₃) δ 13.13, 25.71, 25.97, 31.73, 38.46, 50.79, 100.5, 113.4, 119.3, 128.6, 131.8, 135.1, 139.5, 143.5, 159.6, 163.8. MS (ESI) *m/z* 432.1 (M+1)⁺.

§ 3.5 References

1. Errington J., Daniel R. A., Scheffers D-J. Cytokinesis in bacteria. *Microbiol. Mol. Biol. Rev.* **2003**, *67*, 52-65.
2. Respicio L., Nair P. A., Huang Q., Burcu A., Tracz S., Truglio J. J., Kisker C., Ralieggh D. P., Ojima I., Knudson D. L., Tonge P. J., Slayden R. A. Characterizing septum inhibition in *Mycobacterium tuberculosis* for novel drug discovery. *Tuberculosis* **2008**, *88*, 420-429.
3. Slayden R. A., Knudson D. L., Belisle J. T. Identification of cell cycle regulators in *Mycobacterium tuberculosis* by inhibition of septum formation and global transcriptional analysis. *Microbiology* **2006**, *152*, 1789-1797.
4. Vollmer, W. The prokaryotic cytoskeleton: A putative target for inhibitors and antibiotics? *Appl. Microbiol. Biotech.*, **2006**, *73*, 37-47.
5. Kumar, K.; Awasthi, D.; Berger, W. T.; Tonge, P. J.; Slayden, R. A.; Ojima, I., Discovery of anti-TB agents that target the cell-division protein FtsZ. *Future Med. Chem.* **2010**, *2*, 1305-1323.
6. Awasthi, D.; Kumar, K.; Ojima, I., Therapeutic potential of FtsZ inhibition: a patent perspective. *Expert Opin. Ther. Patents* **Early Online** (2011).
7. Kumar, K.; Awasthi, D.; Lee, S.-Y.; Zanardi, I.; Ruzsicska, B.; Knudson, S.; Tonge, P. J.; Slayden, R. A.; Ojima, I., Novel Trisubstituted Benzimidazoles, Targeting *Mtb* FtsZ, as a New Class of Antitubercular Agents. *J. Med. Chem.* **2011**, *54*, 374-381.
8. Huang, Q.; Kirikae, F.; Kirikae, T.; Pepe, A.; Amin, A.; Respicio, L.; Slayden, R. A.; Tonge, P. J.; Ojima, I., Targeting FtsZ for Antituberculosis Drug Discovery: Noncytotoxic Taxanes as Novel Antituberculosis Agents. *J. Med. Chem.* **2006**, *49*, 463-466.
9. White, E. L.; Ross, L. J.; Reynolds, R. C.; Seitz, L. E.; Moore, G. D.; Borhani, D. W. Slow polymerization of *Mycobacterium tuberculosis* FtsZ. *J. Bacteriol.* **2000**, *182*, 4028-4034.
10. Jaiswal, R.; Beuria, T. K.; Mohan, R.; Mahajan, S. K.; Panda, D., Totarol inhibits bacterial cytokinesis by perturbing the assembly dynamics of FtsZ. *Biochemistry* **2007**, *46*, 4211-4220.

11. Shields, C. J.; Falvey, D. E.; Schuster, G. B.; Buchardt, O.; Nielsen, P. E., Competitive singlet-singlet energy transfer and electron transfer activation of aryl azides: application to photo-cross-linking experiments. *J. Org. Chem.* **1988**, *53*, 3501-3507.
12. Merrill, S. H.; Unruh, C. C., Photosensitive azide polymers. *J. Appl. Polymer Sci.* **1963**, *7*, 273-279.
13. Rai, D.; Singh, J. K.; Roy, N.; Panda, D., Curcumin inhibits FtsZ assembly: an attractive mechanism for its antibacterial activity. *Biochem. J.* **2008**, *410*, 147-155.

Chapter IV

Discovery of Novel Trisubstituted Benzimidazole-Based Antibacterial Agents Against Other Pathogens

Table of Contents

§ 4.1 Introduction.....	113
§ 4.2 Compounds targeting FtsZ from other pathogens	115
§ 4.3 Results and discussion:	123
§ 4.3.1 Preliminary screening against different bacterial strains	123
§ 4.3.2 Ex-vivo efficacy of hit benzimidazoles against <i>B.thailandensis</i> and <i>F. tularensis</i>	125
§ 4.3.3 Resynthesis of 2,5,6-trisubstituted hit benzimidazoles for accurate MIC ₉₉ <i>determination</i>	127
§ 4.4 Conclusion	131
§ 4.5 Experimental Section.....	132
§ 4.6 References.....	139

§ 4.1 Introduction

Bacterial infections due to pathogens such as methicillin-resistant *Staphylococcus aureus* (MRSA), vancomycin-resistant *enterococci* (VRE), *F. tularensis*, *Y. pestis*, *B. thailandensis*, and others have re-emerged as major health concerns throughout the world. Infections due to VRE and MRSA are a particular nosocomial problem in hospitalized or immuno-compromised individuals as well as healthcare professionals.^{1,2,3} These organisms are often resistant to multiple antibiotics. In the past two decades, there has been a rapid increase in the incidence of VRE and MRSA infections. Community-acquired (CA) MRSA infections among young persons have emerged in several areas worldwide during the last decade which represents a new challenge for healthcare professionals.⁴ According to the Center for Disease Control and Prevention (CDC), the estimated number of people developing invasive MRSA infection in 2005 was about 94,360, while approximately 18,650 people died during a hospital stay related to these MRSA infections in the United States.² In spite of the serious situation, there are only a small number of FDA-approved therapeutic drugs including, linezolid, daptomycin, tigecycline, quinupristin, platensimycin, clindamycin available to treat these infections. However, these drugs have been found to show limited efficacy and furthermore, drug resistance has already been observed.⁵

Francisella tularensis is a highly virulent gram-negative bacterium and the causative agent of tularemia.⁶ Due to its high virulence and difficult diagnosis, *F. tularensis* is classified as a Class A agent pathogen by the U.S. government.⁷ Tularemia can be treated to a certain extent by a cocktail of antibiotics such as streptomycin, gentimycin, doxycycline, and ciprofloxacin.^{8,9}

Yersinia pestis is another gram-negative rod-shaped bacterium, belonging to the *enterobacteriaceae* family.⁶ *Y. pestis* infection takes three main forms, i.e., pneumonic, septicemic, and the notorious bubonic plagues, which have been responsible for a number of high-mortality epidemics in the past.^{6,10} More recently, *Y. pestis* has gained attention as a possible biological warfare agent and CDC has classified it as a category A pathogen requiring preparation for a possible terrorist attack.¹¹ About 14% (1 in 7) of all plague cases in the United States are fatal. Globally, the WHO reports 1,000 to 3,000 cases of plague every year.¹² The traditional first line treatment for *Y. pestis* has been streptomycin, chloramphenicol, tetracycline, and fluoroquinolones.^{13,14} In addition, there are various other neglected diseases caused by bacterial infections such as buruli ulcer, trachoma, leprosy, cholera, lyme disease, etc., which

need special attention due to their highly epidemic nature in areas such as Africa, Asia, and Russia.¹⁵

The treatment regimen for above mentioned infections are still limited to rather classical antibacterial drugs that target cell wall biosynthesis, nucleic acid synthesis, protein synthesis, etc.¹⁶ Furthermore, the widespread bacterial resistance to existing therapeutics due to poor drug compliance has been a crucial obstacle in finding suitable and more efficient treatments. Therefore, in order to circumvent the adaptive genetic machinery of bacteria, there is a pressing requirement for the identification of novel therapeutic targets. As mentioned in previous chapters, FtsZ offers an excellent therapeutic target since the disruption of cell division would lead to the inhibition/arrest of bacterial growth (**Figure IV-1**).^{17,18}

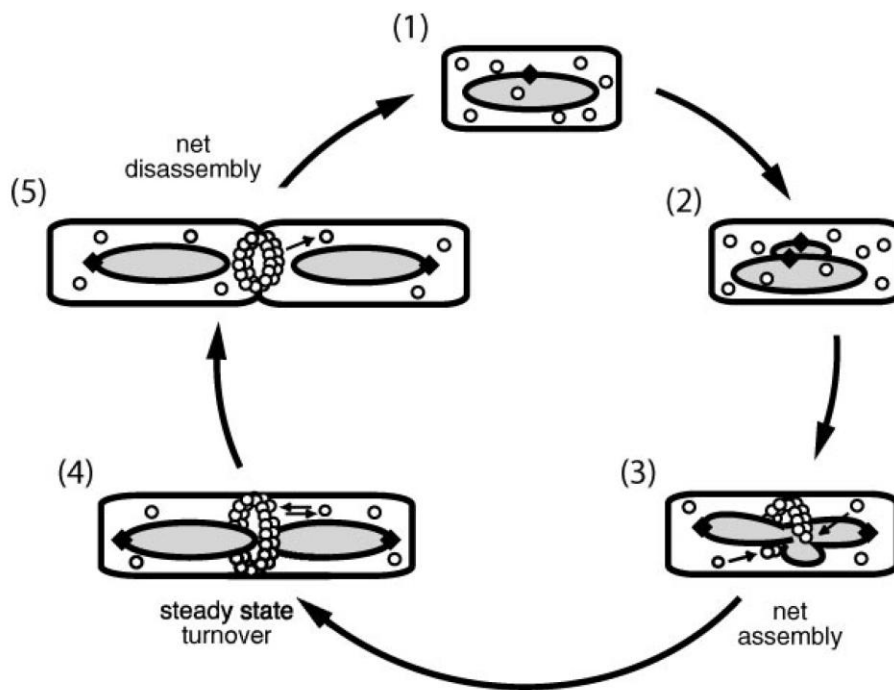


Figure IV-1. Graphic representation of Z-ring formation and cell division.¹⁹

(1) Bacterial cell before the beginning of cell division with FtsZ (O) scattered in the cell and undergoing continuous nucleotide exchange between GTP-bound FtsZ and GDP-bound FtsZ with rapid equilibrium, favoring GTP-bound FtsZ. A circular chromosome with a single origin of replication (◆) is located at midcell. (2-4) After chromosome replication initiates, the origins of replication separate and move to opposite poles of the cell. After completion of replication, the chromosomes separate, leaving a nucleoid-free space. (3) Z-ring formation coincides with chromosome segregation. (5) During cytokinesis the Z-ring constricts leading to septum formation. Complete disassembly of the Z-ring forms the daughter cells.

FtsZ offers a significant potential advantage over traditional targets as it is a highly conserved protein in prokaryotes. Thus, in addition to being pathogen specific, FtsZ inhibitors

could potentially be developed as broad-spectrum antibacterial agents for the treatment of a variety of bacterial infections.²⁰ Since FtsZ is an essential and conserved protein for bacterial cell division, it is believed that escaping the FtsZ-targeted compounds by mutating the protein may be demanding for bacteria, suggesting that resistance mechanisms against compounds developed for FtsZ inhibition may not be widespread in nature.^{21,22} Furthermore, extensive structural and functional homology^{23,24,25} between FtsZ and tubulin provides an opportunity to use known tubulin/microtubules (de)stabilizer as an excellent starting point for the development of novel antibacterial agents. Considering the limited sequence homology between tubulin and FtsZ at protein level, compounds specific to FtsZ should have no appreciable cytotoxicity to eukaryotic cells.²⁶ As described in previous chapters, a number of active trisubstituted benzimidazoles against *Mtb* FtsZ have already discovered. Therefore, our library of trisubstituted benzimidazoles was screened against various pathogens to identify broad-spectrum inhibitors of FtsZ assembly.

§ 4.2 Compounds targeting FtsZ from other pathogens

Representative FtsZ inhibitors for bacterial strains other than *Mtb* are summarized in **Tables IV-1 & IV-2**. The structures of these FtsZ inhibitors are shown in **Figure IV-2** and **Figure IV-3**. These inhibitors have relevance to the discovery and development of broad-spectrum FtsZ inhibitors since FtsZ structure is well conserved in all bacterial species.

Zantrins

A high throughput (HTP) protein-based screening of 18,320 molecules lead to the identifications of five structurally diverse compounds named “zantrins”, which inhibited *E. coli* FtsZ GTPase activity by 50 % at 4-25 μ M concentration.^{17, 27} Zantrins were also examined for inhibitory activity against FtsZ orthologue from *Mtb*. Majority of zantrins inhibited the GTPase activity of *Mtb* FtsZ with IC₅₀ values in the range of 50-70 μ M.

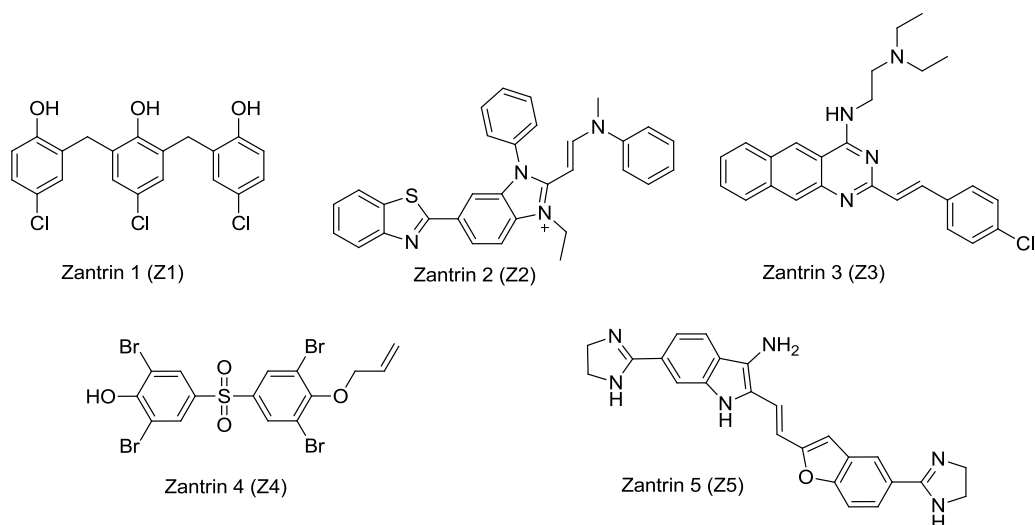


Figure IV-2. FtsZ inhibitors against pathogens other than *Mtb*

It was proposed that these FtsZ-destabilizing zantrins (**Z1** and **Z4**) may bind to a pocket between two FtsZ subunits to block the loop T7 of one monomer to come in optimal contact with GTP bound to the T1-T6 loops of the neighboring monomer, which is essential for polymerization.²⁸ In contrast, some zantrins (**Z2**, **Z3** and **Z5**) appeared to stabilize the FtsZ assembly by contracting the movement of T3 loop that causes a bend in the filament upon GTP hydrolysis.

Viriditoxin

Viriditoxin, a potent *E. coli* FtsZ inhibitor, was identified from a pool of more than 100,000 extracts of microbial fermentation broths and plants using FtsZT65C-fluorescein polymerization assay.²⁹ It exhibited *E. coli* FtsZ polymerization inhibition with an IC₅₀ of 8.2 µg/mL and GTPase inhibition with an IC₅₀ of 7 µg/mL. Furthermore, Viriditoxin was also evaluated for its broad-spectrum antibacterial activity. It inhibited the growth of *S. aureus* and MRSA with MIC values of 4-8 µg/mL and *enterococcus faecalis* and VRE with MIC values of 2-16 µg/mL.

GTP analogues

Lappchen *et al.* designed a novel inhibitor of *E. coli* FtsZ, 8-bromoguanosine-5'-triphosphate (BrGTP), based on the natural substrate GTP.³⁰ GTPase assay and polymerization

assay indicated that BrGTP is a reversible competitive inhibitor of *E. coli* FtsZ. Paradis-Bleau *et al.* synthesized a library of GTP analogues with core structures composed of a guanine-like moiety linked to an alanine side chain (GAL analogues).³¹ All the GAL analogues moderately inhibited the GTPase activity of *Pseudomonas aeruginosa* FtsZ (IC₅₀ 450 μM ~ 2.6 mM).

Sanguinarine

Sanguinarine, a benzophenanthridine alkaloid derived from the rhizomes of *Sanguinaria canadensis*, is known to have a broad range of antimicrobial activity (**Figure IV-3**).³² Beuria *et al.* reported that sanguinarine inhibited cytokinesis in both gram-positive and gram-negative bacteria by arresting *E. coli* FtsZ assembly.³³ Sanguinarine inhibited the extent of light scattering developing from FtsZ polymerization. Electron microscopic images of FtsZ polymer treated with sanguinarine indicated reduced thickness and significantly shorter lengths of FtsZ bundles.

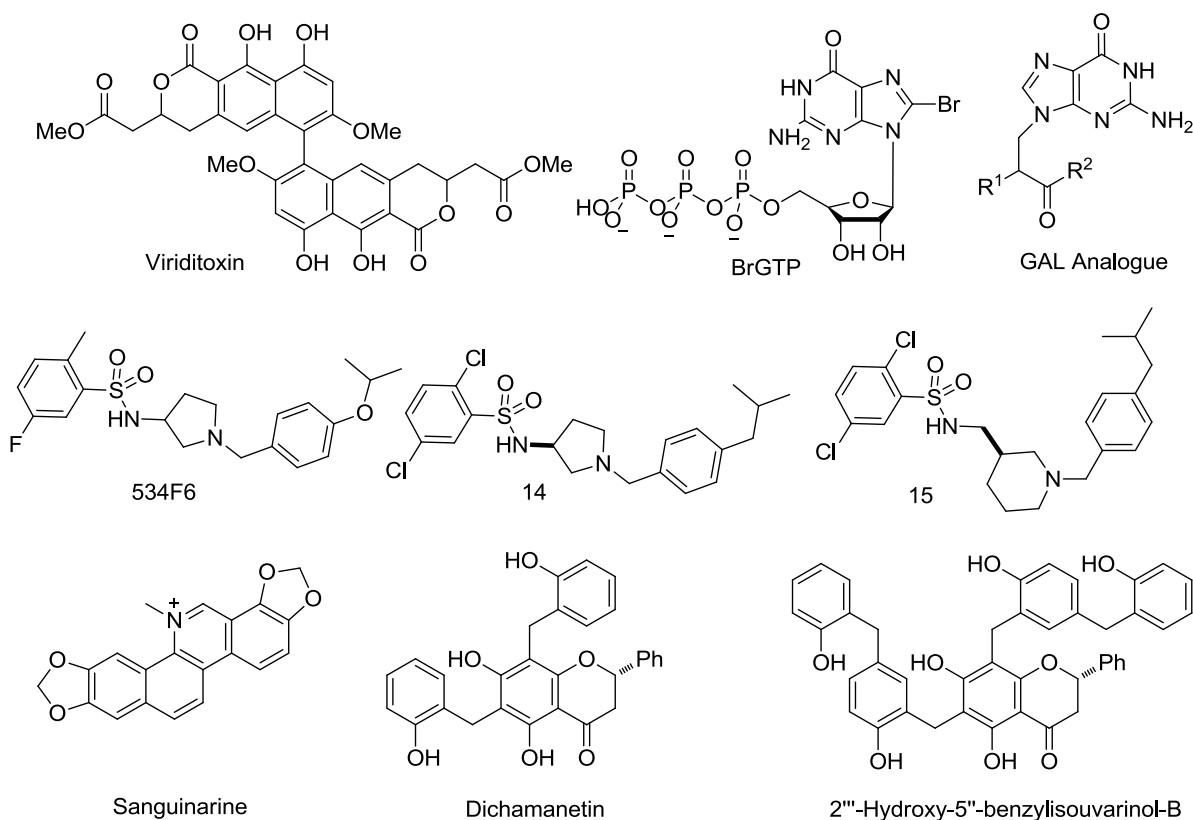


Figure IV-3. FtsZ inhibitors of bacteria other than *Mtb*

Table IV-1. Compounds targeting FtsZ of bacteria other than *Mtb*

	Compound	Target Organism	Mode of action	MIC/IC ₅₀ (cell growth inhibition)
1	Viriditoxin	<i>E. Coli</i> , <i>S. aureus</i> , <i>MRSA</i> , <i>VRE</i> , <i>Enterococcus faecilis</i>	Inhibits GTPase and FtsZ polymerization	4-8 µg/mL (<i>S. aureus</i> and <i>MRSA</i>) 2-16 µg/mL (<i>enterococcus faecalis</i> and <i>VRE</i>)
2	Zantrins	<i>Mtb</i> , <i>E. coli</i> , <i>MRSA</i> , <i>VRE</i>	Inhibits GTPase, Z1, Z2, Z4 destabilizes FtsZ polymer, Z5 stabilizes FtsZ assembly	-
3	GTP analogues 1. BrGTP	<i>E. coli</i>	Inhibits GTPase and FtsZ polymerization Assay in reversible competitive mode	-
	2.GAL Analogues	<i>E. Coli</i> , <i>S. aureus</i>	Inhibits GTPase activity (<i>E. coli</i> FtsZ),	0.4-20 mg/mL (<i>S. aureus</i>)
4	Sanguinarine	<i>B. subtilis</i> , <i>E. coli</i>	Inhibits FtsZ assembly and protofilament bundling, thinner and shorter FtsZ protofilaments (<i>E. coli</i>)	-
5	<i>N</i> -Benzyl-3-sulfonamidopyrrolidine	<i>E. Coli</i>	Lethal cell filamentation, moderate inhibition of GTPase activity, No effect on FtsZ polymerization	Compound 14 -10 µM Compound 15-20 µM
6	(±)-Dichamanetin	<i>S. aureus</i> , <i>B. subtilis</i> , <i>M. smegmatis</i> , <i>E. coli</i>	Inhibits GTPase activity of <i>E. coli</i> FtsZ	1.7-3.4 µM (<i>S. aureus</i> , <i>B. subtilis</i> , <i>M. smegmatis</i> , <i>E. coli</i>)
7	(±)-2''''-Hydroxy-5''''-benzylisouvarinol-B	<i>S. aureus</i> , <i>B. subtilis</i> , <i>M. smegmatis</i> , <i>E. coli</i>	Inhibits GTPase activity of <i>E. coli</i> FtsZ	2.3-10.7 µM (<i>S. aureus</i> , <i>B. subtilis</i> , <i>M. smegmatis</i> , <i>E. coli</i>)

***N*-Benzyl-3-sulfonamidopyrrolidines**

A high define HTP (HTP) screening of a library of compounds at the Broad Institute of Harvard University and Mass Institute of Tech (MIT) identified several compounds that caused lethal cell filamentation in *E. coli* without significantly inhibiting the GTPase activity of FtsZ.³⁴ For example, the lead compound, **534F6 (Figure IV-3)**, displayed only weak inhibition (20 %) of *E. coli* FtsZ GTPase activity at 100 µM concentration and no effect on FtsZ polymerization. Based on this lead compound, an optimized library of 45 compounds was synthesized and

evaluated against *E. coli* and compound **14** was found to be the most potent with MIC value of 10 μM . *E. coli* culture treated with 5 μM of compound **14** and 10 μM of compound **15** showed extensive filamentation.

(±)-Dichamanetin and (±)-2''-hydroxy-5''-benzylisouvarinol-B

Dichamanetin and 2''-hydroxy-5''-benzylisouvarinol-B, polyphenolic natural products, were isolated from *U. chamae* and *X. afticana*, respectively (**Figure IV-3**).^{35,36} These compounds show a high level of activity against gram-positive bacteria, such as, *S. aureus*, *B. subtilis*, *M. smegmatis* and *E. coli*, with MIC values in the range of 1.7-3.4 μM for dichamanetin and 2.3-10.7 μM for hydroxybenzylisouvarinol-B.³⁷ Dichamanetin and hydroxybenzylisouvarinol-B were found to be potent GTPase inhibitors of *E. coli* FtsZ (IC₅₀ 8-12 μM).³⁸

Cinnamaldehyde

Cinnamaldehyde, a natural product, was shown to exhibit broad-spectrum anti-bacterial activity (MIC: 1 $\mu\text{g/mL}$ for *E. coli*; 0.5 $\mu\text{g/mL}$ for *B. subtilis*; 0.25 $\mu\text{g/mL}$ for *MRSA*).³⁹ *E. coli* FtsZ polymerization and GTPase activity were strongly inhibited with an IC₅₀ value of 6.86 \pm 2.2 μM and 5.81 \pm 2.2 μM , respectively. Electron microscopy images and confocal imaging of live *E. coli* cells with GFP-tagged FtsZ further confirmed the reduction in Z-ring formation. STD-NMR in conjunction with AutoDock computer modeling suggested that cinnamaldehyde binds around the T7 loop in the FtsZ monomer, inducing conformational change that block optimal contact with the GTP binding T1-T6 loop in a neighboring monomer.

3-{5-[4-Oxo-2-thioxo-3-(3-trifluoromethylphenyl)-thiazolidin-5-ylidene methyl]-furan-2-yl}-benzoic acid (OTBA)

Beuria *et al.* screened their library of 81 compounds with 29 diverse scaffolds using a sedimentation assay of *E. coli* FtsZ polymer, and found that OTBA promoted *E. coli* FtsZ assembly *in vitro* and inhibited the *B. subtilis* cell proliferation, leading to filamentation (MIC 2 μM).⁴⁰ The light scattering assay showed that OTBA enhanced the extent of *E. coli* FtsZ and *B. subtilis* FtsZ polymerization by 3-fold. Electron microscopic analysis showed that the thickness of FtsZ bundles was increased in the presence of cinnamaldehyde. Inhibition in GTPase activity

was also observed. It was proposed that OTBA inhibited the Z-ring dynamics by promoting the assembly and stability of FtsZ protofilaments.

Curcumin

Curcumin is a naturally occurring polyphenolic compound that has been used as an important dietary ingredient for centuries. Curcumin has also shown antibacterial activity against a number of gram-positive and gram-negative bacteria. Rai *et al.* reported that curcumin induced the filamentation of *B. subtilis* 168 cells, and inhibited the cell proliferation of *B. subtilis* and *E. coli* (MIC: 17 ± 3 μM for *B. subtilis*; 100 μM for *E. coli*).⁴¹ Immunofluorescence microscopy indicated the inhibition of Z-ring formation without any effect on segregation and organization of the nucleoids. Curcumin was found to inhibit FtsZ polymerization, while enhancing GTPase activity. The result indicated that curcumin decreased the stability of FtsZ protofilaments by increasing its GTPase activity.

Berberine

Berberine is a natural product isolated from various species of *Berberis*. Berberine inhibits the over growth of pathogenic gram-positive as well as gram-negative bacteria such as *B. subtilis*, *Staphylococcus aureus*, *E. coli* and *MRSA*.^{42,43,44} Domadia *et al.* showed that berberine inhibited FtsZ assembly (IC₅₀ 10 ± 2.5 μM) and GTPase activity (IC₅₀ 16.01 ± 5 μM).⁴⁵ Electron microscopy images further supported the destabilization of FtsZ protofilaments by berberine, wherein FtsZ filaments were found to be thin, short and curved. Fluorescence study of FtsZ-bound TNP-GTP (TNP = 2,4,6-trinitro-2,5-cyclohexadienylidene) implied that the binding site of berberine was in the vicinity of GTP binding pocket, overlapping with hydrophobic residues of the active site of FtsZ, which was supported by AutoDock and saturation transfer difference (STD)-NMR.

Stathmin-derived I19L peptide

Clement *et al.* showed I19L, a peptide derived from the N-terminal region of stathmin, hampered tubulin polymerization.⁴⁶ Since tubulin and FtsZ exhibit similar folding patterns, the effect of I19L on FtsZ polymerization was also studied.⁴⁷ Sedimentation assay on *E. coli* FtsZ

showed that I19L co-sedimented mainly with FtsZ bundles and thereby affected the bundling of FtsZ. A combination of docking studies and Saturation Transfer Difference–NMR (STD-NMR) experiments indicated a possible binding site of I19L in *E. coli* FtsZ near the GTP binding pocket.

4,6-Diamidino-2-phenylindole (DAPI)

Extending the study on tubulin-DAPI binding,^{48,49,50} Nova *et al.* investigated the characterization of DAPI interaction with *E. coli* FtsZ.⁵¹ Polymerization kinetics indicated that DAPI binding increased FtsZ polymer stability in a concentration dependent manner. The GTPase assay illustrated that DAPI behaved as a non-competitive inhibitor of *E. coli* FtsZ with a K_i of $29.4 \pm 0.3 \mu\text{M}$. Anisotropy fluorescence measurements suggested that the binding of one mole of DAPI per mole of *E. coli* FtsZ was responsible for the bundling of protofilaments and the inhibition of GTPase activity.

PC58538 and PC170942

Stokes *et al.* screened a library of 105,000 synthetic compounds against *B. subtilis* by adopting newly designed microtiter plate assay in combination with phase-contrast microscopy, and identified **PC58538**.⁵² The FtsZ GTPase assay showed that **PC58538** inhibited FtsZ assembly in a dose-dependent manner (IC_{50} 362 μM ; K_i 82 μM). **PC170942**, an analog of **PC58538**, was found to be more potent than its parent molecule (IC_{50} 44 μM ; K_i 10 μM). In addition, fluorescent imaging of GFP-FtsZ expressing *B. subtilis*, treated with **PC58538** (128 $\mu\text{g/mL}$) lacked the band of FtsZ-GFP formed at the midpoint of the untreated cell.

PC190723

Ohashi *et al.* reported the effect of 3-methoxybenzamide (3-MBA) on septation via inhibition of FtsZ cytokinesis.⁵³ Haydon *et al.* designed and screened more than 500 analogs of 3-MBA against various pathogenic bacterial strains and found that **PC190723** exhibited potent antibacterial activity against *B. subtilis*, *MRSA* and *MDRSA* with MIC values in the range of 0.5-1 $\mu\text{g/mL}$.⁵⁴ **PC190723** inhibited the GTPase activity of *S. aureus* FtsZ in a dose dependent

manner (IC₅₀ 55 ng/mL). The docking study of **PC190723** suggested that the interaction of **PC190723** with H7 could contribute to the inhibition of GTPase activity.

Table IV-2. Compounds targeting FtsZ for bacteria other than *Mtb*

	Compound	Target species	Mode of action	MIC/IC ₅₀ (cell growth inhibition)
1	Cinnamaldehyde	<i>E. coli</i> , <i>B. subtilis</i> , <i>MRSA</i>	Inhibits GTPase activity, FtsZ polymerization and FtsZ protofilament bundling (<i>E. coli</i>); reduction in Z-ring/unit cell; conformational change blocking optimal contact with the GTP binding T1-T6 loop in a neighboring monomer	1 µg/mL (<i>E. coli</i>) 0.5 µg/mL (<i>B. subtilis</i>) 0.25 µg/mL (<i>MRSA</i>)
2	OTBA	<i>E. coli</i> , <i>B. subtilis</i>	Inhibition of GTPase activity and enhanced FtsZ polymerization (<i>E. coli</i> and <i>B. subtilis</i>); promoting assembly and stabilization of FtsZ polymer.	2 µM (<i>B. subtilis</i>)
3	Curcumin	<i>E. coli</i> , <i>B. subtilis</i>	Filamentation of <i>B. subtilis</i> 168 cells, inhibition of Z-ring formation without affecting organization of nucleoids; inhibition of FtsZ polymerization and enhancement of GTPase assay (<i>E. coli</i>)	17 µM against (<i>B. Subtilis</i>) 100 µM (<i>E. coli</i>)
4	Berberine	<i>E. coli</i> , <i>B. subtilis</i> , <i>S. aureus</i>	Inhibits GTPase and FtsZ polymerization (<i>E. coli</i>); destabilization of FtsZ assembly-thin, short and curved FtsZ protofilaments; binding site in the vicinity of GTP binding site.	-
5	PC190723	<i>B. subtilis</i> , <i>S. aureus</i>	Inhibits GTPase activity of <i>S. aureus</i> FtsZ by possible interaction with H7 (docking study); discrete foci throughout the elongated <i>B. subtilis</i> 168 cell, indicating mislocalization of Z-ring.	0.5-1 µg/mL against <i>B. subtilis</i> , <i>S. aureus</i> , <i>MRSA</i> , <i>MDRSA</i>
6	PC58538 and PC170942	<i>B. subtilis</i> , <i>S. aureus</i> , <i>MRSA</i>	Long aseptate filaments; inhibition of GTPase activity in a dose dependent manner.	<i>B. subtilis</i> 168 PC58538 128 µg/mL PC170942 16 µg/mL <i>S. Aureus</i> PC170942 64 µg/mL
7	DAPI	<i>E. coli</i>	Enhancing FtsZ protofilament stability while inhibiting GTPase activity; bundling of FtsZ protofilament	
8	Stathmin-derived I19L peptide	<i>E. coli</i>	Inhibition of FtsZ polymerization, bundling of FtsZ protofilaments; proposed binding site near GTP binding pocket.	-

§ 4.3 Results and discussion

§ 4.3.1 Preliminary screening against different bacterial strains

As discussed previously, FtsZ is a highly conserved and ubiquitous protein in various bacterial strains. Therefore, in collaboration with Professor Slayden's laboratory at Colorado State University, a library of trisubstituted benzimidazoles (~1000 compounds) was screened against several pathogens other than *Mtb*. Remarkably, a large number of compounds showed significant activity exhibiting greater than 90 % growth inhibition at 1 $\mu\text{g/mL}$ against *F. tularensis* (Figure IV-4).

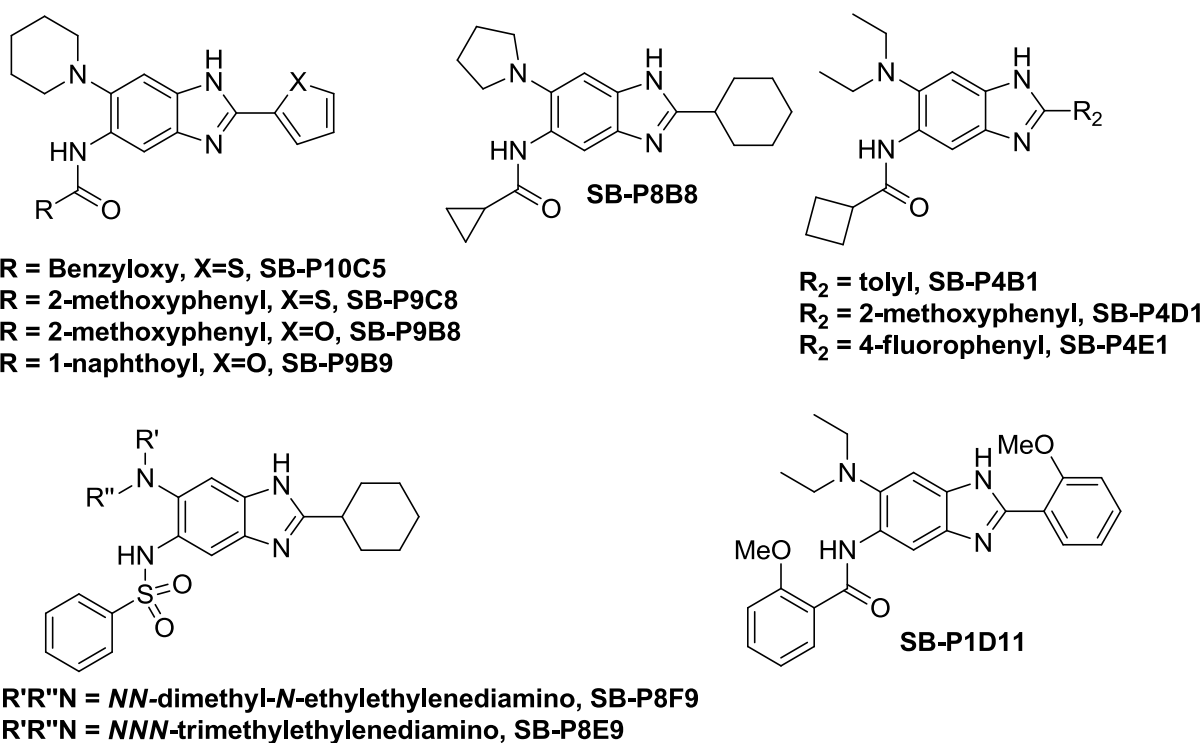


Figure IV-4. Structures of 2,5,6-trisubstituted benzimidazoles against *F. tularensis* at 1 $\mu\text{g/mL}$ with > 90 % growth inhibition

Unexpectedly, in comparison to *Mtb* FtsZ inhibitors where we identified only one 2,5,7-trisubstituted benzimidazole **SB-P5C1**, there were a large number of 2,5,7-trisubstituted benzimidazole hits against *F. tularensis* (Figure IV-5).

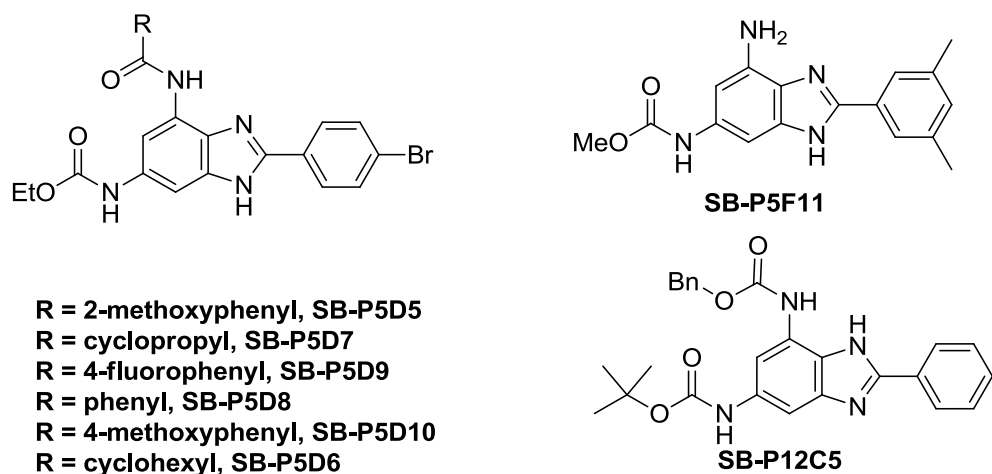


Figure IV-5. Structures of 2,5,7-trisubstituted benzimidazoles against *F. tularensis* at 1 $\mu\text{g/mL}$ with > 90 % growth inhibition

In addition, several hits against *F. tularensis* exhibiting 50-60 % growth inhibition at 0.2 $\mu\text{g/mL}$ were also identified (**Figure IV-6**).

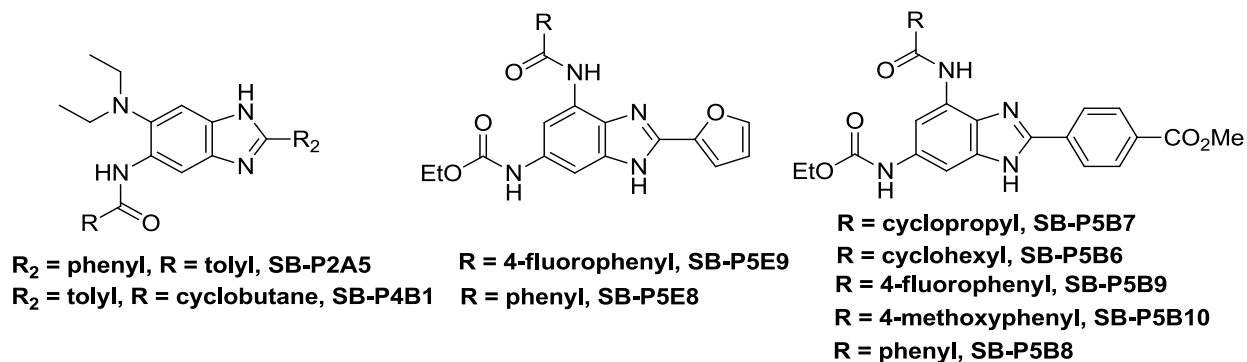


Figure IV-6. Structures of hit benzimidazoles against *F. tularensis* with 40-50 % growth inhibition 0.2 $\mu\text{g/mL}$

Furthermore, several of these benzimidazoles showed moderate growth inhibitory activities (50-80 %) at 1 $\mu\text{g/mL}$ against *Y. pestis* and *B. thailandensis* as well (**Figure IV-7 and Figure IV-8**).

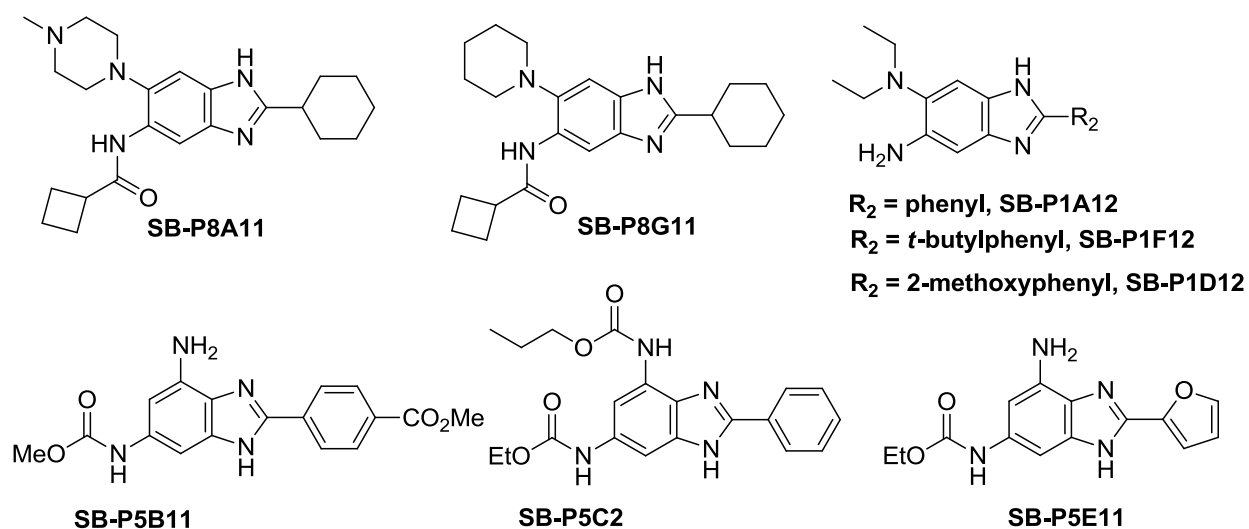


Figure IV-7. Structures of hit benzimidazoles against *Y. pestis*

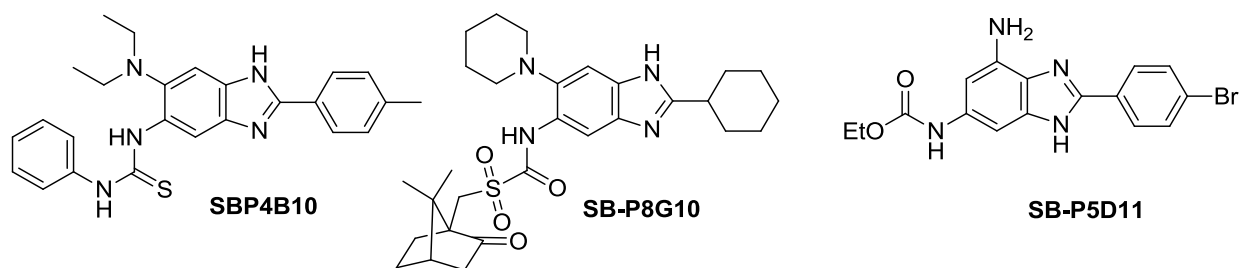


Figure IV-8. Structures of hit benzimidazoles against *B. thailandensis*

§ 4.3.2 *Ex-vivo* efficacy of hit benzimidazoles against *B.thailandensis* and *F. tularensis*

Since a good number of lead compounds active against *F. tularensis* and *B. thailandensis* was identified, *ex-vivo* efficacy of these compounds were evaluated. The effect of three active benzimidazoles, **SB-P8G10**, **SB-P4B10** and **SB-P5D11** on *B. thailandensis* Bt38 efflux mutant infection of RAW macrophages was studied. As shown in the **Figure IV-5**, **SB-P8G10** and **SB-P4B10** significantly reduced the *B. thailandensis* growth *ex vivo* at 25 $\mu\text{g/mL}$ and 10 $\mu\text{g/mL}$, respectively (**Figure IV-9**). **SB-P4B10** and **SB-P5D11** would probably have been more effective at higher concentrations, but RAW cell toxicity of these compounds, which was found to be 25 $\mu\text{g/mL}$, prevented testing at higher concentrations. Since these assays were done by using compounds from the plate which are not analytically pure, the assays will be repeated with pure

compounds to obtain more accurate results. Nevertheless, **SB-P8G10** at 25 $\mu\text{g/mL}$ resulted in a 2 log reduction in *B. thailandensis* compared to untreated control cells.

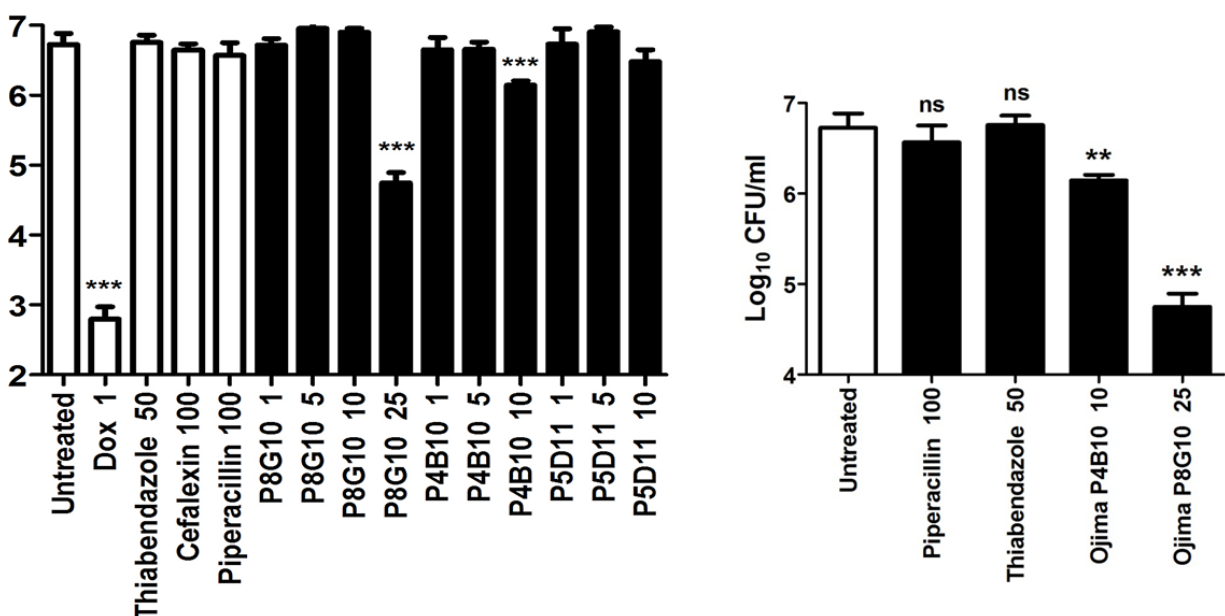


Figure IV-9. Effect of benzimidazoles on *B. thailandensis* Bt38 efflux mutant infection of RAW macrophages

RAW macrophages infected with *B. thailandensis* Bt38 efflux mutants were treated with various benzimidazoles and different concentrations. After the treatment duration the cells were homogenized and transferred to 7H11 agar plates for CFU enumeration.(ns: non-significant reduction in log₁₀CFU)

Similarly, lead compounds active against *F. tularensis*, **SB-P9C8**, **SB-P9B8**, **SB-P8B8**, **SB-P9B9**, and **SB-P10C5**, were subjected to ex-vivo efficacy assay against *F. tularensis* LVS (live vaccine strain) ex vivo infection of RAW macrophages. With the exception of **SB-P8B8**, the compounds were highly effective in reducing infection at the concentration range of 10-50 $\mu\text{g/mL}$ (**Figure IV-10**). There was a 2-3 Log reduction in the colony forming units (CFU) per mL which is considered to be significant. The assays strongly suggest that these compounds are very effective in controlling infections in macrophages. As mentioned before, these assays will be repeated using analytically pure compounds to confirm the results.

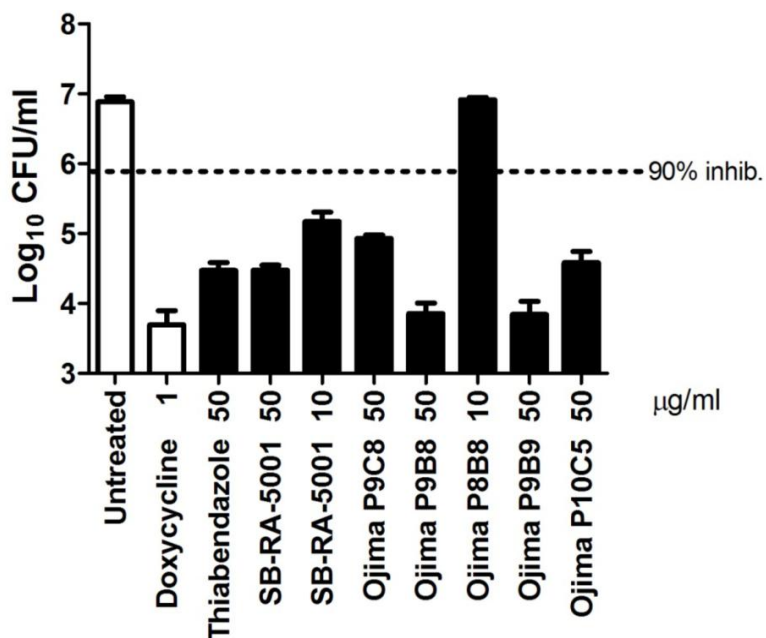
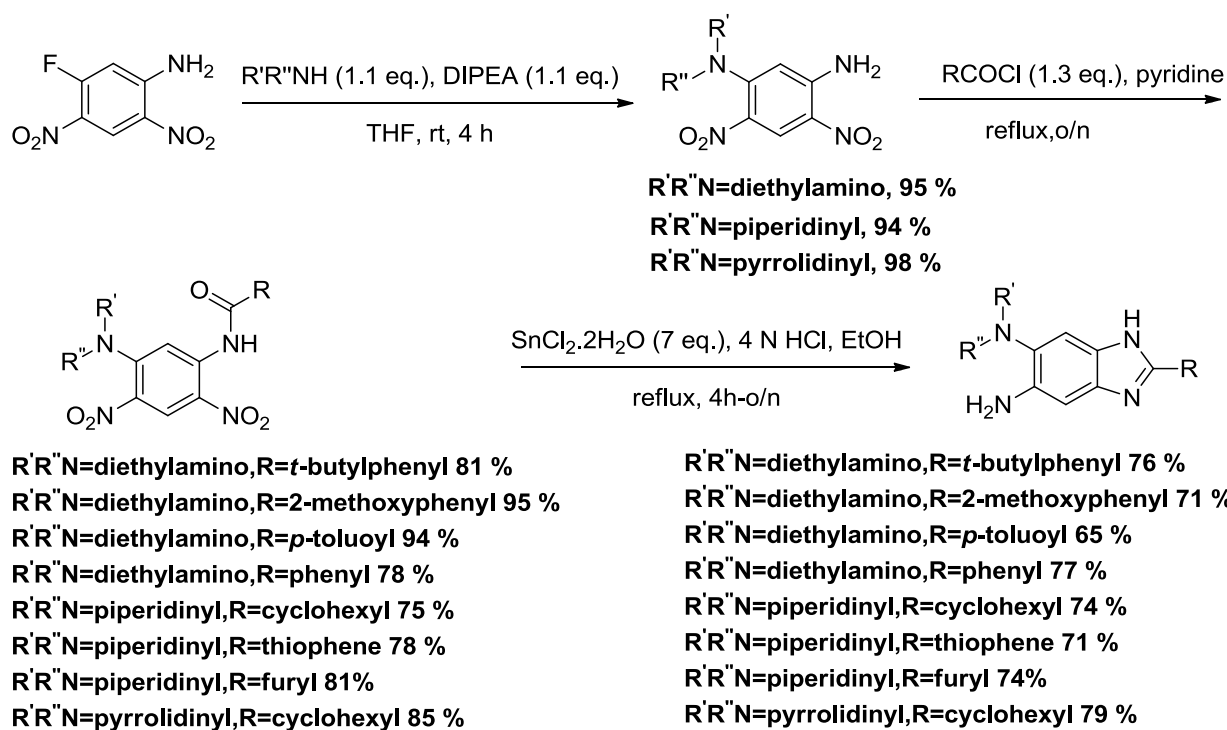


Figure IV-10. Effect of benzimidazoles on *F. tularensis* LVS infection of raw macrophages

RAW macrophages infected with *F. tularensis* LVS were treated with various benzimidazoles and different concentrations. After the treatment duration the cells were homogenized and transferred to 7H11 agar plates for CFU enumeration.

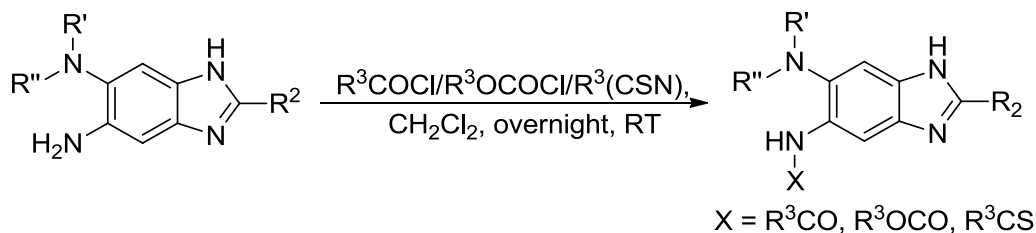
§ 4.3.3 Resynthesis of 2,5,6-trisubstituted hit benzimidazoles for accurate MIC₉₉ determination:

For accurate MIC determination, the 2,5,6-trisubstituted benzimidazole intermediates required for the final acylation to obtain the library of analytically pure active compounds were resynthesized. **Scheme IV-1** outlines the synthesis described in the **Chapter II** (refer to chapter-II for synthesis and characterization details of the intermediates).



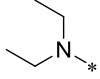
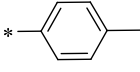
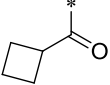
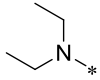
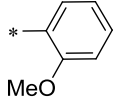
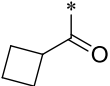
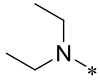
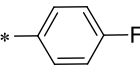
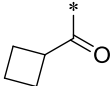
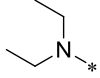
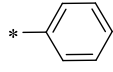
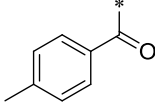
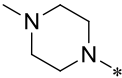
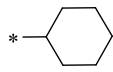
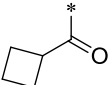
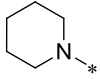
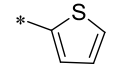
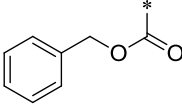
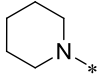
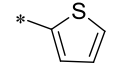
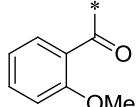
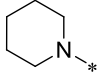
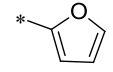
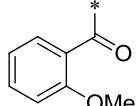
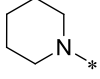
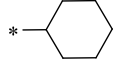
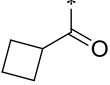
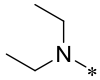
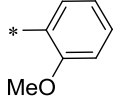
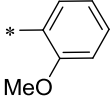
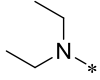
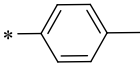
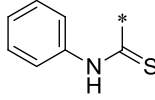
Scheme IV-1. Synthesis of 2,5,6-trisubstituted benzimidazole intermediates

These intermediates were then used for the final acylation to generate the hit benzimidazoles in relatively moderate yield, as outlined in **Scheme IV-2 (Table IV-3)**.



Scheme IV-2. Synthesis of hit compounds

Table IV-3. Re-synthesis of the hit compounds

Entry	Compound	R'R''	R ₂	X	Yield
IV-1	SB-P4B1				58%
IV-2	SB-P4D1				42 %
IV-3	SB-P4E1				48 %
IV-4	SB-P2A5				44 %
IV-5	SB-P8A11				51 %
IV-6	SB-P10C5				48 %
IV-7	SB-P9C8				52 %
IV-8	SB-P9B8				56 %
IV-9	SB-P8G11				57 %
IV-10	SB-P1D11				54 %
IV-11	SB-P4B10				45 %

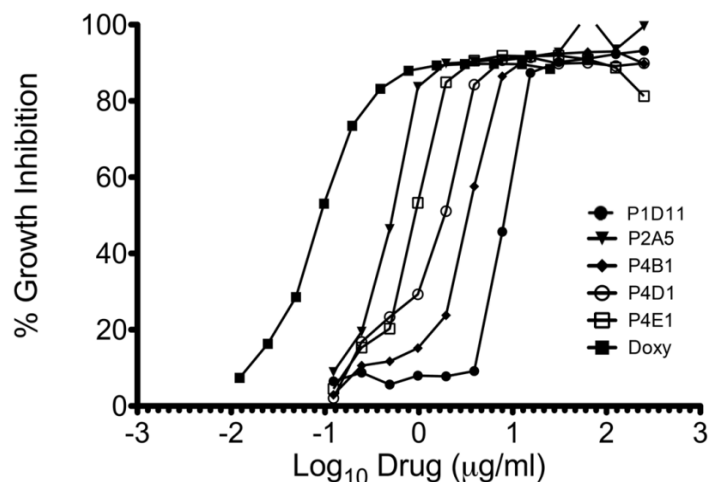


Figure IV-11. Percent growth inhibition of *F. tularensis* LVS 110408 by lead benzimidazoles

The analytically pure re-synthesized active compounds were sent to our collaborator Prof. Slayden's laboratory for accurate MIC determination using Alamar Blue Assay. The results for the first few compounds indicated that most of the lead benzimidazoles inhibited *F. tularensis* LVS 110408 growth with MIC₉₀ values in the range of 1.8-12.9 µg/mL (Figure IV-11 & Figure IV-12).

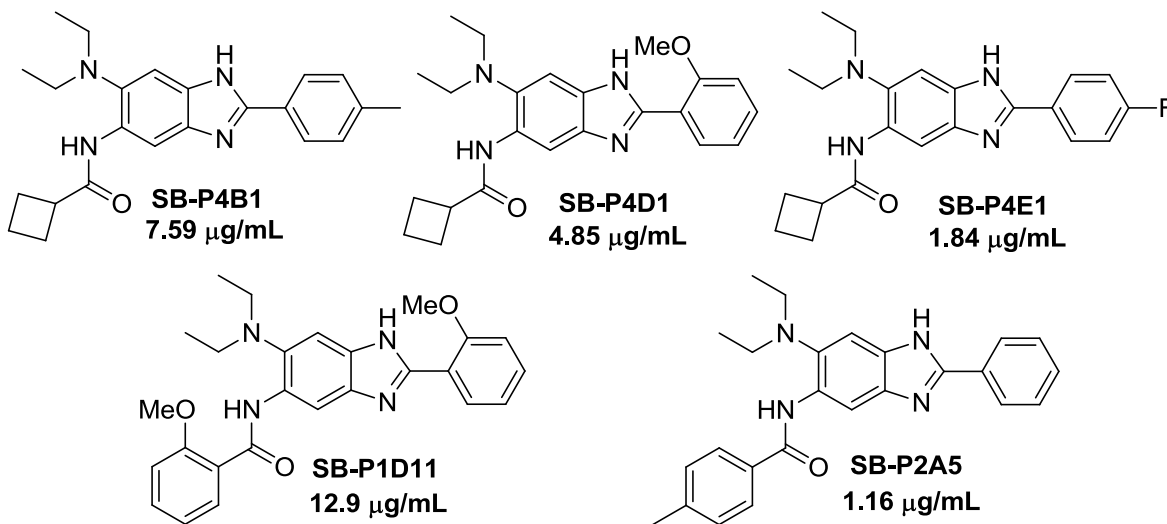


Figure IV-12. MIC₉₀ of lead benzimidazoles against *F. tularensis* LVS 110408

§ 4.4 Conclusion

As FtsZ is a highly conserved protein in different bacterial strains, in-house libraries of trisubstituted benzimidazoles were screened against several pathogens. Remarkably, a large number of hit compounds against *F. tularensis*, *Y. pestis*, *B. thailandensis* exhibiting greater than 90 % growth inhibition at 1 µg/mL was identified. Based on more accurate alamar blue assay, analytically pure compounds exhibited MIC₉₀ values in the range of 1.16-12.9 µg/mL against *F. tularensis*. Ex-vivo efficacy data indicated that **SB-P8G10** and **SB-P4B10** significantly reduced the *B. thailandensis* growth at 25 µg/mL and 10 µg/mL, respectively. Furthermore, with the exception of **SB-P8B8**, several compounds were highly effective in reducing *F.tularensis* LVS infection at the concentration range of 10-50 µg/mL. There was a 2-3 Log reduction in the colony forming units (CFU) per mL which is considered to be exceedingly significant.

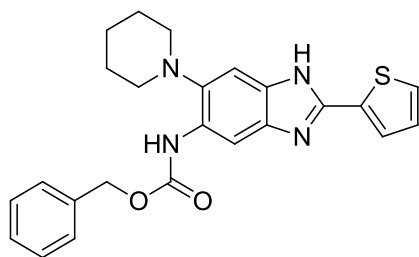
§ 4.5 Experimental Section

Methods: ^1H and ^{13}C NMR spectra were measured on a Varian 300, 400 or 500 MHz NMR spectrometer. Melting points were measured on a Thomas Hoover Capillary melting point apparatus and are uncorrected. TLC was performed on Merck DCalufolien with Kieselgel 60F-254 and column chromatography was carried out on silica gel 60 (Merck; 230-400 mesh ASTM). High-resolution mass spectra were obtained from Mass Spectrometry Laboratory, University of Illinois at Urbana-Champaign, Urbana, IL. Purity was determined by Agilent 1100 series HPLC assembly.

Materials: The chemicals were purchased from Sigma Aldrich Co., Synquest Inc. and purified before use by standard methods. Tetrahydrofuran was freshly distilled from sodium metal and benzophenone. Dichloromethane was also distilled immediately prior to use under nitrogen from calcium hydride.

Synthesis of analytically pure trisubstituted benzimidazoles

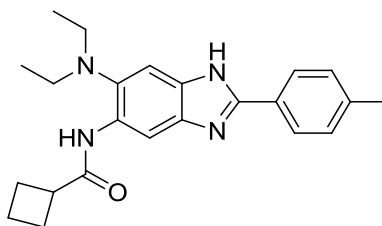
5-Benzoyloxycarbonylamino-6-piperidinyl-2-thiophen-1H-benzo[d]imidazole (SB-P10C5, IV6).



To a solution of 5-amino-2-thiophenyl-6-(*N*-piperidinyl)-1*H*-benzo[d]imidazole (200 mg, 0.67 mmol) in dichloromethane (10 mL) was added a solution of *N*-benzyloxycarbonyloxysuccinimide (167 mg, 0.67 mmol) in dichloromethane (5 mL) dropwise at room temperature. After the addition, the reaction mixture was stirred at room temperature overnight. After the completion of the reaction, the reaction mixture was concentrated under reduced pressure. The crude was purified via flash chromatography on silica gel (gradient 20-40% ethyl acetate/hexanes) to give **SB-P10C5 (IV-6)** as white solid (206 mg, 48 % yield): mp 105-107 °C; ^1H NMR (400 MHz, CDCl_3) δ 1.69 (m, 6 H), 2.72 (broad s, 4 H), 5.22 (s, 2 H), 6.93

(t, 1 H, $J = 3.9$ Hz), 7.27 (d, 1 H, $J = 4.8$ Hz), 7.37 (m, 6 H), 8.21 (s, 1 H), 8.27 (s, 1 H); ^{13}C NMR (100 MHz, CDCl_3) δ 24.12, 25.80, 27.03, 54.60, 66.97, 101.2, 109.9, 126.5, 127.8, 128.1, 128.2, 128.4, 128.7, 130.1, 133.0, 136.5, 139.8, 147.0, 153.9, 171.3, 173.6; HRMS (ESI) m/z calcd for $\text{C}_{24}\text{H}_{24}\text{N}_4\text{O}_2\text{SH}^+$: 433.1698, Found: 433.1698 ($\Delta = -0.0$ ppm).

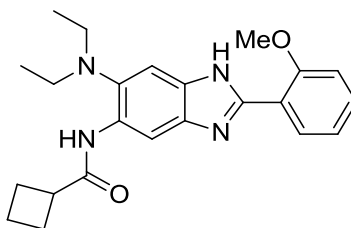
6-*N,N*-Diethylamino-5-(cyclobutanamido)-2-tolyl-1*H*-benzo[d]imidazole (SB-P4B1, IV-1):



To a solution of 5-amino-6-*N,N*-diethylamino-2-(4-methylphenyl)-1*H*-benzo[d]imidazole (115 mg, 0.39 mmol) in dichloromethane (5 mL) was added a solution of cyclobutanecarbonyl chloride (0.45 mL, 0.39 mmol) in dichloromethane (4 mL) dropwise at room temperature. After the addition, the reaction mixture was stirred at room temperature overnight. After the completion of the reaction, the reaction mixture was washed with saturated solution of sodium bicarbonate. The organic layer was dried over anhydrous magnesium sulfate, filtered and concentrated under reduced pressure. The crude was purified by flash chromatography on silica gel (gradient: 20-40% ethyl acetate/hexanes) to give **SB-P4B1 (IV-1)** as a white solid (85 mg, 58 %): mp >200 °C; ^1H NMR (400 MHz, CDCl_3) δ 0.92 (t, 6 H, $J = 7.2$ Hz), 1.83 (m, 1 H), 1.95 (m, 1 H), 2.22-2.37 (m, 7 H), 2.92 (q, 4 H, $J = 7.2$ Hz), 3.29 (m, 1 H), 7.17 (d, 2 H, $J = 8$ Hz), 7.52 (s, 1 H), 7.99 (d, 2 H, $J = 8$ Hz), 8.79 (s, 1 H), 9.40 (s, 1 H); ^{13}C NMR (100 MHz, CDCl_3) δ 12.90, 17.93, 21.27, 25.69, 41.44, 50.30, 101.6, 112.7, 126.6, 127.4, 129.3, 132.0, 133.1, 135.5, 139.6, 152.6, 173.1; HRMS (ESI) m/z calcd for $\text{C}_{23}\text{H}_{28}\text{N}_4\text{OH}^+$: 377.2341, Found: 377.2341 ($\Delta = 0.5$ ppm).

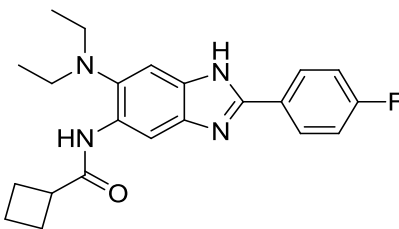
Similar procedure was used for the synthesis of following compounds.

5-Cyclobutanamido-2-(2-methoxyphenyl)-6-*N,N*-diethylamino-1*H*-benzo[d]imidazole(SB-P4D1, IV-2)



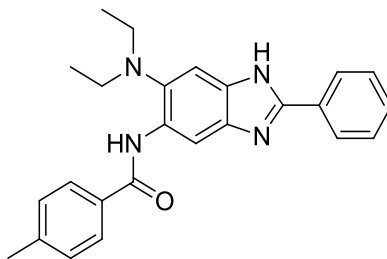
White solid; 42 % yield; mp 110-112 °C; ¹HNMR (400 MHz, CDCl₃) δ 0.95 (t, 6 H, *J* = 7.2 Hz), 1.93 (m, 1 H), 2.01 (m, 1 H), 2.28 (m, 2 H), 2.35 (m, 2 H), 2.96 (m, 4 H, *J* = 7 Hz), 3.23 (m, 1 H), 4.07 (s, 3 H), 7.05 (d, 1 H, *J* = 8 Hz), 7.10 (t, 1 H, *J* = 8 Hz), 7.39 (m, 1 H), 7.59 (s, 1 H), 8.51 (d, 1 H, *J* = 7.6 Hz), 8.69 (s, 1 H), 9.26 (s, 1 H); ¹³C NMR (100 MHz, CDCl₃) δ 12.90, 18.01, 25.53, 41.40, 50.35, 55.94, 100.4, 111.4, 113.1, 117.9, 121.6, 129.6, 130.8, 132.6, 135.5, 149.8, 156.6, 172.8; HRMS (ESI) *m/z* calcd for C₂₃H₂₈N₄O₂H⁺: 393.2289, Found: 393.2291 (Δ = -0.5 ppm).

5-Cyclobutanamido-2-(4-fluorophenyl)-6-*N,N*-diethylamino-1*H*-benzo[d]imidazole (SB-P4E1, IV-3)



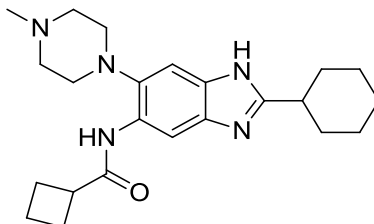
White solid; 48 % yield; mp 170-172 °C; ¹HNMR (400 MHz, CDCl₃) δ 0.93 (t, 6 H, *J* = 7.2 Hz), 1.81 (m, 1 H), 2.02 (m, 1 H), 1.35-2.19 (m, 4 H), 2.94 (q, 4 H, *J* = 7 Hz), 3.30 (m, 1 H), 7.06 (t, 2 H, *J* = 8.8 Hz), 7.55 (s, 1 H), 8.08 (m, 2 H), 8.78 (s, 1 H), 9.41 (s, 1 H); ¹³C NMR (100 MHz, CDCl₃) δ 12.91, 17.96, 25.71, 41.44, 50.32, 101.7, 112.9, 115.6, 115.9, 126.4, 128.7, 132.2, 133.2, 135.9, 139.3, 162.6, 164.8, 173.3; HRMS (ESI) *m/z* calcd for C₂₂H₂₅N₄FOH⁺: 381.2091, Found: 381.2090 (Δ = -0.3 ppm).

5-cyclobutanamido-2-(4-fluorophenyl)-6-*N,N*-diethylamino-1*H*-benzo[d]imidazole (SB-P2A5, IV-4)



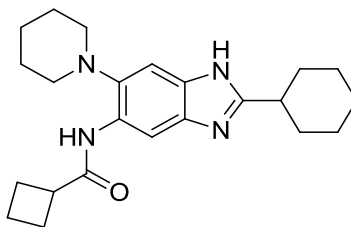
White solid; 44 % yield; mp > 200 °C; ¹H NMR (400 MHz, CDCl₃) δ 0.96 (t, 6 H, *J* = 7.2 Hz), 2.44 (s, 3 H), 3.02 (q, 4 H, *J* = 7 Hz), 7.09 (t, 2 H, *J* = 7.6 Hz), 7.24 (m, 3 H), 7.64 (s, 1 H), 7.84 (d, 2 H, *J* = 8.4 Hz), 7.94 (d, 2 H, *J* = 7.6 Hz), 9.14 (s, 1 H), 10.36 (s, 1 H); ¹³C NMR (100 MHz, CDCl₃) δ 12.98, 21.48, 50.53, 101.6, 113.3, 126.5, 127.0, 128.5, 129.3, 129.6, 129.9, 132.3, 132.5, 133.1, 135.9, 142.1, 152.5, 165.6; HRMS (ESI) *m/z* calcd for C₂₅H₂₆N₄OH⁺: 399.2185, Found: 399.2184 (Δ = - 0.3 ppm).

5-Cyclobutanamido-2-cyclohexyl-6-(*N*-methylpiperazino)-1*H*-benzo[d]imidazole(SB-8A11, IV-5)



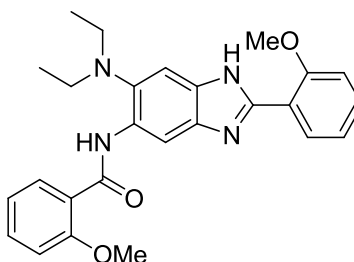
White solid; 51 % yield; mp > 200 °C; ¹H NMR (400 MHz, CDCl₃) δ 1.24-1.36 (m, 4 H), 1.5-1.94 (m, 6 H), 2.08 (m, 3 H), 2.29-2.40 (m, 7 H), 2.64 (broad s, 4 H), 2.81-2.91 (m, 5 H), 3.31 (m, 1 H), 7.48 (s, 1 H), 8.57 (s, 1 H), 8.91 (s, 1 H); ¹³C NMR (100 MHz, CDCl₃) δ 17.95, 25.74, 26.00, 31.71, 38.37, 41.35, 45.96, 52.67, 55.98, 102.4, 110.1, 128.8, 131.9, 137.2, 159.4, 173.0; HRMS (ESI) *m/z* calcd for C₂₃H₃₃N₅OH⁺: 396.2763, Found: 396.2769 (Δ = 1.5 ppm).

5-Cyclobutanamido-2-cyclohexyl-6-piperidinyl-1H-benzo[d]imidazole (SB-P8G11, IV-9)



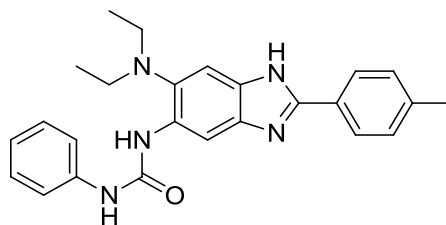
White solid; 57 % yield; mp > 200 °C; ¹H NMR (400 MHz, CDCl₃) δ 1.29-1.36 (m, 3 H), 1.63-1.83 (m, 9 H), 2.05 (m, 1 H), 2.08 (m, 3 H), 2.32-2.45 (m, 5 H), 2.84 (m, 5 H), 3.31 (m, 1 H), 7.47 (s, 1 H), 8.59 (s, 1 H), 9.05 (s, 1 H); ¹³C NMR (100 MHz, CDCl₃) δ 17.96, 23.92, 25.76, 26.03, 27.15, 31.75, 38.40, 41.44, 54.47, 101.9, 110.1, 128.8, 131.8, 138.1, 138.9, 159.2, 173.1; HRMS (ESI) *m/z* calcd for C₂₃H₃₂N₄OH⁺: 381.2654, Found: 381.2654 (Δ = -0.0 ppm).

5-(2-methoxybenzamido)-2-(2-methoxyphenyl)-6-*N,N*-diethylamino-1H-benzo[d]imidazole (SB-P1D11, IV-10)



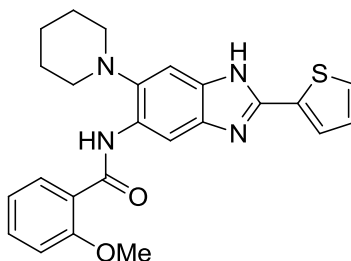
White solid; 54 % yield; mp > 200 °C; ¹H NMR (400 MHz, CDCl₃) δ 0.96 (t, 6 H, *J* = 7.2 Hz), 3.10 (q, 4 H, *J* = 7 Hz), 4.04 (s, 3 H), 4.06 (s, 3 H), 7.04 (t, 2 H, *J* = 7.6 Hz), 7.09 (q, 2 H, *J* = 7.2 Hz), 7.39 (t, 1 H, *J* = 3.2 Hz), 7.45 (t, 1 H, *J* = 3.2 Hz), 7.65 (s, 1 H), 8.35 (d, 1 H, *J* = 8 Hz), 8.54 (d, 1 H, *J* = 8 Hz), 9.00 (s, 1 H), 11.50 (s, 1 H); ¹³C NMR (100 MHz, CDCl₃) δ 12.32, 50.54, 55.62, 55.89, 101.8, 111.2, 111.5, 113.3, 117.9, 121.2, 121.6, 122.6, 129.6, 130.8, 132.4, 132.7, 133.9, 135.9, 149.8, 155.6, 157.2, 162.8; HRMS (ESI) *m/z* calcd for C₂₆H₂₈N₄O₃H⁺: 445.2240, Found: 445.2240 (Δ = -0.0 ppm).

5-(phenylurea)-6-*N,N*-diethylamino-2-tolyl-1*H*-benzo[d]imidazole (SB-P4B10, IV-11)



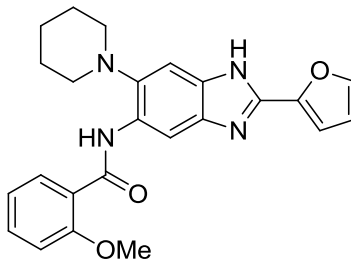
White solid; 45 % yield; mp > 200 °C; ¹H NMR (400 MHz, CDCl₃) δ 0.53 (t, 6 H, *J* = 7.2 Hz), 2.30 (s, 3 H), 2.56 (q, 4 H, *J* = 7 Hz), 7.18 (d, 2 H, *J* = 8 Hz), 7.23-31 (m, 3 H), 7.39 (m, 2 H), 7.95 (d, 2 H, *J* = 8 Hz), 8.18 (s, 1 H), 9.34 (s, 1 H), 10.04 (s, 1 H); ¹³C NMR (100 MHz, CDCl₃) δ 11.86, 21.37, 49.17, 102.7, 112.5, 126.3, 126.5, 126.9, 127.5, 129.5, 132.3, 136.3, 140.4, 152.5, 176.5; HRMS (ESI) *m/z* calcd for C₂₅H₂₇N₅OH⁺: 413.2261, Found: 413.2261 (Δ = 0.0 ppm).

5-(2-Methoxybenzamido)-6-piperidinyl-2-thiophen-1*H*-benzo[d]imidazole(SB-P9C8, IV-7).



White solid; 52 % yield; mp 165-167 °C; ¹H NMR (400 MHz, CDCl₃) δ 1.65 (m, 6 H), 2.74 (broad s, 4 H), 4.01 (s, 3 H), 6.71 (t, 1 H, *J* = 3.6 Hz), 7.01 (m, 2 H), 7.17 (d, 1 H, *J* = 4.8 Hz), 7.37 (d, 1 H, *J* = 3.2 Hz), 7.43 (m, 2 H), 8.89 (s, 1 H), 10.70 (s, 1 H); ¹³C NMR (100 MHz, CDCl₃) δ 23.87, 26.65, 54.39, 56.16, 104.0, 109.6, 111.5, 121.3, 122.6, 126.1, 127.1, 127.5, 129.5, 132.1, 132.9, 133.6, 139.6, 140.8, 147.6, 157.3, 164.0; HRMS (ESI) *m/z* calcd for C₂₄H₂₄N₄O₂SH⁺: 433.1698, Found: 433.1699 (Δ = 0.2 ppm).

5-(2-methoxybenzamido)-2-furyl-6-piperidinyl-1*H*-benzo[d]imidazole (SB-P9B8, IV8)



White solid; 56 % yield; mp 155-157 °C; ^1H NMR (400 MHz, CDCl_3) δ 1.66 (m, 6 H), 2.74 (broad s, 4 H), 4.06 (s, 3 H), 6.32 (d, 1 H, $J = 3.6$ Hz), 6.97 (d, 2 H, $J = 3.6$ Hz), 7.06 (m, 2 H), 7.42 (s, 1 H), 7.51 (t, 1 H, $J = 8.4$ Hz), 9.01 (s, 1 H), 10.81 (s, 1 H); ^{13}C NMR (100 MHz, CDCl_3) δ 23.86, 26.62, 54.33, 56.20, 104.1, 109.6, 111.5, 111.8, 121.3, 122.6, 126.1, 129.8, 131.4, 132.5, 132.9, 139.2, 140.9, 142.9, 144.1, 145.7, 157.3, 163.9; HRMS (ESI) m/z calcd for $\text{C}_{24}\text{H}_{24}\text{N}_4\text{O}_3\text{H}^+$: 417.1927, Found: 417.1924 ($\Delta = -0.7$ ppm).

§ 4.6 References

1. Leavis Helen, L.; Willems Rob, J. L.; Top, J.; Spalburg, E.; Mascini Ellen, M.; Fluit Ad, C.; Hoepelman, A.; de Neeling Albert, J.; Bonten Marc, J. M., Epidemic and nonepidemic multidrug-resistant *Enterococcus faecium*. *Emerg. Infect. Dis.* **2003**, *9*, 1108-15.
2. Klevens, R. M.; Morrison, M. A.; Nadle, J.; Petit, S.; Gershman, K.; Ray, S.; Harrison, L. H.; Lynfield, R.; Dumyati, G.; Townes, J. M.; Craig, A. S.; Zell, E. R.; Fosheim, G. E.; McDougal, L. K.; Carey, R. B.; Fridkin, S. K., Invasive methicillin-resistant *Staphylococcus aureus* infections in the United States. *JAMA* **2007**, *298*, 1763-1771.
3. Loffler, C. A.; MacDougall, C., Update on prevalence and treatment of methicillin-resistant *Staphylococcus aureus* infections. *Expert Rev. Anti-Infect. Ther.* **2007**, *5*, 961-981.
4. Maltezou, H. C.; Giamarellou, H., Community-acquired methicillin-resistant *Staphylococcus aureus* infections. *Int. J. Antimicrob. Agents* **2006**, *27*, 87-96.
5. Tsiodras, S.; Gold, H. S.; Sakoulas, G.; Eliopoulos, G. M.; Wennersten, C.; Venkataraman, L.; Moellering, R. C.; Ferraro, M. J., Linezolid resistance in a clinical isolate of *Staphylococcus aureus*. *Lancet* **2001**, *358*, 207-208.
6. Ryan, K. J.; Ray, C. G., *Sherris Medical Microbiology: An Introduction to Infectious Diseases*. McGraw Hill: 2004; p 488-490.
7. Oyston, P. C. F.; Sjoestedt, A.; Titball, R. W., Tularemia: bioterrorism defence renews interest in *Francisella tularensis*. *Nat. Rev. Microbiol.* **2004**, *2*, 967-978.
8. "Tularemia: FAQ About Tularemia". CDC. Available at http://www.cdc.gov/tularemia/Tul_Fact.html.
9. Enderlin, G.; Morales, L.; Jacobs, R. F.; Cross, J. T., Streptomycin and alternative agents for the treatment of tularemia: review of the literature. *Clin. Infect. Dis.* **1994**, *19*, 42-7.
10. Morelli, G.; Song, Y.-J.; Mazzoni, C. J.; Eppinger, M.; Roumagnac, P.; Wagner, D. M.; Feldkamp, M.; Kusecek, B.; Vogler, A. J.; Li, Y.-J.; Cui, Y.-J.; Thomson, N. R.; Jombart, T.; Leblois, R.; Lichtner, P.; Rahalison, L.; Petersen, J. M.; Balloux, F.; Keim, P.; Wirth, T.; Ravel, J.; Yang, R.-F.; Carniel, E.; Achtman, M., *Yersinia pestis* genome sequencing identifies patterns of global phylogenetic diversity. *Nat. Genet.* **2010**, *42*, 1140-1143.
11. "Plague:FAQ about Plague". CDC. Available at <http://www.bt.cdc.gov/agent/plague/faq.asp>.

12. Dennis, D. T.; Gage, K. L.; Gratz, N.; Poland, J. D.; Tokhomirov, E., Plague Manual: World Health Organization. Geneva Switzerland. **1999**, 172.
13. Meyer, K. F., Modern therapy of plague. *J. Am. Med. Assoc.* **1950**, *144*, 982-5.
14. Wagle, P. M., Recent advances in the treatment of bubonic plague. *Indian J. Med. Sci.* **1948**, *2*, 489-494.
15. Hotez, P. J.; Molyneuz, D. H.; Fenwick, A.; Kumaresan, J.; Sachs, S. E.; Sachs, J. D.; Savioli, L., Control of neglected tropical diseases. *N. Engl. J. Med.* **2007**, *357*, 1018-1027.
16. Miller, J. R.; Waldrop, G. L., Discovery of novel antibacterials. *Expert Opin. Drug Discovery* *5*, 145-154.
17. Margalit, D. N.; Romberg, L.; Mets, R. B.; Hebert, A. M.; Mitchison, T. J.; Kirschner, M. W.; RayChaudhuri, D., Targeting cell division: Small-molecule inhibitors of FtsZ GTPase perturb cytokinetic ring assembly and induce bacterial lethality. *Proc. Natl. Acad. Sci.* **2004**, *101*, 11821-11826.
18. Vollmer, W., The prokaryotic cytoskeleton: A putative target for inhibitors and antibiotics? *Appl. Microbiol. Biotechnol.* **2006**, *73*, 37-47.
19. Romberg, L.; Levin, P. A., Assembly dynamics of the bacterial cell division protein FtsZ: Poised at the edge of stability. *Annu. Rev. Microbiol.* **2003**, *57*, 125-154.
20. Lock, R. L.; Harry, E. J., Cell-division inhibitors: new insights for future antibiotics. *Nat. Rev. Drug Discovery* **2008**, *7*, 324-338.
21. Margolin, W., Themes and variations in prokaryotic cell division. *FEMS Microbiol. Rev.* **2000**, *24*, 531-548.
22. Rothfield, L.; Justice, S.; Garcia-Lara, J., Bacterial cell division. *Annu. Rev. Genet.* **1999**, *33*, 423-448.
23. Erickson, H. P.; Taylor, D. W.; Taylor, K. A.; Bramhill, D., Bacterial cell division protein FtsZ assembles into protofilament sheets and minirings, structural homologs of tubulin polymers. *Proc. Natl. Acad. Sci.* **1996**, *93*, 519-23.
24. Lowe, J.; Amos, L. A., Crystal structure of the bacterial cell-division protein FtsZ. *Nature* **1998**, *391*, 203-6.
25. Lowe, J.; Amos, L. A., Tubulin-like protofilaments in Ca²⁺-induced FtsZ sheets. *Embo J* **1999**, *18*, 2364-71.

26. Nogales, E.; Downing, K. H.; Amos, L. A.; Lowe, J., Tubulin and FtsZ form a distinct family of GTPases. *Nat. Struc. Biol.* **1998**, *5*, 451-458.
27. Margalit, D. N.; Romberg, L.; Mets, R. B.; Hebert, A. M.; Mitchison, T. J.; Kirschner, M. W.; RayChaudhuri, D., Targeting cell division: Small-molecule inhibitors of FtsZ GTPase perturb cytokinetic ring assembly and induce bacterial lethality. *Proc. Natl. Acad. Sci.* **2004**, *101*, 13969.
28. Scheffers, D.-J.; de Wit, J. G.; den Blaauwen, T.; Driessen, A. J. M., GTP Hydrolysis of Cell Division Protein FtsZ: Evidence that the Active Site Is Formed by the Association of Monomers. *Biochemistry* **2002**, *41*, 521-529.
29. Wang, J.; Galgoci, A.; Kodali, S.; Herath, K. B.; Jayasuriya, H.; Dorso, K.; Vicente, F.; Gonzalez, A.; Cully, D.; Bramhill, D.; Singh, S., Discovery of a small molecule that inhibits cell division by blocking FtsZ, a novel therapeutic target of antibiotics. *J. Biol. Chem.* **2003**, *278*, 44424-44428.
30. Lappchen, T.; Hartog Aloysius, F.; Pinas Victorine, A.; Koomen, G.-J.; den Blaauwen, T., GTP analogue inhibits polymerization and GTPase activity of the bacterial protein FtsZ without affecting its eukaryotic homologue tubulin. *Biochemistry* **2005**, *44*, 7879-84.
31. Laeppchen, T.; Pinas, V. A.; Hartog, A. F.; Koomen, G.-J.; Schaffner-Barbero, C.; Andreu, J. M.; Trambaiolo, D.; Loewe, J.; Juhem, A.; Popov, A. V.; den Blaauwen, T., Probing FtsZ and Tubulin with C8-Substituted GTP Analogs Reveals Differences in Their Nucleotide Binding Sites. *Chem. Biol.* **2008**, *15*, 189-199.
32. Godowski, K. C., Antimicrobial action of sanguinarine. *J. Clin. Dent.* **1989**, *1*, 96-101.
33. Beuria, T. K.; Santra, M. K.; Panda, D., Sanguinarine Blocks Cytokinesis in Bacteria by Inhibiting FtsZ Assembly and Bundling. *Biochemistry* **2005**, *44*, 16584-16593.
34. Mukherjee, S.; Robinson, C. A.; Howe, A. G.; Mazor, T.; Wood, P. A.; Uргаonkar, S.; Hebert, A. M.; RayChaudhuri, D.; Shaw, J. T., N-Benzyl-3-sulfonamidopyrrolidines as novel inhibitors of cell division in *E. coli*. *Bioorg. Med. Chem. Lett.* **2007**, *17*, 6651-6655.
35. Anam, E. M., 2''''-Hydroxy-3''-benzyluvarinol,2''''-hydroxy-5''''-benzylisouvarinol-A and 2''-hydroxy-5''-benzylisouvarinol-B: three novel tetra-C-benzylated flavanones from the root extract of *Xylopiа africana* (Benth.) Oliver (Annonaceae). *Indian J. Chem., Sect. B: Org. Chem. Incl. Med. Chem.* **1994**, *33B*, 1009-11.

36. Hufford, C. D.; Lasswell, W. L., Jr., Antimicrobial activities of constituents of *Uvaria chamae*. *Lloydia* **1978**, *41* (2), 156-60.
37. Leegaard, T. M.; Caugant, D. A.; Froholm, L. O.; Hoiby, E. A., Apparent differences in antimicrobial susceptibility as a consequence of national guidelines. *Clin. Microbiol. Infect.* **2000**, *6*, 290-293.
38. Uргаonkar, S.; La Pierre, H. S.; Meir, I.; Lund, H.; Ray Chaudhuri, D.; Shaw, J. T., Synthesis of Antimicrobial Natural Products Targeting FtsZ: (+-)-Dichamanetin and (+-)-2"-Hydroxy-5"-benzylisouvarinol-B. *Org. Lett.* **2005**, *7*, 5609-5612.
39. Domadia, P.; Swarup, S.; Bhunia, A.; Sivaraman, J.; Dasgupta, D., Inhibition of bacterial cell division protein FtsZ by cinnamaldehyde. *Biochem. Pharmacol.* **2007**, *74*, 831-840.
40. Beuria, T. K.; Singh, P.; Surolia, A.; Panda, D., Promoting assembly and bundling of FtsZ as a strategy to inhibit bacterial cell division: A new approach for developing novel antibacterial drugs. *Biochem. J.* **2009**, *423*, 61-69.
41. Rai, D.; Singh, J. K.; Roy, N.; Panda, D., Curcumin inhibits FtsZ assembly: an attractive mechanism for its antibacterial activity. *Biochem. J.* **2008**, *410*, 147-155.
42. Villinski, J. R.; Dumas, E. R.; Chai, H.-B.; Pezzuto, J. M.; Angerhofer, C. K.; Gafner, S., Antibacterial Activity and Alkaloid Content of *Berberis thunbergii*, *Berberis vulgaris* and *Hydrastis canadensis*. *Pharm. Biol.* **2003**, *41*, 551-557.
43. Yu, H.-H.; Kim, K.-J.; Cha, J.-D.; Kim, H.-K.; Lee, Y.-E.; Choi, N.-Y.; You, Y.-O., Antimicrobial Activity of Berberine Alone and in Combination with Ampicillin or Oxacillin Against Methicillin-Resistant *Staphylococcus aureus*. *J. Med. Food* **2005**, *8*, 454-461.
44. Hwang, B. Y.; Roberts, S. K.; Chadwick, L. R.; Wu, C. D.; Kinghorn, A. D., Antimicrobial constituents from goldenseal (the rhizomes of *Hydrastis canadensis*) against selected oral pathogens. *Planta Medica* **2003**, *69*, 623-627.
45. Domadia, P. N.; Bhunia, A.; Sivaraman, J.; Swarup, S.; Dasgupta, D., Berberine Targets Assembly of *Escherichia coli* Cell Division Protein FtsZ. *Biochemistry* **2008**, *47*, 3225-3234.
46. Clement, M.-J.; Jourdain, I.; Lachkar, S.; Savarin, P.; Gigant, B.; Knossow, M.; Toma, F.; Sobel, A.; Curmi, P. A., N-Terminal Stathmin-like Peptides Bind Tubulin and Impede Microtubule Assembly. *Biochemistry* **2005**, *44*, 14616-14625.

47. Clement, M.-J.; Kuoch, B.-t.; Ha-Duong, T.; Joshi, V.; Hamon, L.; Toma, F.; Curmi, P. A.; Savarin, P., The Stathmin-Derived I19L Peptide Interacts with FtsZ and Alters Its Bundling. *Biochemistry* **2009**, *48*, 9734-9744.
48. Arbildua, J. J.; Brunet, J. E.; Jameson, D. M.; Lopez, M.; Nova, E.; Lagos, R.; Monasterio, O., Fluorescence resonance energy transfer and molecular modeling studies on 4',6-diamidino-2-phenylindole (DAPI) complexes with tubulin. *Protein Sci.* **2006**, *15*, 410-419.
49. Bonne, D.; Heusele, C.; Simon, C.; Pantaloni, D., 4',6-Diamidino-2-phenylindole, a fluorescent probe for tubulin and microtubules. *J. Biol. Chem.* **1985**, *260*, 2819-25.
50. Ortiz, M.; Lagos, R.; Monasterio, O., Interaction between the C-terminal peptides of tubulin and tubulin S detected with the fluorescent probe 4',6-diamidino-2-phenylindole. *Arch. Biochem. Biophys.* **1993**, *303*, 159-64.
51. Nova, E.; Montecinos, F.; Brunet, J. E.; Lagos, R.; Monasterio, O., 4',6-Diamidino-2-phenylindole (DAPI) induces bundling of Escherichia coli FtsZ polymers inhibiting the GTPase activity. *Arch. Biochem. Biophys.* **2007**, *465*, 315-319.
52. Stokes, N. R.; Sievers, J.; Barker, S.; Bennett, J. M.; Brown, D. R.; Collins, I.; Errington, V. M.; Foulger, D.; Hall, M.; Halsey, R.; Johnson, H.; Rose, V.; Thomaidis, H. B.; Haydon, D. J.; Czaplewski, L. G.; Errington, J., Novel Inhibitors of Bacterial Cytokinesis Identified by a Cell-based Antibiotic Screening Assay. *J. Biol. Chem.* **2005**, *280*, 39709-39715.
53. Ohashi, Y.; Chijjiwa, Y.; Suzuki, K.; Takahashi, K.; Nanamiya, H.; Sato, T.; Hosoya, Y.; Ochi, K.; Kawamura, F., The lethal effect of a benzamide derivative, 3-methoxybenzamide, can be suppressed by mutations within a cell division gene, ftsZ, in Bacillus subtilis. *J. Bacteriol.* **1999**, *181*, 1348-1351.
54. Haydon, D. J.; Stokes, N. R.; Ure, R.; Galbraith, G.; Bennett, J. M.; Brown, D. R.; Baker, P. J.; Barynin, V. V.; Rice, D. W.; Sedelnikova, S. E.; Heal, J. R.; Sheridan, J. M.; Aiwale, S. T.; Chauhan, P. K.; Srivastava, A.; Taneja, A.; Collins, I.; Errington, J.; Czaplewski, L. G., An Inhibitor of FtsZ with Potent and Selective Anti-Staphylococcal Activity. *Science* **2008**, *321*, 1673-1675.

Chapter V

Synthesis of CMPF for Dual-Targeting Taxoid Conjugate

Table of Contents

§ 5.1. Introduction.....	145
§ 5.2 Results and Discussion.....	150
§ 5.2.1 <i>Synthesis of CMPF derivatives</i>	150
§ 5.2.2 <i>Evaluation of binding affinity of CMPF derivatives to human serum albumin (HSA)</i>	151
§ 5.4 Conclusion	152
§ 5.5 Experimental Section.....	153
§5.6 References	159

§ 5.1. Introduction

Cancer is the collection of diseases which is characterized by the uncontrolled growth of undifferentiated cells known as tumor cells. Despite successful research in discovering antitumor drugs such as discodermolide, epothilone, doxorubicin, there is still no significant reduction in the death rates caused due to cancer. Cancer is the second leading cause of death in the U.S causing 7 million deaths every year—or 12.5% of deaths worldwide.¹

One of the key problems associated with conventional chemotherapy is its inability to differentiate between the tumor cells and healthy cells because of their similar physiological and biochemical processes. This lack of selectivity not only leads to undesirable side effects such as hair loss, liver and kidney damage, and bone marrow defects but also lowers drug efficiency. In order to achieve effective tumor specific drug delivery, it is required to understand the basic difference between the physiological and biochemical processes of normal and malignant cells. Rapidly growing tumor cells require large amount of nutrients and vitamins in comparison to normal cells. Therefore, tumor cells overexpress certain receptors which are specific to folic acid^{2,3}, biotin⁴, benzamide-riboside⁵, intestinal oligopeptides⁶, hyaluronic acid, monoclonal antibodies⁷ etc. These tumor specific receptors can be used as targets to selectively deliver cytotoxic agents into malignant cell.⁸ Consequently, the cytotoxic warheads can be attached to tumor targeting moieties through a suitable linker to form a drug conjugate (**Figure V-1**).

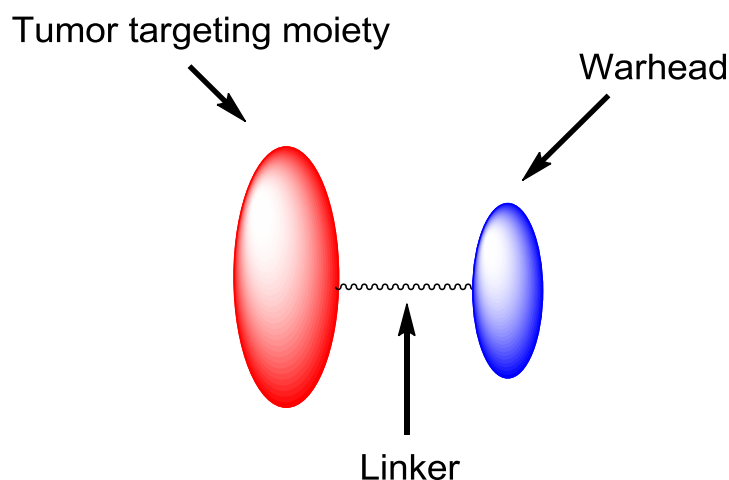


Figure V-1. Basic structure of drug conjugate

Before internalization, the drug conjugate should be non-toxic and the linker should be stable during circulation. Many linkers like peptides, hydrazones, esters etc. have been designed and successfully used for drug delivery.⁹ In Ojima research laboratory, disulfide linkers, which are cleaved inside the tumor cells through disulfide exchange with intracellular thiol such as glutathione, are used. Based on the results from preclinical models, disulfide linkers have been found to be more efficient in comparison to several other linkers.^{10,11}

Another morphological difference between the malignant and normal cells is defective tumor vasculature and under developed lymphatic drainage system which cause abnormal molecular and fluid transport in malignant cells.¹² This phenomenon of enhanced permeability and retention of large molecules and lipids in solid tumors is termed ‘enhanced permeability and retention’ (EPR) or passive effect as they are receptor independent.¹² Thus, macromolecular cytotoxic agents or cytotoxic macromolecular drug conjugates may be expected to show enhanced degree of selectivity to malignant cell. Various approaches have been investigated to generate macromolecular cytotoxic drug conjugates by using synthetic polymers¹³, dendrimers, proteins, carbon nanotubes¹⁴ etc. as macromolecule components. One of the promising approaches is the use of endogenous proteins like albumin, transferrin as macromolecular conjugates. The advantage with endogenous proteins lies in the fact that they can easily be taken up by malignant cells providing additional selectivity.¹⁵

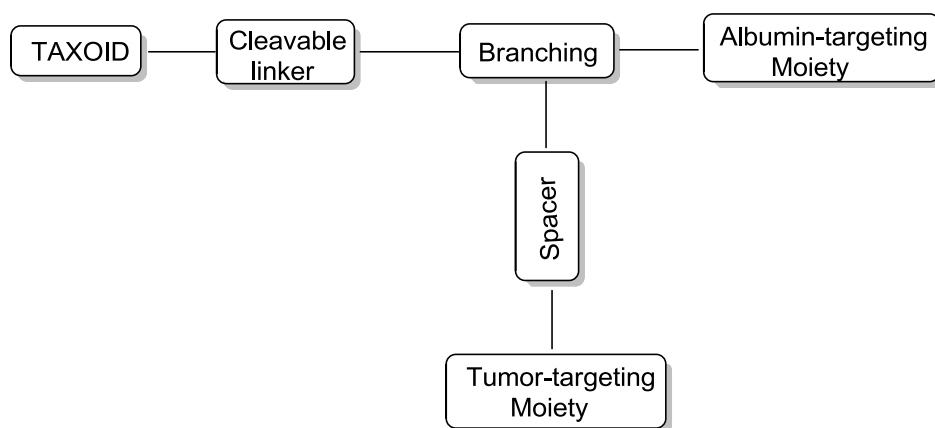


Figure V-2. Dual targeting taxoid conjugate

Albumin is the most abundant blood plasma protein which helps the transportation of long chain fatty acids. In recent studies, it was shown that malignant cells exhibit enhanced albumin uptake.¹⁶ Hence, an albumin-targeting conjugate containing the

cytotoxic component can be another effective approach towards achieving drug specificity.¹⁷ On the basis of these findings, dual-targeting taxoid conjugate composed of cytotoxic warhead, tumor targeting moiety, albumin targeting moiety, linker and spacer has been proposed (**Figure V-2**). The dual-targeting taxoid conjugates are designed to target the tumor cells at two different levels. As discussed earlier, tumor targeting moieties direct the drug conjugate to the overexpressed receptors on the tumor cells where upon internalization the active drug is released. The other aspect of dual-targeting is the presence of albumin targeting moieties. The attachment of drug conjugate to albumin will generate a macromolecular conjugate. According to the EPR effect, the macromolecular drug conjugate will show enhanced permeability and retention to the cancer cells.¹²

An endogenous ligand, 3-carboxy-4-methyl-5-propyl-2-furanpropanoic acid (CMPF) will be used as albumin-targeting moiety because of its favored water solubility and high binding affinity ($K_A=4.6 \times 10^6 M^{-1}$) to albumin.¹⁸ As both the carboxyl groups in CMPF are required for the efficient binding to albumin, it can be attached to the conjugate by introducing an amino group at the propyl terminal. In the previous work by Ojima lab, different CMPF derivatives were prepared (**Figure V-3**) and their binding affinity to bovine serum albumin (BSA) and human serum albumin (HSA) was evaluated using isothermal titration calorimetry (ITC). Except for the fluorescent CMPF derivative, other derivatives either showed very weak or negligible binding affinity. This led to the assumption that the presence of a polar amino group affects the binding of CMPF derivative to albumin.

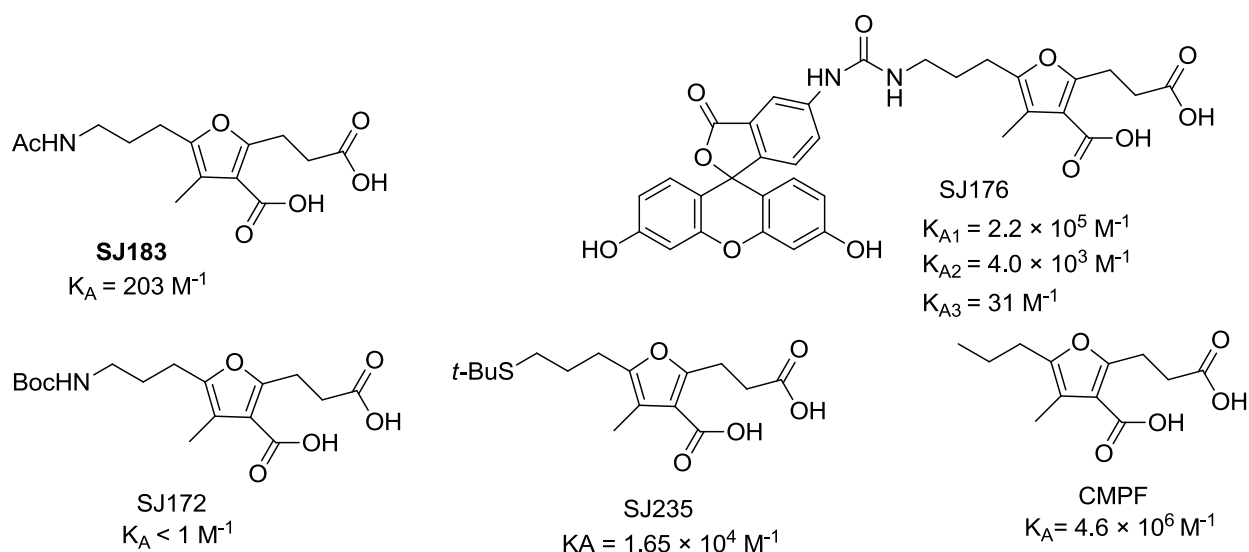


Figure V-3. Derivatives of CMPF with their binding affinities to albumin

This study led to the suggestion that a *tert*-butylthiol derivative of CMPF can tolerate the polarity of the molecule. Unfortunately, the binding affinity of *tert*-butylthiol derivative of CMPF was weaker than that of CMPF and higher than that of **SJ183** or **SJ172** (**Figure V-4**). This implied that the propyl group on CMPF is important for strong binding. The results suggested that increasing the hydrophobicity of the propyl arm by longer alkyl chain may enhance the binding affinity of CMPF.

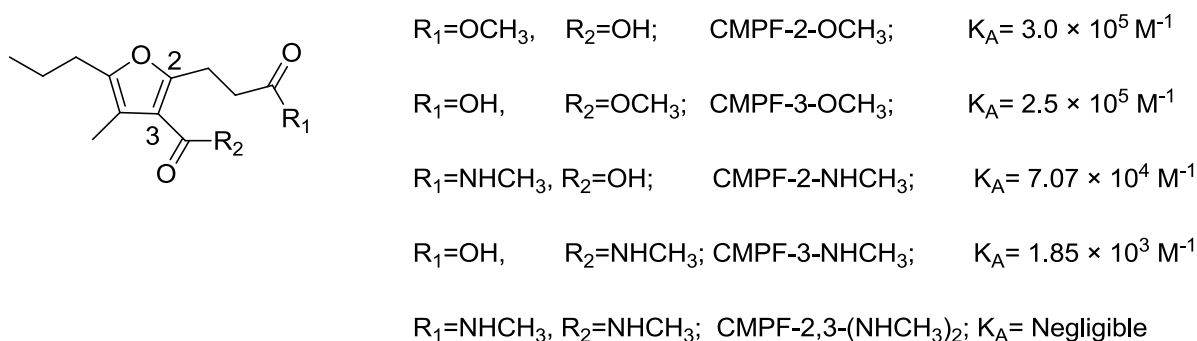


Figure V-4. Binding affinity of methyl ester and N-methyl amide derivatives of CMPF to HSA.

In order to come up with alternative attachment site to the drug conjugate, the binding affinity of methyl ester and *N*-methylamide-CMPF derivatives were evaluated using ITC. The mono-amides showed weaker binding than the corresponding esters and the bis-amide showed no activity. The binding affinity of CMPF-2-NHMe ($7.07 \times 10^4 M^{-1}$) was higher than that of CMPF-3-NHMe ($1.85 \times 10^3 M^{-1}$) (**Figure V-4**). Though the binding affinity of CMPF-2-NHMe is 24 times weaker than that of the parent CMPF, the binding mode was still conserved. Thus CMPF may be attached to the dual-targeting conjugate through the amide linkage at the 2-position of CMPF (**Figure V-5**).

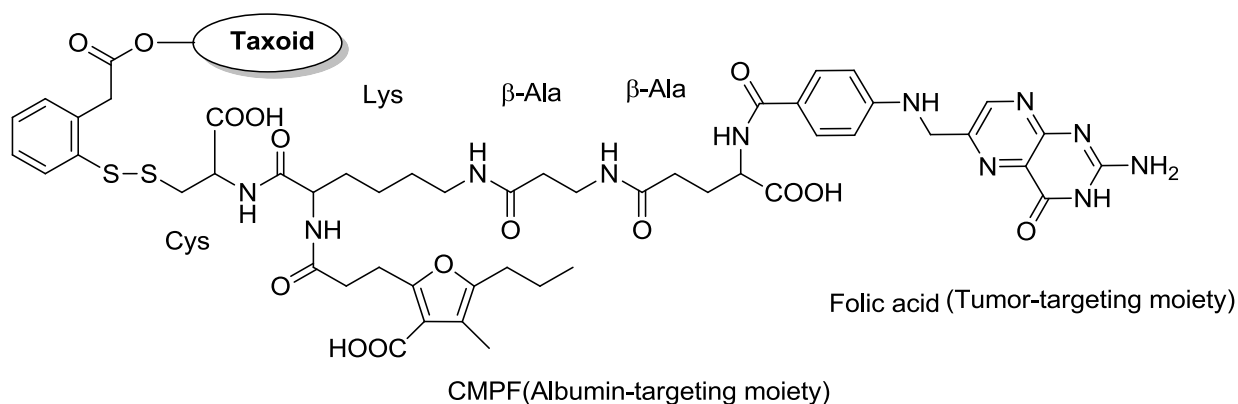
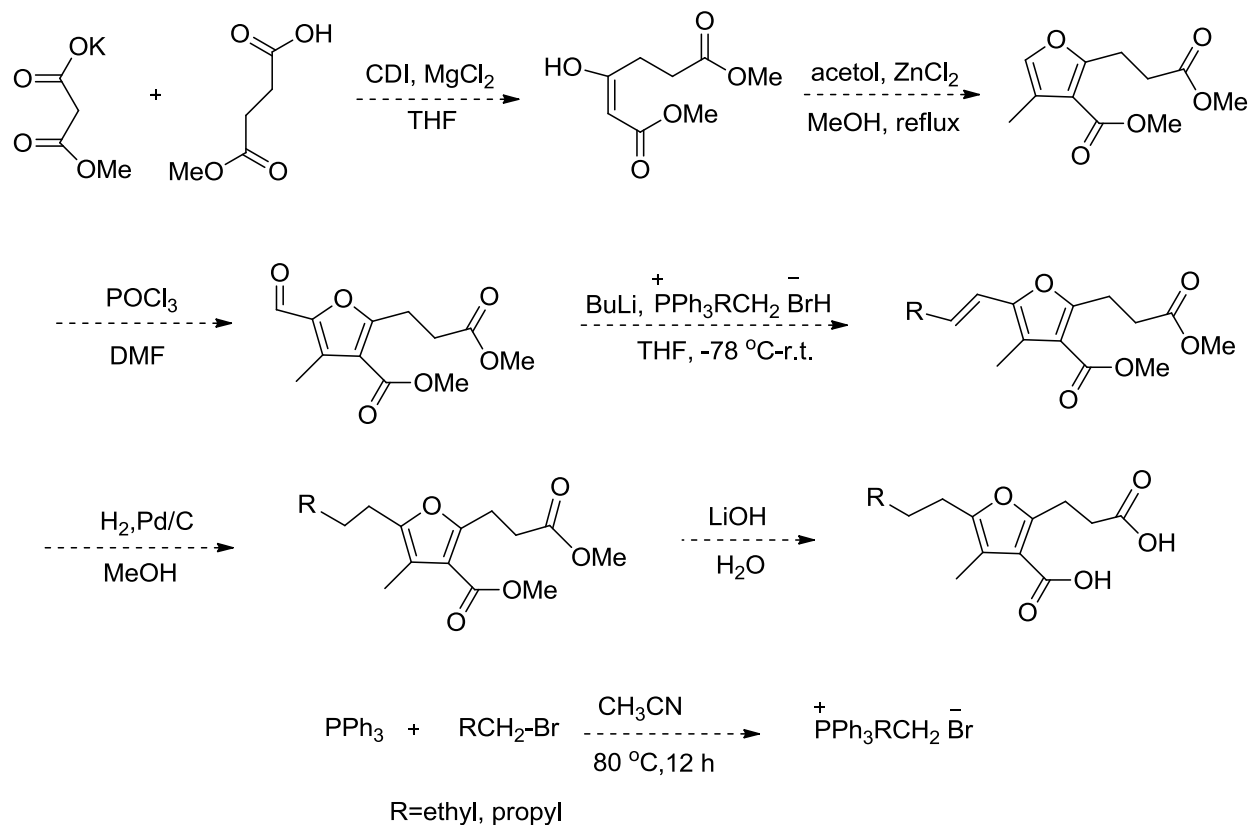


Figure V-5. Dual targeting taxoid conjugate containing folic acid and CMPF

As previously discussed, the propyl arm in CMPF cannot be replaced with polar or bulky substituents. It is suggested that the substitution of the propyl arm by longer alkyl chains may improve the binding affinity. Accordingly, synthesis of CMPF derivatives having one and two carbon units more than parent CMPF molecule at the position-5 was proposed (**Scheme V-1**). Subsequently, their binding affinity to albumin will also be evaluated by ITC.

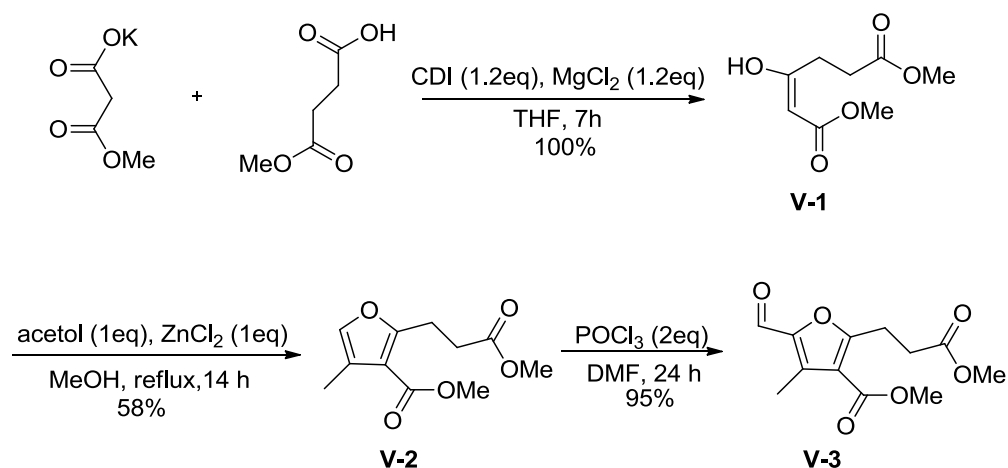


Scheme V-1. Proposed synthesis of CMPF analogues

§ 5.2 Results and Discussion

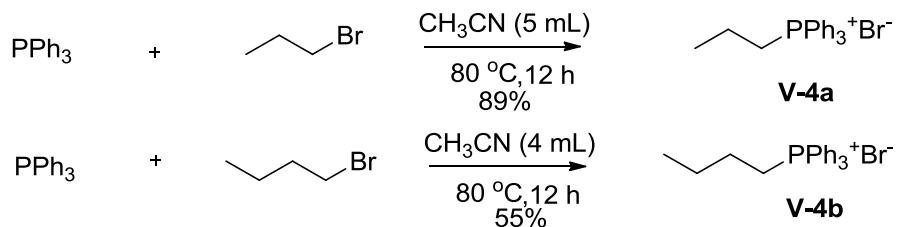
§ 5.2.1 Synthesis of CMPF derivatives

The synthesis of CMPF derivatives started with the preparation of Methyl 5-Formyl-2-(3-methoxy-3-oxopropyl)-4-methylfuran-3-carboxylate (**V-3**).¹⁹ The condensation of potassium 3-methoxy-3-oxopropanoate with 4-methoxy-4-oxobutanoic acid in the presence of *N,N'*-carbonyldiimidazole and magnesium chloride gave 3-oxohexanedioic acid dimethyl ester **V-1** in quantitative yield. Zinc chloride-catalyzed coupling of **V-1** with acetol gave **V-2** in 58% yield.^{20,21} Using Vilsmeier-Hack formylation, previously stirred solution of phosphorous oxychloride in *N,N'*-dimethylformamide was added to **V-2** to generate **V-3** in 94% yield (Scheme V-2).



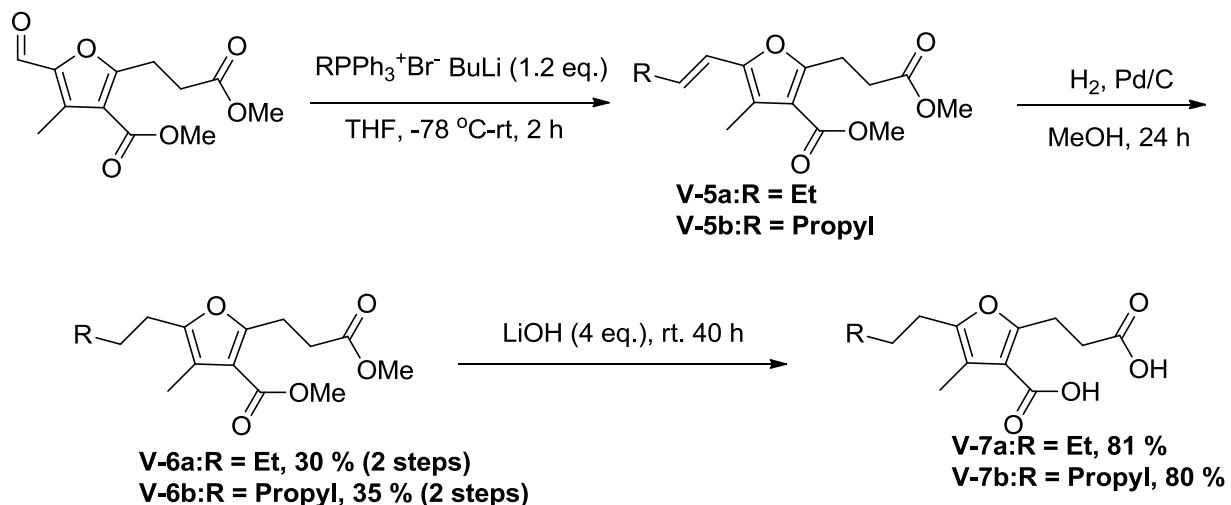
Scheme V-2. Synthesis of CMPF precursor

Alkyltriphenylphosphonium salts were synthesized by refluxing alkyl bromide and triphenylphosphine in acetonitrile. Propyltriphenylphosphonium bromide **V-4a** and butyltriphenylphosphonium bromide **V-4b** were obtained in 89% and 55% yields, respectively (Scheme V-3).



Scheme V-3. Synthesis of alkyltriphenylphosphonium salts

Alkyltriphenylphosphonium salts **V-4a** and **V-4b** were treated with n-BuLi to form the corresponding phosphorous ylides. To these phosphonium salts, **V-3** was added in THF at -78 °C to form **V-5a** and **V-5b**. These products were subjected to ambient pressure hydrogenation to form **V-6a** and **V-6b** with two steps yield of 70 % and 71 %, respectively. Subsequent hydrolysis of **V-6a** and **V-6b** with aqueous LiOH gave the final CMPF derivatives **V-7a** and **V-7b** (Scheme V-4).



Scheme V-4. Synthesis of CMPF analogues

§ 5.2.2 Evaluation of binding affinity of CMPF derivatives to human serum albumin (HSA)

In order to evaluate the effect of substitution at the 5-position, it is necessary to evaluate their binding affinities to HSA by ITC. ITC is a thermodynamic technique that allows the study on the interactions of two species. When these two species interact, heat is either generated or absorbed. By measuring the heat of absorption/generation, binding constants (K), reaction stoichiometry (n), and thermodynamic parameters including enthalpy (ΔH) and entropy (ΔS) can be accurately determined.

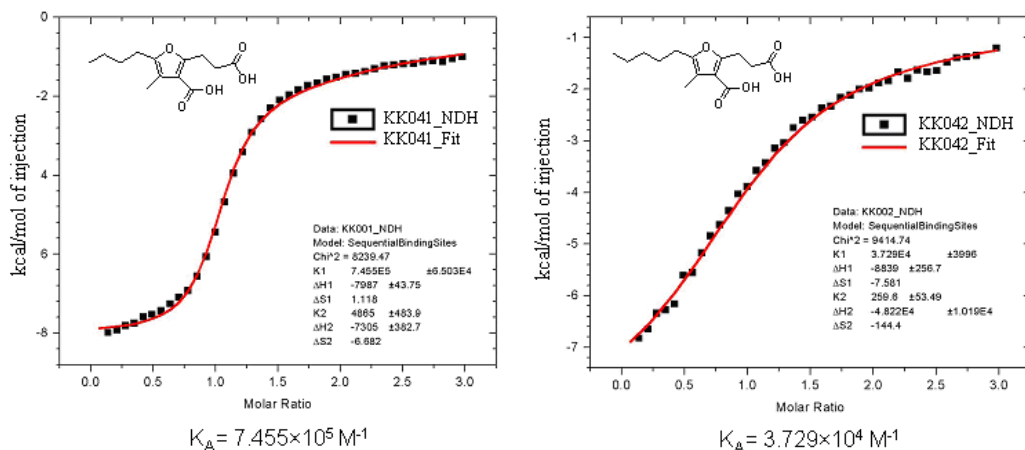


Figure V-6. ITC Measurements of CMPF derivatives

Phosphate buffer of pH 7.4 was used to prepare the solution of HSA and CMPF derivatives **V-7a** and **V-7b**. The concentrations of HSA and ligands (CMPF derivatives) used for the ITC measurement were 0.1 mM and 2 mM. The binding constants of **V-7a** and **V-7b** to HSA were measured to be $K_A = 7.45 \times 10^5 \text{ M}^{-1}$ and $K_A = 3.729 \times 10^4 \text{ M}^{-1}$ respectively (**Figure V-6**). On comparing the binding constants for these derivatives with that of the parent CMPF molecule, we observed that the binding constant of **V-7a** was one sixth of parent CMPF whereas that of **V-7b** was almost negligible. The increase in the hydrophobicity of the propyl arm by adding one carbon unit showed significant decrease in the binding constant. The binding constant of CMPF derivative having additional two carbon units was negligible in comparison to parent CMPF molecule.

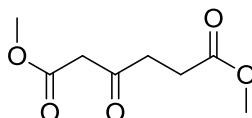
§ 5.4 Conclusion

An endogenous ligand, 3-carboxy-4-methyl-5-propyl-2-furanpropanoic acid (CMPF) is known to bind to albumin and can be used as a tumor targeting moiety because of its favored water solubility and high binding affinity to albumin. Several CMPF analogues were designed and synthesized for targeted drug delivery using multi-step organic synthesis in excellent yield. The binding affinity of these analogues to albumin was also studied. In comparison to CMPF, the binding constant of **V-7a** was one sixth of that of CMPF whereas that of **V-7b** was almost negligible. It was concluded that the increase in the hydrophobicity of the propyl arm by adding one carbon unit showed significant decrease in the binding constant.

§ 5.5 Experimental Section

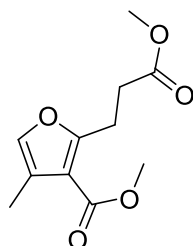
General Methods: All chemicals were obtained from commercial sources. Tetrahydrofuran and dichloromethane were dried by passing through drying columns on the Innovative Technologies, Inc. solvent purification system. NMR spectra were recorded on a Varian 300 NMR spectrometer or a Varian 400 NMR spectrometer. The ^1H and ^{13}C spectra were calibrated using residual solvent peak as the internal standard (CDCl_3 : 7.26/77.00ppm). The ^{31}P spectra were not calibrated. Melting points were measured on a Thomas Hoover Capillary melting point apparatus and are uncorrected. TLC was performed on Merck DC-alufolien with Kieselgel 60F-254 and column chromatography was carried out on silica gel 60 (Merck; 230-400 mesh ASTM). Isothermal titration calorimetry was performed on MicroCal Instrument at 37 °C. The concentration of human serum albumin and ligands were 0.1 mM and 2 mM respectively in phosphate buffer of pH7.4. The solutions were degassed in a mild vacuum for 5-10 min prior to each measurement. The size of the measurement cell is 1.43 mL and the solution of the ligand was added at 5 μL increments to reach up to 10 equivalents of ligand to albumin.

1,6-dimethyl-3-oxohexanediote (**V-1**):¹⁹



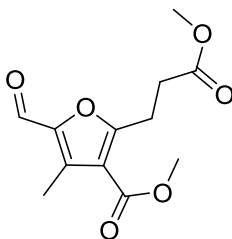
To a solution of succinic acid monomethyl ester (3.09 g, 23.44 mmol) in dry THF (20 mL) was added *N,N'*-carbonyldiimidazole (4.56 g, 28.12 mmol) at 0 °C. The reaction flask was removed from the ice bath and stirred for 1 h under nitrogen atmosphere. The carbon dioxide was released. To the reaction mixture MgCl_2 (2.67 g, 28.12 mmol) was added followed by potassium malonate monomethyl ester (4.39 g, 28.12 mmol) and the suspension was stirred at 45 °C under nitrogen for 7.5 h. The reaction was quenched with 1M H_2SO_4 (30 mL), extracted with EtOAc, dried over MgSO_4 and solvent was evaporated. The crude product was purified by column chromatography on silica gel (20 – 35 % EtOAc in hexanes) to afford **V-1** as colorless oil (4.41 g, 100 % yield): ^1H NMR (300 MHz, CDCl_3) δ 2.60 (t, 2 H, $J = 7.5$ Hz), 2.85 (t, 2 H, $J = 7.5$ Hz), 3.65 (s, 3 H), 3.49 (s, 1 H), 3.72 (s, 3 H); ^{13}C NMR (75 MHz, CDCl_3) δ 27.66, 37.38, 51.87, 52.39, 167.3, 172.7, 200.8. All data are in agreement with literature values.¹⁹

Methyl 2-(3-methoxy-3-oxopropyl)-4-methylfuran-3-carboxylate (V-2):²¹



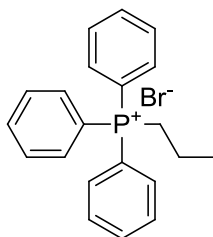
To a solution of **V-1** (4.17 g, 22.1 mmol) and hydroxyacetone (1.64 g, 1 equiv.) in MeOH (2 mL) was added ZnCl₂ (2.97 g, 22.1 mmol). The mixture was stirred at 65 °C under nitrogen. After 14 h the reaction mixture was cooled down, quenched with water (20 mL) followed by extraction with EtOAc (3×) and dried over MgSO₄. The crude product was purified by column chromatography on silica gel (5 - 7 % EtOAc in hexanes) to afford **V-2** as colorless oil (2.91 g, 58 % yield): ¹H NMR (300 MHz, CDCl₃) δ 2.12 (s, 3 H), 2.67 (t, 2 H, *J* = 7.6 Hz), 3.27 (t, 2 H, *J* = 7.8 Hz), 3.68 (s, 3 H), 3.82 (s, 3 H). All data are consistent with the literature values.²¹

Methyl 5-Formyl-2-(3-methoxy-3-oxopropyl)-4-methylfuran-3-carboxylate (V-3):²⁵



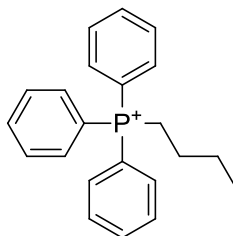
Phosphorous oxychloride (2.32 mL, 24.84 mmol) was stirred in DMF (51 mL) at 0 °C for 1 h. The solution was stirred into a flask with **V-2** (2.81 g, 12.42 mmol) and stirred for 24 h at room temperature. The solution was poured into ice-cold water (600 mL) followed by saturated aqueous solution of NaHCO₃ (120 mL). After stirring for 1 h the solution was extracted four times with EtOAc and dried over MgSO₄. The crude product was purified and column chromatography on silica gel (20 – 35 % EtOAc in hexanes) to give **V-3** (2.93 g, 95 % yield) ¹H NMR (300 MHz, CDCl₃) δ 2.52 (s, 3 H), 2.76 (t, 2 H, *J* = 7.6), 3.37 (t, 2 H, *J* = 7.5), 3.87 (s, 3 H), 9.72 (s, 3 H); ¹³C NMR (75 MHz, CDCl₃) δ 9.93, 23.9, 30.98, 51.57, 51.81, 116.2, 134.6, 147.3, 163.3, 165.5, 172.0, 177.08; MS(*m/z*) 255.08 [M⁺].

Propyltriphenylphosphonium bromide (V-4a):²²



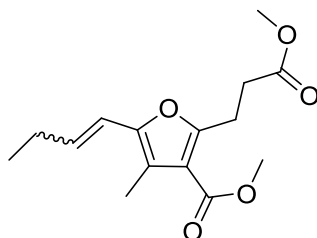
A solution of PPh₃ (3.00 g, 11.43 mmol) and bromopropane (1.24 mL, 13.71 mmol) in acetonitrile (5 mL) was refluxed under nitrogen for 12 h. After cooling to room temperature, ether 10 mL was added gradually. The product was precipitated and **V-4a** collected (3.91 g, 89 % yield): ¹H NMR (300 MHz, CDCl₃) δ 1.22 (t, 3H, *J* = 7.3Hz), 1.68 (m, 2 H), 3.75 (m, 2 H), 7.86-7.26 (m, 15 H); ¹³C NMR (75 MHz, CDCl₃) δ 15.05, 16.32, 23.96, 24.61, 117.4, 118.6, 130.2, 130.4, 133.3, 133.5, 134.8, 134.9; ³¹P NMR (121 MHz, CDCl₃) δ 25.18. All data are in agreement with literature values.²³

Butyltriphenylphosphonium bromide (V-4b):²²



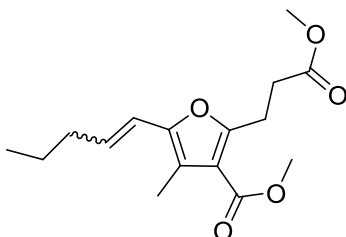
The same procedure were used for the synthesis of **V-4b** (1.99 g, 55 % yield): ¹H NMR (300 MHz, CDCl₃) δ 0.91 (t, 3 H, *J* = 7Hz), 1.59 (m, 2 H), 1.69 (m, 2 H), 3.8 (m, 2 H), 7.9- 7.4 (m, 15 H); ¹³C NMR (75 MHz, CDCl₃) δ 13.63, 22.13, 23.49, 23.70, 24.42, 24.48, 117.5, 118.6, 130.3, 133.4, 133.5, 134.9; ³¹P NMR (300 MHz, CDCl₃) δ 25.39. All data are in agreement with literature values.²³

Methyl 5-(but-1-enyl)-2-(3-methoxy-3-oxopropyl)-4-methylfuran-3-methylcarboxylate (V-5a):²⁴



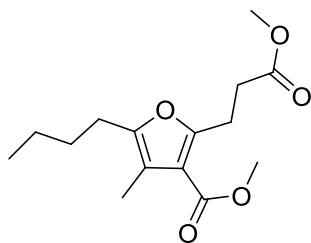
To a solution of propyltriphenylphosphonium bromide (130.96 mg, 0.34 mmol) in THF (2 mL) under inert atmosphere at $-78\text{ }^{\circ}\text{C}$ was slowly added *n*-BuLi in hexanes (1.6 M, 0.34 mmol). After stirring for 35 min a solution of **V-3** (72 mg, 0.280 mmol) in THF (0.55 mL) was added and the mixture was stirred for 1 h at $-78\text{ }^{\circ}\text{C}$ and then 2 h at $0\text{ }^{\circ}\text{C}$. The reaction was quenched with phosphate buffer (5 mL, pH=3 - 4), extracted with 1:1 EtOAc/hexanes (3 \times) and dried with MgSO_4 . The crude product was purified by flash chromatography (gradient 10 – 20 % EtOAc in hexanes) and the fractions were evaporated in the dark to give the product **V-5a** as a mixture of *E/Z* regioisomers. The wet product was immediately subjected to the next step.

Methyl 2-(3-methoxy-3-oxopropyl)-4-methyl-5-(pent-1-enyl)furan-3-methylcarboxylate (V-5b):²⁴



The same procedure was used for the synthesis of **V-5b** and the wet product was immediately used in the next step. Butyltriphenylphosphonium bromide (202.22 mg, 0.50 mmol, 1.2 equiv. to **V-3**) in THF (3 mL), *n*-BuLi in hexanes (1.6 M, 1 equiv. to butyltriphenylphosphonium bromide), **V-3** (107.3 mg, 0.280 mmol) in THF (0.82 mL).

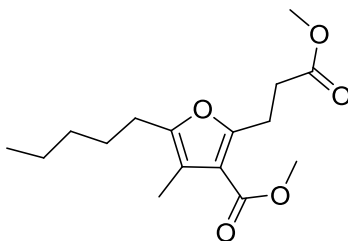
Methyl 5-butyl-2-(3-methoxy-3-oxopropyl)-4-methylfuran-3-carboxylate (V-6b):



To a solution of **V-5b** from the previous step in EtOH (5 mL) was carefully added 10 % Pd/C (15 mg) and the suspension was vigorously stirred under 1 atm of H_2 for 24 h. The catalyst was filtered off through celite and the crude product was purified by column chromatography on silics gel (gradient 10 – 20 % EtOAc in hexanes) to give **V-6b** as colorless oil (44.6 mg, 35.6 % yield): $^1\text{H NMR}$ (300 MHz, CDCl_3) δ 0.88 (t, 3 H, $J = 6.9$ Hz), 1.27 (m, 4 H), 1.54 (m, 2 H), 2.05

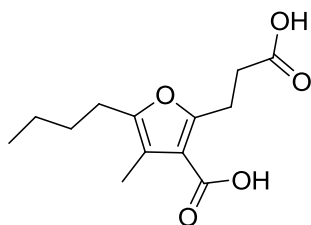
(s, 3 H), 2.49 (t, 2 H, $J = 7.5$), 2.66 (t, 2 H, $J = 7.6$ Hz), 3.24 (t, 2 H, $J = 7.8$ Hz), 3.68 (s, 3 H), 3.80 (s, 3 H).

Methyl 2-(3-methoxy-3-oxopropyl)-4-methyl-5-pentylfuran-3-carboxylate (V-6a):



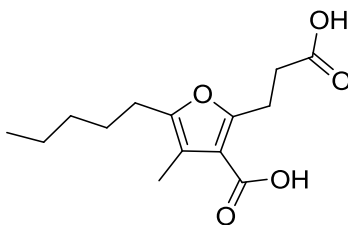
Same procedure was used for the synthesis of **V-6a** (24.0 mg, 30% yield). ^1H NMR (300 MHz, CDCl_3): δ 0.89 (t, 3 H, $J = 7.2$ Hz), 1.30 (m, 2 H), 1.55 (m, 2 H), 2.05 (s, 3 H), 2.50 (t, 2 H, $J = 7.2$ Hz), 2.65 (t, 2 H, $J = 7.9$ Hz), 3.24 (t, 2 H, $J = 7.8$ Hz), 3.68 (s, 3 H), 3.80 (s, 3 H).

5-butyl-2-(2-carboxyethyl)-4-methylfuran-3-carboxylic acid (V-7a):



To **V-6a** (20.5 mg, .07 mmol) was added 1 M aqueous solution of LiOH (0.36 ml, 0.36 mmol). The emulsion was stirred at room temperature for 42 h. The solution was washed three times with 30 % EtOAc in hexanes and then acidified with a few drops of concentrated aqueous HCl. The precipitated product was extracted with EtOAc, dried over MgSO_4 and the solvent was evaporated to yield the product **V-7a** (15.1 mg, 81 % yield): mp. 115-120 °C; ^1H NMR (300 MHz, CDCl_3) δ 0.91 (t, 3 H, $J = 7.2$ Hz), 1.30 (m, 2 H), 1.55 (m, 2 H), 2.07 (s, 3 H), 2.52 (t, 2 H, $J = 7.3$ Hz), 2.72 (t, 2 H, $J = 7.8$ Hz), 3.31 (t, 2 H, $J = 7.6$ Hz); ^{13}C NMR (100 MHz, CDCl_3) δ 9.61, 13.75, 22.12, 23.63, 25.17, 30.41, 32.12, 113.3, 114.8, 151.0, 160.0, 170.2, 178.5; MS (ESI) m/z 255.1 ($\text{M}+1$) $^+$

2-(2-carboxyethyl)-4-methylfuran-5-pentyl-3-carboxylic acid (V-7b):



The same procedure was used for the synthesis of **V-7b** (25.2 mg, 80 % yield): mp. 107-109 °C; ^1H NMR (300 MHz, CDCl_3) δ 0.88 (t, 3 H, $J = 6.7$ Hz), 1.29 (m, 4 H), 1.57 (m, 2 H), 2.07 (s, 3 H), 2.51 (t, 2 H, $J = 7.6$ Hz), 2.71 (t, 2 H, $J = 7.6$ Hz), 3.31 (t, 2 H, $J = 7.8$ Hz); ^{13}C NMR (100 MHz, CDCl_3) δ 9.63, 13.97, 22.34, 23.95, 25.42, 27.95, 31.20, 32.05, 113.2, 114.9, 151.06, 160.0, 170.5, 178.9; MS (ESI) m/z 269.2 ($\text{M}+1$) $^+$

§ 5.6 References

1. Cancer facts and figures. *American Cancer Society*, 2009.
2. Weitman, S. D.; Lark, R. H.; Coney, L. R.; Fort, D. W.; Frasca, V.; Zurawski, V. R., Jr.; Kamen, B. A., Distribution of the folate receptor GP38 in normal and malignant cell lines and tissues. *Cancer Res.* **1992**, *52*, 3396-3401.
3. Lee, E. S.; Na, K.; Bae, Y. H., Polymeric micelle for tumor pH and folate-mediated targeting. *J. Control. Release* **2003**, *91*, 103-113.
4. Na, K.; Lee, T. B.; Park, K.-H.; Shin, E.-K.; Lee, Y.-B.; Choi, H.-K., Self-assembled nanoparticles of hydrophobically-modified polysaccharide bearing vitamin H as a targeted anti-cancer drug delivery system. *Eur. J. Pharm. Sci.* **2003**, *18*, 165-173.
5. Szekeres, T.; Sedlak, J.; Novotny, L., Benzamide riboside, a recent inhibitor of inosine 5'-monophosphate dehydrogenase induces transferrin receptors in cancer cells. *Curr. Med. Chem.* **2002**, *9*, 759-764.
6. Schally, A. V.; Szepeshazi, K.; Nagy, A.; Comaru-Schally, A. M.; Halmos, G., New approaches to therapy of cancers of the stomach, colon and pancreas based on peptide analogs. *Cell Mol. Life Sci.* **2004**, *61*, 1042-1068.
7. Wu, X.; Ojima, I., Tumor specific novel taxoid-monoclonal antibody conjugates. *Curr. Med. Chem.* **2004**, *11*, 429-438.
8. Jaracz, S.; Chen, J.; Kuznetsova, L. V.; Ojima, I., Recent advances in tumor-targeting anticancer drug conjugates. *Bioorg. Med. Chem.* **2005**, *13*, 5043-5054.
9. Chen, J.; Jaracz, S.; Zhao, X.; Chen, S.; Ojima, I., Antibody-cytotoxic agent conjugates for cancer therapy. *Expert Opin. Drug Delivery* **2005**, *2*, 873-890.
10. Kigawa, J.; Minagawa, Y.; Kanamori, Y.; Itamochi, H.; Cheng, X.; Okada, M.; Oishi, T.; Terakawa, N., Glutathione concentration may be a useful predictor of response to second-line chemotherapy in patients with ovarian cancer. *Cancer* **1998**, *82*, 697-702.
11. Liu, C.; Tadayoni, B. M.; Bourret, L. A.; Mattocks, K. M.; Derr, S. M.; Widdison, W. C.; Kedersha, N. L.; Ariniello, P. D.; Goldmacher, V. S.; Eradication of large colon tumor xenografts by targeted delivery of maytansinoids. *Proc. Natl. Acad. Sci.* **1996**, *93*, 8618-8623.

12. Maeda, H.; Fang, J.; Inutsuka, T.; Kitamoto, Y., Vascular permeability enhancement in solid tumor: various factors, mechanisms involved and its implications. *Int. Immunopharmacol.* **2003**, *3*, 319-328.
13. Jelinkova, M.; Strohalm, J.; Etrych, T.; Ulbrich, K.; Rihova, B., Starlike vs. Classic Macromolecular Prodrugs: Two Different Antibody-Targeted HPMA Copolymers of Doxorubicin Studied in Vitro and in Vivo as Potential Anticancer Drugs. *Pharm. Res.* **2003**, *20*, 1558-1564.
14. Bianco, A., Carbon nanotubes for the delivery of therapeutic molecules. *Expert Opin. Drug Delivery* **2004**, *1*, 57-65.
15. Kratz, F.; Beyer, U., Serum proteins as drug carriers of anticancer agents: a review. *Drug Del.* **1998**, *5*, 281-299.
16. Wunder, A.; Stehle, G.; Sinn, H.; Schrenk, H. H.; Hoff-Biederbeck, D.; Bader, F.; Friedrich, E. A.; Peschke, P.; Maier-Borst, W.; Heene, D. L., Enhanced albumin uptake by rat tumors. *Int. J. Onco.* **1997**, *11*, 497-507.
17. Schlicker, A.; Peschke, P.; Sinn, H.; Hahn, E. W., Albumin as a carrier system for delivering drugs to solid tumors. *J. Pharm. Sci. Tech.* **2000**, *54*, 442-448.
18. Henderson, S. J.; Lindup, W. E., Interaction of 3-carboxy-4-methyl-5-propyl-2-furanopropanoic acid, an inhibitor of plasma protein binding in uremia, with human albumin. *Biochem. Pharmacol.* **1990**, *40*, 2543-2548.
19. Pfordt, J.; Thoma, H.; Spittler, G., Identification, structure elucidation, and synthesis of previously unknown urofuranic acids in human blood. *Liebigs Annalen der Chemie* **1981**, 2298-2308.
20. Brooks, D. W.; De Lee, N. C.; Peevey, R., Remote substituent effects in microbial reductions of 3-ketoglutarate and 3-ketoadipate esters. *Tet. Lett.* **1984**, *25*, 4623-4626.
21. Nudelman, A.; Nudelman, A., Convenient syntheses of d-aminolevulinic acid. *Synthesis* **1999**, *4* 568-570.
22. Jain, D. V. S.; Chadha, R., Kinetics of the reaction between triphenylphosphine and some haloalkanes. *Ind. J. Chem.* **1991**, *30A*, 929-35.
23. <http://www.aist.go.jp/RIODB/SDBS/> (National Institute of Advanced Industrial Science and Technology, date of access)

24. Wittig, G.; Schollkopf, U., Triphenylphosphinemethylene as an olefin-forming reagent. I. *Chem. Ber.* **1954**, *97*, 1318-1330.
25. Vilsmeier, A.; Haack, A., Action of phosphorus halides on alkylformanilides. A new method for the preparation of secondary and tertiary p-alkylaminobenzaldehydes. *Ber.* **1927**, *60B*, 119-22.

Chapter VI

Synthesis of Taxoid-Based Antitubercular Agents for Co-Crystallization With FtsZ and X-ray Study

Table of Contents

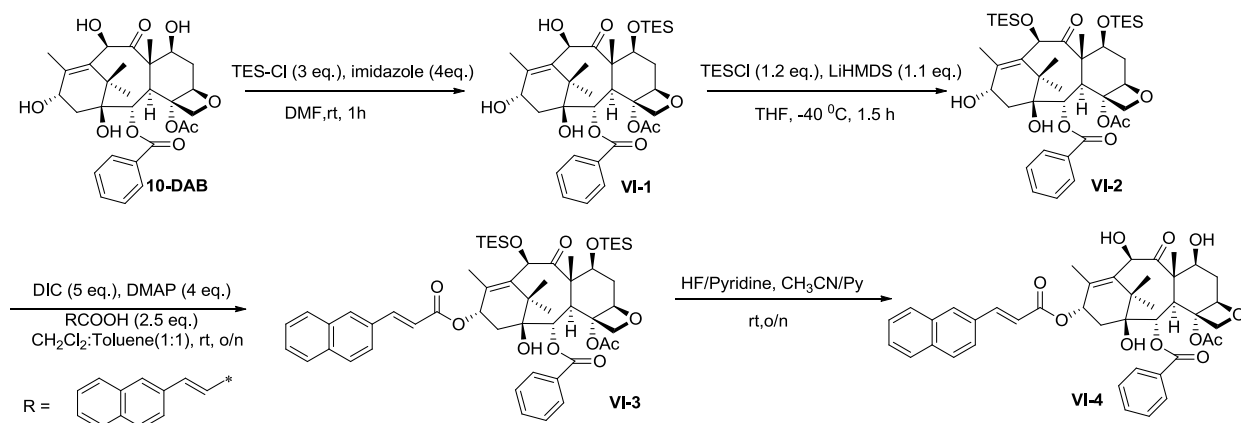
§ 6.1 Introduction.....	163
§ 6.2 Results and discussions.....	166
§ 6.3 Conclusion	167
§ 6.4 Experimental Section.....	168
§ 6.5 References	172

Table VI-1. Antimicrobial activities of taxanes against drug-sensitive and multidrug-resistant *Mtb* strains^a

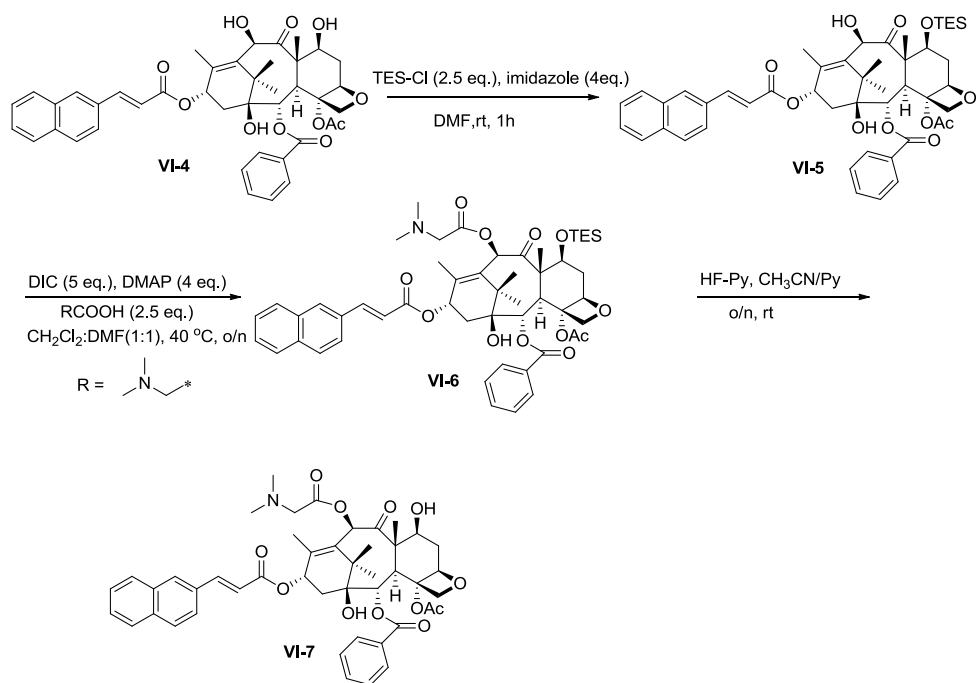
	Taxanes	MIC <i>Mtb.</i> (μM)		Cytotoxicity (IC_{50} , μM)	
1	Paclitaxel	40	40	0.019	0.028
2	SB-T-0032	5	1.25	0.65	0.65
3	SB-RA-2001	5	2.5	4.5	15.7
4	SB-RA-5001	2.5	1.25	>80	>80
5	SB-RA-5001MeO6	2.5	2.5	>80	>80
6	SB-RA-5011	2.5	1.25	>80	>80
7	SB-RA-5012	2.5	1.25	>80	>80

M. tuberculosis H37Rv is sensitive to all antibiotics tested. *M. tuberculosis* IMCJ946.K2 is resistant to nine drugs including INH, REF, EB, streptomycin, kanamycin, ethionamid, *p*-aminosalicylic acid, cycloserine and enviomycin. MCF7 and A549 cells: human breast and non-small cell lung cancer cell lines, respectively.

In collaboration with Dr. Lowe, we decided to carry out the co-crystallization of FtsZ with some of the active taxoid-based anti-TB agents to get some information about the binding site of the taxanes-based anti-TB agents. The synthesis of taxoid-based anti-TB agents are shown below (Scheme VI-1 and VI-2).⁵



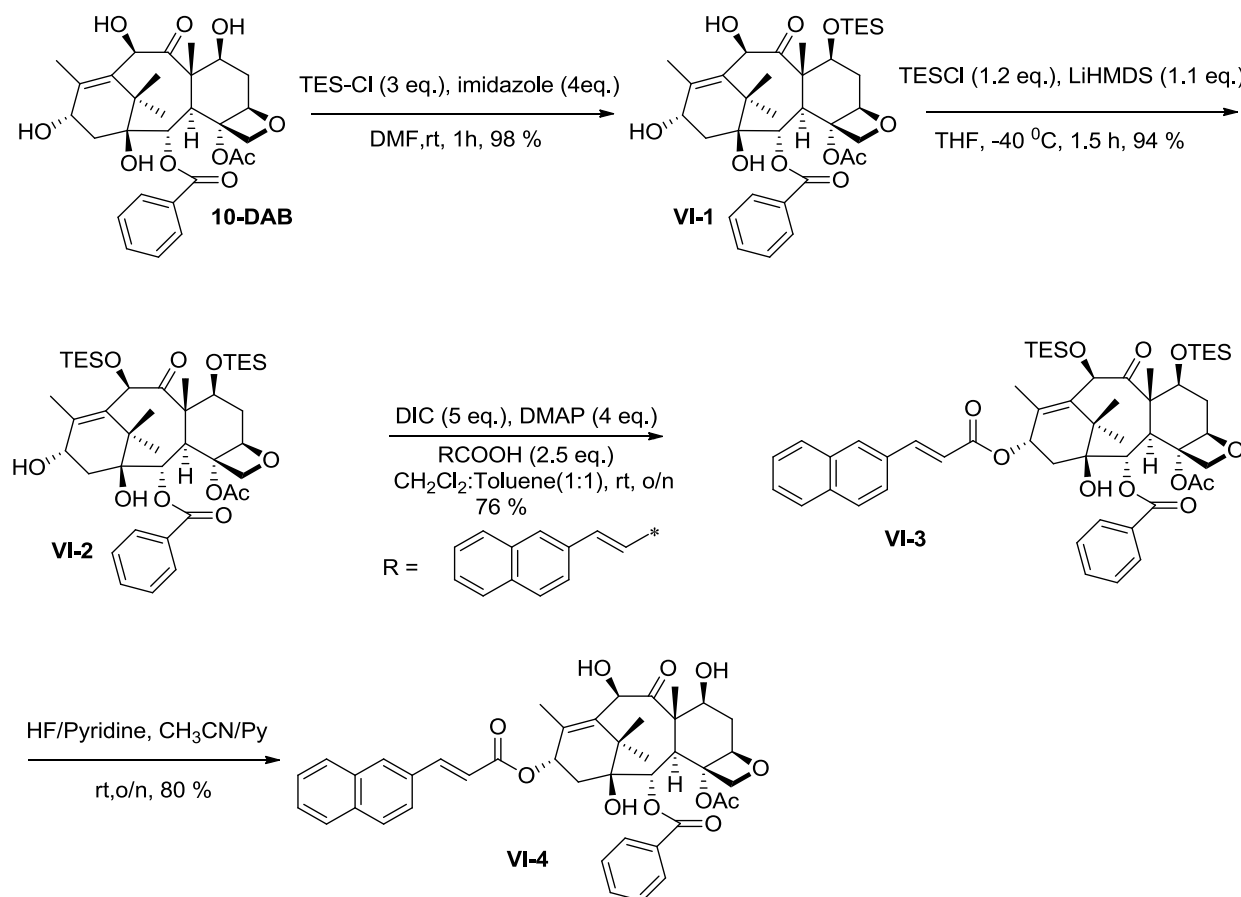
Scheme VI-1. Synthesis of SB-RA-2001



Scheme VI-2. Synthesis of SB-RA-200101

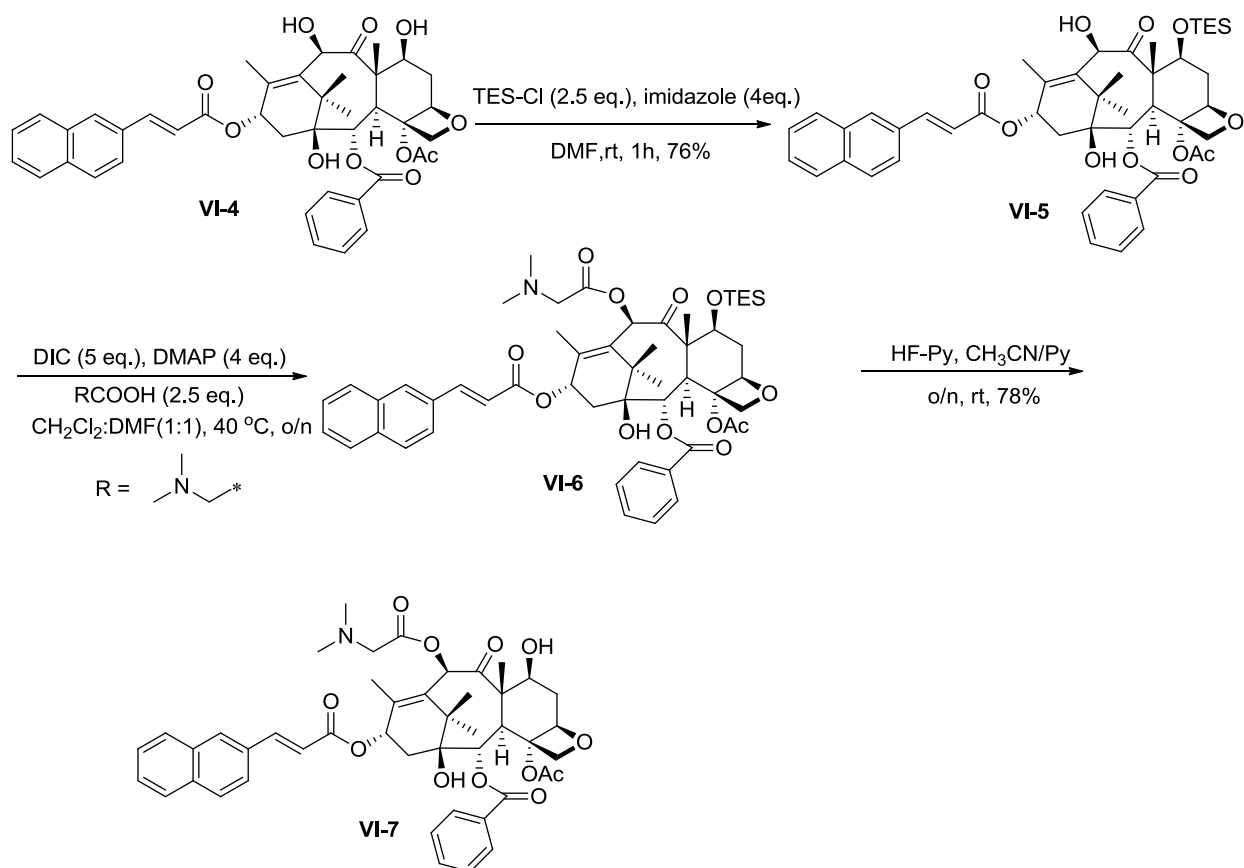
§ 6.2 Results and discussions

Starting with 10-DAB, C-7 hydroxy protection by TES chloride was carried out followed by C-10 hydroxy protection with TES chloride to obtain **VI-2** in 94 % yield. C-13 coupling of compound **VI-2** with naphthoyl acrylic acid and subsequent deprotection of C-7 and C-10 hydroxy groups lead to **VI-4** (**SB-RA-2001**) (**Scheme VI-3**).



Scheme VI-3. Synthesis of SB-RA-2001 (VI-4)

C-7 hydroxy of **VI-4** was protected by TES chloride followed by C-10 coupling with *N,N*-dimethyl glycine to afford compound **VI-6**. Finally, deprotection of C-7 TES group with HF/pyridine generated compound **VI-7** (**Scheme VI-4**).



Scheme VI-4. Synthesis of SB-RA-200101 (VI-7)

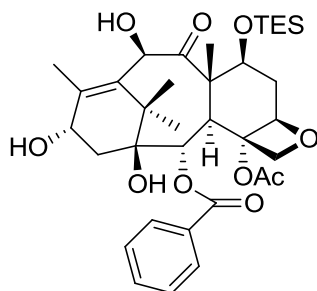
§ 6.3 Conclusion

In order to determine the binding site of taxane-based anti-TB agents (previously discovered in our lab), the co-crystallization of FtsZ with taxane is planned to be studied in collaboration with Dr. Lowe. Two taxane-based anti-TB agents were synthesized using multi-step synthetic methodologies developed in our laboratory.

§ 6.4 Experimental Section

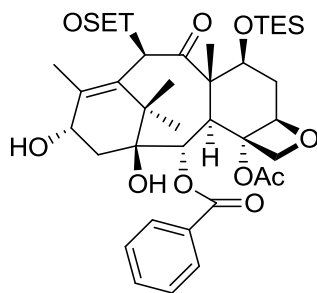
Materials: All chemicals were obtained from commercial sources. Tetrahydrofuran and dichloromethane were dried by passing through drying columns on the Innovative Technologies, Inc. solvent purification system. NMR spectra were recorded on a Varian 300 NMR spectrometer or a Varian 400 NMR spectrometer. The ^1H and ^{13}C spectra were calibrated using residual solvent peak as the internal standard (CDCl_3 : 7.26/77.00ppm). Melting points were measured on a Thomas Hoover Capillary melting point apparatus and are uncorrected. TLC was performed on Merck DC-alufolien with Kieselgel 60F-254 and column chromatography was carried out on silica gel 60 (Merck; 230-400 mesh ASTM).

7- (triethylsilyl)-10-deacetylbaccatin III (VI-1)⁵:



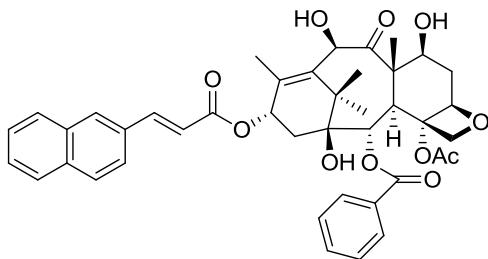
To a solution of 10-DAB (500 mg, 0.918 mmol) and imidazole (249.8 mg, 3.67 mmol) in dry *N,N*-dimethylformamide (17.5 mL) was added chlorotriethylsilane (0.46 mL, 2.75 mmol) dropwise via syringe at room temperature, and then the reaction mixture was stirred for 1 h at room temperature and diluted with EtOAc (60 mL). The mixture was washed with water (15 mL x 3), brine (10 mL), dried over anhydrous MgSO_4 and concentrated in *vacuo*. The crude product was purified on a silica gel column using hexanes/EtOAc (2/1 followed by 1/1) as the eluant to give **VI-1** as a white solid (568 mg, 96 % yield). ^1H NMR (300 MHz, CDCl_3) δ 0.5 (m, 6H), 0.97 (m, 9H), 1.21 (s, 3H), 1.58 (s, 3H), 1.73 (s, 3 H), 1.85 (dt, 1 H), 1.99 (s, 3 H), 2.23 (s, 3 H), 2.24 (s, 3 H), 2.47 (ddd, 1 H), 3.94 (d, 1 H, $J = 7.4$ Hz), 4.14 (d, 1 H, $J = 8.4$ Hz), 4.32 (d, 1 H, $J = 8.1$ Hz), 4.41 (d, 1 H, $J = 6.3$ Hz), 4.84 (t, 1 H), 4.94 (d, 1 H, $J = 8.4$ Hz), 5.14 (s, 1 H), 5.19 (s, 1 H), 5.58 (d, 1 H, $J = 7.2$ Hz), 7.40 (t, 2 H), 7.54 (t, 1 H), 8.10 (d, 2 H); ^{13}C NMR (75 MHz, CDCl_3) δ 5.1, 6.7, 9.9, 15.1, 19.5, 22.6, 26.8, 37.2, 38.6, 42.7, 47.0, 57.9, 67.9, 72.9, 74.7, 74.8, 76.5, 78.8, 80.7, 84.2, 128.6, 129.4, 130.0, 133.6, 135.1, 141.9, 167.0, 170.7, 210.3. All data are in agreement with literature values.⁵

7, 10-Bis (triethylsilyl)-10-deacetylbaccatin III (VI-2)⁵:



To a solution of **VI-1** (568 mg, 0.862 mmol) in THF was added LiHMDS (0.85 mL of 1.2 M solution) at -40 °C. After the reaction mixture was stirred for 10 min, TES chloride (.173 mL, 1.03 mmol) was added dropwise at -40 °C. The mixture was warmed to 0 °C over a period of 30-60 min and then concentrated in *vacuo*. Purification of the crude product by silica gel chromatography (hexanes/EtOAc = 4/1 to 1/1) afforded **VI-2** as white solid (626 mg, 94 % yield). All data are in agreement with literature values.⁵

13-[3-(2-Naphthyl)prop-2-enoyl]-10-deacetylbaccatin III (VI-4)⁵:

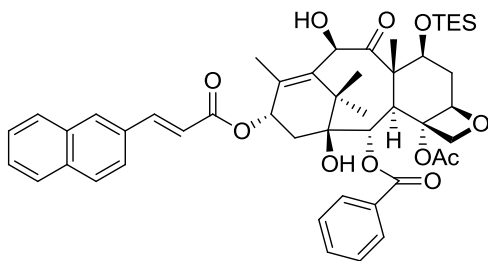


To a solution of 7, 10-Bis (triethylsilyl)-10-deacetylbaccatin III (354 mg, 0.457 mmol), DMAP (279 mg, 2.28 mmol) and the corresponding acid (199 mg, 0.457 mmol) in toluene/dichloromethane (1/1) was added DIC (403 mg, 3.199 mmol) at room temperature with stirring. After stirring for 10-15 h, the solvent was evaporated *in vacuo*. Purification of the crude product by short silica gel chromatography using ethyl acetate/hexane (4:1) as eluant afforded TES protected C-13 coupling product **VI-3** contaminated by DIC-acid complex, which were directly used in the next step.

To a solution of TES protected C-13 coupling product **VI-3** (334 mg, 0.350 mmol) in a (1:1) mixture of pyridine and acetonitrile (4 mL/100mg of starting material) at 0 °C was added a 70 % solution of HF in pyridine (1 mL/100 mg of starting material) with stirring. After stirring overnight at room temperature, the reaction was quenched with NaHCO₃ solution and extracted

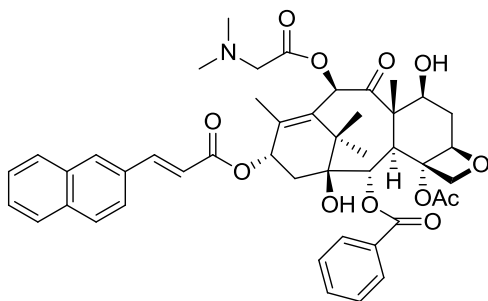
with ethyl acetate. The combined organic layers were washed with a saturated solution of copper sulfate and with water, then dried over magnesium sulfate, filtered and concentrated. Purification of the crude product by silica gel chromatography (hexanes/EtOAc = 1/1) afforded to afford **VI-4** as white solid (Yield: 75 %); $^1\text{H NMR}$ (300 MHz, CDCl_3) δ 1.15 (s, 3H), 1.26 (s, 3H), 1.70 (m, 2H), 1.79 (s, 3H), 1.93 (m, 1H), 2.09 (s, 3H), 2.24 (m, 1H), 2.30 (s, 3H), 2.46 (dd, $J = 9.2, 16.0$ Hz, 1H), 2.65 (m, 1H), 4.02 (d, 1H, $J = 7.0$ Hz), 4.26 (m, 4H), 4.99(d, 1H, $J = 8.3\text{Hz}$), 5.31(s, 1H), 5.71 (d, 1H, $J = 7.0$ Hz), 6.19 (m, 1H), 6.61 (d, 1H, $J = 16.0$ Hz), 7.51 (m, 4H), 7.60 (m, 3H), 7.70 (d, 1H, $J = 9.2$ Hz), 7.89 (m, 2H), 8.03(m, 3H).); $^{13}\text{C NMR}$ (100 MHz, CDCl_3) δ 9.8, 15.1, 2.02, 22.6, 26.5, 36.5, 37.1, 42.9, 46.8, 57.7, 70.3, 72.1, 74.7, 76.6, 79.0, 81.0, 84.1, 117.1, 123.1, 126.4, 127.6, 127.8, 128.6, 128.9, 129.2, 130.0, 130.5, 131.4, 133.3, 134.4, 135.8, 139.3, 143.9, 146.6, 166.3, 166.9, 211.5. All data are in agreement with literature values.⁵

7-triethylsilyl-13-[3-(2-naphthyl)prop-2-enoyl]-10-deacetylbaaccatin III (VI-5)⁵:



To a solution of 13-[3-(2-naphthyl)prop-2-enoyl]-10-deacetylbaaccatin III (150 mg, 0.206mmol) and imidazole (42 mg, 0.517 mmol) in *N,N*-dimethylformamide (DMF, 4 mL) was added chlorotriethylsilane (0.087 mL, 0.898 mmol) dropwise via syringe at 0 °C. The reaction mixture was stirred for 1 h at room temperature and diluted with EtOAc (50 mL). The mixture was then washed with H₂O (20 mL x 3), brine (20 mL), dried over anhydrous MgSO₄ and concentrated. The crude product was purified on a silica gel column using hexanes/EtOAc (1/1) as eluant to give 7-triethylsilyl-13-[3-(2-naphthyl)prop-2-enoyl]-10-deacetylbaaccatin III **VI-5** as a white solid (130 mg, 75%): $^1\text{H NMR}$ (300 MHz, CDCl_3) δ 0.81 (m, 6H), 1.00 (m, 9H), s, 3H), 1.26 (s, 3H), 1.70 (m, 2H), 1.79 (s, 3H), 1.93 (m, 1H), 2.09 (s, 3H), 2.24 (m, 1H), 2.30 (s, 3H), 2.46 (dd, 1H, $J = 9.2, 16.0$ Hz), 2.65 (m, 1H), 4.02 (d, 1H, $J = 7.0$ Hz), 4.26 (m, 3H), 4.51(m, 1H), 4.99(d, 1H, $J = 8.3\text{Hz}$), 5.31(s, 1H), 5.71 (d, 1H, $J = 7.0$ Hz), 6.19 (m, 1H), 6.61 (d, 1H, $J = 16.0$ Hz), 7.51 (m, 4H), 7.60(m, 3H), 7.70 (d, 1H, $J = 9.2$ Hz), 7.89 (m, 2H), 8.03(m, 3H). All data are in agreement with literature values.⁵

10-*N,N*-Dimethylglycyl-13-[3-(2-naphthyl) prop-2-enoyl]-10-deacetylbaccatin III (VI-7)⁵:



To a magnetically stirred solution of **VI-5** (150 mg, 0.178 mmol) in dry DMF/CH₂Cl₂ (1/2) were added *N,N*-dimethyl glycine (55.29 mg, 0.536 mmol), DMAP (0.89 mmol), and DIC (0.89 mmol) at room temperature under N₂. After stirring for overnight, the solvent was removed on a rotary evaporator and the residue was purified by short silica gel chromatography using ethyl acetate/hexane (2:1) as eluent to afford TES protected C- 10 coupling product **VI-6** contaminated by DIC-acid complex, which were directly used in the next step.

To a solution of TES protected C-10 coupling product **VI-6** in a (1:1) mixture of pyridine and acetonitrile (4 mL/100mg of starting material) at 0 °C was added a 70 % solution of HF in pyridine (1 mL/100 mg of starting material) with stirring. After stirring overnight at room temperature, the reaction was quenched with NaHCO₃ solution and extracted with ethyl acetate. The combined organic layers were washed with a saturated solution of copper sulfate and with water, then dried over magnesium sulfate, filtered and concentrated. Purification of the crude product by silica gel chromatography (hexanes/EtOAc/TEA = 1/2/0.1) afforded to afford **VI-7** as white solid. Yield: 78%; ¹H NMR (300 MHz, CDCl₃) δ 1.15 (s, 1 H), 1.26 (s, 3H), 1.70 (m, 2H), 1.79 (s, 3H), 1.93 (m, 1H), 2.09 (s, 3H), 2.24 (m, 7H), 2.30 (s, 3H), 2.46 (dd, 1H, *J* = 9.2, 16.0 Hz), 2.65 (m, 1H), 3.45 (s, 2H), 3.91 (d, 1H, *J* = 7.0 Hz), 4.26 (m, 4H), 4.52(m, 1H), 5.02(d, 1H, *J* = 8.3Hz), 5.71 (d, 1H, *J* = 7.0 Hz), 6.24 (m,1H), 6.43(s, 1H), 6.63 (d, 1H, *J* = 16.0 Hz), 7.49 (m, 4H), 7.58(m, 3H), 7.71 (d, 1H, *J*= 9.2 Hz), 7.90 (m, 2H), 8.09 (m, 3H); ¹³C NMR (100 MHz, CDCl₃) δ 9.5, 15.9, 22.0, 22.9, 27.3, 35.7, 36.3, 36.5, 36.9, 43.3, 46.1, 58.9, 66.4, 70.4, 72.9, 75.3, 76.6, 76.7, 79.7, 81.4, 84.8, 117.1, 123.4, 127.2, 127.9, 128.1, 128.9, 128.9, 129.2, 129.5, 130.3, 130.8, 131.6, 133.4, 133.5, 133.9, 134.7, 143.8, 147.0, 150.3, 156.4, 195 159.8, 166.6, 167.2, 170.0, 182.2, 206.0. All data are in agreement with literature values.⁵

§ 6.5 References

1. Sarcina, M.; Mullineaux, C.W.; Effects of tubulin assembly inhibitors on cell division in prokaryotes in vivo. *FEMS Microbiol. Lett.* **2000**, *191*, 25-29.
2. de Pereda, J.M.; Leynadier, D.; Evangelio, J.A.; Chacon, P.; Andreu J.M.; Tubulin secondary structure analysis, limited proteolysis sites, and homology to FtsZ. *Biochemistry* **1996**, *35*, 14203-14215.
3. White, E.L.; Suling, W.J.; Ross, L.J.; Seitz, L.E.; Reynolds, R.C.; 2-Alkoxy-carbonylaminopyridines: inhibitors of Mycobacterium tuberculosis FtsZ. *J. Antimicrob. Chemother.* **2002**, *50*, 111-114.
4. Reynolds, R.C.; Srivastava, S.; Ross, L.J.; Suling, W.J.; White, E.L.; A new 2-carbamoyl pteridine that inhibits mycobacterial FtsZ. *Bioorg. Med. Chem. Lett.* **2004**, *14*, 3161-3164.
5. Huang, Q.; Kirikae, F.; Kirikae, T.; Pepe, A.; Amin, A.; Respicio, L. *et al.* Targeting FtsZ for Antituberculosis Drug Discovery: Noncytotoxic Taxanes as Novel Antituberculosis Agents. *J. Med. Chem.* **2006**, *49*, 463-466.
6. Appendino, G; Danieli, B.; Jakupovic, J.; Belloro, E.; Scambia, G.; Bombardelli, E. The chemistry and occurrence of taxane derivatives. XXX. Synthesis and evaluation of C-seco paclitaxel analogs. *Tet. Lett.* **1997**, *38*, 4273-4276.
7. Taraboletti, G.; Micheletti, G.; Rieppi, M.; Poli, M.; Turatto, M.; Rossi, C.. Antiangiogenic and antitumor activity of IDN 5390, a new taxane derivative. *Clin. Cancer Res.* **2002**, *8*, 1182-1188.

Bibliography

Chapter I

1. Bloom, B. R.; Murray, C. J., Tuberculosis: commentary on a reemergent killer. *Science* **1992**, *257* (5073), 1055-64.
2. Tuberculosis: Basic TB facts. Center for Disease Control and Prevention (CDC). Available from: <http://www.cdc.gov/tb/topic/basics/default.htm>.
3. Tuberculosis: Data and Country Profiles. World Health Organization (WHO) Available from: http://www.who.int/tb/publications/global_report/2010/en/index.html.
4. Raviglione, M. C., Issues facing TB control (7). Multiple drug-resistant tuberculosis. *Scott. Med. J.* **2000**, *45*, 52-5.
5. Miller, J. R.; Waldrop, G. L., Discovery of novel antibacterials. *Expert Opin. Drug Discovery* *5*, 145-154.
6. Tuberculosis: What is TB? National Institute of Allergy and Infectious Diseases (NIAID). Available from: <http://www.niaid.nih.gov/topics/tuberculosis/understanding/whatistb/Pages/default.aspx>.
7. Margalit, D. N.; Romberg, L.; Mets, R. B.; Hebert, A. M.; Mitchison, T. J.; Kirschner, M. W.; RayChaudhuri, D., Targeting cell division: Small-molecule inhibitors of FtsZ GTPase perturb cytokinetic ring assembly and induce bacterial lethality. *Proc. Nat. Acad. Sci.* **2004**, *101*, 11821-11826.
8. Vollmer, W., The prokaryotic cytoskeleton: A putative target for inhibitors and antibiotics? *Appl. Microbiol. Biotechnol.* **2006**, *73*, 37-47.
9. Ben-Yehuda, S.; Losick, R., Asymmetric cell division in *B. subtilis* involves a spiral-like intermediate of the cytokinetic protein FtsZ. *Cell* **2002**, *109*, 257-266.
10. Goehring, N. W.; Beckwith, J., Diverse paths to midcell: assembly of the bacterial cell division machinery. *Curr. Biol.* **2005**, *15*, R514-R526.
11. Leung, A. K. W.; White, E. L.; Ross, L. J.; Reynolds, R. C.; DeVito, J. A.; Borhani, D. W., Structure of Mycobacterium tuberculosis FtsZ Reveals Unexpected, G Protein-like Conformational Switches. *J. Mol. Biol.* **2004**, *342*, 953-970.
12. Moller-Jensen, J.; Loewe, J., Increasing complexity of the bacterial cytoskeleton. *Curr. Opin. Cell Biol.* **2005**, *17*, 75-81.
13. Thanedar, S.; Margolin, W., FtsZ Exhibits Rapid Movement and Oscillation Waves in Helix-like Patterns in *Escherichia coli*. *Curr. Biol.* **2004**, *14*, 1167-1173.
14. Erickson Harold, P.; Anderson David, E.; Osawa, M., FtsZ in bacterial cytokinesis: cytoskeleton and force generator all in one. *Microbiol. Mol. Biol Rev.* **2010**, *74*, 504-28.

15. Respicio, L.; Nair, P. A.; Huang, Q.; Anil, B.; Tracz, S.; Truglio, J. J.; Kisker, C.; Raleigh, D. P.; Ojima, I.; Knudson, D. L.; Tonge, P. J.; Slayden, R. A., Characterizing septum inhibition in *Mycobacterium tuberculosis* for novel drug discovery. *Tuberculosis* **2008**, *88*, 420-429.
16. Slayden, R. A.; Knudson, D. L.; Belisle, J. T., Identification of cell cycle regulators in *Mycobacterium tuberculosis* by inhibition of septum formation and global transcriptional analysis. *Microbiology* **2006**, *152*, 1789-1797.
17. Adams, D. W.; Errington, J., Bacterial cell division: assembly, maintenance and disassembly of the Z ring. *Nat. Rev. Microbiol.* **2009**, *7*, 642-653.
18. Margolin, W., Themes and variations in prokaryotic cell division. *FEMS Microbiol. Rev.* **2000**, *24*, 531-548.
19. Mukherjee, A.; Lutkenhaus, J., Dynamic assembly of FtsZ regulated by GTP hydrolysis. *EMBO J.* **1998**, *17*, 462-469.
20. Dajkovic, A.; Mukherjee, A.; Lutkenhaus, J., Investigation of regulation of FtsZ assembly by SulA and development of a model for FtsZ polymerization. *J. Bacteriol.* **2008**, *190*, 2513-2526.
21. Chen, Y.; Bjornson, K.; Redick, S. D.; Erickson, H. P., A rapid fluorescence assay for FtsZ assembly indicates cooperative assembly with a dimer nucleus. *Biophys. J.* **2005**, *88*, 505-514.
22. Caplan, M. R.; Erickson, H. P., Apparent Cooperative Assembly of the Bacterial Cell Division Protein FtsZ Demonstrated by Isothermal Titration Calorimetry. *J. Biol. Chem.* **2003**, *278*, 13784-13788.
23. Romberg, L.; Simon, M.; Erickson, H. P., Polymerization of FtsZ, a bacterial homolog of tubulin. Is assembly cooperative? *J. Biol. Chem.* **2001**, *276*, 11743-11753.
24. Popp, D.; Iwasa, M.; Erickson, H. P.; Narita, A.; Maeda, Y.; Robinson, R. C., Suprastructures and Dynamic Properties of *Mycobacterium tuberculosis* FtsZ. *J. Biol. Chem.* **2010**, *285*, 11281-11289.
25. Popp, D.; Narita, A.; Iwasa, M.; Maeda, Y.; Robinson, R. C., Molecular mechanism of bundle formation by the bacterial actin ParM. *Biochem. Biophys. Res. Commun.* **2010**, *391*, 1598-1603.
26. Li, Z.; Trimble, M. J.; Brun, Y. V.; Jensen, G. J., The structure of FtsZ filaments in vivo suggests a force-generating role in cell division. *EMBO J.* **2007**, *26*, 4694-4708.
27. Erickson, H. P., The ftsZ protofilament and attachment of ZipA - structural constraints on the FtsZ power stroke. *Curr. Opin. Cell Biol.* **2001**, *13*, 55-60.
28. Pichoff, S.; Lutkenhaus, J., Unique and overlapping roles for ZipA and FtsA in septal ring assembly in *Escherichia coli*. *EMBO J* **2002**, *21*, 685-693.

29. Geissler, B.; Elraheb, D.; Margolin, W., A gain-of-function mutation in *ftsA* bypasses the requirement for the essential cell division gene *zipA* in *Escherichia coli*. *Proc. Nat. Acad. Sci.* **2003**, *100*, 4197-4202.
30. Anderson, D. E.; Gueiros-Filho, F. J.; Erickson, H. P., Assembly dynamics of FtsZ rings in *Bacillus subtilis* and *Escherichia coli* and effects of FtsZ-regulating proteins. *J. Bacteriol.* **2004**, *186*, 5775-5781.
31. Stricker, J.; Maddox, P.; Salmon, E. D.; Erickson, H. P., Rapid assembly dynamics of the *Escherichia coli* FtsZ-ring demonstrated by fluorescence recovery after photobleaching. *Proc. Nat. Acad. Sci.* **2002**, *99*, 3171-3175.
32. Errington, J.; Daniel, R. A.; Scheffers, D.-J., Cytokinesis in bacteria. *Microbiol. Mol. Biol. Rev.* **2003**, *67*, 52-65.
33. Romberg, L.; Levin, P. A., Assembly Dynamics of The Bacterial Cell Division Protein FtsZ: Poised at the Edge of Stability. *Annu. Rev. Microbiol.* **2003**, *57*, 125 - 54.
34. Romberg, L.; Mitchison, T. J., Rate-Limiting Guanosine 5'-Triphosphate Hydrolysis during Nucleotide Turnover by FtsZ, a Prokaryotic Tubulin Homologue Involved in Bacterial Cell Division. *Biochemistry* **2004**, *43*, 282-288.
35. Huecas, S.; Andreu, J. M., Polymerization of Nucleotide-free, GDP- and GTP-bound Cell Division Protein FtsZ: GDP Makes the Difference. *FEBS Lett.* **2004**, *569*, 43 - 48.
36. Lu, C.; Reedy, M.; Erickson, H. P., Straight and curved conformations of FtsZ are regulated by GTP hydrolysis. *J. Bacteriol.* **2000**, *182*, 164-170.
37. Mukherjee, A.; Saez, C.; Lutkenhaus, J., Assembly of an FtsZ mutant deficient in GTPase activity has implications for FtsZ assembly and the role of the Z ring in cell division. *J. Bacteriol.* **2001**, *183*, 7190-7197.
38. Oliva, M. A.; Trambaiolo, D.; Loewe, J., Structural Insights into the Conformational Variability of FtsZ. *J. Mol. Biol.* **2007**, *373*, 1229-1242.
39. Osawa, M.; Anderson, D. E.; Erickson, H. P., Reconstitution of Contractile FtsZ Rings in Liposomes. *Science* **2008**, *320*, 792-794.
40. Yanagisawa, M.; Imai, M.; Taniguchi, T., Shape Deformation of Ternary Vesicles Coupled with Phase Separation. *Phys. Rev. Lett.* **2008**, *100*, 148102/1-148102/4.
41. Zhu, T. F.; Szostak, J. W., Coupled Growth and Division of Model Protocell Membranes. *J. Am. Chem. Soc.* **2009**, *131*, 5705-5713.
42. de Pereda, J. M.; Leynadier, D.; Evangelio, J. A.; Chacon, P.; Andreu, J. M., Tubulin secondary structure analysis, limited proteolysis sites, and homology to FtsZ. *Biochemistry* **1996**, *35*, 14203-14215.

43. Nogales, E.; Wang, H. W., Structural Mechanisms Underlying Nucleotide-Dependent Self-Assembly of Tubulin and Its Relatives. *Curr. Opin. Struct. Biol.* **2006**, *16*, 221 - 229.
44. Lock, R. L.; Harry, E. J., Cell-division inhibitors: new insights for future antibiotics. *Nat. Rev. Drug Discovery* **2008**, *7*, 324-338.
45. Rothfield, L.; Justice, S.; Garcia-Lara, J., Bacterial cell division. *Annu. Rev. Genet.* **1999**, *33*, 423-448.
46. Haydon, D. J.; Stokes, N. R.; Ure, R.; Galbraith, G.; Bennett, J. M.; Brown, D. R.; Baker, P. J.; Barynin, V. V.; Rice, D. W.; Sedelnikova, S. E.; Heal, J. R.; Sheridan, J. M.; Aiwale, S. T.; Chauhan, P. K.; Srivastava, A.; Taneja, A.; Collins, I.; Errington, J.; Czaplowski, L. G., An Inhibitor of FtsZ with Potent and Selective Anti-Staphylococcal Activity. *Science* **2008**, *321*, 1673-1675.
47. Kumar, K.; Awasthi, D.; Berger, W. T.; Tonge, P. J.; Slayden, R. A.; Ojima, I., Discovery of anti-TB agents that target the cell-division protein FtsZ. *Future Med. Chem.* **2010**, *2*, 1305-1323.
48. Kapoor, S.; Panda, D., Targeting FtsZ for antibacterial therapy: a promising avenue. *Expert Opin. Ther. Targets* **2009**, *13*, 1037-1051.
49. Huang, Q.; Tonge Peter, J.; Slayden Richard, A.; Kirikae, T.; Ojima, I., FtsZ: a novel target for tuberculosis drug discovery. *Curr. Top. Med. Chem.* **2007**, *7*, 527-43.
50. Erickson, H. P.; Taylor, D. W.; Taylor, K. A.; Bramhill, D., Bacterial cell division protein FtsZ assembles into protofilament sheets and minirings, structural homologs of tubulin polymers. *Proc. Nat. Acad. Sci.* **1996**, *93*, 519-23.
51. Lowe, J.; Amos, L. A., Crystal structure of the bacterial cell-division protein FtsZ. *Nature* **1998**, *391*, 203-6.
52. Lowe, J.; Amos, L. A., Tubulin-like protofilaments in Ca²⁺-induced FtsZ sheets. *EMBO J* **1999**, *18*, 2364-71.
53. Lappchen, T.; Hartog Aloysius, F.; Pinas Victorine, A.; Koomen, G.-J.; den Blaauwen, T., GTP analogue inhibits polymerization and GTPase activity of the bacterial protein FtsZ without affecting its eukaryotic homologue tubulin. *Biochemistry* **2005**, *44*, 7879-84.
54. Huang, Q.; Kirikae, F.; Kirikae, T.; Pepe, A.; Amin, A.; Respicio, L.; Slayden, R. A.; Tonge, P. J.; Ojima, I., Targeting FtsZ for Antituberculosis Drug Discovery: Noncytotoxic Taxanes as Novel Antituberculosis Agents. *J. Med. Chem.* **2006**, *49*, 463-466.
55. Constantine, G. H.; Karchesy, J. J.; Franzblau, S. G.; LaFleur, L. E., (+)-Totarol from *Chamaecyparis nootkatensis* and activity against *Mycobacterium tuberculosis*. *Fitoterapia* **2001**, *72*, 572-574.

56. Kubo, I.; Muroi, H.; Himejima, M., Antibacterial activity of totarol and its potentiation. *J. Nat. Prod.* **1992**, *55*, 1436-40.
57. Jaiswal, R.; Beuria, T. K.; Mohan, R.; Mahajan, S. K.; Panda, D., Totarol inhibits bacterial cytokinesis by perturbing the assembly dynamics of FtsZ. *Biochemistry* **2007**, *46*, 4211-4220.
58. Sarcina, M.; Mullineaux, C. W., Effects of tubulin assembly inhibitors on cell division in prokaryotes in vivo. *FEMS Microbiol. Lett.* **2000**, *191*, 25-29.
59. White, E. L.; Suling, W. J.; Ross, L. J.; Seitz, L. E.; Reynolds, R. C., 2-Alkoxy-carbonylaminopyridines: inhibitors of Mycobacterium tuberculosis FtsZ. *J. Antimicrob. Chemother.* **2002**, *50*, 111-114.
60. Reynolds, R. C.; Srivastava, S.; Ross, L. J.; Suling, W. J.; White, E. L., A new 2-carbamoyl pteridine that inhibits mycobacterial FtsZ. *Bioorg. Med. Chem. Lett.* **2004**, *14*, 3161-3164.
61. Georg, G. I.; Chen, T. T.; Ojima, I.; Wyas, D. M.; Editors, *Taxane Anticancer Agents: Basic Science and Current Status. ACS Symp. Ser., 1995; 583; p 353.* 1995; p 353 pp.
62. Kingston, D. G. I.; Jagtap, P. G.; Yuan, H.; Samala, L., The chemistry of taxol and related taxoids. *Prog. Chem. Org. Nat. Prod.* **2002**, *84*, 53-225.
63. Ojima, I.; Bounaud, P.-Y.; Bernacki, R. J., Designing taxanes to treat multidrug-resistant tumors. *Mod. Drug Discovery* **1999**, *2*, 45,47-48,51-52.
64. Brooks, T. A.; Kennedy, D. R.; Gruol, D. J.; Ojima, I.; Baer, M. R.; Bernacki, R. J., Structure-activity analysis of taxane-based broad-spectrum multidrug resistance modulators. *Anticancer Res.* **2004**, *24*, 409-415.
65. Brooks Tracy, A.; Minderman, H.; O'Loughlin Kieran, L.; Pera, P.; Ojima, I.; Baer Maria, R.; Bernacki Ralph, J.; Brooks, T., Taxane-based reversal agents modulate drug resistance mediated by P-glycoprotein, multidrug resistance protein, and breast cancer resistance protein. *Mol. Cancer Ther.* **2003**, *2*, 1195-205.
66. Minderman, H.; Brooks, T. A.; O'Loughlin, K. L.; Ojima, I.; Bernacki, R. J.; Baer, M. R., Broad-spectrum modulation of ATP-binding cassette transport proteins by the taxane derivatives ortataxel (IDN-5109, BAY 59-8862) and tRA96023. *Cancer Chemother. Pharmacol.* **2004**, *53*, 363-369.
67. Ojima, I.; Borella, C. P.; Wu, X.; Bounaud, P.-Y.; Oderda, C. F.; Sturm, M.; Miller, M. L.; Chakravarty, S.; Chen, J.; Huang, Q.; Pera, P.; Brooks, T. A.; Baer, M. R.; Bernacki, R. J., Design, Synthesis and Structure-Activity Relationships of Novel Taxane-Based Multidrug Resistance Reversal Agents. *J. Med. Chem.* **2005**, *48*, 2218-2228.
68. Ojima, I.; Bounaud, P.-Y.; Bernacki, R. J., New weapons in the fight against cancer. *Chemtech* **1998**, *28*, 31-36.

69. Ojima, I.; Bounaud, P.-Y.; Oderda, C. F., Recent strategies for the treatment of multi-drug resistance in cancer cells. *Expert Opin. Ther. Pat.* **1998**, *8*, 1587-1598.
70. Ojima, I.; Bounaud, P.-Y.; Takeuchi, C.; Pera, P.; Bernacki, R. J., New taxanes as highly efficient reversal agents for multi-drug resistance in cancer cells. *Bioorg. Med. Chem. Lett.* **1998**, *8*, 189-194.
71. Appendino, G.; Danieli, B.; Jakupovic, J.; Belloro, E.; Scambia, G.; Bombardelli, E., The chemistry and occurrence of taxane derivatives. XXX. Synthesis and evaluation of C-seco paclitaxel analogs. *Tet. Lett.* **1997**, *38*, 4273-4276.
72. Taraboletti, G.; Micheletti, G.; Rieppi, M.; Poli, M.; Turatto, M.; Rossi, C.; Borsotti, P.; Roccabianca, P.; Scanziani, E.; Nicoletti, M. I.; Bombardelli, E.; Morazzoni, P.; Riva, A.; Giavazzi, R., Antiangiogenic and antitumor activity of IDN 5390, a new taxane derivative. *Clin. Cancer Res.* **2002**, *8*, 1182-1188.

Chapter II

1. Bloom B. R., Murray C. J. Tuberculosis: commentary on a reemergent killer. *Science* **1992**, *257*, 1055-1064.
2. Tuberculosis: Data and Country Profiles. World Health Organization (WHO)
Available from:
http://www.who.int/tb/publications/global_report/2010/en/index.html.
3. Romberg, L.; Levin, P. A. Assembly dynamics of the bacterial cell division protein FtsZ: Poised at the Edge of Stability. *Annu. Rev. Microbiol.* **2003**, *57*, 125-154
4. Errington, J.; Daniel, R. A.; Scheffers, D.-J., Cytokinesis in bacteria. *Microbiol. Mol. Biol. Rev.* **2003**, *67*, 52-65.
5. Adams, D. W.; Errington, J., Bacterial cell division: assembly, maintenance and disassembly of the Z ring. *Nat. Rev. Microbiol.* **2009**, *7*, 642-653.
6. Vollmer, W., The prokaryotic cytoskeleton: A putative target for inhibitors and antibiotics? *Appl. Microbiol. Biotechnol.* **2006**, *73*, 37-47.
7. Respicio, L.; Nair, P. A.; Huang, Q.; Anil, B.; Tracz, S.; Truglio, J. J.; Kisker, C.; Raleigh, D. P.; Ojima, I.; Knudson, D. L.; Tonge, P. J.; Slayden, R. A., Characterizing septum inhibition in Mycobacterium tuberculosis for novel drug discovery. *Tuberculosis* **2008**, *88*, 420-429.
8. Slayden, R. A.; Knudson, D. L.; Belisle, J. T., Identification of cell cycle regulators in Mycobacterium tuberculosis by inhibition of septum formation and global transcriptional analysis. *Microbiology*, **2006**, *152*, 1789-1797.
9. de Pereda, J. M.; Leynadier, D.; Evangelio, J. A.; Chacon, P.; Andreu, J. M., Tubulin secondary structure analysis, limited proteolysis sites, and homology to FtsZ. *Biochemistry* **1996**, *35*, 14203-14215.

10. Nogales, E.; Wang, H. W., Structural Mechanisms Underlying Nucleotide-Dependent Self-Assembly of Tubulin and Its Relatives. *Curr. Opin. Struct. Biol.* **2006**, *16*, 221 - 229.
11. Kumar, K.; Awasthi, D.; Berger, W. T.; Tonge, P. J.; Slayden, R. A.; Ojima, I., Discovery of anti-TB agents that target the cell-division protein FtsZ. *Future Med. Chem.* **2010**, *2*, 1305-1323.
12. Kapoor, S.; Panda, D., Targeting FtsZ for antibacterial therapy: a promising avenue. *Expert Opin. Ther. Targets* **2009**, *13*, 1037-1051.
13. Huang, Q.; Tonge Peter, J.; Slayden Richard, A.; Kirikae, T.; Ojima, I., FtsZ: a novel target for tuberculosis drug discovery. *Curr. Top. Med. Chem.* **2007**, *7*, 527-43.
14. Huang, Q.; Kirikae, F.; Kirikae, T.; Pepe, A.; Amin, A.; Respicio, L.; Slayden, R. A.; Tonge, P. J.; Ojima, I., Targeting FtsZ for Antituberculosis Drug Discovery: Noncytotoxic Taxanes as Novel Antituberculosis Agents. *J. Med. Chem.* **2006**, *49*, 463-466.
15. Sarcina, M.; Mullineaux, C. W., Effects of tubulin assembly inhibitors on cell division in prokaryotes in vivo. *FEMS Microbiol. Lett.* **2000**, *191*, 25-9.
16. White, E. L.; Ross, L. J.; Reynolds, R. C.; Seitz, L. E.; Moore, G. D.; Borhani, D. W. Slow polymerization of Mycobacterium tuberculosis FtsZ. *J. Bacteriol.* **2000**, *182*, 4028-34.
17. White, E. L.; Suling, W. J.; Ross, L. J.; Seitz, L. E.; Reynolds, R. C. 2-Alkoxy-carbonylaminopyridines: inhibitors of *Mycobacterium tuberculosis* FtsZ. *J. Antimicrob. Chemother.* **2002**, *50*, 111-114.
18. Reynolds, R. C.; Srivastava, S.; Ross, L. J.; Suling, W. J.; White, E. L. A new 2-carbamoyl pteridine that inhibits mycobacterial FtsZ. *Bioorg. Med. Chem. Lett.* **2004**, *14*, 3161-3164.
19. Slayden, R. A.; Lee, R. E.; Barry, C. E., Isoniazid Effects Multiple Components of the Type II Fatty Acid Synthase System of Mycobacterium tuberculosis. *Mol. Microbiol.* **2000**, *38*, 514-525.
20. Collins, L.; Franzblau, S. G., Microplate Alamar blue assay versus BACTEC 460 system for high-throughput screening of compounds against Mycobacterium tuberculosis and Mycobacterium avium. *Antimicrob. Agents Chemother.* **1997**, *41*, 1004-1009.
21. Elkin, V. V.; Tolkacheva, L. N.; Chernysheva, N. B.; Karmanova, I. B.; Konyushkin, L. D.; Semenov, V. V., Hydrogenation on palladium-containing granulated catalysts 3. Synthesis of aminobenzimidazoles by catalytic hydrogenation of dinitroanilines. *Russ. Chem. Bull.* **2007**, *56*, 1216-1226.

Chapter III

1. Errington J., Daniel R. A., Scheffers D.-J. Cytokinesis in bacteria. *Microbiol. Mol. Biol. Rev.* **2003**, *67*, 52-65.
2. Respicio L., Nair P. A., Huang Q., Burcu A., Tracz S., Truglio J. J., Kisker C., Ralieghe D. P., Ojima I., Knudson D. L., Tonge P. J., Slayden R. A. Characterizing septum inhibition in Mycobacterium tuberculosis for novel drug discovery. *Tuberculosis* **2008**, *88*, 420-429.
3. Slayden R. A., Knudson D. L., Belisle J. T. Identification of cell cycle regulators in Mycobacterium tuberculosis by inhibition of septum formation and global transcriptional analysis. *Microbiology* **2006**, *152*, 1789-1797.
4. Vollmer, W. The prokaryotic cytoskeleton: A putative target for inhibitors and antibiotics? *Appl. Microbiol. Biotech.*, **2006**, *73*, 37-47.
5. Kumar, K.; Awasthi, D.; Berger, W. T.; Tonge, P. J.; Slayden, R. A.; Ojima, I., Discovery of anti-TB agents that target the cell-division protein FtsZ. *Future Med. Chem.* **2010**, *2*, 1305-1323.
6. Awasthi, D.; Kumar, K.; Ojima, I., Therapeutic potential of FtsZ inhibition: a patent perspective. *Expert Opin. Ther. Patents* **Early Online** (2011).
7. Kumar, K.; Awasthi, D.; Lee, S.-Y.; Zanardi, I.; Ruzsicska, B.; Knudson, S.; Tonge, P. J.; Slayden, R. A.; Ojima, I., Novel Trisubstituted Benzimidazoles, Targeting Mtb FtsZ, as a New Class of Antitubercular Agents. *J. Med. Chem.* **2011**, *54*, 374-381.
8. Huang, Q.; Kirikae, F.; Kirikae, T.; Pepe, A.; Amin, A.; Respicio, L.; Slayden, R. A.; Tonge, P. J.; Ojima, I., Targeting FtsZ for Antituberculosis Drug Discovery: Noncytotoxic Taxanes as Novel Antituberculosis Agents. *J. Med. Chem.* **2006**, *49*, 463-466.
9. White, E. L.; Ross, L. J.; Reynolds, R. C.; Seitz, L. E.; Moore, G. D.; Borhani, D. W. Slow polymerization of Mycobacterium tuberculosis FtsZ. *J. Bacteriol.* **2000**, *182*, 4028-4034.
10. Jaiswal, R.; Beuria, T. K.; Mohan, R.; Mahajan, S. K.; Panda, D., Totarol inhibits bacterial cytokinesis by perturbing the assembly dynamics of FtsZ. *Biochemistry* **2007**, *46*, 4211-4220.
11. Shields, C. J.; Falvey, D. E.; Schuster, G. B.; Buchardt, O.; Nielsen, P. E., Competitive singlet-singlet energy transfer and electron transfer activation of aryl azides: application to photo-cross-linking experiments. *J. Org. Chem.* **1988**, *53*, 3501-3507.
12. Merrill, S. H.; Unruh, C. C., Photosensitive azide polymers. *J. Appl. Polymer Sci.* **1963**, *7*, 273-279.

Chapter IV

1. Leavis Helen, L.; Willems Rob, J. L.; Top, J.; Spalburg, E.; Mascini Ellen, M.; Fluit Ad, C.; Hoepelman, A.; de Neeling Albert, J.; Bonten Marc, J. M., Epidemic and nonepidemic multidrug-resistant *Enterococcus faecium*. *Emerg. Infect. Dis.* **2003**, *9*, 1108-15.
2. Klevens, R. M.; Morrison, M. A.; Nadle, J.; Petit, S.; Gershman, K.; Ray, S.; Harrison, L. H.; Lynfield, R.; Dumyati, G.; Townes, J. M.; Craig, A. S.; Zell, E. R.; Fosheim, G. E.; McDougal, L. K.; Carey, R. B.; Fridkin, S. K., Invasive methicillin-resistant *Staphylococcus aureus* infections in the United States. *JAMA* **2007**, *298*, 1763-1771.
3. Loffler, C. A.; MacDougall, C., Update on prevalence and treatment of methicillin-resistant *Staphylococcus aureus* infections. *Expert Rev. Anti-Infect. Ther.* **2007**, *5*, 961-981.
4. Maltezou, H. C.; Giamarellou, H., Community-acquired methicillin-resistant *Staphylococcus aureus* infections. *Int. J. Antimicrob. Agents* **2006**, *27*, 87-96.
5. Tsiodras, S.; Gold, H. S.; Sakoulas, G.; Eliopoulos, G. M.; Wennersten, C.; Venkataraman, L.; Moellering, R. C.; Ferraro, M. J., Linezolid resistance in a clinical isolate of *Staphylococcus aureus*. *Lancet* **2001**, *358*, 207-208.
6. Ryan, K. J.; Ray, C. G., *Sherris Medical Microbiology: An Introduction to Infectious Diseases*. McGraw Hill: 2004; p 488-490.
7. Oyston, P. C. F.; Sjoestedt, A.; Titball, R. W., Tularemia: bioterrorism defence renews interest in *Francisella tularensis*. *Nat. Rev. Microbiol.* **2004**, *2*, 967-978.
8. "Tularemia: FAQ About Tularemia". CDC. Available at http://www.cdc.gov/tularemia/Tul_Fact.html.
9. Enderlin, G.; Morales, L.; Jacobs, R. F.; Cross, J. T., Streptomycin and alternative agents for the treatment of tularemia: review of the literature. *Clin. Infect. Dis.* **1994**, *19*, 42-7.
10. Morelli, G.; Song, Y.-J.; Mazzoni, C. J.; Eppinger, M.; Roumagnac, P.; Wagner, D. M.; Feldkamp, M.; Kusecek, B.; Vogler, A. J.; Li, Y.-J.; Cui, Y.-J.; Thomson, N. R.; Jombart, T.; Leblois, R.; Lichtner, P.; Rahalison, L.; Petersen, J. M.; Balloux, F.; Keim, P.; Wirth, T.; Ravel, J.; Yang, R.-F.; Carniel, E.; Achtman, M., *Yersinia pestis* genome sequencing identifies patterns of global phylogenetic diversity. *Nat. Genet.* **2010**, *42*, 1140-1143.
11. "Plague:FAQ about Plague". CDC. Available at <http://www.bt.cdc.gov/agent/plague/faq.asp>.
12. Dennis, D. T.; Gage, K. L.; Gratz, N.; Poland, J. D.; Tokhomirov, E., *Plague Manual: World Health Organization*. Geneva Switzerland. **1999**, 172.
13. Meyer, K. F., Modern therapy of plague. *J. Am. Med. Assoc.* **1950**, *144*, 982-5.
14. Wagle, P. M., Recent advances in the treatment of bubonic plague. *Indian J. Med. Sci.* **1948**, *2*, 489-494.
15. Hotez, P. J.; Molyneuz, D. H.; Fenwick, A.; Kumaresan, J.; Sachs, S. E.; Sachs, J. D.;

- Savioli, L., Control of neglected tropical diseases. *N. Engl. J. Med.* **2007**, *357*, 1018-1027.
16. Miller, J. R.; Waldrop, G. L., Discovery of novel antibacterials. *Expert Opin. Drug Discovery* **5**, 145-154.
 17. Margalit, D. N.; Romberg, L.; Mets, R. B.; Hebert, A. M.; Mitchison, T. J.; Kirschner, M. W.; RayChaudhuri, D., Targeting cell division: Small-molecule inhibitors of FtsZ GTPase perturb cytokinetic ring assembly and induce bacterial lethality. *Proc. Natl. Acad. Sci.* **2004**, *101*, 11821-11826.
 18. Vollmer, W., The prokaryotic cytoskeleton: A putative target for inhibitors and antibiotics? *Appl. Microbiol. Biotechnol.* **2006**, *73*, 37-47.
 19. Romberg, L.; Levin, P. A., Assembly dynamics of the bacterial cell division protein FtsZ: Poised at the edge of stability. *Annu. Rev. Microbiol.* **2003**, *57*, 125-154.
 20. Lock, R. L.; Harry, E. J., Cell-division inhibitors: new insights for future antibiotics. *Nat. Rev. Drug Discovery* **2008**, *7*, 324-338.
 21. Margolin, W., Themes and variations in prokaryotic cell division. *FEMS Microbiol. Rev.* **2000**, *24*, 531-548.
 22. Rothfield, L.; Justice, S.; Garcia-Lara, J., Bacterial cell division. *Annu. Rev. Genet.* **1999**, *33*, 423-448.
 23. Erickson, H. P.; Taylor, D. W.; Taylor, K. A.; Bramhill, D., Bacterial cell division protein FtsZ assembles into protofilament sheets and minirings, structural homologs of tubulin polymers. *Proc. Natl. Acad. Sci.* **1996**, *93*, 519-23.
 24. Lowe, J.; Amos, L. A., Crystal structure of the bacterial cell-division protein FtsZ. *Nature* **1998**, *391*, 203-6.
 25. Lowe, J.; Amos, L. A., Tubulin-like protofilaments in Ca²⁺-induced FtsZ sheets. *Embo J* **1999**, *18*, 2364-71.
 26. Nogales, E.; Downing, K. H.; Amos, L. A.; Lowe, J., Tubulin and FtsZ form a distinct family of GTPases. *Nat. Struct. Biol.* **1998**, *5*, 451-458.
 27. Margalit, D. N.; Romberg, L.; Mets, R. B.; Hebert, A. M.; Mitchison, T. J.; Kirschner, M. W.; RayChaudhuri, D., Targeting cell division: Small-molecule inhibitors of FtsZ GTPase perturb cytokinetic ring assembly and induce bacterial lethality. *Proc. Natl. Acad. Sci.* **2004**, *101*, 13969.
 28. Scheffers, D.-J.; de Wit, J. G.; den Blaauwen, T.; Driessen, A. J. M., GTP Hydrolysis of Cell Division Protein FtsZ: Evidence that the Active Site Is Formed by the Association of Monomers. *Biochemistry* **2002**, *41*, 521-529.
 29. Wang, J.; Galgoci, A.; Kodali, S.; Herath, K. B.; Jayasuriya, H.; Dorso, K.; Vicente, F.; Gonzalez, A.; Cully, D.; Bramhill, D.; Singh, S., Discovery of a small molecule that inhibits cell division by blocking FtsZ, a novel therapeutic target of antibiotics. *J. Biol. Chem.* **2003**, *278*, 44424-44428.

30. Lappchen, T.; Hartog Aloysius, F.; Pinas Victorine, A.; Koomen, G.-J.; den Blaauwen, T., GTP analogue inhibits polymerization and GTPase activity of the bacterial protein FtsZ without affecting its eukaryotic homologue tubulin. *Biochemistry* **2005**, *44*, 7879-84.
31. Laeppchen, T.; Pinas, V. A.; Hartog, A. F.; Koomen, G.-J.; Schaffner-Barbero, C.; Andreu, J. M.; Trambaiolo, D.; Loewe, J.; Juhem, A.; Popov, A. V.; den Blaauwen, T., Probing FtsZ and Tubulin with C8-Substituted GTP Analogs Reveals Differences in Their Nucleotide Binding Sites. *Chem. Biol.* **2008**, *15*, 189-199.
32. Godowski, K. C., Antimicrobial action of sanguinarine. *J. Clin. Dent.* **1989**, *1*, 96-101.
33. Beuria, T. K.; Santra, M. K.; Panda, D., Sanguinarine Blocks Cytokinesis in Bacteria by Inhibiting FtsZ Assembly and Bundling. *Biochemistry* **2005**, *44*, 16584-16593.
34. Mukherjee, S.; Robinson, C. A.; Howe, A. G.; Mazor, T.; Wood, P. A.; Uргаonkar, S.; Hebert, A. M.; RayChaudhuri, D.; Shaw, J. T., N-Benzyl-3-sulfonamidopyrrolidines as novel inhibitors of cell division in E. coli. *Bioorg. Med. Chem. Lett.* **2007**, *17*, 6651-6655.
35. Anam, E. M., 2''''-Hydroxy-3'''-benzyluvarinol,2''''-hydroxy-5''''-benzylisouvarinol-A and 2'''-hydroxy-5''-benzylisouvarinol-B: three novel tetra-C-benzylated flavanones from the root extract of *Xylopia africana* (Benth.) Oliver (Annonaceae). *Indian J. Chem., Sect. B: Org. Chem. Incl. Med. Chem.* **1994**, *33B*, 1009-11.
36. Hufford, C. D.; Lasswell, W. L., Jr., Antimicrobial activities of constituents of *Uvaria chamae*. *Lloydia* **1978**, *41* (2), 156-60.
37. Leegaard, T. M.; Caugant, D. A.; Froholm, L. O.; Hoiby, E. A., Apparent differences in antimicrobial susceptibility as a consequence of national guidelines. *Clin. Microbiol. Infect.* **2000**, *6*, 290-293.
38. Uргаonkar, S.; La Pierre, H. S.; Meir, I.; Lund, H.; Ray Chaudhuri, D.; Shaw, J. T., Synthesis of Antimicrobial Natural Products Targeting FtsZ: (+)-Dichamanetin and (+)-2'''-Hydroxy-5''-benzylisouvarinol-B. *Org. Lett.* **2005**, *7*, 5609-5612.
39. Domadia, P.; Swarup, S.; Bhunia, A.; Sivaraman, J.; Dasgupta, D., Inhibition of bacterial cell division protein FtsZ by cinnamaldehyde. *Biochem. Pharmacol.* **2007**, *74*, 831-840.
40. Beuria, T. K.; Singh, P.; Surolia, A.; Panda, D., Promoting assembly and bundling of FtsZ as a strategy to inhibit bacterial cell division: A new approach for developing novel antibacterial drugs. *Biochem. J.* **2009**, *423*, 61-69.
41. Rai, D.; Singh, J. K.; Roy, N.; Panda, D., Curcumin inhibits FtsZ assembly: an attractive mechanism for its antibacterial activity. *Biochem. J.* **2008**, *410*, 147-155.
42. Villinski, J. R.; Dumas, E. R.; Chai, H.-B.; Pezzuto, J. M.; Angerhofer, C. K.; Gafner, S., Antibacterial Activity and Alkaloid Content of *Berberis thunbergii*, *Berberis vulgaris* and *Hydrastis canadensis*. *Pharm. Biol.* **2003**, *41*, 551-557.
43. Yu, H.-H.; Kim, K.-J.; Cha, J.-D.; Kim, H.-K.; Lee, Y.-E.; Choi, N.-Y.; You, Y.-O.,

- Antimicrobial Activity of Berberine Alone and in Combination with Ampicillin or Oxacillin Against Methicillin-Resistant *Staphylococcus aureus*. *J. Med. Food* **2005**, *8*, 454-461.
44. Hwang, B. Y.; Roberts, S. K.; Chadwick, L. R.; Wu, C. D.; Kinghorn, A. D., Antimicrobial constituents from goldenseal (the rhizomes of *Hydrastis canadensis*) against selected oral pathogens. *Planta Medica* **2003**, *69*, 623-627.
 45. Domadia, P. N.; Bhunia, A.; Sivaraman, J.; Swarup, S.; Dasgupta, D., Berberine Targets Assembly of *Escherichia coli* Cell Division Protein FtsZ. *Biochemistry* **2008**, *47*, 3225-3234.
 46. Clement, M.-J.; Jourdain, I.; Lachkar, S.; Savarin, P.; Gigant, B.; Knossow, M.; Toma, F.; Sobel, A.; Curmi, P. A., N-Terminal Stathmin-like Peptides Bind Tubulin and Impede Microtubule Assembly. *Biochemistry* **2005**, *44*, 14616-14625.
 47. Clement, M.-J.; Kuoch, B.-t.; Ha-Duong, T.; Joshi, V.; Hamon, L.; Toma, F.; Curmi, P. A.; Savarin, P., The Stathmin-Derived I19L Peptide Interacts with FtsZ and Alters Its Bundling. *Biochemistry* **2009**, *48*, 9734-9744.
 48. Arbildua, J. J.; Brunet, J. E.; Jameson, D. M.; Lopez, M.; Nova, E.; Lagos, R.; Monasterio, O., Fluorescence resonance energy transfer and molecular modeling studies on 4',6-diamidino-2-phenylindole (DAPI) complexes with tubulin. *Protein Sci.* **2006**, *15*, 410-419.
 49. Bonne, D.; Heusele, C.; Simon, C.; Pantaloni, D., 4',6-Diamidino-2-phenylindole, a fluorescent probe for tubulin and microtubules. *J. Biol. Chem.* **1985**, *260*, 2819-25.
 50. Ortiz, M.; Lagos, R.; Monasterio, O., Interaction between the C-terminal peptides of tubulin and tubulin S detected with the fluorescent probe 4',6-diamidino-2-phenylindole. *Arch. Biochem. Biophys.* **1993**, *303*, 159-64.
 51. Nova, E.; Montecinos, F.; Brunet, J. E.; Lagos, R.; Monasterio, O., 4',6-Diamidino-2-phenylindole (DAPI) induces bundling of *Escherichia coli* FtsZ polymers inhibiting the GTPase activity. *Arch. Biochem. Biophys.* **2007**, *465*, 315-319.
 52. Stokes, N. R.; Sievers, J.; Barker, S.; Bennett, J. M.; Brown, D. R.; Collins, I.; Errington, V. M.; Foulger, D.; Hall, M.; Halsey, R.; Johnson, H.; Rose, V.; Thomaidis, H. B.; Haydon, D. J.; Czaplewski, L. G.; Errington, J., Novel Inhibitors of Bacterial Cytokinesis Identified by a Cell-based Antibiotic Screening Assay. *J. Biol. Chem.* **2005**, *280*, 39709-39715.
 53. Ohashi, Y.; Chijiwa, Y.; Suzuki, K.; Takahashi, K.; Nanamiya, H.; Sato, T.; Hosoya, Y.; Ochi, K.; Kawamura, F., The lethal effect of a benzamide derivative, 3-methoxybenzamide, can be suppressed by mutations within a cell division gene, *ftsZ*, in *Bacillus subtilis*. *J. Bacteriol.* **1999**, *181*, 1348-1351.
 54. Haydon, D. J.; Stokes, N. R.; Ure, R.; Galbraith, G.; Bennett, J. M.; Brown, D. R.; Baker, P. J.; Barynin, V. V.; Rice, D. W.; Sedelnikova, S. E.; Heal, J. R.; Sheridan, J. M.;

Aiwale, S. T.; Chauhan, P. K.; Srivastava, A.; Taneja, A.; Collins, I.; Errington, J.; Czaplewski, L. G., An Inhibitor of FtsZ with Potent and Selective Anti-Staphylococcal Activity. *Science* **2008**, *321*, 1673-1675.

Chapter V

1. Cancer facts and figures. *American Cancer Society*, 2009.
2. Weitman, S. D.; Lark, R. H.; Coney, L. R.; Fort, D. W.; Frasca, V.; Zurawski, V. R., Jr.; Kamen, B. A., Distribution of the folate receptor GP38 in normal and malignant cell lines and tissues. *Cancer Res.* **1992**, *52*, 3396-3401.
3. Lee, E. S.; Na, K.; Bae, Y. H., Polymeric micelle for tumor pH and folate-mediated targeting. *J. Control. Release* **2003**, *91*, 103-113.
4. Na, K.; Lee, T. B.; Park, K.-H.; Shin, E.-K.; Lee, Y.-B.; Choi, H.-K., Self-assembled nanoparticles of hydrophobically-modified polysaccharide bearing vitamin H as a targeted anti-cancer drug delivery system. *Eur. J. Pharm. Sci.* **2003**, *18*, 165-173.
5. Szekeres, T.; Sedlak, J.; Novotny, L., Benzamide riboside, a recent inhibitor of inosine 5'-monophosphate dehydrogenase induces transferrin receptors in cancer cells. *Curr. Med. Chem.* **2002**, *9*, 759-764.
6. Schally, A. V.; Szepeshazi, K.; Nagy, A.; Comaru-Schally, A. M.; Halmos, G., New approaches to therapy of cancers of the stomach, colon and pancreas based on peptide analogs. *Cell Mol. Life Sci.* **2004**, *61*, 1042-1068.
7. Wu, X.; Ojima, I., Tumor specific novel taxoid-monoclonal antibody conjugates. *Curr. Med. Chem.* **2004**, *11*, 429-438.
8. Jaracz, S.; Chen, J.; Kuznetsova, L. V.; Ojima, I., Recent advances in tumor-targeting anticancer drug conjugates. *Bioorg. Med. Chem.* **2005**, *13*, 5043-5054.
9. Chen, J.; Jaracz, S.; Zhao, X.; Chen, S.; Ojima, I., Antibody-cytotoxic agent conjugates for cancer therapy. *Expert Opin. Drug Delivery* **2005**, *2*, 873-890.
10. Kigawa, J.; Minagawa, Y.; Kanamori, Y.; Itamochi, H.; Cheng, X.; Okada, M.; Oishi, T.; Terakawa, N., Glutathione concentration may be a useful predictor of response to second-line chemotherapy in patients with ovarian cancer. *Cancer* **1998**, *82*, 697-702.
11. Liu, C.; Tadayoni, B. M.; Bourret, L. A.; Mattocks, K. M.; Derr, S. M.; Widdison, W. C.; Kedersha, N. L.; Ariniello, P. D.; Goldmacher, V. S.; Eradication of large colon tumor xenografts by targeted delivery of maytansinoids. *Proc. Natl. Acad. Sci.* **1996**, *93*, 8618-8623.
12. Maeda, H.; Fang, J.; Inutsuka, T.; Kitamoto, Y., Vascular permeability enhancement in solid tumor: various factors, mechanisms involved and its implications. *Int. Immunopharmacol.* **2003**, *3*, 319-328.
13. Jelinkova, M.; Strohalm, J.; Etrych, T.; Ulbrich, K.; Rihova, B., Starlike vs. Classic Macromolecular Prodrugs: Two Different Antibody-Targeted HPMA Copolymers of

- Doxorubicin Studied in Vitro and in Vivo as Potential Anticancer Drugs. *Pharm. Res.* **2003**, *20*, 1558-1564.
14. Bianco, A., Carbon nanotubes for the delivery of therapeutic molecules. *Expert Opin. Drug Delivery* **2004**, *1*, 57-65.
 15. Kratz, F.; Beyer, U., Serum proteins as drug carriers of anticancer agents: a review. *Drug Del.* **1998**, *5*, 281-299.
 16. Wunder, A.; Stehle, G.; Sinn, H.; Schrenk, H. H.; Hoff-Biederbeck, D.; Bader, F.; Friedrich, E. A.; Peschke, P.; Maier-Borst, W.; Heene, D. L., Enhanced albumin uptake by rat tumors. *Int. J. Onco.* **1997**, *11*, 497-507.
 17. Schlicker, A.; Peschke, P.; Sinn, H.; Hahn, E. W., Albumin as a carrier system for delivering drugs to solid tumors. *J. Pharm. Sci. Tech.* **2000**, *54*, 442-448.
 18. Henderson, S. J.; Lindup, W. E., Interaction of 3-carboxy-4-methyl-5-propyl-2-furanopropanoic acid, an inhibitor of plasma protein binding in uremia, with human albumin. *Biochem. Pharmacol.* **1990**, *40*, 2543-2548.
 19. Pfordt, J.; Thoma, H.; Spitteller, G., Identification, structure elucidation, and synthesis of previously unknown urofuranic acids in human blood. *Liebigs Annalen der Chemie* **1981**, 2298-2308.
 20. Brooks, D. W.; De Lee, N. C.; Peevey, R., Remote substituent effects in microbial reductions of 3-ketoglutarate and 3-ketoadipate esters. *Tet. Lett.* **1984**, *25*, 4623-4626.
 21. Nudelman, A.; Nudelman, A., Convenient syntheses of d-aminolevulinic acid. *Synthesis* **1999**, *4* 568-570.
 22. Jain, D. V. S.; Chadha, R., Kinetics of the reaction between triphenylphosphine and some haloalkanes. *Ind. J. Chem.* **1991**, *30A*, 929-35.
 23. <http://www.aist.go.jp/RIODB/SDBS/> (National Institute of Advanced Industrial Science and Technology, date of access)
 24. Wittig, G.; Schollkopf, U., Triphenylphosphinemethylene as an olefin-forming reagent. *I. Chem. Ber.* **1954**, *97*, 1318-1330.
 25. Vilsmeier, A.; Haack, A., Action of phosphorus halides on alkylformanilides. A new method for the preparation of secondary and tertiary p-alkylaminonobenzaldehydes. *Ber.* **1927**, *60B*, 119-22.

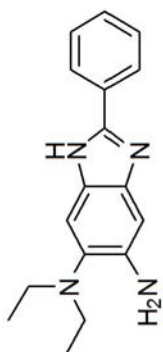
Chapter VI

1. Sarcina, M.; Mullineaux, C.W.; Effects of tubulin assembly inhibitors on cell division in prokaryotes in vivo. *FEMS Microbiol. Lett.* **2000**, *191*, 25-29.
2. de Pereda, J.M.; Leynadier, D.; Evangelio, J.A.; Chacon, P.; Andreu J.M.; Tubulin secondary structure analysis, limited proteolysis sites, and homology to FtsZ. *Biochemistry* **1996**, *35*, 14203-14215.

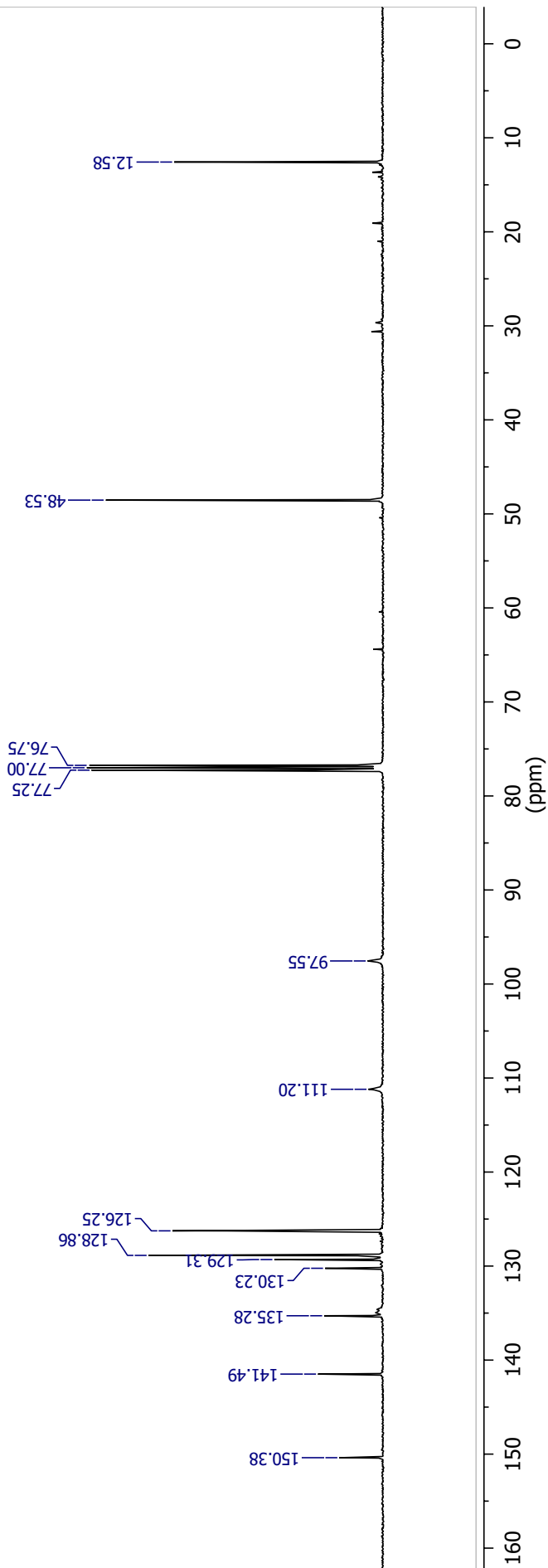
3. White, E.L.; Suling, W.J.; Ross, L.J.; Seitz, L.E.; Reynolds, R.C.; 2-Alkoxy-carbonylaminopyridines: inhibitors of Mycobacterium tuberculosis FtsZ. *J. Antimicrob. Chemother.* **2002**, *50*, 111-114.
4. Reynolds, R.C.; Srivastava, S.; Ross, L.J.; Suling, W.J.; White, E.L.; A new 2-carbamoyl pteridine that inhibits mycobacterial FtsZ. *Bioorg. Med. Chem. Lett.* **2004**, *14*, 3161-3164.
5. Huang, Q.; Kirikae, F.; Kirikae, T.; Pepe, A.; Amin, A.; Respicio, L. *et al.* Targeting FtsZ for Antituberculosis Drug Discovery: Noncytotoxic Taxanes as Novel Antituberculosis Agents. *J. Med. Chem.* **2006**, *49*, 463-466.
6. Appendino, G.; Danieli, B.; Jakupovic, J.; Belloro, E.; Scambia, G.; Bombardelli, E. The chemistry and occurrence of taxane derivatives. XXX. Synthesis and evaluation of C-seco paclitaxel analogs. *Tet. Lett.* **1997**, *38*, 4273-4276.
7. Taraboletti, G.; Micheletti, G.; Rieppi, M.; Poli, M.; Turatto, M.; Rossi, C.. Antiangiogenic and antitumor activity of IDN 5390, a new taxane derivative. *Clin. Cancer Res.* **2002**, *8*, 1182-1188.

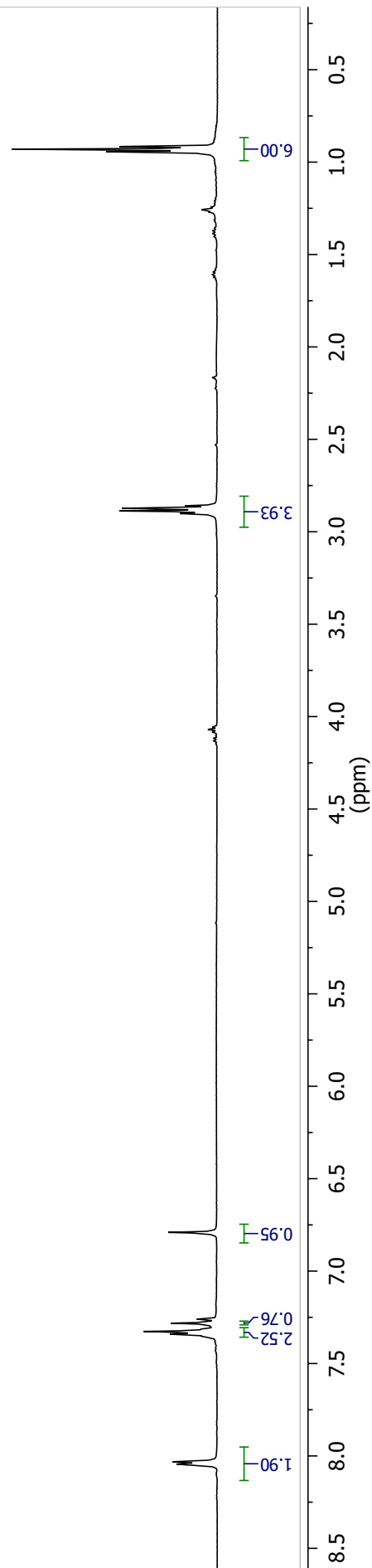
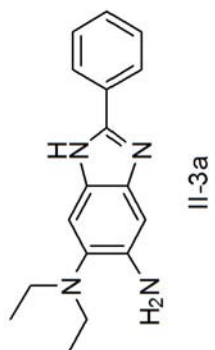
APPENDICES

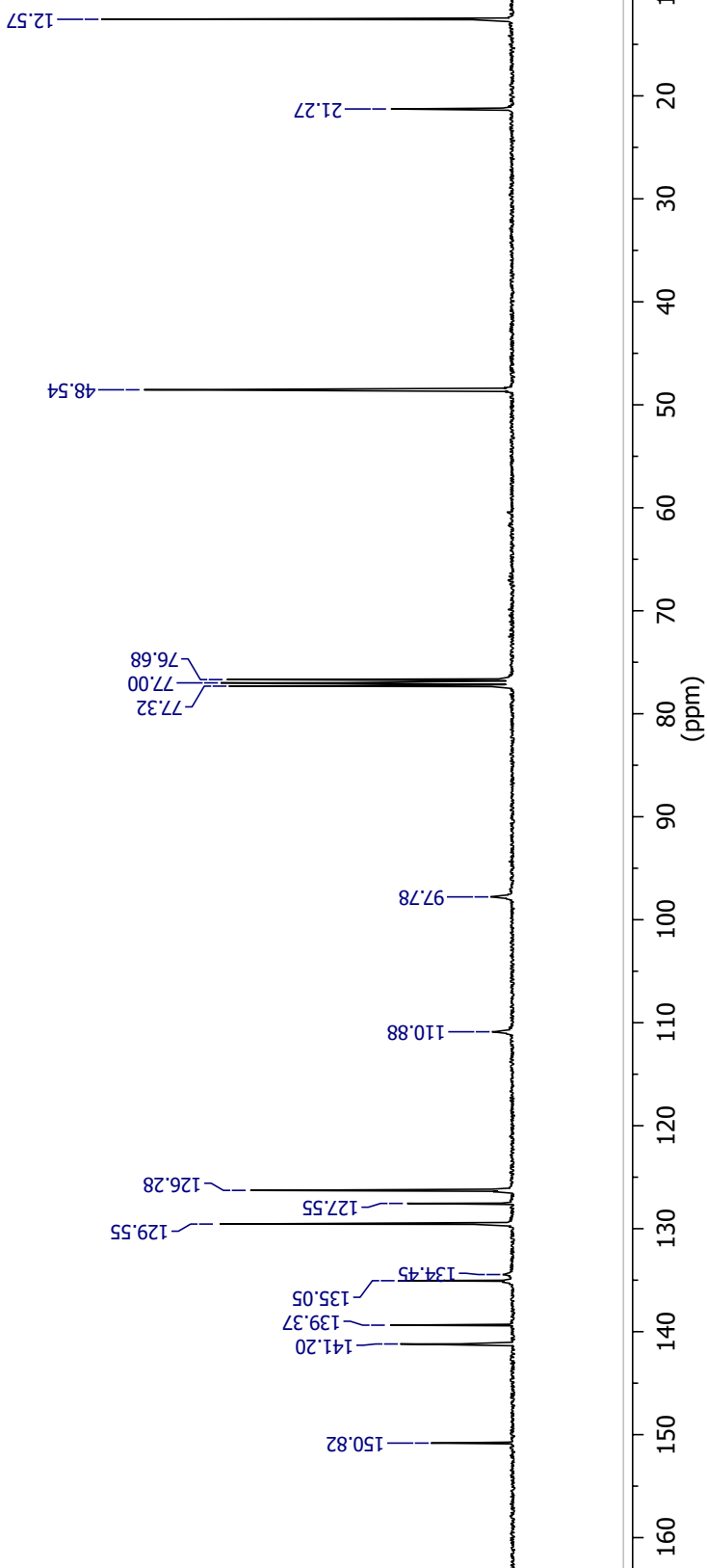
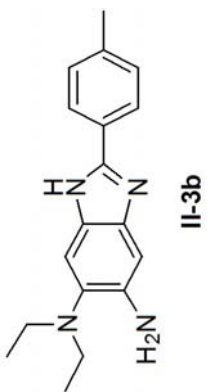
A1. Appendix Chapter II.....	189
A2. Appendix Chapter III.....	286
A3. Appendix Chapter IV.....	288
A4. Appendix Chapter V.....	310
A5. Appendix Chapter VI	314

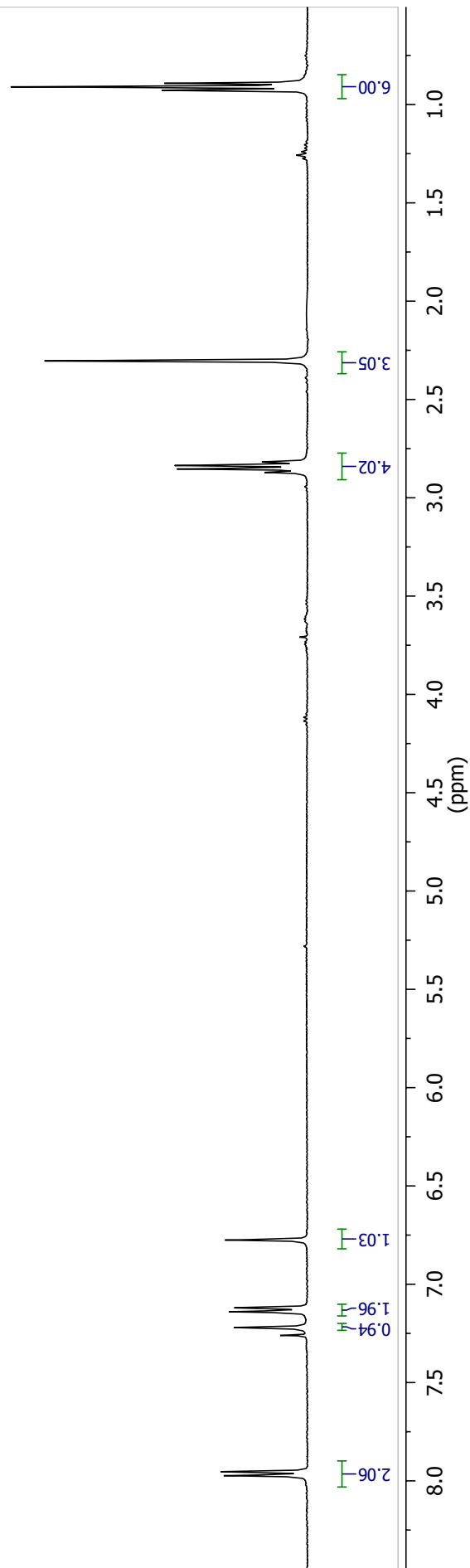
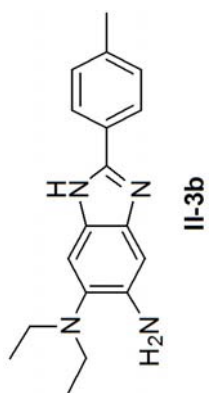


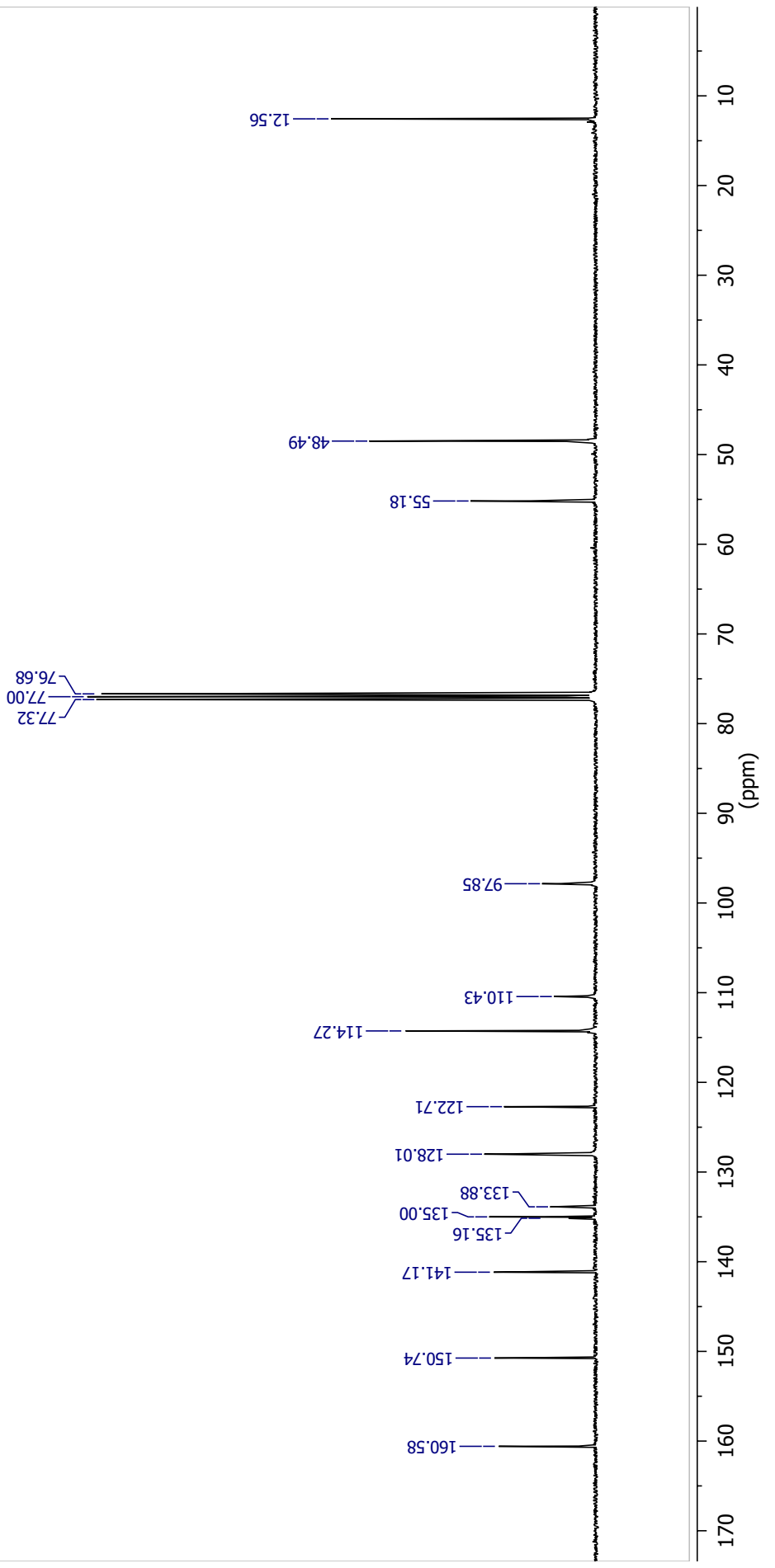
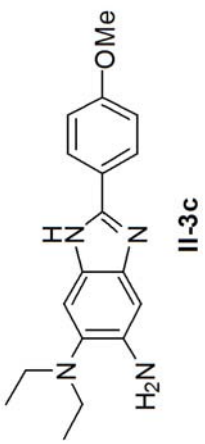
II-3a

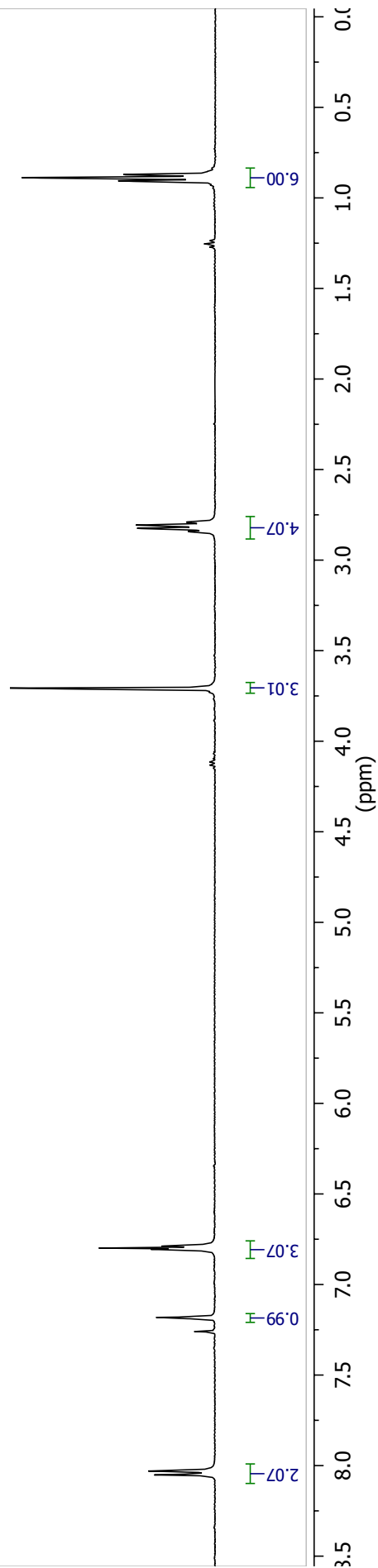
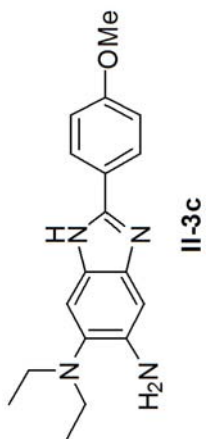


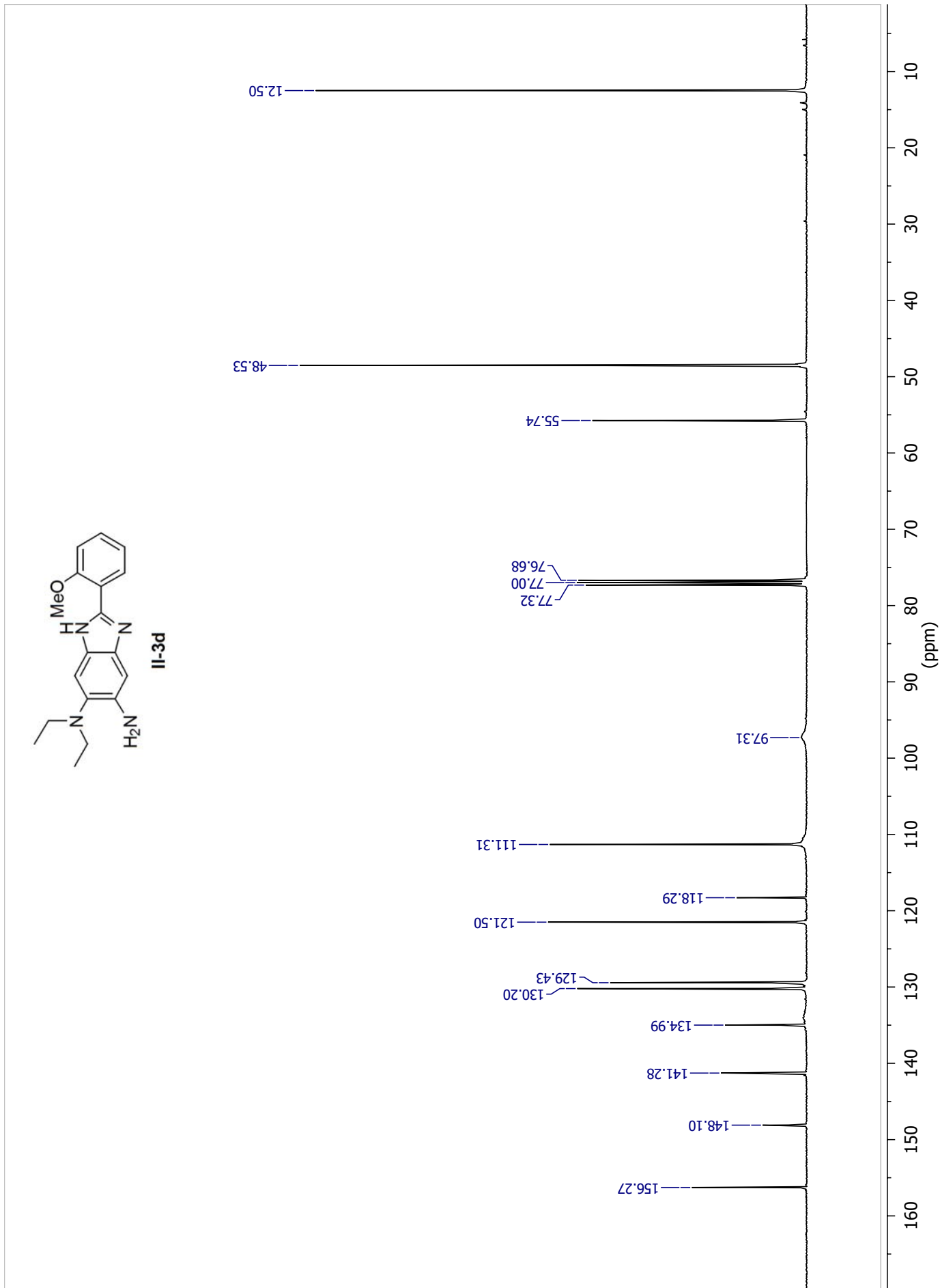


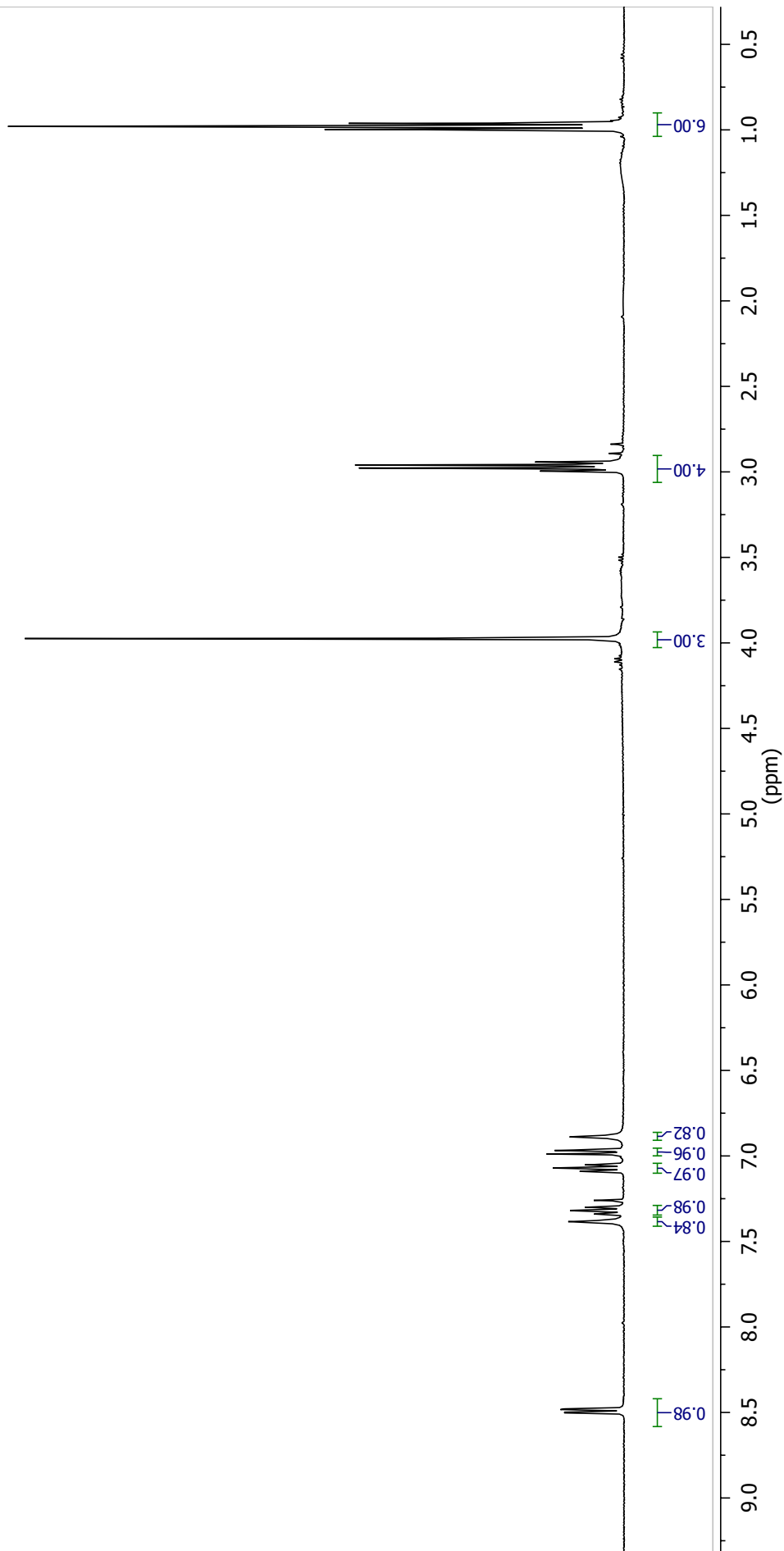
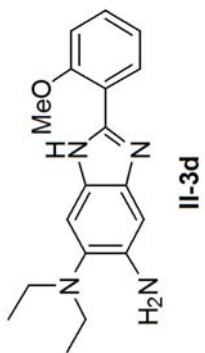


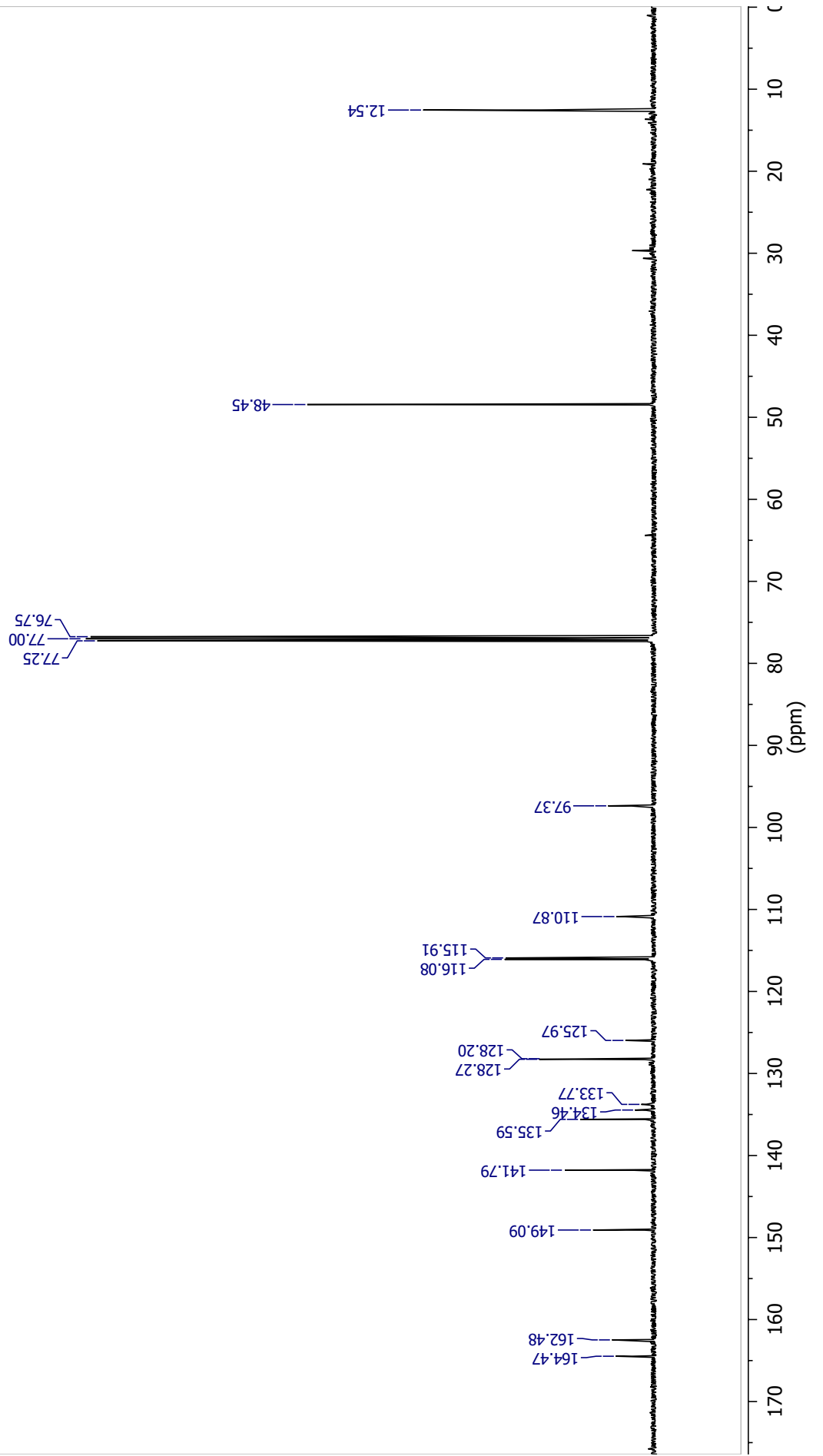
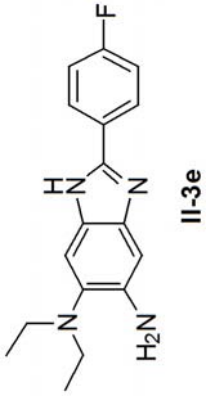


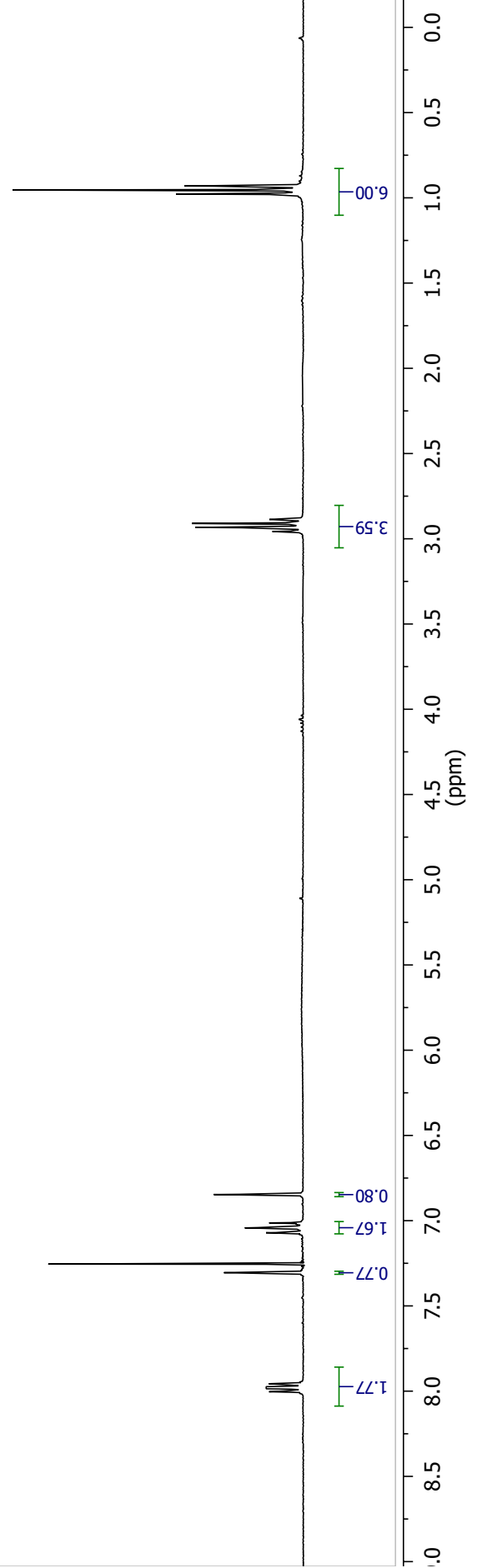
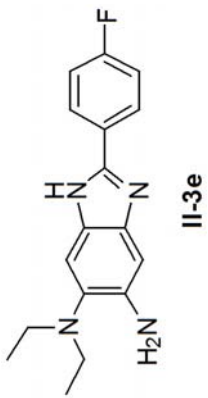


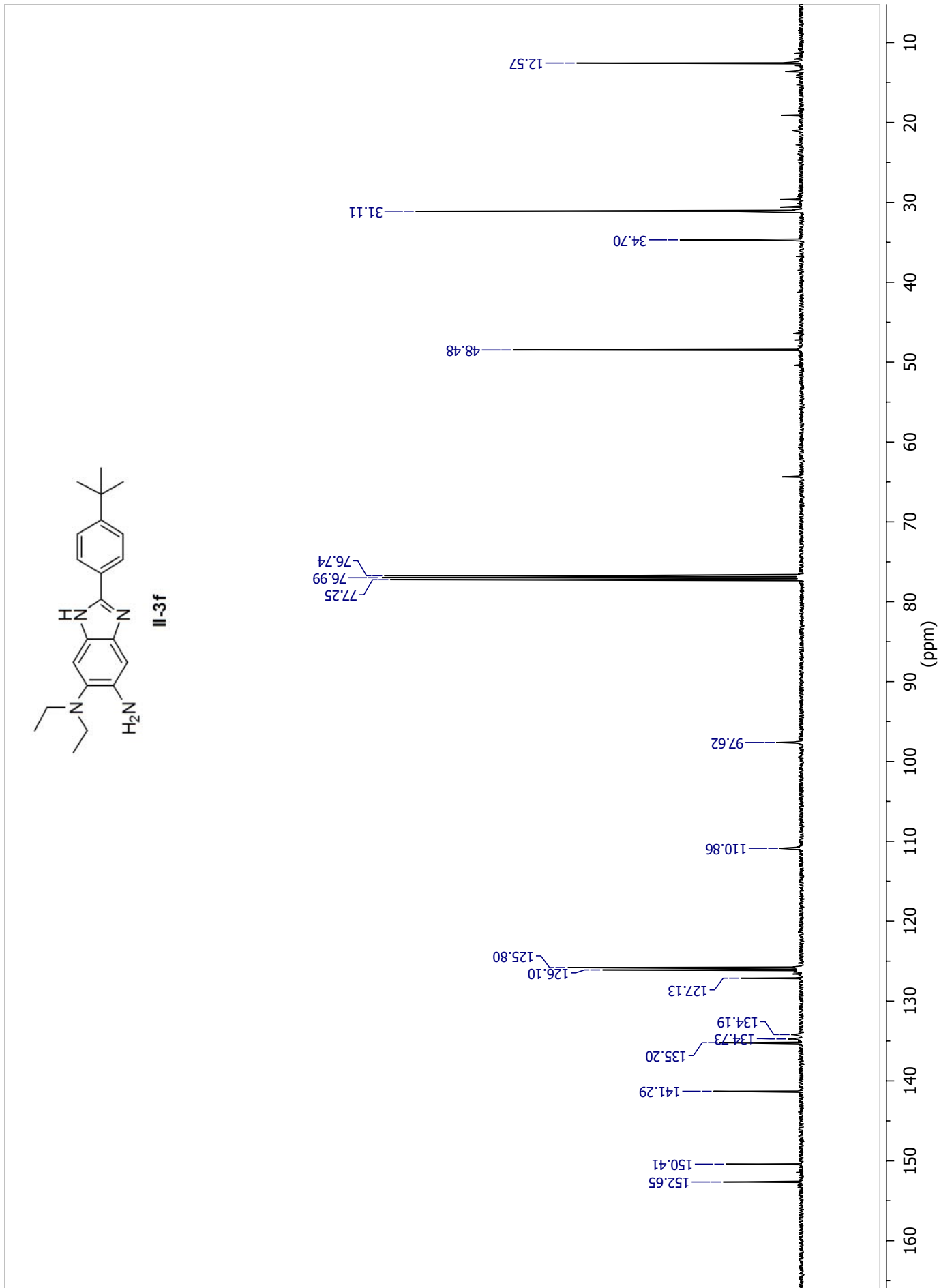


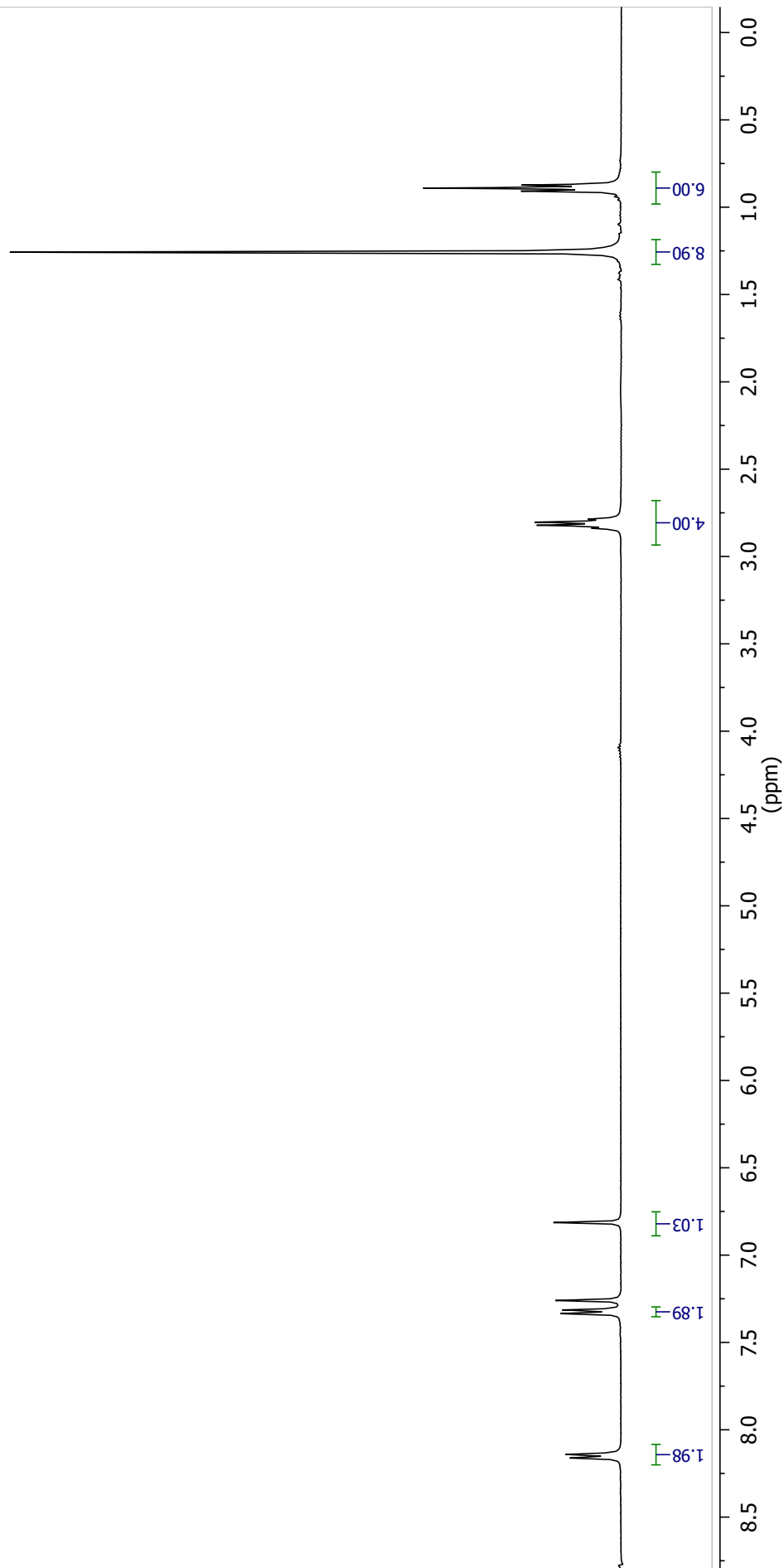
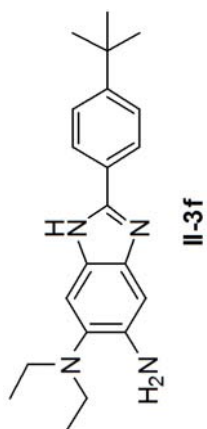


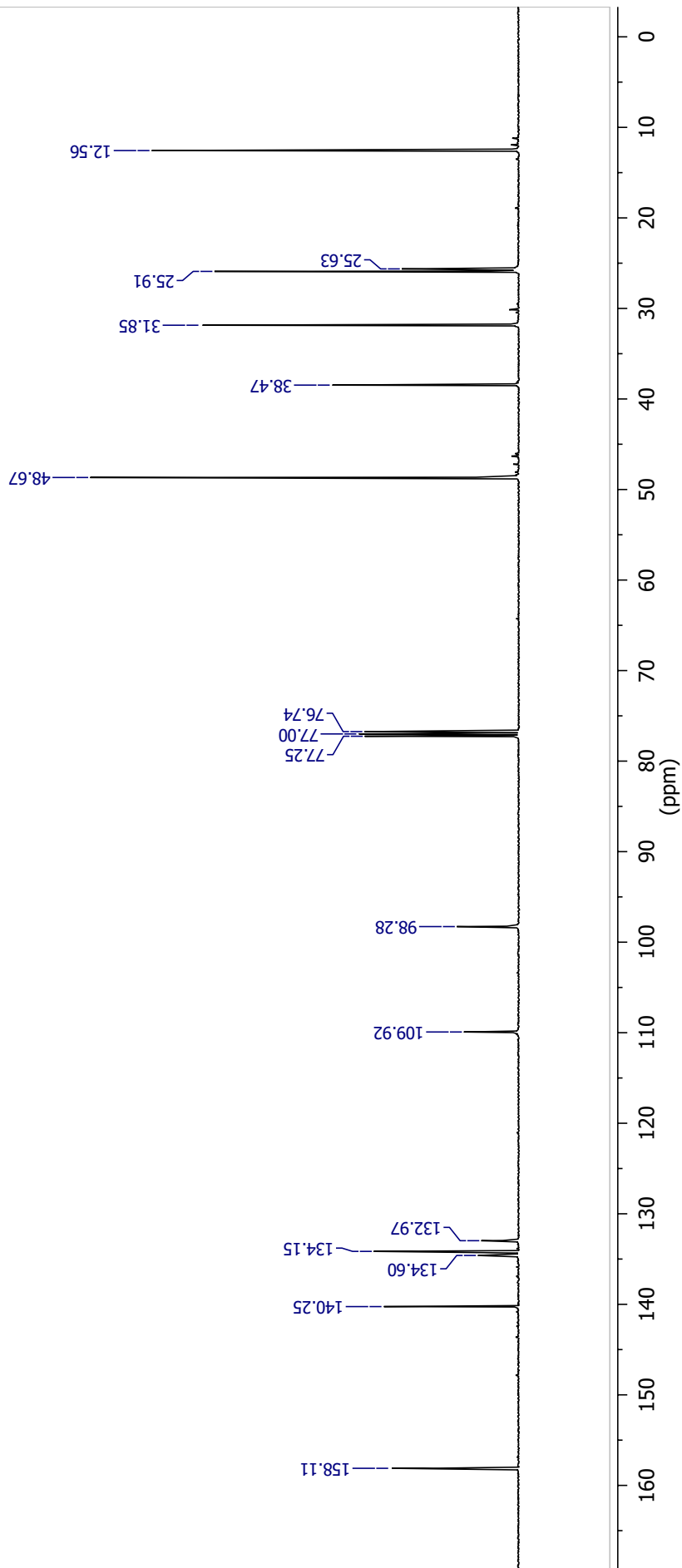
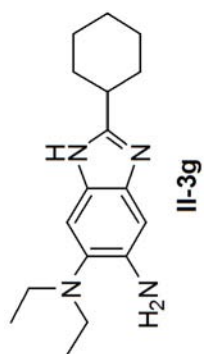


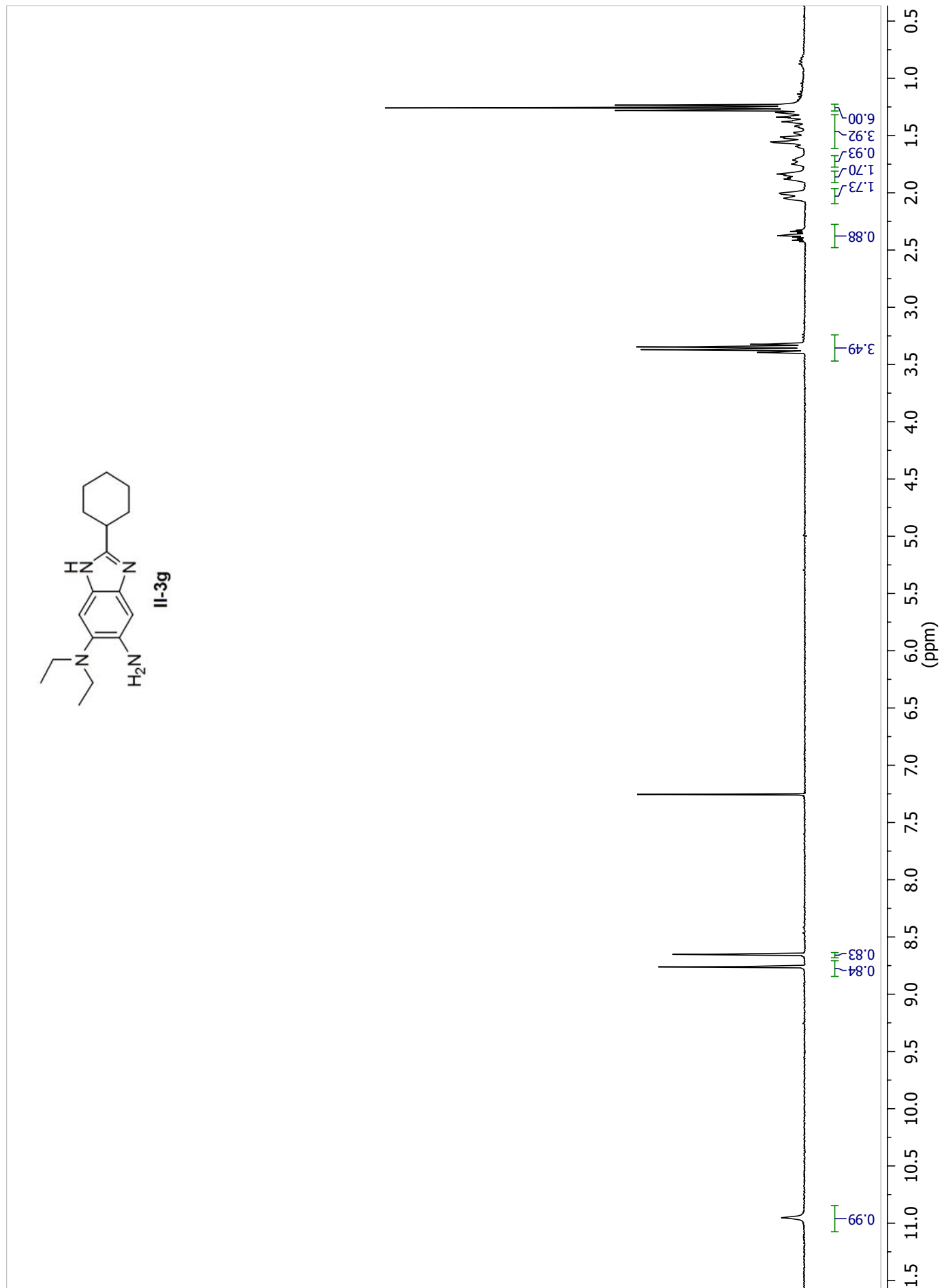
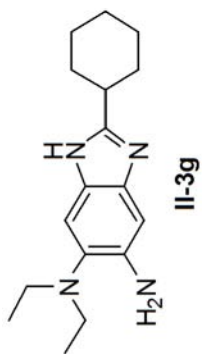


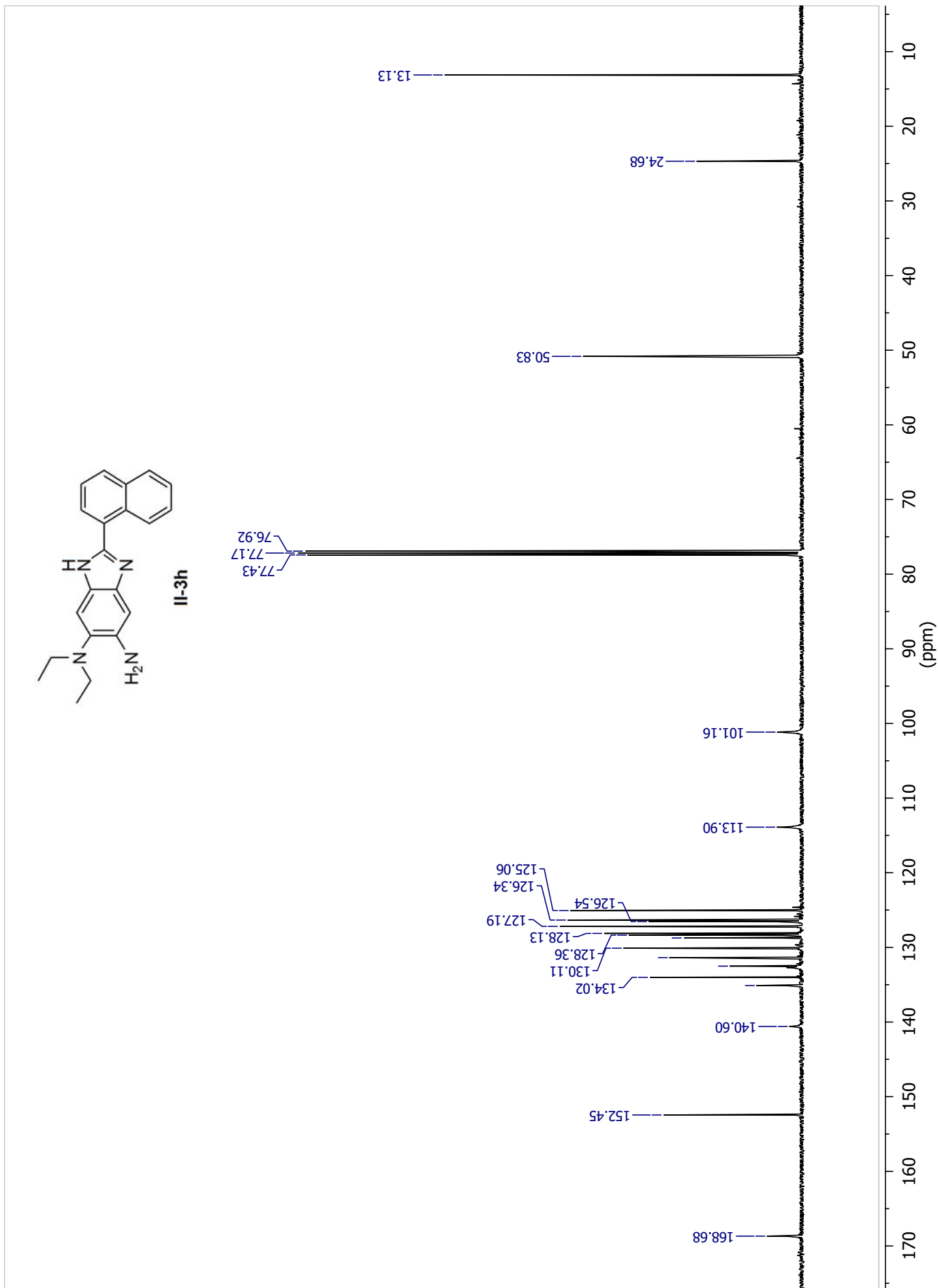


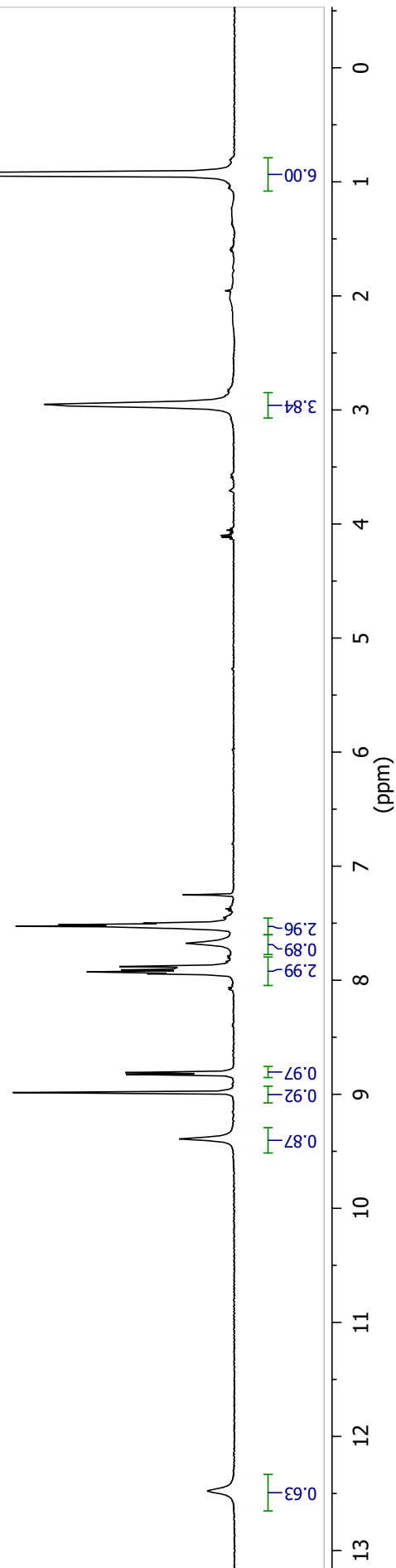
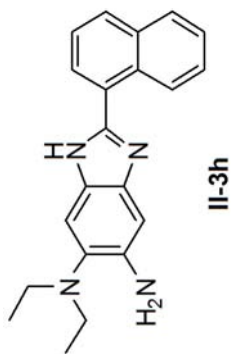


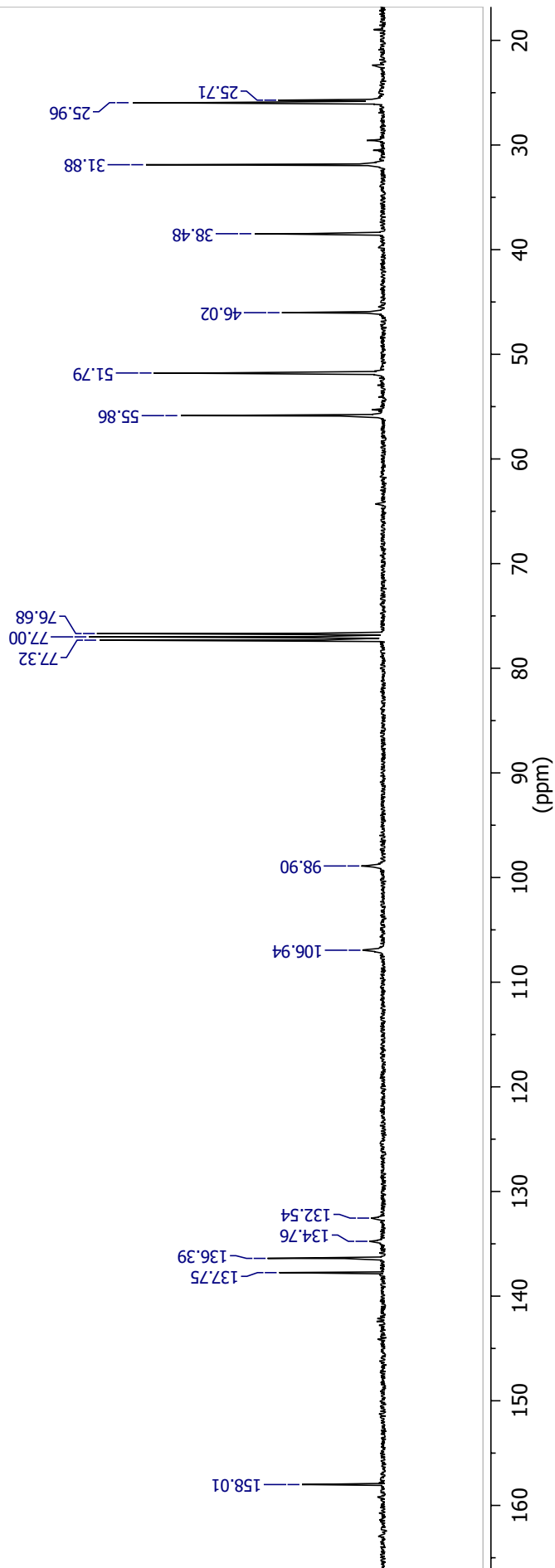
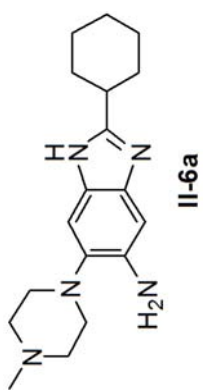


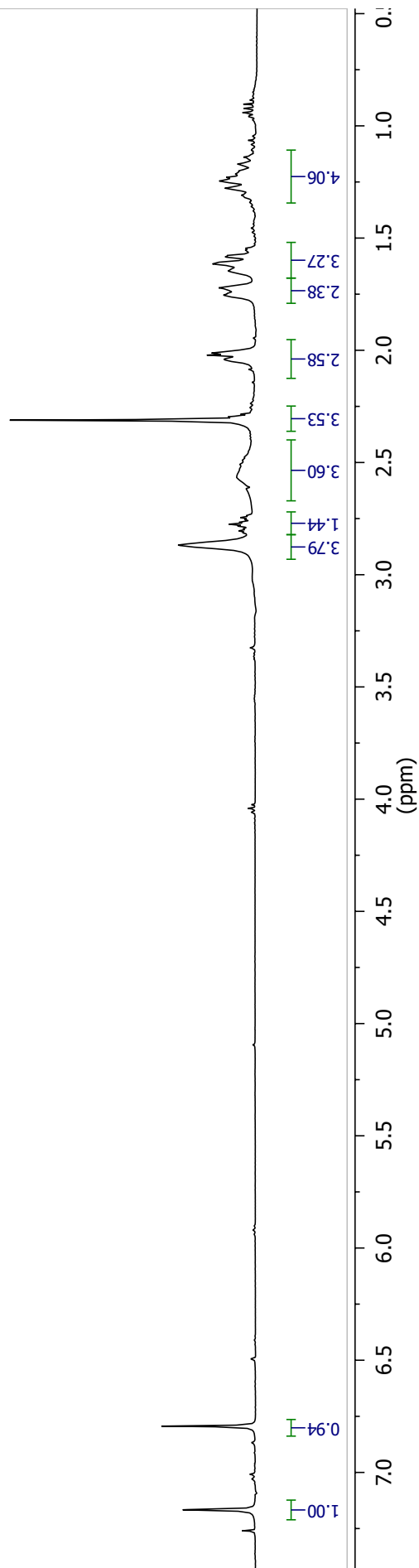
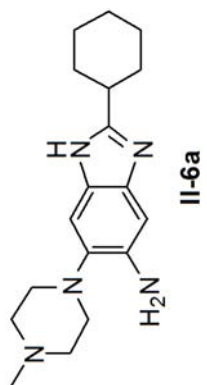


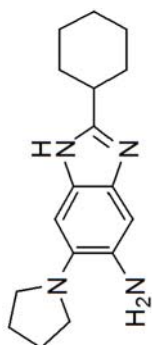




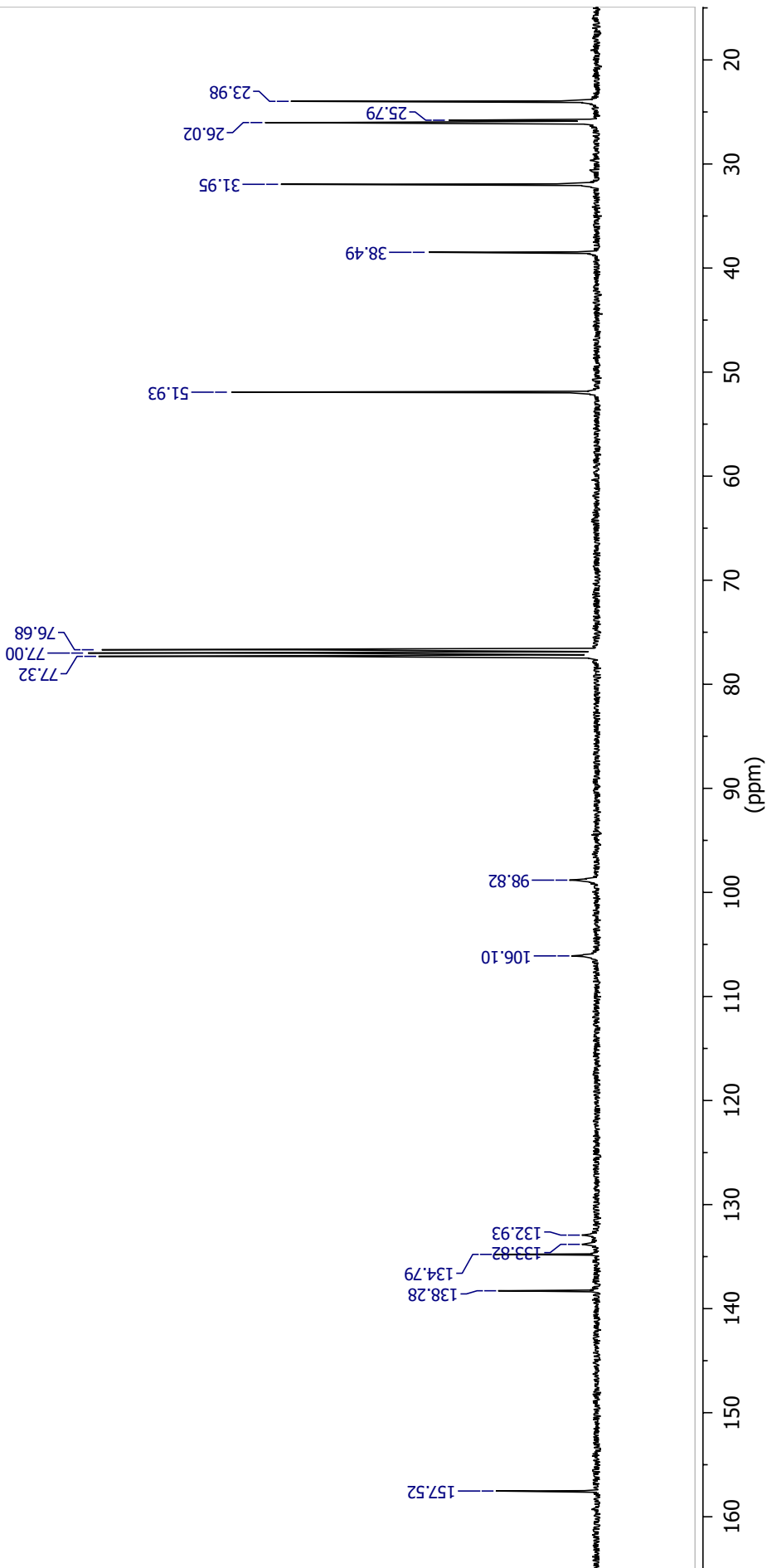


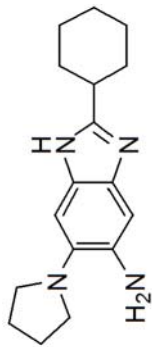




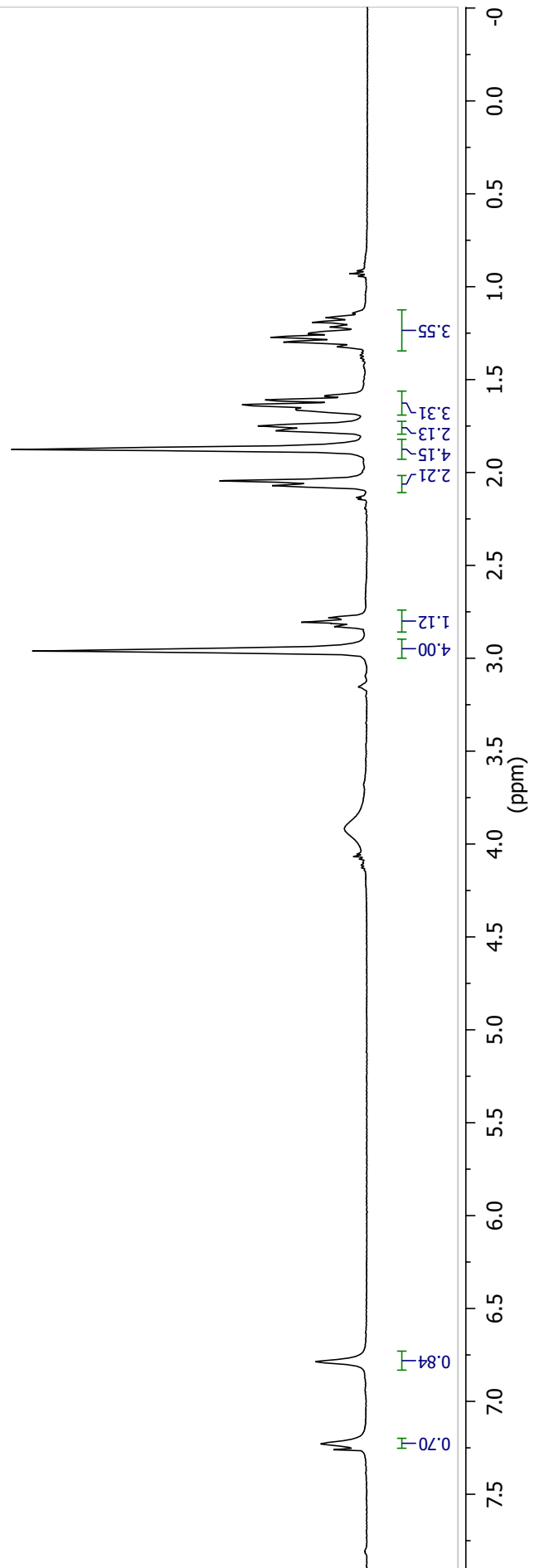


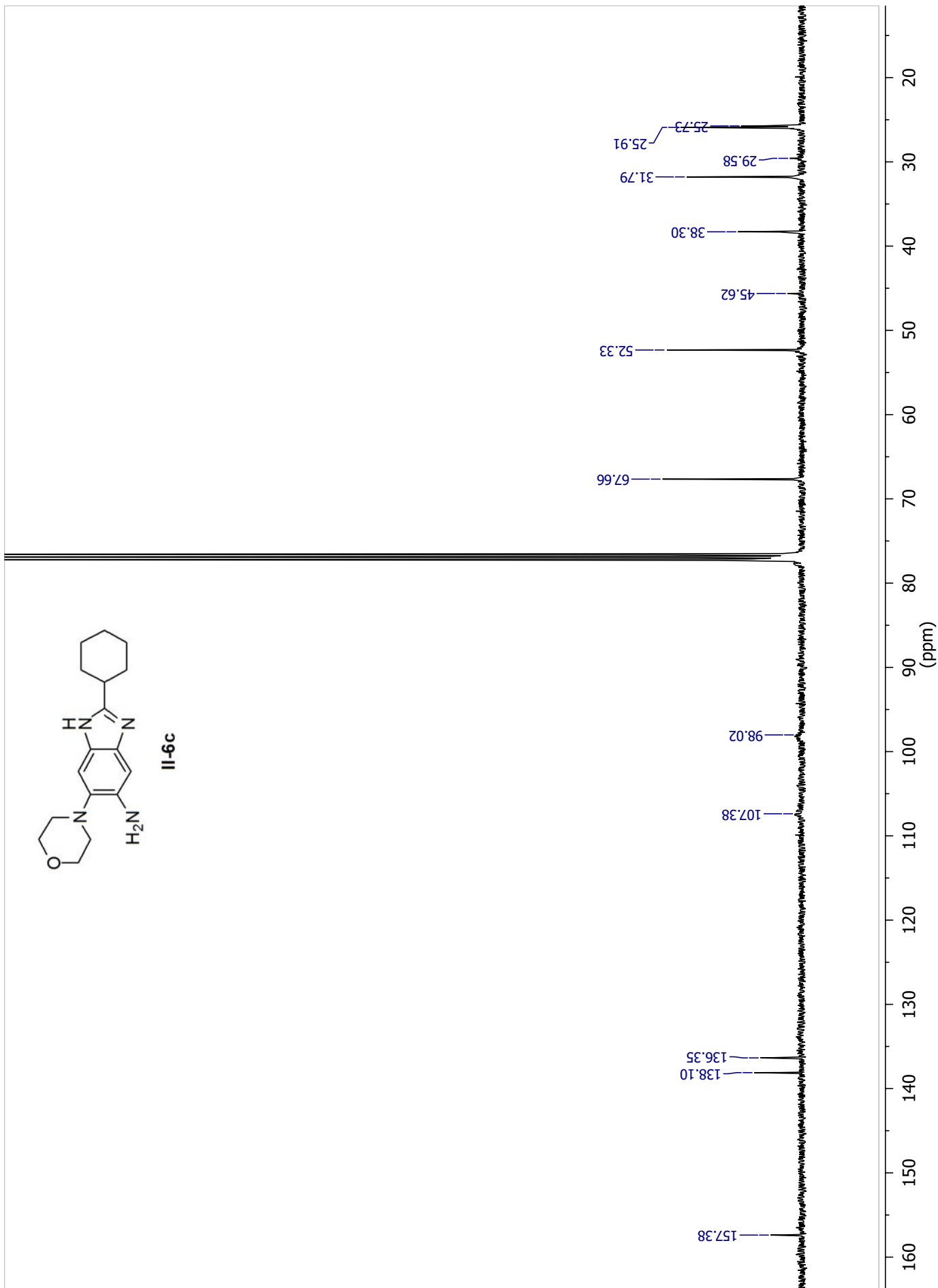
II-9-b

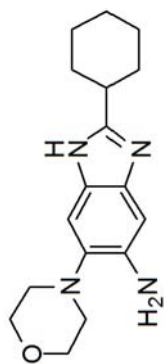




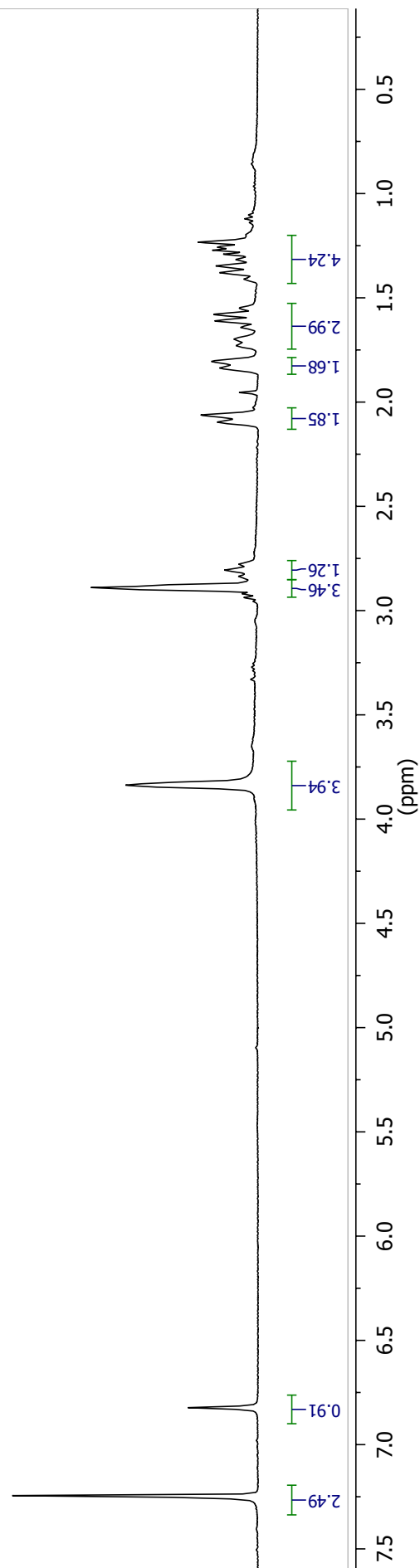
II-6b

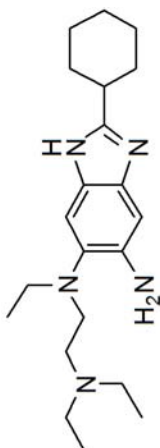




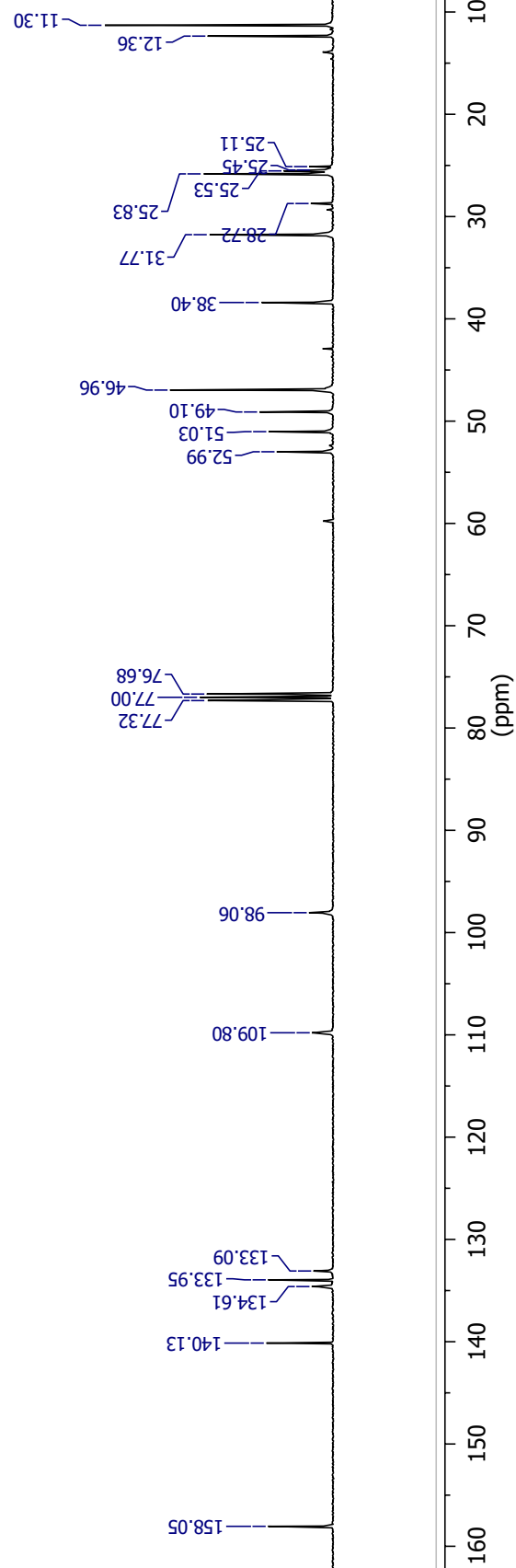


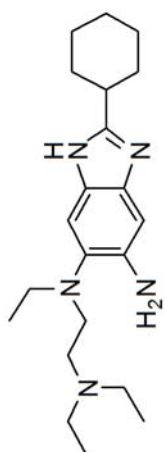
II-6c



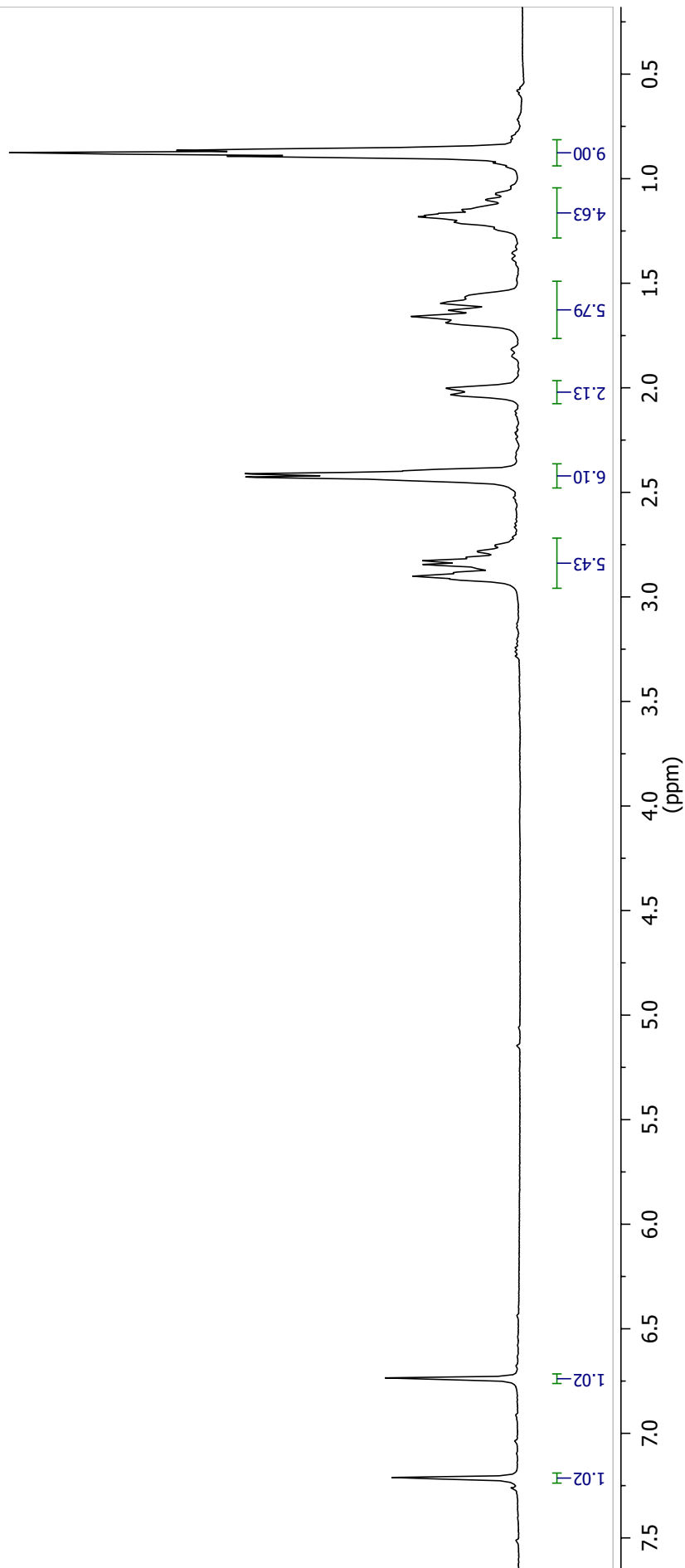


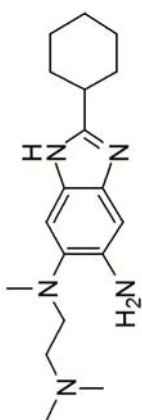
II-6d



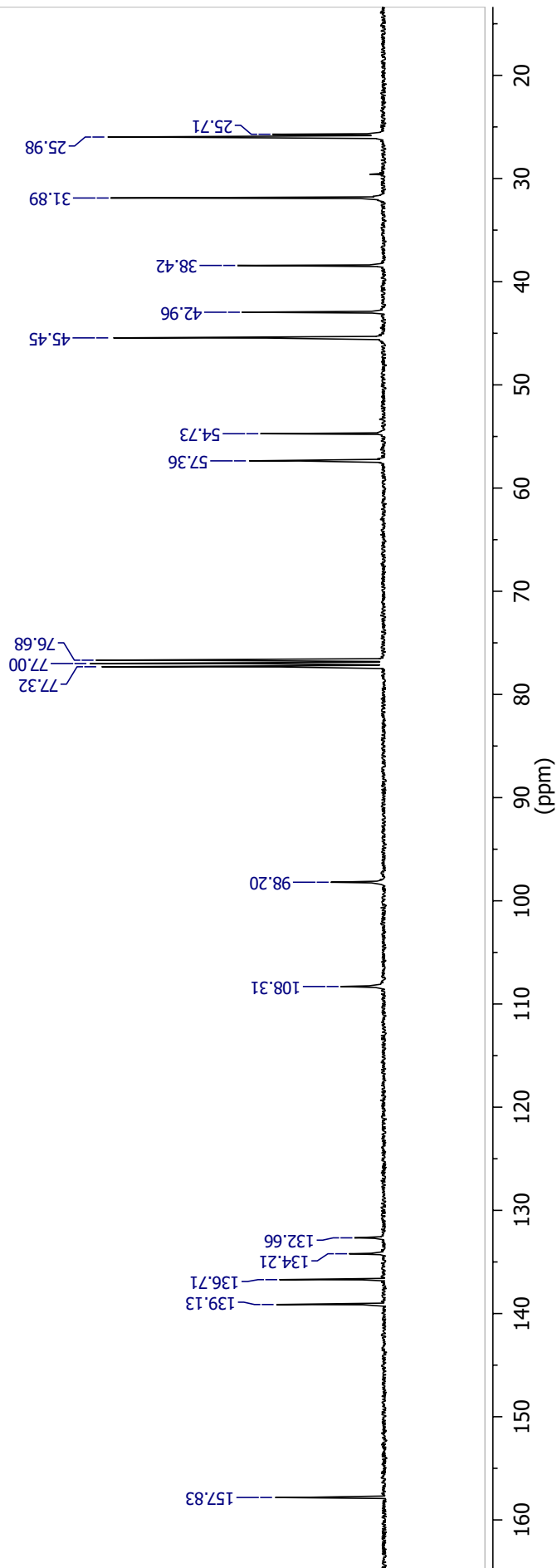


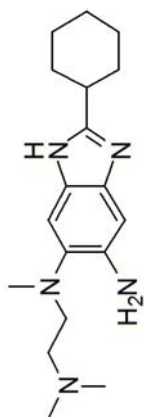
II-6d



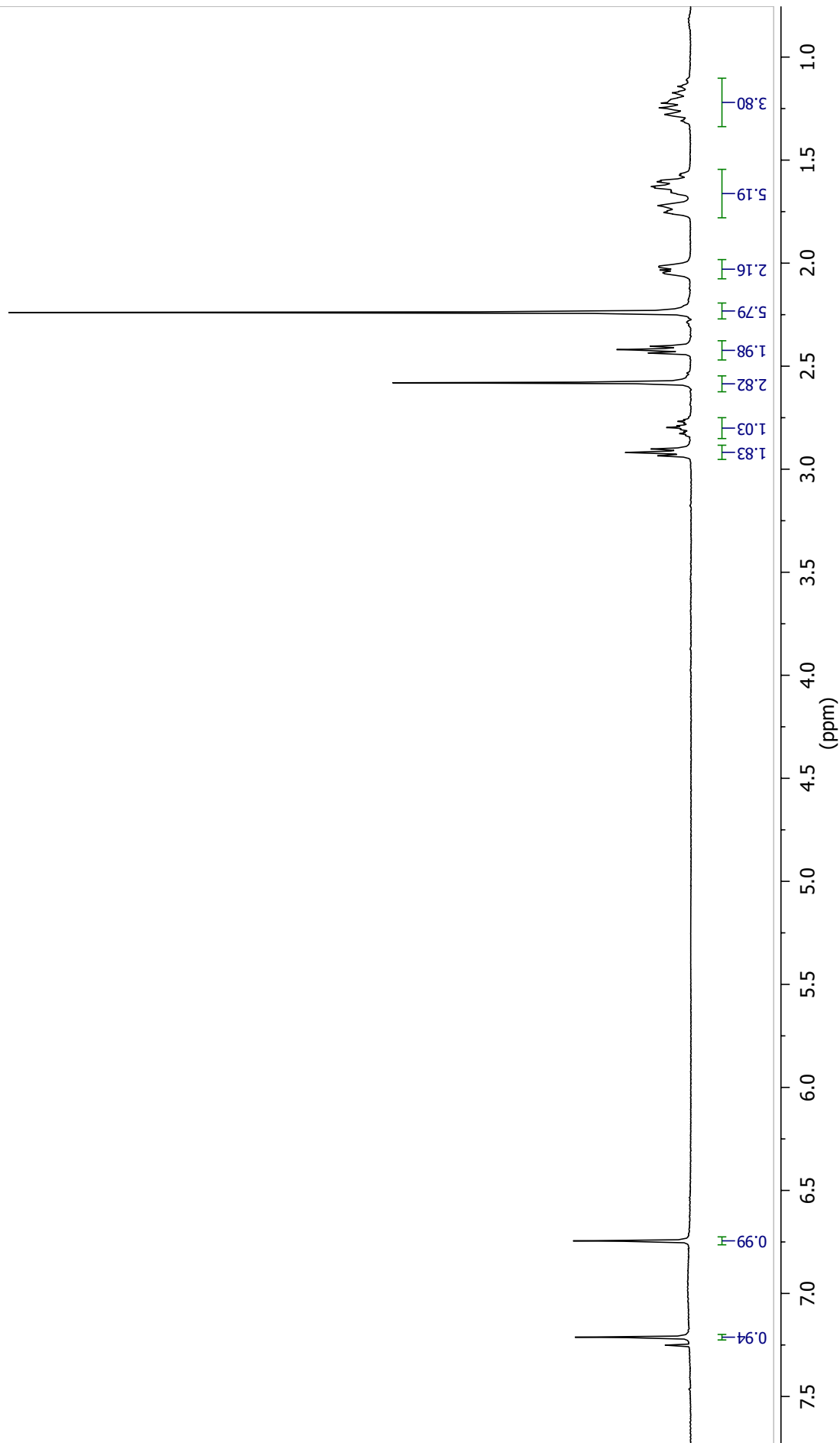


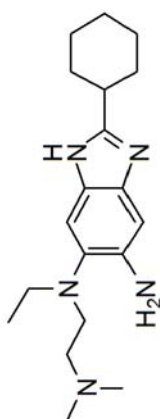
II-6e



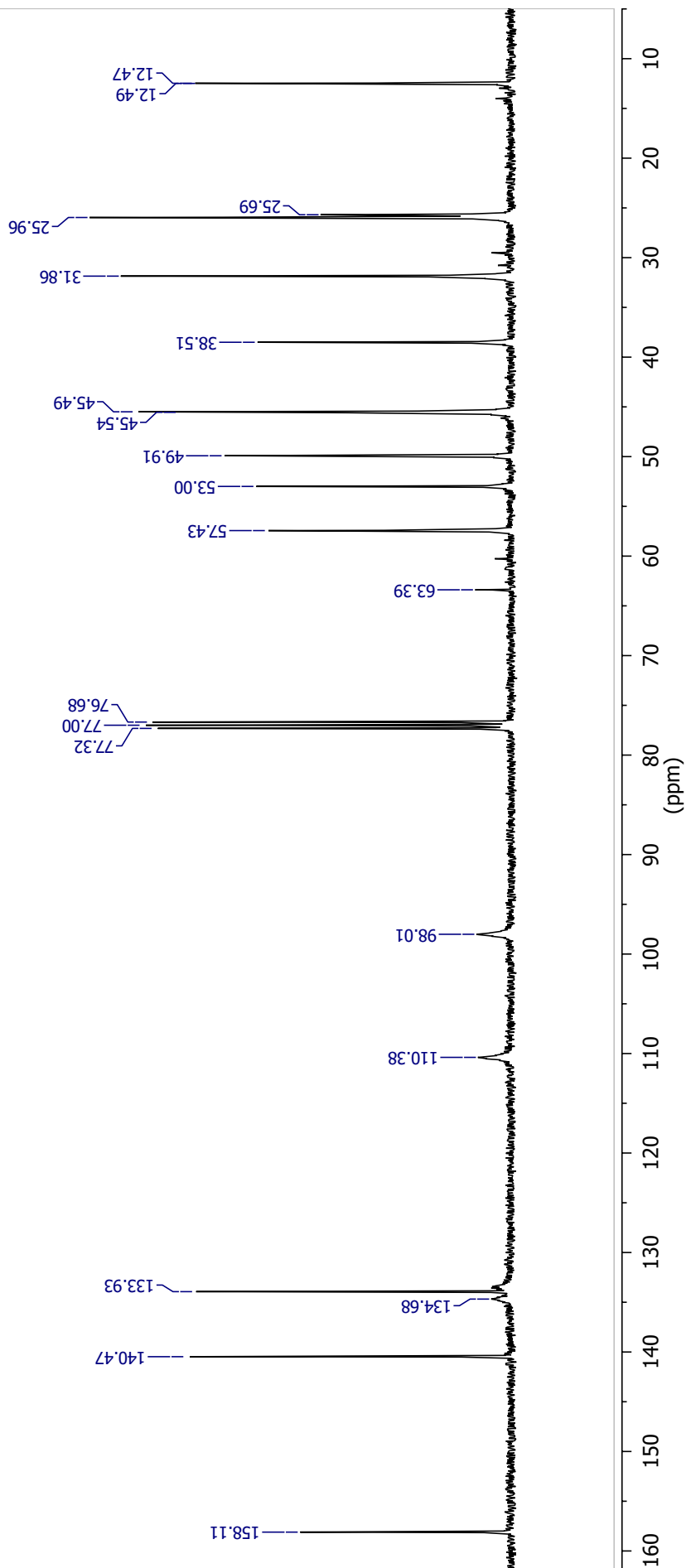


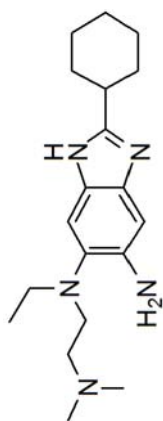
II-6e



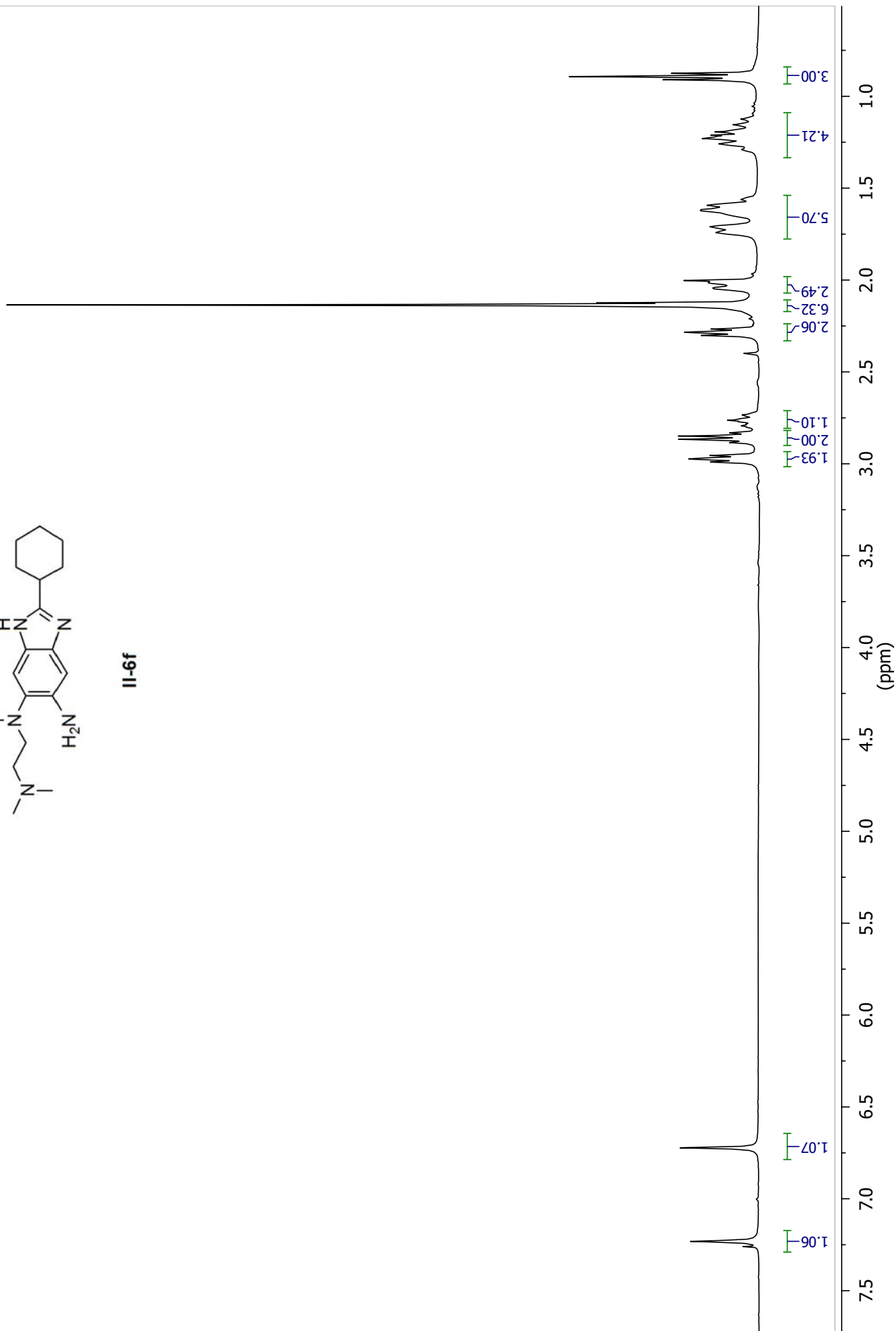


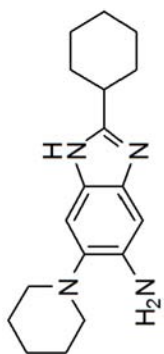
II-6f



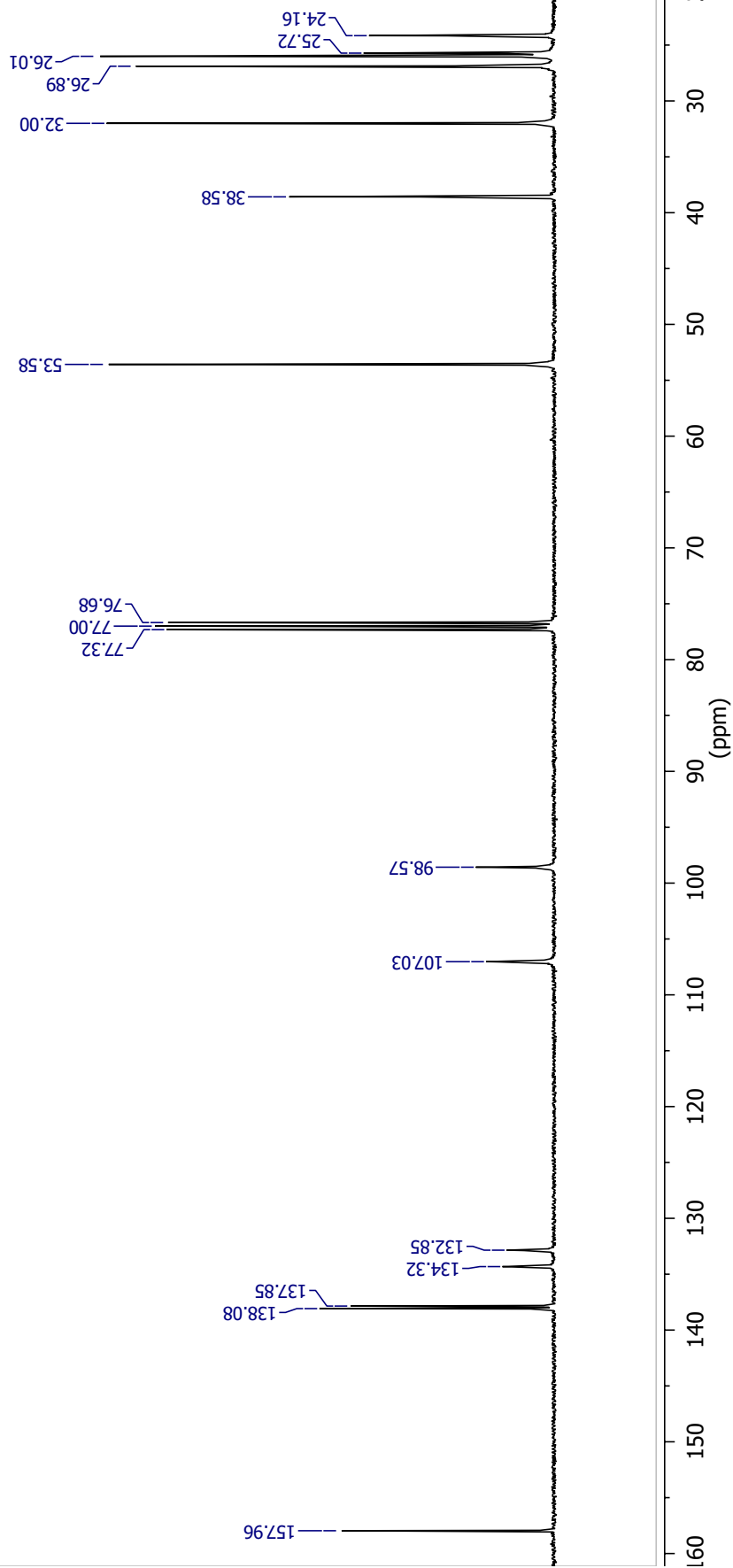


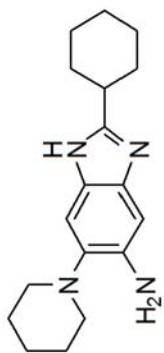
II-6f



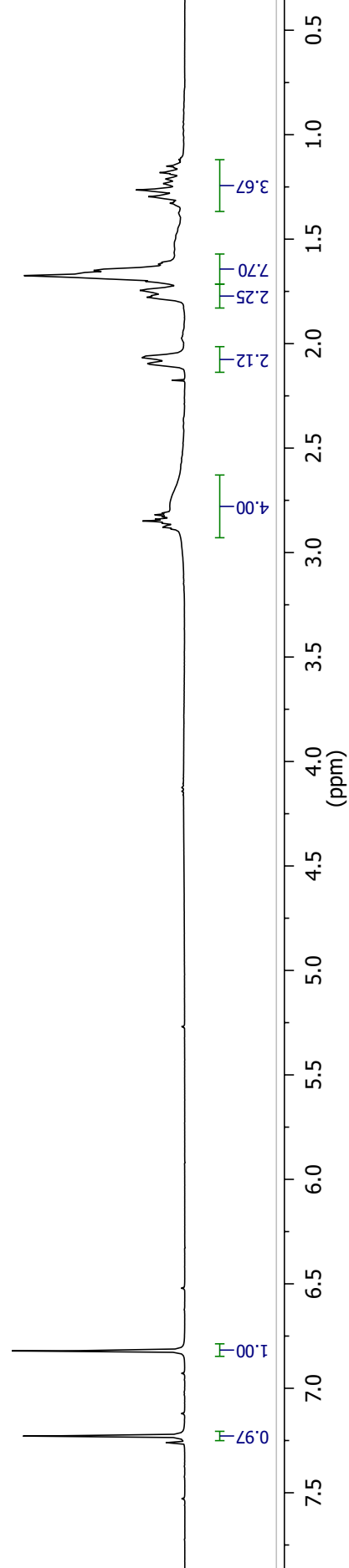


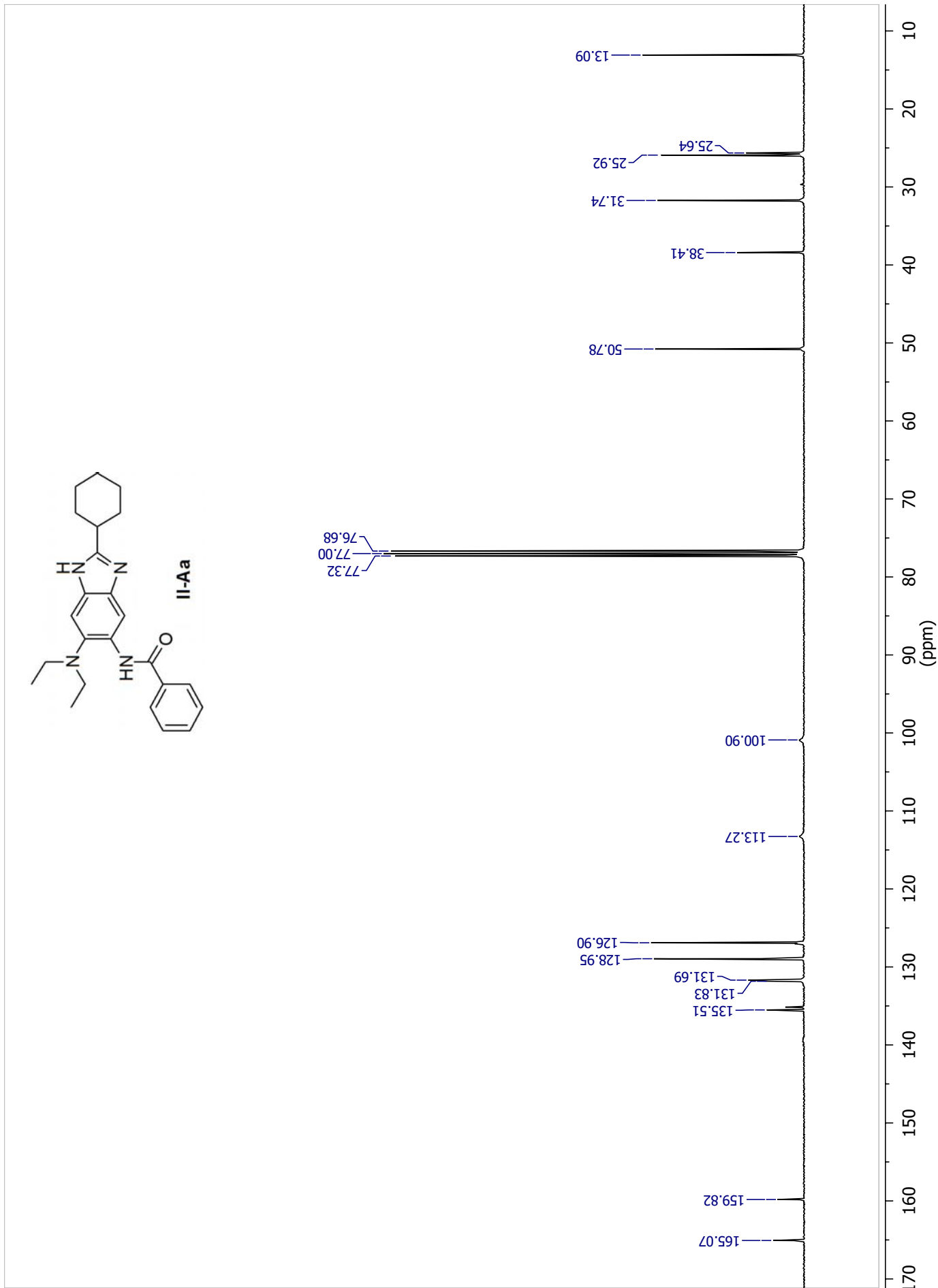
II-6g

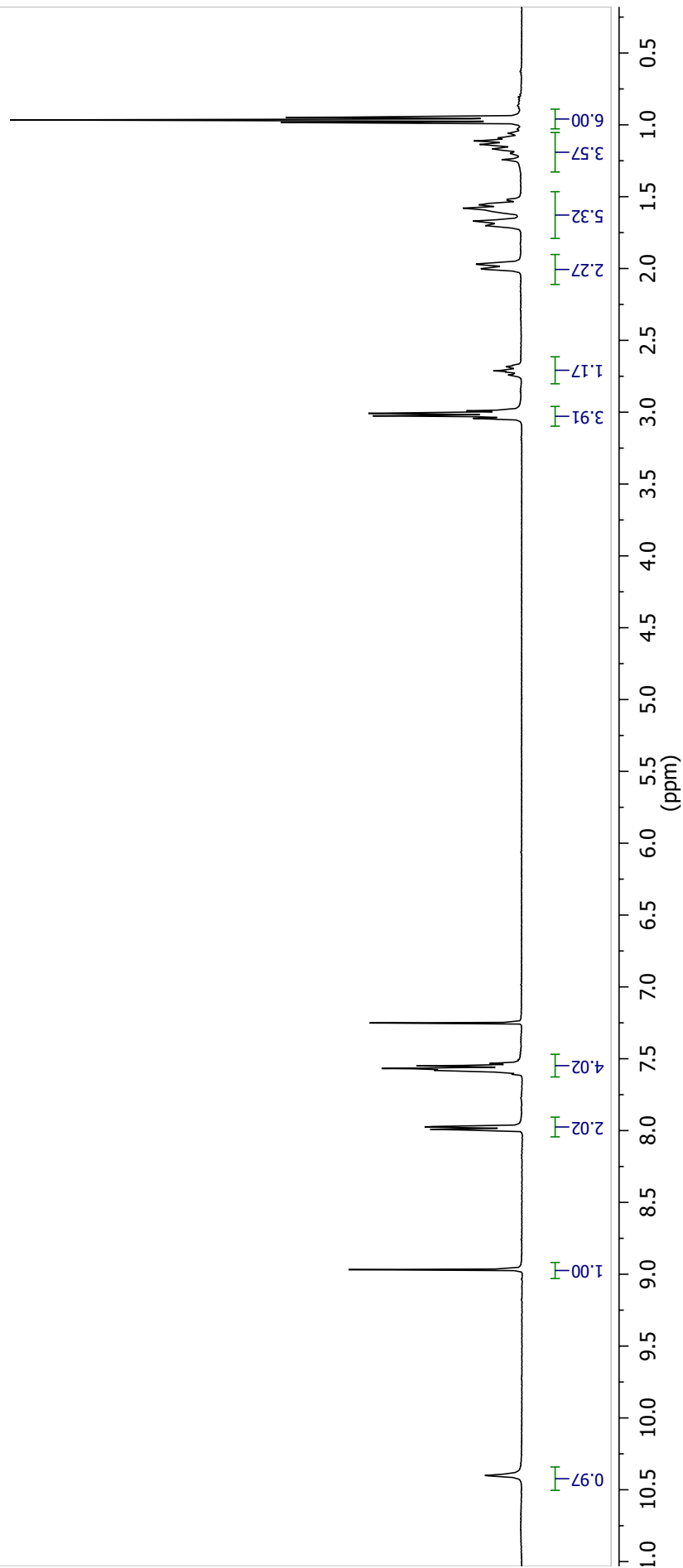
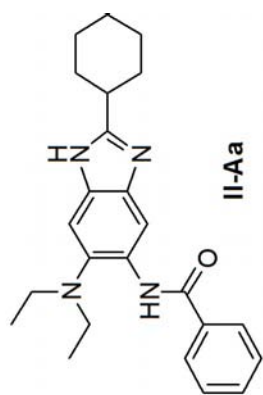


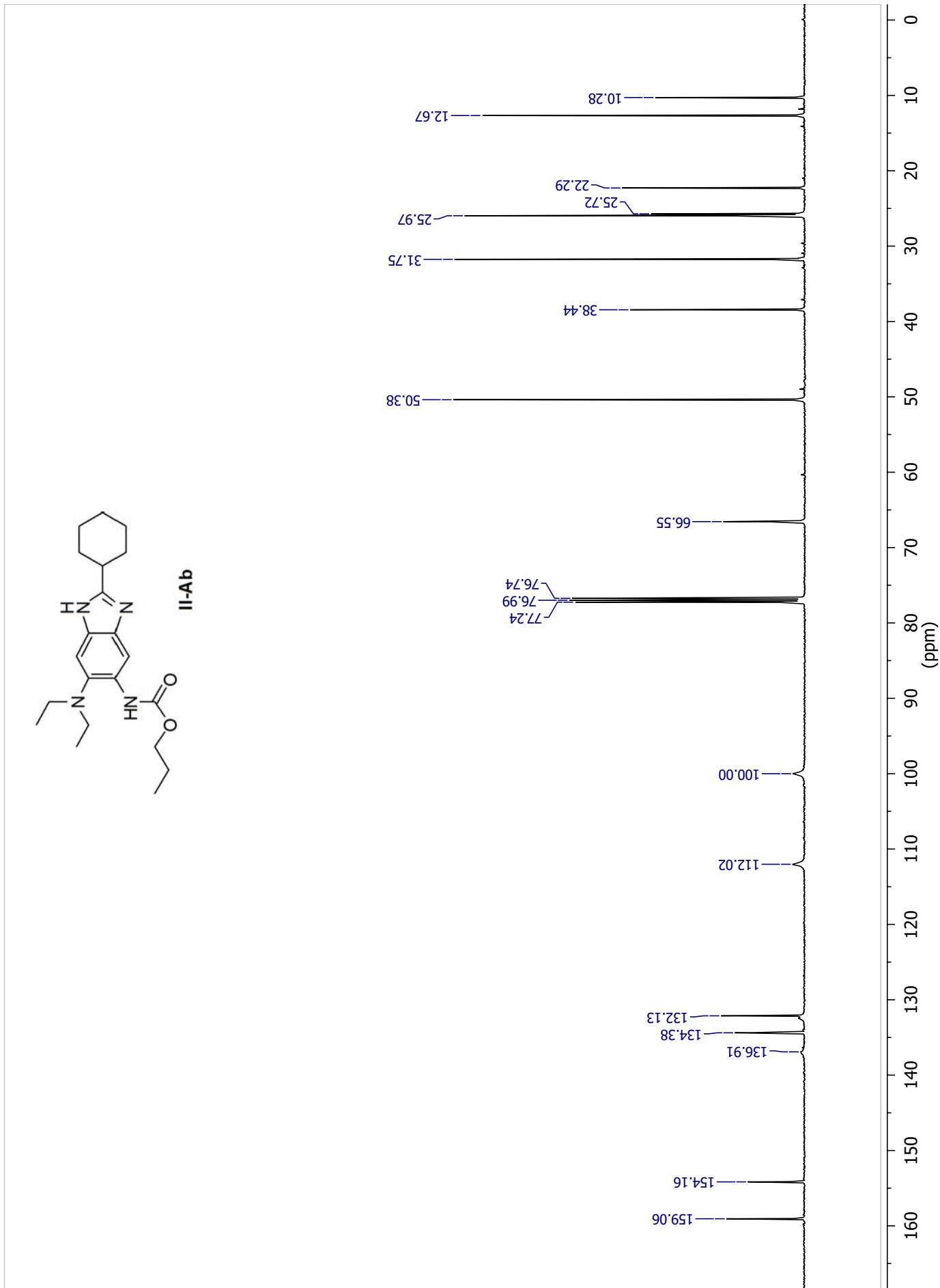


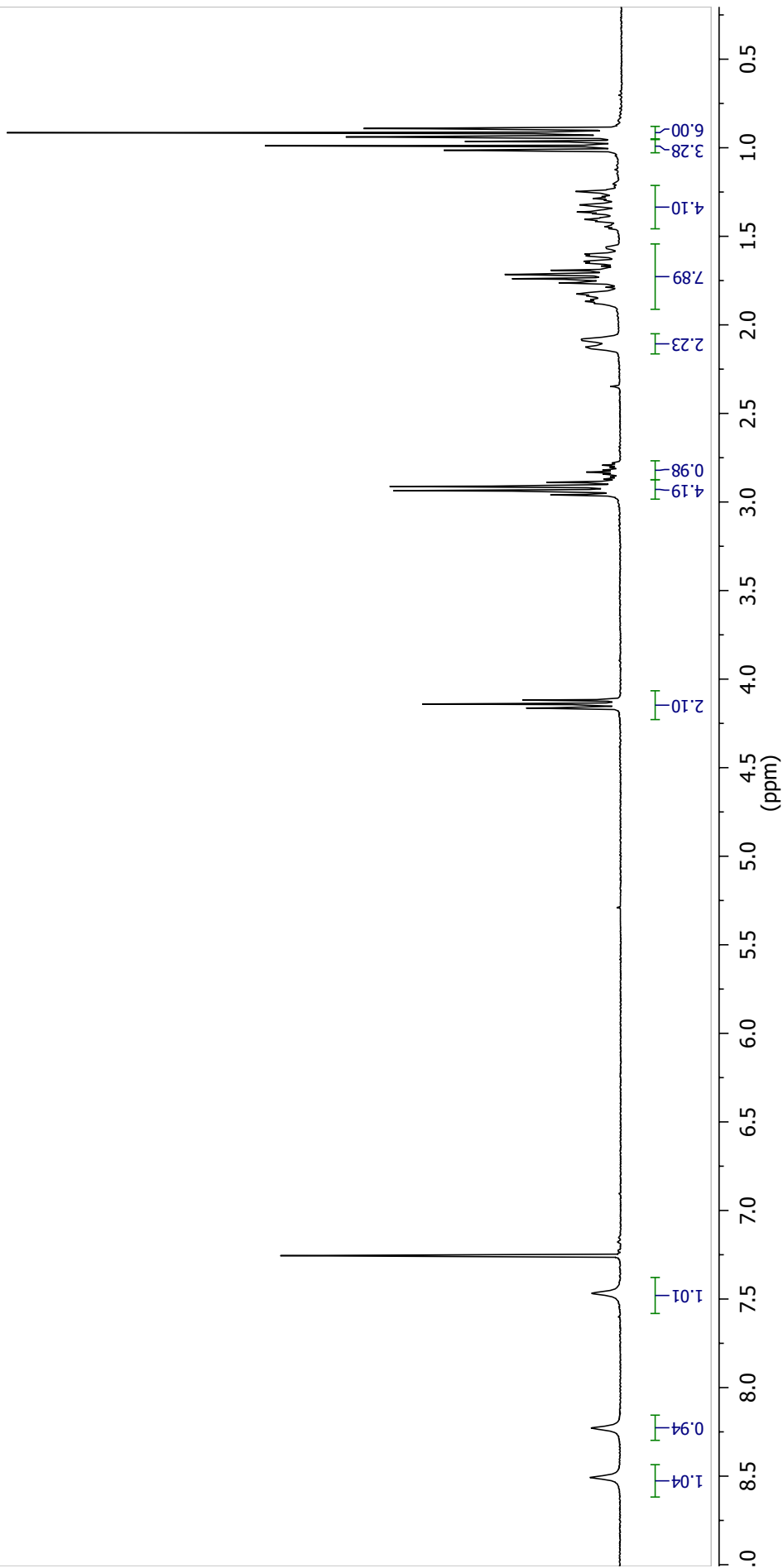
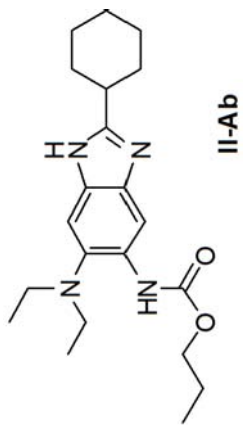
II-6g

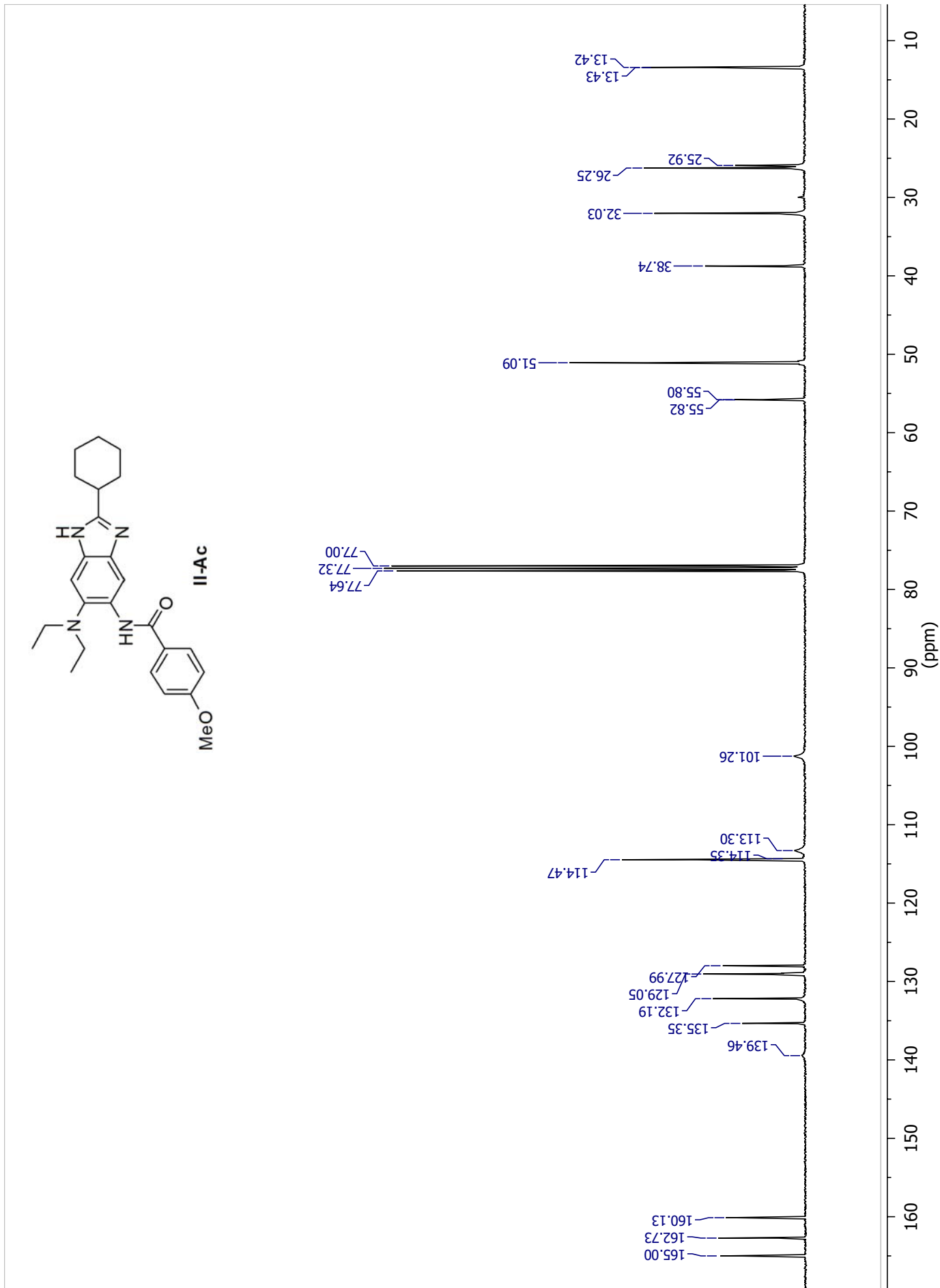


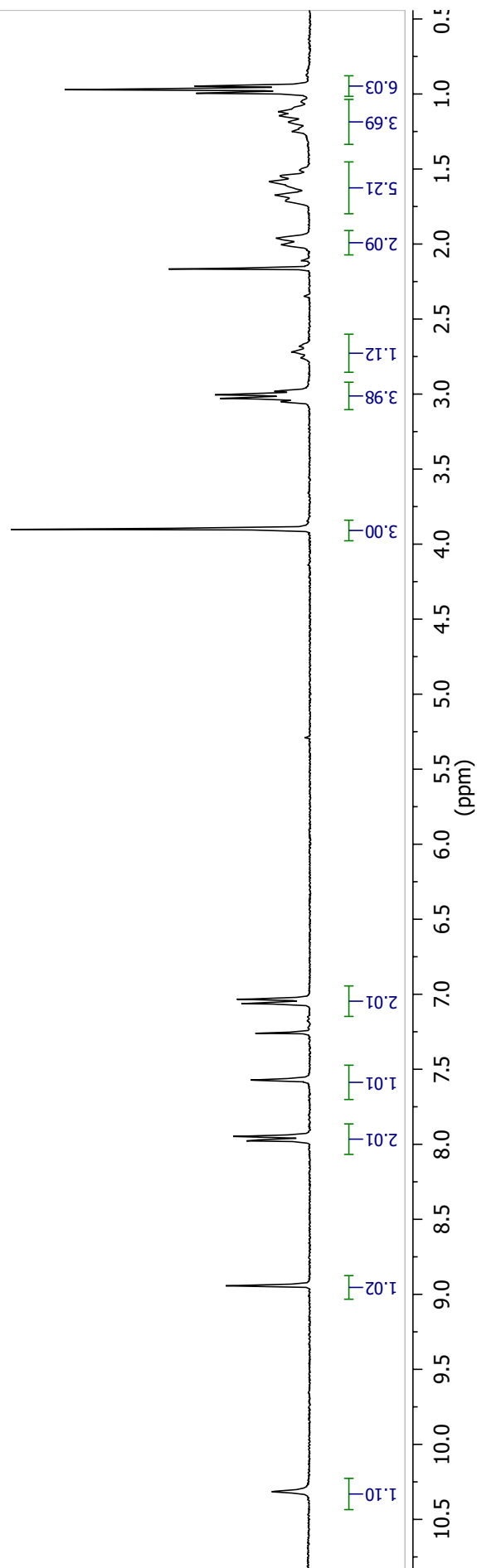
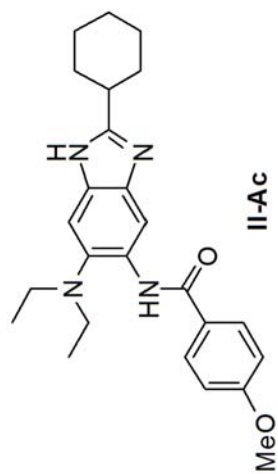


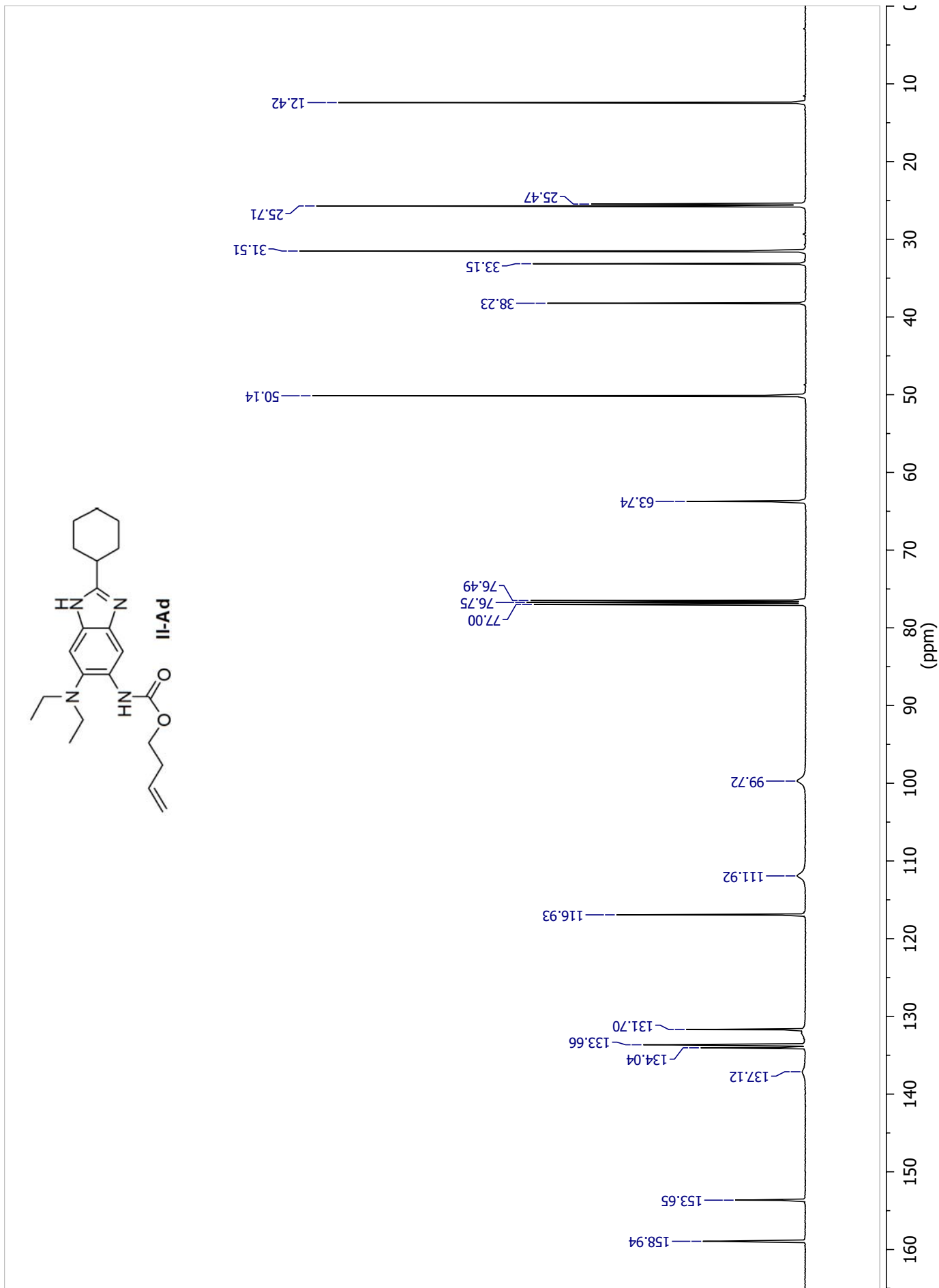


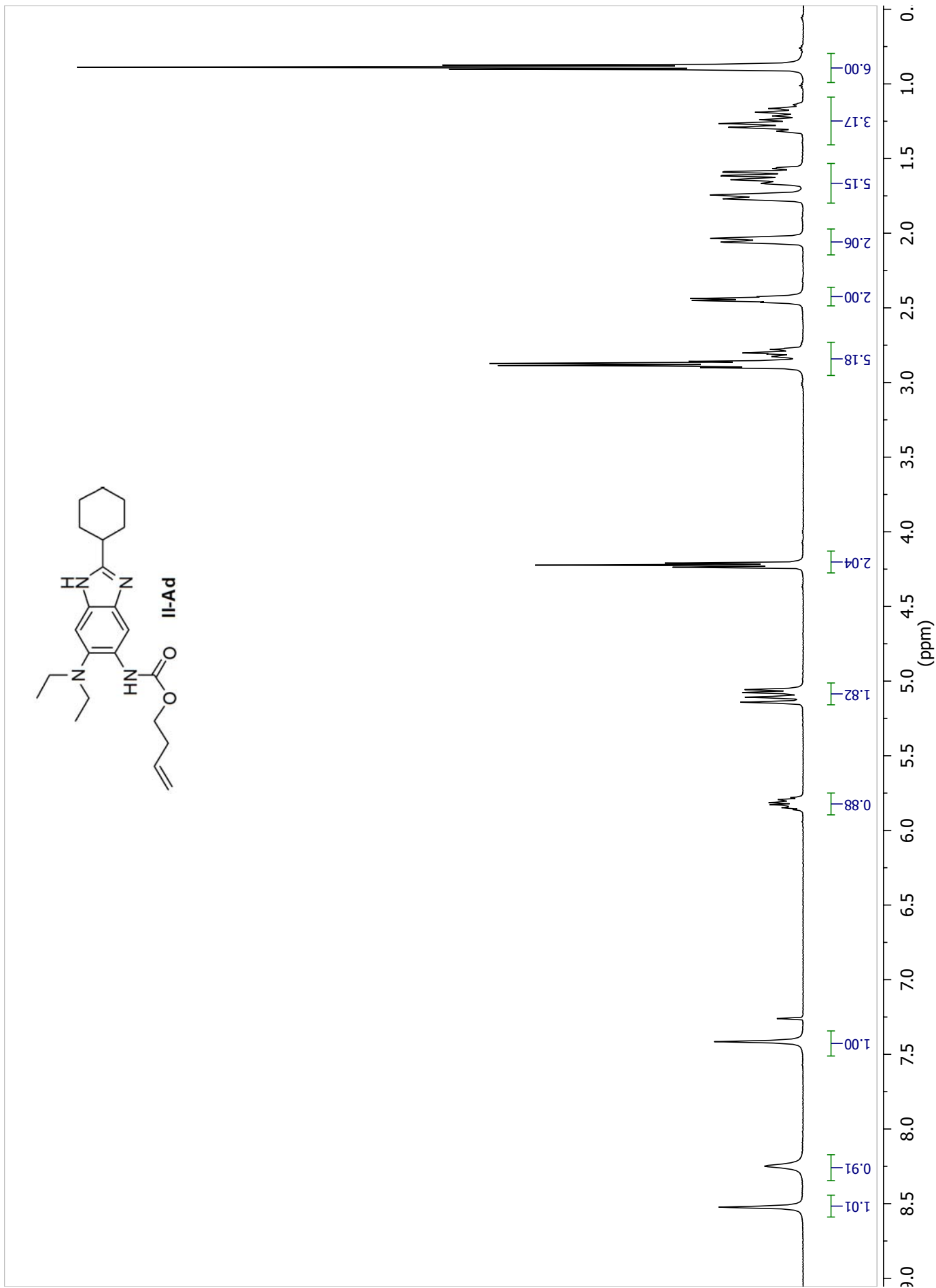


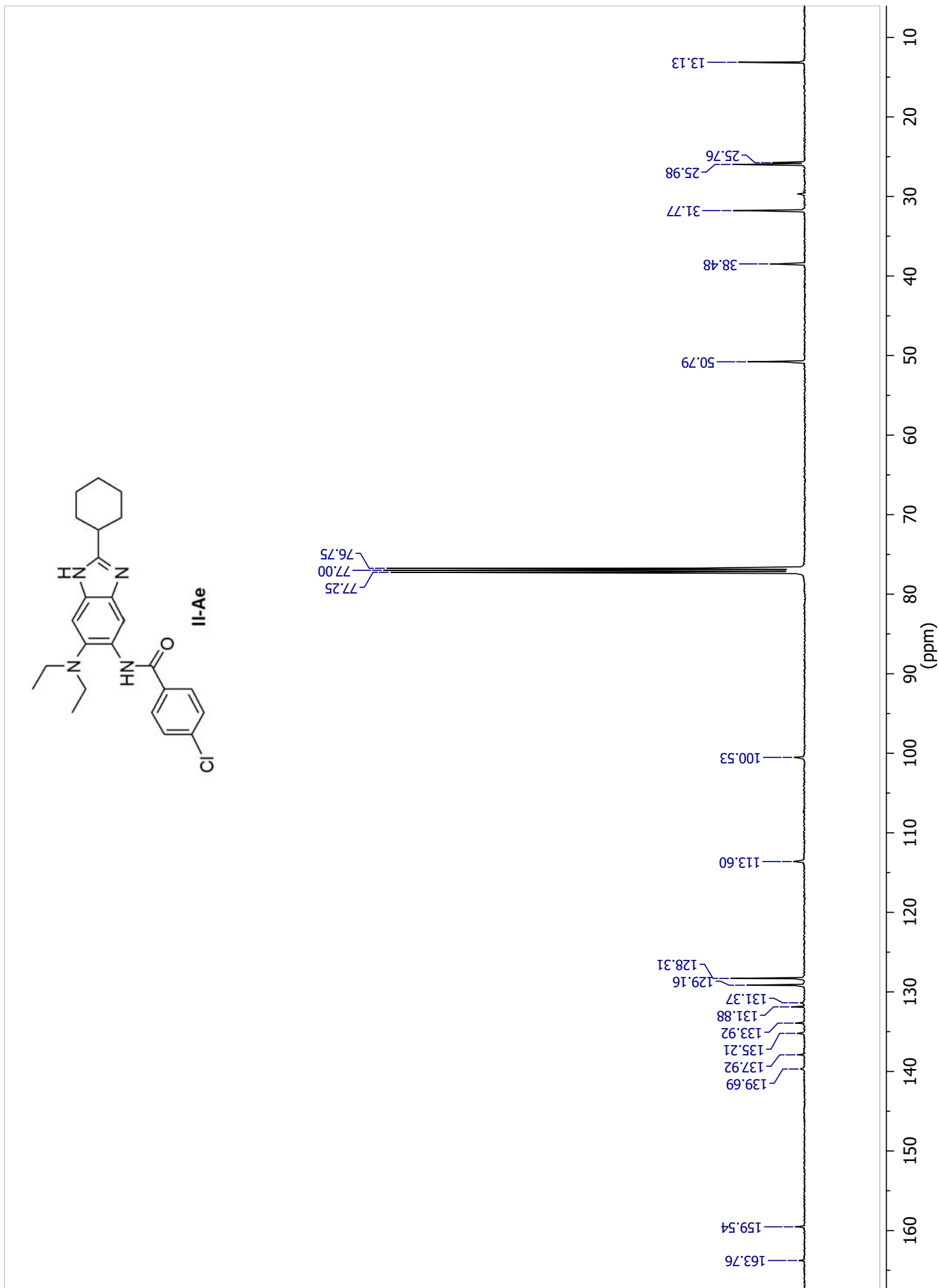


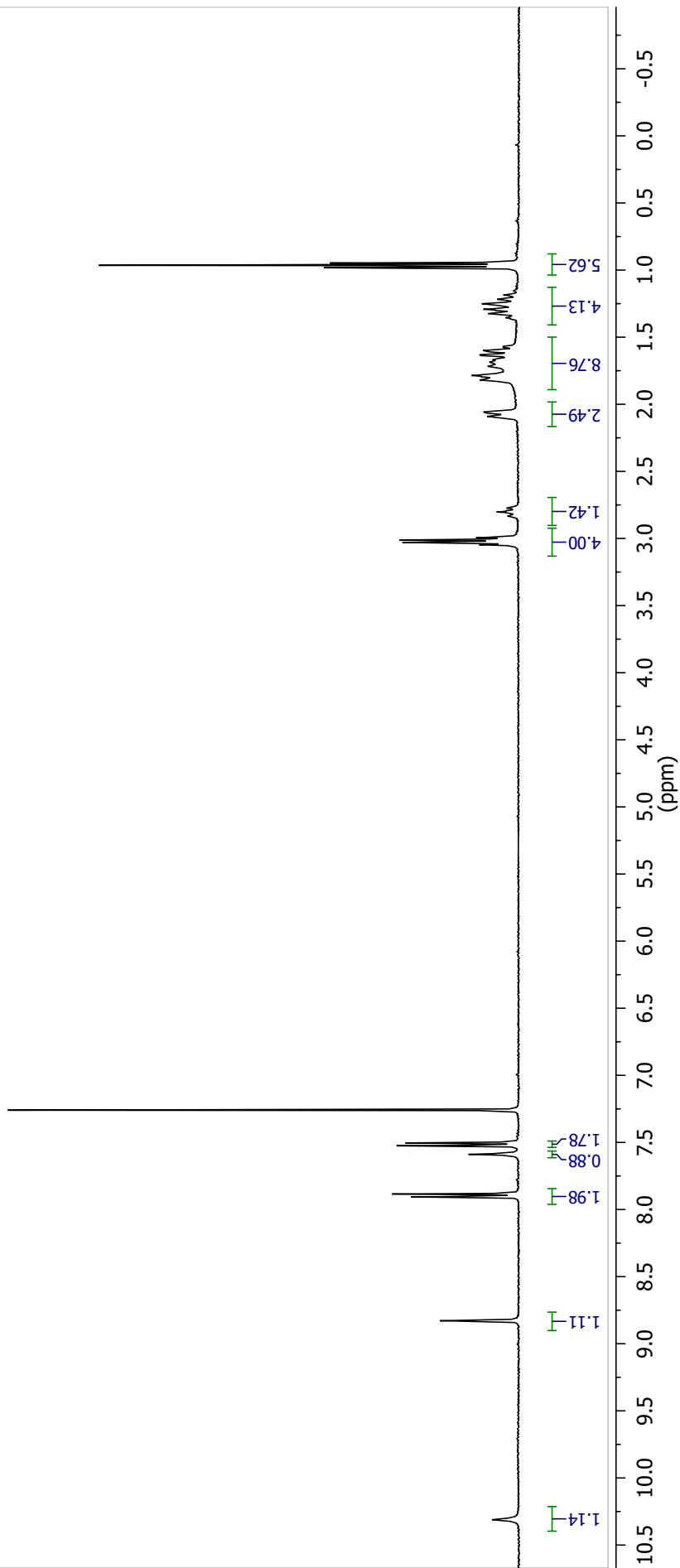
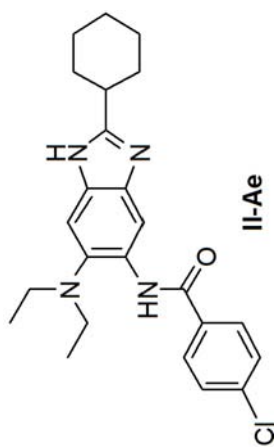


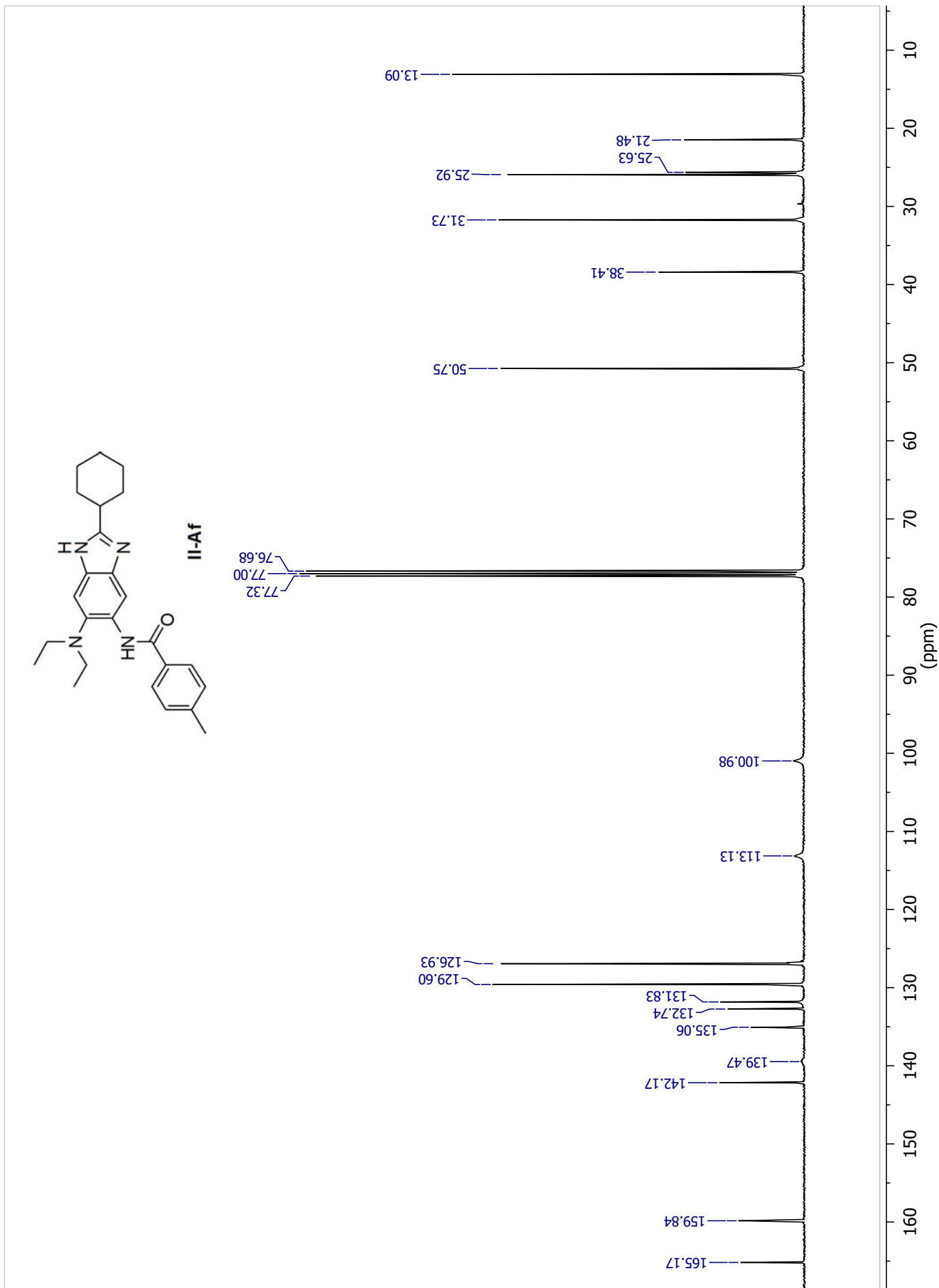


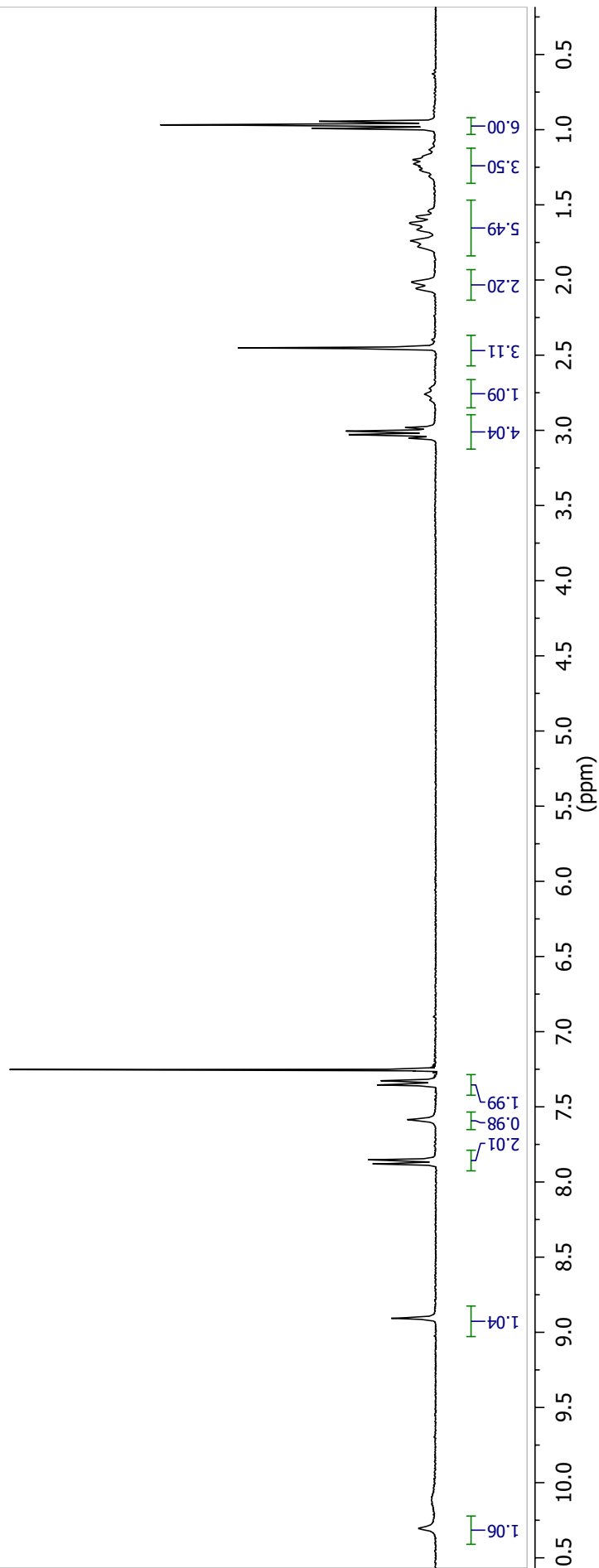
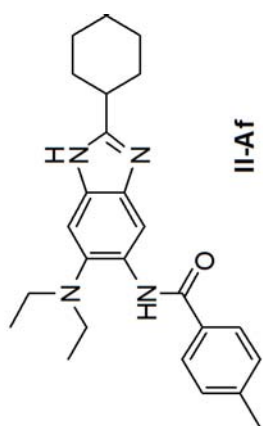


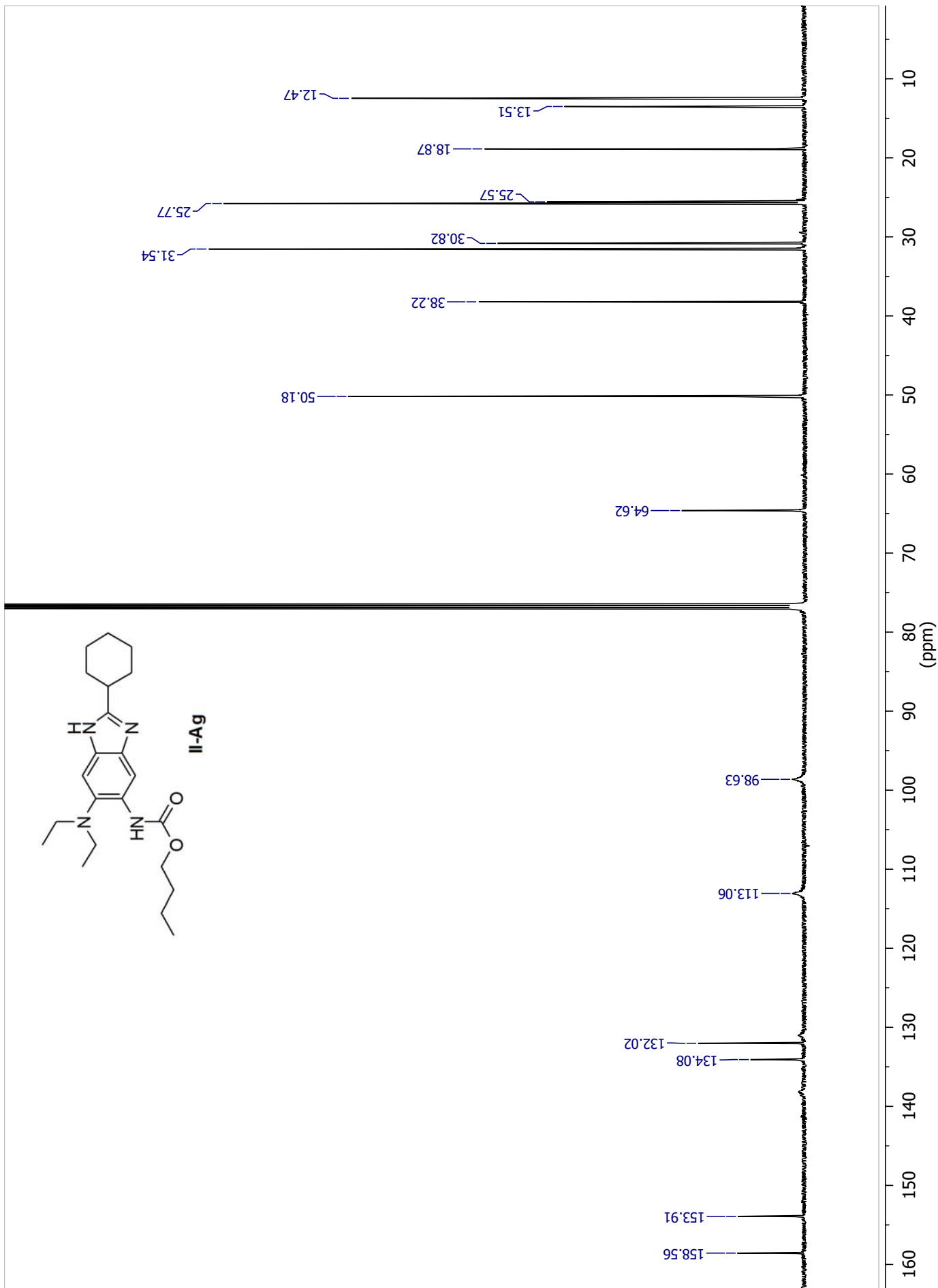


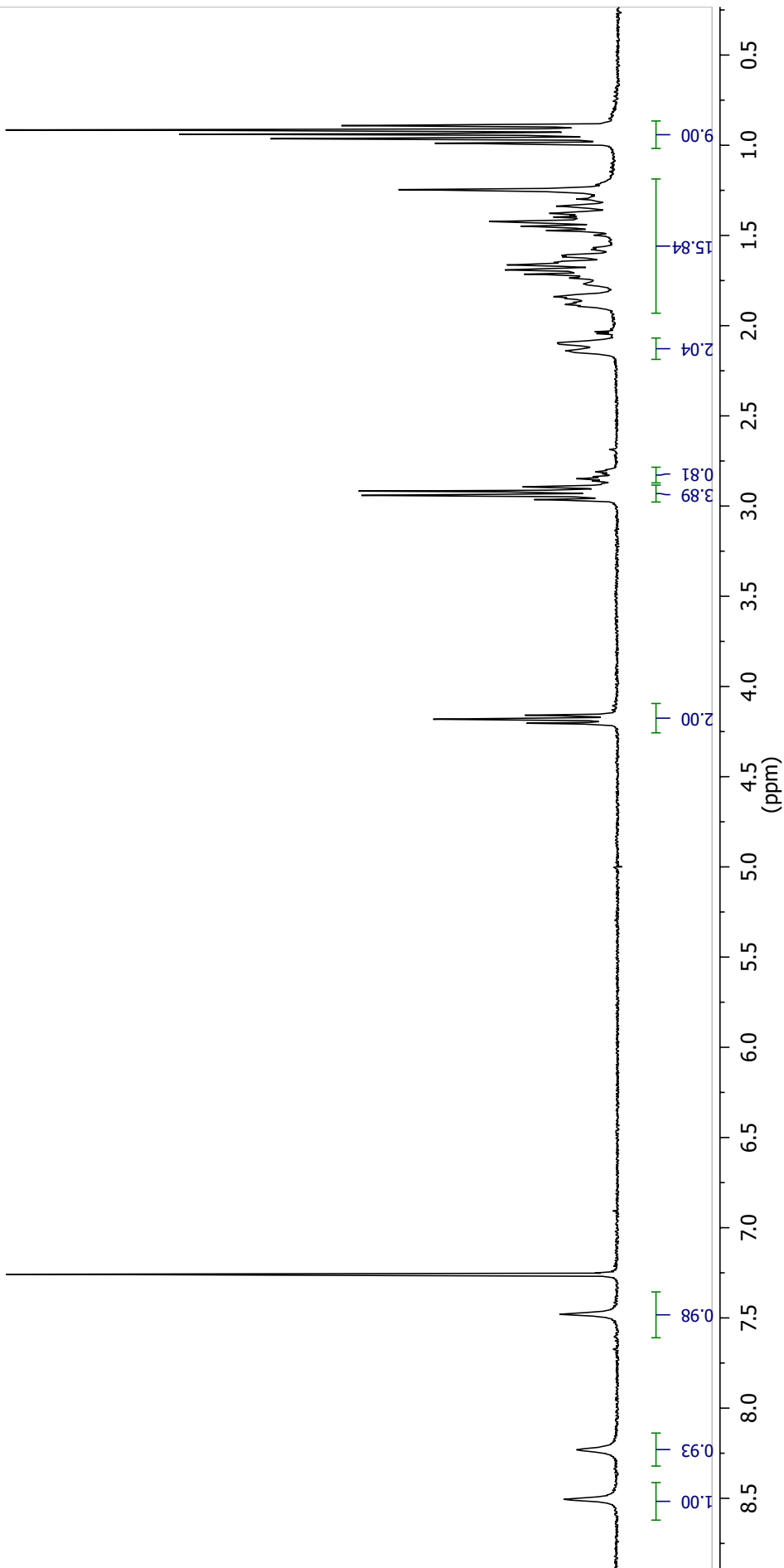
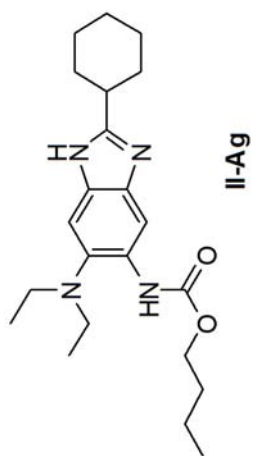


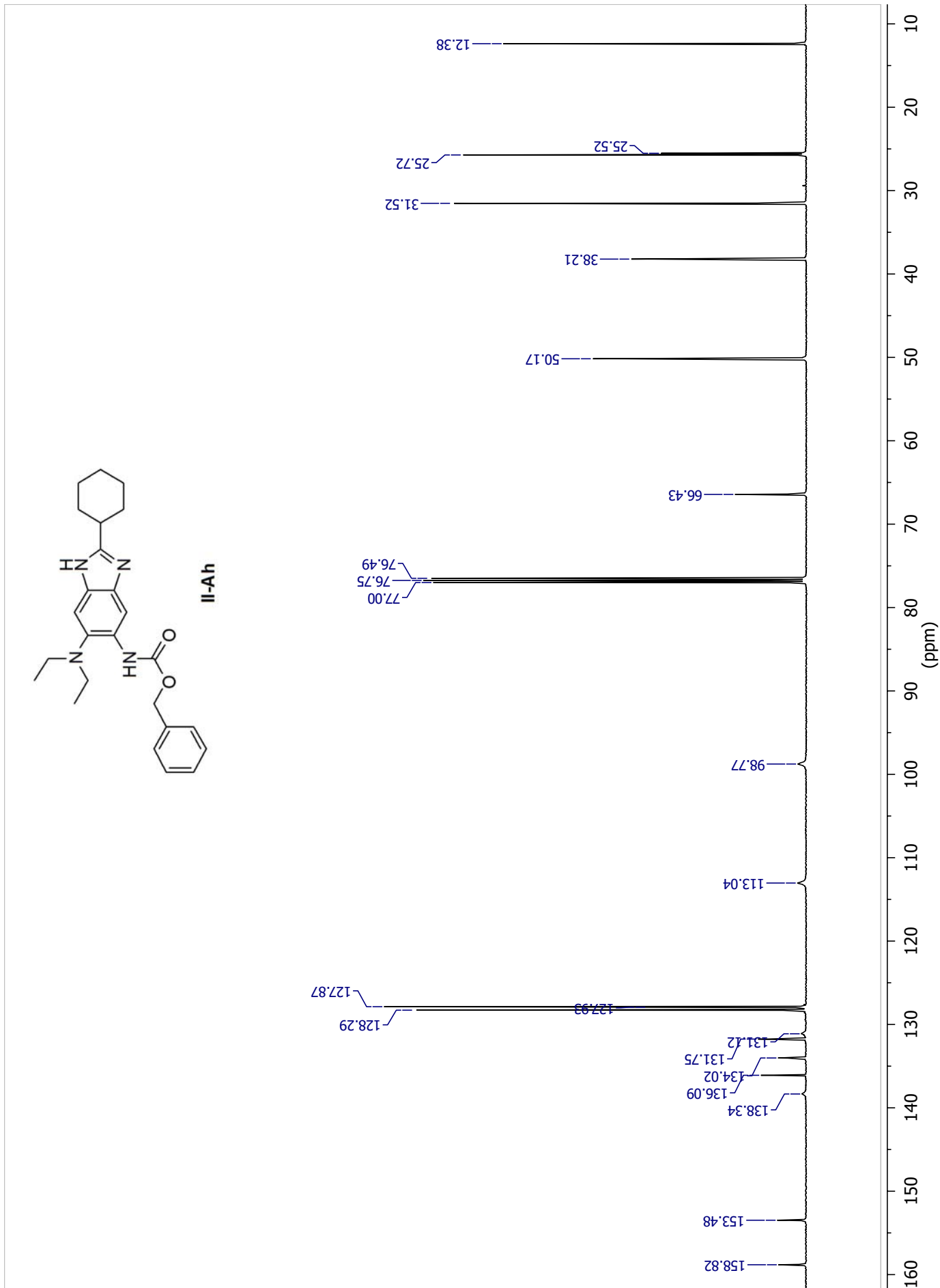


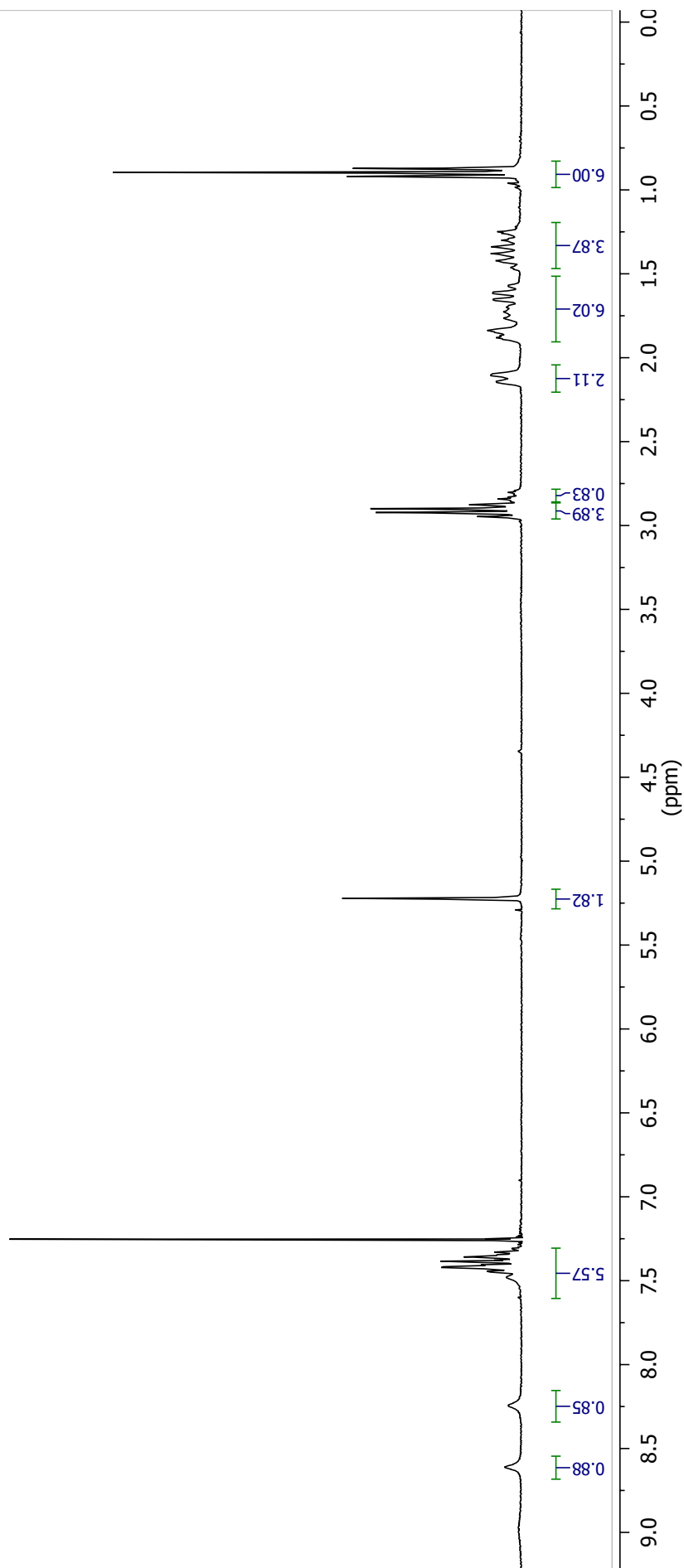
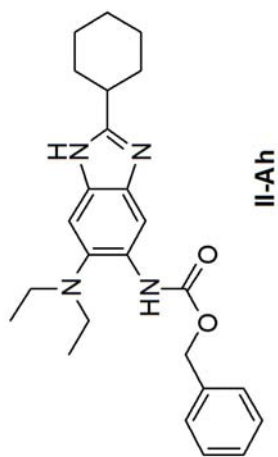


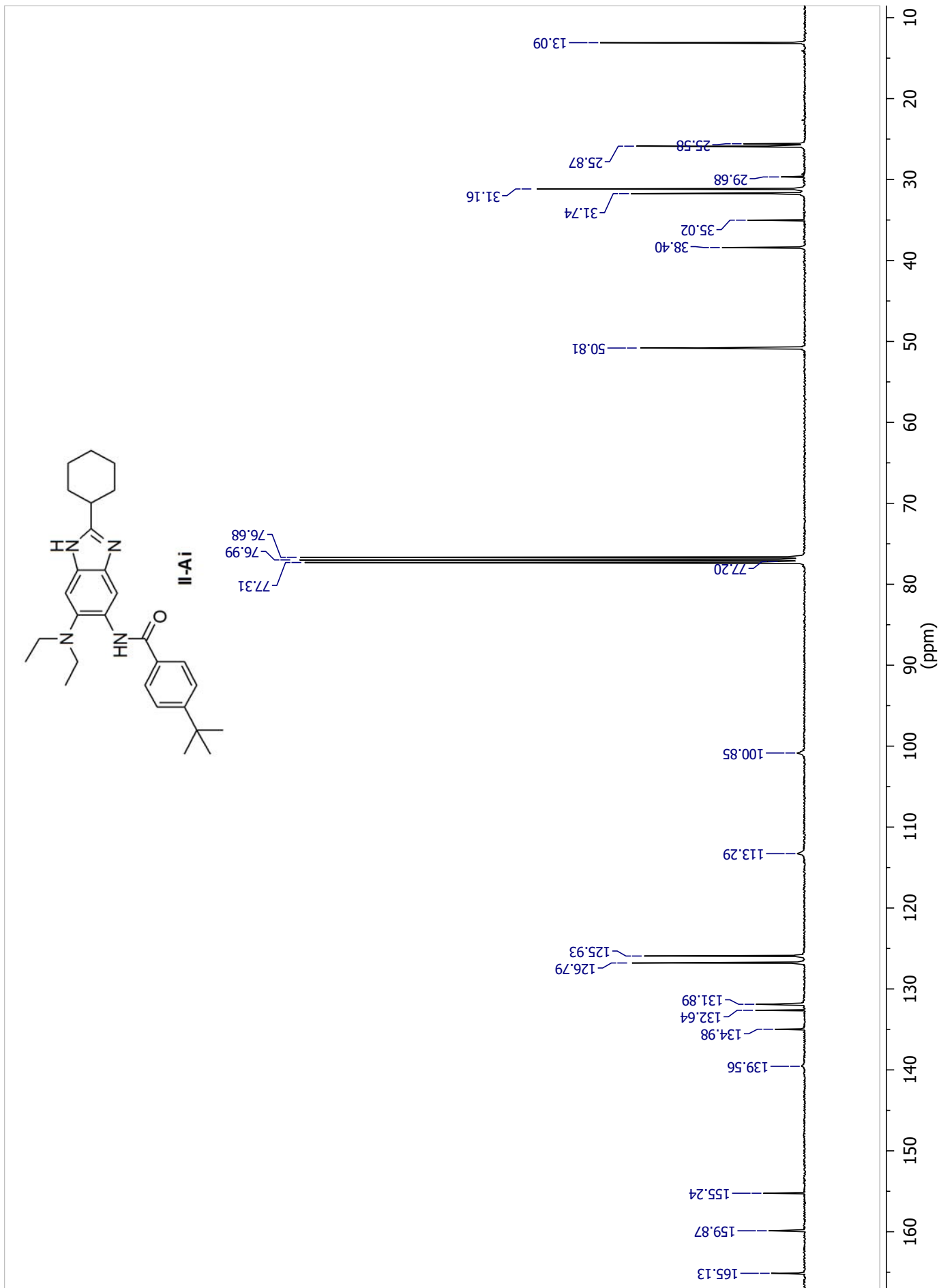


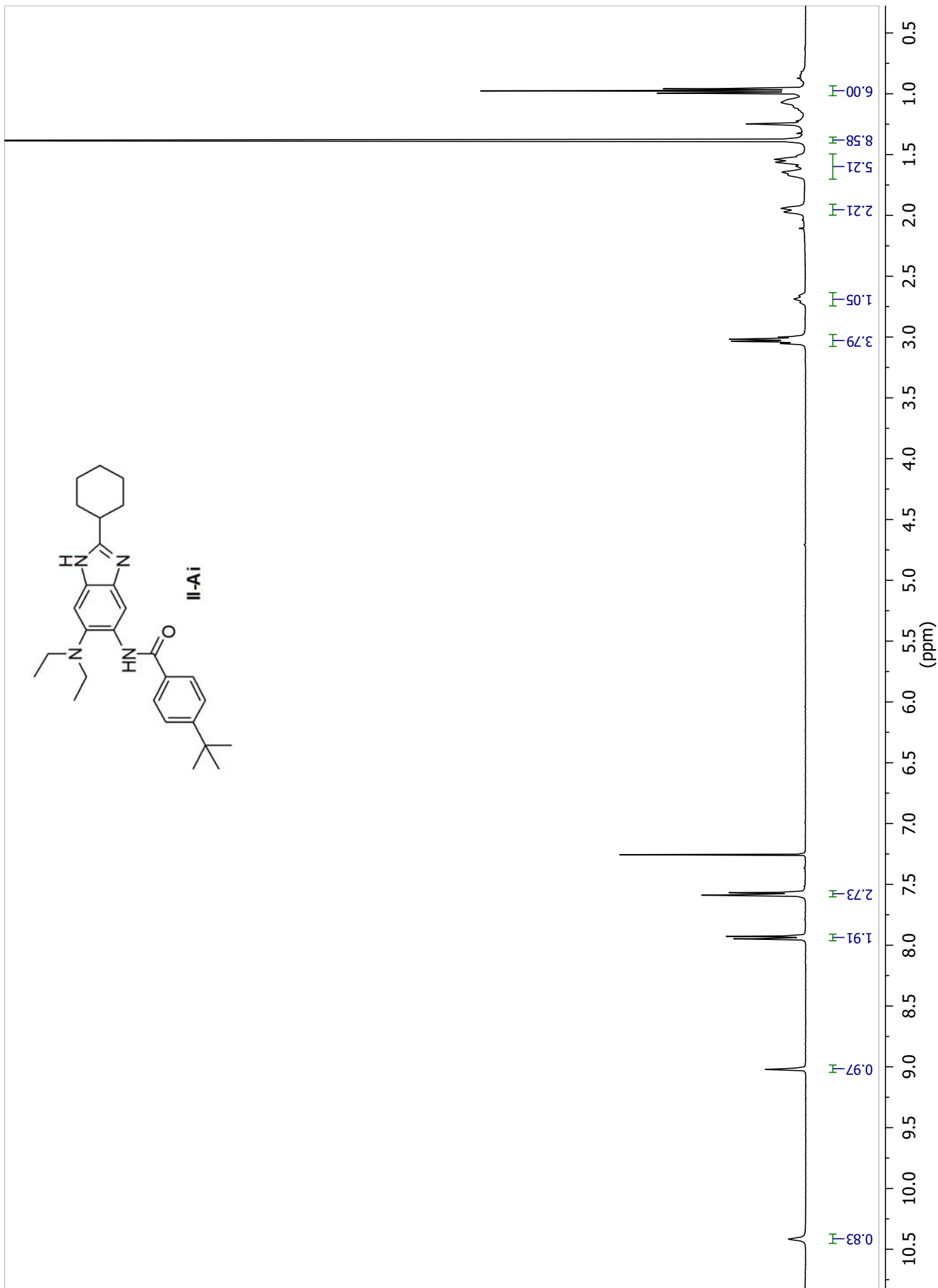


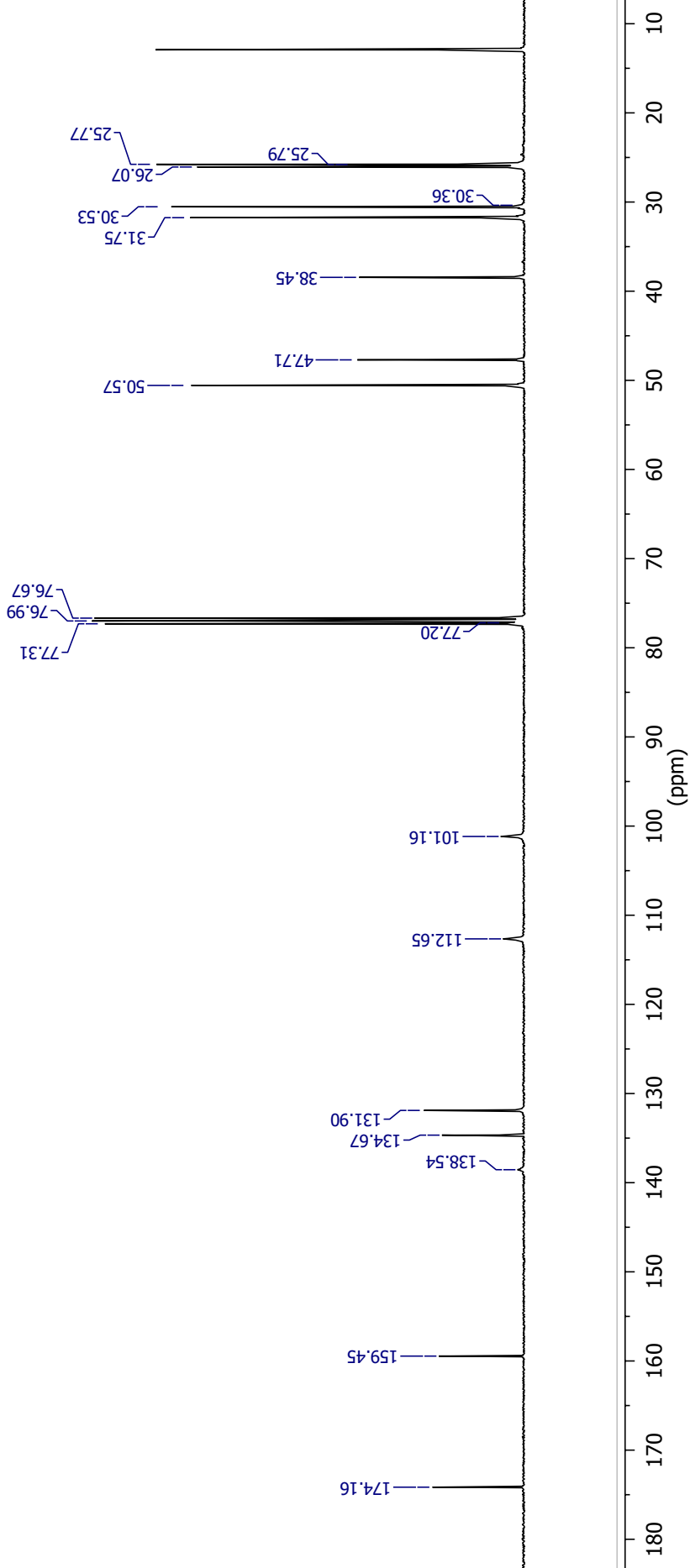
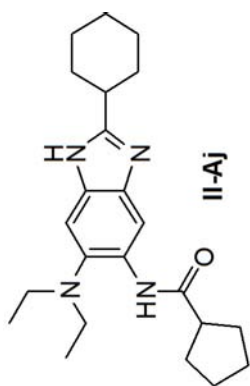


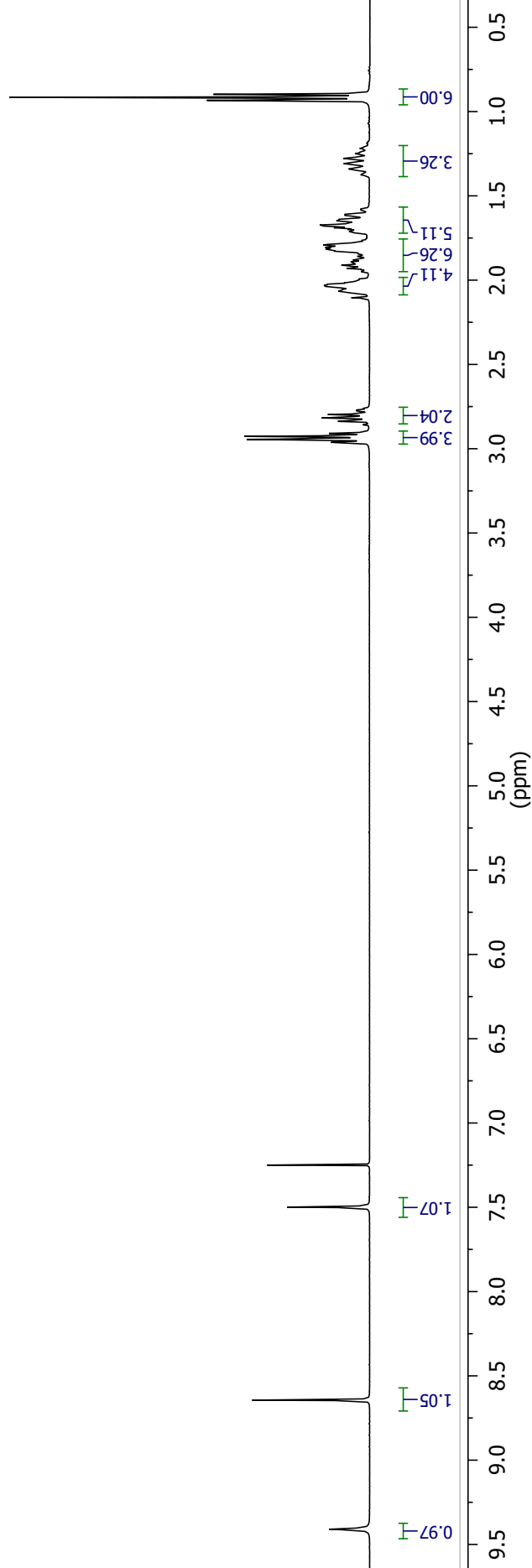
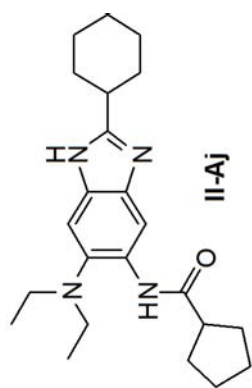


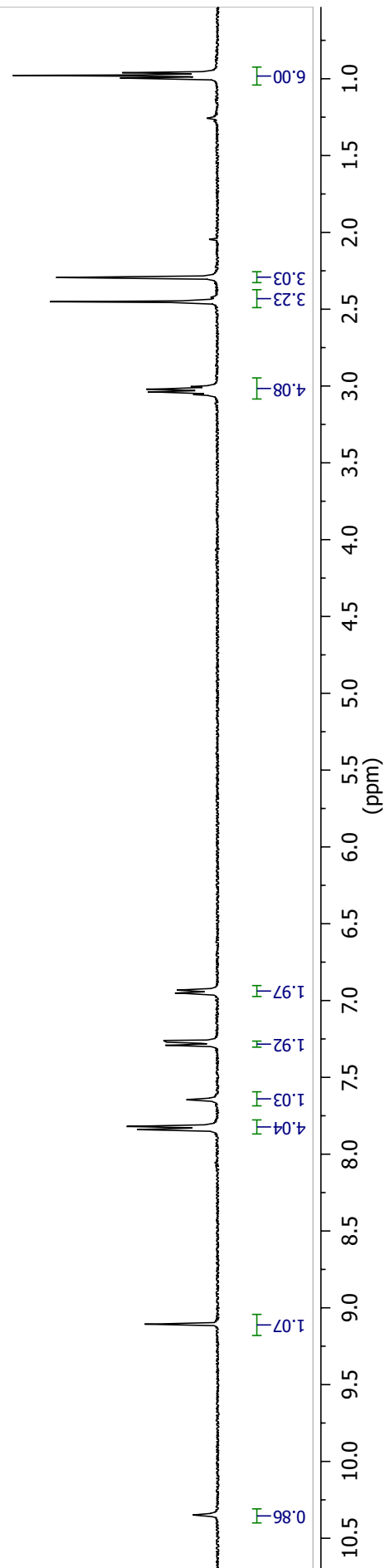
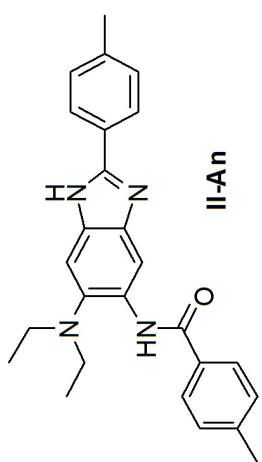


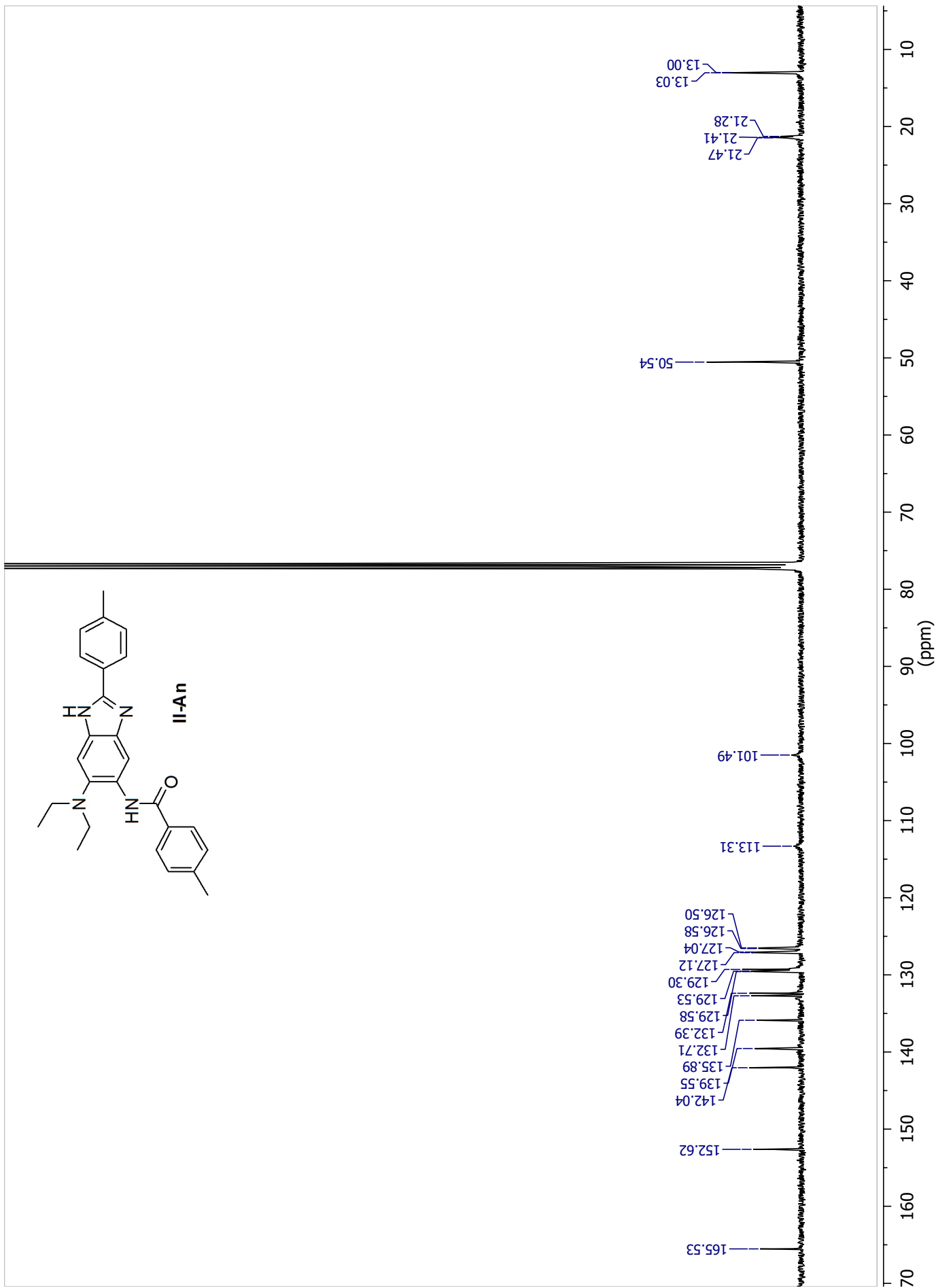


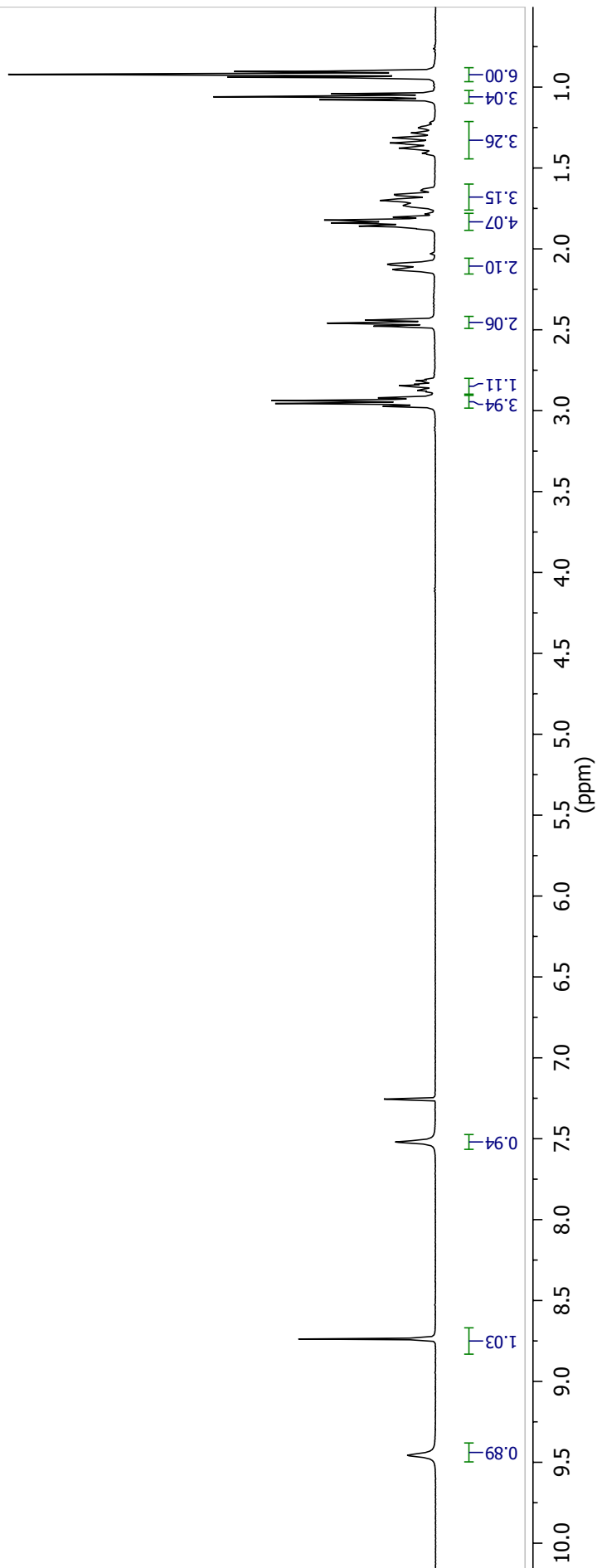
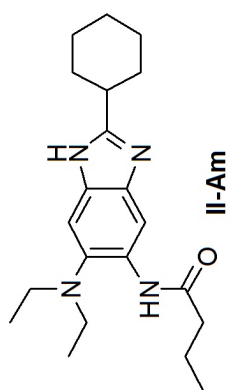


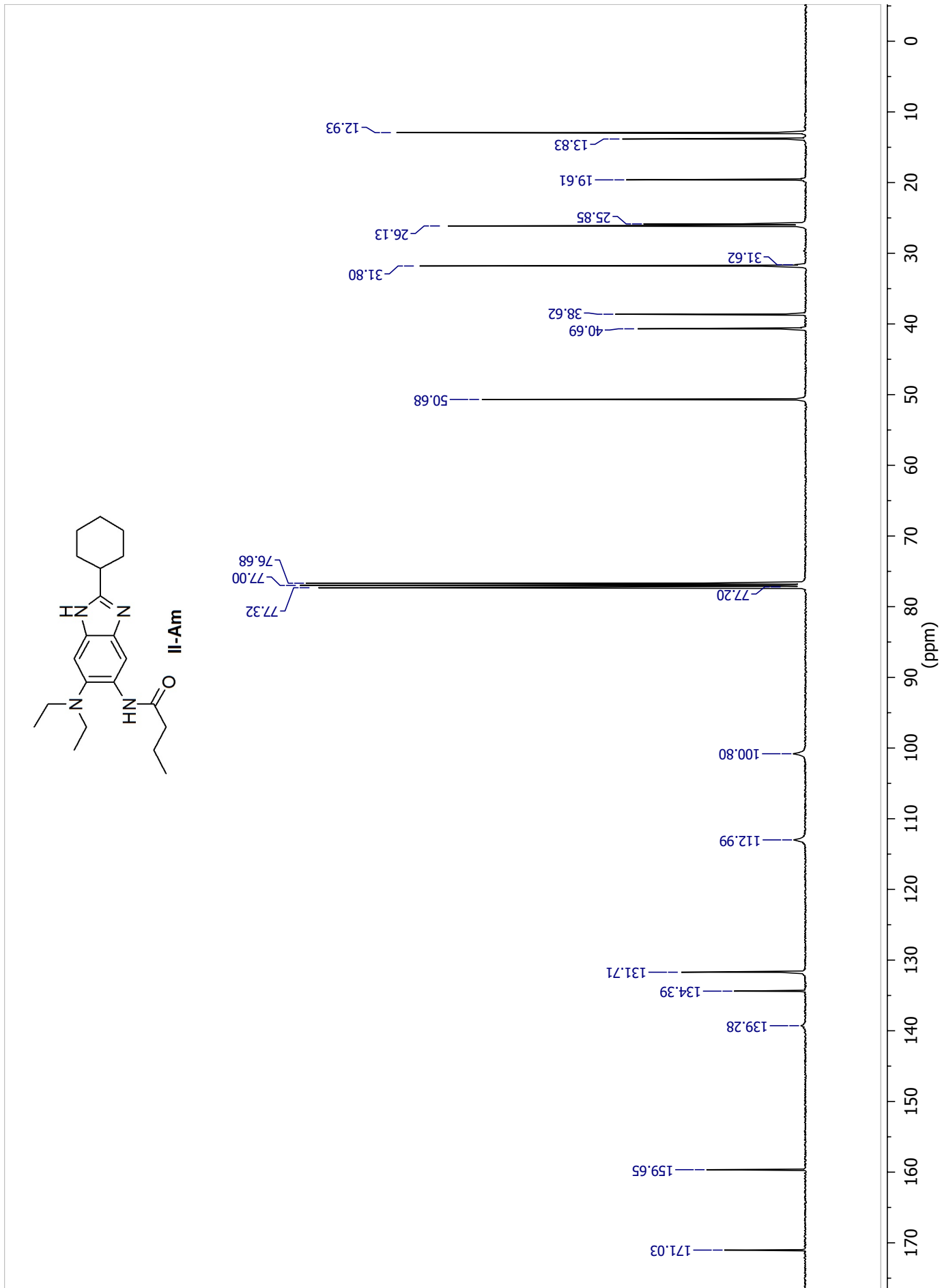


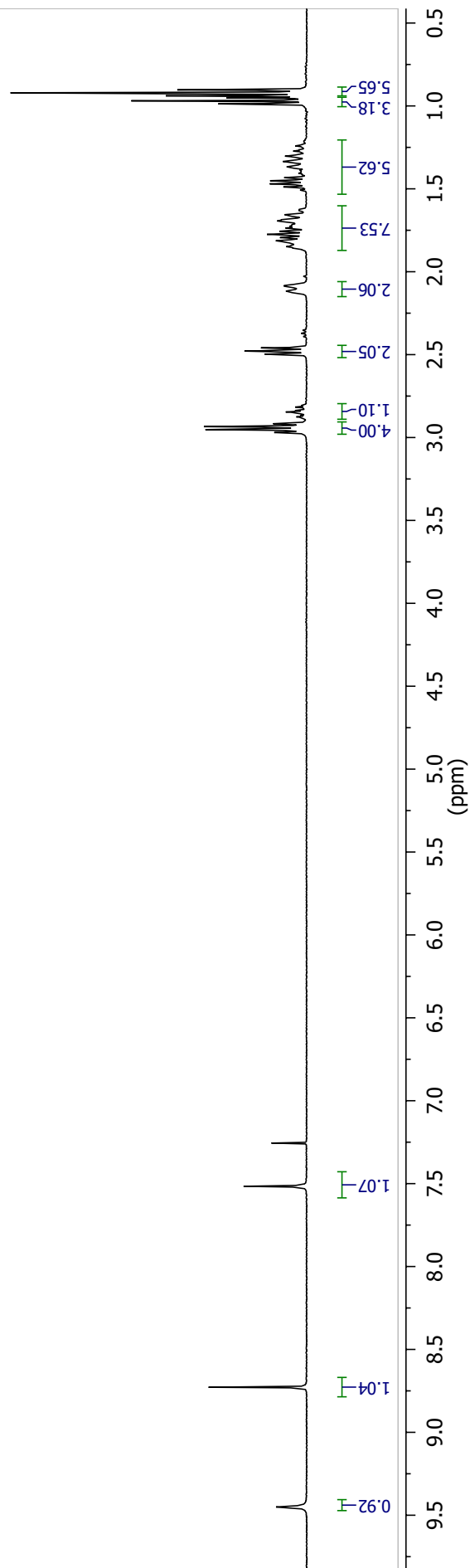
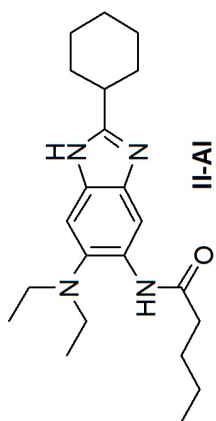


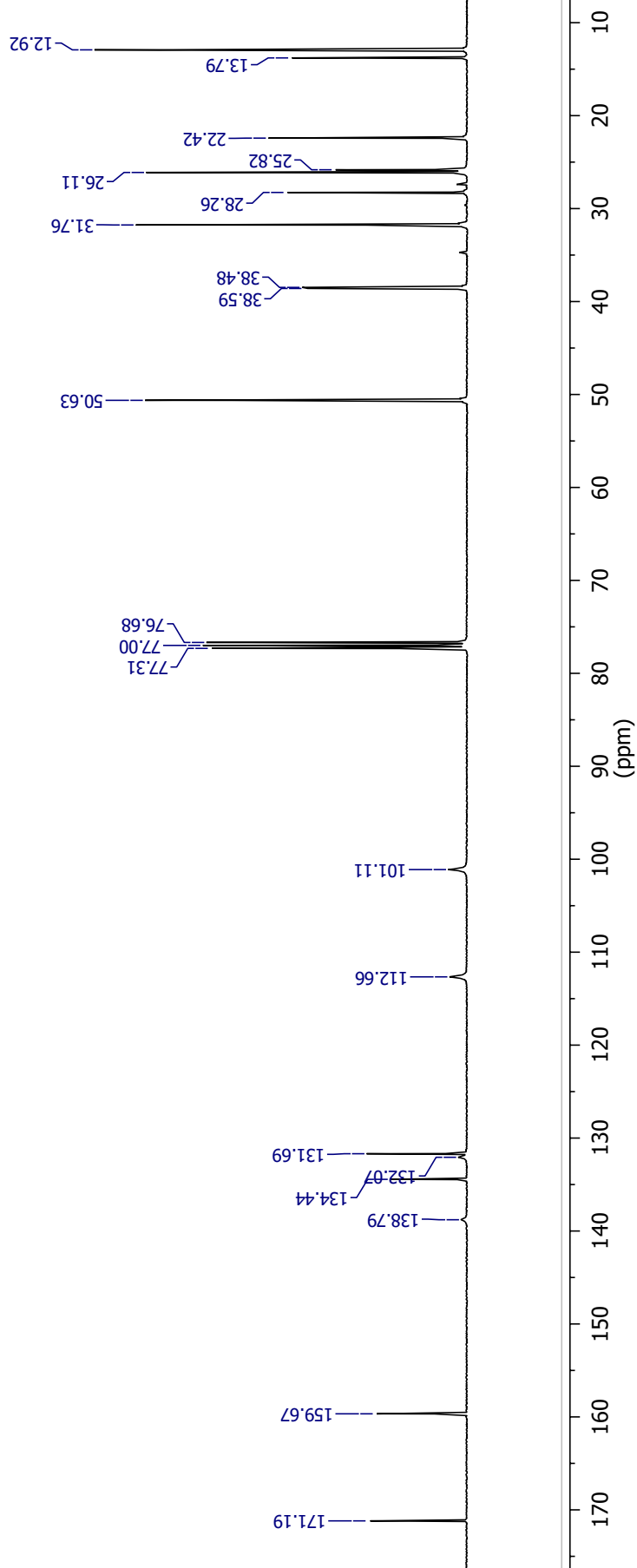
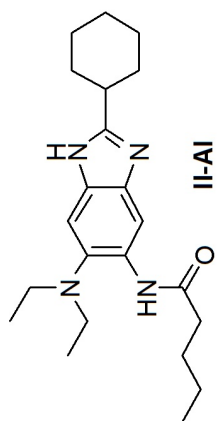


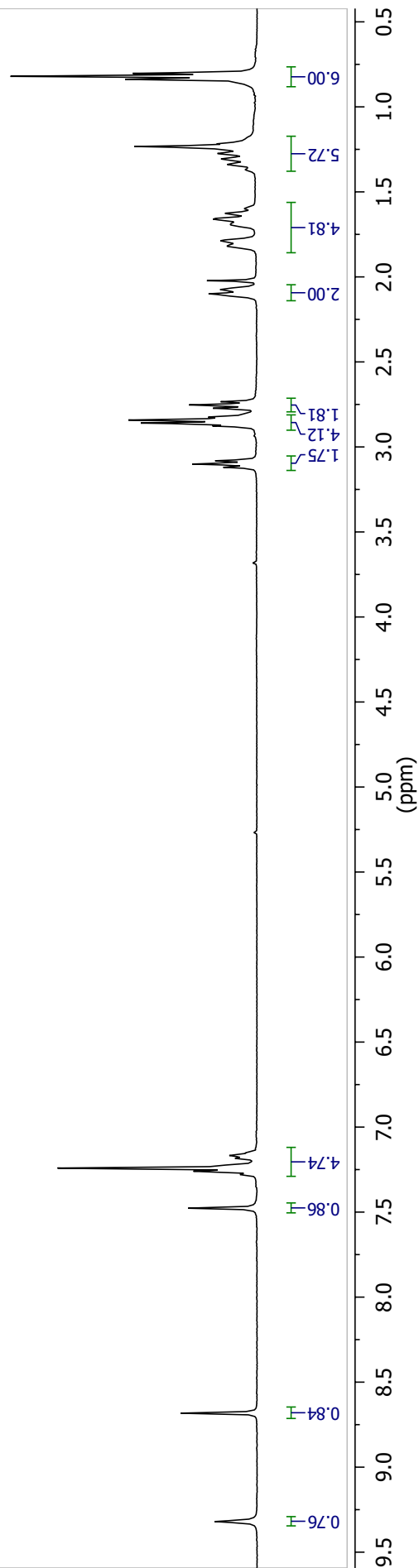
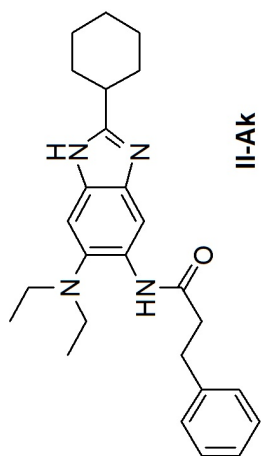


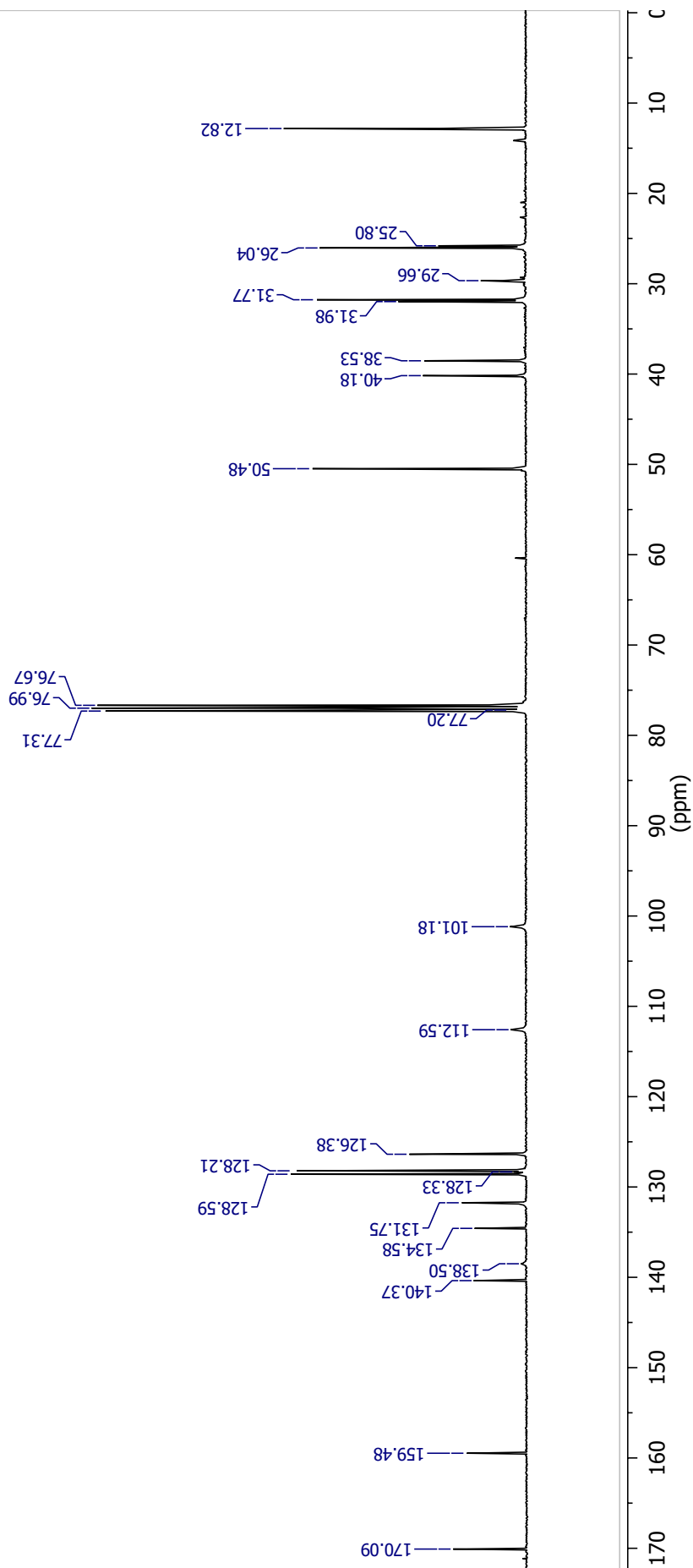
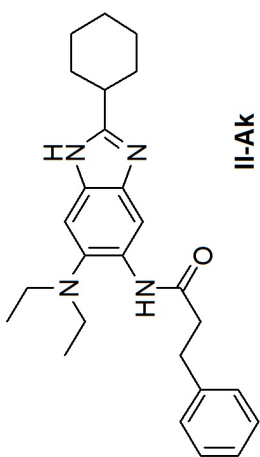


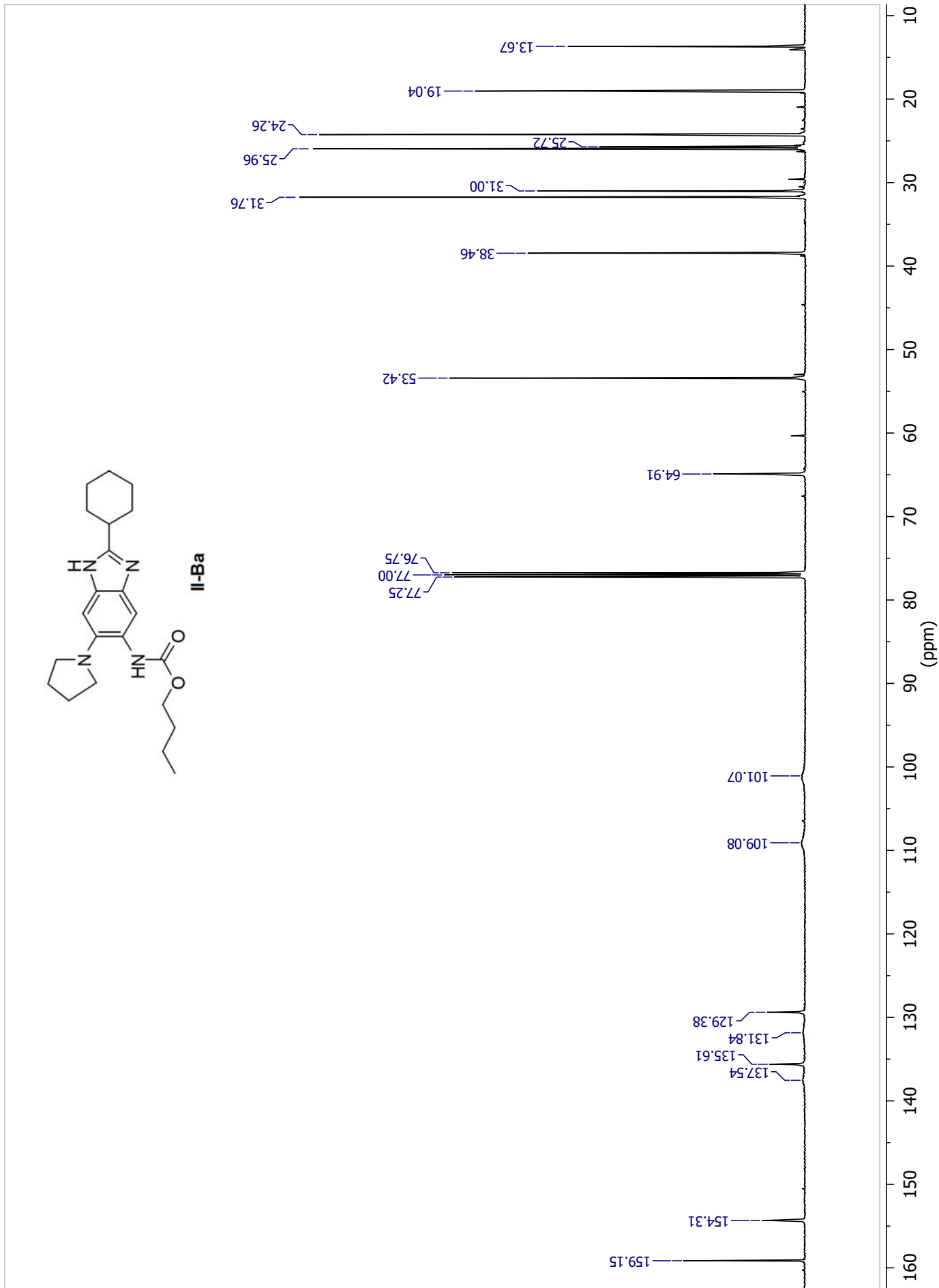


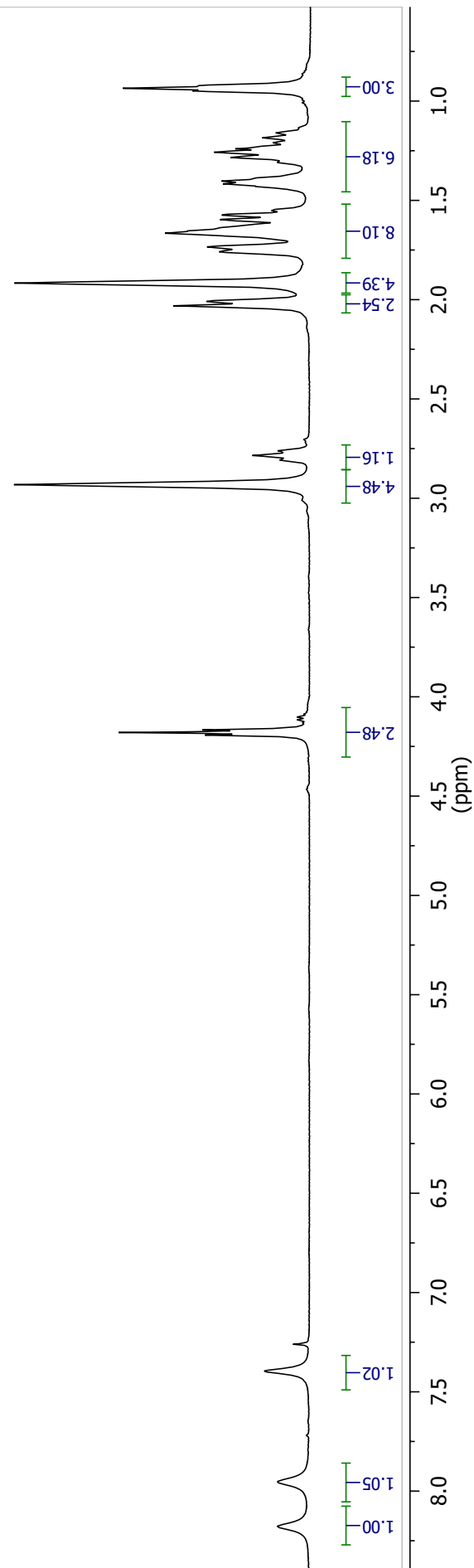
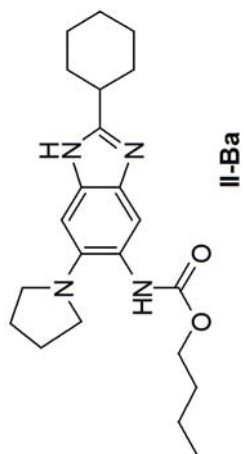


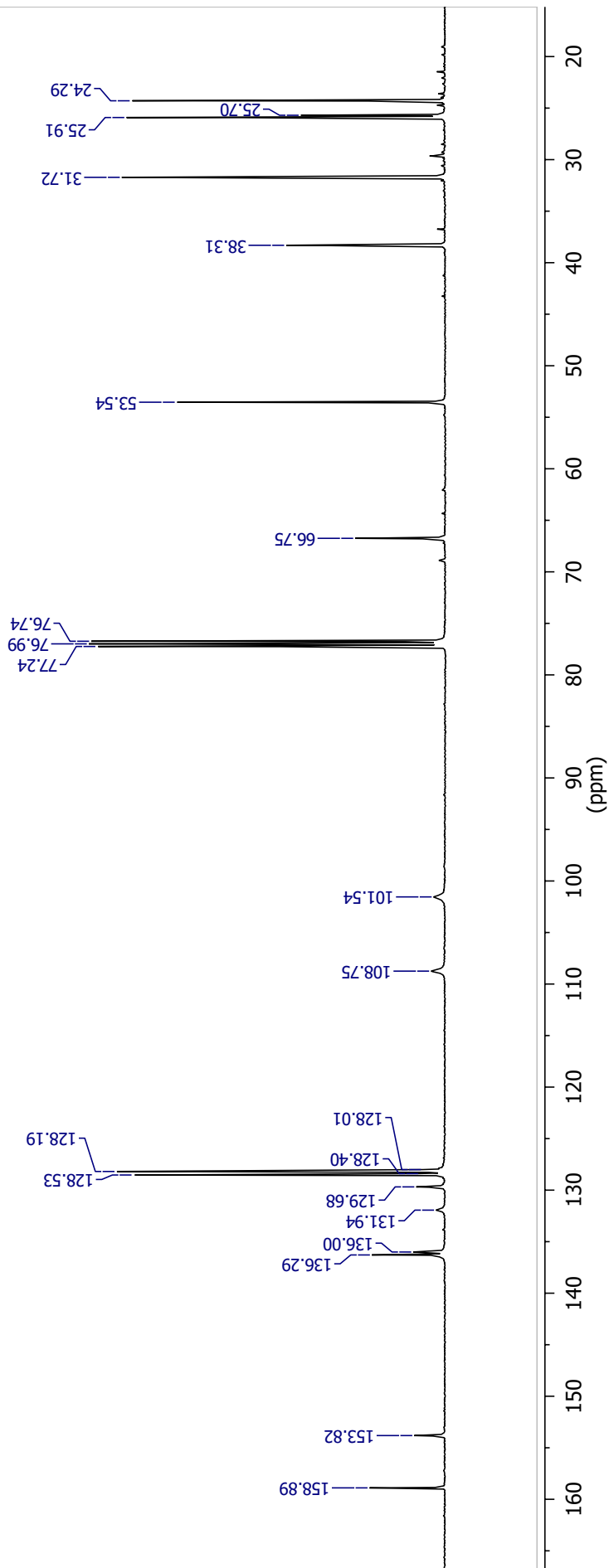
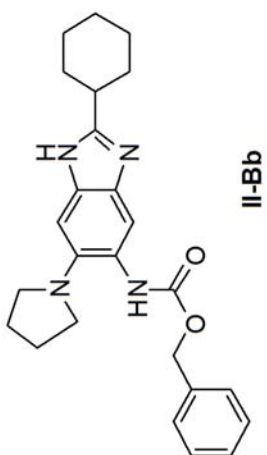


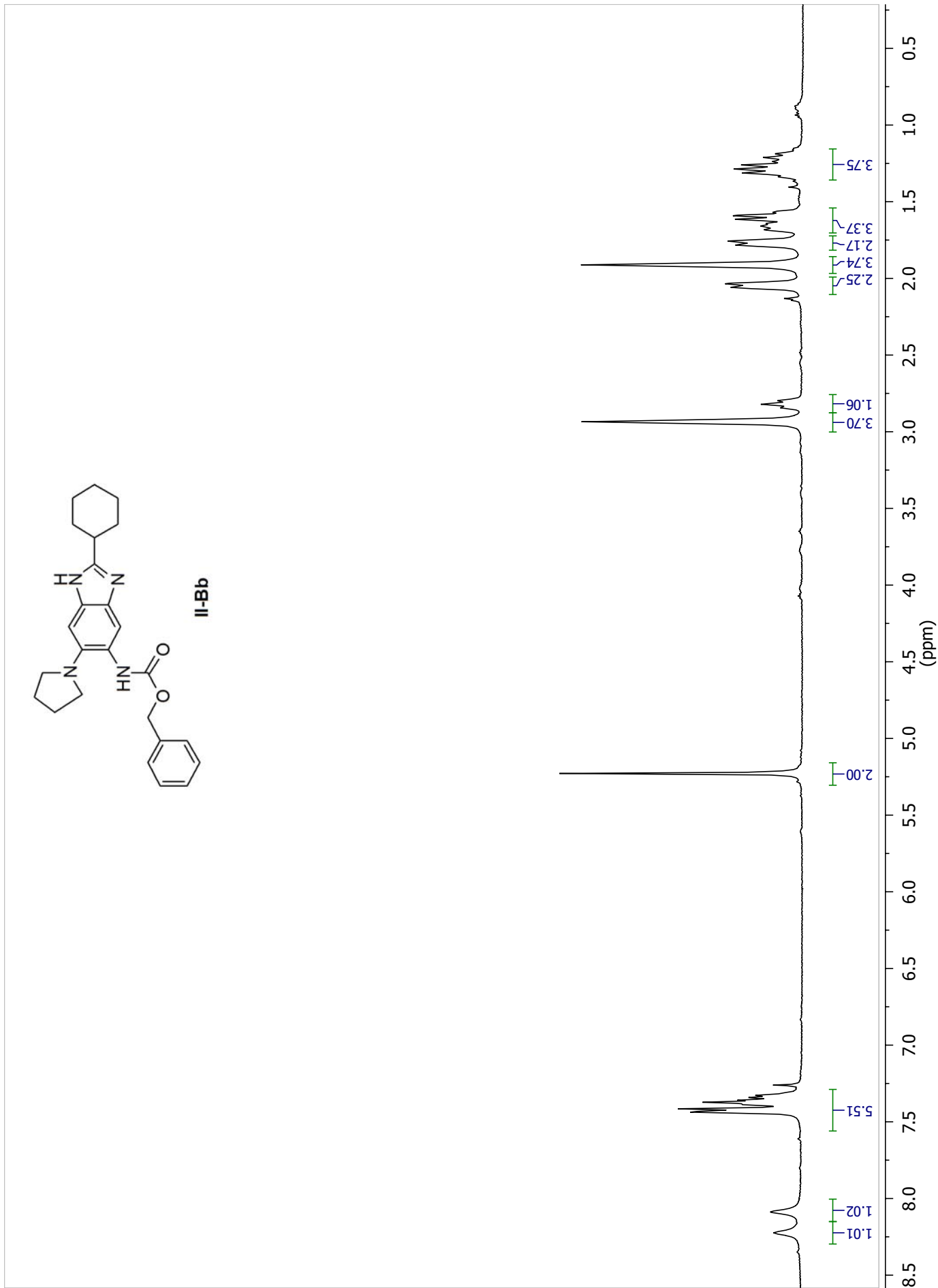


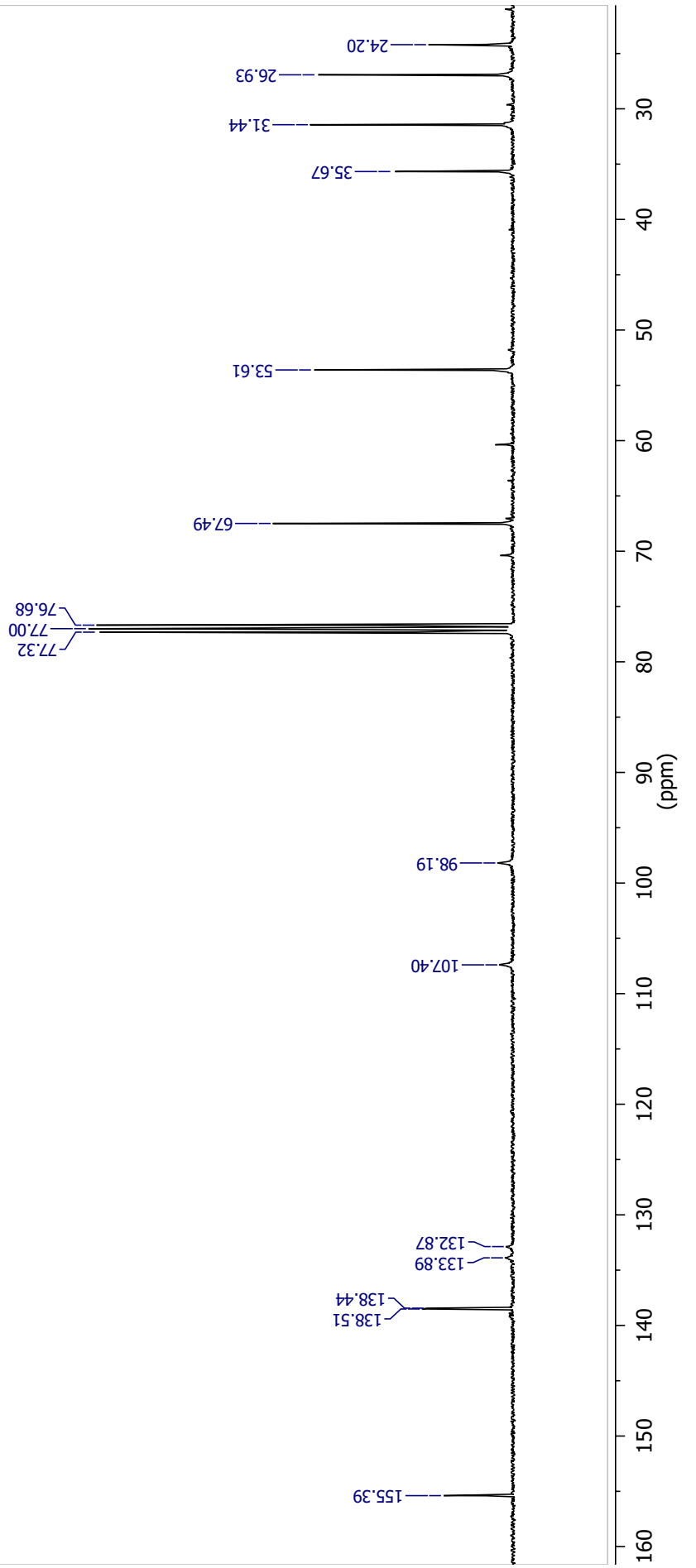
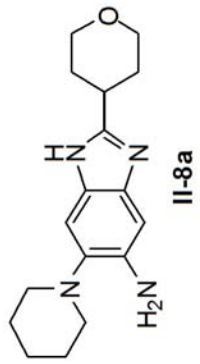


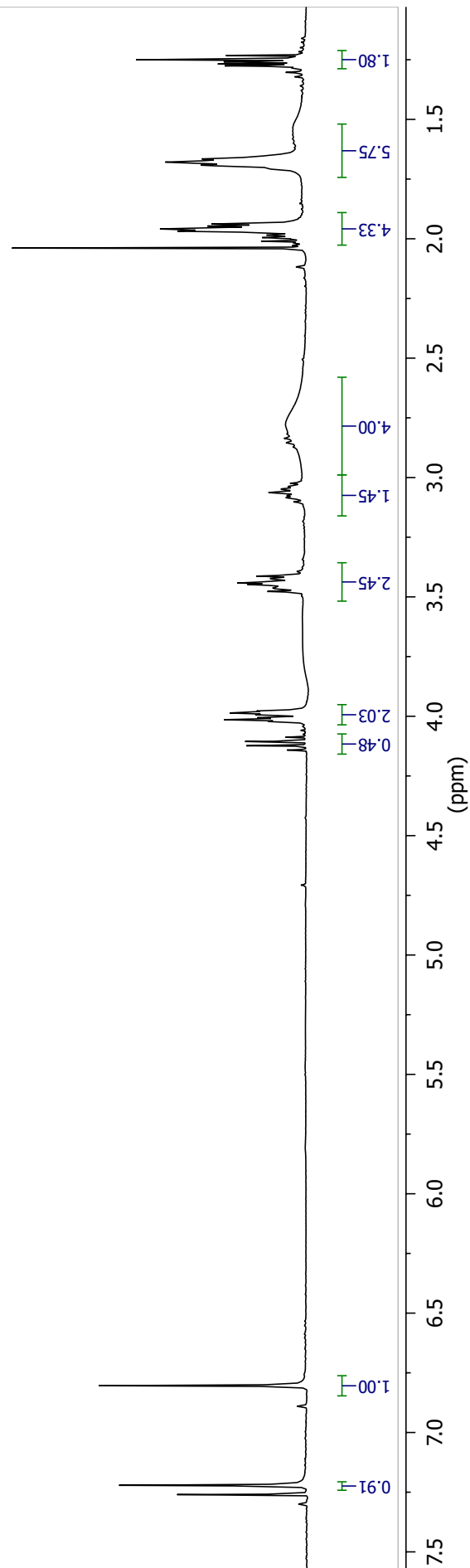
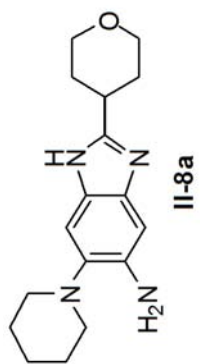


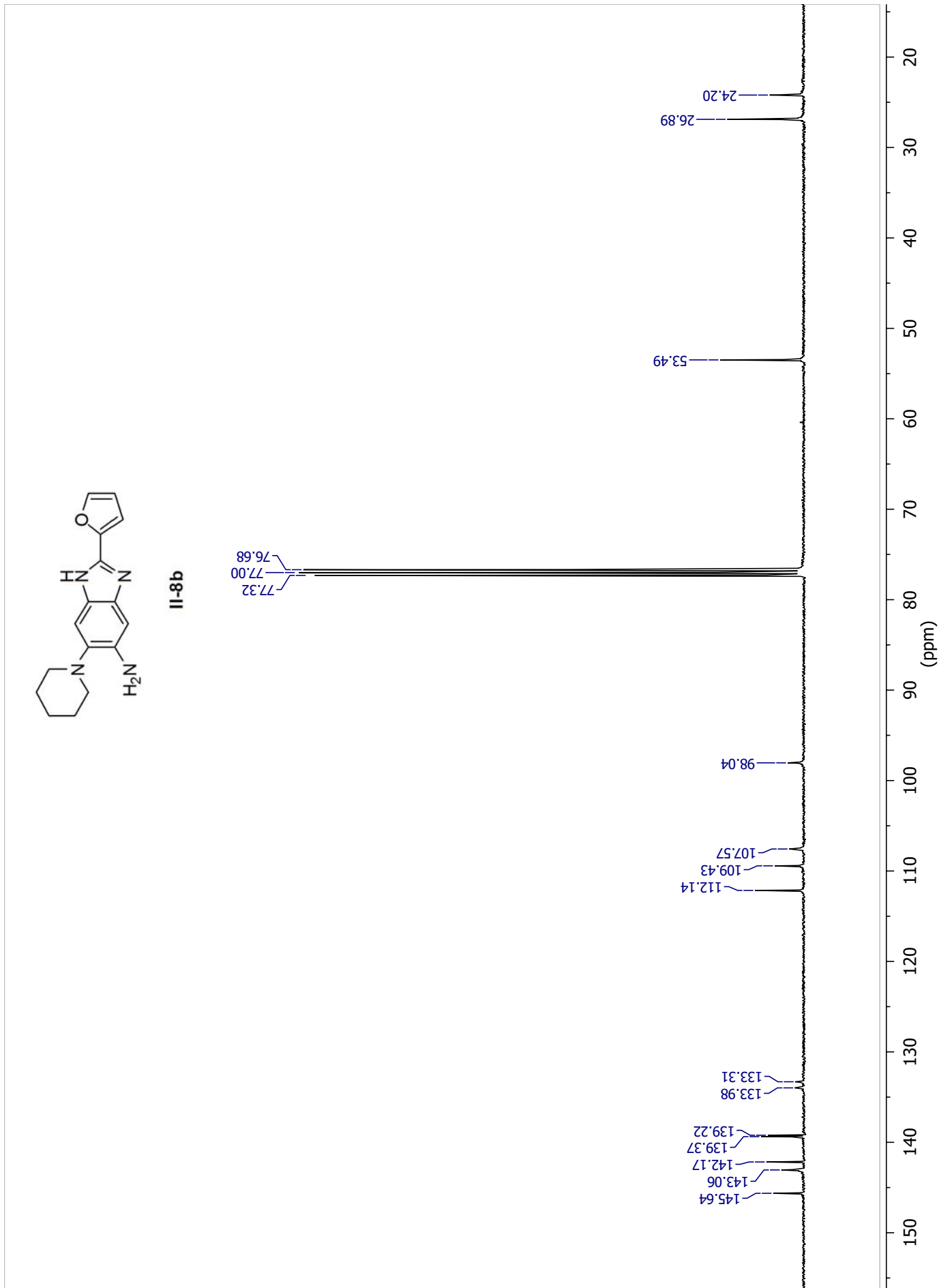


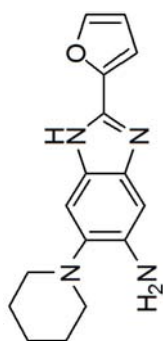




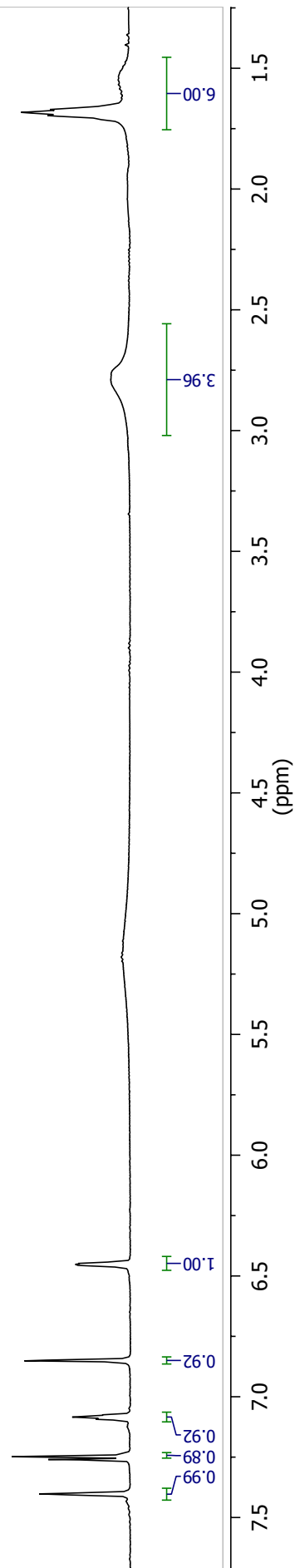


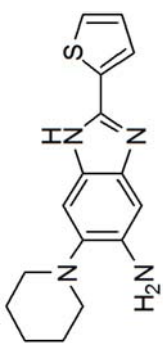




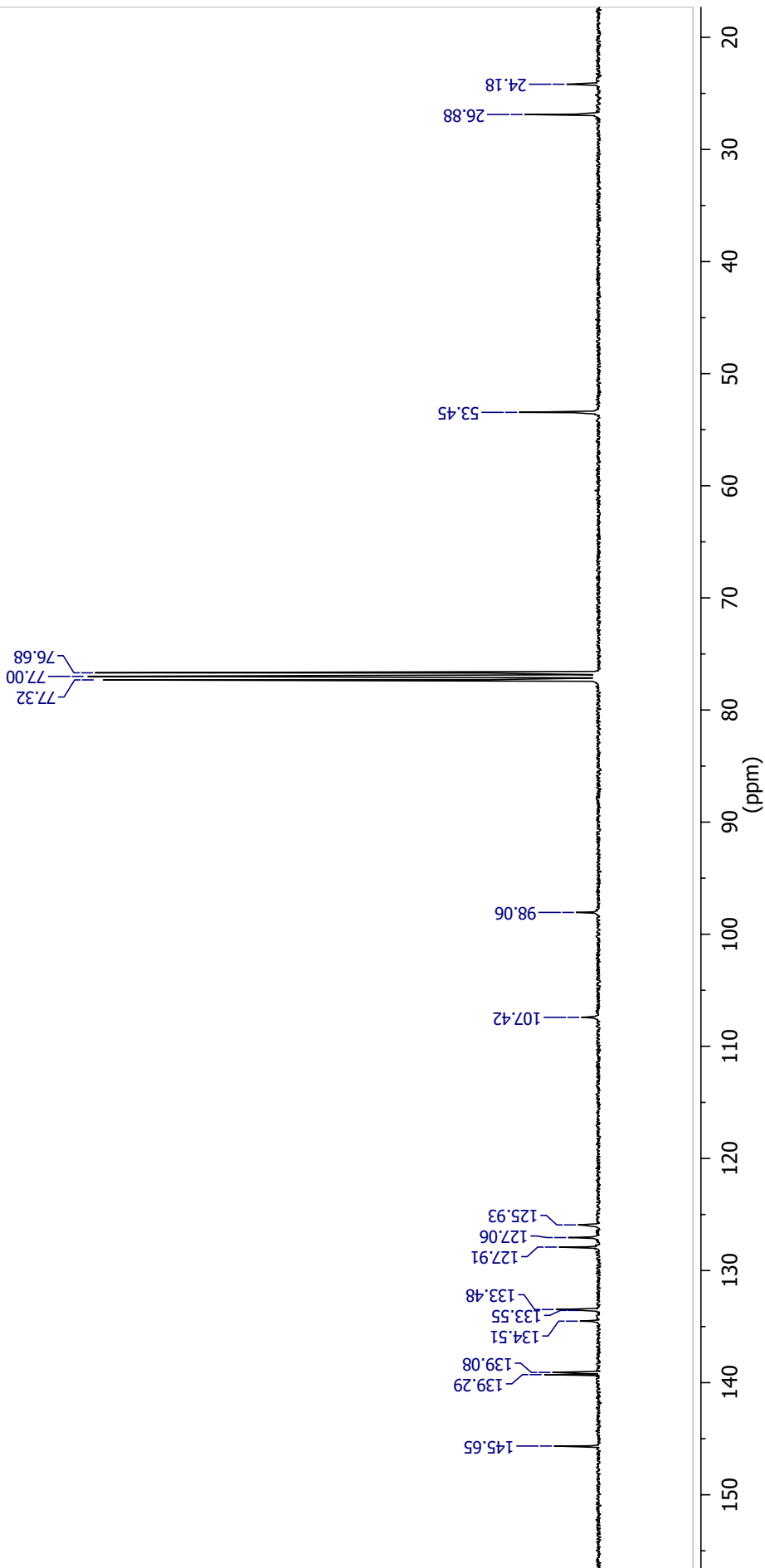


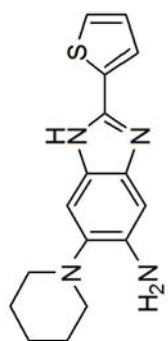
II-8b



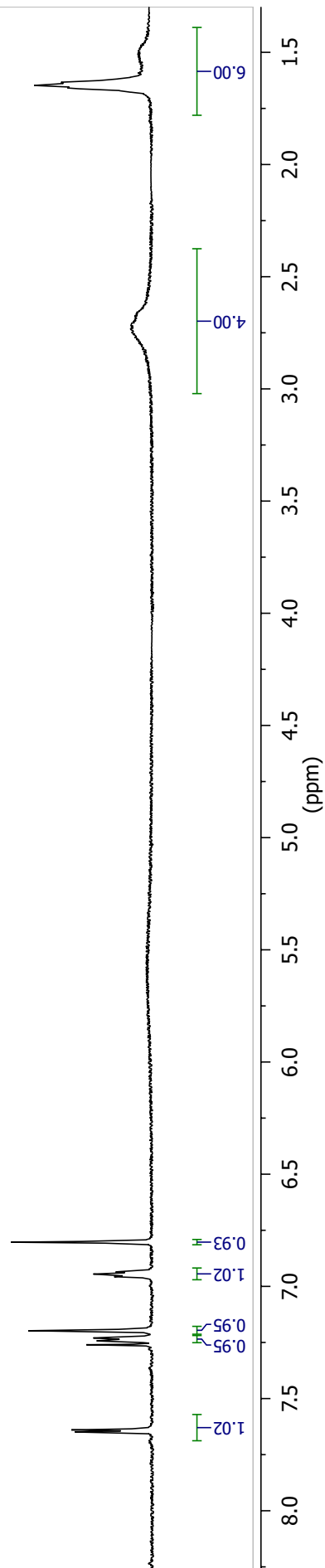


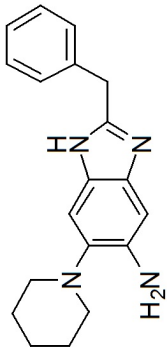
II-8c



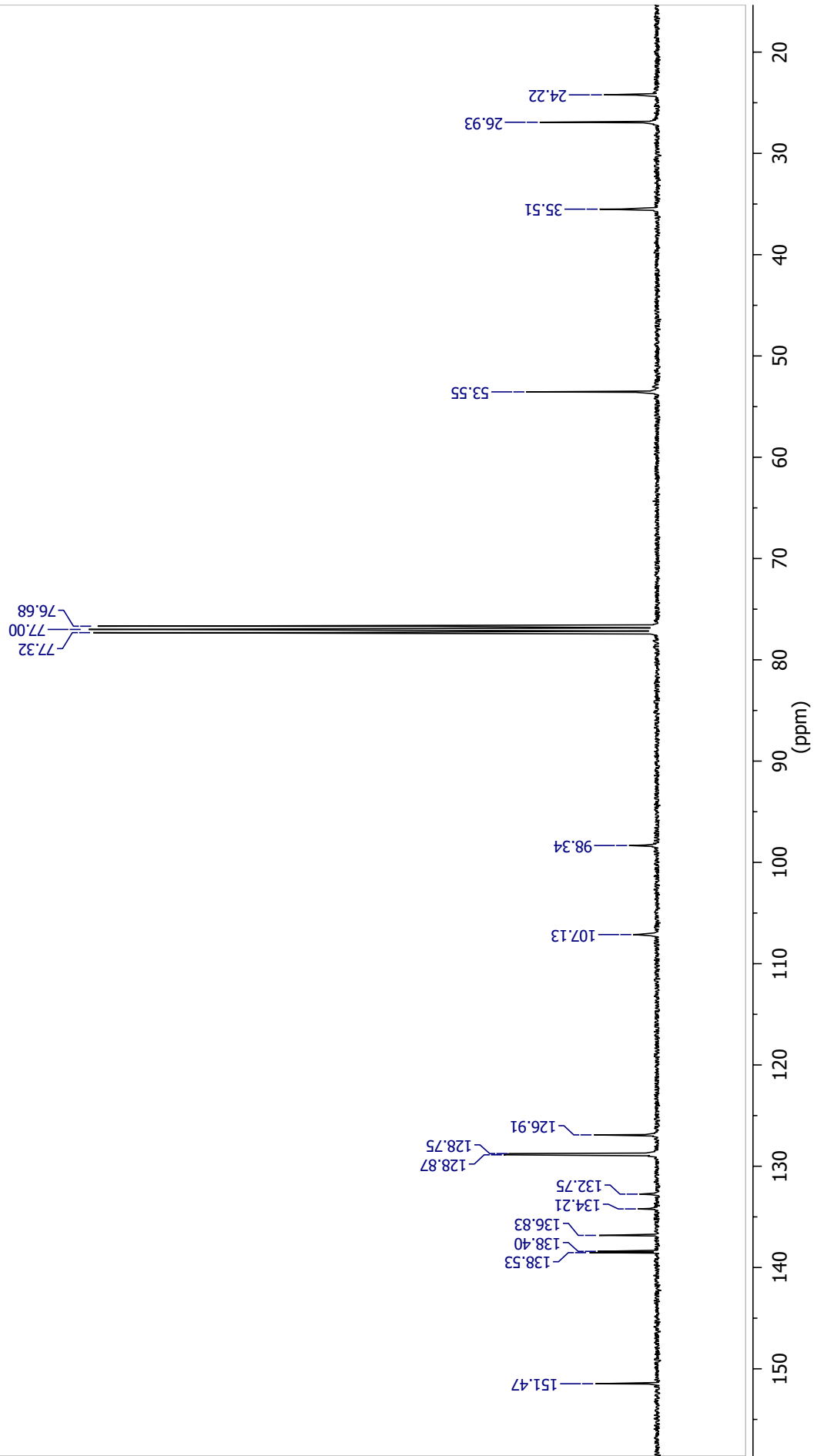


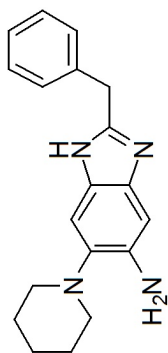
II-8c



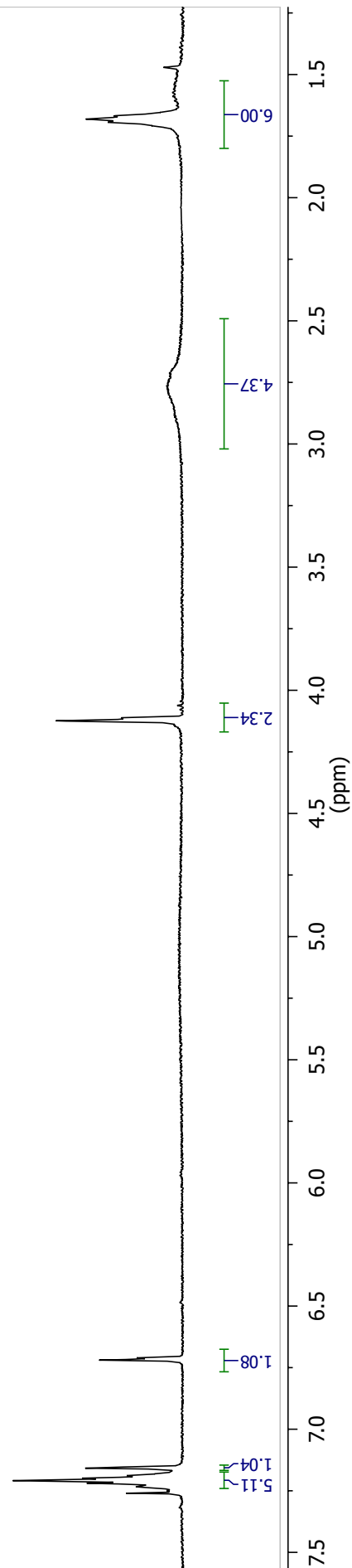


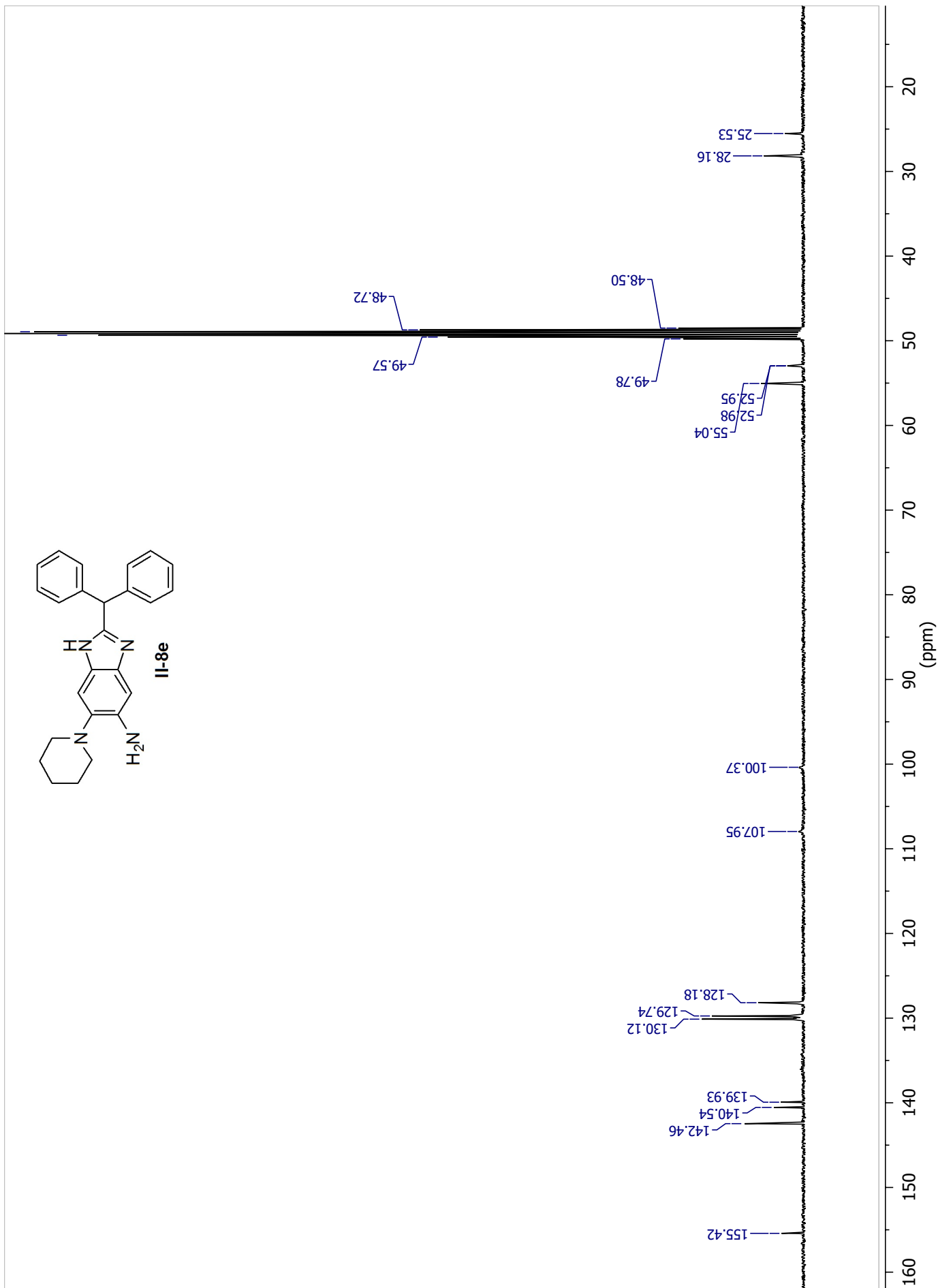
II-8-II

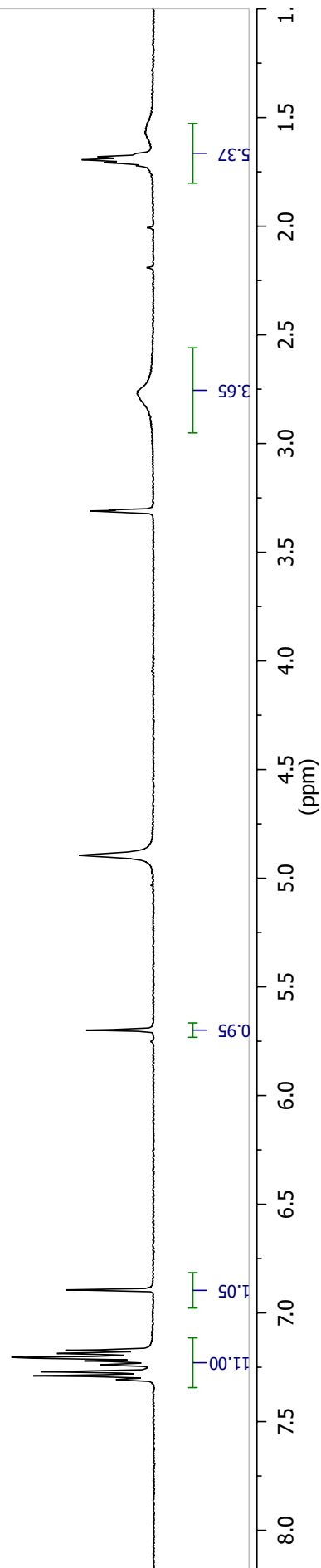
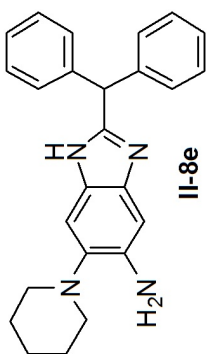


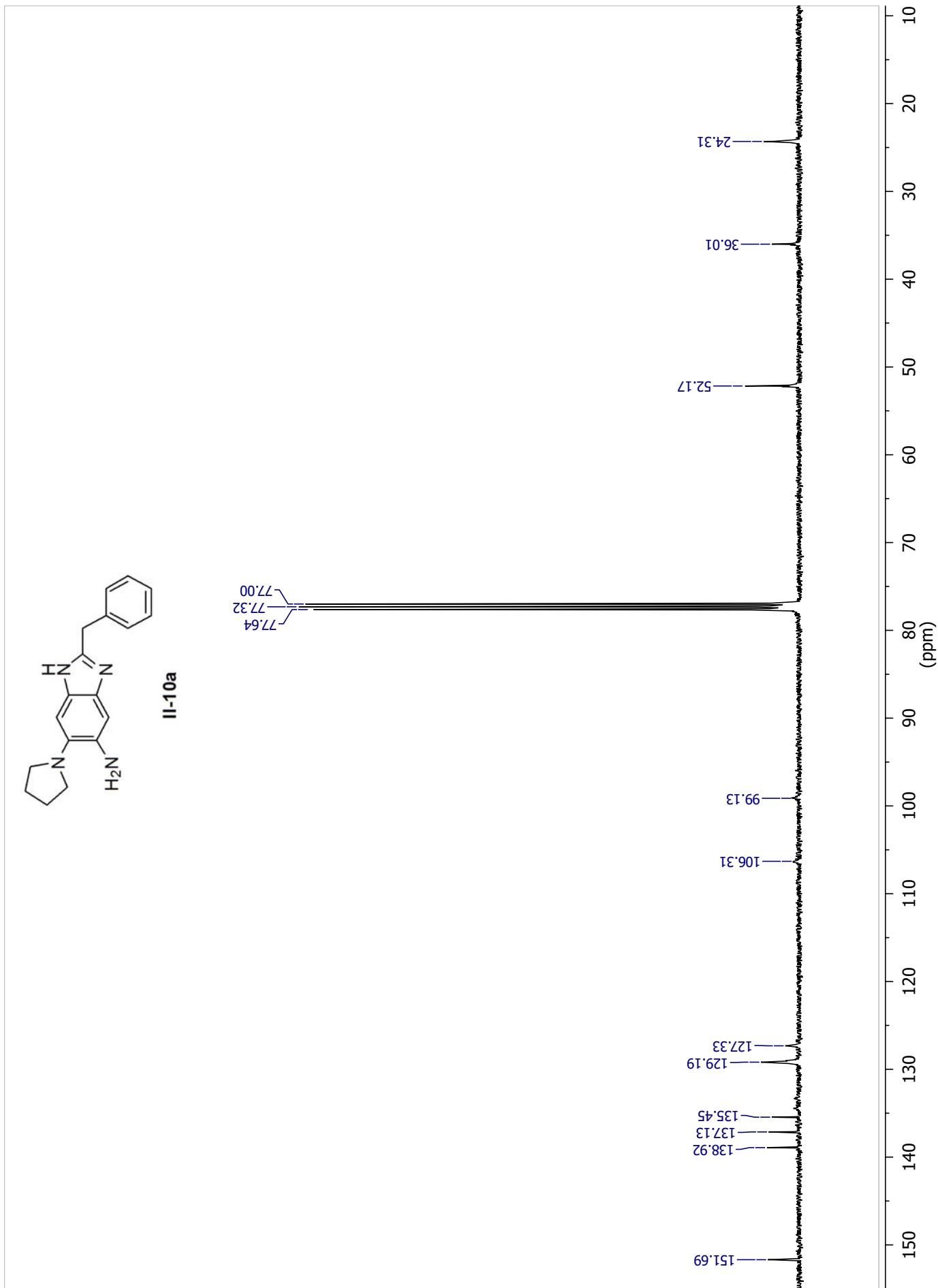


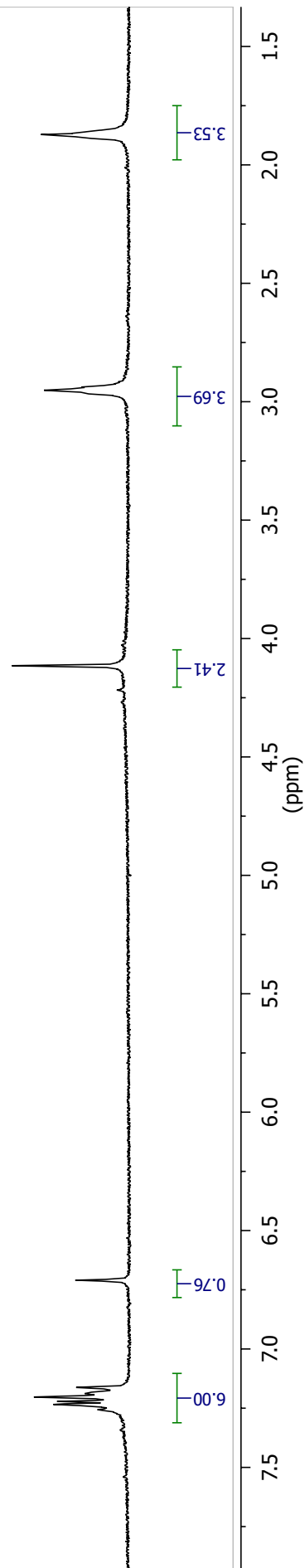
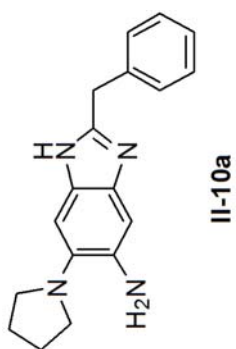
II-8d

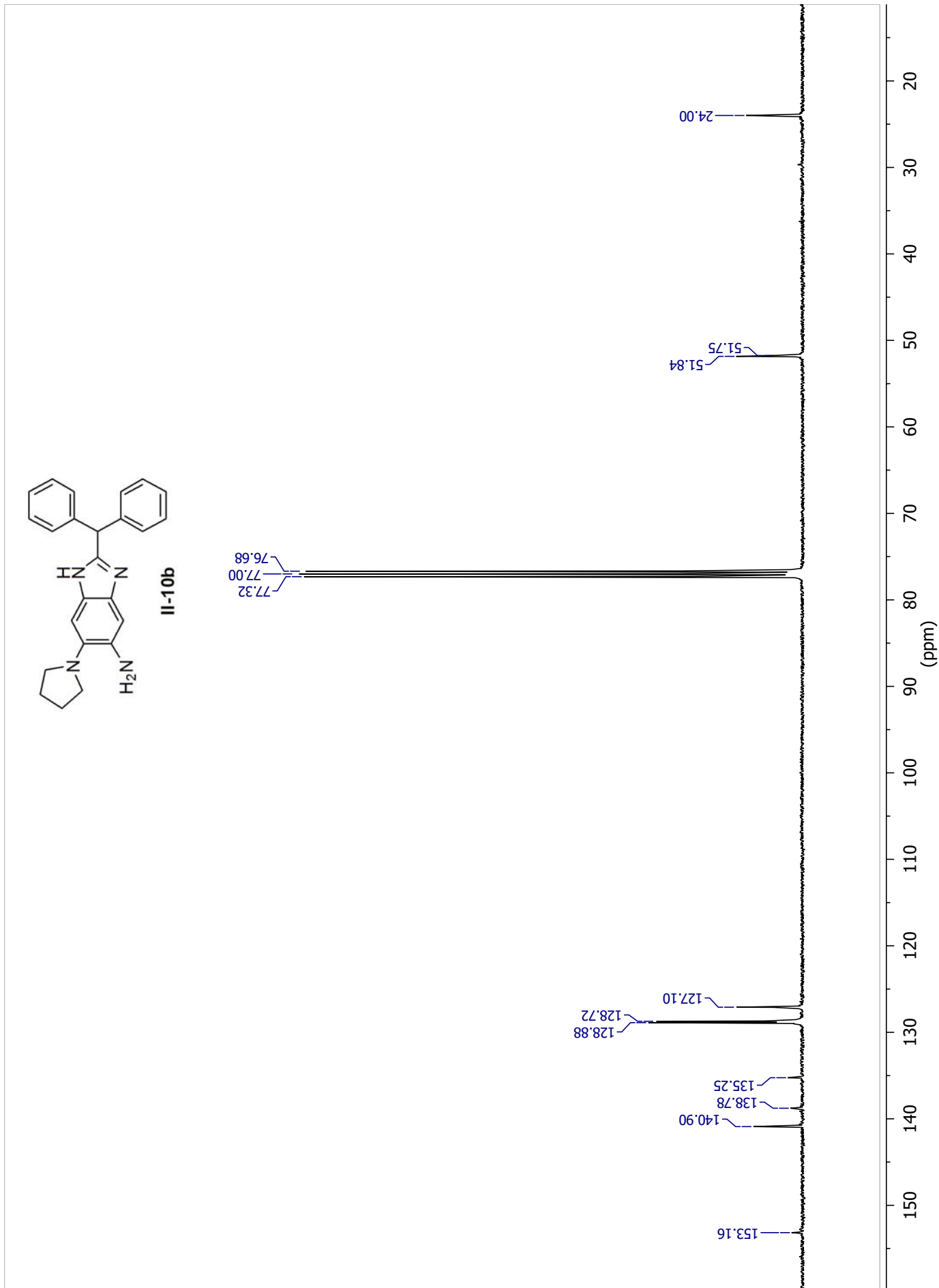


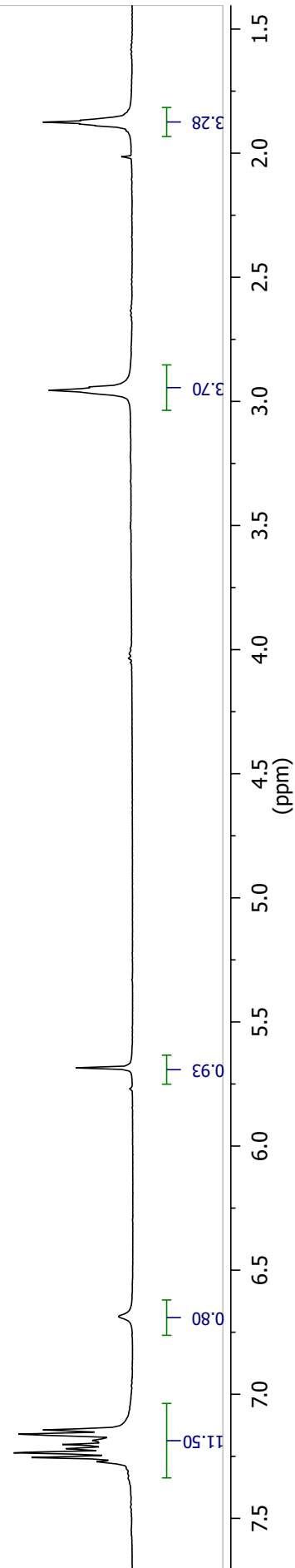
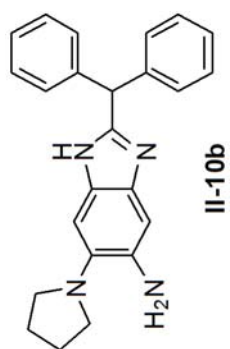


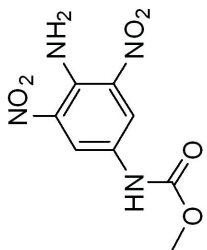




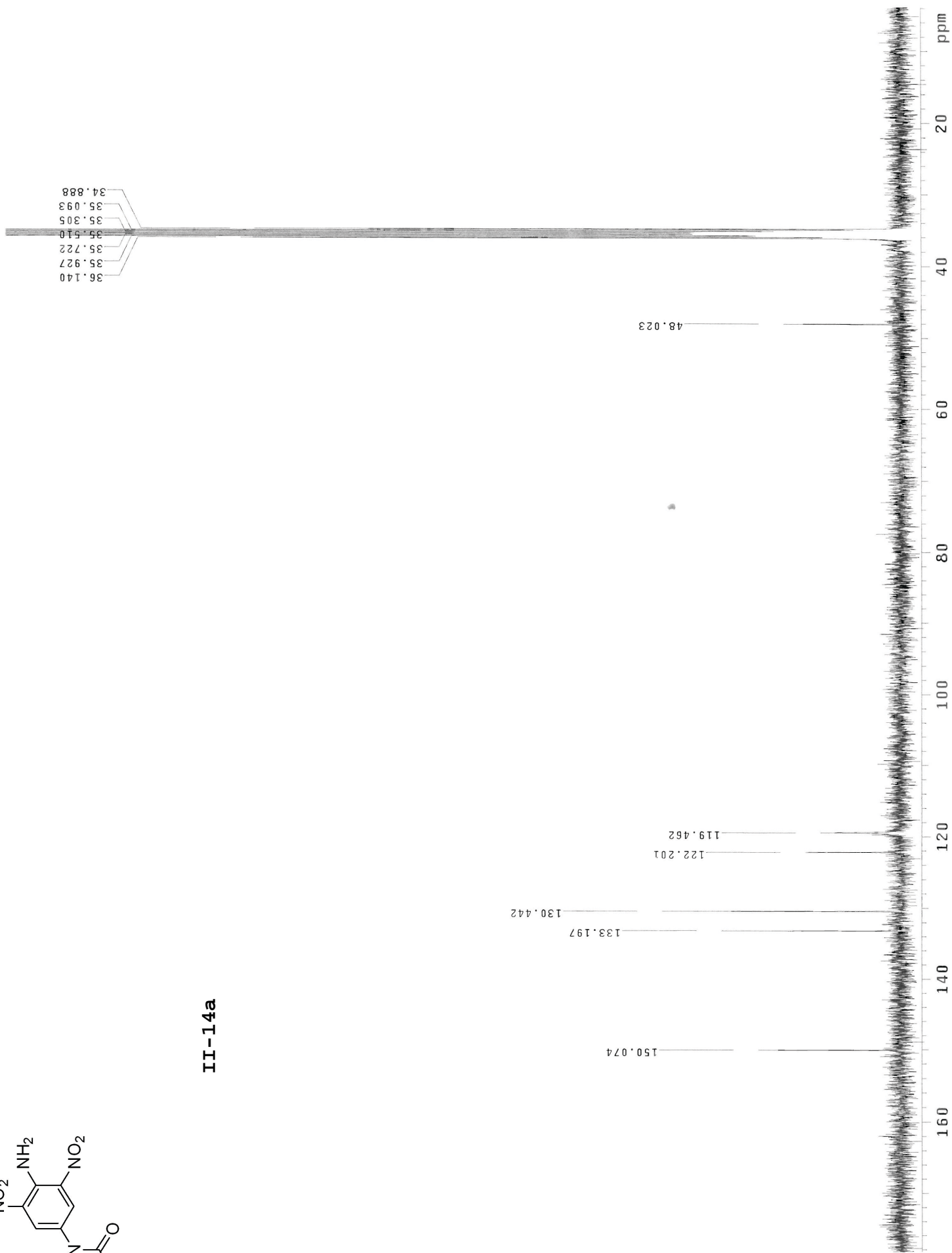


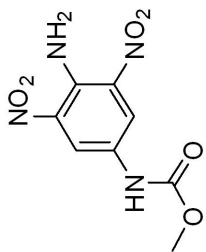




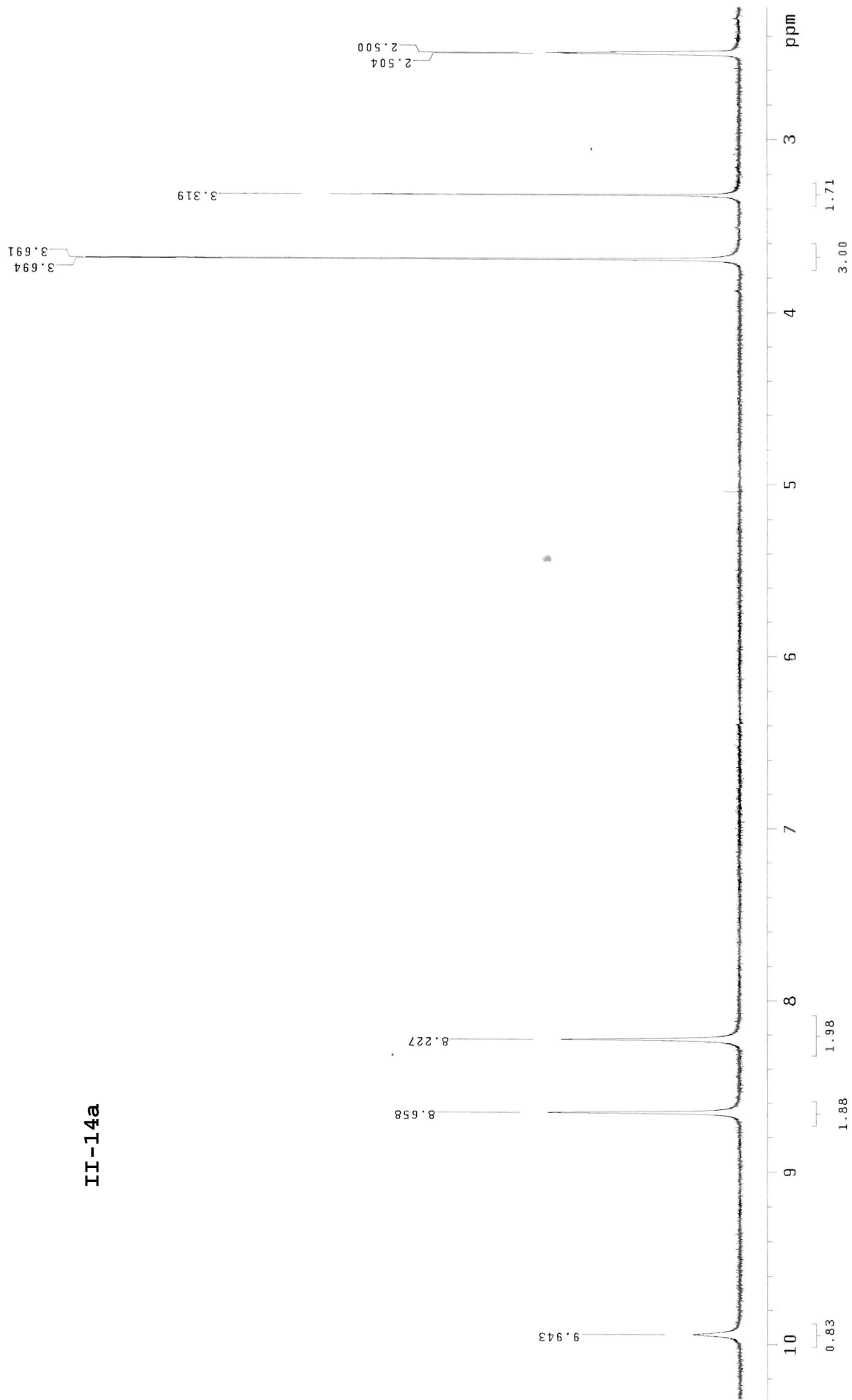


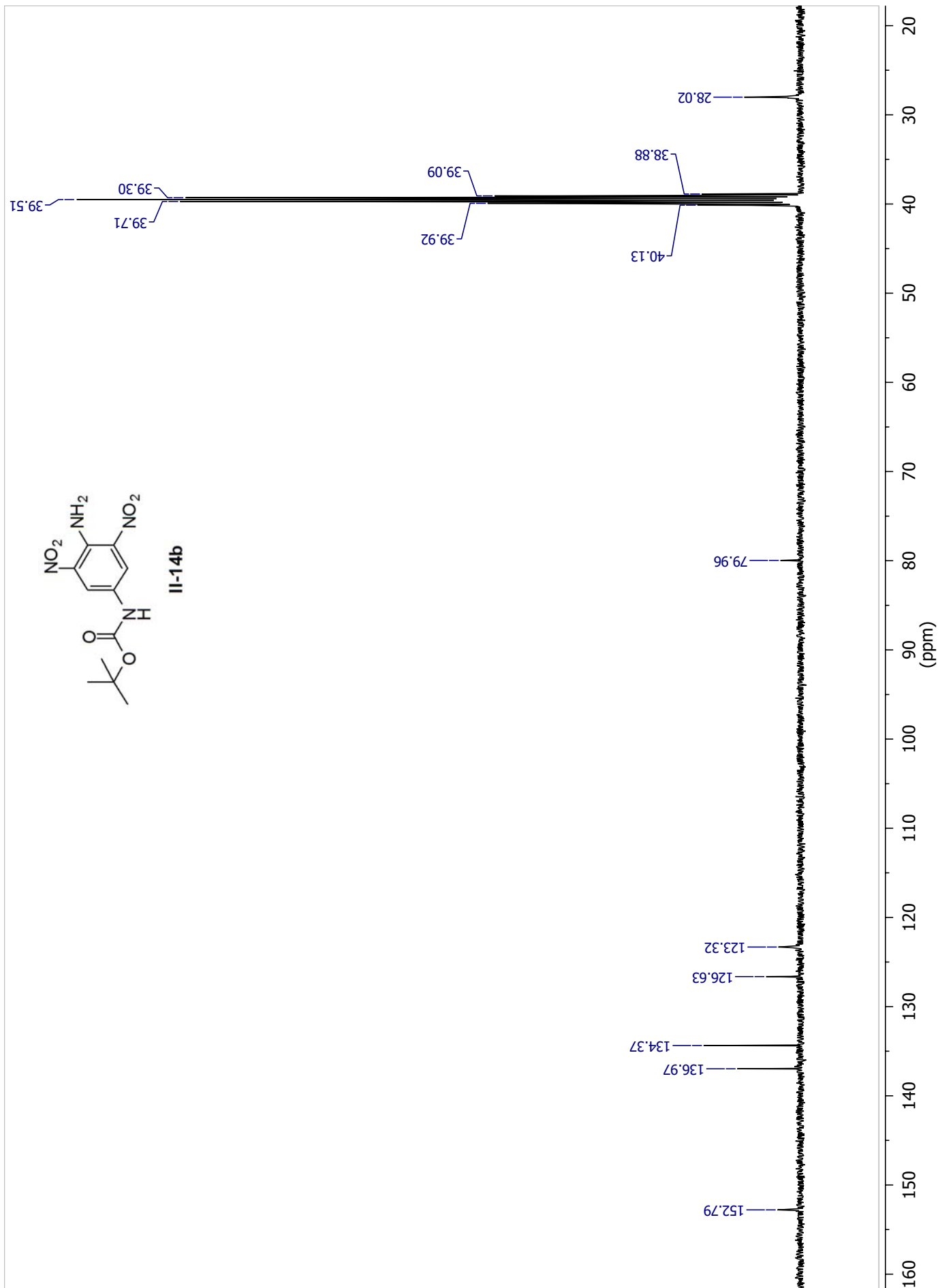
II-14a

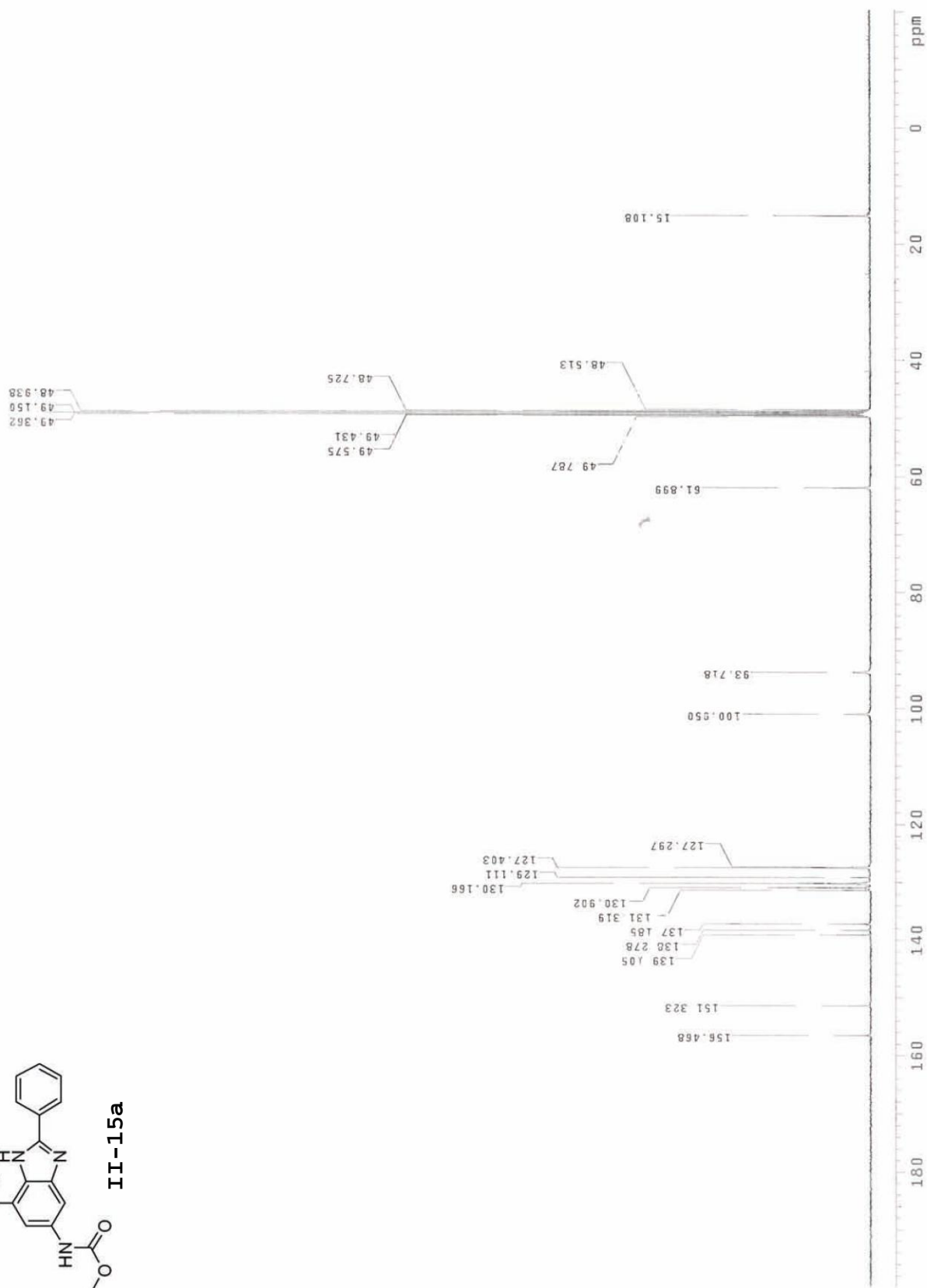
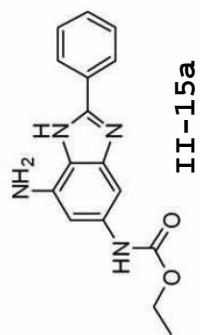


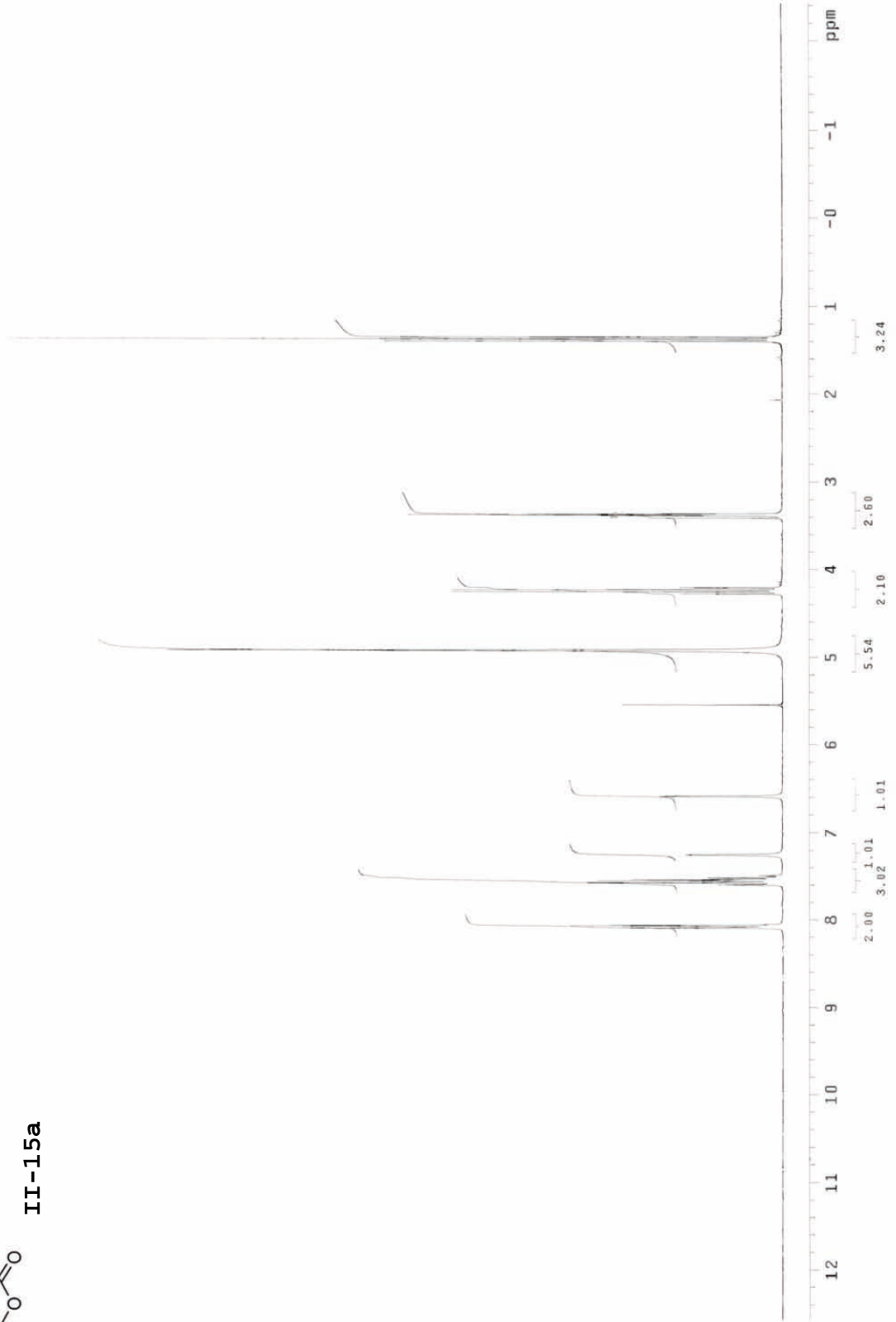
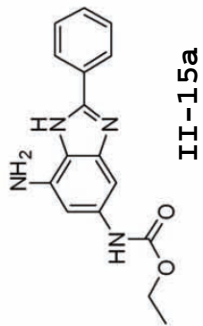


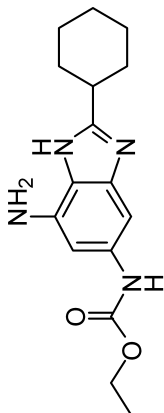
II-14a



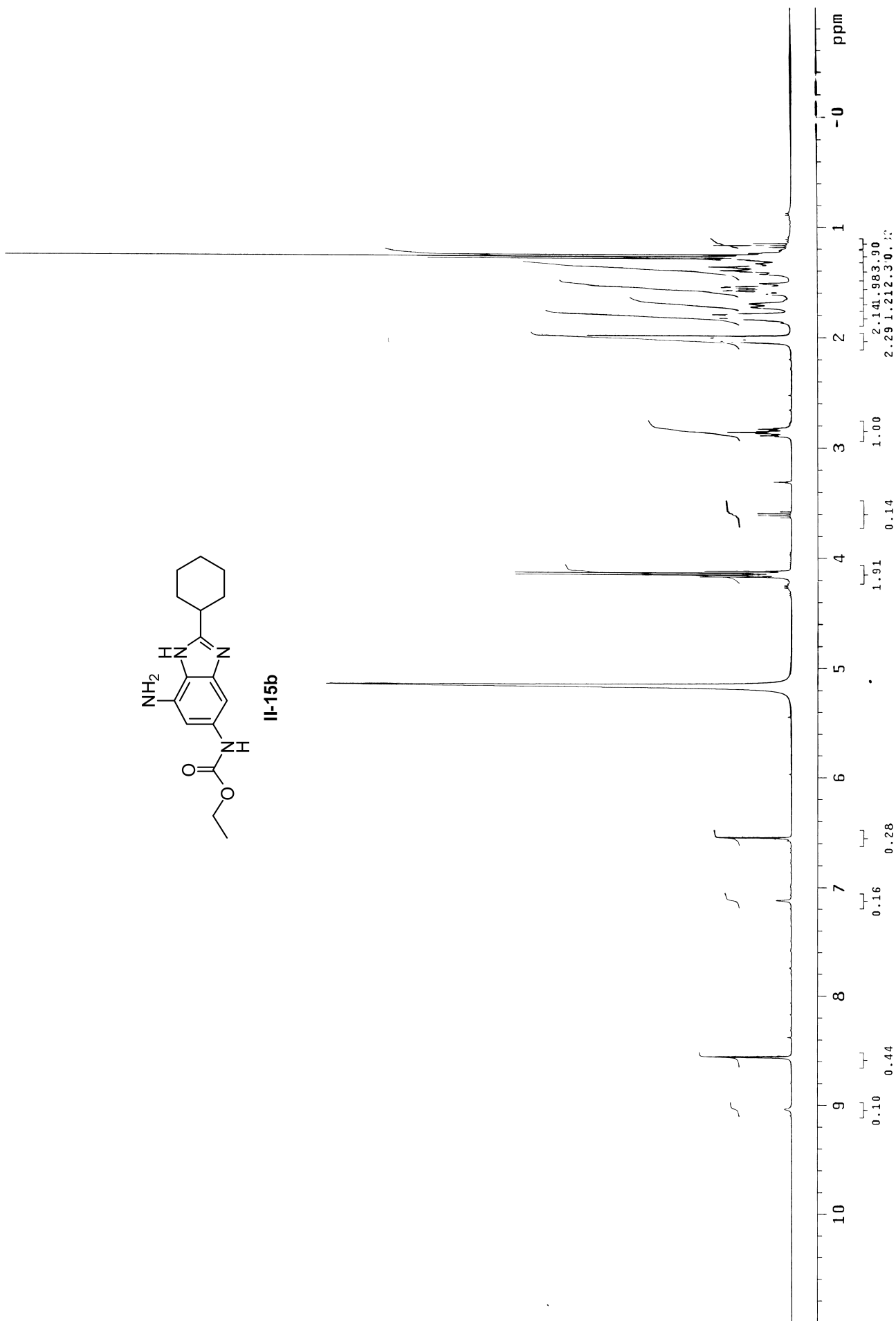


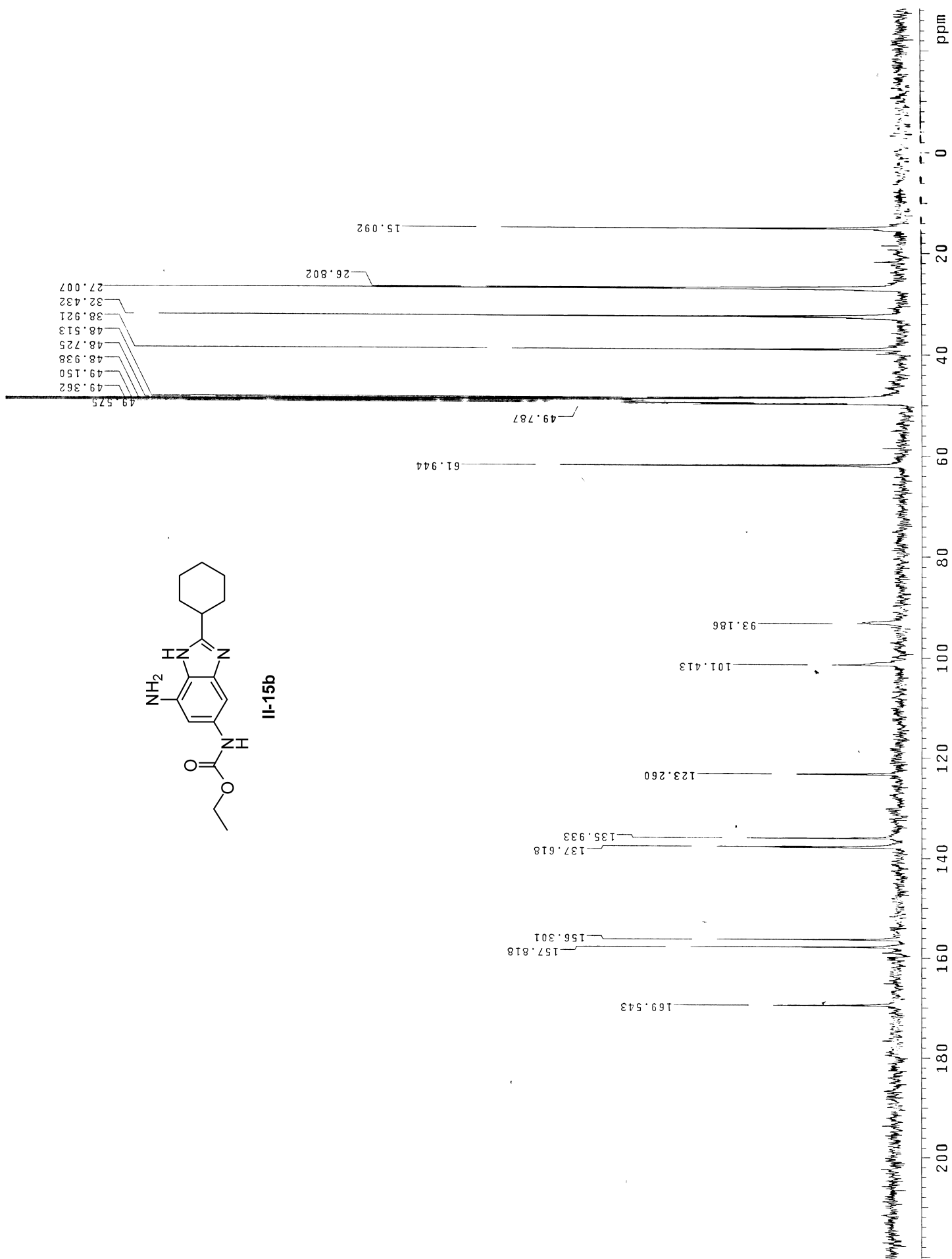


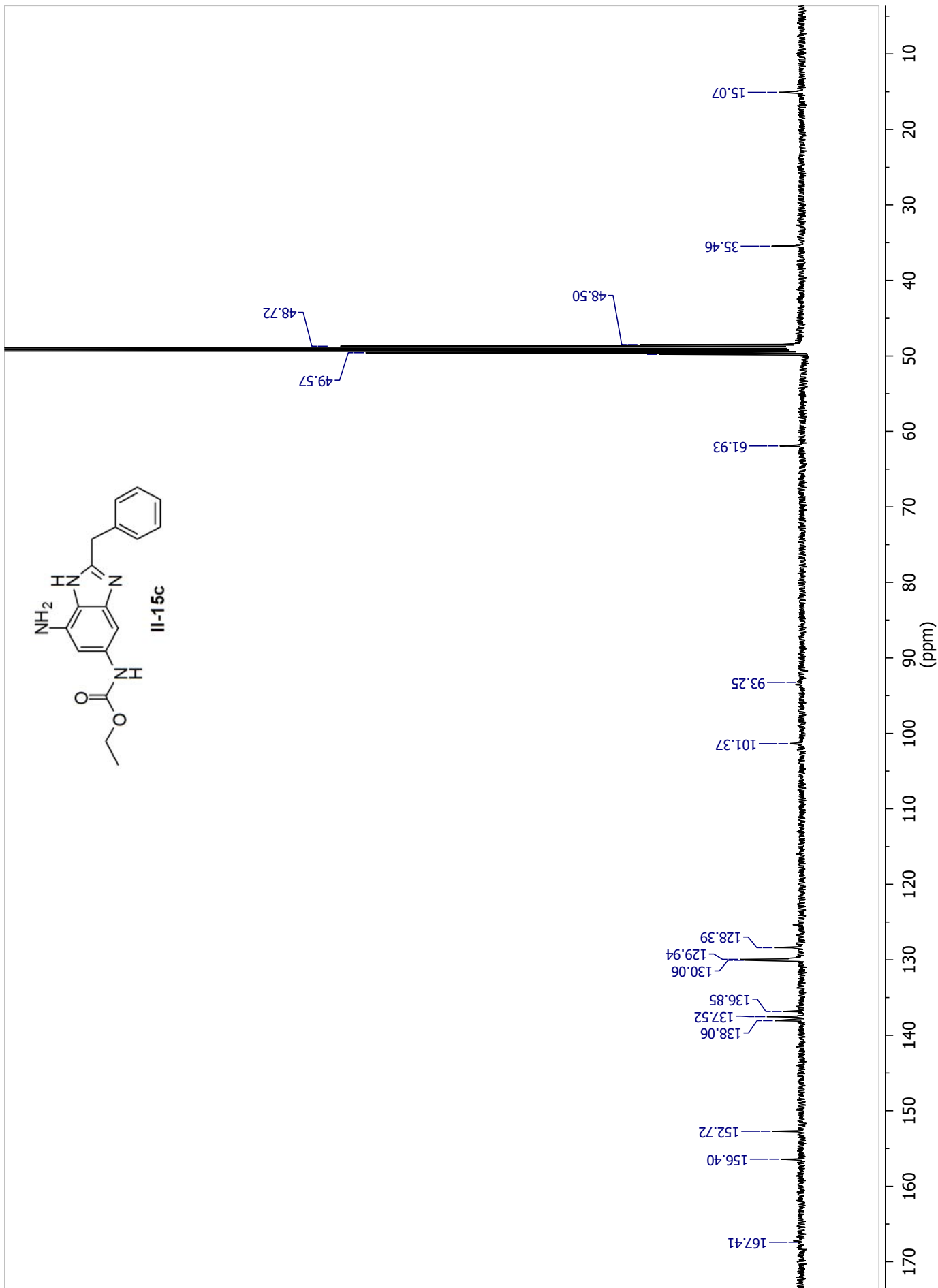


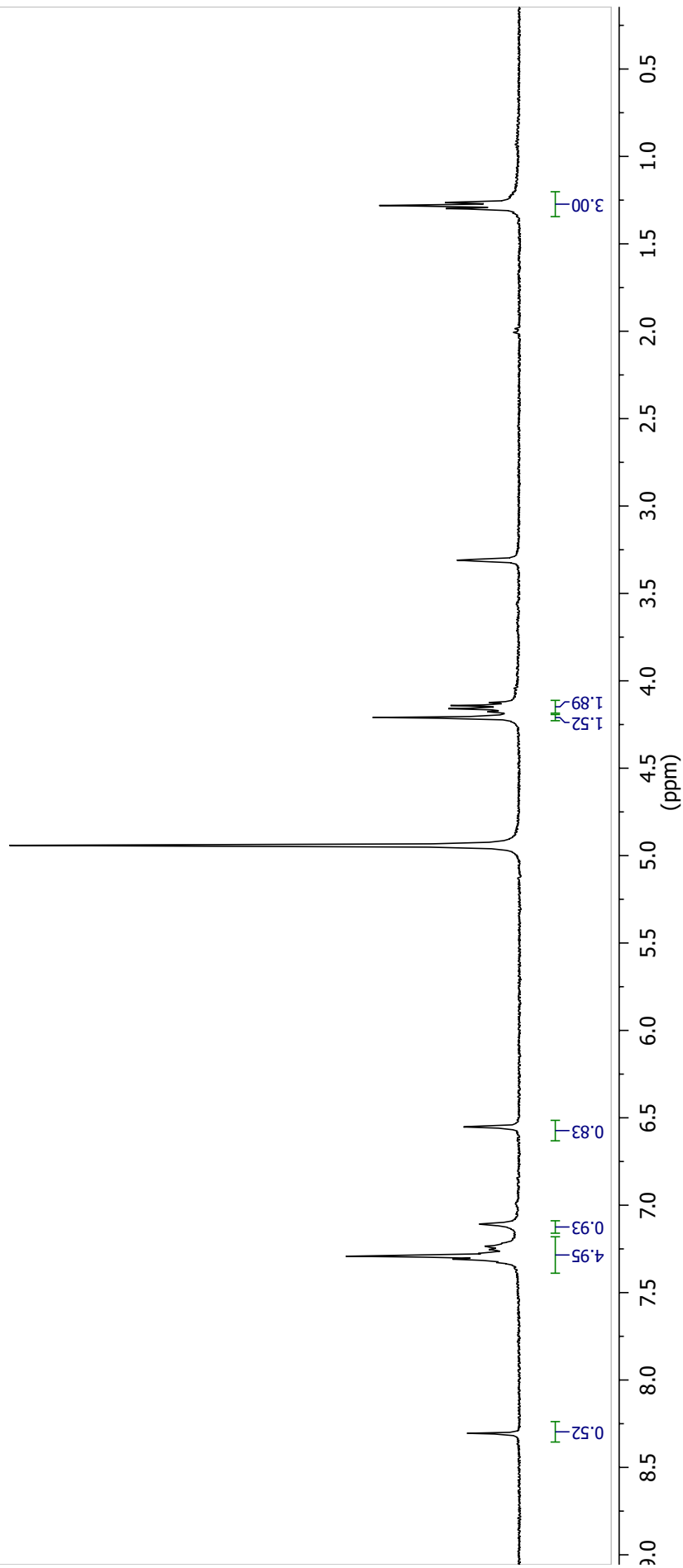
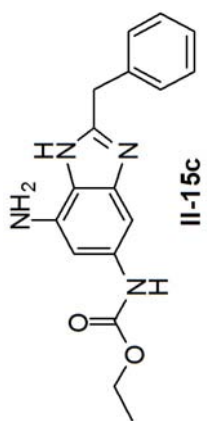


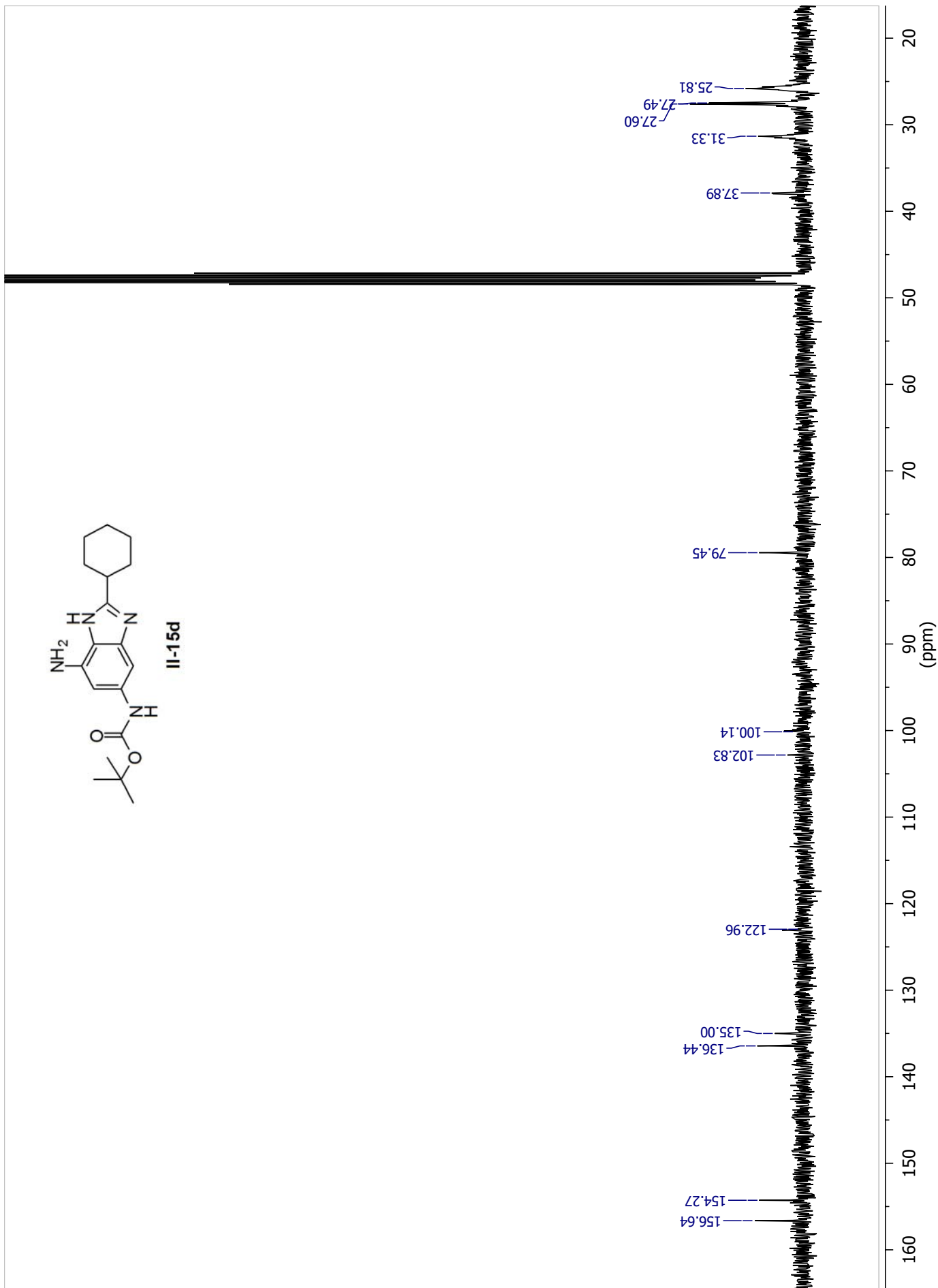
II-15b

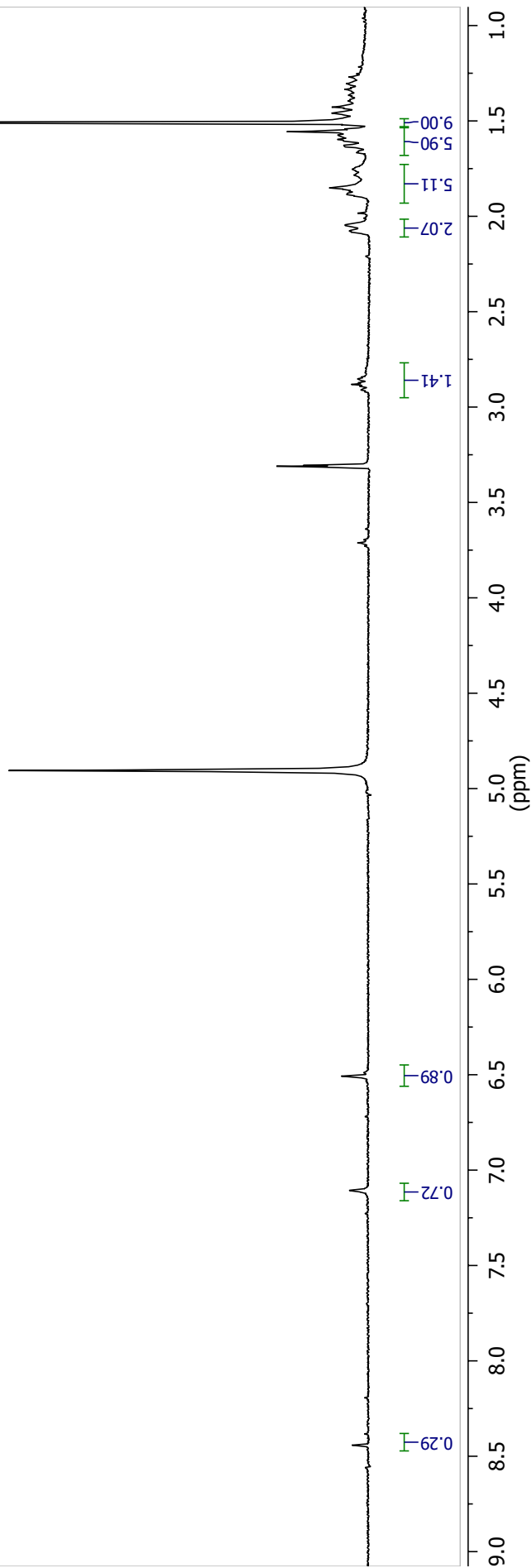
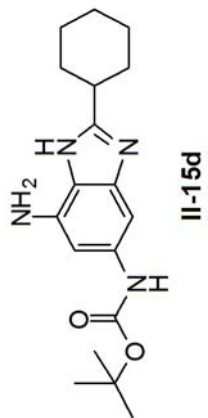


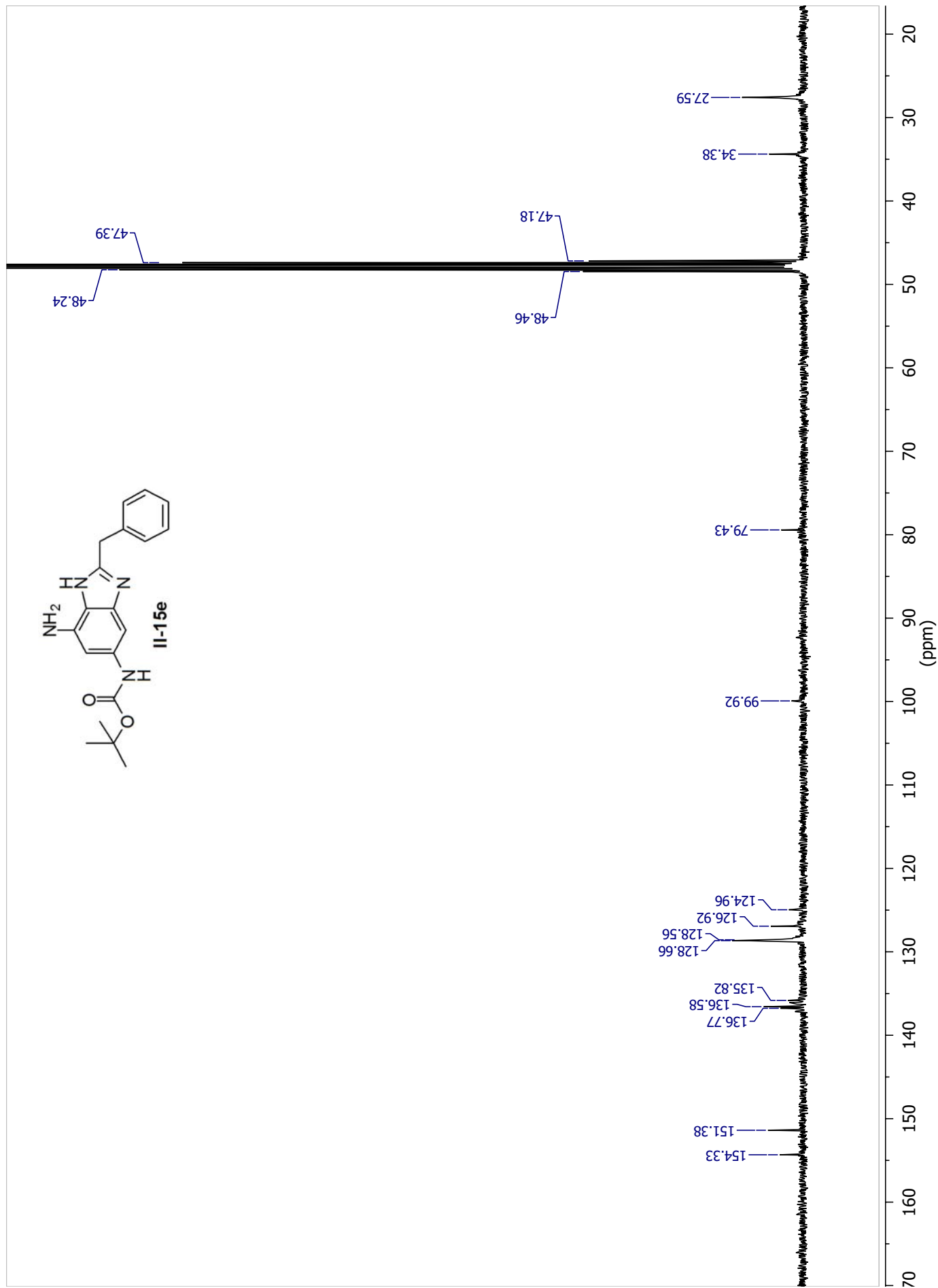


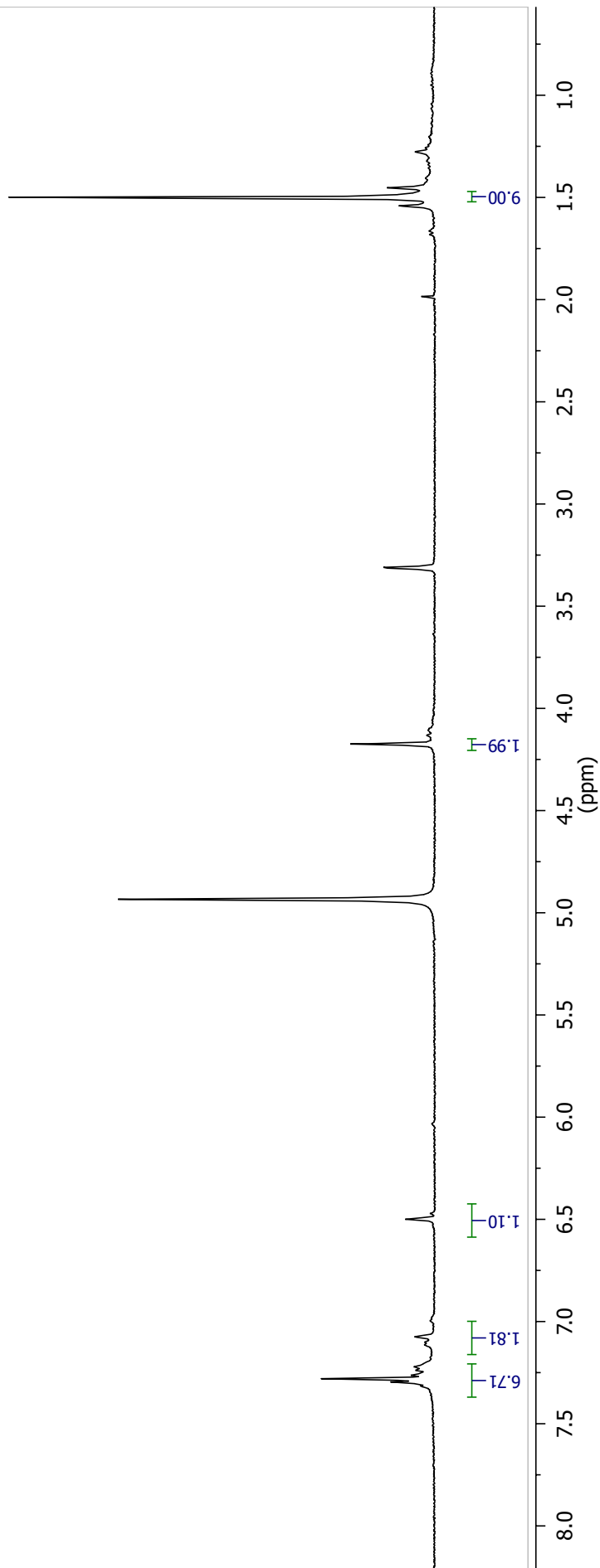
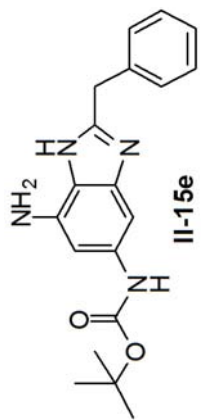


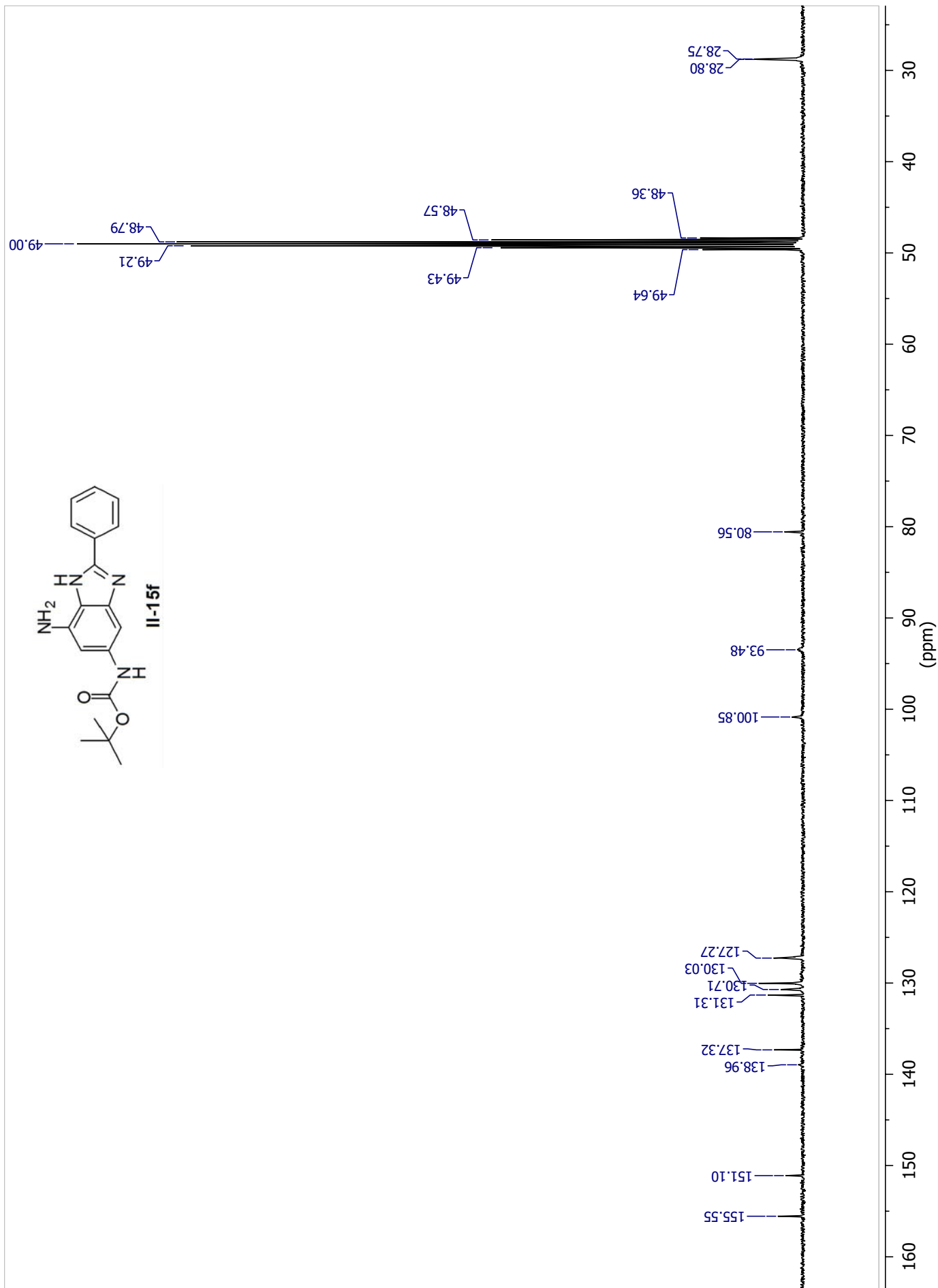


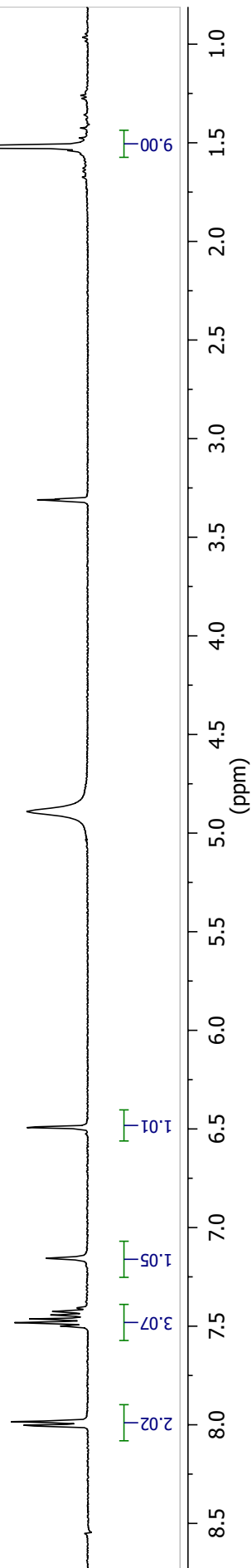
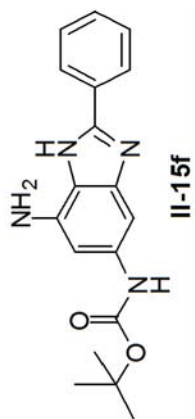


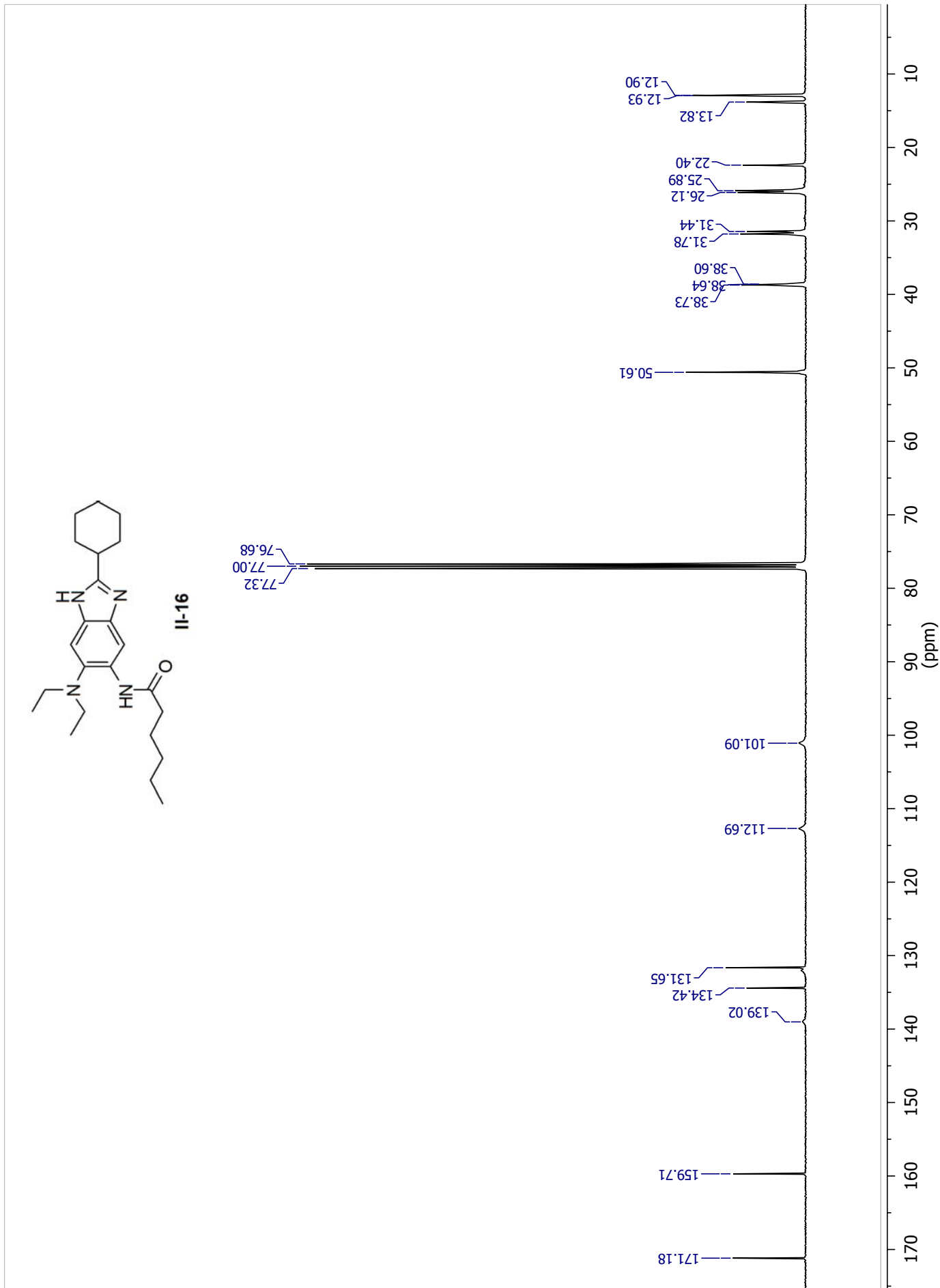


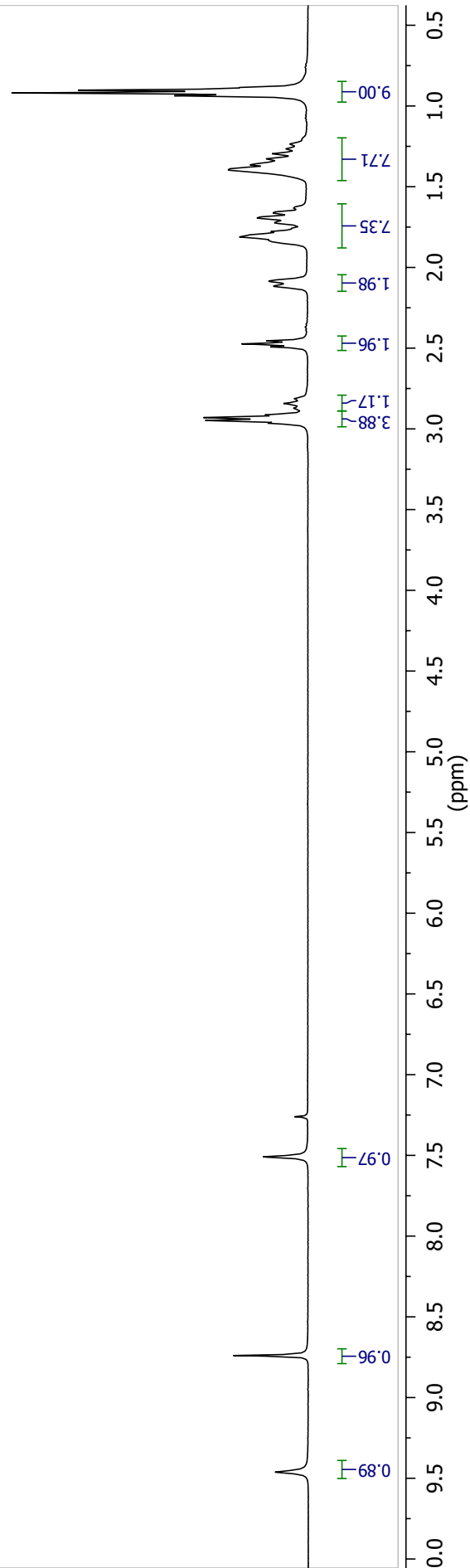
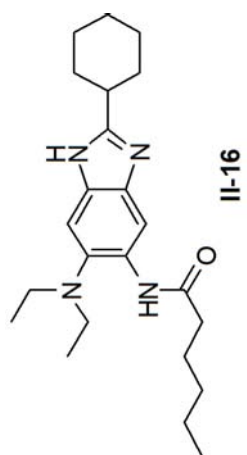


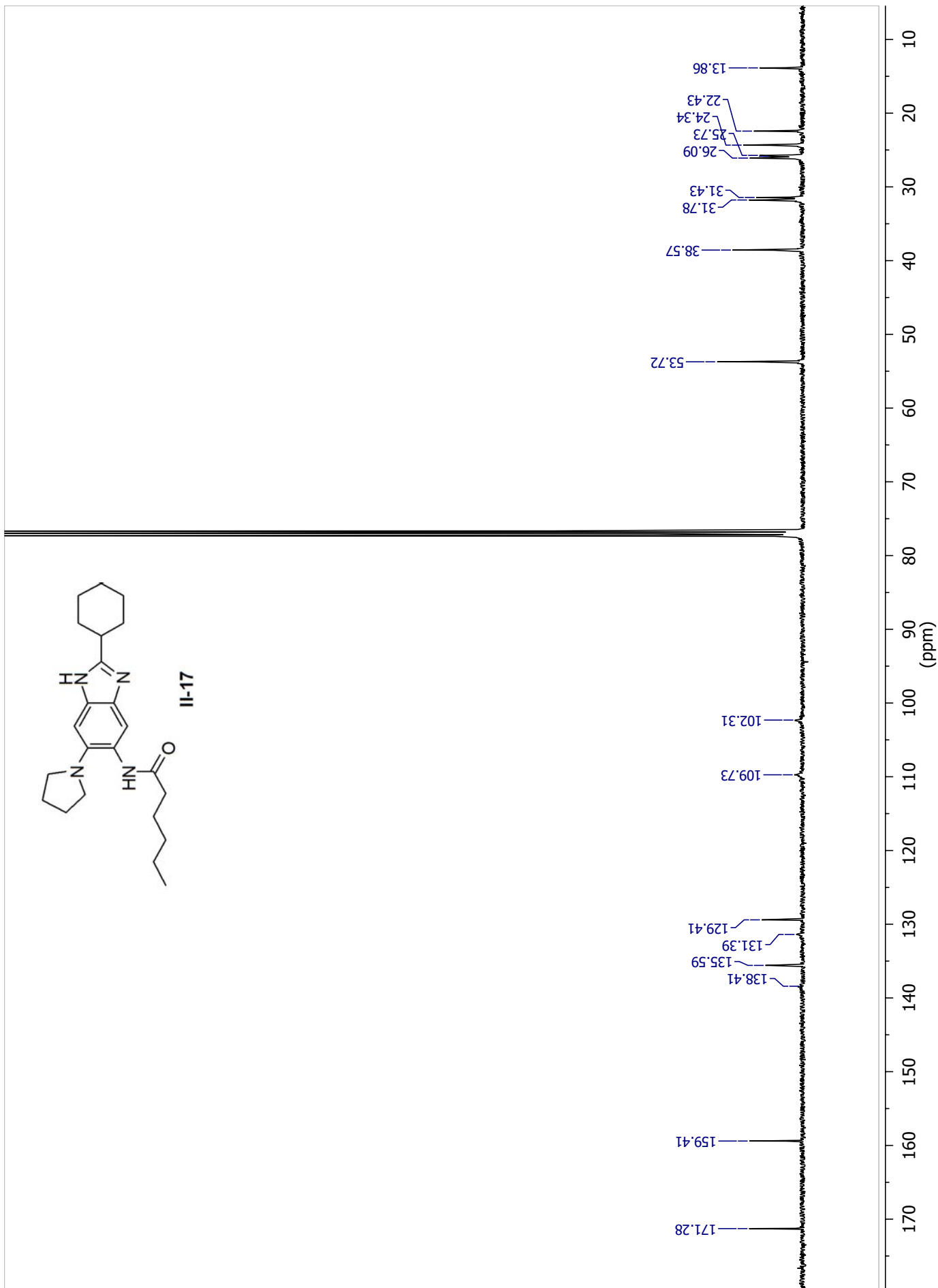


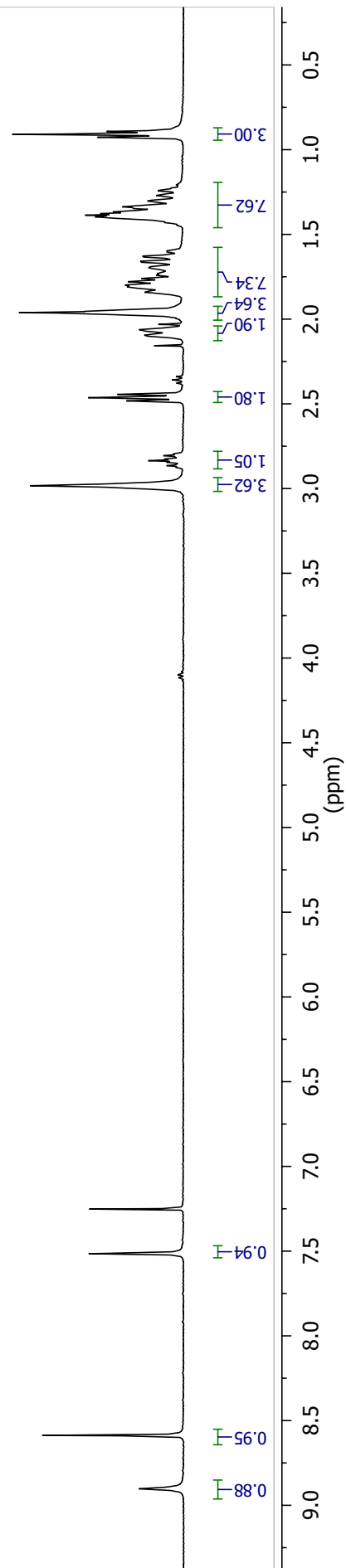
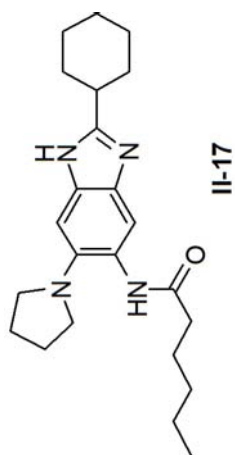


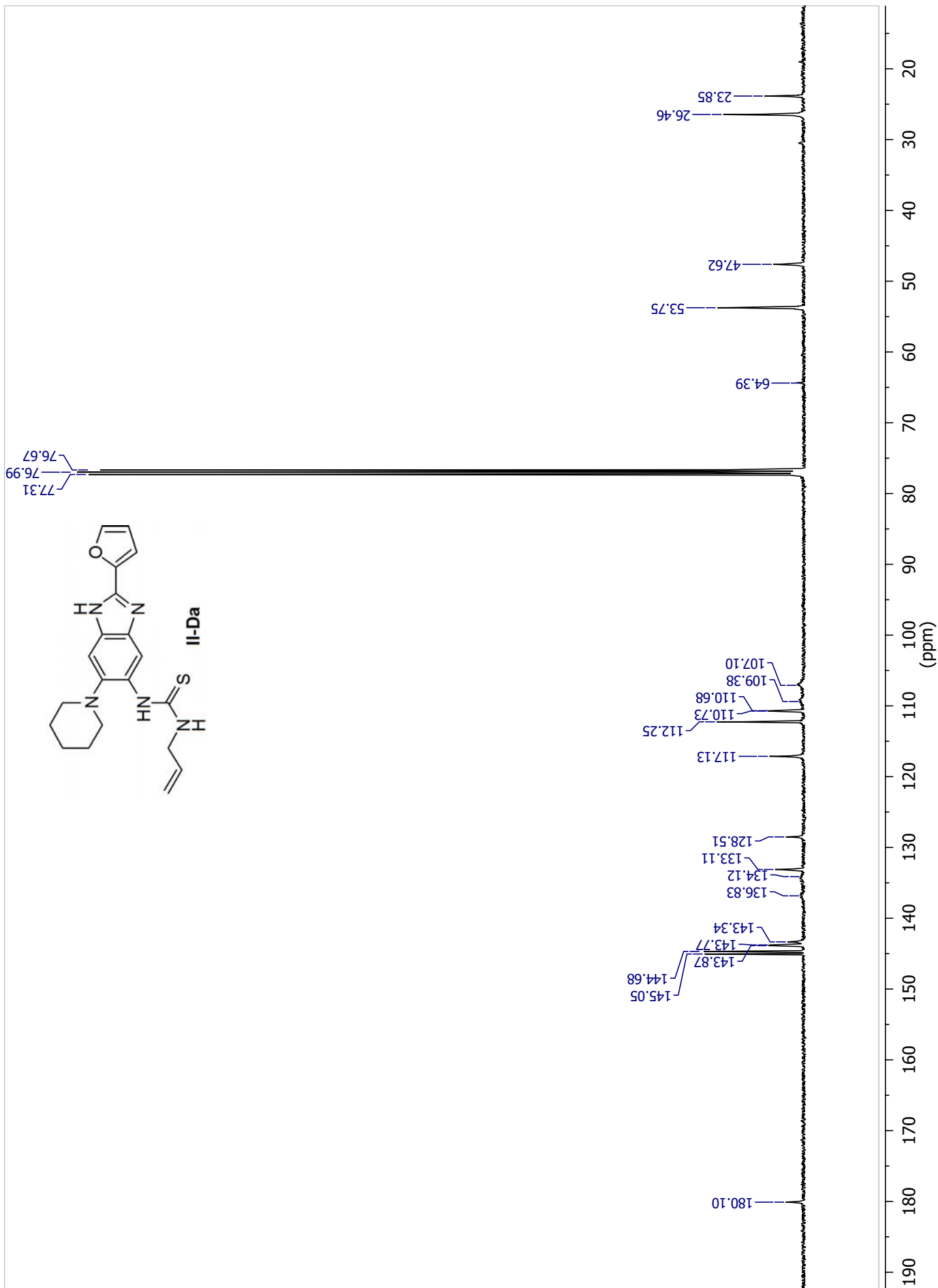


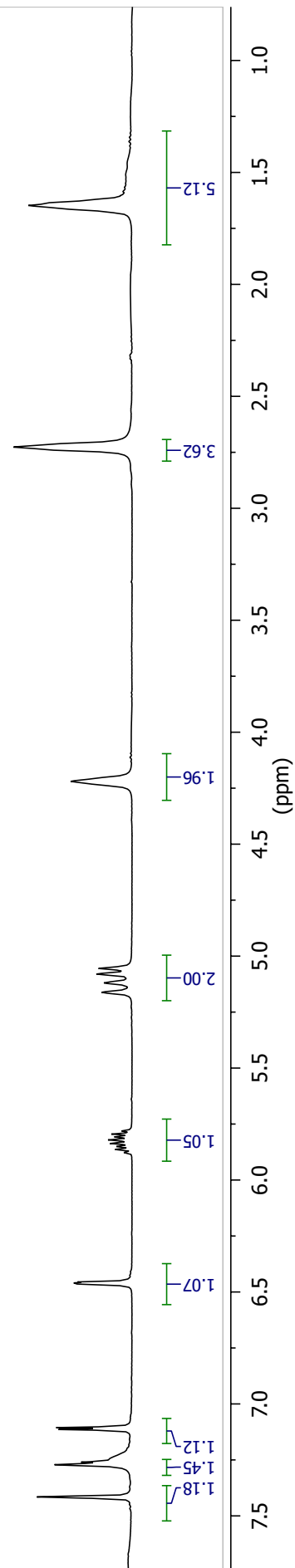
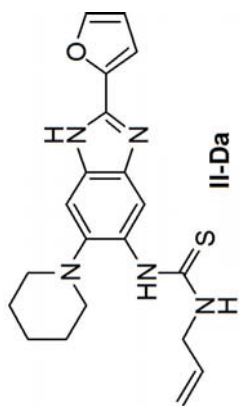


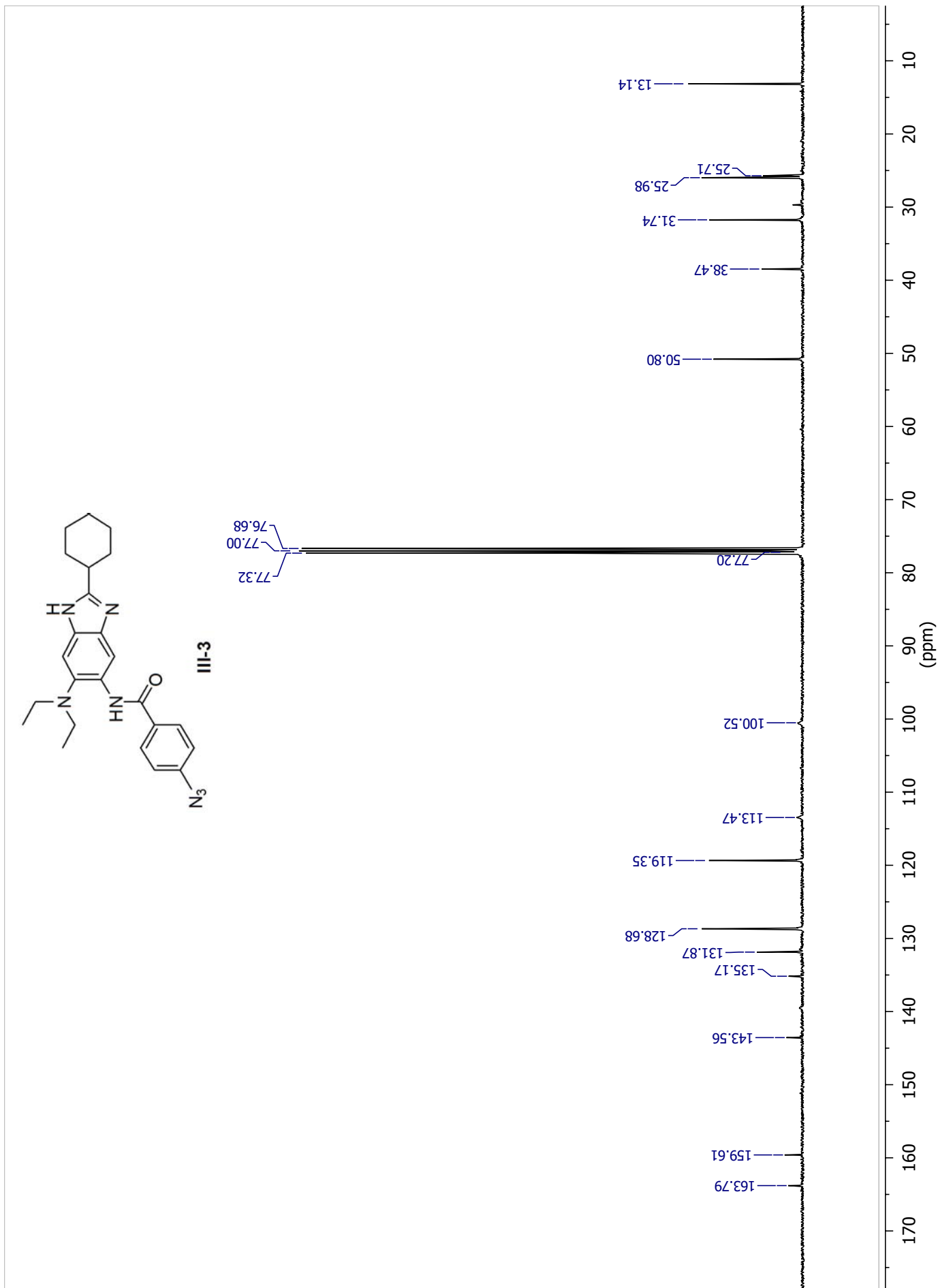


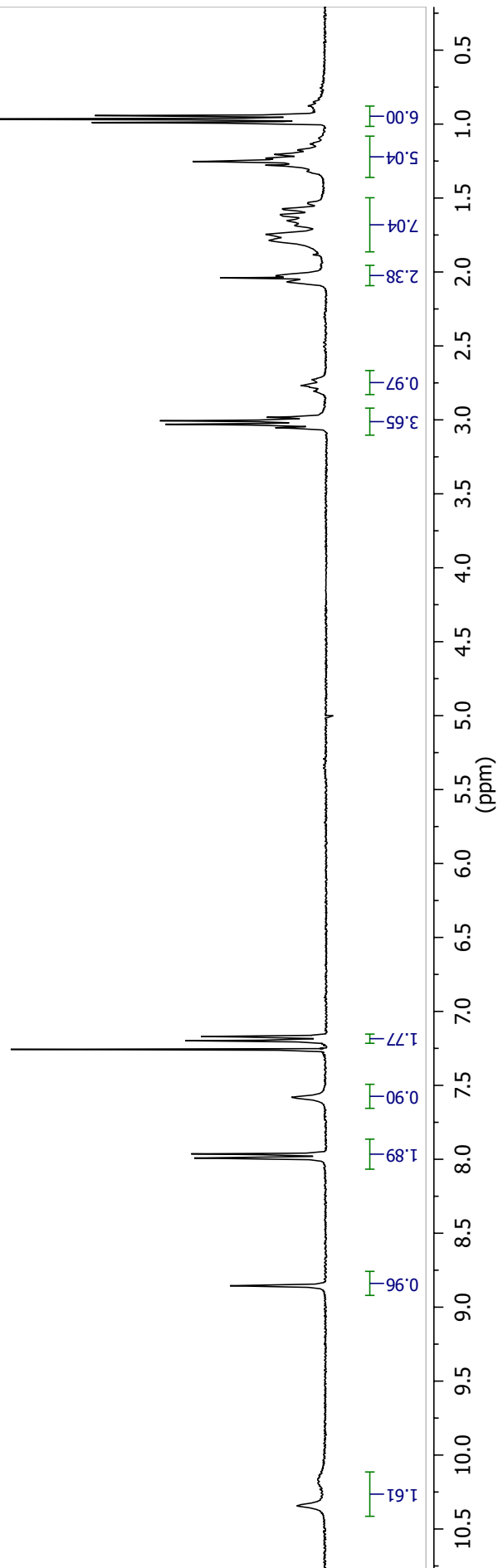
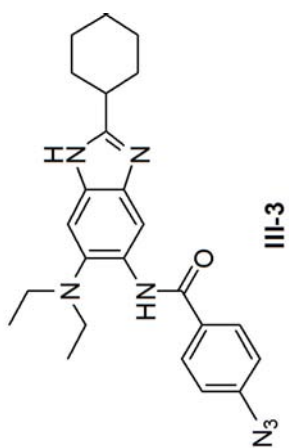


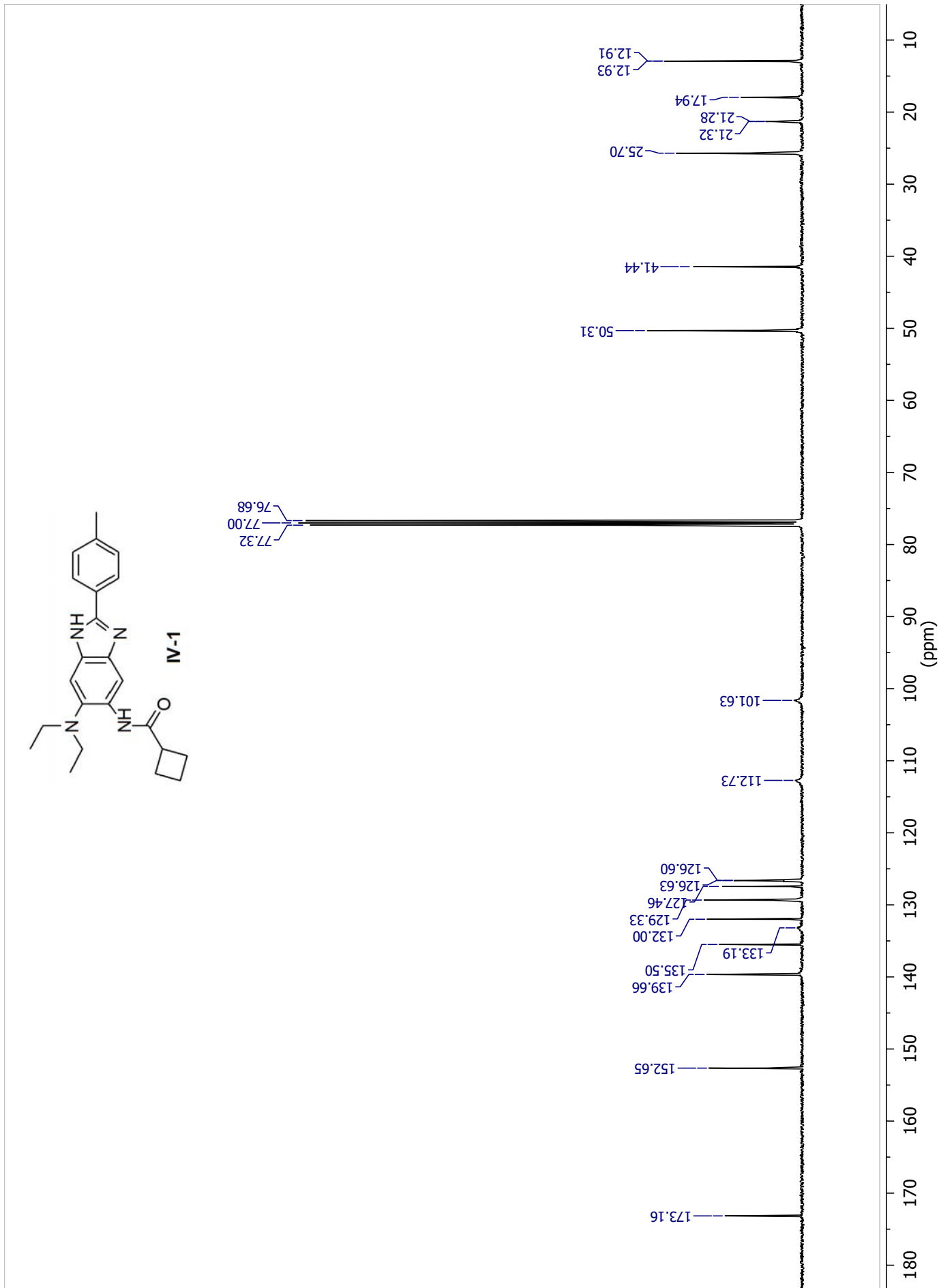


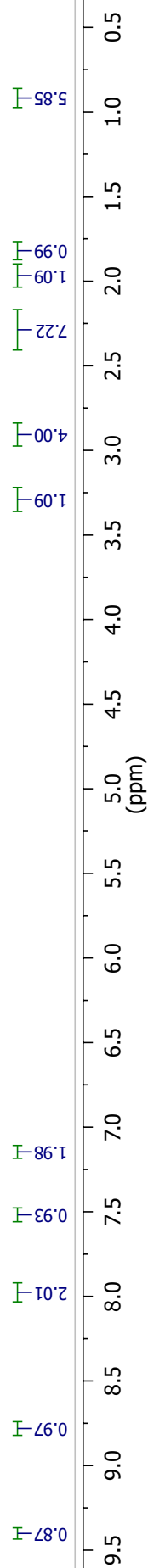
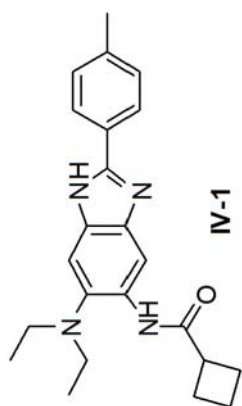


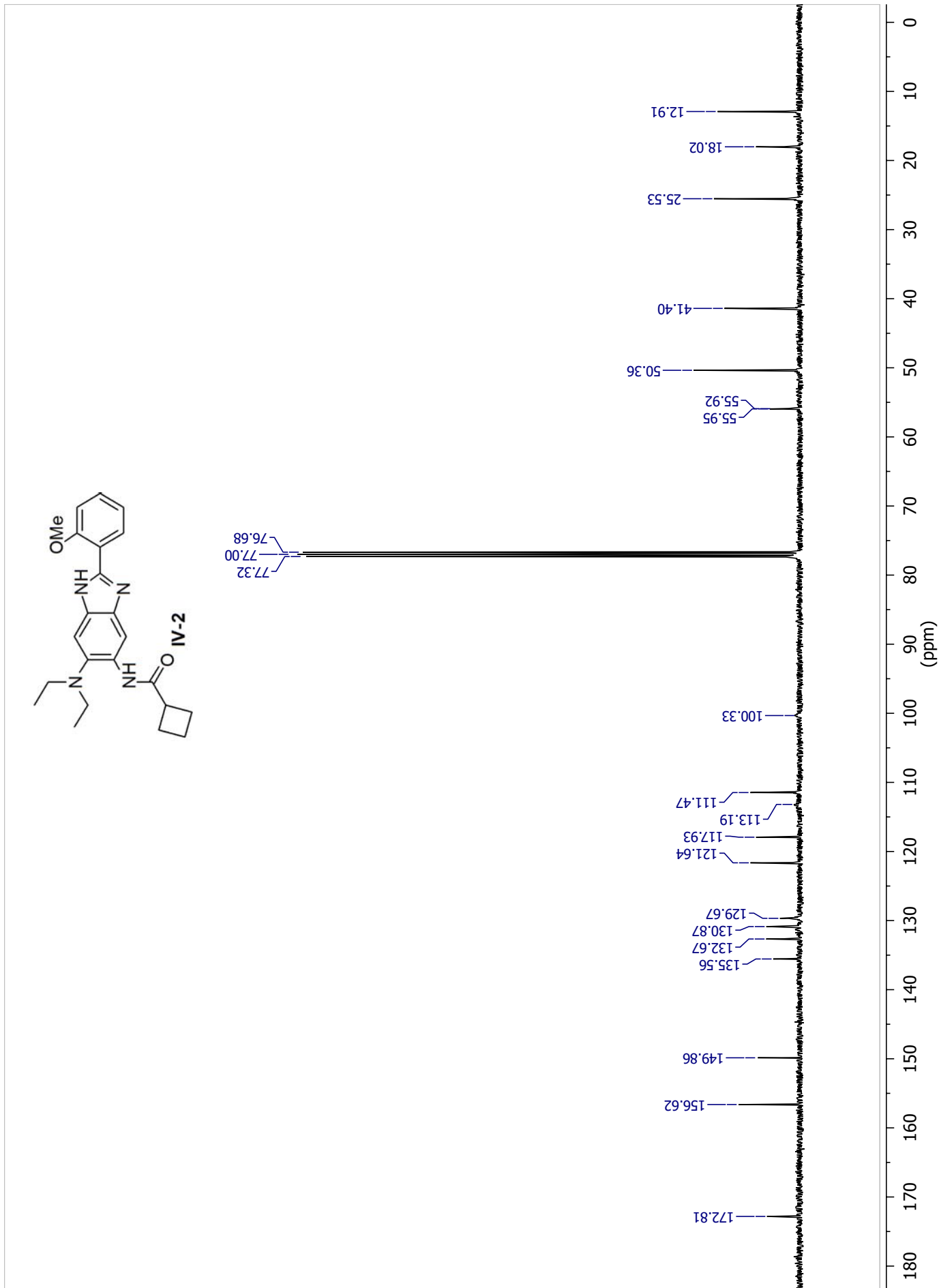


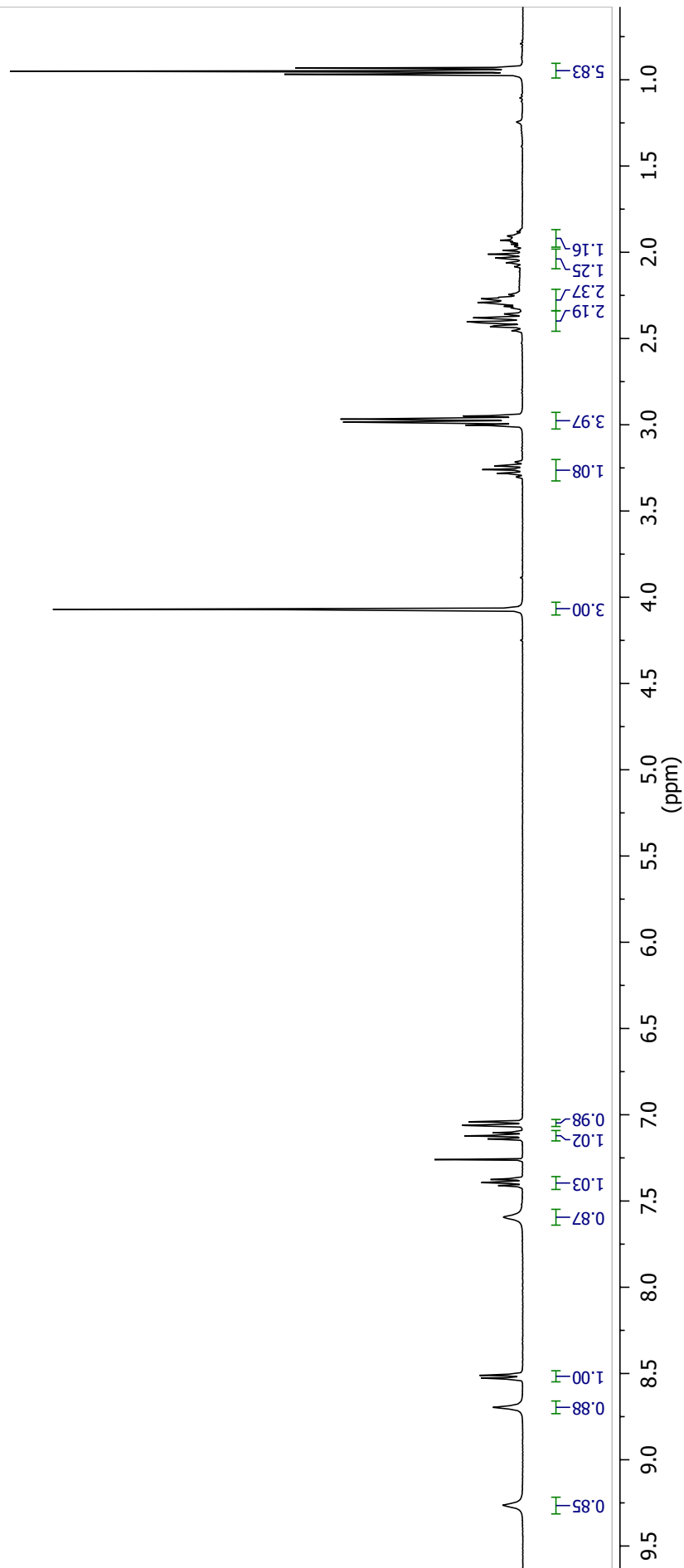
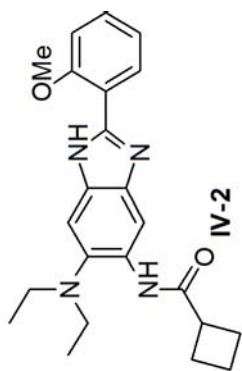


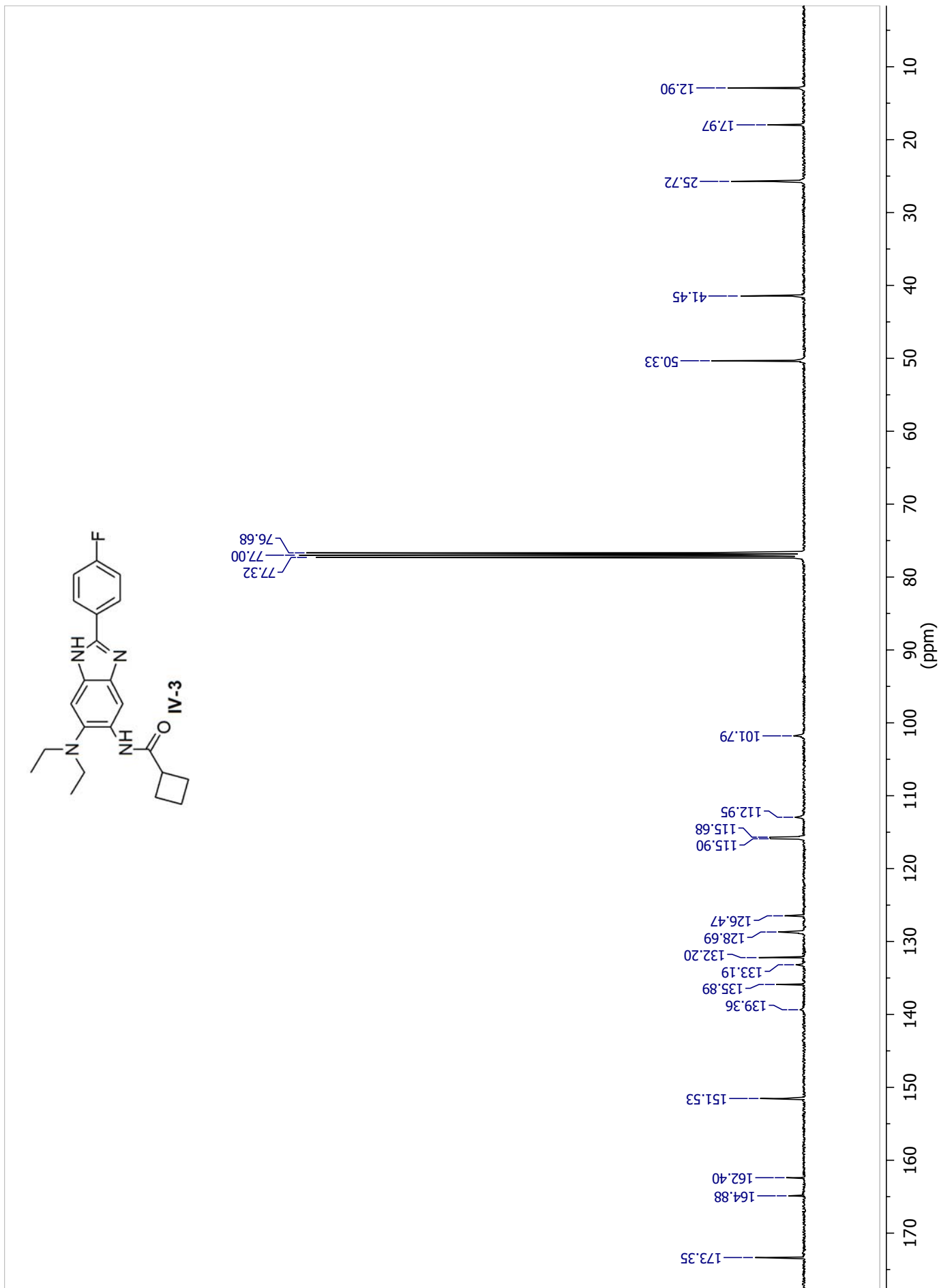


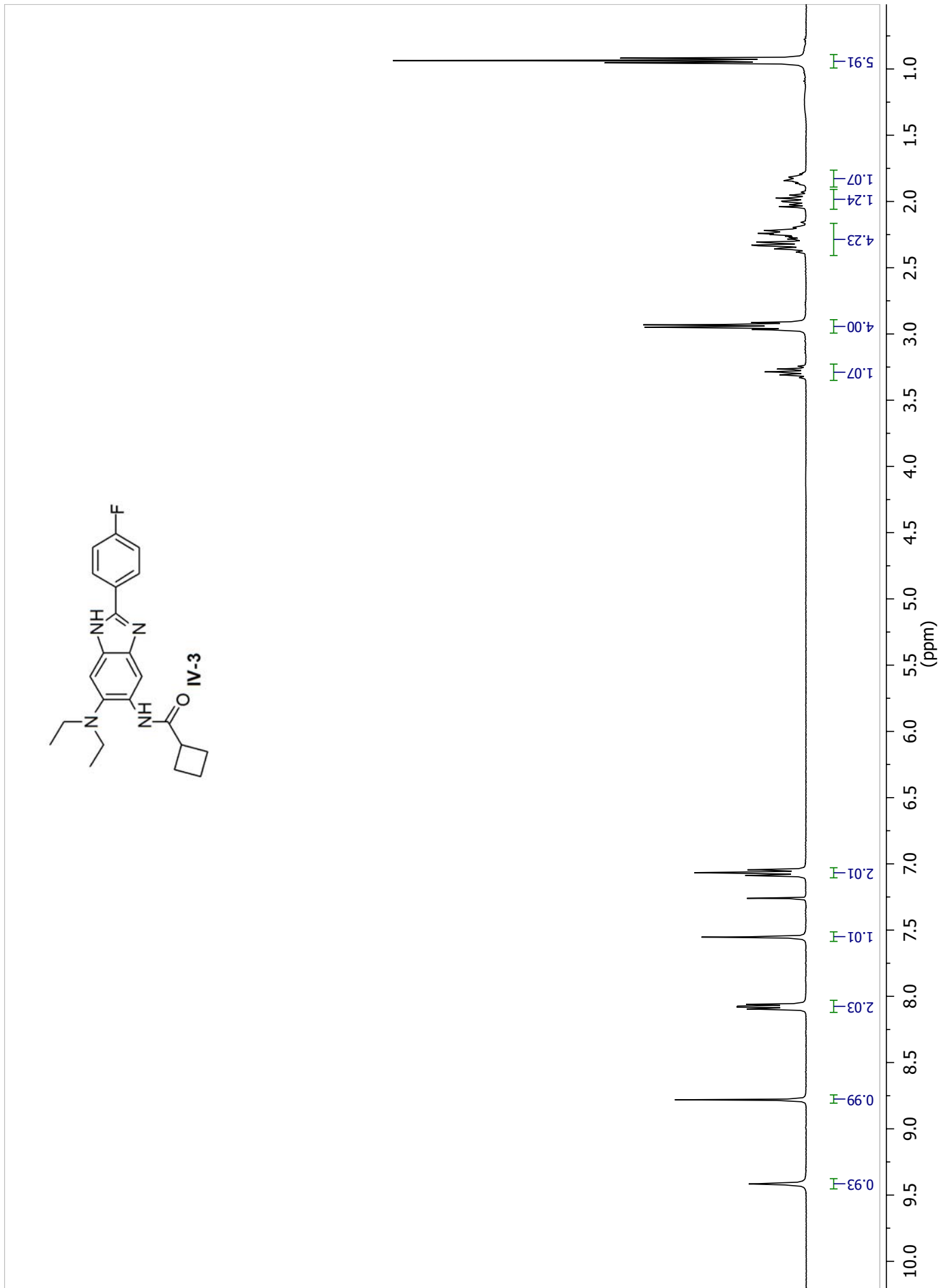


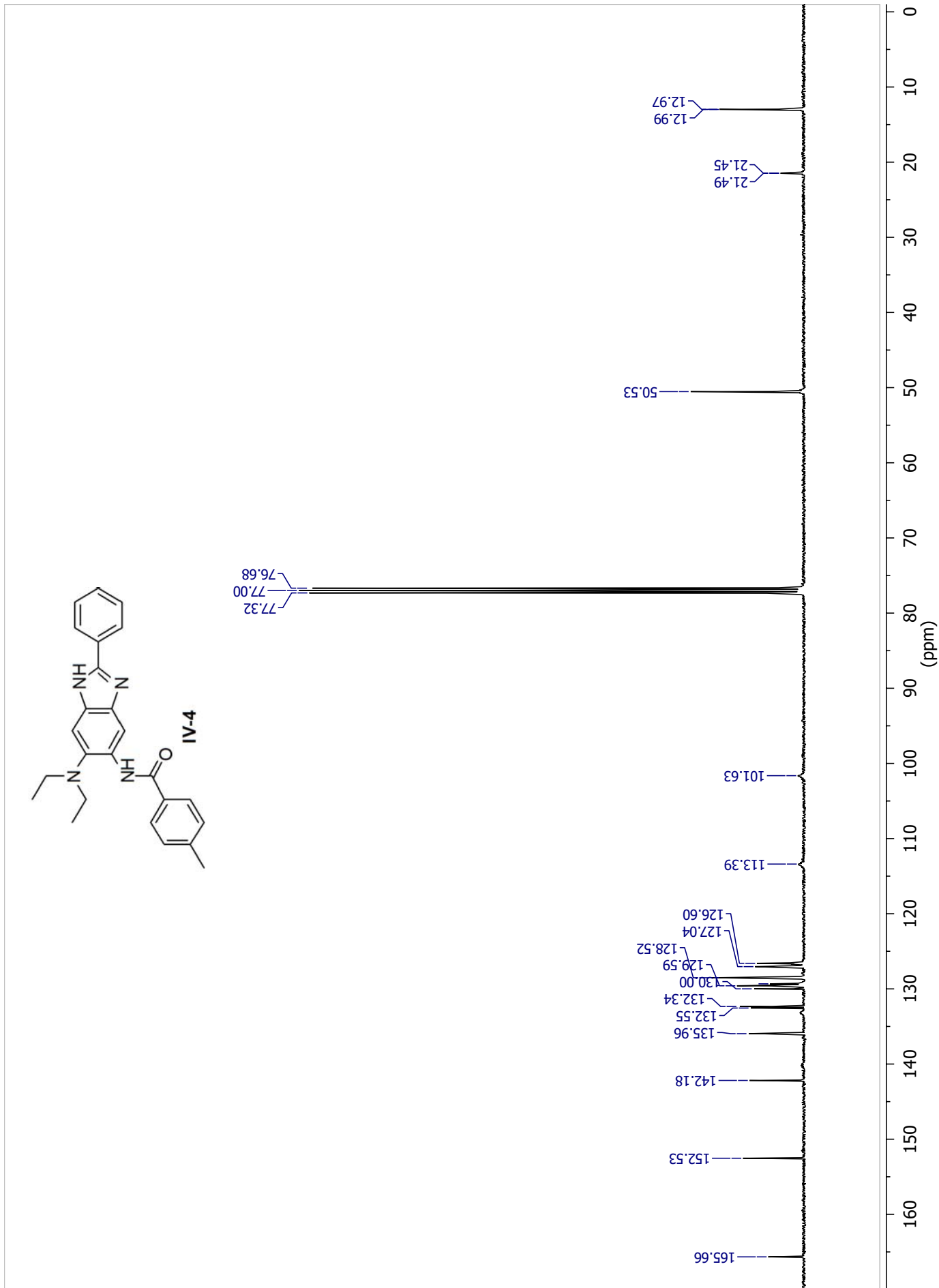


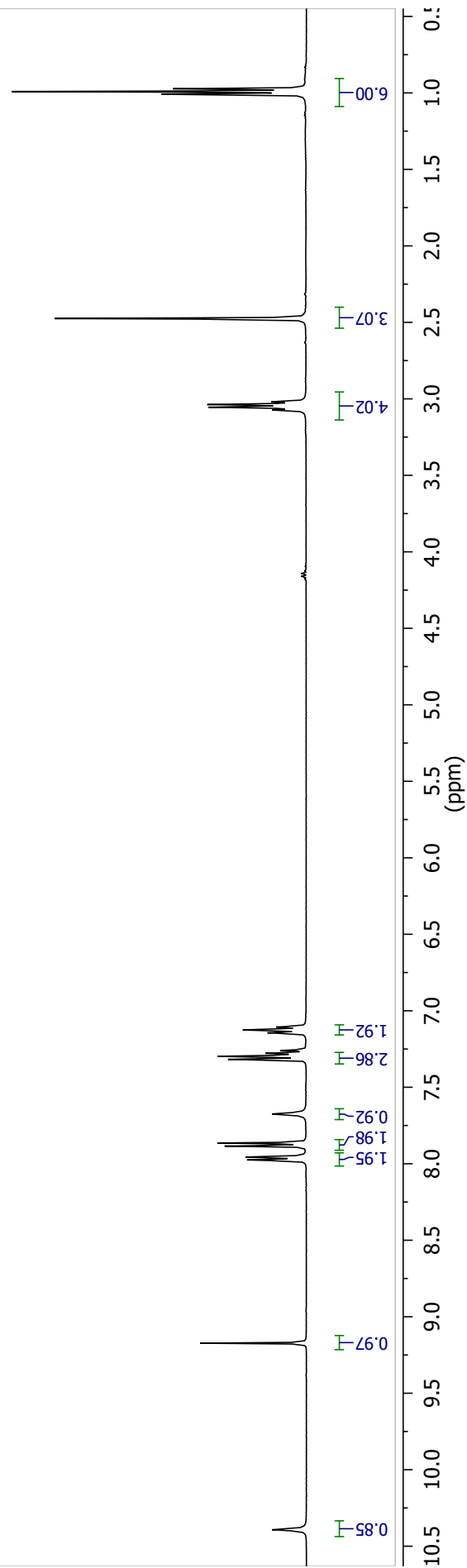
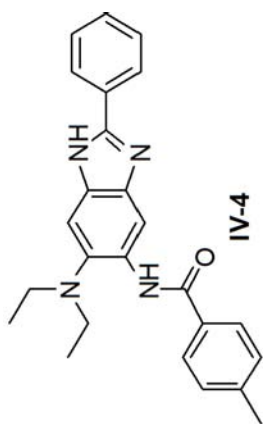


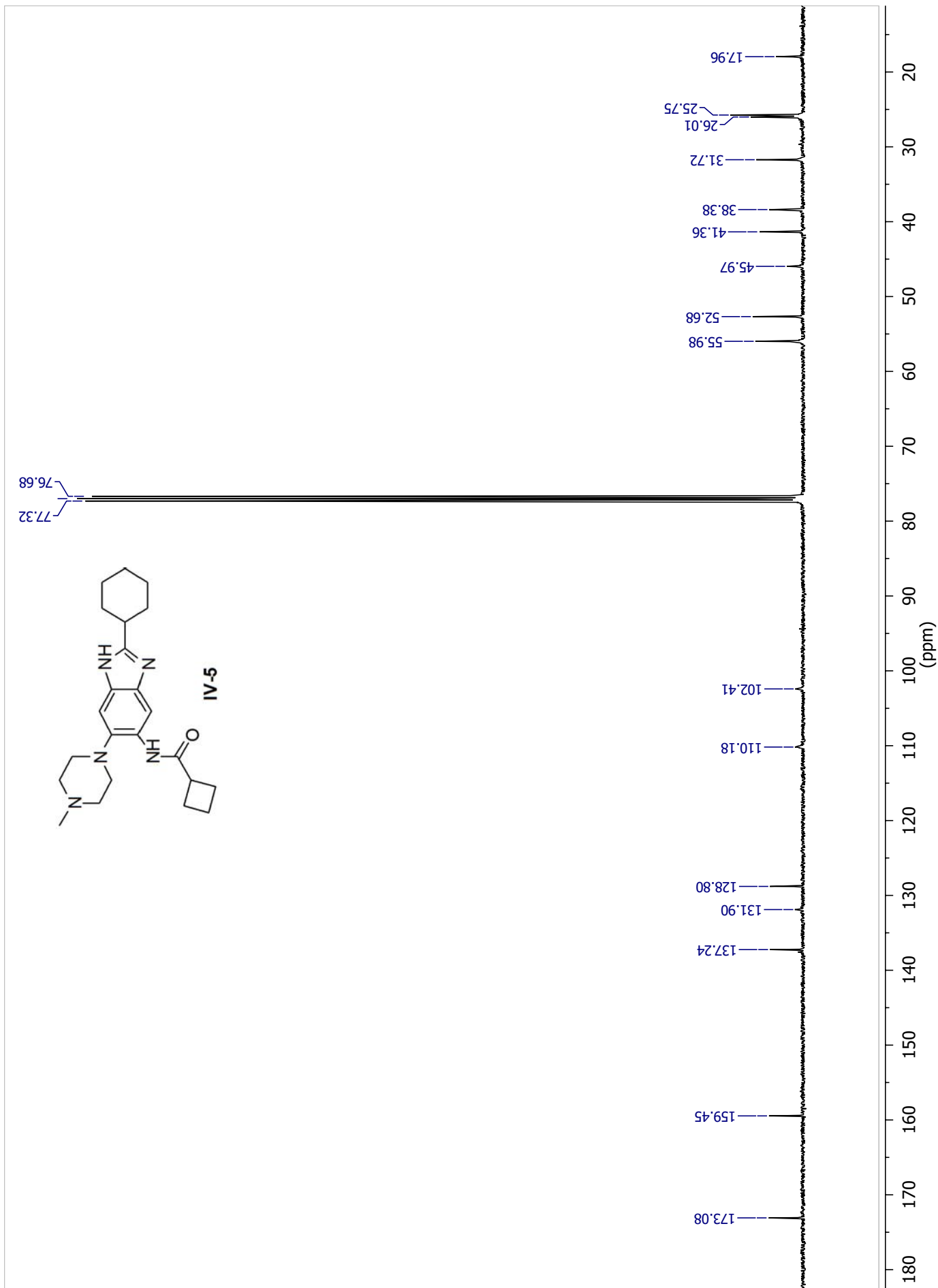


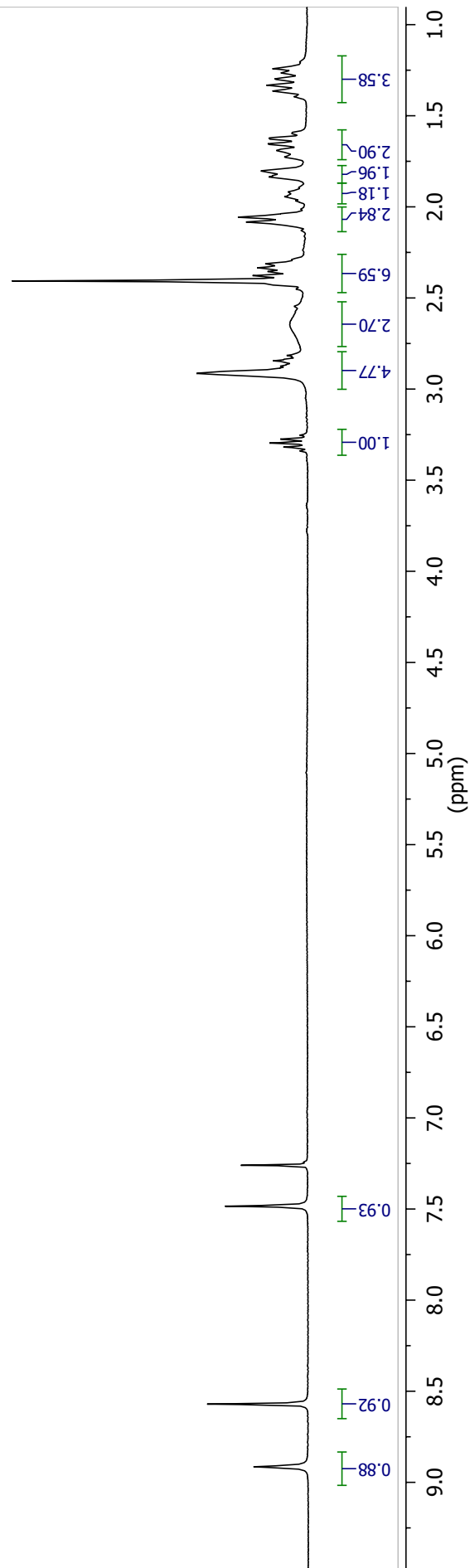
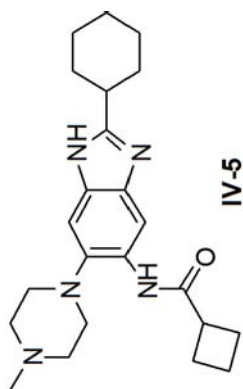


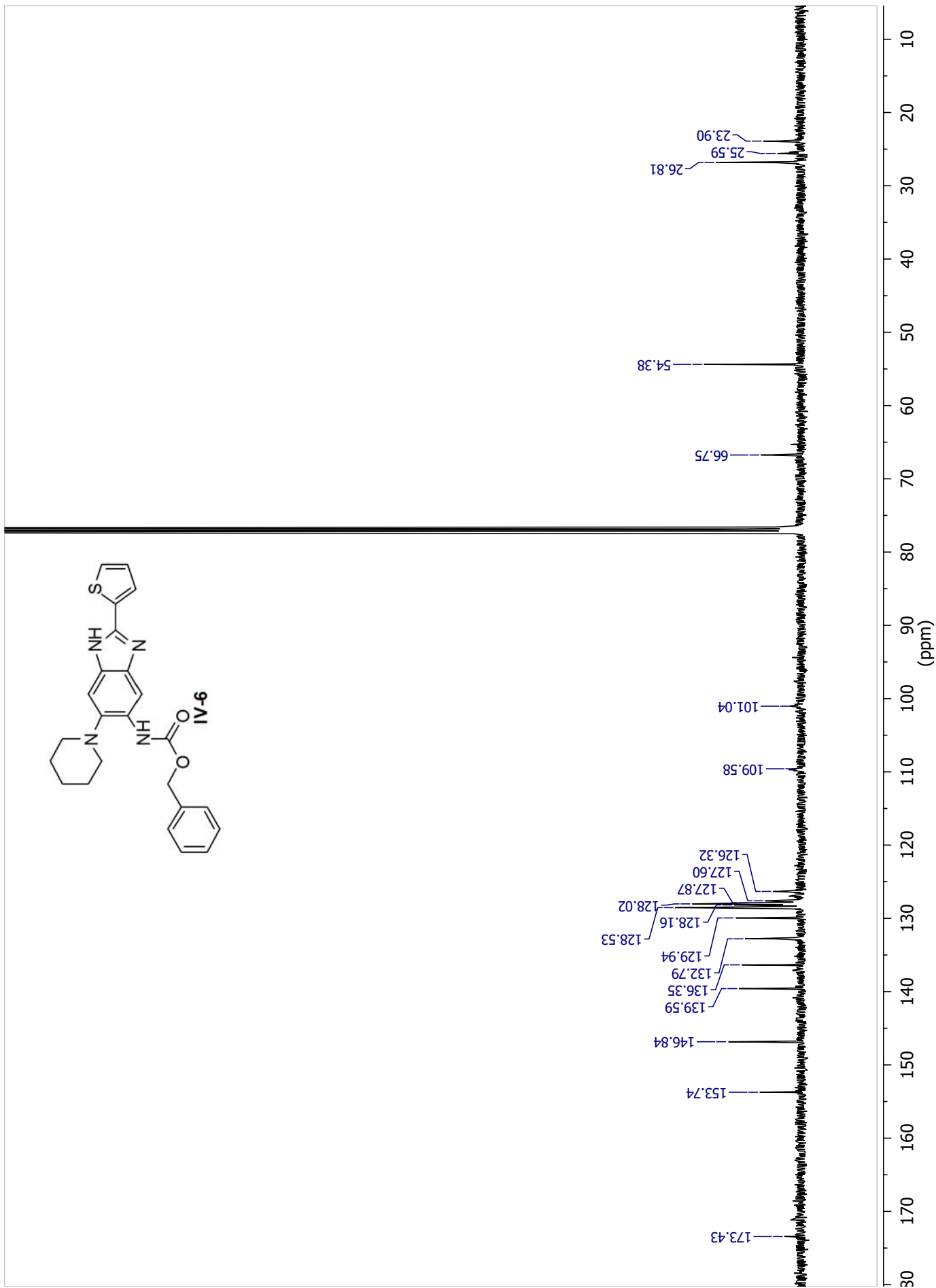


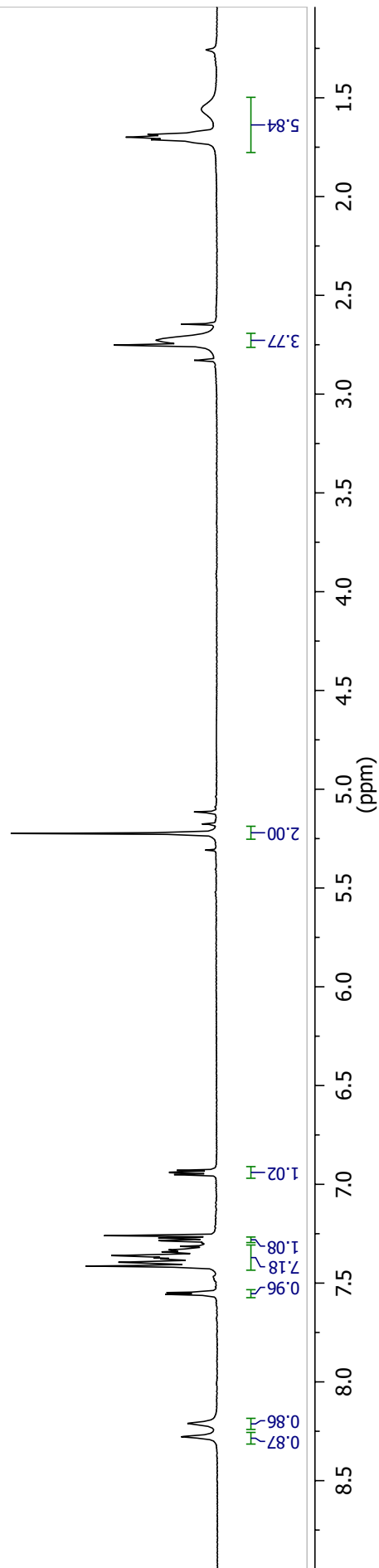
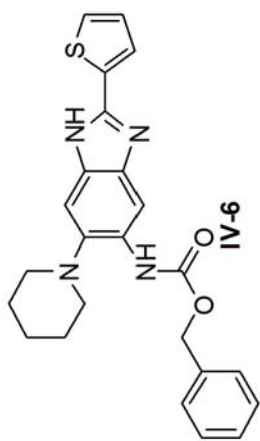


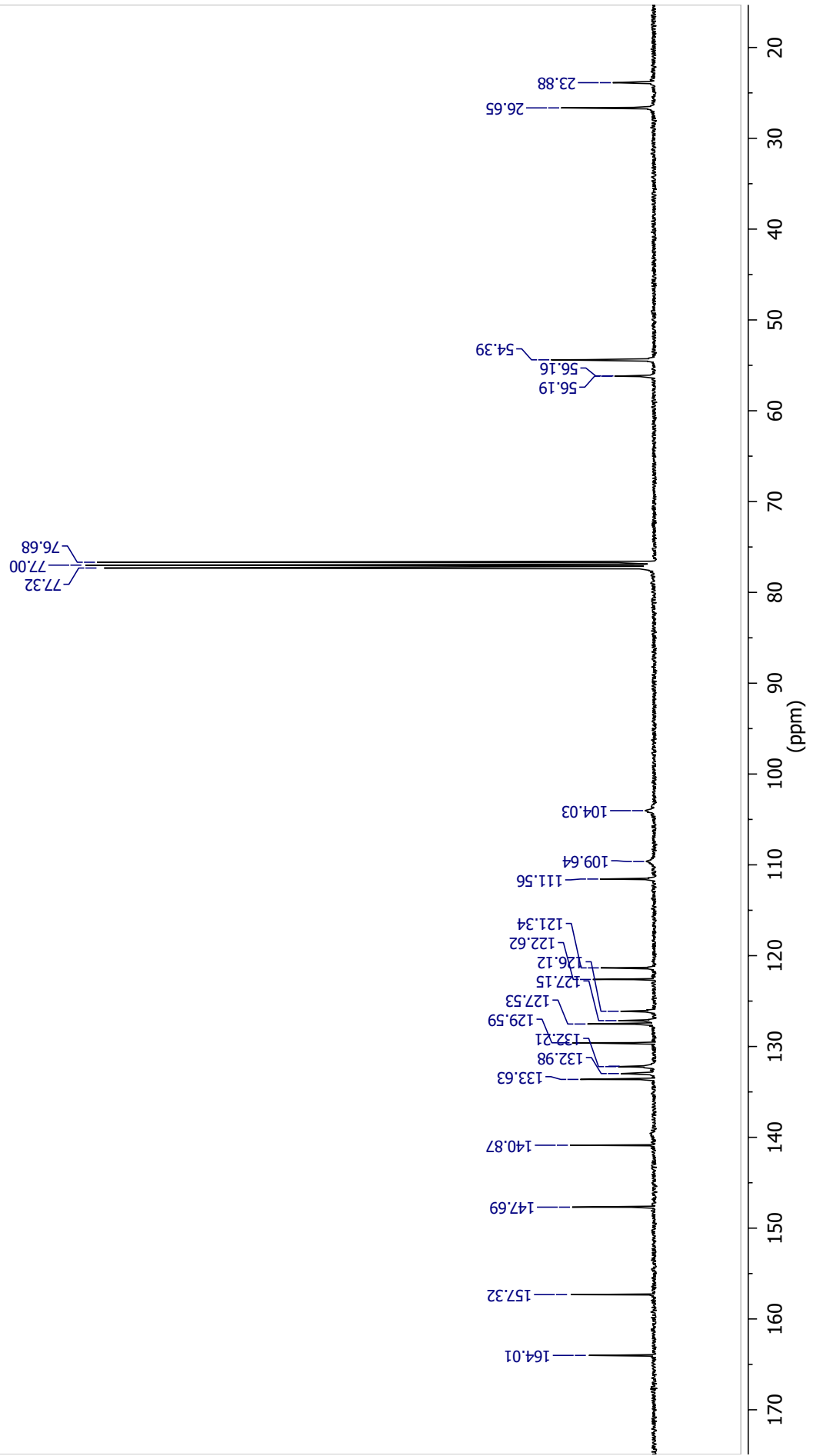
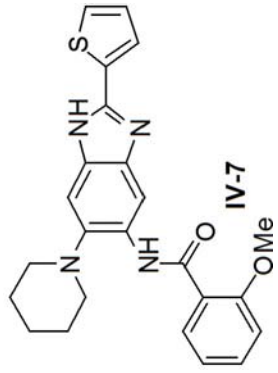


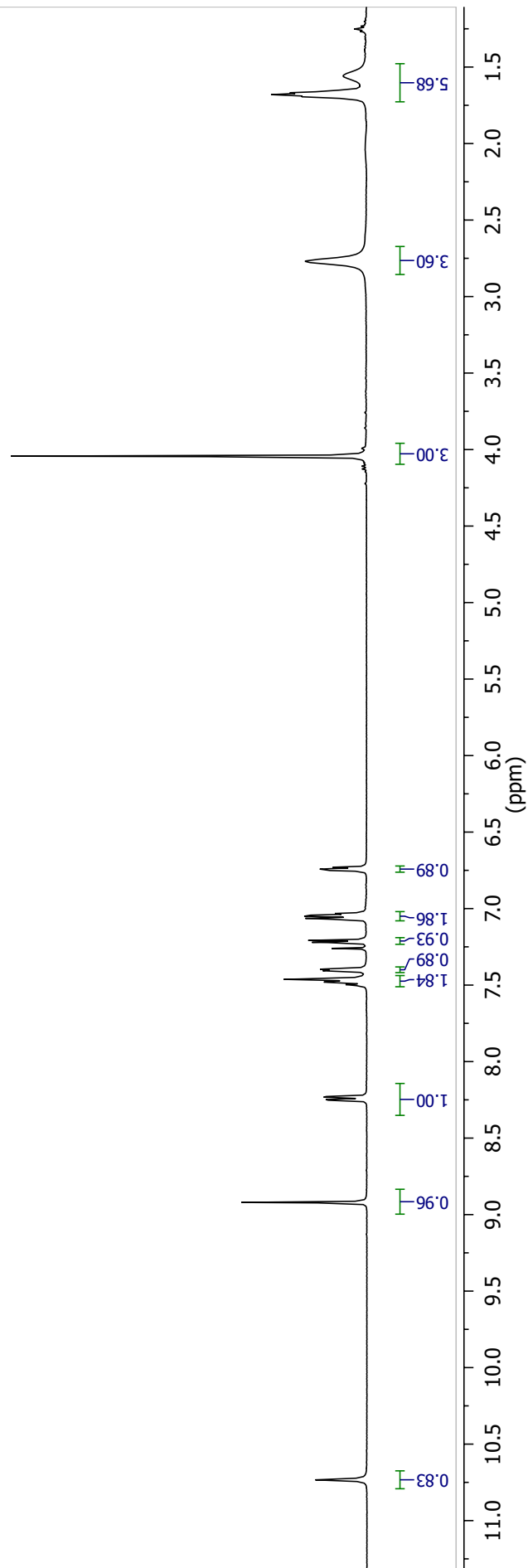
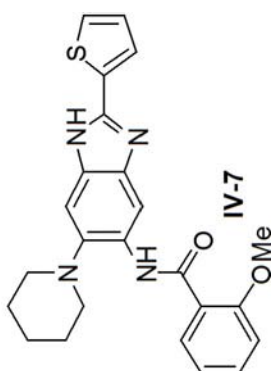


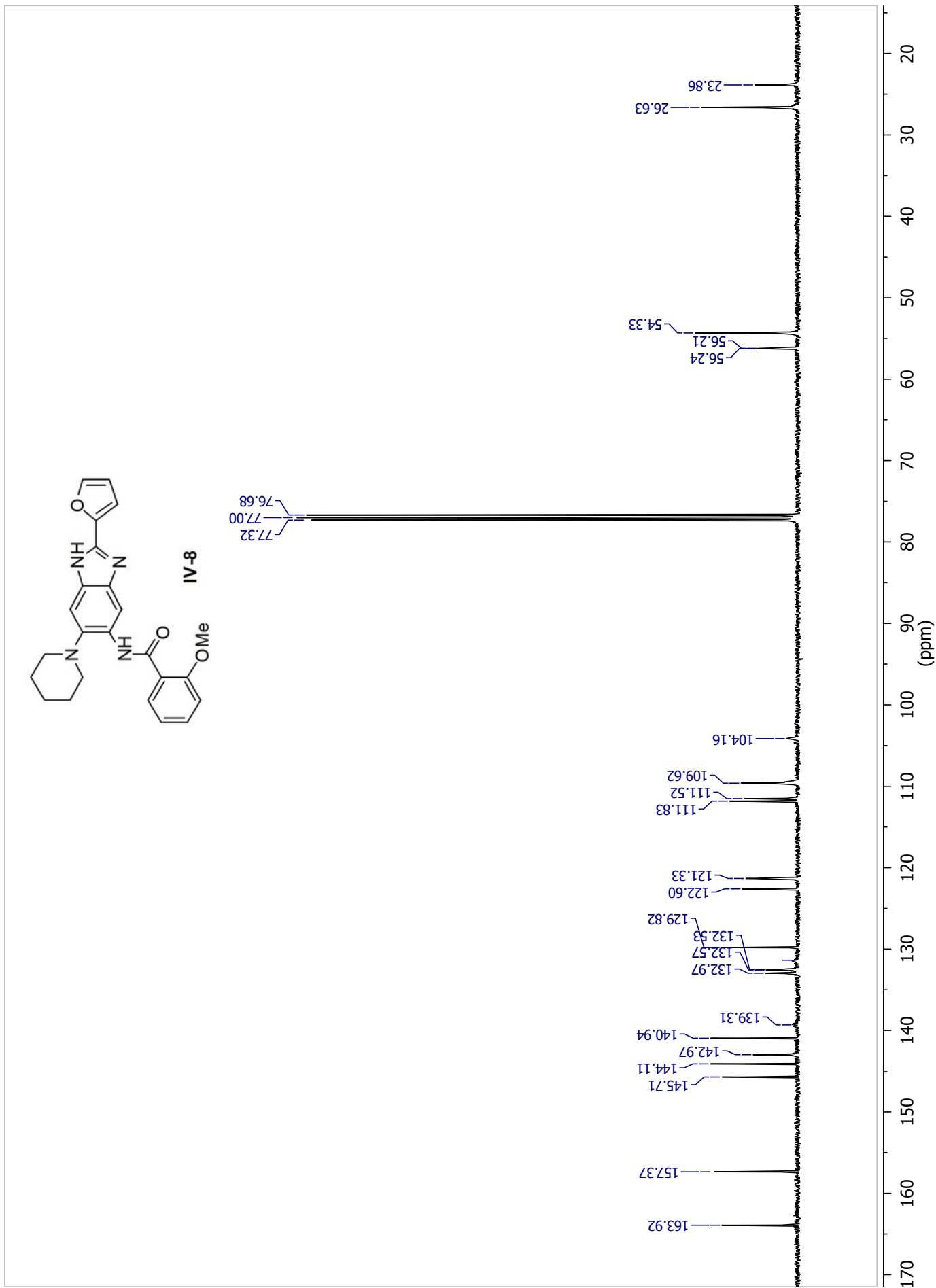


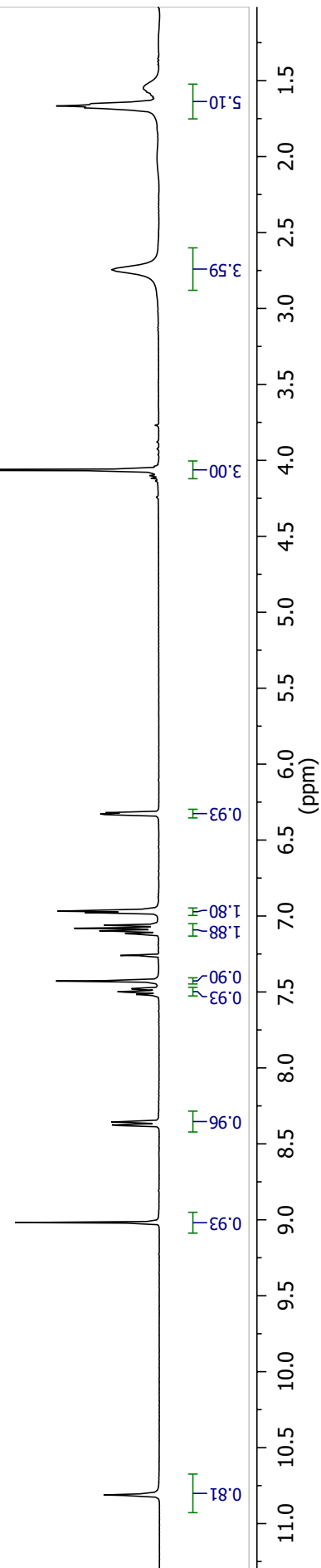
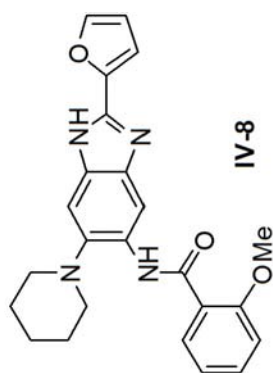


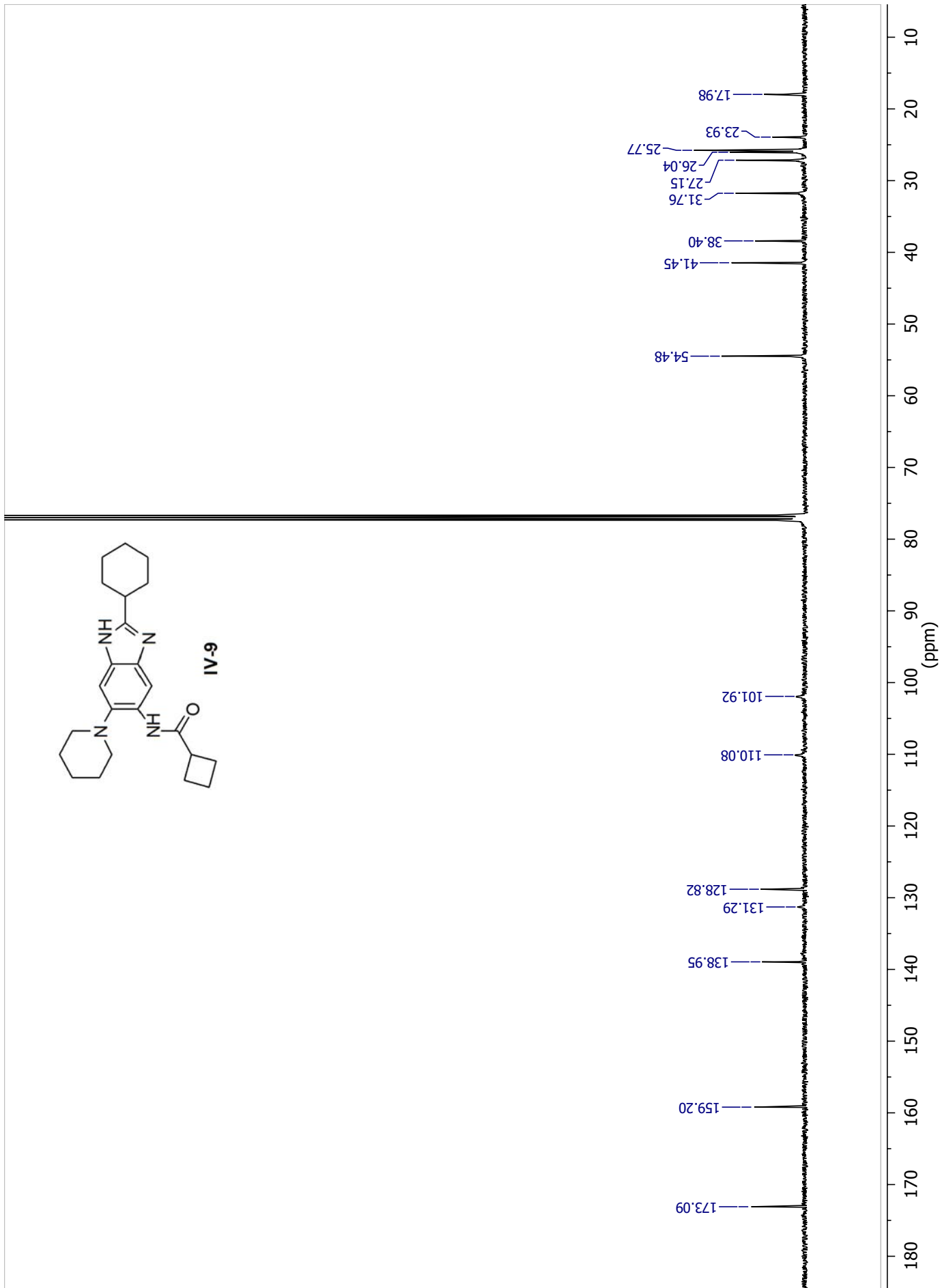


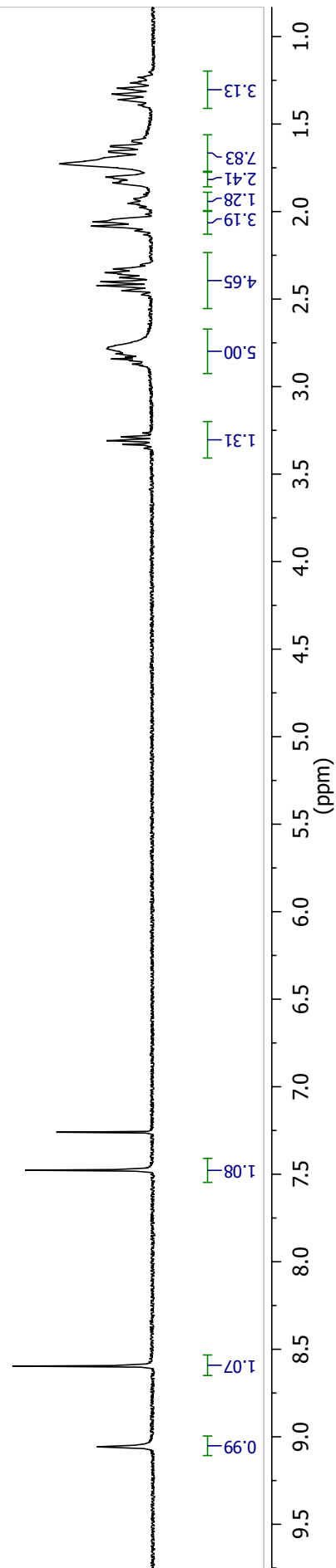
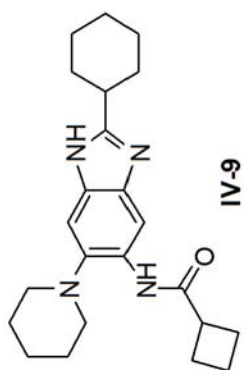


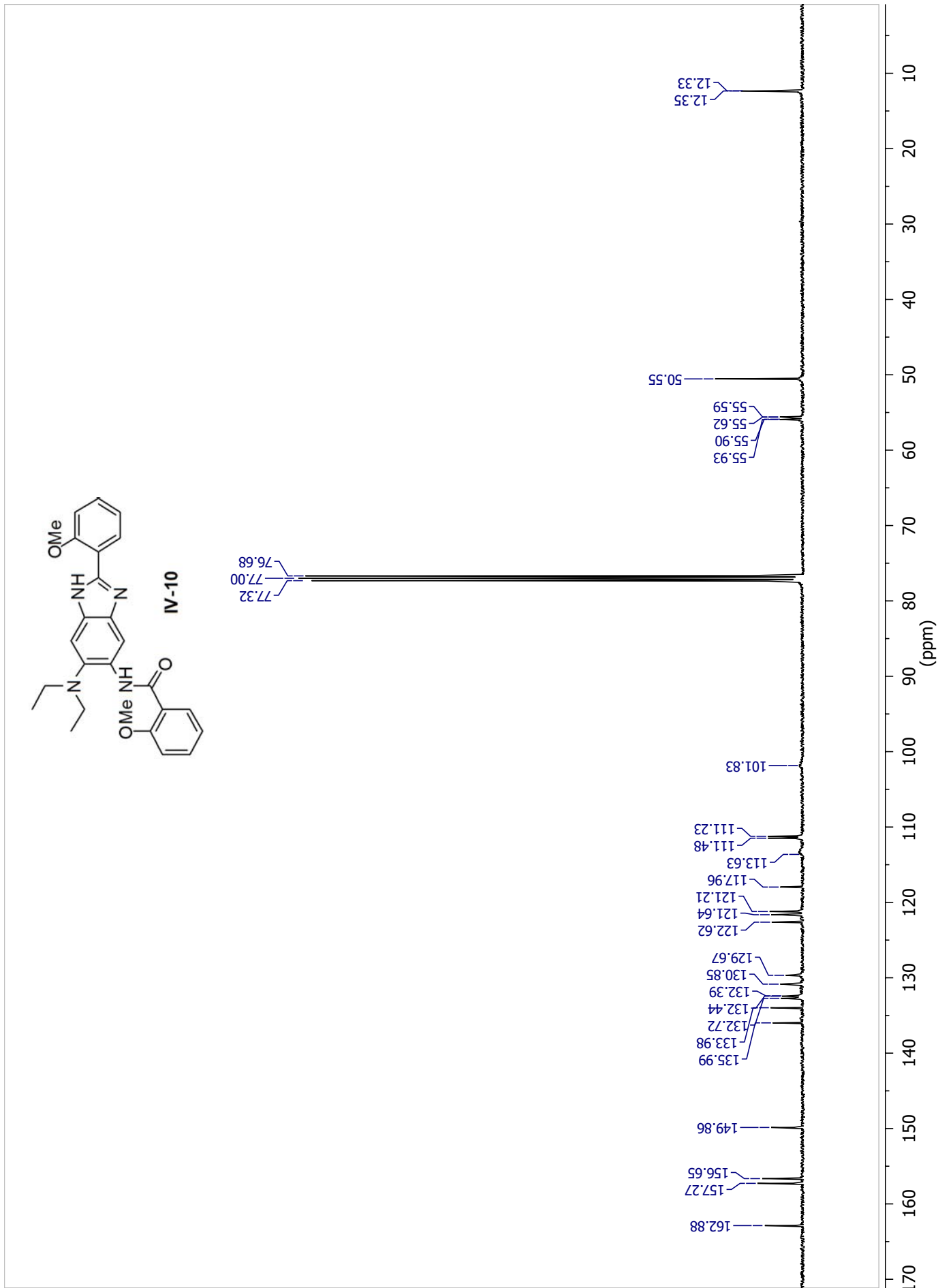


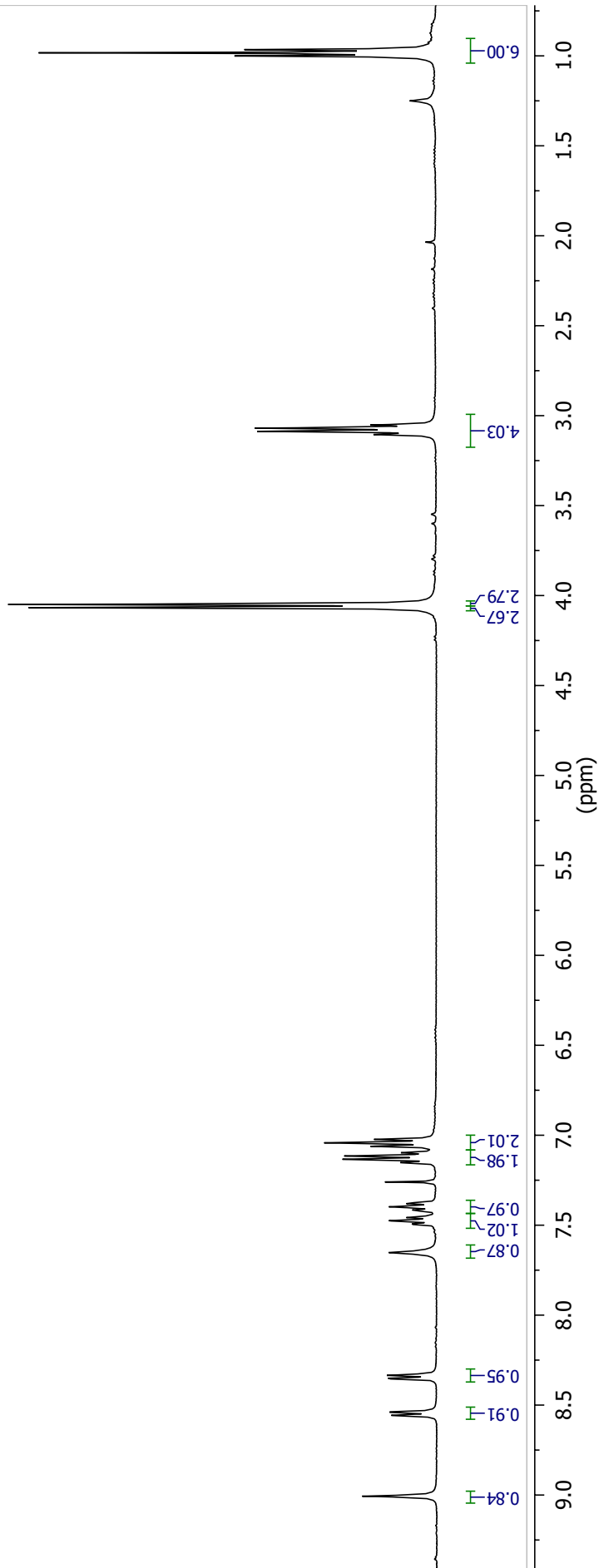
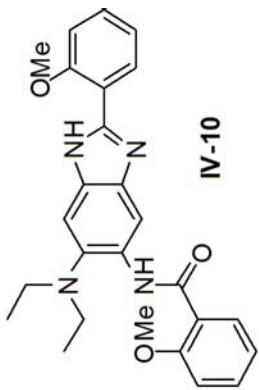


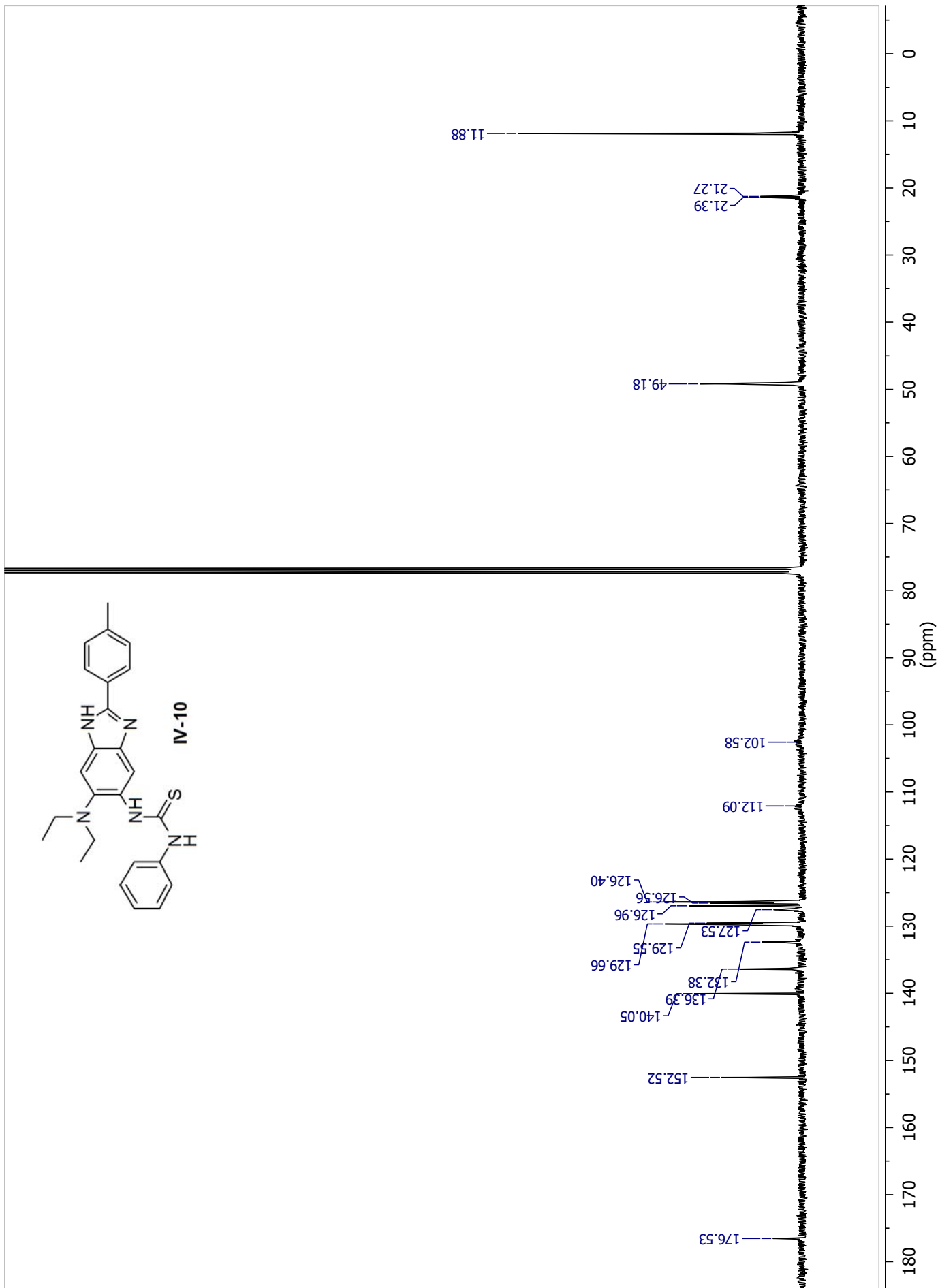


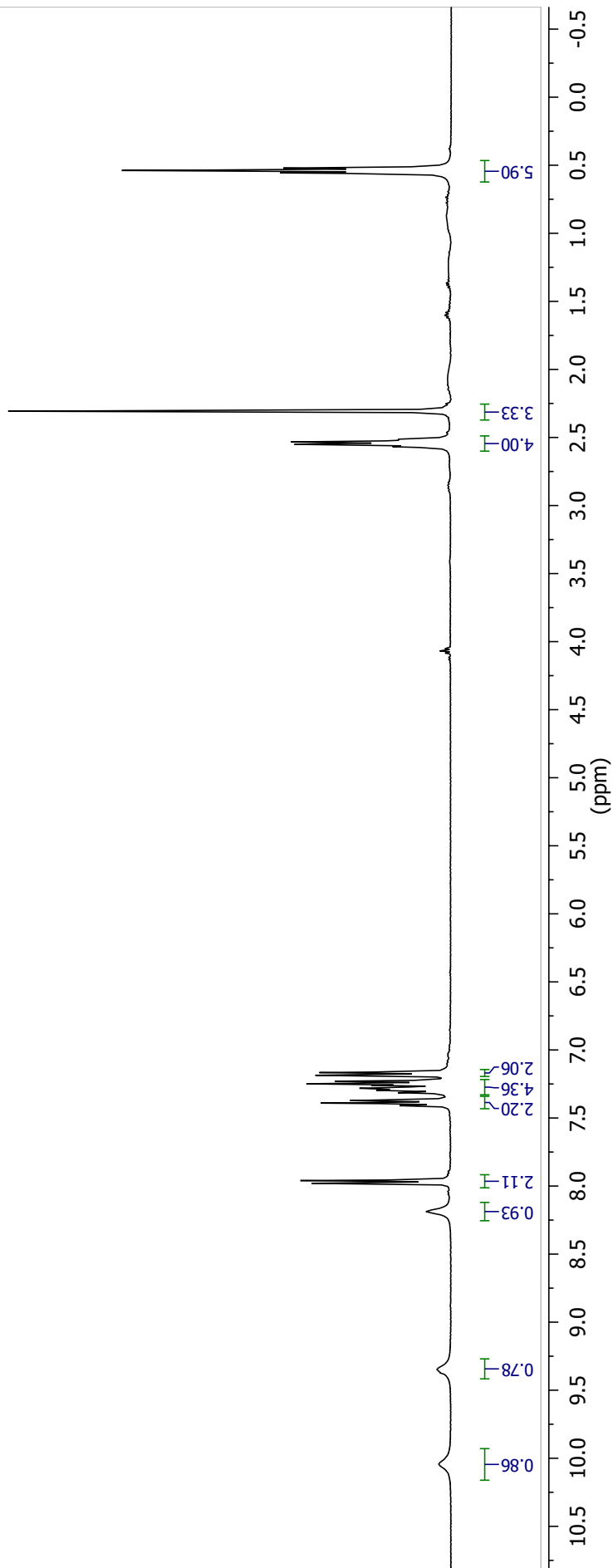
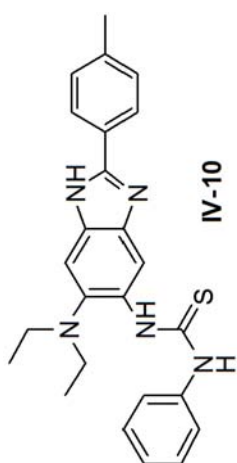


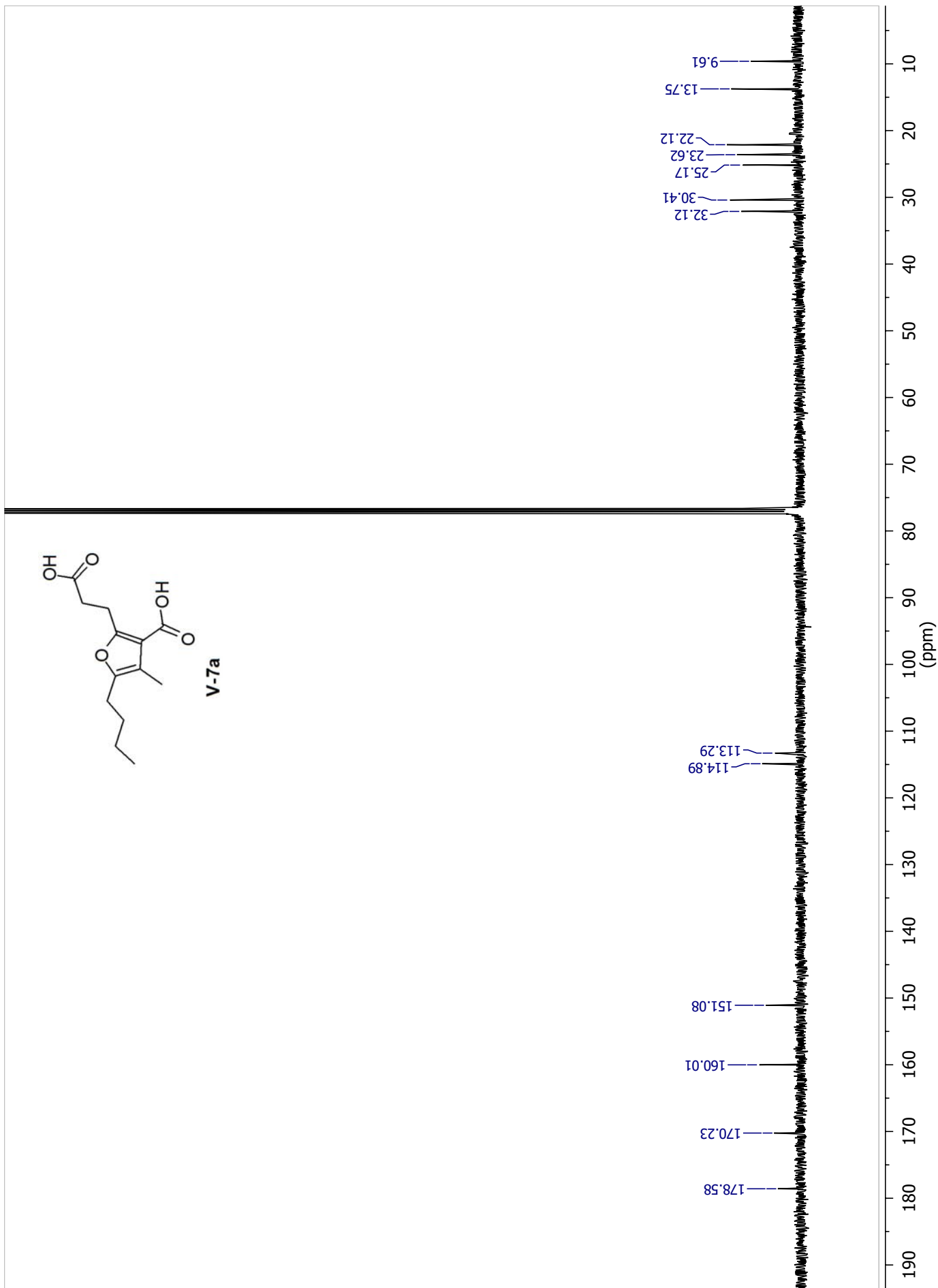


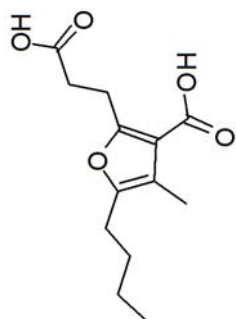












V-7a

